EXTREME BENTHIC COMMUNITIES IN THE AGE OF GLOBAL CHANGE

EDITED BY: Roberto Sandulli, Jeroen Ingels, Daniela Zeppilli, Andrew Kvassnes Sweetman, Sarah Louise Mincks, Furu Mienis and Chih-Lin Wei

PUBLISHED IN: Frontiers in Marine Science

frontiers Research Topics

Frontiers eBook Copyright Statement

The copyright in the text of individual articles in this eBook is the property of their respective authors or their respective institutions or funders. The copyright in graphics and images within each article may be subject to copyright of other parties. In both cases this is subject to a license granted to Frontiers.

The compilation of articles constituting this eBook is the property of Frontiers.

Each article within this eBook, and the eBook itself, are published under the most recent version of the Creative Commons CC-BY licence. The version current at the date of publication of this eBook is CC-BY 4.0. If the CC-BY licence is updated, the licence granted by Frontiers is automatically updated to the new version.

When exercising any right under the CC-BY licence, Frontiers must be attributed as the original publisher of the article or eBook, as applicable.

Authors have the responsibility of ensuring that any graphics or other materials which are the property of others may be included in the CC-BY licence, but this should be checked before relying on the CC-BY licence to reproduce those materials. Any copyright notices relating to those materials must be complied with.

Copyright and source acknowledgement notices may not be removed and must be displayed in any copy, derivative work or partial copy which includes the elements in question.

All copyright, and all rights therein, are protected by national and international copyright laws. The above represents a summary only. For further information please read Frontiers' Conditions for Website Use and Copyright Statement, and the applicable CC-BY licence.

ISSN 1664-8714
ISBN 978-2-88966-482-5
DOI 10.3389/978-2-88966-482-5

About Frontiers

Frontiers is more than just an open-access publisher of scholarly articles: it is a pioneering approach to the world of academia, radically improving the way scholarly research is managed. The grand vision of Frontiers is a world where all people have an equal opportunity to seek, share and generate knowledge. Frontiers provides immediate and permanent online open access to all its publications, but this alone is not enough to realize our grand goals.

Frontiers Journal Series

The Frontiers Journal Series is a multi-tier and interdisciplinary set of open-access, online journals, promising a paradigm shift from the current review, selection and dissemination processes in academic publishing. All Frontiers journals are driven by researchers for researchers; therefore, they constitute a service to the scholarly community. At the same time, the Frontiers Journal Series operates on a revolutionary invention, the tiered publishing system, initially addressing specific communities of scholars, and gradually climbing up to broader public understanding, thus serving the interests of the lay society, too.

Dedication to Quality

Each Frontiers article is a landmark of the highest quality, thanks to genuinely collaborative interactions between authors and review editors, who include some of the world's best academicians. Research must be certified by peers before entering a stream of knowledge that may eventually reach the public - and shape society; therefore, Frontiers only applies the most rigorous and unbiased reviews.
Frontiers revolutionizes research publishing by freely delivering the most outstanding research, evaluated with no bias from both the academic and social point of view. By applying the most advanced information technologies, Frontiers is catapulting scholarly publishing into a new generation.

What are Frontiers Research Topics?

Frontiers Research Topics are very popular trademarks of the Frontiers Journals Series: they are collections of at least ten articles, all centered on a particular subject. With their unique mix of varied contributions from Original Research to Review Articles, Frontiers Research Topics unify the most influential researchers, the latest key findings and historical advances in a hot research area! Find out more on how to host your own Frontiers Research Topic or contribute to one as an author by contacting the Frontiers Editorial Office: frontiersin.org/about/contact

EXTREME BENTHIC COMMUNITIES IN THE AGE OF GLOBAL CHANGE

Topic Editors:
Roberto Sandulli, University of Naples Parthenope, Italy
Jeroen Ingels, Florida State University, United States
Daniela Zeppilli, Institut Français de Recherche pour l'Exploitation de la Mer (IFREMER), France
Andrew Kvassnes Sweetman, Heriot-Watt University, United Kingdom
Sarah Louise Mincks, University of Alaska Fairbanks, United States
Furu Mienis, Royal Netherlands Institute for Sea Research (NIOZ), Netherlands
Chih-Lin Wei, National Taiwan University, Taiwan

Citation: Sandulli, R., Ingels, J., Zeppilli, D., Sweetman, A. K., Mincks, S. L., Mienis, F., Wei, C.-L., eds. (2021). Extreme Benthic Communities in the Age of Global Change. Lausanne: Frontiers Media SA. doi: 10.3389/978-2-88966-482-5

Table of Contents

frontiers in Marine Science

EDITORIAL
published: 11 January 2021
doi: 10.3389/fmars.2020.609648

Editorial: Extreme Benthic Communities in the Age of Global Change

Roberto Sandulli[1,2†], Jeroen Ingels[3†], Daniela Zeppilli[4†], Andrew Kvassnes Sweetman[5†], Sarah Hardy Mincks[6†], Furu Mienis[7†] and Wei Chin-Lin[8†]*

[1] Laboratory of Marine Ecology, Department of Science and Technology, University of Naples "Parthenope", Naples, Italy, [2] National Interuniversity Consortium for Marine Sciences, Rome, Italy, [3] Coastal and Marine Laboratory, Florida State University, St Teresa, FL, United States, [4] IFREMER Centre Brest REM/EEP/LEP, ZI de la Pointe du Diable, CS10070, Plouzané, France, [5] The Lyell Centre for Earth and Marine Science, Heriot-Watt University, Edinburgh, United Kingdom, [6] College of Fisheries and Ocean Sciences, University of Alaska Fairbanks, Fairbanks, AK, United States, [7] Nederlands Institut Voor Onderzoek der Zee Royal Netherlands Institute for Sea Research and Utrecht University, Den Burg, Netherlands, [8] Institute of Oceanography, National Taiwan University, Taipei, Taiwan

Keywords: benthos, global change, extreme environment, biodiversity, ecosystem functioning

Editorial on the Research Topic

Extreme Benthic Communities in the Age of Global Change

The sea floor represents the largest solid ecosystem on our Planet. This heterogeneous realm consists of many different features shaped by millions of years of geological and chemical events, and biological and environmental evolution. "Extreme" benthic environments, defined as having abiotic conditions that demand organisms and resident communities be adapted in order to survive and thrive, are widespread and offer many opportunities for investigating the biological responses and adaptations of organisms to "abnormal" life conditions. At the same time, these adapted organisms may give insights into future ecosystem responses, as today's extreme ecosystems can be considered natural analogs of "normal" environments that may change under future climate change conditions. With continuing climate change and increased anthropogenic pressures, very few seafloor areas will remain untouched. Hence the future of the benthos will depend on how organisms, species, populations and communities will respond. Benthic communities are especially useful in long-term comparative investigations such as studying the effects of climate change and other pressures because most of their species are sessile or have low mobility, can be long-lived, and integrate the effects of environmental change over time. In addition, macro-, meio-, and microbenthos of hard and soft bottoms are found in almost any marine environment, including the most hostile or unusual, rendering them ideal to assess the impacts of environmental change and other pressures, as well as effects of multiple, simultaneous pressures. The continuous discovery of communities in extreme environments and the study of their variability, heterogeneity, and their relation to climate change and anthropogenic impacts, are slowly expanding as more evidence and long-term observations become increasingly available.

The present Special Issue of Frontiers in Marine Science aims at providing a significant contribution to understanding more of the above-mentioned topics. The issue contains 13 diverse scientific contributions from all over the world on many fundamental questions related to benthos in extreme environments, and how these environments and their biota respond to global change and human pressures.

Several papers have focused on chemosynthetic systems in shallow and deep water, covering hydrothermal vents and vent fields, illustrating the diversity of research conducted in these unique ecosystems. On one hand, some studies are demonstrating unique organism distributions, connectivity, and adaptations, while documenting undiscovered biodiversity with new species

OPEN ACCESS

Edited and reviewed by:
Jacob Carstensen, Aarhus University, Denmark

****Correspondence:***
Roberto Sandulli
roberto.sandulli@uniparthenope.it

† These authors have contributed equally to this work

Specialty section:
This article was submitted to Global Change and the Future Ocean, a section of the journal Frontiers in Marine Science

Received: *23 September 2020*
Accepted: *14 December 2020*
Published: *11 January 2021*

Citation:
Sandulli R, Ingels J, Zeppilli D, Sweetman AK, Hardy Mincks S, Mienis F and Chin-Lin W (2021) Editorial: Extreme Benthic Communities in the Age of Global Change. Front. Mar. Sci. 7:609648. doi: 10.3389/fmars.2020.609648

descriptions. On the other hand, other studies show that these systems are or will be subject to human pressures, including climate change, before we fully understand how they function and how their biodiversity is driven by the biotics and abiotics surrounding them. Åström et al. provide a thorough review of cold seeps benthic ecology in the Arctic, suggesting that chemosynthetic systems, operating on different spatial and temporal cycles than the surficial photosynthetic counterpart, may act as spatio-temporal bridges or refugia for benthic communities subject to climate change such as warming, and subsequent mismatches in phenologies and energy demands vs. surface supply (bentho-pelagic coupling). Along the Arctic Mid-Ocean Ridge, Ramirez-Llodra et al. examined benthic communities on inactive sulfide mounds (2,600 m depth), characterized by sponge and stalked crinoid fields, recognized as Vulnerable Marine Ecosystems. This has implications for marine management and conservation since these mounds may be targeted for deep-sea mining in the future. Spedicato et al. also draw attention to deep-sea mining by showing how meiofauna and nematodes are useful in describing the environmental heterogeneity, mainly in terms of substratum type and geochemistry, of hydrothermal vent fields along the Mid-Atlantic Ridge, which may be exploited for seafloor massive sulfide extraction. Food availability, geochemical settings, and biotic interactions were distinct drivers of the meiofauna communities. Cepeda et al. showed that, within meiofauna, kinorhynchs showed particular affinity with cold seep conditions (low oxygen, high sulfide, and methane) likely caused by reduced competition for space and resources by other organisms in these extreme environments. They also describe three new "mud dragon" species, indicating that much of the deep-sea diversity remains undescribed. Moving into shallow-water chemosynthetic environments, Donnarumma et al. studied Secca delle Fumose, a hydrothermal vent system in the Mediterranean, showing that communities are adapted to the specific conditions of these vent systems, with resistant species and communities that are different from control sites outside the vent area. Further work on chemosynthetic species is presented by Eilertsen et al., who described a new species of *Osedax* from the Arctic Mid-Ocean Ridge. Few extreme ecosystems speak to the imagination as whale falls in the deep sea; the authors mimicked such food falls by deploying cow bones near a hydrothermal vent and observing dense aggregations of the newly described bone-eating worm, feasting on the lipids stored within. A prime example of how limited availability of energy in the oligotrophic deep-sea pushes evolution to exploit alternative chemosynthetic niches.

It is well-accepted that energy is limited in the deep sea, that, apart from the above-mentioned chemosynthetic habitats, appears to be mainly reliant on the scarce, intermittent cascading of organic matter and other compounds from surface waters. How are deep-sea communities adapted to this oligotrophy, that, other than darkness, low temperatures and high pressure, poses additional challenges to metabolism, physiology, and behavior? McClain et al. brings novel insight into this field, proposing an eco-evolutionary adaptive theory of the metabolic niche, whereby deep-sea species are adapted to specific energy regimes which scale with biodiversity patterns. They present 10 hypotheses centered around metabolic niches, energy demand, biodiversity, and biogeography, concluding that benthic deep-sea invertebrates with high energy demands are located in areas with higher chemical availability being their distributions linked to geographic patterns of chemical energy availability. These findings suggest that species are likely adapted to specific energy regimes and imply a relation between adaptation and biogeographical distributions and patterns. An alternative view to geographic distributions and "energy" in the deep sea is provided by Castellan et al. on the distribution of the temperate coral *Dendrophyllia cornigera* across the Atlantic Ocean and whole Mediterranean. By analyzing temperature recordings at the collection sites they documented that this eurybathic coral lives between ∼7 and 17°C, which may present an advantage for its survival in a warming ocean.

Much of the deep sea remains un- or under-explored. As deep-sea science progresses, so do the technologies used to study it. This is particularly important in light of global change and anthropogenic impacts; ecosystems are changing before we have a chance to study their communities in detail. Ríos et al. focused on rock sponge aggregations in the Cantabrian Sea, where they took physical samples and imagery to fine tune improved methodologies to calculate biomass and volume of sponge assemblages. Their image-based approach aimed at developing better techniques to avoid destructive sampling in studying these vulnerable habitats. An image-based approach was also used by Meyer et al., who documented megabenthic communities of the Sognefjord. A seaward sill in the fjord causes stratification, resulting in limited variability of abiotic factors in the deep basin, which provided a unique opportunity to study their effect on benthic community composition. Their study showed that highly-stratified fjords can hold stable communities (diversity, richness).

Submarine canyons, much like fjords, offer strong connections between land and sea. This is demonstrated in Liao et al., who studied the Gaoping Submarine Canyon off SW Taiwan. This canyon is fed by a mountain river with extremely high sediment loads. Transport of sediments through the canyon system results in a high-energy system that poses extreme challenges to the resident nematode communities that respond to the strong bottom currents, with reduced taxonomic, trophic and functional diversity and maturity. Their findings also suggest strong heterogeneity in the canyon system, with some degree of local extinction and dispersal limitation.

Apart from the phenomena associated with climate change, marine benthic ecosystems are exposed to human activities and disturbances, including several types of pollution with impacts on a global scale. Enough evidence has accumulated to demonstrate that the "remote" deep sea and the Antarctic have—in spite of their long-thought status as pristine environments—not remained unaffected. Using nematode and copepod communities, Stark et al. studied spatial variation and human impacts at Casey Station in East Antarctica. They found that these communities respond strongly to their immediate environment, and to large spatial scale contrasts. In addition, nematode and copepod communities markedly responded to metals concentrations (as proxy for historical anthropogenic

pollution), providing further evidence that they can be useful indicators of environmental changes in Antarctic ecosystems.

We are enhancing our understanding of our ocean and its ecosystems, but society also recognizes the impacts climate change and human activities are having; with newly emerging Blue Economies and increased reliance on ocean resources, sustainability is key in order to maintain healthy oceans for future generations. Useful in this process is having the ability to concretize the value of marine ecosystem services and the benefits they provide to humankind. This approach is used by the final study in this special issue, Barnes et al., who combined observations of benthic life around seamounts of the Ascension Islands with the calculation of Blue Carbon Natural Capital. Despite their young age, small size and isolation, these seamounts can provide meaningful ecosystem services and their conservation does generate a quantifiable economic return.

The studies in this special issue cover shallow and deep-water areas, ecosystems fed by chemosynthetic and photosynthetic energy, and species, populations, and communities across a large size spectra, from meiofauna to megafauna. They also enhance our understanding of ecosystems that challenge ocean life, while being subjected to pressures resulting from global change to anthropogenic activities. It is expected that under global change conditions, extreme ecosystems will be especially affected, because of the specific organism-to-community adaptations evolved in such systems. Global change is occurring on time scales much shorter than those required for the formation of extreme ecosystems and the bio-ecological evolutionary pathways that run alongside it. Future changes may modify population dynamics over time and space, and alter the phenology and the geographical distribution of benthic communities and species. These modifications can result in habitat loss and species extinctions, with consequences for biogeochemical fluxes, ecological interactions and cascades, ecosystem functioning, and biodiversity. Energy availability is likely to change in benthic ecosystems, posing additional challenges to well-adapted organisms. In addition to global change, anthropogenic activities are compounding the pressures on marine communities. As we enter the UN Decade of Ocean Science for Sustainable Development, the focus lies on developing the scientific research required to ensure the health and sustainable use of our oceans. The diversity of contributions in this special issue shows that we are only scratching the surface with regards to understanding biodiversity in extreme environments, and the complexities of biological and ecological interactions, as well as the nature of their change in the Anthropocene. However, it also shows their unique value to scientific comprehension of how ecosystems are changing, and the benefits to humankind that are at stake.

AUTHOR CONTRIBUTIONS

All authors listed have made a substantial, direct and intellectual contribution to the work, and approved it for publication.

Conflict of Interest: The authors declare that the research was conducted in the absence of any commercial or financial relationships that could be construed as a potential conflict of interest.

Copyright © 2021 Sandulli, Ingels, Zeppilli, Sweetman, Hardy Mincks, Mienis and Chin-Lin. This is an open-access article distributed under the terms of the Creative Commons Attribution License (CC BY). The use, distribution or reproduction in other forums is permitted, provided the original author(s) and the copyright owner(s) are credited and that the original publication in this journal is cited, in accordance with accepted academic practice. No use, distribution or reproduction is permitted which does not comply with these terms.

frontiers in Marine Science

ORIGINAL RESEARCH
published: 07 November 2019
doi: 10.3389/fmars.2019.00663

Extremes in Benthic Ecosystem Services; Blue Carbon Natural Capital Shallower Than 1000 m in Isolated, Small, and Young Ascension Island's EEZ

David K. A. Barnes[1], Chester J. Sands[1], Andrew Richardson[2] and Ness Smith[3]*

[1] British Antarctic Survey, NERC, Cambridge, United Kingdom, [2] Conservation Department, Ascension Island Government, Georgetown, United Kingdom, [3] South Atlantic Environmental Research Institute, Stanley, Falkland Islands

Biodiversity tends to decrease with increasing isolation and reduced habitat size, and increase with habitat age. Ascension Island and its seamounts are small, isolated and relatively young, yet harbor patchily dense life. Large areas of these waters are soon to be designated as a major Marine Protected Area. Given the remote location there are few local threats to the region. However, global climate related stressors (e.g., temperature and acidification) and arguably plastic pollution are key issues likely to impact ecosystem services. We evaluate the accumulated carbon in benthos around Ascension Island's EEZ shallower than 1000 m using data collected over two research cruises in 2015 and 2017 through seabed mapping, seabed camera imagery and collections of benthos using a mini-Agassiz trawl. Benthos shallower than 1000 m essentially comprises the coastal waters around Ascension Island and three seamounts (Harris-Stewart, Grattan, and Unnamed). There is considerable societal benefit from benthic carbon storage and sequestration through its mitigation value buffering climate change. This service is often termed "blue carbon." Overall we estimate that there is at least 43,000 t of blue carbon, on the 3% of Ascension Island EEZ's seabed which is <1000 m, mainly in the form of cold coral reefs. Two thirds of that occurs around the main island of Ascension, but it is very unevenly distributed on the seabed. Seabed roughness (e.g., rocky outcrops) seems most important for the development of blue carbon hotspots. About 21% of the total blue carbon is considered to be sequestered (removed from the carbon cycle for 100+ years) = 9000 t Carbon. At the 2019 Shadow Price of Carbon the proportion of CO_2 considered sequestered is £29–59. As 9000 t C this is equivalent to 33,070 t CO_2, which in 2019 is valued at approximately £1–2 million. With time, this increases with rising value of carbon, but also annual increment of carbon deposition, to £2–4 million by 2030. Thus even when biogeographic values of isolation, size and age are least favorable to biodiversity, the natural capital stock and future services of benthic ecosystems can be considerable and generate quantifiable economic return on their conservation.

Keywords: blue carbon, ecosystem services, natural capital, Atlantic Islands, cold corals, Ascension Island, Marine Protected Area

OPEN ACCESS

Edited by:
Furu Mienis, Royal Netherlands Institute for Sea Research (NIOZ), Netherlands

Reviewed by:
Andrew J. Davies, University of Rhode Island, United States
Nova Mieszkowska, University of Liverpool, United Kingdom

****Correspondence:***
David K. A. Barnes
dkab@bas.ac.uk

Specialty section:
This article was submitted to Global Change and the Future Ocean, a section of the journal Frontiers in Marine Science

Received: *24 May 2019*
Accepted: *10 October 2019*
Published: *07 November 2019*

Citation:
Barnes DKA, Sands CJ, Richardson A and Smith N (2019) Extremes in Benthic Ecosystem Services; Blue Carbon Natural Capital Shallower Than 1000 m in Isolated, Small, and Young Ascension Island's EEZ. Front. Mar. Sci. 6:663. doi: 10.3389/fmars.2019.00663

INTRODUCTION

Ascension Island is a very isolated, young and small land mass sitting just south of the equator at −7°56 latitude and −14°22 longitude. It is approximately 2,250 km from the east coast of South America and 1,600 km from the west coast of Africa, with the nearest landmass being St. Helena, approximately 1,200 km to the south-east. Biogeographically these factors would all suggest low biodiversity. Such extreme locations are often the furthest from anthropogenic impacts and have very high ratios of Exclusive Economic Zones (EEZ) to land area. There are dense patches of life around Ascension Island coast and associated seamounts, in the shallows and important cold coral stands in deeper water (Nolan et al., 2017). The large EEZ around Ascension Island is likely to have considerable natural capital and ongoing ecosystem services derived from it. Two decades ago the global value of ecosystem services was estimated at US$30 trillion per year (Constanza et al., 1997). Since then understanding and demonstration of ecosystem services value has rapidly increased (Balmford et al., 2002; de Groot et al., 2012). Marine ecosystem service valuations, particularly within deep sea environments are, however, more challenging and there have been few attempts to value services provided by benthic ecosystems (Foley et al., 2010; Jobstvogt et al., 2014). The EEZ's of remote islands largely consist of deep sea ecosystems, and such places are a current focus for designation of very large Marine Protected Areas (VLMPA), such as those designated around Easter Island (by Chile) and Pitcairn Island (by United Kingdom) in the Pacific, and those implemented around South Georgia and the South Sandwich Islands and the South Orkney Islands in the Southern Ocean (Trathan et al., 2014). In the South Atlantic too, there is support for a no-take VLMPA around Ascension Island which was officially announced by the United Kingdom Government in March 2019 and which is also supported by the Island Council, subject to funding. Designation of these VLMPAs are not without controversy as it can involve finance losses (e.g., from closing or reducing commercial fishing) and incur costs (e.g., from monitoring, managing threats and policing use). It is not always clear how societal value can be demonstrated from VLMPAs and the ecosystem services they protect, although significant progress has recently been made (Adams, 2014[1]) and has started to address the considerable values provided by marine carbon capture and storage.

Blue carbon is that captured through photosynthesis and held within marine (mainly coastal) ecosystems. The International blue carbon initiative of the United Nations Environment Programme[2] argues that the 2% of global area represented by coast is responsible for half of global carbon sequestration and that it is much more efficient at storage than forest (Duarte et al., 2005). There are powerful arguments for why we need to understand and measure blue carbon. As the difficulty and cost of mitigation or reduction of climate change and it's drivers (such as CO_2) is becoming clear all carbon capture mechanisms need consideration. Because it is a highly efficient, naturally occurring and manageable mechanism (Duarte et al., 2005) the scientific profile of measuring blue carbon has risen rapidly. To date measuring blue carbon has focused on assessment of how much carbon is captured and stored by accessible and efficient sinks, such as mangrove, salt marsh and seagrass beds (Murdiyarso et al., 2015). As in the current study this has mainly been carried out by sampling to estimate the density of organisms in a location and then estimating the portion of carbon within the organisms (% of loss on ignition).

Blue carbon can be important even in cold waters, such as on Southern Ocean continental shelves, where the pace of marine growth is slow, providing a negative feedback against climate change (Barnes, 2015; Barnes et al., 2018a). The MPAs around the remote South Orkney Islands and South Georgia and the South Sandwich Islands have low levels of blue carbon storage but still have key roles in such ecosystem services because of their large shelf areas (Barnes et al., 2016). To date little is known of the marine benthic biodiversity and potential ecosystem services from 100 to 1000 m around most remote Atlantic archipelagos, except for their commercial demersal fish and crustacean stocks. To progress this regionally consultation workshops were held, as part of a wider natural capital assessment programme[3], for Ascension Island in February 2017 and June 2018, which resulted in the identification of priority areas to investigate. In June 2018, with an upcoming decision on a potential VLMPA designation under the UK Blue Belt Programme[4], assessment of the marine environment was considered a high priority, in particular services such as blue carbon storage on the seabed within Ascension Island's EEZ.

Blue carbon is captured when algae fix carbon from CO_2 (from the atmosphere but dissolved in water), most of which is recycled on death by microbial breakdown. However, some is stored when it sinks to the seabed or is eaten by animals to be incorporated into tissues and skeletons (see Barnes and Sands, 2017). When such organismal storage (removed from the carbon cycle) is longer than 100 years, either through long life or burial, it can be termed sequestered. At this point the amount of blue carbon (standing stock) or natural capital can be allocated a monetary value; Social Cost of Carbon (SCC) or shadow price of carbon (SPC). This varies between nations, years, discount rate and even model types. Our assessment of Ascension Island's benthic blue carbon aimed to answer the questions; How much blue carbon is there on Ascension Island's seabeds? what biodiversity contains this? and what is its economic value? This should provide a first blue carbon baseline within 1000 m depth prior to the VLMPA establishment. These findings contribute evidence to a program of natural capital assessments (NCA) being implemented by the UK Joint Nature Conservation Committee (JNCC) and conducted by the South Atlantic Environmental Research Institute (SAERI) in the UK South Atlantic Overseas Territories.

[1]See e.g., www.ecosystemvaluation.org, www.openchannels.org, www.naturalcapitalproject.org.

[2]http://thebluecarboninitiative.org/

[3]http://jncc.defra.gov.uk/page-7443

[4]https://www.gov.uk/government/publications/the-blue-belt-programme

MATERIALS AND METHODS

Our method attempted to link seabed mapping (to characterize the study area < 1000 m depth), underwater imagery (to determine the variety of habitats and density of types of organisms) and trawl (to collect biological specimens to determine identification and carbon content). Combining these techniques can produce standing stocks of carbon held in marine organisms, by habitat, by major area (Barnes and Sands, 2017). An economic value can be placed on whatever total result is found by applying a standardized, internationally recognized value of carbon sequestered per unit mass.

The mid-Atlantic ocean study area was the coast of Ascension Island and three nearby seamounts (**Figure 1**). We used seabed mapping (multibeam swath – data available in Fremand and Barnes, 2019), imaging and targeted specimen collection to firstly assess benthic organism presence in the shallowest 1000 m of Ascension Island's EEZ (**Figure 2**). We took 421 Shelf Underwater Camera System (SUCS) images around Ascension Island and 271 SUCS images at three nearby seamounts. Identification of specimens from imagery was supported by seven Agassiz tows around Ascension Island and six around the seamounts. All biological specimens visible in images were identified and recorded to at least Phylum and Class level. Most image specimens were identifiable to much higher taxonomic resolution with access to trawled specimens, which could be examined under microscope by experts. Given the breadth of taxonomic diversity, expert identifications for all material collected within a reasonable time frame was not possible. Instead we identified everything as belonging to a functional group as per Barnes and Sands (2017) as it provides an ecological context to the diversity that is more meaningful than the higher taxonomic levels of Phylum and Class. The thirteen function groups are defined as follows: suspension feeder pioneers (SP), climax suspension feeders (SC), sedentary suspension feeders (SS), deposit feeding crawlers (DC), deposit feeding vermiform (DV), deposit feeding, shelled burrowers (DS), calcareous grazers (GC), scavenger/predator, sessile soft bodied (PS), scavenger/predator, sessile calcareous (PC), scavenger/predator, mobile soft bodied (PM), scavenger/predator, mobile calcareous (PL), scavenger/predator, arthropod (PA), and flexible strategy (FS) (**Table 1**). We used previously peer-reviewed methodology (Barnes and Sands, 2017) to estimate the amount of blue carbon stored in ecosystems using a three step process from data collected on the 2015 and 2017 scientific voyages of the RRS James Clark Ross (cruise numbers JR864 and JR16-NG). The first step comprised analysis of the 692 highly accurate (405.7 × 340.6 mm, 12MB, 5 MegaPixel, ±0.1 mm see **Supplementary Table S1**) images of the seabed to identify animals and their density. Thus for each image the number of specimens of each functional group were recorded, along with the substratum size. This suite of animal identity and density information was collated into a spreadsheet, with a row per image and column per animal identity. To this was added corresponding physical and oceanographic contextual information from multibeam swath and five CTD casts around Ascension and three casts at the seamounts (the positions of CTDs and Agassiz tows are given in **Supplementary Table S2**). From these depth, sea temperature, salinity, oxygen and chlorophyll content were added and substratum type (Wentworth scale) was added by viewing each image. The shadow length on substrata (in each image) was measured to score rugosity (seabed roughness) on a scale of <1, 1–10, 11–20, 21–30, 31–40, and 41+ mm. To convert densities of functional groups per image to carbon per m^2, we first multiplied up the image area to 1 m^2, then multiplied these densities by the mean amount of carbon held by each functional group. These mean values were derived by measuring organic content of specimens collected (from collection using a bespoke mini-Agassiz trawl) by weighing after drying them at 70°C for 12 h, and gained ash mass by weight following 480°C incineration for 12 h. We used carbon composition as 50% of organic mass and 12% of carbonate (following Barnes and Sands, 2017). These measures gave a series of carbon masses for each functional group so that mean values could be calculated for each functional group.

Blue carbon per area data was tested for normality and heterogeneity of variance and then subject to ANOVA to explore which parameters might be driving variability. The ANOVA on the estimated organismal carbon data per image used three factors; rugosity (six levels), site (four levels) and substratum (three levels). The rugosity levels are explained above, the sites were Ascension island and three seamounts and the substratum was hard, soft and mixed. We added 13 rows of data derived from shallow water seabed images (from Barnes, 2015) at the same location to give a sample size of 421 + 271 + 13 = 705. Assemblage structure was explored visually using non-metric Multidimensional Scaling (nMDS) in R [R Core Team (2014). R: A language and environment for statistical computing. R Foundation for Statistical Computing, Vienna, Austria[5]] and the package Vegan (Dixon, 2003).

Functional Groups of Benthos From Images

Our main apparatus was a non-invasive, high resolution, fiber optic SUCS imaging system. This bespoke equipment has an advantage over most other systems of being quantitative and (tested to be) mm accurate over its entire field of view. This is because the camera is; (a) always perpendicular to the seabed, whatever the orientation of the seabed, (b) has a neutral focal length (i.e., not wide or telephoto) and this allows a flat (rather than dome) port to minimize distortion, and (c) the powerful, live controlled dual angle lighting system enables setting a middle aperture diameter (F stop), minimizing lens distortion. These features facilitate accurate measurement in any plane and accurate density determinations. Raw presence numbers for each functional group were standardized (corrected for the total *n* of benthos sample numbers) into proportion of all benthic fauna (**Table 1**). These were then further standardized to density/m^2 (**Table 1**).

Scaling Up From Images

We scaled up our blue carbon per area results to the total area < 1000 m deep of Ascension Island and its three seamounts.

[5]http://www.R-project.org/

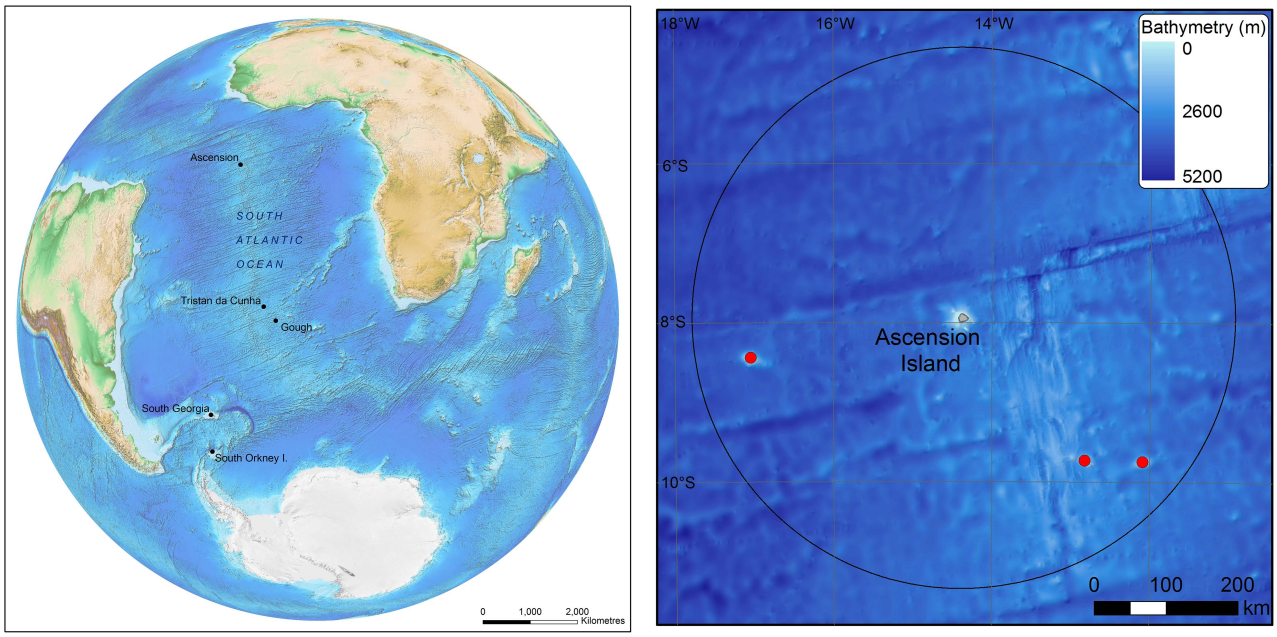

FIGURE 1 | The position of Ascension Island in the South Atlantic (left) and the island and seamounts (red dots) within it's Exclusive Economic Zone. Bathymetric data is GEBCO held by the British Oceanographic Data Centre (The GEBCO_2014 Grid, version 20150318, www.gebco.net).

To do this we used Arcview GIS to calculate the area of seabed (329 km^2 around Ascension, 267 km^2 of seamounts and just 16 km^2 we did not map) using publicly available bathymetry information (held by the British Oceanographic and Polar Data Centres). Estimating sequestration is difficult, especially so from imagery and with large scaling factors, so error could be considerable. Our estimates were driven by chance of burial, so any evidence of this or just nearby sediment was taken into account, as of course was how much of each benthic item was skeleton and what form this takes (e.g., hard coral polyps are more likely to fossilize than sea cucumbers). There are many diverse ways of estimating error associated with such work, one of which is change with increased sampling (particularly pertinent to deep water work, given that we sampled considerably less than 1% of relevant seabed). In our study the last three sites (of 21 at Ascension Island) altered our estimate of sequestered carbon there by ∼3% each, which changed our overall estimate (for all regional seabed < 1000 m) by ∼1.5% each (see **Supplementary Table S3**).

To calculate scaling factors for zoobenthic blue carbon estimates we first multiplied up the proportion of surveyed seabed at each rugosity level for each location. We assumed that the proportion of these rugosity levels were representative of unsurveyed areas < 1000 m depth. This assumption was made on the basis that increased sample number altered the proportion of rugosity levels by relatively small amounts (6, 3, and 1% change in rugosity estimates by adding last three, last two and last sites to total sites, respectively). So for example 57.5% of Ascension Island's surveyed seabed < 1000 m depth had a rugosity level of 1–10 mm. Thus we multiplied the total area of Ascension Island's shelf (328.5 km^2) × 0.575 = 188.8 km^2 of shelf with this level of rugosity. This was multiplied by mean carbon storage for each rugosity level at each location (**Table 6**), so for Ascension island's 1–10 mm rugosity area, this was 188.8 × 40.7 (g m^2 or t km^2) = 7,687 t km^2. This was repeated for each rugosity level at all < 1000 m depth locations.

RESULTS

Thirteen functional groups of benthic organisms were identified in the images recorded by the SUCS. Overall frequencies of each functional group varied considerably between each of the four sites, with more than half of them rare at any site (**Table 1**). Flexible feeding strategists (many ophiuroids/brittlestars) dominated numbers of benthic organisms around Ascension Island and Grattan seamount, though sessile scavenger/predators such as corals were also very abundant. In contrast sessile suspension feeders (ascidians, bryozoans, brachiopods, some polychete worms and sponges) were the most numerous benthos at Stewart-Harris and Unnamed seamounts. Thus we observed biodiversity was broadly organized into two patterns; brittlestar (FS) and coral (PC) dominated at Ascension Island and Grattan seamount compared to a more mixed suspension feeder assemblage at the other two seamounts investigated. However, images could also be separated into large areas of little apparent zoobenthic carbon, areas of substantial blue carbon in living benthos and lastly banks of blue carbon in dead calcareous skeletons (**Figure 3**).

Using non-metric Multidimensional Scaling (nMDS) showed that two dimensional plots were a reasonable representations of multidimensional structure for each of

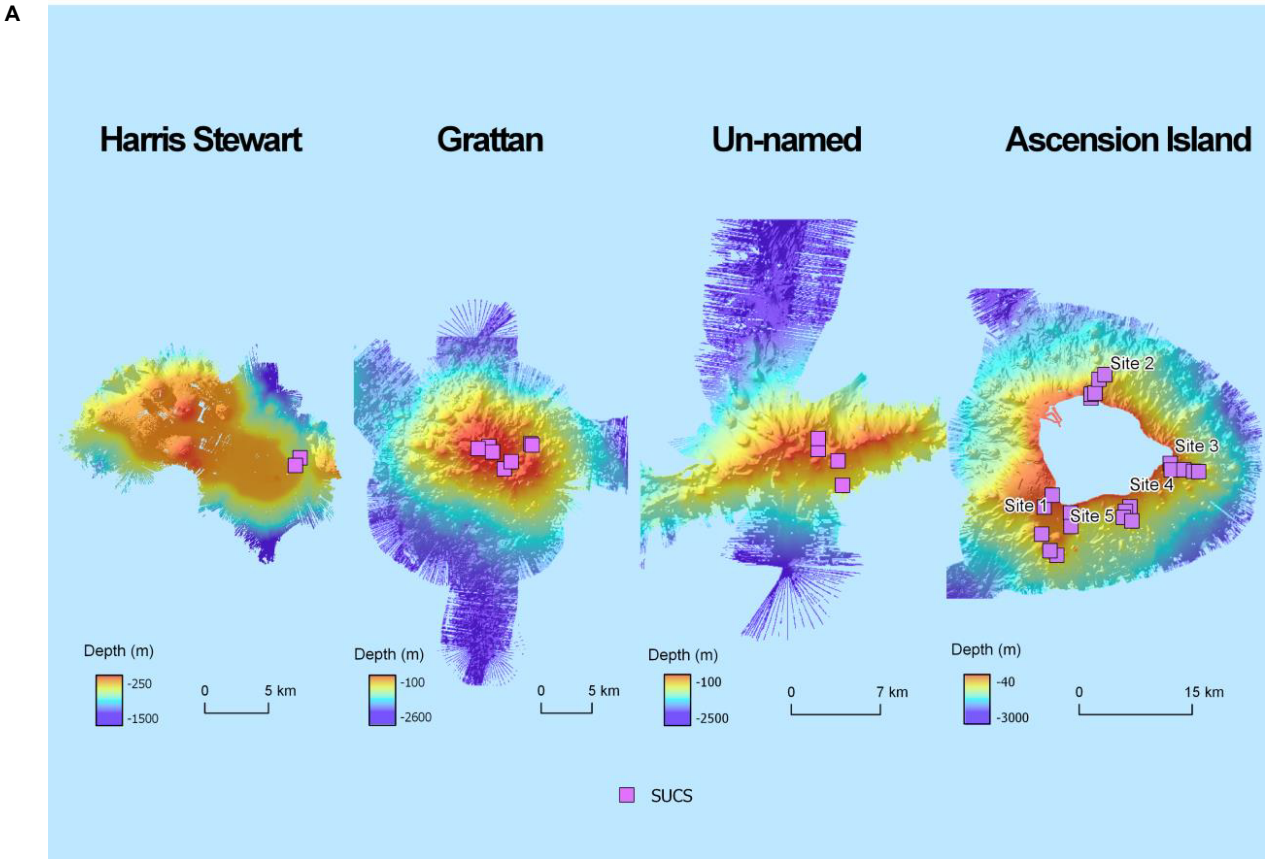

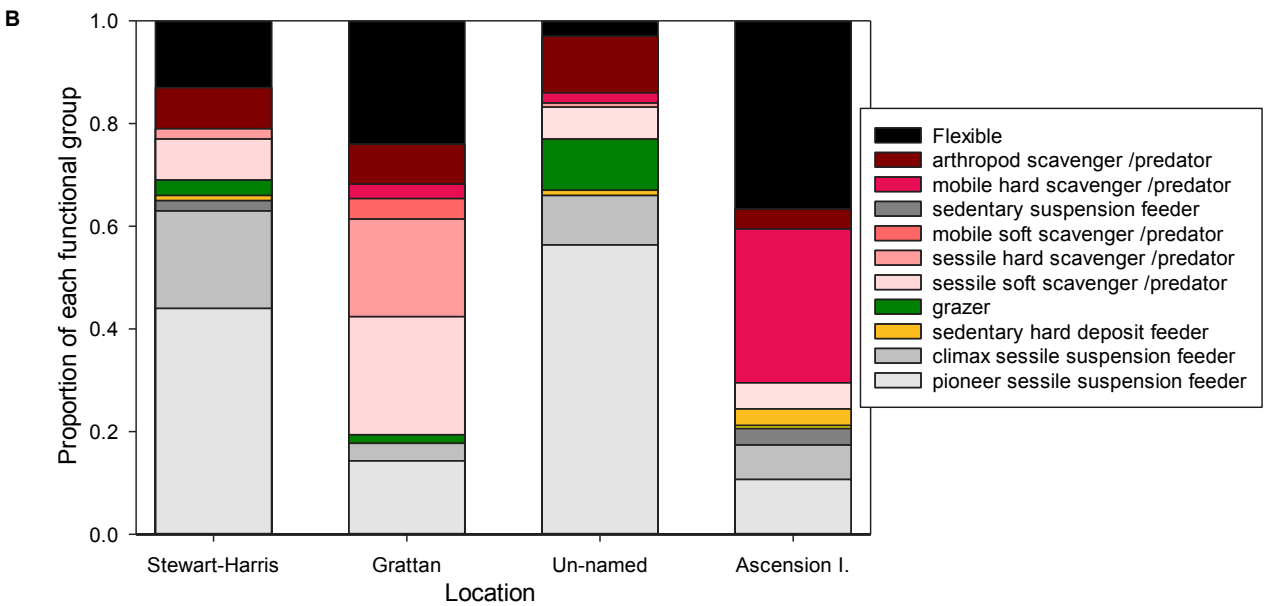

FIGURE 2 | (A) The expeditions of RRS James Clark Ross in 2015 and 2017 were the first to map the seabed around Ascension and it's EEZ seamounts. The pink squares represent sites where imagery was collected using the Shelf Underwater Camera System (SUCS). **(B)** The proportion of individuals in images from each functional group per location.

TABLE 1 | Occurrence of each biodiversity functional group by site.

Site	SP	SC	SS	DC	DV	DS	GC	PS	PC	PM	PL	PA	FS
A													
Asc	361	167	61	2	3	9	109	172	899	3	85	130	1325
StH	105	46	4	–	–	2	8	18	5	–	–	31	20
Gra	162	37	–	3	–	4	19	263	216	5	32	89	306
UNa	300	510	–	1	–	2	54	33	2	–	13	60	16
B													
Asc	0.11	0.05	0.02	–	–	–	0.03	0.05	**0.27**	–	0.03	0.04	**0.40**
StH	**0.48**	**0.21**	0.02	–	–	0.01	0.04	0.08	0.02	–	–	0.14	0.09
Gra	0.14	0.03	–	–	–	–	0.02	**0.23**	0.19	–	0.03	0.08	**0.27**
UNa	**0.56**	0.10	–	–	–	–	0.10	0.06	0.01	–	0.02	0.11	0.03
C													
Asc	6.21	2.87	1.05	–	0.03	0.05	1.88	2.96	15.5	–	1.46	2.24	22.81
StH	18.1	7.94	0.69	–	–	0.35	1.38	3.11	0.86	–	–	5.35	3.45
Gra	8.15	1.86	–	0.15	–	0.2	0.96	19.9	10.87	0.25	1.61	4.48	15.4
UNa	25.6	4.35	–	0.09	–	0.17	4.6	2.81	0.17	–	1.11	5.12	1.36

*The sites are <1000 m depth at each of Ascension Island (Asc), Stewart–Harris (StH), Grattan (Gra), and Unnamed (Una). The data are number of **(A)**, proportion of **(B)** and density/m^2 of **(C)** individuals in each functional group. The bold values refer to the highest values in each row (i.e., the dominant functional groups).*

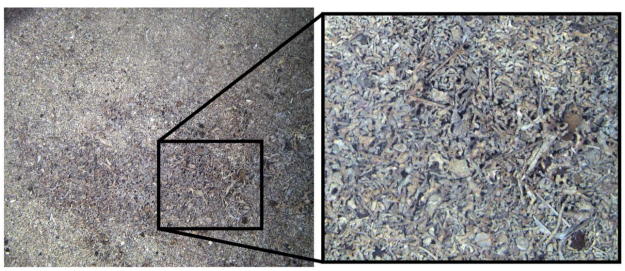

FIGURE 3 | A SUCS image of seabed around Ascension Island's coast showing extensive build-up of carbonate from dead coral, echinoid echinoderms, sponges, mollusks, and bryozoans.

habitats, sites and substratum rugosity, but a high number of (SUCS) images with no or few faunal components forces the clustering to the center of each plot. What little structure observed was mainly in Ascension Island's highly rugose rocky environments. Rather than by island/seamount, this density data can be investigated by habitat or other key factors such as seabed rugosity (roughness or level of 3D structuring).

Carbon Storage

We found zoobenthic carbon stored by mean individuals of each functional group across each of the four study sites ranged from 0.02 to 9.8 g (**Table 2**) with a mean of ∼1.4 g. However, when multiplied by density the most important functional groups were sessile, calcareous predators (corals) at Ascension and Grattan seamount and sessile suspension feeders at Stewart-Harris and Unnamed seamounts (**Table 2**). Hard corals and sessile suspension feeders accounted for approximately 30–34 and 19–26 g m^2 at each of Ascension Island and Grattan seamount vs. the other two seamounts, respectively. These totaled for each site as 41.1–74.6 g per m^2 of living fauna (highest around Ascension Island) and a further 4–55 g per m^2 in dead calcareous skeletal remains (again highest around Ascension Island). Of

TABLE 2 | Estimates of carbon held by live zoobenthos, in **(A)** grams per individual and **(B)** grams per m^2 per functional group per site.

Site	SP	SC	SS	DC	DV	DS	GC	PS	PC	PM	PL	PA	FS
A													
Asc	1.00	1.37	1.07		1.67	9.80	2.82	1.17	2.21		4.21	0.85	0.52
StH	1.06	0.87	1.06			1.77	2.78	1.08	2.09			0.90	0.02
Gra	0.84	1.10		0.93		1.80	3.02	0.43	2.74	2.32	3.22	0.92	0.08
UNa	1.02	1.29		0.89		3.18	3.07	1.62	2.29		4.86	0.69	0.02
B													
Asc	6.18	3.94	1.12	0.03	0.05	0.49	5.3	3.46	**34.2**		6.14	1.9	11.8
StH	**19.1**	6.9	0.73			0.62	3.83	3.35	1.8			4.79	0.05
Gra	6.82	2.05		0.14		0.36	2.9	8.5	**29.8**	0.58	5.18	4.12	1.28
UNa	**26.1**	5.61		0.08		0.54	**14.1**	4.56	0.39		5.39	3.52	0.03

The bold values refer to the highest values in each row (i.e., the dominant functional groups).

the four sites with seabeds shallower than 1000 m, Ascension Island had more stored carbon than the seamounts. Of substrata, hard surfaces had more stored carbon, principally in the form of *Lophelia* coral outcrops. There were very high levels of variability of zoobenthic carbon storage, within and between study sites, ranging from > 1.2 kg m^2 to none per image detectable by imaging. ANOVA of our data showed that whilst site (Ascension and the three seamounts) and substratum type (measured as hard, soft or mixed) were significant terms, most variability was explained by rugosity (**Table 3**).

The proportion of area surveyed at each site, of each rugosity type was calculated and this was converted to area (km^2) for each surveyed site (columns 3–8 of **Table 4**). The mean values across the three surveyed seamounts were then scaled up to the total area of all seamount area (row 3 of **Table 4**). Of the 610.7 km^2 total area < 1000 m in depth, **Table 4** shows most was of low rugosity. Mean values of blue carbon storage estimates per km^2 (shown in **Table 5**) by rugosity level and site showed how important high rugosity is to blue carbon build-up. Although zoobenthic carbon showed clear increase with seabed rugosity, there was considerable variation at each rugosity level, at both Ascension and the nearby seamounts (**Figure 4**, upper plots). Mean values of zoobenthic carbon (solid circles, **Figure 4**) by rugosity level did, however, show a more linear increase.

At Ascension we estimated that ∼27% of stored zoobenthic carbon can be considered sequestered locked up for 100+ years (on the basis of how much carbon is in very old corals or dead skeletons). Based on such estimates, similar relationships were apparent between rugosity and carbon sequestration (**Figure 4**, lower plots) as with storage. No relationships were apparent at site level, probably due to such high variability in sequestration at rugosity level 1 (in turn likely a function of high variation in substratum nature within sites) (**Figure 4**, lower right plot). This is important because it stopped meaningful analysis using seabed multibeam characteristics (because SWATH data was gridded at 25 m scale).

TABLE 3 | ANOVA of zoobenthic carbon storage on Ascension Island seabeds <1000 m deep.

Source	DF	Adj. SS	Adj. MS	*F*	*P*
Rugosity	5	857037	171407	**12.3**	0.001
Site	3	251100	83700	6	0.001
Substratum	2	155591	77796	5.6	0.004
Error	695	9721061	13987		
Total	705	11473501			

The bold value refers to the highest value in the row (i.e., the dominant factor).

TABLE 4 | Areas in km^2 less than 1000 m deep around Ascension by each rugosity level.

		Estimated substratum rugosity in mm					
Site	**Area**	**0–1**	**1–10**	**11–20**	**21–30**	**31–40**	**41+**
Ascension	328.5	2.3	187.4	70.6	34.9	25.0	8.3
Surveyed seamounts	265.8	20.6	122.6	65.7	30.4	10.8	15.7
Unsurveyed seamount	16.4	1.3	7.5	4.1	1.9	0.7	1.0
EEZ total (<1000 m)	610.7	24.2	317.5	140.4	67.2	36.5	25.0

Only 16.4 km^2 of a total of 610.7 km^2 was unsurveyed by the research cruises JR864 and JR16-NG.

TABLE 5 | Zoobenthic carbon storage by rugosity and area, in tonnes per km^2.

		Substratum rugosity in mm					
Site	**Mean**	**0–1**	**1–10**	**11–20**	**21–30**	**31–40**	**41+**
Ascension	**83**	2	41	87	**181**	**225**	**272**
Stewart-H	**45**	ND	35	50	47	ND	ND
Grattan	**63**	24	65	49	52	67	**154**
Unnamed	**61**	ND	25	71	**111**	**132**	**199**

At some sites we found no seabed with particular rugosity levels, which we indicate as No Data (ND). Mean values across all rugosities are shown left (low in value because high rugosity levels were rare). The bold values refer to the highest values in each row (i.e., the dominant rugosity levels).

Scaling Up Carbon Storage to Shelf Areas of Ascension Island's EEZ

One rugosity level and one site dominated the study samples in the region. Much (52%) of the <1000 m depth seabed we imaged in Ascension Island's EEZ was low in rugosity (1–10mm). On average we estimate that this supports ∼41 t C km^2 (see row 2, column 4, of **Table 5**) comprising just 29% of total zoobenthic carbon (12,519 t see last row, column 4 of **Table 6**). More than half of the seabed < 1000 m in Ascension Island's EEZ is the immediate coast around the main island (53.7%), which supports disproportionally high (65% [27890/43045 see **Table 6**]) of Ascension's EEZ benthic blue carbon. Thus substratum rugosity and geography were the key factors behind blue carbon standing stock (Natural Capital).

Overall we estimate that Ascension Island's < 1000 m area supports ∼43,000 t of blue carbon (**Table 6**), mainly as *Lophelia* cf. *pertusa* (cold coral) reefs as well as abundant echinoids such as the cidaroid *Cidaris cidaris*. This standing stock is patchy and sequestration possibilities similarly so, and likely to vary considerably with depth, proximity and nature of soft substrata, and proximity and nature of blue carbon sources. We found that ∼21% of all organismal carbon on the seabed in our samples was held by old living and dead corals or part buried animal skeletons. Our mean estimate of carbon *in situ* for <100 years (meeting the UN definition for "sequestered") was thus ∼21% of living standing stock (∼9,000 t C).

DISCUSSION

How Does Ascension Island Blue Carbon Natural Capital Compare With Elsewhere?

As with most work sampling deep water habitats, especially in remote regions, our results from Ascension region involve scaling up from very small sample areas (692 × 0.14 m^2), from few sites (21 at Ascension and 13 at the three seamounts). Trailing

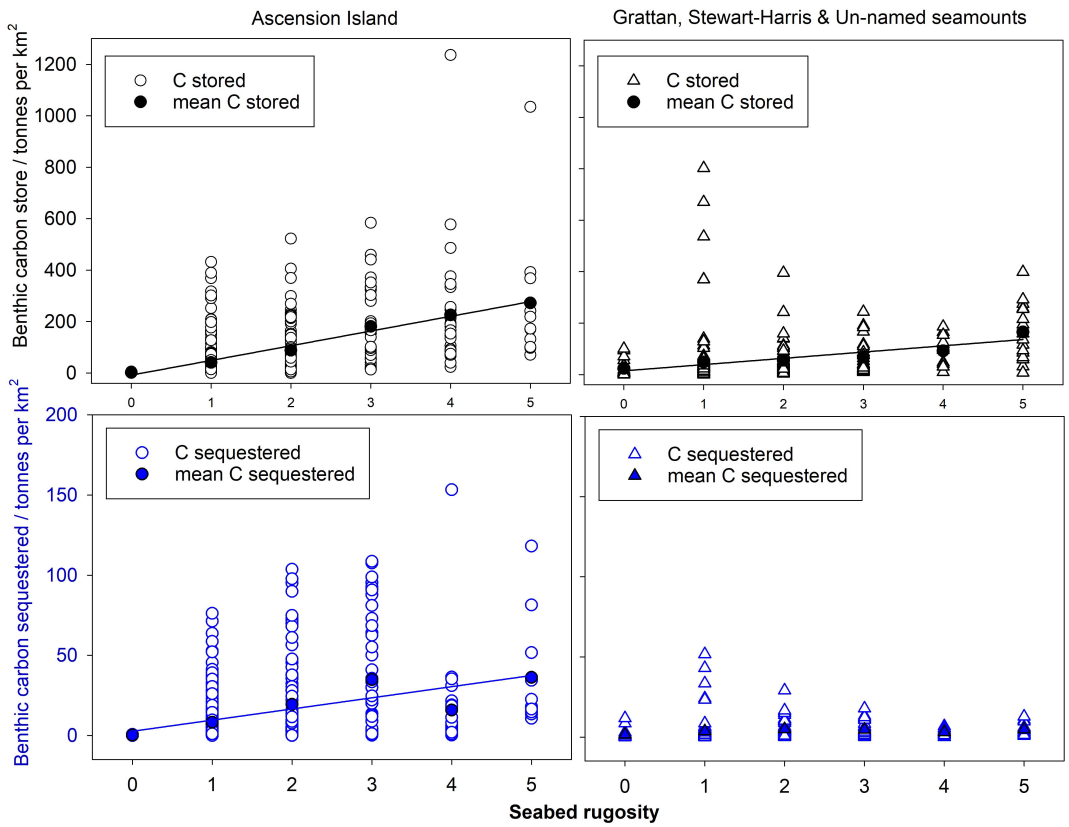

FIGURE 4 | Zoobenthic carbon storage and sequestration with rugosity levels in Ascension Island EEZ waters.

our camera between actual samples, in live view mode, enabled observation of ∼100 times the sampled area of seabed. During that non-sampled extra seabed observed we saw no obviously new habitats. Our paucity of seabed sampling was also only supported by 8 CTD casts and 13 Agassiz tows, all of which is scant to characterize > 600 km^2 of seabed < 1000 m depth. However, the weeks of *in situ* research time and funding required for a large capable research vessel and crew to be there, and even more to get there, means that this still represents by far the most considerable investigation of deep seabed around Ascension. Whilst small, this was a step change by an order of magnitude in terms of information collected. Ascension's remoteness and political sensitivity means that more comprehensive deep water sampling may not follow for many decades. Nevertheless it is with this backdrop of uncertainty that any comparisons with more sampled and better known areas must be made.

It is clear from the current study that blue carbon occurring within the top 1000 m of seabed in the Ascension Island EEZ is extremely unevenly distributed across multiple spatial scales, supporting initial observations (Nolan et al., 2017). Within our Ascension EEZ data, the highest levels of variability occurred on the cm to m scale (associated with rugosity). Other important spatial scales were larger at 10s of meters (associated with different substratum types and 10–100 km (associated with seamount/island identity). However, above the spatial scale of Ascension EEZ, that of 1000s of kilometers (associated with different archipelagos and continents) there can be even higher levels of blue carbon variability. This scale is associated with different continents, oceans and major climatic regimes. Overall, the Ascension Island EEZ (<1000 m depth) is estimated to support 70 t carbon km^2, an order of magnitude more than the South Orkney Islands (8 t c km^2) which are considered as a polar blue carbon hotspot (Barnes et al., 2016). There are few continental shelves where accurate estimates have been produced. Standing stock of shelf around another isolated location, South Georgia (Barnes and Sands, 2017), is probably half that of the South Orkney Islands. Despite being productive, the remotest South Sandwich Islands may have as little as 1% of Ascension EEZ benthic blue carbon per unit area. In terms of stored

TABLE 6 | Zoobenthic carbon storage by rugosity and area, in tonnes.

		Substratum rugosity in mm					
Site	**Total**	**0–1**	**1–10**	**11–20**	**21–30**	**31–40**	**41+**
Ascension	27890	4	7687	6177	6141	5617	2263
Stewart-H	3917	0	796	2313	788	20	0
Grattan	5445	299	2741	648	441	203	1114
Unnamed	5559	0	1163	1750	1076	712	857
Unsurveyed	233	1	131	73.4	18	2	8
EEZ total (<1000 m)	43045	304	12519	10963	8464	6554	4242

The last row shows totals by rugosity level and overall (left-most).

carbon though it is clearly small in comparison with moderate forests or production of blue carbon in mangroves or kelp forests (Murdiyarso et al., 2015; Krause-Jensen and Duarte, 2016). It may be more important in terms of conversion of blue carbon stored to sequestration. Our estimated value of ∼9,000 t C sequestered for <1000 m depth is low but a high proportion (21%) of standing stock. This does not imply that conversion rate of carbon storage to carbon sequestration is 21%. Conversion rate is likely to be much lower (possibly by an order of magnitude). Much of the carbon that we consider sequestered could have been there for hundreds or even thousands of years, so it is a cumulative build up. Much of the fast growth is by organisms less likely to sequester, either because they are in high energy habitats of the shallows or because they mainly comprise soft tissues which are easily consumed on death by other macrobes or broken down in the microbial loop (and thus the carbon is recycled rather than sequestered). However, our 9,000 t C total value of sequestered carbon is likely to be a considerable underestimate, because it does not take into account sequestration of primary or secondary production into >1000 m depths.

What Is the Magnitude of Ongoing Blue Carbon Ecosystem Services?

The current study estimated standing stock or natural capital of existing zoobenthic blue carbon around Ascension island's <1000 m depth zone. In addition to standing stock information, estimation on ongoing carbon storage requires growth performance data or key zoobenthos store and sequesters, and environmental horizon scanning (for change in likely conditions influencing performance). Various literature has estimated growth rates of calcifying benthos such as corals, and shown that they vary considerably even within species between locations, depths and water masses (Vecsei, 2004; Van Oevelen et al., 2009; Roberts et al., 2010; Sabatier et al., 2012). We used a conservative estimate of 0.1 $g.m^{-2}.day^{-1}$ across benthic taxa, which in line with cold coral literature is slow compared to global mean reef production 2.5–7.4 $g.m^{-2}.day^{-1}$ (Vecsei, 2004) or 2.2 $g.m^{-2}.day^{-1}$ of the nearest Caribbean reefs (Mallela, 2013). The value of 0.1 g carbon $m^{-2}.day^{-1}$ was only applied to seabed areas which had at least 10 g carbon living zoobenthic estimated standing stock. However, using this as a whole environment carbon accumulation rate has several problems, all of which are underestimates. This value does not include near surface primary production standing stock or sequestration export nor does it include the nearshore faunal standing stock or export, which we estimate to be in the region of ∼18 g carbon m^2 (see accompanying Excel worksheet) and is likely to grow very much quicker (Vecsei, 2004; Mallela, 2013). Thus our production estimation is very conservative.

We estimated that 506 of the 692 SUCS images contained less than 10 g C m^2 of live fauna. Thus we considered that only 692 − 506 = 186 of the 692 were significant generators of blue carbon. We thus applied our growth rate (0.1 $g.m^{-2}.day^{-1}$) to 186/692 = 26.9% of Ascension Island's < 1000 m depth area (610.7 km^2); 0.269 × 610.5 = 164.3 km^2. The calculation we used was thus 0.1 t Carbon km^2 × 164 km^2 × 365 (days) = blue carbon stock generation = ∼6000 $t.yr^{-1}$ in the < 1000 m area of the Ascension Island EEZ. Our estimate of 6000 $t.yr^{-1}$ of sequestered carbon for the area <1000 m deep in Ascension Island's EEZ is equivalent to ∼14% of our blue carbon standing stock estimate in that same area.

Geographic Variability in Blue Carbon and Drivers Influencing This

The productivity, standing stock and drivers of blue carbon sinks are likely to vary in many different ways, even within a single "type" such as kelp forests (Bell et al., 2015). The current work only investigated blue carbon over a wider and deeper bathymetric range than most literature (but see Armstrong et al., 2012), yet still constituted a mere 1% of Ascension Island's EEZ. Assuming that the abyssal seabed around Ascension is typical, it is likely to be very low in biomass and blue carbon per unit area. Thus the Ascension EEZ well illustrates the extremes of geographic variability in blue carbon distribution. As much as 99% of Ascension EEZ could be within the <1% of the seabed shallower than 1000 m. Even within that, most blue carbon seems to be around Ascension Island's coast and, even within that, most is associated with the 10% of the seabed which is rough and complex. We found areas where there was three orders of magnitude variability in estimated blue carbon standing stock within tens of meters apart.

The extreme variability over multiple spatial scales makes isolating which factors are causal of variation extremely challenging. However, the location and nature of most of the dead calcareous skeletal remains (mainly around Ascension Island), suggests that there has not been considerable temporal variation, unlike other blue carbon sources (e.g., Krumhansl et al., 2016). Likewise the growth rate estimates suggests slow growth and build-up of the cold coral reefs in Ascension Island waters. We think that the prevailing reasons for such sparse and patchy blue carbon are (1) isolation from nearest larval supply and (2) recruitment conditions for young. Isolation is important because Ascension and its associated seamounts are far apart, and all very far apart from other nearest adult concentrations for larval supply. This is exacerbated by them being small in area and relatively young. Thus local retention of larvae is probably very important to development of biomass and thereby blue carbon, but during the process of SUCS image capture we observed considerable water movement across all depths and locations. In addition to high water movement, imaging using SUCS showed some sand at every site and location. Thus recruitment conditions involve unstable soft sediments and "sand blasted" hard surfaces, which may be partly why rugosity emerged as such a strong factor. Roughness slows water down (allowing larvae to settle) and provides protection from particles being driven against surfaces by current. We think most areas of blue carbon importance establish and develop close to adult supply sources (i.e., downstream of previous or current biomass) where the seabed is rough to maximize recruitment success.

Neither temperature nor a proxy of primary production (phytoplankton) emerged as explanatory factors, however, there is good reason to suspect that both of these could still be

important drivers but complicated and confounded in various ways. High marine biomass is typically associated with coral reefs, which in Ascension EEZ are in shallow warm waters but also in deep cold waters. However, that is only where there is enough hard surface to establish and even then only (perhaps by chance) in some of those areas (Nolan et al., 2017). Where shelf seabeds are in contact with phytoplankton blooms, such as round Ascension Island's coast they can be very important for suspension feeders and their predators (but not so much for many other carbon rich benthos). However, the depth of algal blooms vary between locations and strongly with time. Our two surveys were both far too brief to establish durations, depths and nature of these blooms.

Threats to Ascension Island's Biodiversity and Blue Carbon

Marine biodiversity and blue carbon ecosystem services face very considerable, increasing and diverse threats (Ling et al., 2009; Krumhansl et al., 2016; Barnes et al., 2018a). We considered three main threats to Ascension Island EEZ's biodiversity and blue carbon ecosystem services, how to monitor for these and any potential mitigation. It was not apparent from our 2015 and 2017 surveys that there were immediate strong impacts or threats (Nolan et al., 2017). However, given the remote nature of the seabed we surveyed, most of the threats are likely to be quite diverse and global in nature. Local threats to blue carbon are likely to only influence marine life around the main island of Ascension's coast (rather than beyond to seamounts).

Despite small population and remoteness, pollution is a consideration. For example plastic pollution was evident on the sea surface and seabed, and there is evidence that is increasing considerably (Barnes et al., 2018b). Plastic entanglement of coral was seen, albeit only apparent in 0.5% of samples. Plastic can mechanically damage biota, increase disease susceptibility and decrease efficiency and slow growth through being ingested. Whilst this appears to be an increasing issue in Ascension waters, most have no local source nor obvious solution (although nearby landfill sites could be made more secure to wind blowing material into the nearby ocean). Refueling and human coastal use also provide some pollution threat, mainly to shallow coral assemblages in bays.

As with many remote locations much of the increasing threat is climate change related in the form of pH decrease (acidification), temperature stress and other physio-chemical ocean change. Whilst thermal tolerance issues are probably most severe for shallow biota, acidification is probably the most serious issue for most blue carbon storing biodiversity, not least because of reduced sequestration potential. Even if organisms can buffer decreased pH whilst alive (at the cost of somatic growth or reproductive potential), the chances of burial of their carbon stored are reduced because of increased dissolution, and large build-ups of ancient calcareous reef remains will be increasingly dissolved.

Across oceans the drastic reduction of fish populations through fishing, and bycatch from bottom fishing or birds near the surface is a major, long-recognized and rising problem (Jackson et al., 2001). There are few coastal environments on the planet where fishing would not be high amongst threats but around Ascension it is unlikely that regional fishing provides much threat since it is small scale and pelagic, apart from gear loss (plastic pollution). Although gear loss (ghost fishing) has been found around other Atlantic Islands and seamounts we did not encounter any on our 2015 and 2017 surveys. Best practice for monitoring blue carbon (high carbon storing biodiversity) health and performance is likely to be through regular surveys, by SCUBA in shallows and research ship in deeper waters. These are expensive financially, in time and expertise, and deeper work would require multibeam, deep cameras and limited targeted physical collections (to monitor temporal growth effects) but there are few such vessels passing Ascension Island. Furthermore we could not find multibeam (SWATH) signatures for centers of blue carbon interest (for example Topographic Position Index) at 25 m data gridding scale (Nolan et al., 2017). The resolution of such systems at that depth make them unlikely to provide rapid "remote" monitoring solution. Monitoring and stewardship of blue carbon has costs but this ecosystem itself has a calculable value in societal benefit, and estimating this provides context against costs and shows return for conservation (Zarate-Barrera and Maldonado, 2015; Barnes et al., 2016).

What Is the (Shadow Carbon Cost) Value of Sequestration by Ascension EEZ's Marine Life?

There is a very wide range of estimate methods and thus estimates for Social Cost of Carbon (SCC) and shadow price of carbon (SPC) between nations, years, discount rate and even models. We report using 2019 values in £ GBP Sterling, based on the High level commission on Carbon prices[6]. This places a value of approximately US$39–78 per tonne CO_2 in 2019. In United Kingdom, these translate to GBP £29–59 per tonne CO_2 (2019). It is important to note that this value increases considerably with time so that any value presented in this report needs to be rescaled for any year it is read other than 2019.

We estimate that blue carbon storage by marine biodiversity in <1000 m depth across Ascension Island's EEZ totals at ∼43,000 t (∼28,000 t around Ascension Island and 15,000 t around the three offshore seamounts). This 43,000 t of blue carbon stock held by benthic biodiversity there is estimated to capture an additional 6,000 t per year (but will also have losses in respiration and microbial breakdown). We estimate that ∼21% of that stored zoobenthic carbon can be considered sequestered (9,000 t). 43,000 t C is equivalent of 158,000 t CO_2 and the fully sequestered 9,000 t C is equivalent to 33,070 t CO_2. Thus the 2019 lower value of this blue carbon sequestered is 33,070 × 29 = £960,000 and the upper value is £1.9 million. Each year this value increases with both increased value of carbon but also annual increment of carbon deposition, such that 2030 lower and upper values of sequestered blue carbon are estimated to be £2.1–£4.3 million. This valuation does not take into account if there is any underlying trend in the change of rates of sequestration (e.g., increase or decrease in blue carbon capture,

[6]https://static1.squarespace.com/static/54ff9c5ce4b0a53decccfb4c/t/59244eed17bffc0ac256cf16/1495551740633/CarbonPricing_Final_May29.pdf

storage and sequestration is response to physical changes in the environment). Monitoring using data here as baseline should be able to address this potential source of error. Total valuation did not include the surrounding deep seabed production and sequestration, yet that is by far most of Ascension Island's EEZ. Deep water blue carbon storage is little known anywhere in the world and unmeasured around Ascension but even if it is only 5% of that above 1000 m, it would double the total value of the EEZ standing stock.

Countries which commit to protecting and improving their ecosystems that act as carbon sinks are able to access international carbon mitigation financing streams such as Reducing Emissions through Decreased Deforestation (REDD +)and National Appropriate Mitigation Actions (NAMAs) as well as to implement programs and policies at a national level. Whilst most of these schemes are terrestrially based, there are promising market mechanisms for marine – or "Blue Carbon" – trading including the United Nations Framework Convention on Climate Change (UNFCCC) and EU Emissions Trading System (Roger Ullman et al., 2013). In the United Kingdom, the Shelf Sea Biogeochemistry Research Programme is exploring how carbon credits could be implemented through the amount of carbon stored within its territorial waters. In protecting its benthic carbon through the designation of its VLMPA, Ascension Island Government could potentially draw on these future Blue Carbon trading mechanisms.

DATA AVAILABILITY STATEMENT

The datasets generated for this study are available on request to the corresponding author.

AUTHOR CONTRIBUTIONS

All authors were involved conceptually in the project and contributed to the writing of the manuscript. DB and CS led the fieldwork and analysis. AR contributed to the lab work.

FUNDING

National Geographic Pristine Seas funded one of the two expeditions, whilst Blue Marine Foundation funded the other. JNCC and SAERI commissioned and funded the analyses.

ACKNOWLEDGMENTS

We thank the Foreign and Commonwealth Office (FCO) which managed Conflict, Stability and Security Fund (CSSF), and Joint Nature Conservation Committee (JNCC) for funding analyses. We would also like to thank the National Geographic Pristine Seas, Blue Marine Foundation, and the Natural Environment Research Council for funding the two field expeditions. Finally, we thank the officers and crew of RRS James Clark Ross for all their tireless effort in helping to make JR864 and JR16-NG so successful.

SUPPLEMENTARY MATERIAL

The Supplementary Material for this article can be found online at: https://www.frontiersin.org/articles/10.3389/fmars.2019.00663/full#supplementary-material

REFERENCES

Adams, W. M. (2014). The value of valuing nature. *Science* 346, 549–551. doi: 10.1126/science.1255997

Armstrong, C. W., Foley, N. S., Tinch, R., and van den Hove, S. (2012). Services from the deep: steps towards valuation of deep sea goods and services. *Ecosyst. Serv.* 2, 2–13. doi: 10.1016/j.ecoser.2012.07.001

Balmford, A., Bruner, A., Cooper, P., Costanza, R., Farber, S., Green, R. E., et al. (2002). Economic reasons for conserving nature. *Science* 297, 950–953. doi: 10.1126/science.1073947

Barnes, D. K. A. (2015). Antarctic sea ice losses drive gains in benthic carbon drawdown. *Curr. Biol.* 25, R789–R790. doi: 10.1016/j.cub.2015.07.042

Barnes, D. K. A., Fleming, A., Sands, C. J., Quartino, M. L., and Deregibus, D. (2018a). Icebergs, sea ice, blue carbon and antarctic feedbacks. *Phil. Trans. R. Soc. A* 376:20170176. doi: 10.1098/rsta.2017.0176

Barnes, D. K. A., Ireland, L., Hogg, O. T., Morley, S., Enderlein, P., and Sands, C. J. (2016). Why is the south orkney island shelf (the world's first high seas marine protected area) a carbon immobilization hotspot? *Glob. Change Biol.* 22, 1110–1120. doi: 10.1111/gcb.13157

Barnes, D. K. A., Morley, S. A., Bell, J., Brewin, P., Brigden, K., Collins, M., et al. (2018b). Marine plastics threaten giant Atlantic marine protected areas. *Curr. Bio.* 28, R1121–R1122. doi: 10.1016/j.cub.2018.08.064

Barnes, D. K. A., and Sands, C. J. (2017). Functional group diversity is key to Southern ocean benthic carbon pathways. *PLoS One* 12:e0179735. doi: 10.1371/journal.pone.0179735

Bell, T. W., Cavanaugh, K. C., Reed, D. C., and Siegel, D. A. (2015). Geographical variability in the controls of giant kelp biomass dynamics. *J. Biogeog.* 42, 2010–2021. doi: 10.1111/jbi.12550

Constanza, R., d'Arge, R., de Groot, R., Farber, S., Grasso, M., Hannon, B., et al. (1997). The value of the world's ecosystem services and natural capital. *Nature* 387, 253–260. doi: 10.1126/sciadv.1601880

de Groot, R., Brander, R., van der Ploeg, S., Costanza, R., Bernard, F., Braat, L., et al. (2012). Global estimates of the value of ecosystems and their services in monetary units. *Ecosyst. Serv.* 1, 50–61. doi: 10.1016/j.ecoser.2012.07.005

Dixon, P. (2003). VEGAN, a package of functions for community ecology. *J. Veg. Sci.* 14, 927–930. doi: 10.1111/j.1654-1103.2003.tb02228.x

Duarte, C. M., Middelburg, J. J., and Caraco, N. (2005). Major role of marine vegetation on the oceanic carbon cycle. *Biogeosciences* 2, 1–8. doi: 10.1371/journal.pone.0052932

Foley, N., van Rensburg, T., and Armstrong, W. C. (2010). The ecological and economic value of cold-water coral ecosystems. *Ocean Coast. Manag.* 53, 313–326. doi: 10.1016/j.ocecoaman.2010.04.009

Fremand, A., and Barnes, D. (2019). *A Bathymetric Compilation of Ascension Island, 2000-2017 (Version 1.0) [Data Set]. UK Polar Data Centre. Natural Environment Research Council, UK Research & Innovation.* Available at: https://doi.org/10.5285/afba710f-dab1-4a63-867b-520177388224

Jackson, J. B. C., Kirby, M. X., Berger, W. H., Bjorndal, K. A., Botsford, L. W., Bourque, B. J., et al. (2001). Historical overfishing and the recent collapse of coastal ecosystems. *Science* 293, 629–638.

Jobstvogt, N., Townsend, M., Witte, U., and Hanley, N. (2014). How can we identify and communicate the ecological value of deep-sea ecosystem services? *PLoS One* 9:e100646. doi: 10.1371/journal.pone.0100646

Krause-Jensen, D., and Duarte, C. M. (2016). Substantial role of macroalgae in marine carbon sequestration. *Nat. Geosci.* 9, 737–742. doi: 10.1007/s13280-016-0849-7

Krumhansl, K. A., Okamoto, D. K., Rassweiler, A., Novak, M., Bolton, J. J., Cavanaugh, K. C., et al. (2016). Global patterns of kelp forest change over the past half-century. *Proc. Natl. Acad. Sci. U.S.A.* 113, 13785–13790.

Ling, S. D., Johnson, C. R., Frusher, S. D., and Ridgway, K. R. (2009). Overfishing reduces resilience of kelp beds to climate-driven catastrophic phase shift. *Proc. Natl. Acad. Sci. U.S.A.* 106, 22341–22345. doi: 10.1073/pnas.0907529106

Mallela, J. (2013). Calcification by reef-building sclerobionts. *PLoS One* 8:e60010. doi: 10.1371/journal.pone.0060010

Murdiyarso, D., Purbopuspito, J., Kauffman, J. B., Warren, M. W., Sasmito, S. D., Donato, D. C., et al. (2015). The potential of Indonesian mangrove forests for global climate change mitigation. *Nat. Clim. Change* 5, 1089–1092. doi: 10.1186/s13021-017-0080-2

Nolan, E. T., Barnes, D. K. A., Brown, J., Downes, K., Enderlein, P., Gowland, E., et al. (2017). Biological and physical characterization of the seabed surrounding Ascension Island from 100–1000 m. *J. Mar. Biol. Ass. U.K.* 97, 647–659. doi: 10.1017/S0025315417000820

R Core Team (2014). *R: A Language and Environment for Statistical Computing*. Vienna, Austria: R Foundation for Statistical Computing. Available at: http://www.R-project.org/

Roberts, J. M., Wheeler, A. J., Freiwald, A., and Cairns, S. J. (2010). *Cold-Water Corals. The Biology and Geology of Deep-Sea Coral Habitats*. Cambridge: Cambridge University press.

Roger Ullman, R., Bilbao-Bastida, V., and Grimsditch, G. (2013). Including blue carbon in climate market mechanisms. *Ocean Coast. Manag.* 83, 15–18. doi: 10.1016/j.ocecoaman.2012.02.009

Sabatier, P., Reyss, J.-L., Hall-Spencer, J. M., Colin, C., Frank, N., and Tisnerat-Laborde, N. (2012). 210Pb-226Ra chronology reveals rapid growth rate of *Madrepora oculata* and *Lophelia pertusa* on world's largest cold-water coral reef. *Biogeosciences* 9, 1253–1265. doi: 10.5194/bg-9-1253-2012

Trathan, P. N., Collins, M. A., Grant, S. M., Belchier, M., Barnes, D. K. A., Brown, J., et al. (2014). The south georgia and the south sandwich Islands MPA: protecting a biodiverse oceanic island chain situated in the flow of the antarctic circumpolar current. *Adv. Mar. Biol.* 69, 15–78. doi: 10.1016/B978-0-12-800214-8.00002-5

Van Oevelen, D., Duineveld, G., Lavaleye, M., Mienis, F., Soetaert, K., and Heip, C. H. R. (2009). The cold-water coral community as a hot spot for carbon cycling on continental margins: a food-web analysis from rockall bank (northeast Atlantic). *Limnol. Oceanogr.* 54, 1829–1844. doi: 10.4319/lo.2009.54.6.1829

Vecsei, A. (2004). A new estimate of global reefal carbonate production including the fore-reefs. *Glob. Planet. Change* 43, 1–18. doi: 10.1016/j.gloplacha.2003.12.002

Zarate-Barrera, T. G., and Maldonado, J. H. (2015). Valuing blue carbon: carbon sequestration benefits provided by the marine protected areas in Colombia. *PLoS One* 10:e0126627. doi: 10.1371/journal.pone.0126627

Conflict of Interest: The authors declare that the research was conducted in the absence of any commercial or financial relationships that could be construed as a potential conflict of interest.

Copyright © 2019 Barnes, Sands, Richardson and Smith. This is an open-access article distributed under the terms of the Creative Commons Attribution License (CC BY). The use, distribution or reproduction in other forums is permitted, provided the original author(s) and the copyright owner(s) are credited and that the original publication in this journal is cited, in accordance with accepted academic practice. No use, distribution or reproduction is permitted which does not comply with these terms.

frontiers in Marine Science

ORIGINAL RESEARCH
published: 08 November 2019
doi: 10.3389/fmars.2019.00692

The Yellow Coral *Dendrophyllia cornigera* in a Warming Ocean

Giorgio Castellan[1,2], *Lorenzo Angeletti*[1]*, *Marco Taviani*[1,3,4] *and Paolo Montagna*[5,6,7]

[1] Institute of Marine Sciences, National Research Council, Bologna, Italy, [2] Department for the Cultural Heritage, University of Bologna, Ravenna, Italy, [3] Department of Biology, Woods Hole Oceanographic Institution, Woods Hole, MA, United States, [4] Stazione Zoologica Anton Dohrn, Naples, Italy, [5] Institute of Polar Sciences, National Research Council, Bologna, Italy, [6] Laboratoire des Sciences du Climat et de l'Environnement, Gif-sur-Yvette, France, [7] Lamont Doherty Earth Observatory, Columbia University, Palisades, NY, United States

Ocean warming is expected to impinge detrimentally on marine ecosystems worldwide up to impose extreme environmental conditions capable to potentially jeopardize the good ecological status of scleractinian coral reefs at shallow and bathyal depths. The integration of literature records with newly acquired remotely operated vehicle (ROV) data provides an overview of the geographic distribution of the temperate coral *Dendrophyllia cornigera* spanning the eastern Atlantic Ocean to the whole Mediterranean Sea. In addition, we extracted temperature values at each occurrence site to define the natural range of this coral, known to maintain its physiological processes at 16°C. Our results document a living temperature range between ∼7°C and 17°C, suggesting that the natural thermal tolerance of this eurybathic coral may represent an advantage for its survival in a progressively warming ocean.

Keywords: coral ecosystems, *Dendrophyllia cornigera*, mesophotic zone, global change, coral survival, future ocean

OPEN ACCESS

Edited by:
Roberto Sandulli,
Università degli Studi di Napoli Parthenope, Italy

Reviewed by:
Christine Ferrier-Pagès,
Scientific Centre of Monaco, Monaco
Giorgio Bavestrello,
University of Genoa, Italy

***Correspondence:**
Lorenzo Angeletti
lorenzo.angeletti@bo.ismar.cnr.it

Specialty section:
This article was submitted to Global Change and the Future Ocean, a section of the journal Frontiers in Marine Science

Received: *02 September 2019*
Accepted: *28 October 2019*
Published: *08 November 2019*

Citation:
Castellan G, Angeletti L, Taviani M and Montagna P (2019) The Yellow Coral Dendrophyllia cornigera in a Warming Ocean. Front. Mar. Sci. 6:692. doi: 10.3389/fmars.2019.00692

INTRODUCTION

More efficient remote-sensing technologies, advanced SCUBA diving techniques, increasing quality of ROV (Remotely Operated Vehicles) images, and maneuverability have sensibly bettered our in-depth understanding of shallow-to-deep marine habitats. In the Mediterranean Sea, scleractinian corals populate all depths: (i) zooxantellate corals in shallow waters (with *Cladocora caespitosa* as the major bioconstructor); (ii) zooxanthellate and azooxanthellate corals at intermediate depths, approximately between 30 and 200 m (e.g., *Dendrophyllia cornigera* and *D. ramea*); and (iii) azooxanthellate cold-water corals (CWCs) below 200 m depth, mostly dominated by *Madrepora oculata* and *Desmophyllum pertusum* (=*Lophelia pertusa*: Addamo et al., 2016).

However, to date, relatively little information is available on mesophotic-to-twilight coral habitats, though these are known to be defined by specific environmental factors and characterized by high level of biodiversity (Loya et al., 2018; Corriero et al., 2019).

Although our perception of how global climate changes are affecting marine environments is still limited, there is a growing awareness that these may negatively influence marine ecosystems (Poloczanska et al., 2013; Gattuso et al., 2015). This holds true, in particular, for coral biocostructions, known for supporting and enhancing biodiversity, and providing unique ecosystems services (Hoegh-Guldberg et al., 2017). According to the Fifth Assessment Report (AR5) of the Intergovernmental Panel on Climate Change (IPCC) the current global climate change is proceeding at an unprecedented pace compared to those occurred in the geological history

(Pachauri et al., 2014). The surface ocean temperatures have increased of about 1°C since the beginning of the 20th century (0.89°C over the period 1901–2012, Pachauri et al., 2014). Available forecasts provide quantitative scenarios of the possible future state of the ocean, prospecting that oceans will be warmer, more acidic and stratified, less productive, and oxygenated than at present by the end of the 21st century (Pachauri et al., 2014). If these predictions come true, stenoecius marine organisms will be facing extreme conditions in the near future, calling for adaptation or failure. Warming ocean temperatures may influence corals fitness and physiological processes, leading to variations in their abundance and distribution (Hughes et al., 2018). Decreasing ocean pH may alter coral calcification capacity and metabolism, though with responses that appear to be species-specific (McCulloch et al., 2012; Rodolfo-Metalpa et al., 2015; Movilla, 2019).

The consequences of global changes have already been observed at tropical latitudes, where coral reefs have experienced several mass bleaching events (e.g., in 1998, 2002, and 2006), with the largest event recorded in 2016 (Lough et al., 2018). Globally, 90% of all reefs is expected to experience severe bleaching with annual incidence by 2055 (Hooidonk et al., 2014). The Mediterranean Sea is also strongly influenced by climate change, with future warming expected to exceed global rates by 25% (Lionello and Scarascia, 2018). Here, global changes are threatening coral ecosystems by exacerbating bleaching events in temperate zooxanthellate species (Kersting et al., 2013), inducing mass mortality of circalittoral coral communities due to heat waves (Coma et al., 2009), and emphasizing the reduction of food supply and oxygen availability for deep-sea corals related to ocean stratification and the restriction of water recycle (Levin and Bris, 2015).

Dendrophyllia cornigera, the yellow coral, is a considerable component of both mesophotic and deep coral ecosystems in the Mediterranean Sea, extending its bathymetric range up to participate to deep-sea ecosystems dominated by white cold-water corals (Roberts et al., 2009; Angeletti et al., 2014; Taviani et al., 2017; Altuna and Poliseno, 2019; Aymà et al., 2019; Chimienti et al., 2019; Puig and Gili, 2019; Rueda et al., 2019). This coral species was observed also as part of the mesophotic-to-deep coral communities in the Atlantic, from the Azores to the Bay of Biscay (Rodolfo-Metalpa et al., 2015). The spatial distribution of *D. cornigera* (**Figure 1**), and the wide range of environments that this species populates, suggest that it may have less restrictive environmental needs to settle and grow compared to those of other CWCs, mainly restricted to temperature between 4°C and 13°C (Roberts et al., 2006). In several studies investigating the biological response of different deep-sea corals (mainly *M. oculata*, *D. pertusum*, and *D. cornigera*) to the increasing sea water temperature, *D. pertusum* showed decreased fitness performances at 15°C (Brooke et al., 2013) while *M. oculata* appeared more tolerant (Orejas et al., 2011). The same thermal treatments applied on specimens of *D. cornigera* revealed an higher ability to capture preys (zooplankton) and an increase in the growth and respiration rates at temperature regimes up to over 16°C (Gori et al., 2014; Reynaud and Ferrier-Pagès, 2019). However, information about the spatial distribution of *D. cornigera* and its temperature preferences from *in situ* observations are still poor and fragmented, lessening our capability to make predictions regarding the fate of this species in relation with global changes. In this study, we quantify *D. cornigera* occurrences based on 16 ROV video transects performed in 8 sites spanning different areas of the Mediterranean Sea. These data have been integrated with published *D. cornigera* records to get a comprehensive picture of the distribution of *D. cornigera* and of how its abundance varies in relation with depth. Finally, we determine the temperature range of its occurrence. Our contribution aims at providing the first comprehensive overview on the geographic and bathymetric distribution of *D. cornigera*, strongly focusing to the definition of its thermal tolerance range with *in situ* observation, and speculating about possible response in face of global ocean warming.

MATERIALS AND METHODS

Benthic Community Data

Data come from the analysis of 16 ROV videos collected during 8 oceanographic cruises carried out from 2010 to 2017 in 6 different areas (**Supplementary Table S1**): 9 from the Adriatic Sea (Bari Canyon, off Monopoli and off Montenegro); 6 in the Ionian Sea (Amendolara Seamount and Santa Maria di Leuca); and 1 in the Tyrrhenian Sea (Nora Canyon) (**Figure 1A**). We analyzed the videos using ArcGIS and Adelie software. The navigation data were simplified using Gaussian smoothing and synchronized with the high-definition ROV videos. The benthic communities were mapped by randomly extracting a frame every 10 s, obtaining over 9700 seafloor images. After removing poor-quality frames, the remaining images were analyzed for the taxonomic identification of sessile megabenthic fauna and to determine *D. cornigera* sites.

Literature Records

The ROV data were integrated with previous information on the distribution of *D. cornigera* from available peer-reviewed publications, national and international reports obtained from principal scientific databases (such as ISI Web of Knowledge, Scopus, Google Scholar). We selected only works reporting the geographic position and the depth of the coral occurrences. In older publications, benthic samples were collected using dredges, hauls or other devices, making it impossible to identify the precise coordinates and depths of the samples. We therefore decided to exclude sites without a precise location and with an uncertainty in the sampling depth greater than 100 m, which could generate a bias in the temperature analysis.

Temperature Ranges

Seawater temperature values at water depths close to the *D. cornigera* sites were sourced from the World Ocean Atlas 2013 version 2 (WOA13v2) dataset at 0.25° (Locarnini et al., 2013). For each site, we extracted seasonal temperature values (winter: January–March; spring: April–June; summer: July–September; autumn: October–December) at the closest available depth to

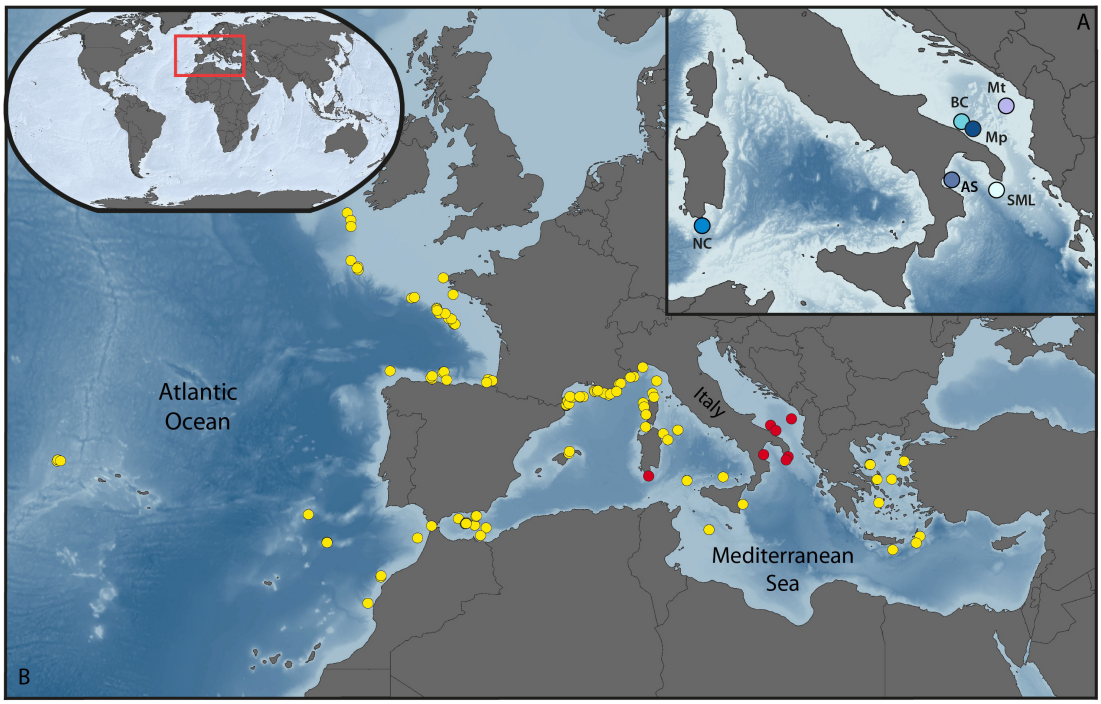

FIGURE 1 | *Dendrophyllia cornigera* distribution. **(A)** Detailed view of the sites explored by the ROV dives. BC, Bari Canyon (272–510 m depth); SML, off Santa Maria di Leuca (119–498 m depth); AS, Amendolara Seamount (133–205 m depth); NC, Nora Canyon (441–463 m depth); Mt, off Montenegro (433–504 m depth); Mp, off Monopoli (463–494 m depth). **(B)** Locations of *D. cornigera* published records (yellow dots, for reference see **Supplementary Table S1**), and occurrences obtained from ROV video transects (red dots).

that of *D. cornigera* records. Temperatures were extracted at the minimum and maximum depth values for those literature records missing a unique depth value but characterized by a range. The annual minimum and maximum temperature of each *D. cornigera* records were calculated, providing the overall temperature range.

RESULTS

Geographic and Bathymetric Distribution of *Dendrophyllia cornigera*

The 16 ROV dives explored 90,054 m^2 of seabed in the depth range comprised between 119 and 510 m. Overall, the analysis of the benthic communities revealed a notable presence of *D. cornigera* within the 6 investigated areas, with 61 sites having at least one colony of the yellow coral, for a total of 116 colonies (**Supplementary Table S2**). The Ionian dives revealed the highest number of *D. cornigera* specimens (83 colonies in 42 sites). In particular, the Amendolara Seamount area hosts the highest value documented, 67 colonies distributed in 35 sites, while dives performed off Santa Maria di Leuca show the lowest abundance in the Ionian Sea (16 colonies in 7 sites). The occurrences are significantly lower in the Adriatic Sea, where a total of 14 sites host 22 colonies. Here, 5 coral sites were identified in the Bari Canyon area and off Monopoli, which present 6 and 12 colonies, respectively, while dives performed off Montenegro show only one colony for each of the 4 sites. In the Nora Canyon (South Sardinia), 11 colonies were observed in 5 sites along the transect.

Most of the coral occurrences fall within the 100–200 m depth range, where 32 sites and 61 specimens were counted (**Figure 2**). At this depth, transects performed along the Amendolara Seamount largely contribute to the abundance observed (29 sites and 58 colonies), while Santa Maria di Leuca dives display much lower values (3 sites and 3 colonies). A second peak of abundance is present between 400 and 500 m depth, with a total of 20 sites hosting 42 colonies. Within this bathymetric range, we identified sites with *D. cornigera* specimens in all the explored areas, with the exception of Amendolara Seamount area. The highest number of sites were detected in Nora Canyon and off Monopoli areas (5 coral sites each), while a greater number of specimens (13 colonies) was reported in the Santa Maria di Leuca area.

Literature Records

The selection of published documents reporting geographic and bathymetric locations of *D. cornigera* resulted in 36 publications, from 1948 to 2018, and a total of 120 coral records (**Figure 1B**). With the exception of two documents targeting both Mediterranean and Atlantic regions, the majority of the selected publications refer to the Mediterranean Sea (27 out of 36; **Figure 1B** and **Supplementary Table S3**). Overall, 81 *D. cornigera* occurrences are reported in the Mediterranean region, with a decreasing trend toward the eastern basin: 18 publications (57 records) for the western Mediterranean, 5 publications

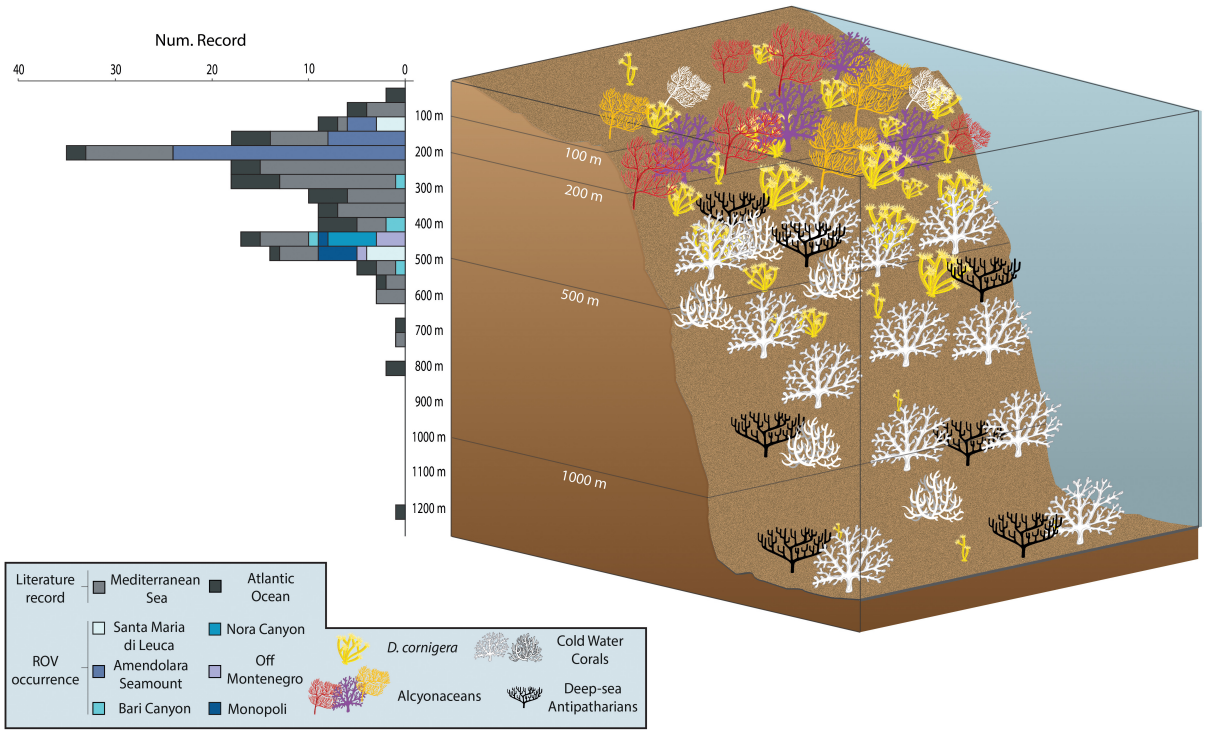

FIGURE 2 | Bathymetric distribution of *D. cornigera* records. 3D schematic representation showing the bathymetric distribution, and the number of *D. cornigera* records from literature review and ROV analysis performed in this study, by depth range.

(16 records) for the central Mediterranean, and 6 publications (8 records) for the eastern Mediterranean, mainly in the Aegean Sea (**Figure 1B**).

The Mediterranean *D. cornigera* records encompass a bathymetric range between 70–100 m and 733 m (**Figure 2** and **Supplementary Table S2**). The majority falls within 200–300 m depth (29 records), with fewer occurrences in the range 100–200 m (15 records), and 300–400 m (13 records).

A much lower number of records concerns the Atlantic Ocean, with 39 sites reported in 9 publications and a bathymetric range spanning from 30 to 1200 m (**Figure 2**). As for the Mediterranean Sea, a great part of the records (26 of 39) are located between 100 and 400 m depth, but with the highest value between 300 and 400 m depth (10 records).

Finally, we integrated the literature records with the new ROV occurrences from the present study, obtaining a total number of 181 *D. cornigera* records for the Atlantic-Mediterranean region.

Temperature Range

The seawater temperatures close to the coral sites show a wide variability ranging from ∼7°C to ∼17°C (**Figure 3**). More than 80% of the coral records occur between ∼13°C and ∼15°C and a second peak of abundance (ca. 15%) was detected between ∼10°C and ∼13°C (**Figure 3A**).

Temperature values show a clear separation between the Atlantic and Mediterranean sites, with the exception of few sites located along the Moroccan coast and off the Azores (**Figure 3B**). The Mediterranean sites are characterized by well-defined temperature ranges, varying from 12.89°C to 15.55°C. Temperature variations at any individual site are wider at shallower depths and gradually decrease going deeper. The overall range of temperature is wider for the Atlantic sites (from 6.93°C in the Bay of Biscay at 1200 m to 16.59°C off the Azores at 91 m), and the temperature variation does not seem directly related to depth, with few deep sites showing up to 1°C seasonal amplitude.

DISCUSSION

Despite *D. cornigera* being commonly recognized as an occasional species in CWCs ecosystems dominated by *M. oculata* and *D. pertusum* (Chimienti et al., 2019; Rueda et al., 2019, with references therein), corals of the genus *Dendrophyllia* are a consistent component of temperate coral ecosystems since at least the Miocene. *Dendrophyllia* corals from this geological period have been observed with high abundances in on-land Mediterranean CWCs fossil occurrences, being also present in the Pliocene and the Early-Middle Pleistocene records (Vertino et al., 2019). At the Pliocene-Pleistocene boundary, the diversity of dendrophylliids remarkably decreased, starting the "golden age" of *Lophelia*-dominated bioconstructions. To date, most of the *D. cornigera* rubble facies in the Mediterranean Sea date back to the Late Pleistocene, implying a greater development of this species in the recent geological time (Vertino et al., 2014).

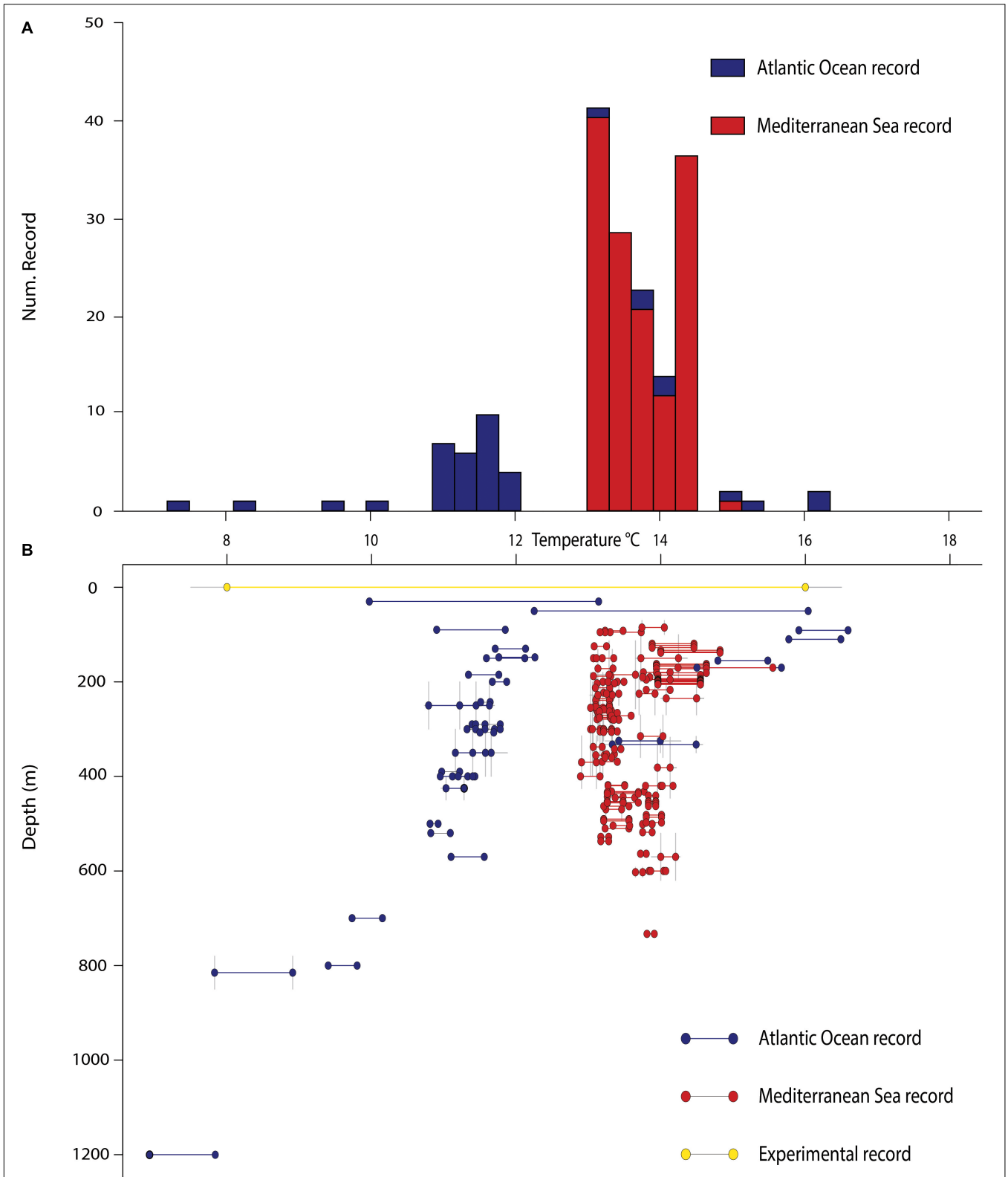

FIGURE 3 | Frequency histogram and temperature annual variability of *D. cornigera* sites by water depth. **(A)** Number of *D. cornigera* records by temperature. **(B)** Temperature variability ranges defined by annual minimum and maximum values for each *D. cornigera* site and related with water depth. Yellow bar represents the temperature interval observed from in-tank experiment (Gori et al., 2014); horizontal gray lines represent the uncertainty value related with temperature, while the vertical ones stand for those ralated with depth.

Through the combined analysis of the new ROV videos and the available literature records, we obtained a comprehensive view of the modern geographic distribution of *D. cornigera*, which extends from the Azores and the eastern Atlantic coast to the whole Mediterranean Sea (**Figure 1**), in agreement with previously published information (Gori et al., 2014). The lower number of *D. cornigera* records in the southern Ionian Sea and the Levantine Basin could be an artifact reflecting the paucity of scientific publications on these areas compared to the available literature for the western Mediterranean Sea and the eastern Atlantic Ocean. In principle, this lack of information could bias the present-day *D. cornigera* distribution, with existing gaps not necessarily associated to unsuitable conditions.

The geographic and bathymetric distribution of temperate scleractinian corals reflects different environmental factors. Radiation levels (for zooxanthellate corals only), geomorphologic and hydrological conditions, seawater temperature and dissolved nutrient, and oxygen concentration are among the major drivers controlling the temperate coral growth (Roberts et al., 2009). In particular, seawater temperature seems to play a major role in determining and limiting the distribution of zooxanthellate and azooxanthellate scleractinian corals (Coma et al., 2009; Roberts et al., 2009; Kersting et al., 2013). *C. caespitosa*, a significant zooxanthellate scleractinian reef-builder in the Mediterranean Sea, populates shallow waters down to 40 m depth in a temperature range of ∼14–25°C (Montagna et al., 2007; Rodolfo-Metalpa et al., 2008). Several studies have investigated the environmental factors controlling *C. caespitosa* distribution. Under suboptimal conditions, such as high light intensity and irregular food source, *C. caespitosa* shows the ability to upregulate its heterotrophy and maintain the symbiosis, presenting light-adapted symbiotic zooxanthellae (*Symbiodinium* Clade A) (Rodolfo-Metalpa et al., 2008; Hoogenboom et al., 2010). Seawater temperature, on the contrary, clearly influences the distribution of *C. caespitosa* and causes bleaching events (Kersting et al., 2013).

Temperature also affects the distribution of azooxanthellate CWC, with most of the species living within ∼4–14°C temperature range (Roberts et al., 2006; Taviani et al., 2017). In the Mediterranean Sea, CWCs find suitable conditions to settle below ∼200 m depth, where the temperature is typically lower than 14°C. The near-homeothermic conditions of the deep Mediterranean Sea, that does not get colder than 12°C (Lejeusne et al., 2010), allow CWCs to populate the seabed over 1000 m depth (Mastrototaro et al., 2010).

Field observations and results from culturing experiments in aquaria reveal a higher thermal tolerance of *D. cornigera* compared to CWCs species. Studies testing the physiological responses of several CWCs to different temperatures show the absence of significant physiological changes in *D. cornigera* at temperatures up to 16°C (Gori et al., 2014). *In situ* annual temperature ranges are in line with these experimental results and confirm that this coral is well adapted to relatively warm temperature conditions (**Figure 3**). A further line of evidence comes from the bathymetric distribution of *D. cornigera*, which extends from 30 to 1200 m depth. The highest number of occurrences are observed between 100 and 200 m depth (53 coral sites) (**Figure 2**). These depths probably present the most suitable temperature conditions for the coral (from 13.80 ± 0.05°C to 14.35 ± 0.08°C in the Mediterranean Sea and from 12.89 ± 0.64°C to 13.47 ± 0.71°C in the Atlantic Ocean) (**Figure 3A**). Therefore, the tolerance to high temperature allows *D. cornigera* to settle at shallower depths, where temperatures are too warm for more sensitive temperate coral species.

A natural tolerance to warm conditions seems to be shared by corals in family Dendrophylliidae, genus *Dendrophyllia*. For instance, *Dendrophyllia ramea*, presents a patchy distribution in the Mediterranean Sea, having been observed in the Adriatic Sea (Kružić et al., 2002), and the Levantine Basin (Salomidi et al., 2010; Orejas et al., 2017). The environmental and ecological factors regulating the distribution of *D. ramea* are still poorly known, but available information suggest that this species preferentially thrives in the shallower layers of the water column (approximately from 20 to 150 m), thus requiring warmer conditions (Orejas et al., 2019). In addition, *Eguchipsammia fistula* (family Dendrophylliidae) has been reported in the Red Sea at intermediate depths (230–270 m) at 21.6°C and *Dendrophyllia* sp. even deeper (570–640 m) in the same basin at 21.5°C (Roder et al., 2013).

The bathymetric distribution of *D. cornigera* shows a notable peak of abundance between 300 and 400 m, with temperature ranging from 13.24 ± 0.05°C to 13.39 ± 0.05°C in the Mediterranean Sea and 11.73 ± 0.34°C to 12.14 ± 0.41°C in the Atlantic Ocean, indicating the capability of this coral to colonize also deeper and colder layers.

The Mediterranean Sea is experiencing a gradual warming, from the surface down to the deepest layers, as a result of global climate changes (Vargas-Yáñez et al., 2008). The IPCC documented an increasing trend in Mediterranean Sea surface temperature of 0.66°C from 1950 to 2009 (Pachauri et al., 2014). Current predictions, based on different Representative Concentration Pathways (RCPs), indicate a temperature increase from 0.5°C to 2.6°C for the end of the 21st century (Shaltout and Omstedt, 2014). The raise of seawater temperature over its actual range of variability will probably push temperate coral ecosystems beyond the range of natural temperature, potentially influencing their fitness and survival. In-tank experiments testing the response of *C. caespitosa* to warm conditions reported coral tissue necrosis or mortality appearing at 26–28°C (Kersting et al., 2013). The warming of the seawater temperature over the thermal tolerance of *C. caespitosa* at its distribution depth (from 0 to ∼40 m) may lead to an increase in the intensity and frequency of bleaching events (Rodolfo-Metalpa et al., 2006). *Cladocora caespitosa* cannot escape these warmer conditions moving deeper along the water column because of its specific trophic needs (i.e., radiation levels for photosynthesis). As a consequence, this warming might in principle reduce the extent of *C. caespitosa* reefs, enhancing the importance of coral ecosystems composed by species with higher thermal tolerance and playing a similar ecological role.

The increase in temperature is taking place also in the deep Mediterranean Sea. The most conservative predictions for the 2016–2035 period forecast a temperature increase of about

0.035°C per year for the 150–350 m depth layer (Ozer et al., 2017). Applying this rate of increase to the current thermal conditions of the *D. cornigera* sites between 150 and 350 m depth, the seawater temperature value will be ∼0.7°C warmer in 2035 (from 14.23 ± 0.04°C to 14.61 ± 0.07°C) than present-day (from 13.57 ± 0.04°C to 13.94 ± 0.07°C). Deep-sea warming will probably lead to the exceeding of CWCs thermal limits in the shallower part of their bathymetric range, strongly threatening their survival and influencing their distribution (Gori et al., 2014; Maier et al., 2019).

Global change influences several environmental drivers of paramount importance for temperate corals. Ocean acidification is thought to be a major threat to coral ecosystems, reducing the amount of carbonate ions [CO_3^{2-}] available in seawater. Predictions anticipate that ca. 70% of known CWCs reefs will be exposed to waters corrosive to aragonite before the end of 21st century (Tittensor et al., 2010) up to evoking negative to counteractive scenarios for their eventual survival (Maier et al., 2011; McCulloch et al., 2012; Gammon et al., 2018). However, some studies reveal that net calcification rates, as well as dissolution rates of exposed skeleton and respiration rates of different deep-sea coral species, do not significantly change when exposed to high seawater pCO_2, with *D. cornigera* showing no physiological alterations (Movilla et al., 2014; Rodolfo-Metalpa et al., 2015; Reynaud and Ferrier-Pagès, 2019).

Climate change may also affect nutrient concentrations and food sources, which are of primarily importance for CWCs distribution and survival (Lionello and Scarascia, 2018). The Mediterranean Sea is markedly oligotrophic and characterized by a strong stratification of the water column during summer, resulting in high temperatures, and low food availability (e.g., Zabala and Ballesteros, 1989). In deep-sea habitats, where food availability may be extremely heterogeneous in time and space (Mienis et al., 2009), benthic ecosystems are under strong nutritional forcing, leading to a "summer dormancy" in many benthic suspension feeders (Lejeusne et al., 2010). Global warming is intensifying water column stratification, producing a 40% lengthening of summer conditions (Coma et al., 2009) and influencing the fundamental biological processes that require high-energy investments, such as coral growth and reproduction. Opportunistic trophic behavior has been observed in *D. pertusum* (Mueller et al., 2014) and recent studies demonstrated a high trophic plasticity of *D. cornigera*, which favors the wide distribution of this coral in areas with variable food availability (Gori et al., 2018).

However, the big question remains: will the yellow coral *D. cornigera* have an edge in the race against global ocean warming? Our results suggest that the natural thermal tolerance of the mesophotic-bathyal coral *D. cornigera* will likely prove to be an advantage in the survival struggle in a progressively warming ocean. We anticipate that *D. cornigera* could experiment in principle an increase of its horizontal and vertical distribution range, perhaps even taking advantage in the long term of a concomitant decline of more thermal-sensitive reef-forming calcareous organisms.

DATA AVAILABILITY STATEMENT

The raw data supporting the conclusions of this manuscript will be made available by the authors, without undue reservation, to any qualified researcher.

AUTHOR CONTRIBUTIONS

GC analyzed the data and wrote the manuscript together with MT, LA, and PM. All authors contributed to the discussion and preparation of the manuscript.

FUNDING

This work was partly supported by the EU F.P. VII Projects HERMIONE (contract no. 226354), CoCoNet (contract no. 287844), MISTRALS/PALEOMEX/COFIMED and Convenzione MATTM-CNR per i Programmi di Monitoraggio per la Direttiva sulla Strategia Marina (MSFD, Art. 11, Dir. 2008/56/CE), and is part of the DG Environment programme IDEM (grant agreement no. 11.0661/2017/750680/SUB/EN V.C2) and the MIUR-PRIN GLIDE.

ACKNOWLEDGMENTS

We thank captain, crew, and scientific staff of R/V Urania and Minerva Uno cruises for their skillful and efficient cooperation during operations at sea (ISMAR-Bologna scientific contribution no. 2000).

SUPPLEMENTARY MATERIAL

The Supplementary Material for this article can be found online at: https://www.frontiersin.org/articles/10.3389/fmars.2019.00692/full#supplementary-material

REFERENCES

Addamo, A. M., Vertino, A., Stolarski, J., García-Jiménez, R., Taviani, M., and Machordom, A. (2016). Merging scleractinian genera: the overwhelming genetic similarity between solitary *Desmophyllum* and colonial *Lophelia*. *BMC Evol. Biol.* 16:108. doi: 10.1186/s12862-016-0654-8

Altuna, A., and Poliseno, A. (2019). "Taxonomy, genetics and biodiversity of Mediterranean deep-sea corals and cold-water corals," in *Mediterranean Cold-Water Corals: Past, Present and Future*, eds C. Orejas and C. Jiménez (Cham, CH: Springer International Publishing), 121–156. doi: 10.1007/978-3-319-91608-8_14

Angeletti, L., Taviani, M., Canese, S., Foglini, F., Mastrototaro, F., Argnani, A., et al. (2014). New deep-water cnidarian sites in the southern Adriatic Sea. *Mediterr. Mar. Sci.* 15, 263–273. doi: 10.12681/mms.558

Aymà, A., Aguzzi, J., Canals, M., Company, J. B., Lastras, G., Mecho, A., et al. (2019). "Occurrence of living cold-water corals at large depths within

submarine canyons of the northwestern Mediterranean Sea," in *Mediterranean Cold-Water Corals: Past, Present and Future*, eds C. Orejas and C. Jiménez (Cham, CH: Springer International Publishing), 271–284. doi: 10.1007/978-3-319-91608-8-26

Brooke, S., Ross, S. W., Bane, J. M., Seim, H. E., and Young, C. M. (2013). Temperature tolerance of the deep-sea coral *Lophelia pertusa* from the southeastern United States. *Deep Sea Res. Part II* 92, 240–248. doi: 10.1016/j.dsr2.2012.12.001

Chimienti, G., Bo, M., Taviani, M., and Mastrototaro, F. (2019). "Occurrence and biogeography of Mediterranean cold-water corals," in *Mediterranean Cold-Water Corals: Past, Present and Future*, eds C. Orejas and C. Jiménez (Cham, CH: Springer International Publishing), 213–243. doi: 10.1007/978-3-319-91608-8_19

Coma, R., Ribes, M., Serrano, E., Jiménez, E., Salat, J., and Pascual, J. (2009). Global warming-enhanced stratification and mass mortality events in the Mediterranean. *PNAS* 106, 6176–6181. doi: 10.1073/pnas.0805801106

Corriero, G., Pierri, C., Mercurio, M., Marzano, C. N., Tarantini, S. O., Gravina, M. F., et al. (2019). A Mediterranean mesophotic coral reef built by non-symbiotic scleractinians. *Sci. Rep.* 9:3601. doi: 10.1038/s41598-019-40284-4

Gammon, M. J., Tracey, D. M., Marriott, P. M., Cummings, V. J., and Davy, S. K. (2018). The physiological response of the deep-sea coral *Solenosmilia variabilis* to ocean acidification. *PeerJ* 6:e5236. doi: 10.7717/peerj.5236

Gattuso, J. -P., Magnan, A., Billé, R., Cheung, W. W. L., Howes, E. L., Joos, F., et al. (2015). Contrasting futures for ocean and society from different anthropogenic CO2 emissions scenarios. *Science* 349:4722. doi: 10.1126/science.aac4722

Gori, A., Reynaud, S., Orejas, C., Gili, J. -M., and Ferrier-Pagès, C. (2014). Physiological performance of the cold-water coral *Dendrophyllia cornigera* reveals its preference for temperate environments. *Coral Reefs* 33, 665–674. doi: 10.1007/s00338-014-1167-9

Gori, A., Tolosa, I., Orejas, C., Rueda, L., Viladrich, N., Grinyó, J., et al. (2018). Biochemical composition of the cold-water coral *Dendrophyllia cornigera* under contrasting productivity regimes: insights from lipid biomarkers and compound-specific isotopes. *Deep Sea Res. I* 141, 106–117. doi: 10.1016/j.dsr.2018.08.010

Hoegh-Guldberg, O., Poloczanska, E. S., Skirving, W., and Dove, S. (2017). Coral reef ecosystems under climate change and ocean acidification. *Front. Mar. Sci.* 4:158. doi: 10.3389/fmars.2017.00158

Hoogenboom, M., Rodolfo-Metalpa, R., and Ferrier-Pagès, C. (2010). Co-variation between autotrophy and heterotrophy in the Mediterranean coral *Cladocora caespitosa*. *J. Exp. Biol.* 213, 2399–2409. doi: 10.1242/jeb.040147

Hooidonk, R. V., Maynard, J. A., Manzello, D., and Planes, S. (2014). Opposite latitudinal gradients in projected ocean acidification and bleaching impacts on coral reefs. *Glob. Chang. Biol.* 20, 103–112. doi: 10.1111/gcb.12394

Hughes, T. P., Kerry, J. T., Baird, A. H., Connolly, S. R., Dietzel, A., Eakin, C. M., et al. (2018). Global warming transforms coral reef assemblages. *Nature* 556, 492–496. doi: 10.1038/s41586-018-0041-2

Kersting, D. K., Bensoussan, N., and Linares, C. (2013). Long-term responses of the endemic reef- builder *Cladocora caespitosa* to Mediterranean warming. *PLoS One* 8:e70820. doi: 10.1371/journal.pone.0070820

Kružić, P., Zibrowius, H., and Pozar-Domac, A. (2002). Actiniaria and Scleractinia (Cnidaria, Anthozoa) from the Adriatic Sea (Croatia): first records, confirmed occurrences and significant range extensions of certain species. *Ital. J. Zool.* 69, 345–353. doi: 10.1080/11250000209356480

Lejeusne, C., Chevaldonné, P., Pergent-Martini, C., Boudouresque, C. F., and Pérez, T. (2010). Climate change effects on a miniature ocean: the highly diverse, highly impacted Mediterranean Sea. *Trends Ecol. Evol.* 25, 250–260. doi: 10.1016/j.tree.2009.10.009

Levin, L. A., and Bris, N. L. (2015). The deep ocean under climate change. *Science* 350, 766–768. doi: 10.1126/science.aad0126

Lionello, P., and Scarascia, L. (2018). The relation between climate change in the Mediterranean region and global warming. *Reg. Environ. Chang.* 18, 1481–1493. doi: 10.1007/s10113-018-1290-1

Locarnini, R. A., Mishonov, A. V., Antonov, J. I., Boyer, T. P., Garcia, H. E., Baranova, O. K., et al. (2013). World Ocean Atlas 2013, Volume 1: Temperature. Washington D.C: National Oceanic and Atmospheric Administration (NOAA). doi: 10.1007/s10113-018-1290-1

Lough, J. M., Anderson, K. D., and Hughes, T. P. (2018). Increasing thermal stress for tropical coral reefs: 1871–2017. *Sci. Rep.* 8:6079. doi: 10.1038/s41598-018-24530-9

Loya, Y., Puglise, K. A., and Bridge, T. C. L. (2018). *Mesophotic Coral Ecosystems*. Cham, CH: Springer International Publishing. doi: 10.1007/978-3-319-92735-0

Maier, C., Watremez, P., Taviani, M., Weinbauer, M. G., and Gattuso, J. P. (2011). Calcification rates and the effect of ocean acidification on Mediterranean cold-water corals. *Proc. R. Soc. B Biol. Sci.* 279, 1716–1723. doi: 10.1098/rspb.2011.1763

Maier, C., Weinbauer, M. G., and Gattuso, J.-P. (2019). "Fate of Mediterranean scleractinian cold-water corals as a result of global climate change. a synthesis," in *Mediterranean Cold-Water Corals: Past, Present and Future*, eds C. Orejas and C. Jiménez (Cham, CH: Springer International Publishing), 517–529. doi: 10.1007/978-3-319-91608-8-44

Mastrototaro, F., D'Onghia, G., Corriero, G., Matarrese, A., Maiorano, P., Panetta, P., et al. (2010). Biodiversity of the white coral bank off Cape Santa Maria di Leuca (Mediterranean Sea): an update. *Deep Sea Res. II* 57, 412–430. doi: 10.1016/j.dsr2.2009.08.021

McCulloch, M., Falter, J., Trotter, J., and Montagna, P. (2012). Coral resilience to ocean acidification and global warming through pH up-regulation. *Nat. Clim. Chang.* 2, 623–627. doi: 10.1038/nclimate1473

Mienis, F., de Stigter, H. C., de Haas, H., and van Weering, T. C. E. (2009). Near-bed particle deposition and resuspension in a cold-water coral mound area at the Southwest Rockall Trough margin, NE Atlantic. *Deep Sea Res. I* 56, 1026–1038. doi: 10.1016/j.dsr.2009.01.006

Montagna, P., McCulloch, M., Mazzoli, C., Silenzi, S., and Odorico, R. (2007). The non-tropical coral *Cladocora caespitosa* as the new climate archive for the Mediterranean Sea: high-resolution (˜ weekly) trace element systematics. *Quat. Sci. Rev.* 26, 441–462. doi: 10.1016/j.quascirev.2006.09.008

Movilla, J., Orejas, C., Calvo, E., Gori, A., Lopez-Sanz, A., Grinyo, J., et al. (2014). Differential response of two Mediterranean cold-water coral species to ocean acidification. *Coral Reefs* 33, 675–686. doi: 10.1007/s00338-014-1159-9

Movilla, J. (2019). "A case study: variability in the calcification response of Mediterranean cold-water corals to ocean acidification," in *Mediterranean Cold-Water Corals: Past, Present and Future*, eds C. Orejas and C. Jiménez (Cham, CH: Springer International Publishing), 531–533. doi: 10.1007/978-3-319-91608-8_45

Mueller, C. E., Larsson, A. I., Veuger, B., Middelburg, J. J., and Van Oevelen, D. (2014). Opportunistic feeding on various organic food sources by the cold-water coral *Lophelia pertusa*. *Biogeosciences* 11, 123–133. doi: 10.5194/bg-11-123-2014

Orejas, C., Ferrier-Pagès, C., Reynaud, S., Gori, A., Beraud, E., Tsounis, G., et al. (2011). Long-term growth rates of four Mediterranean cold-water coral species maintained in aquaria. *Mar. Ecol. Prog. Ser.* 429, 57–65. doi: 10.3354/meps09104

Orejas, C., Gori, A., Jiménez, C., Riviera, J., Lo Iacono, C., Hadjioannou, L., et al. (2017). First in situ documentation of a population of the coral *Dendrophyllia ramea* off cyprus (Levantine Sea) and evidence of human impacts. *Galaxea CRS* 19, 15–16. doi: 10.3755/galaxea.19.1_15

Orejas, C., Taviani, M., Ambroso, S., Andreou, V., Bilan, M., Bo, M., et al. (2019). "Cold-water corals in aquaria: advances and challenges. A focus on the Mediterranean," in *Mediterranean Cold-Water Corals: Past, Present and Future*, eds C. Orejas and C. Jiménez (Cham, CH: Springer International Publishing), 435–471. doi: 10.1007/978-3-319-91608-8-38

Ozer, T., Gertman, I., Kress, N., Silverman, J., and Herut, B. (2017). Interannual thermohaline (1979–2014) and nutrient (2002–2014) dynamics in the Levantine surface and intermediate water masses, SE Mediterranean Sea. *Glob. Planet. Chang.* 151, 60–67. doi: 10.1016/j.gloplacha.2016.04.001

Pachauri, R. K., Allen, M. R., Barros, V. R., Broome, J., Cramer, W., Christ, R., et al. (2014). *Climate Change 2014: Synthesis Report. Contribution of Working Groups I, II and III to the Fifth Assessment Report of the Intergovernmental Panel on Climate Change*. Geneva: IPCC.

Poloczanska, E. S., Brown, C. J., Sydeman, W. J., Kiessling, W., Schoeman, D. S., Moore, P. J., et al. (2013). Global imprint of climate change on marine life. *Nat. Clim. Chang.* 3, 919–925. doi: 10.1038/nclimate1958

Puig, P., and Gili, J.-M. (2019). "Submarine canyons in the Mediterranean: a shelter for cold-water corals," in *Mediterranean Cold-Water Corals: Past, Present*

and Future, eds C. Orejas and C. Jiménez (Cham, CH: Springer International Publishing), 285–289. doi: 10.1007/978-3-319-91608-8_27

Reynaud, S., and Ferrier-Pagès, C. (2019). "Biology and ecophysiology of Mediterranean cold–water corals," in *Mediterranean Cold-Water Corals: Past, Present and Future*, eds C. Orejas and C. Jiménez (Cham, CH: Springer International Publishing), 391–404. doi: 10.1007/978-3-319-91608-8-35

Roberts, J. M., Wheeler, A., Freiwald, A., and Cairns, S. (2009). *Cold-Water Corals: The Biology and Geology of Deep-Sea Coral Habitats*. Cambridge: Cambridge University Press.

Roberts, J. M., Wheeler, A. J., and Freiwald, A. (2006). Reefs of the deep: the biology and geology of cold-water coral ecosystems. *Science* 312, 543–547. doi: 10.1126/science.1119861

Roder, C., Berumen, M. L., Bouwmeester, J., Papathanassiou, E., Al-Suwailem, A., and Voolstra, C. R. (2013). First biological measurements of deep-sea corals from the Red Sea. *Sci. Rep.* 3:2802. doi: 10.1038/srep02802

Rodolfo-Metalpa, R., Montagna, P., Aliani, S., Borghini, M., Canese, S., Hall-Spencer, J. M., et al. (2015). Calcification is not the Achilles' heel of cold-water corals in an acidifying ocean. *Glob. Chang. Biol.* 21, 2238–2248. doi: 10.1111/gcb.12867

Rodolfo-Metalpa, R., Peirano, A., Houlbrèque, F., Abbate, M., and Ferrier-Pagès, C. (2008). Effects of temperature, light and heterotrophy on the growth rate and budding of the temperate coral *Cladocora caespitosa*. *Coral Reefs* 27, 17–25. doi: 10.1007/s00338-007-0283-1

Rodolfo-Metalpa, R., Richard, C., Allemand, D., and Ferrier-Pagès, C. (2006). Growth and photosynthesis of two Mediterranean corals, *Cladocora caespitosa* and *Oculina patagonica*, under normal and elevated temperatures. *J. Exp. Biol.* 209, 4546–4556. doi: 10.1242/jeb.02550

Rueda, J. L., Urra, J., Aguilar, R., Angeletti, L., Bo, M., García-Ruiz, C., et al. (2019). "Cold-water coral associated fauna in the Mediterranean Sea and adjacent areas," in *Mediterranean Cold-Water Corals: Past, Present and Future*, eds C. Orejas and C. Jiménez (Cham, CH: Springer International Publishing), 295–333. doi: 10.1007/978-3-319-91608-8_29

Salomidi, M., Zibrowius, H., Issaris, Y., and Milionis, K. (2010). *Dendrophyllia* in Greek waters, Mediterranean Sea, with the first record of *D. ramea* (Cnidaria, Scleractinia) from the area. *Mediterr. Mar. Sci.* 11, 189–194. doi: 10.12681/mms.102

Shaltout, M., and Omstedt, A. (2014). Recent sea surface temperature trends and future scenarios for the Mediterranean Sea. *Oceanologia* 56, 411–443. doi: 10.5697/oc.56-3.411

Taviani, M., Angeletti, L., Canese, S., Cannas, R., Cardone, F., Cau, A., et al. (2017). The "Sardinian cold-water coral province" in the context of the Mediterranean coral ecosystems. *Deep Sea Res. II* 145, 61–78. doi: 10.1016/j.dsr2.2015.12.008

Tittensor, D. P., Baco, A. R., Hall-Spencer, J. M., Orr, J. C., and Rogers, A. D. (2010). Seamounts as refugia from ocean acidification for cold-water stony corals. *Mar. Ecol.* 31, 212–225. doi: 10.1111/j.1439-0485.2010.00393.x

Vargas-Yáñez, M., Jesús García, M., Salat, J., García-Martínez, M. C., Pascual, J., and Moya, F. (2008). Warming trends and decadal variability in the Western Mediterranean shelf. *Glob. Plan. Chang.* 63, 177–184. doi: 10.1016/j.gloplacha.2007.09.001

Vertino, A., Stolarski, J., Bosellini, F. R., and Taviani, M. (2014). "Mediterranean corals through time: from miocene to present," in *The Mediterranean Sea: Its History and Present Challenges*, eds S. Goffredo and Z. Dubinsky (Dordrecht: Springer), 257–274. doi: 10.1007/978-94-007-6704-1-14

Vertino, A., Taviani, M., and Corselli, C. (2019). "Spatio-temporal distribution of Mediterranean cold-water corals," in *Mediterranean Cold-Water Corals: Past, Present and Futureed*, eds C. Orejas and C. Jiménez (Cham, CH: Springer International Publishing), 67–83. doi: 10.1007/978-3-319-91608-8_9

Zabala, M., and Ballesteros, E. (1989). Surface-dependent strategies and energy flux in benthic marine communities or, why corals do not exist in the Mediterranean. *Sci. Mar.* 53, 3–17.

Conflict of Interest: The authors declare that the research was conducted in the absence of any commercial or financial relationships that could be construed as a potential conflict of interest.

Copyright © 2019 Castellan, Angeletti, Taviani and Montagna. This is an open-access article distributed under the terms of the Creative Commons Attribution License (CC BY). The use, distribution or reproduction in other forums is permitted, provided the original author(s) and the copyright owner(s) are credited and that the original publication in this journal is cited, in accordance with accepted academic practice. No use, distribution or reproduction is permitted which does not comply with these terms.

frontiers in Marine Science

ORIGINAL RESEARCH
published: 08 November 2019
doi: 10.3389/fmars.2019.00685

Environmental and Benthic Community Patterns of the Shallow Hydrothermal Area of Secca Delle Fumose (Baia, Naples, Italy)

Luigia Donnarumma[1,2], Luca Appolloni[1,2], Elena Chianese[1], Renato Bruno[3], Elisa Baldrighi[4], Rosanna Guglielmo[5], Giovanni F. Russo[1,2], Daniela Zeppilli[4] and Roberto Sandulli[1,2]*

[1] Laboratory of Marine Ecology, Department of Science and Technology, University of Naples "Parthenope", Naples, Italy, [2] National Interuniversity Consortium for Marine Sciences, Rome, Italy, [3] EEP/SPICI Group/UMR 8198, Department of Sciences et Technologies, University of Lille, Villeneuve-d'Ascq, France, [4] IFREMER, Centre Brest, REM/EEP/LEP, Plouzané, France, [5] Integrative Marine Ecology Department, Stazione Zoologica Anton Dohrn, Naples, Italy

The occurrence of hydrothermal vent ecosystems at Secca delle Fumose, Pozzuoli Bay (Gulf of Naples), represented an opportunity to study the benthic assemblages under the thermal stress of hydrothermal emissions in a very shallow environment (9–14 m water depth). In autumn 2016, the macrobenthic community was sampled by scuba divers at four sites located in the Baia Underwater Archeological Park. Two sites were characterized by vent emissions (one with white bacterial mat scattered on the bottom and one with a yellow substrate around a geyser opening) and two at about 100 m away, used as control. Sediment and interstitial water environmental variables were measured to determine their influence on the structure of macrobenthic assemblages. A total of 1,954 macrofaunal individuals was found, characterized by great differences in abundance and species richness among sites. This pattern was correlated to the dominance of a particular set of variables that drastically change in a very small spatial scale, from one site to another. The control sites, characterized by the highest percentage of gravel in the sediments (19.67 ± 2.6%) and normal level of major ions such as Ca^{2+}, K^{+}, and Mg^{2+} in the interstitial waters, showed the highest values of sinecological indices. The "white" hydrothermal site exhibited the lowest species richness, abundance and species diversity, influenced by low pH values (∼7.6), high temperatures (∼37.53°C) and by the highest total organic carbon content (TOC 34.78%) in the sediment. The "yellow" hydrothermal site, with sediment TOC equal to 30.03% and interstitial sulfide ions measuring 130.58 *ppm*, showed higher values of sinecological indices than those recorded at the "white" site. Therefore, taxonomic analysis revealed a high turnover between control and vents sites. This highlights the preference for hydrothermal vents by a few resistant species, such as the gastropod *Tritia cuvierii* and the polychaete *Capitella capitata*, confirming the role of the latter species as opportunistic in extreme environments like Secca delle Fumose.

Keywords: shallow hydrothermal vents, interstitial water, sediments, macrofauna, benthos, extreme habitats, Mediterranean Sea

OPEN ACCESS

Edited by:
Rui Rosa,
University of Lisbon, Portugal

Reviewed by:
Ana Colaço,
Marine Research Institute (IMAR), Portugal
Clara Rodrigues,
University of Aveiro, Portugal

****Correspondence:***
Luigia Donnarumma
luigia.donnarumma@uniparthenope.it

Specialty section:
This article was submitted to Global Change and the Future Ocean, a section of the journal Frontiers in Marine Science

Received: *23 April 2019*
Accepted: *24 October 2019*
Published: *08 November 2019*

Citation:
Donnarumma L, Appolloni L, Chianese E, Bruno R, Baldrighi E, Guglielmo R, Russo GF, Zeppilli D and Sandulli R (2019) Environmental and Benthic Community Patterns of the Shallow Hydrothermal Area of Secca Delle Fumose (Baia, Naples, Italy). Front. Mar. Sci. 6:685. doi: 10.3389/fmars.2019.00685

INTRODUCTION

The relationship between environmental factors and benthic communities is of primary importance in determining the structure of biocenoses and their functioning (e.g., Feder et al., 1994; Ellingsen, 2002; Lloret and Marín, 2009; Arribas et al., 2014). A huge variety of marine species and bioconstructions is widely distributed along the bathymetrical gradient, from very shallow to deep-water. Among extreme marine systems, hydrothermal vents have wide global distribution, occurring in all oceanic bottoms, at different latitudes and depths and harboring rich and peculiar biological communities (Parson et al., 1995; Dando et al., 2000). Several studies revealed that the occurrence of benthic organisms in the hydrothermal systems is strongly related to the volcanic fluids that outflow from the bottom, characterized by high concentrations of iron, zinc sulfides and gases, such as CH_4, H_2S, H_2, and CO_2 (e.g., Van Dover and Fry, 1989; Micheli et al., 2002; Hall-Spencer et al., 2008; Martin et al., 2008; Yao et al., 2010). A great biological difference occurs between deep and shallow vents. The former are mainly characterized by chemolithotrophic bacteria using H_2S as energy source, representing the basis for a complex heterotrophic ecosystem, while the latter are composed both by chemolithotrophic bacteria and by communities energetically driven by photosynthetic organisms, such as diatoms and algal-bacterial mats absent in deep-sea vents communities (Vismann, 1991; Lutz and Kennish, 1993; Tarasov et al., 2005; Raghukumar et al., 2008).

In the Mediterranean Sea, very shallow hydrothermal vents were reported for the Tyrrhenian and Aegean Sea, ranging from few meters to about 30 m depth (Dando et al., 1999). They are related to tectonically active coastal zones, where the volcanic fluids are characterized by high temperatures and mainly composed by sulfide and/or CO_2 (Dando et al., 2000). Even though shallow benthic communities include tolerant species to natural or anthropogenic stressors, many studies have suggested that the increasing temperature and sulfides negatively affect a wide variety of benthic assemblages, reducing the water oxygen concentration and producing toxicity to the majority of aerobic species (Caldwell, 1975; Wang and Chapman, 1999; Vaquer-Sunyer and Duarte, 2010, 2011). Similarly, natural CO_2 emissions in seawater produce a change in carbonate chemistry, resulting in a local seawater acidification, which, in turn, impacts on

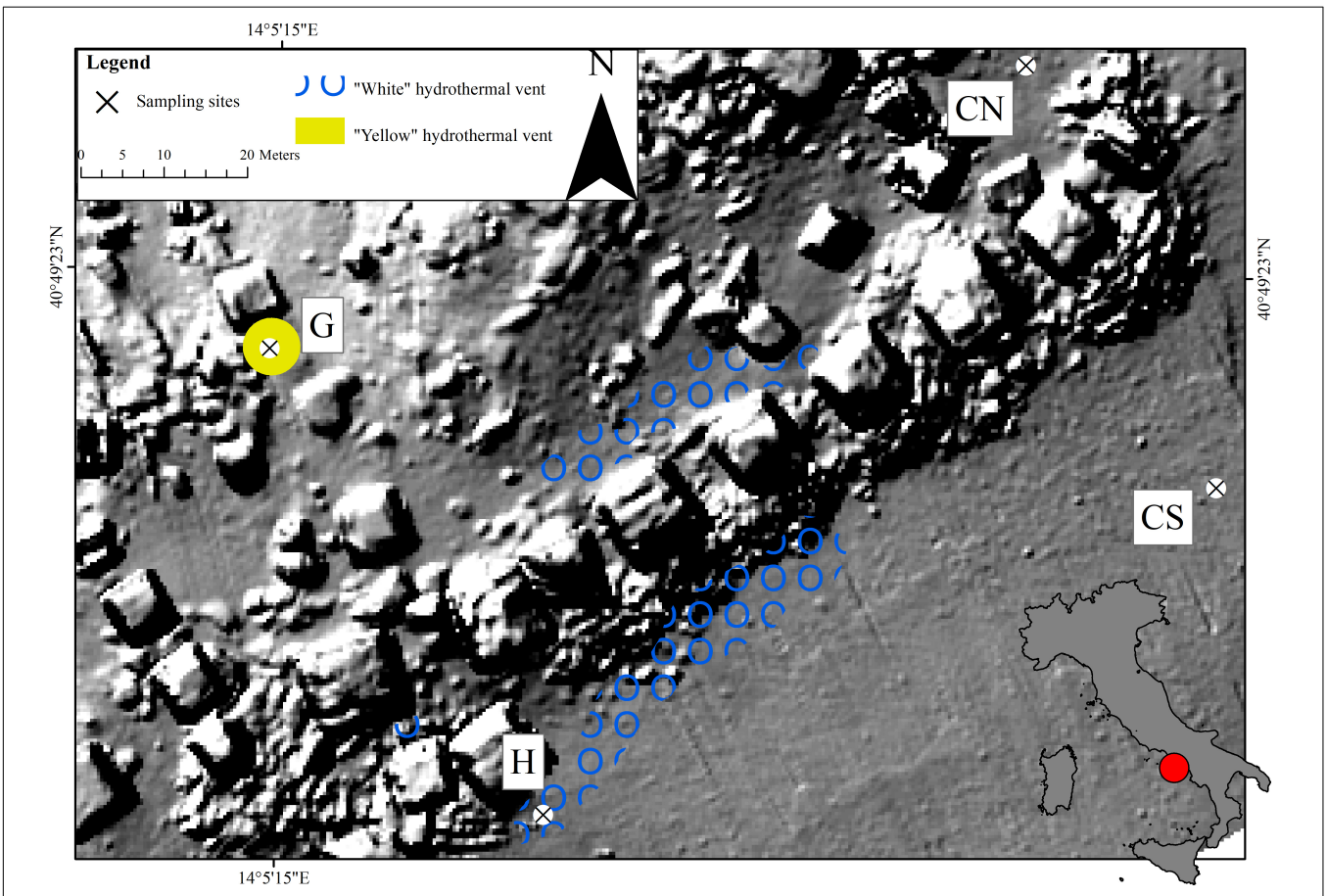

FIGURE 1 | Study area showing the sampling sites (H – White hydrothermal vent; G – Geyser; CN – Control North; CS – Control South) around pillars of the Roman age at Secca delle Fumose (Gulf of Naples, Italy).

calcification and growth processes of many planktic and benthic species (Fabry et al., 2008; Doney et al., 2009; Wicks and Roberts, 2012).

Volcanic emissions, rich in CO_2, were previously reported by Hall-Spencer et al. (2008) for the cold vents of Ischia Island, in the Gulf of Naples (Italy). Here, sulfides are absent while the high percentage of CO_2 (∼90–95%) considerably reduces the seawater pH which negatively affects calcifying organisms (Cigliano et al., 2010; Donnarumma et al., 2014; Lucey et al., 2016; Teixidó et al., 2018).

A few kilometers away from Ischia Island, in the Campi Flegrei caldera, Di Napoli et al. (2016) reported a remarkable variation in seawater pH (∼7.3–8.3) due to the gas-rich hydrothermal fluids occurring in a shallow submarine relief, namely Secca delle Fumose. This area was only recently investigated from a geological (e.g., Tedesco et al., 1990; Passaro et al., 2013) and microbiological (Maugeri et al., 2010), point of view. High-resolution morpho-bathymetric data and archeological surveys indicate that the relief is largely anthropogenic, consisting of a dense aggregation of pillars of the Roman age (first century BC), with a perimeter of 9 m × 9 m and a height of 7 m, mostly standing on a seafloor at 12 m depth where hydrothermal vents occur. Since there is a lack of information concerning the other biological and ecological components, the aims of this paper are: (i) to evaluate the spatial variation of macrobenthic community at the Secca delle Fumose, (ii) to assess the most important abiotic parameters affecting soft-bottom assemblage structure and (iii) to estimate the taxonomic diversity among hydrothermal vents and non-vent sites. To our knowledge, this study represents the first investigation of macrobenthic assemblages inhabiting the shallow hydrothermal systems of Campi Flegrei.

MATERIALS AND METHODS

Site Description

"Secca delle Fumose" (SdF) belongs to the largest degassing structure offshore of the Campi Flegrei caldera. With an extension of approximately 0.14 km^2, is located about 800 m off the coastline in the north-western part of Pozzuoli Bay (Gulf of Naples, Italy) (40°49′23 ″N 14°05′15″E) (Tedesco et al., 1990; Passaro et al., 2013; Di Napoli et al., 2016). In this area, four sampling sites were selected (**Figure 1**), two control sites (CN; CS) and two in proximity of very different vents: a first characterized by white bacterial mats (H) and a second by yellow substrate around a solitary geyser opening (G). The control sites were distant about 65 m each other and 100 m away, in the hydrothermal area, the other two sites were sampled at the same distance from each other.

Sampling Collection and Analytical Procedures

In each site (H, G, CN, and CS) in November 2016, environmental parameters were measured (temperature and pH) and samples for interstitial water chemistry, grain size, total organic carbon (TOC) and sediment macrofauna were collected in triplicate.

Sediment temperature was measured *in situ* by means of an underwater thermometer. Water samples at water/sediment interface were collected for pH evaluation (pH/ORP Meter, HI98171, and probe HI 1230, Hanna instr.). Interstitial water (20 ml) for ions and metals determination was sampled using syringes and kept frozen until analyses; sediment samples were collected for the grain size and TOC analysis, by means

TABLE 1 | Environmental condition of the study area. Data were expressed as percentages or averaged (±S.D.) among three replicates at each site (H; G; CN; CS).

VARIABLES		H	G	CN	CS
Sediment variables					
Temperatures (°C)		37.53 ± 2.28	29.1 ± 2.81	21.8	21.8
pH		7.56 ± 0.05	8	8.1	8.1
TOC (%)		34.78	30.03	17.05	18.14
Gravel (%)		7.41	13.96	17.84	21.52
Sand (%)		90.12	83.40	79.60	76.67
Mud (%)		2.47	2.64	2.57	1.81
Interstitial water variables					
Ions (*ppm*)	Na^+	8668.260 ± 4.5	9973.210 ± 10.5	10776.925 ± 12.5	11120.825 ± 18.7
	Cl^-	19512.965 ± 20.5	23726.385 ± 15.7	26039.500 ± 17.5	25976.560 ± 18.6
	K^+	317.855 ± 7.6	426.340 ± 10.2	407.405 ± 8.5	399.125 ± 6.2
	Mg^{2+}	805.000 ± 7.3	954.705 ± 3.8	1219.475 ± 8.8	1179.500 ± 5.2
	Ca^{2+}	327.500 ± 8.3	472.200 ± 9.5	503.290 ± 9.2	385.725 ± 7.3
	NO_3^-	28.77 ± 0.06	25.50 ± 0.06	26.07 ± 0.03	25.68 ± 0.32
	SO_4^{2-}	3152.300 ± 3.6	2658.500 ± 6.5	3369.880 ± 3.1	3888.500 ± 5.9
	S^{2-}	<lod	130.58	<lod	<lod
Metals (*ppb*)	Zn	33.66 ± 0.51	34.56 ± 3.86	39.09 ± 0.50	33.55 ± 0.50
	Pb	62.02 ± 0.16	31.29 ± 0.52	18.31 ± 0.60	60.02 ± 0.71
	Cd	4.42 ± 0.19	<lod	<lod	4.42 ± 0.18
	Cu	<lod	8.88 ± 0.21	5.25 ± 0.21	<lod

lod (limit of detection): 2 ppm for S^{2-}; 0.8 ppb for Cd; 0.1 ppb for Cu.

of a cylindrical corer (5.5 cm diameter) pushed 10 cm into the sediment.

In the laboratory, interstitial water was filtered with cellulose filters (0.20 μm) and treated with H_2O_2 (100 μl in 10 ml of sample) for the digestion of organic content; samples were then fractioned in two aliquots for ions and metals determination.

For the analysis of major ions concentration, interstitial water samples were analyzed through ICS1100 ion chromatographic system, equipped with a double column system for simultaneous analyses of both anions and cations (Chianese et al., 2019); anions were detected with an AS22 column working with a cell volume of 100 μl and a solution 3.5 mM of sodium carbonate/bicarbonate as eluent, while cations were determined with a CS12A column working with a cell volume of 25 μl and 20 mM methanesulfonic acid solution as eluent. For both anions and cations, calibration curves were calculated using certified multistandard solutions; anions and cations detectable with this method are respectively: Cl^-, F^-, Br^-, NO_2^-, NO_3^-, PO_4^{3-}, SO_4^{2-} (as inorganic species), $HCOO^-$, CH_3COO^-, $C_2O_4^{-2}$ (as organic species) and Li^+, Na^+, K^+, NH_4^+, Ca^{2+}, and Mg^{2+}. In addition the S^{2-} ion was estimated using a chromatographic method, converting it in sulfate ion after oxidation with H_2O_2. Heavy metals (Pb, Cd, Cu, and Zn) were estimated by means of a polarographic method, with a Metrohm 797 VA Computrace; this system uses a multimode working Mercury electrode and an Ag/AgCl electrode as reference. Using this method, metals that are soluble in mercury such as zinc, cadmium, lead, and copper are simultaneously determinable (Chianese et al., 2019). Also in this case, calibration curves were calculated using certified multistandard solutions.

For the grain size analysis (Eleftheriou and McIntyre, 2008), sediment was sieved over a series of 11 sieves with mesh size ranging from 1 cm to 63 μm. Fractions were dried in oven at 60°C for 48 h and weighed; data were expressed as percentages of the total sediment dry weight, differencing it in three size classes: gravel (>2 mm), sand (2 mm <Ø> 0.063 mm), and mud (<0.063 mm). TOC was determined according to Schumacher (2002) and expressed as% of sediment.

As for macrofauna community, samples were collected at each site by scuba-diving operators using an air-lift pump equipped with a 0.5 mm nylon mesh size bag (Benson, 1989; Chemello and Russo, 1997) within a 50 cm × 50 cm frame, reaching a depth of 10 cm in the sediment. In the laboratory, the samples were fixed in 70% ethanol and macrofauna was sorted and analyzed under a stereomicroscope. Macrofauna organisms were analyzed up to the lowest taxonomic level, when possible, and their identification was cross-checked with the World Register of Marine Species (WoRMS Editorial Board, 2018).

Data Analysis

Multivariate ordination by principal component analysis (PCA) was performed on normalized environmental variables in order to determine their distribution patterns among the four sampling sites.

Sinecological indices, such as number of individuals (N) *per* 25 dm^3, species richness (SR), Shannon-Weaver diversity (H′: $\log_2$) and Pielou's evenness (J) were calculated based on three replicate samples for each site. The quantitative (DI, percentage of individuals of a given species upon total individuals collected in the sample) and qualitative dominances (DQ, percentage of species of a given taxon upon the total of species collected in the sample) were also calculated. Differences of sinecological variable among sites were detected by permutational analysis of variance (PERMANOVA; Anderson, 2001a), based on Euclidean distance (Terlizzi et al., 2007). A one-way experimental design with $n = 3$ was involved with the fixed factor Site (four levels). PERMANOVA analysis, based on Bray–Curtis similarity, was also performed in order to assess differences in the structure of community assemblages among sites. 4999 permutations were always applied (Anderson, 2001b) and a PERMANOVA pairwise *t*-test was used in order to evaluate differences between pairs of sites. Prior to analysis, data were log (x + 1) transformed (Clarke and Warwick, 2001) in order to normalize the data.

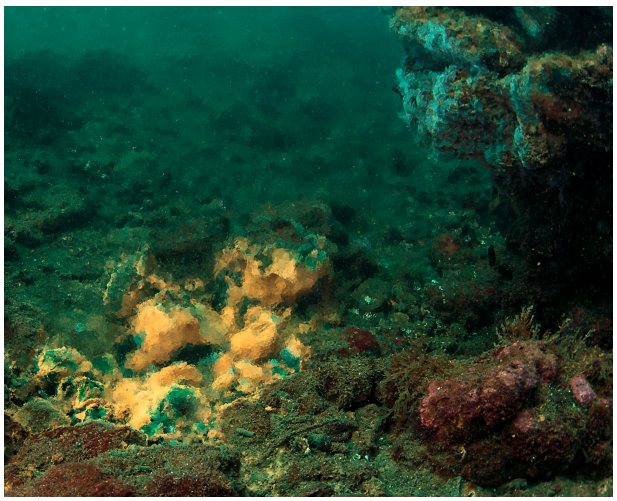

FIGURE 2 | The hydrothermal geyser with surrounding rocky substrate covered by yellow sulfur deposits.

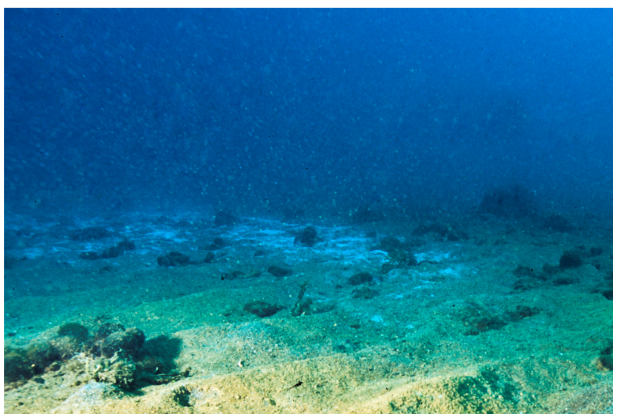

FIGURE 3 | Hydrothermal site with soft bottom covered by a white microbial mat.

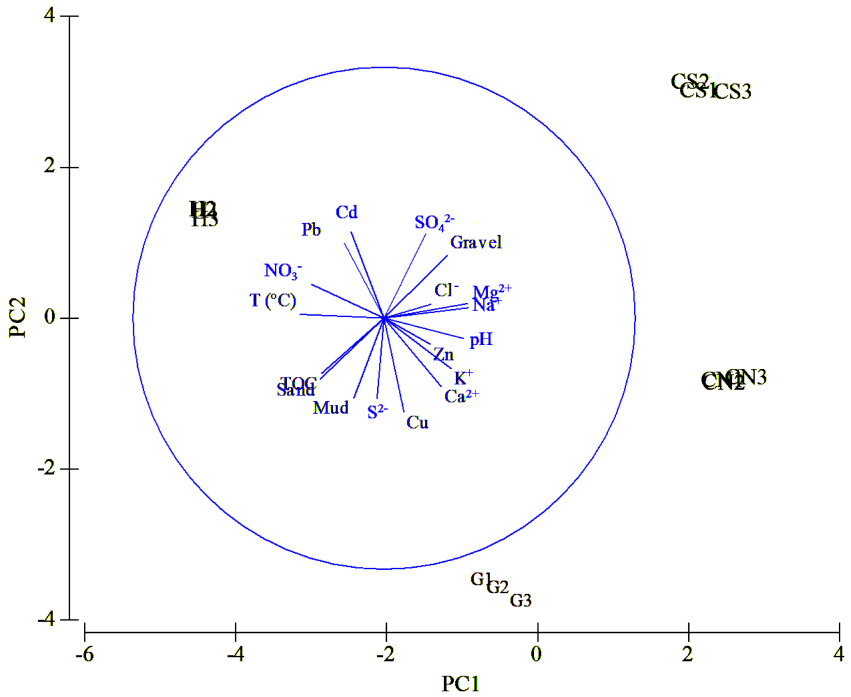

FIGURE 4 | Ordination of environmental variables at the four sites of the Secca delle Fumose using PCA.

To examine the structural variation of benthic communities among sites, canonical analysis of principal coordinates (CAP; Anderson and Willis, 2003) was used and similarity percentage (SIMPER) was calculated among the replicates for each site and, then, it was applied to identify those species that contributed more to the similarity among sites. Only species that cumulatively contributed to 50% to similarity were considered.

Relationships between macrobenthic community composition and environmental variables were tested by distance-based linear modeling analysis routine (distLM, Anderson, 2004). The aim was to identify which variables were mostly related with assemblages and to better explain the biological pattern among sites. Then, distance based redundancy analysis (dbRDA, Legendre and Anderson, 1999) was used to visualize the influence of variables identified by distLM. For distLM analysis, interstitial water variables, expressed in *ppm* and *ppb*, were $\log_{10}$ transformed to better compare different scales (Underwood, 1997). All multivariate analyses were undertaken using the PRIMER-PERMANOVA + v.6 software package (Anderson et al., 2008).

RESULTS

Environmental Variables

Environmental characteristics of SdF are summarized in **Table 1**. A solitary hydrothermal vent (geyser) at G site is present at 10 m depth. The vent opening was about 10 cm in diameter; the hydrothermal fluid temperature reaches ∼80°C at the outlet, while a lower temperature (29.1 ± 2.81°C) and a moderate pH value (8) occurred in the sediment at a distance of 20 cm from the vent center. Rocky substrate surrounding the geyser was covered by yellow sulfur deposits (**Figure 2**), while soft substrate among the rocks presented a TOC content of 30.03%. Interstitial water had a sulfur ion S^{2-} concentration of 130.58 *ppm*. Here, the most abundant ions were sulfate SO_4^{-2} , with a concentration of 2658.500 ± 6.5 *ppm*, and Mg, with a concentration of 954.705 ± 3.8 *ppm*, furthermore, relevant values of metals such as Zn (34.56 ± 3.86 *ppb*) and Pb (31.29 ± 0.52 *ppb*) were detected. About 1 m from the vent, where macrofauna was collected, the sediment was composed by sand (83.40%), gravel (13.96%), and mud (2.64%).

The H site was approximately 65 m from the G site, at a depth of 14 m. The sediment temperature was about 37.53 ± 2.28°C and the pH value 7.56 ± 0.05, indicating an acidified condition, where some gas bubbling occurred. This site was characterized by a soft bottom covered by a white microbial mat (**Figure 3**), with a TOC content of 34.78%. Sediment was mainly composed by sand (90.12%), gravel (7.41%) and mud (2.47%), while interstitial water showed the highest mean value of NO_3^- (28.77 ± 0.06 *ppm*) respect to the other sites, and a high mean value of Pb (62.02 ± 0.16 *ppb*) among metals.

The two control sampling sites (CN and CS) were located respectively to the north and south of Roman pillars and 100 m from G and H at a depth of 9.8 and 12.1 m respectively. In these sites, the gas emissions and the white microbial mat were absent, while the sediment temperature of 21.8°C was comparable to that of sea water column; the pH values (average 8.1) were within the range of normal conditions. The content of the TOC in the sediment varied from 17.05 to 18.14%. The

sediment grain size was characterized by a high percentage of sand (CN 79.60%; CS 76.67%) and a lower content of gravel (CN 17.84%; CS 21.52%) and mud (CN 2.57%; CS 1.81%). High concentrations of heavy metals occurred in the interstitial water in both sites: the CN site was mainly characterized by a Zn content of 39.09 ± 0.50 *ppb*, while CS by Pb concentrations of 60.02 ± 0.71 *ppb*. This latter site presented also the highest mean value of SO_4^{2-} (3888.500 ± 5.9 *ppm*).

The sediment quality characteristics from sampling sites were shown by multivariate PCA (**Figure 4**). In particular, PC1 accounted for 47.5% of variation among sites, and PC1 and PC2 together accounted for 84.5% (**Table 2**). Along the PC1 axis, hydrothermal vent sites (H and G) were separated from the control sites (CN and CS), according to temperature and ion NO_3^-, that were high at the active sites; on the contrary other ions (e.g., Mg^{2+}; Na^+) and pH, were high at control sites (**Figure 4** – PC1). Along the PC2 axis, the graph showed a clear separation between southern (H and CS) and northern (G and CN) sites; the former sites were displaced on the graph according to heavy metals content such as Cd and Pb and the SO_4^{2-} ion; the latter sites according to Cu, S^{2-} ion and% of mud (**Figure 4** – PC2).

Macrofauna Diversity and Community Structure

A total number of 1,954 individuals, belonging to 164 taxa grouped in eight macrobenthic groups, were classified to

TABLE 2 | Principal component loadings for hydrothermal and control sites from PCA of environmental data from four sites sampled at the Secca delle Fumose hydrothermal zone.

PC	Eigenvalues	%Variation	Cum.%Variation
1	**8.54**	**47.5**	**47.5**
2	**6.66**	**37**	**84.5**
Environmental variables		**PC1**	**PC2**
pH		**0.317**	−0.081
T (°C)		**−0.335**	0.015
TOC (%)		−0.250	−0.221
Na^+		**0.337**	0.041
Cl^-		0.189	0.056
Ca^{2+}		0.229	−0.274
K^+		0.269	−0.202
Mg^{2+}		**0.333**	0.058
NO_3^-		**−0.290**	0.135
SO_4^{2-}		0.167	**0.337**
S^{2-}		−0.028	**−0.322**
Zn		0.185	−0.104
Pb		−0.159	**0.299**
Cd		−0.132	**0.345**
Cu		0.080	**−0.376**
Gravel (%)		0.253	0.251
Sand (%)		−0.256	−0.244
Mud (%)		−0.120	**−0.319**

Bold values were considered high (≥ |0.290|).

TABLE 3 | Taxonomic list of total fauna occurring at Secca delle Fumose, with abundance (N) of each taxon at each site (H - White hydrothermal vent; G - Geyser; CN - Control North; CS - Control South).

TAXA	H	G	CN	CS
Nemertea	–	–	5	–
Sipuncula	–	71	58	477
Polychaeta				
Amphictene auricoma (O. F. Müller, 1776)	–	–	1	–
Aphelochaeta marioni (Saint-Joseph, 1894)	–	–	7	–
Aphelochaeta multibranchis (Grube, 1863)	–	–	4	–
Aponuphis bilineata (Baird, 1870)	1	3	26	53
Capitella capitata (Fabricius, 1780)	4	–	–	–
Chrysopetalum debile (Grube, 1855)	–	–	1	1
Dialychone acustica (Claparède, 1870)	–	–	9	–
Diplocirrus glaucus (Malmgren, 1867)	–	–	1	–
Drilonereis filum (Claparède, 1868)	–	–	1	–
Eteone longa (Fabricius, 1780)	–	–	4	–
Euclymene oerstedi (Claparède, 1863)	–	–	5	–
Eulalia sp.	–	–	3	2
Eunice pennata (Müller, 1776)	–	–	–	45
Eunice vittata (Delle Chiaje, 1828)	–	11	81	16
Exogone sp.	–	–	3	–
*Glycera unicornis (*Lamarck, 1818)	–	–	12	2
Harmothoe longisetis (Grube, 1863)	–	2	2	3
Hesionidae indet.	–	–	7	–
Hydroides dianthus (Verrill, 1873)	–	1	–	–
Hydroides uncinata (Phillipi, 1844)	–	–	1	–
Laonice cirrata (M. Sars, 1851)	–	–	1	–
Lepidonotus clava (Montagu, 1808)	–	–	–	2
Levinsenia gracilis (Tauber, 1879)	–	–	7	–
Lumbrineris latreilli (Audouin and Milne-Edwards, 1834)	–	–	7	–
Lysidice unicornis (Grube, 1840)	–	4	4	20
Malmgrenia andreapolis (McIntosh, 1874)	–	–	3	–
Mysta picta (Quatrefages, 1866)	–	–	7	–
Neanthes kerguelensis (McIntosh, 1885)	–	–	–	5
Nereis rava (Ehlers, 1868)	–	6	14	–
Notomastus latericeus (Sars, 1851)	–	1	6	1
Owenia fusiformis (Delle Chiaje, 1844)	–	–	20	–
Perinereis cultrifera (Grube, 1840)	–	7	–	–
Phyllodoce lineata (Claparède, 1870)	–	–	5	–
Pista cristata (Müller, 1776)	–	–	18	–
Platynereis dumerilii (Audouin and Milne Edwards, 1833)	–	1	9	–
Pontogenia chrysocoma (Baird, 1865)	–	–	–	1
Protocirrineris chrysoderma (Claparède, 1868)	–	–	4	–
Protodorvillea kefersteini (McIntosh, 1869)	–	–	9	–
Pseudoleiocapitella fauveli (Harmelin, 1964)	–	–	1	–
Sabellidae indet.	–	–	4	–
Serpula vermicularis (Linnaeus, 1767)	–	3	1	–
Sigambra tentaculata (Treadwell, 1941)	–	–	3	–
Spio filicornis (Müller, 1776)	1	–	–	–
Spiophanes bombyx (Claparède, 1870)	1	–	–	–
Spirobranchus triqueter (Linnaeus, 1758)	–	5	–	–
Sthenelais limicola (Ehlers, 1864)	–	–	–	1
Syllidae indet.	–	–	16	3
Polyplacophora				
Acanthochitona crinita (Pennant, 1777)	–	–	–	1
Acanthochitona fascicularis (Linnaeus, 1767)	–	–	1	1

(Continued)

TABLE 3 | Continued

TAXA	H	G	CN	CS
Callochiton septemvalvis (Montagu, 1803)	–	1	–	–
Leptochiton scabridus (Jeffreys, 1880)	–	–	1	–
Lepidochitona sp.	–	1	10	21
Gastropoda				
Alvania cancellata (da Costa, 1778)	–	1	–	–
Alvania discors (Allan, 1818)	1	3	1	–
Alvania lineata (Risso, 1826)	–	5	–	–
Alvania pagodula (Bucquoy, Dautzenberg, and Dollfus, 1884)	–	–	–	1
Aplysia parvula (Mörch, 1863)	–	–	–	1
Ascobulla fragilis (Jeffreys, 1856)	–	–	1	6
Bela nebula (Montagu, 1803)	–	–	1	–
Bittium latreillii (Payraudeau, 1826)	–	5	1	9
Bolma rugosa (Linnaeus, 1767)	–	–	–	1
Bulla striata (Bruguière, 1792)	–	1	–	–
Caecum auriculatum (de Folin, 1868)	–	1	–	6
Caecum glabrum (Montagu, 1803)	–	–	1	–
Caecum sp.	–	–	–	26
Caecum trachea (Montagu, 1803)	–	–	1	4
Calyptraea chinensis (Linnaeus, 1758)	–	1	3	8
Cerithium vulgatum (Bruguière, 1792)	–	1	1	1
Chrysallida indistincta (Henn and Brazier, 1894)	–	–	–	1
Eulimella sp.	–	–	1	–
Euspira nitida (Donovan, 1804)	–	–	1	–
Fusinus sp.	–	–	–	3
Gibbula ardens (Salis Marschlins, 1793)	–	1	1	–
Gibbula fanulum (Gmelin, 1791)	–	–	–	1
Gibbula guttadauri (Philippi, 1836)	–	–	3	1
Gibbula sp.	–	–	1	–
Haminoea sp.	1	–	–	10
Hexaplex trunculus (Linnaeus, 1758)	–	–	–	5
Mangelia costulata (Risso, 1826)	–	–	2	–
*Mangelia scabrida (*Monterosato, 1890)	–	1	–	–
Manzonia crassa (Kanmacher, 1798)	–	–	1	–
Odostomia sp.	–	–	–	1
Ondina vitrea (Brusina, 1866)	–	–	2	–
Philine sp.	–	–	1	4
Rissoa splendida (Eichwald, 1830)	–	–	1	–
Tectura virginea (O. F. Müller, 1776)	–	–	1	–
Tritia cuvierii (Payraudeau, 1826)	8	15	–	–
Tritia incrassata (Strøm, 1768)	–	7	–	–
Pusia savignyi (Payraudeau, 1826)	–	–	–	2
Pusia tricolor (Gmelin, 1791)	–	–	–	1
Vitreolina sp.	–	–	–	1
Weinkauffia turgidula (Forbes, 1844)	–	–	–	1
Williamia gussoni (Costa O. G., 1829)	–	–	–	2
Bivalvia				
Arca noae (Linnaeus, 1758)	–	1	–	1
Asbjornsenia pygmaea (Lovén, 1846)	–	–	10	–
Cardites antiquatus (Linnaeus, 1758)	–	–	–	3
Centrocardita aculeata (Poli, 1795)	–	–	2	2
Centrocardita sp.	–	1	28	24
Ctena decussata (O. G. Costa, 1829)	–	–	4	9
Dosinia exoleta (Linnaeus, 1758)	–	–	1	–
Flexopecten hyalinus (Poli, 1795)	–	–	1	–
Gari costulata (W. Turton, 1822)	–	–	5	2
Gari tellinella (Lamarck, 1818)	–	–	1	–
Glans trapezia (Linnaeus, 1767)	–	–	1	10
Gouldia minima (Montagu, 1803)	–	1	5	21
Gregariella semigranata (Reeve, 1858)	–	12	1	9
Hiatella arctica (Linnaeus, 1767)	–	40	5	71
Kurtiella bidentata (Montagu, 1803)	–	–	17	8
Laevicardium crassum (Gmelin, 1791)	–	–	1	–
Limaria tuberculata (Olivi, 1792)	–	1	1	–
Loripinus fragilis (Philippi, 1836)	–	–	1	2
Lucinella divaricata (Linnaeus, 1758)	–	–	1	–
Modiolula phaseolina (Philippi, 1844)	–	–	1	–
Moerella donacina (Linnaeus, 1758)	–	–	5	2
Musculus costulatus (Risso, 1826)	–	–	7	–
Musculus subpictus (Cantraine, 1835)	–	–	4	3
Papillicardium papillosum (Poli, 1791)	–	–	1	–
Peronidia albicans (Gmelin, 1791)	–	–	–	1
Polititapes aureus (Gmelin, 1791)	–	–	13	5
Rocellaria dubia (Pennant, 1777)	–	2	1	3
Striarca lactea (Linnaeus, 1758)	–	5	3	11
Thracia villosiuscula (MacGillivray, 1827)	–	–	1	–
*Venus verrucosa (*Linnaeus, 1758)	–	8	7	14
Amphipoda				
Ampithoe ramondi (Audouin, 1826)	–	–	1	–
Apherusa chiereghinii (Giordani- Soika, 1949)	–	–	1	–
Caprellidae	–	–	–	4
Dexamine spinosa (Montagu, 1813)	–	–	3	7
Gammarus sp.	–	–	2	9
Microdeutopus anomalus (Rathke, 1843)	–	–	1	–
Microdeutopus spp.	–	–	2	1
Pereionotus testudo (Montagu, 1808)	–	–	6	12
Pseudolirius kroyeri (Haller, 1897)	–	–	1	–
Perioculodes sp.	1	–	–	–
Decapoda				
Alpheus glaber (Olivi, 1792)	–	1	–	–
Anapagurus bicorniger (A. Milne-Edwards and Bouvier, 1892)	–	2	13	5
Athanas nitescens (Leach, 1813)	–	2	–	–
Clibanarius erythropus (Latreille, 1818)	–	4	–	–
Ebalia deshayesi (Lucas, 1846)	–	–	1	5
Eriphia verrucosa (Forskål, 1775)	–	1	–	–
Galathea sp.	–	2	–	3
Lysmata seticaudata (Risso, 1816)	–	–	2	–
Necallianassa truncata (Giard and Bonnier, 1890)	–	–	1	–
Paguristes eremita (Linnaeus, 1767)	–	–	–	1
*Pagurus cuaensis (*Bell, 1844)	–	3	–	–
Pagurus sp.	1	–	–	–
Pisa armata (Latreille, 1803)	–	–	–	1
*Processa macrophthalma (*Nouvel and Holthuis, 1957)	–	1	–	1
*Sirpus zariquieyi (*Gordon, 1953)	–	–	1	2
Synalpheus gambarelloides (Nardo, 1847)	–	–	1	–
Upogebia stellata (Montagu, 1808)	–	2	–	–
*Xantho pilipes (*A. Milne-Edwards, 1867)	–	4	–	–
Isopoda				
Anthuridae	–	–	3	16
Cymodoce truncata (Leach, 1814)	–	1	14	7
Kupellonura mediterranea (Barnard, 1925)	–	1	2	–

(Continued)

TABLE 3 | Continued

TAXA	H	G	CN	CS
Tanaidacea				
Chondrochelia savignyi (Kroyer, 1842)	–	–	2	10
Cumacea				
ind.	–	–	5	–
Echinoidea				
Echinocyamus pusillus (O. F. Müller, 1776)	–	–	7	7
Holothuroidea				
indet.	–	–	2	2
Ophiuroidea				
Ophiothrix sp.	–	1	–	3
Amphipholis sp.	–	3	4	11
Platyhelminthes	–	–	1	–
Chordata				
Branchiostoma lanceolatum (Pallas, 1774)	–	–	6	1

Dashes indicate absence.

different taxonomic levels as follows: Mollusca (610 ind.), Sipuncula (606 ind.), Polychaeta (513 ind.), Crustacea (172 ind.), Echinodermata (40 ind.), Chordata (7 ind.), Nemertea (5 ind.), and Platyhelminthes (1 ind.) (**Table 3**). The whole benthic community drastically increased in abundance and species richness away from the vent sites (H: DI = 0.97% – DQ = 5.49%; G: DI = 13.20% – DQ = 29.88%) to control sites (CN: DI = 31.58% – DQ = 68.29%; CS: DI = 54.25% – DQ = 48.78%).

The main taxa structuring the benthic community were Mollusca, Sipuncula, Polychaeta and Crustacea, reaching a dominance of 97.28%. With the only exception of Sipuncula, three taxa were detected at all sites, differentially contributing to the communities living at each site (**Figure 5**).

Mollusca showed the highest species richness, being represented by 76 species, belonging to the classes Polyplacophora, Gastropoda, and Bivalvia. Bivalvia was the dominant group in term of abundance (**Figure 5A**), with 400 individuals (65.57%) belonging to 30 species (39.47%). Gastropods were the dominant group in term of species richness (**Figure 5B**), with 41 species (53.94%) and an abundance of 173 individuals (28.36%). Polyplacophores were poorly represented, both in abundance (37 ind.; 6.06%) and species richness (5 sp.; 6.57%).

The highest percentage of mollusks abundance mainly occurred in the control site CS (52.46%), where bivalves were mainly represented by the species *Hiatella arctica* (76 ind.), gastropods by *Caecum* sp. (26 ind.) and polyplacophores by *Lepidochitona* sp. (31 ind.). On the other hand, the lowest percentage of mollusks occurred in H (DI 1.64%) with only three species: *Tritia cuvierii* (8 ind.), *Haminoea* sp. (1 ind.), and *Alvania discors* (1 ind.).

Polychaeta, with a total of 513 individuals belonging to 47 species, were mainly represented by the species *Eunice vittata* (108 ind., 21.05%) and *Aponuphis bilineata* (83 ind., 16.18%). This group was dominant in the control site CN (**Figures 5C,D**), both in abundance (307 ind., 59.84%) and in species richness (36 sp., 76%). The opposite occurred in H, where a total of only seven individuals belonging to four species, among which four individuals of the polychaete *Capitella capitata*, were recorded.

Crustacea were represented by 172 individuals belonging to 33 species, grouped in five orders: Decapoda, Isopoda, Tanaidacea, Amphipoda, and Cumacea. Only five species, represented by the decapod *Anapagurus bicorniger*, the amphipods *Dexamine spinosa* and *Pereionotus testudo*, the isopods *Cymodoce truncata* and Anthuridae indet., reached a dominance of 52.35% of the total crustacean assemblage. The highest percentage of crustaceans individuals was detected in CS (84 ind., 48.84%; **Figure 5E**) and species richness in CN (20 sp., 60.61%; **Figure 5F**), while only 2 species, the decapod *Pagurus* sp. and the amphipod *Perioculodes* sp., occurred in H with only 1 individual.

Among the sinecological indices (**Table 4**), the highest density (N) and species richness (SR) values were recorded in CN and CS, while the lowest values in H, which also showed the lowest values of diversity (H′) and evenness (J). For each index, PERMANOVA test highlighted significant differences among sites, except for Pielou's evenness (J) (**Table 4**). A significant difference was also detected analyzing macrofauna composition (PERMANOVA: $F = 3.411$, $p = 0.0004$). In particular, pairwise comparisons showed differences between hydrothermal vents (G; H) and non-vents (CN; CS) sites, with the highest average similarity among these latter sites (Average similarity 38.30%; **Table 5**). These differences were also evident in the plot of CAP analysis (**Figure 6**), where the three replicates formed consistent clusters for each site. Along the CAP1 axis, vent sites (H and G) were separated from control ones (CN and CS), while along the CAP2 axis the graph showed a clear separation between the southern (H and CS) and northern (G and CN) sites. In particular, H and G were strongly polarized respectively in the positive and negative part of CAP2, while CN and CS were aggregated around the zero value of CAP2, respectively in the positive and negative part. The average multivariate similarity of macrofaunal assemblage composition for each site ranged from 11.94 to 59.92% (**Table 6**), while the similarity of dominant species among sites was 19.62%, attributable to sipunculans, mollusks, and polychaetes (**Table 7**).

Relationship Between Environmental Variables and Macrobenthic Community

The pattern of community structure was significantly correlated with some environmental parameters of sediments and interstitial waters (**Table 8**) and visualized in the dbRDA (**Figure 7**), where vectors indicate the direction of increasing influence of each variable on community changes.

Concerning the first group of variables (**Table 8A** – Marginal tests), gravel, sand, pH, temperature, and TOC explained a significant variation in benthic community when tested individually. In particular, only gravel and pH represented the most important driving factors influencing benthic community distribution among sites (**Table 8A** – Sequential tests), explaining 52.76% of community variation.

As for interstitial water variables, all the investigated ions, with the only exception of S^{2-} in the site G, had a significant effect on community variability (**Table 8B** – Marginal tests), even

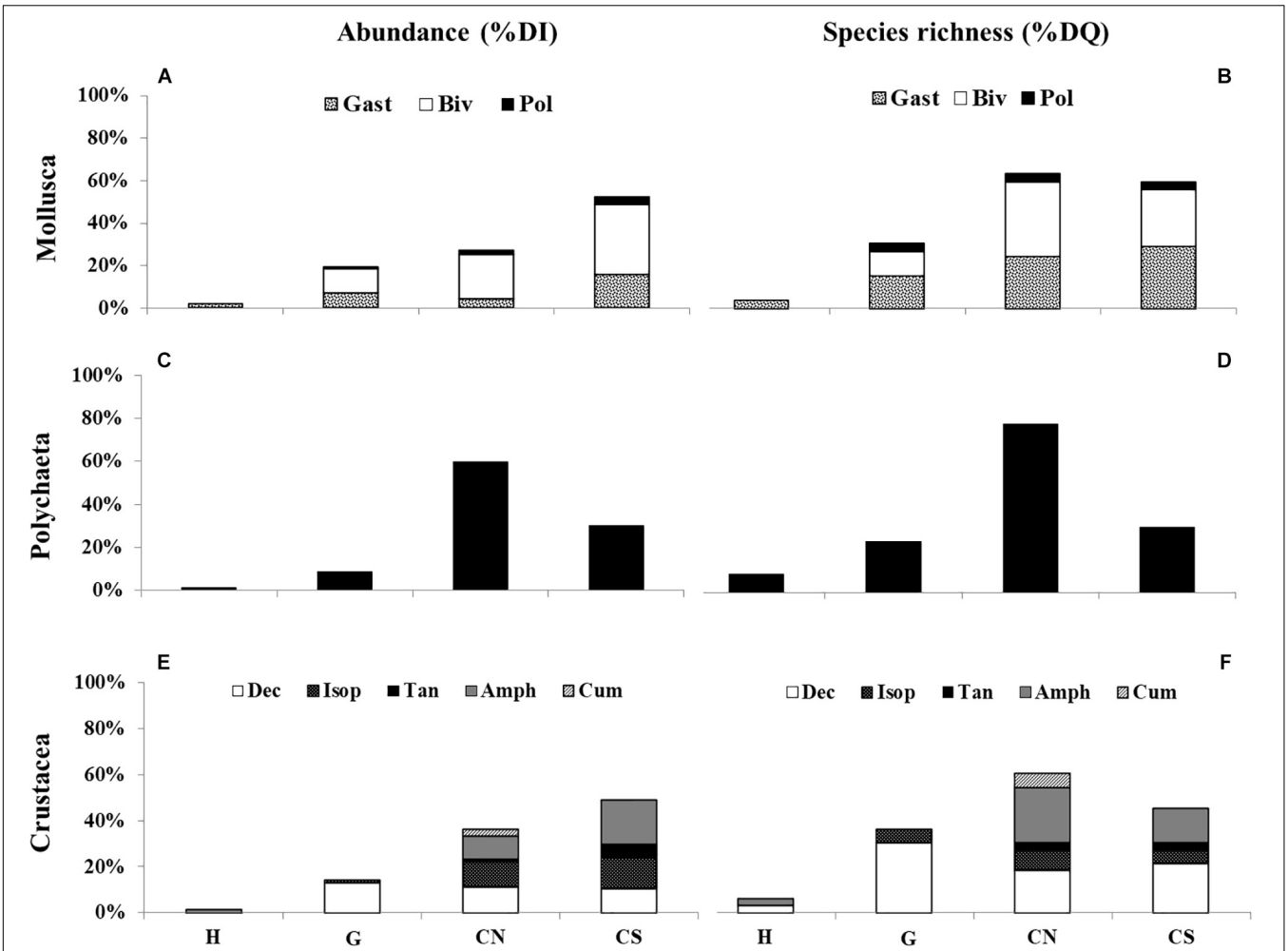

FIGURE 5 | Total contribution to quantitative (Abundance -%DI) and qualitative (Species richness -%DQ) dominances of three taxonomic groups: Mollusca [**(A,B)** Gastropoda (Gast); Bivalvia (Biv); Polyplacophora (Pol)], Polychaeta **(C,D)** and Crustacea [**(E,F)** Decapoda (Dec); Isopoda (Isop); Tanaidacea (Tan); Amphipoda (Amph); Cumacea (Cum)] for each site (H; G; CN; CS).

though the greatest influence was due to the Mg^{2+}, K^{2+}, and Ca^{2+} ions (**Table 8B** – Sequential tests), which explained 56.63% of community variation.

TABLE 4 | Macrofauna assemblage.

Site	SR	N	J	H′
H	3.33 ± 2.08	6.33 ± 5.03	0.56 ± 0.48	1.22 ± 1.07
G	24 ± 12.16	86 ± 50.68	0.78 ± 0.05	3.47 ± 0.82
CN	63 ± 5.29	205.66 ± 50.52	0.87 ± 0.01	5.23 ± 0.18
CS	51.33 ± 10.78	353.33 ± 107.77	0.64 ± 0.05	3.63 ± 0.37
F	29.31	16.314	0.958	16.28
p(perm)	0.0006	0.0004	0.473	0.001

Number of individuals (N) per 25 dm^3, species richness (SR), Shannon-Weaver diversity (H′) and Pielou's evenness (J) measured for each site (H; G; CN; CS) (mean ± SD), and results of PERMANOVA test on Euclidean distance [F: F-value, p(perm): calculated probability value, Unique perms: the number of unique permutations].

DISCUSSION

The hydrothermal vent system at Pozzuoli Bay provides an opportunity to study the macrobenthic assemblages and composition in a shallow extreme environment. Through this work, the macrobenthic community at Secca delle Fumose was investigated for the first time. The results highlighted a strong

TABLE 5 | Results of PERMANOVA pairwise comparisons among sites, using 4999 permutations, and average similarity between sites.

Site	*t*	Unique perms	*p*(MC)	Average similarity (%)
H, G	1.4325	10	0.1286	7.66
H, CN	1.9607	10	0.0344	0.75
H, CS	2.013	10	0.0378	1.28
G, CN	1.9645	10	0.038	18.83
G, CS	1.8827	10	0.0416	24.18
CN, CS	2.0479	10	0.0236	38.30

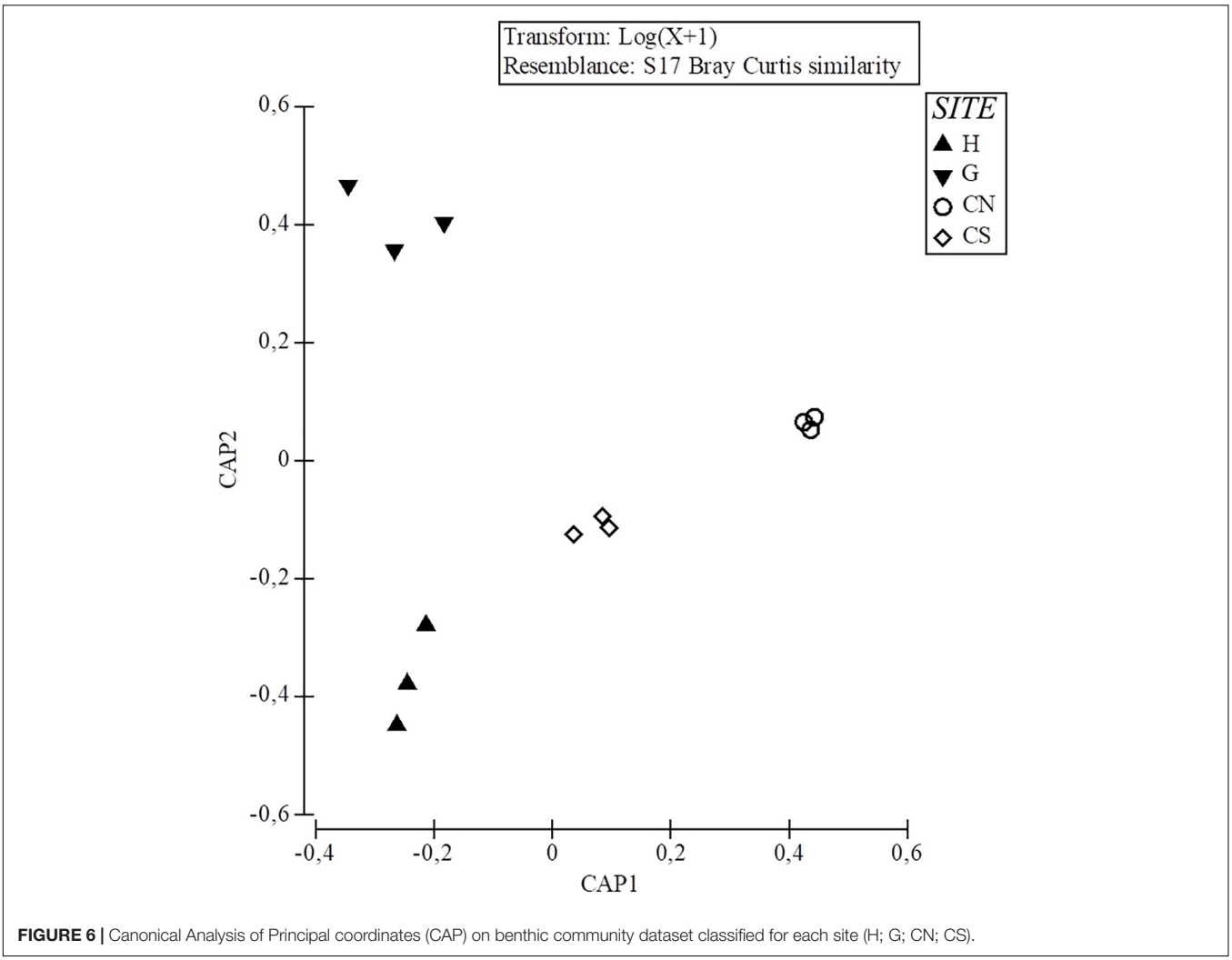

FIGURE 6 | Canonical Analysis of Principal coordinates (CAP) on benthic community dataset classified for each site (H; G; CN; CS).

change in density, species richness and diversity between two non-vent (CN and CS) and two different vent (H and G) sites.

When compared to the hydrothermal sites, the control sites showed higher abundance and species richness, and the environment was characterized by normal pH and ions concentrations (e.g., Ca^{2+}, K^{2+}, and Mg^{2+}), and by a significant percentage of gravelly sediment that markedly affected the macrobenthic composition (DistLM **Table 6**; dbRDA **Figure 7**).

It is well-known that benthic species are functionally and structurally related to the main features of the habitat they reside (e.g., Woodin, 1978; Thrush et al., 1991; Desprez, 2000; Riera et al., 2012; Donnarumma et al., 2018; Casoli et al., 2019). In particular, the taxa composition recorded in the control sites was consistent with a marked occurrence of gravel, which offers microhabitats suitable for settlement and refuge. This is also proven by the high dominance of the byssate bivalve *H. arctica*, which is commonly found on hard substrates, where become strictly aggregated in dense groups (Purchon, 1977). The occurrence of high abundance of gastropod *Caecum* spp. is probably due to the presence of sand in the sediment with only tracks of mud (Fretter and Graham, 1978). Species belonging to the genus *Eunice* (Annelida, Polychaeta) also occurred with a very high abundance in the control area, in agreement with their cosmopolitan nature (George and Hartmann-Schröder, 1985; Dounas and Koukouras, 1989; Gusso et al., 2001; Fauchald et al., 2009), as well as for the crevice-dwelling isopod *C. truncata* and sipunculans, capable of hiding in the narrow cracks of rocks and in empty or fragmented shells (Ferrero-Vicente et al., 2013).

In addition to the relationship between benthic assemblages and structural characteristics of the substrate, the understanding of environment state is also related to the occurrence of sensitive or tolerant species to the environmental changes (Simboura and Zenetos, 2002; Washburn et al., 2016). For instance, the high abundance of *C. truncata* restricted only in the control area might be related to the suitable habitat conditions, as reported for the normal pH conditions at Ischia Island by Cigliano et al. (2010). Conversely, the absence of this species at the geyser site (G) may be due to the crustaceans sulfide sensitivity (Gray et al., 2002), as well as its absence in the white hydrothermal vent (H) could be also related to the metabolic sensitivity of *C. truncata* to high pCO_2 condition (Turner et al., 2016).

TABLE 6 | Results of similarity of percentages test, showing dominant species mostly responsible for the similarity among replicates for each site (Cum%-50% cut-off).

Average similarity	Taxa	Av.Abund	Av.Sim	Sim/SD	Contrib%	Cum.%
CS – 59.92%	SIPUNCULA	5.04	6.97	12.35	11.63	11.63
	Hiatella arctica	3.07	3.75	9.60	6.25	17.88
	Aponuphis bilineata	2.77	3.33	3.49	5.56	23.44
	Centrocardita sp.	2.18	2.93	13.48	4.89	28.34
	Eunice pennata	2.44	2.65	1.32	4.43	32.77
	Lysidice unicornis	1.95	2.39	2.71	3.99	36.75
	Gouldia minima	1.97	2.25	9.98	3.75	40.51
	Lepidochitona sp.	1.87	1.89	5.46	3.15	43.66
	Amphipholis sp.	1.50	1.84	3.87	3.07	46.73
	Haminoea cf hydatis	1.44	1.81	8.19	3.02	49.75
CN – 54.53%	*Eunice vittata*	3.25	3.88	56.62	7.11	7.11
	SIPUNCULA	2.99	3.76	71.54	6.90	14.01
	Centrocardita sp.	2.30	2.81	5.43	5.14	19.16
	Aponuphis bilineata	2.19	2.50	57.02	4.59	23.75
	Owenia fusiformis	2.02	2.50	57.02	4.59	28.34
	Pista cristata	1.92	2.30	6.52	4.22	32.56
	Polititapes aureus	1.65	1.95	6.69	3.58	36.14
	Cymodoce truncata	1.69	1.94	56.62	3.55	39.69
	Glycera unicornis	1.57	1.85	13.34	3.39	43.08
	Hesionidae indet.	1.19	1.46	13.34	2.68	45.77
	Musculus costulatus	1.19	1.46	13.34	2.68	48.45
S – 32.10%	SIPUNCULA	2.93	8.68	5.96	27.05	27.05
	Hiatella arctica	2.23	4.49	1.59	13.99	41.04
H – 11.94%	*Tritia cuvierii*	1.07	11.94	0.58	100	100

Heavy metals (Zn, Cd, Pb, and Cu) occurred in the interstitial waters of sediments at all sampling sites (**Table 1**). However, their low quantity is compatible with the existence of a well-structured macrobenthic assemblage in the control sites, as reported in previous investigations (Bryan, 1976; Yoshida et al., 2002; Raghukumar et al., 2008). Moreover, the presence only in the control sites of the cephalochordate *Branchiostoma lanceolatum* attests to the good quality of the sites, since it is a species sensitive to organic enrichment and polluted water (Simboura and Zenetos, 2002; Rota et al., 2009).

TABLE 7 | Results of similarity of percentages test, showing taxa that mostly contributed to similarity among sites.

Taxa	Av.Abund	Av.Sim	Sim/SD	Contrib%	Cum.%
SIPUNCULA	2.74	2.98	1	15.19	15.19
MOLLUSCA					
Tritia cuvierii (Payraudeau, 1826)	0.6	1.44	0.26	7.34	22.53
Hiatella arctica (Linnaeus, 1767)	1.52	1.27	0.67	6.48	29.01
POLYCHAETA					
Aponuphis bilineata (Baird, 1870)	1.45	1.26	0.97	6.43	35.44
Eunice vittata (Delle Chiaje, 1828)	1.45	0.95	0.64	4.84	40.28
MOLLUSCA					
Centrocardita sp.	1.18	0.78	0.63	3.97	44.25
POLYCHAETA					
Lysidice unicornis (Grube, 1840)	0.87	0.69	0.74	3.52	47.76

Average similarity: 19.62%; Cum%-50% cut-off.

At the two hydrothermal sites (G and H), a drastic decrease of benthic biodiversity was observed. This can be mainly attributable to environmental conditions, in particular to presence of sulfide, high temperatures and seawater pH variations generated by volcanic activity. Moreover, as observed by Tarasov et al. (2005), the hydrothermal fluids in these sites produced a slight reduction of water salinity, measured as Na^+ and Cl^- ions.

Several studies (e.g., Thiermann et al., 1997; Tarasov et al., 1999; Dando, 2010) have reported a decrease of both density and diversity of benthic communities as corresponding to the occurrence of high temperatures and sulfide concentrations, leading to an increase of temperature- and/or sulfide-tolerant species. The same result was also found in the present study where high sediment temperatures and sulfide ions (S^{2-}) occurred at the geyser site (G), resulting in a 69% reduction of taxonomic richness and a 73% reduction in number of individuals compared to control sites. At this geyser site we observed the absence of obligate vent-associated species, which were previously reported for deep-sea vent systems (Tarasov et al., 2005 and reference therein; Schander et al., 2010; Stevens et al., 2015). Our data are consistent with results from other coastal shallow water hydrothermal vents (Dando, 2010; Bianchi et al., 2011). In particular, the fauna around the geyser at the Secca delle Fumose was composed by the most representative species inhabiting the 'background' area (e.g., the polychaetes *E. vittata* and *A. bilineata*,

TABLE 8 | DistLM results comparing benthic community data and environmental variables **(A,B)**.

VARIABLES	Marginal tests			Sequential tests			
	Pseudo-F	*p*	Proportion of variation explained	Pseudo-F	*p*	Proportion of variation explained	Cumulative variation
(A) Sediment variables							
Gravel (%)	3.3023	**0.0028**	0.24825	3.3023	**0.0024**	0.24825	0.24825
Sand (%)	3.3547	**0.0032**	0.2512	1.6102	0.0954	0.11409	0.36234
Mud (%)	1.5694	0.0956	0.13565	0	1	1.45E-15	0.36234
pH	3.408	**0.0068**	0.25418	2.7984	**0.0042**	0.16525	0.52759
Temperatures (°C)	4.7266	**0.0002**	0.32096	1.9971	0.0622	0.10486	0.63245
TOC (%)	3.1083	**0.0056**	0.23713	0.67269	0.7442	3.71E-02	0.6695
(B) Interstitial water variables							
Ca^{2+}	2.3312	**0.0258**	0.18905	2.3312	**0.0244**	0.18905	0.18905
K^{+}	3.2656	**0.0084**	0.24617	2.2943	**0.0274**	0.16474	0.35379
Mg^{2+}	4.5698	**0.0006**	0.31365	3.8457	**0.0014**	0.20979	0.56358
NO_3^-	3.3708	**0.009**	0.2521	1.0131	0.398	5.52E-02	0.61876
SO_4^{2-}	2.1855	**0.034**	0.17935	0.89609	0.5072	4.95E-02	0.6683
S^{2-}	1.7078	0.0796	0.14587	0.50382	0.8168	3.04E-02	0.69866
Zn	1.6187	0.1072	0.13932	1.3074	0.2978	7.42E-02	0.77289
Pb	1.6385	0.1018	0.14078	1.3553	0.302	7.07E-02	0.84356
Cd	1.4394	0.1482	0.12583	1.1787	0.3936	5.80E-02	0.90157
Cu	1.3934	0.1556	0.1223	0.76951	0.5662	4.28E-02	0.94438

Bold data are significantly different at α = 0.05.

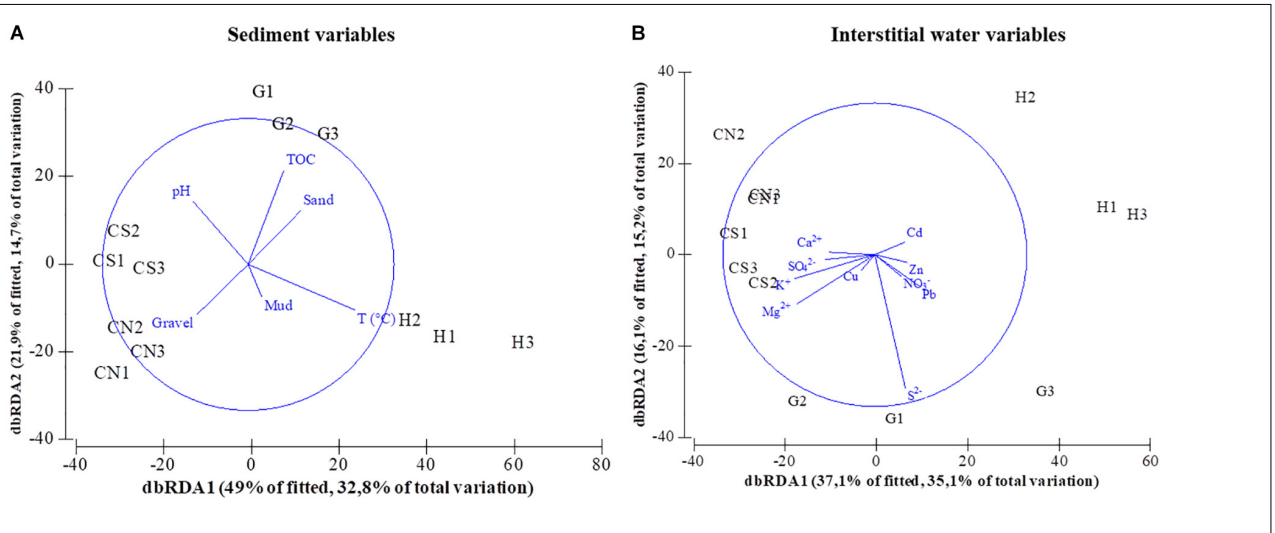

FIGURE 7 | dbRDA plot of benthic community structure fitted to sediment **(A)** and water variables **(B)**, showing each site replicated (H; G; CN; CS).

the bivalves *H. arctica* and *Venus verrucosa*, the ophiuroid *Amphipholis* sp.), but with a very low number of individuals. This benthic assemblage may represent a "simplified" community as suggested by Dando (2010), who defined the living fauna around hydrothermal vent and cold seep sites as a subset of the background biota.

According to Thiermann et al. (1997), the harsh hydrothermal conditions drastically affect the macrobenthic composition, as also observed at the "white" hydrothermal site (H). Here, the lowest species richness (9 sp.) and abundance (19 ind.) are mainly due to the seawater acidification (pH ∼7.6), in agreement with Di Napoli et al. (2016) who recently detected acidic CO_2-rich fluids in the SdF area, and to the high sediment temperature (37.53 ± 2.28°C), that was almost the double of that detected in the control sites (21.8°C). These factors produced a reduction of 83.64% in taxonomic richness and 86.29% in number of individuals if compared with those found around the geyser and a reduction of 93.92 and 97.75% respectively if compared with control sites.

The dominant species in H site were the gastropod *T. cuvierii* (8 ind.) and the opportunistic polychaete *C. capitata* (4 ind.), while the other species, each occurring with only one individual,

could be considered very rare in the hydrothermal area. The occurrence of the vagile nassariid gastropod *T. cuvierii* and the sediment-dwelling polychaete *C. capitata* clearly underlines the faunal similarity of our study area with other shallow-water hydrothermal vents. Indeed, nassariid species *Tritia neritea* (= *Cyclope neritea* Linnaeus, 1758), was among the dominant organisms in hydrothermal vents off Milos in the Aegean Sea (Dando et al., 1995; Southward et al., 1997; Thiermann et al., 1997) and in the Papua New Guinea (Tarasov et al., 1999). Population density of nassarids species is often influenced by food availability (Zhao et al., 2011), similarly the high abundance of *T. cuvierii* in the white hydrothermal site (H) may be due to the high food source consisting in the microbial mat (Cardigos et al., 2005), so as also occurs for the congeneric species *T. neritea* in other vent systems. High TOC concentration in the sediment (**Table 1**) might represent a further food source of this gastropod. The organic enrichment could be responsible for the dominance of the opportunistic polychaete *C. capitata* (Grassle and Grassle, 1976), which is a tolerant species to high temperatures and sulfide concentrations (Gamenick et al., 1998a). This work does not address directly the genetics of *C. capitata* complex (Blake, 2009; Nygren, 2014) that is also reported in hydrothermal vents and sulfidic habitats (Gamenick et al., 1998a,b), nevertheless such complex of sibling species so as for gastropods (e.g., Colognola et al., 1986) will be the focus of future research on its genetic variation under the extreme environmental conditions occurring in the study area.

CONCLUSION

This work represents the first study describing the particular environmental conditions and species composition of macrofauna at the Secca delle Fumose shallow hydrothermal system, an easily accessible coastal area, to evaluate the biological responses in an extreme habitat (i.e., characterized by high temperature, sulfide concentration and low pH condition). The results showed that the studied macrobenthic community appears to be strongly driven by high sediment temperatures, by sulfide concentration around the geyser and by low pH value in the white microbial mat area with the occurrence of some CO_2 gas bubbling. These key factors led to a drastic reduction of biodiversity, compared to the surrounding non-vent area, highlighting the great importance of environmental state in structuring benthic systems. Future studies should also take into account other key elements of ecosystem functioning, such as meiofauna and microfauna communities, for a better understanding of the complex characteristics related to this very shallow extreme environment of the Campi Flegrei area.

DATA AVAILABILITY STATEMENT

This manuscript contains previously unpublished data. The name of the repository and accession number are not available.

ETHICS STATEMENT

The study present in the manuscript involve macrobenthos communities without endangered animal species.

AUTHOR CONTRIBUTIONS

DZ and RS conceived the study. LD wrote the manuscript. LD, LA, EB, RB, DZ, and RS provided samples from the field. EB and RB performed the samples pretreatment. EC provided chemical analysis. LD and RG provided taxonomic analysis. LD and LA performed statistical analysis. DZ, RS, and GR provided the sampling design and improved the manuscript. All the authors read, edited and approved the final manuscript.

FUNDING

Financial support was provided by the project "Prokaryote-nematode Interaction in marine extreme envirONments: a uniquE source for ExploRation of innovative biomedical applications" (PIONEER) funded by the Total Foundation and IFREMER (2016–2019), and by the project Boost Europe – ERC "Extreme marine nematoDes: moDel orgAnisms for a Journey toward the origin and Evolution of metazoan life in our changing planet" (EDDAJE) funded by the Brittany Region and IFREMER (2019).

ACKNOWLEDGMENTS

We are grateful to Soprintendenza of the Underwater Archeological Park of Baia (prot. 5667, 24/10/2016) for the authorization to sampling. We are thankful to Dr. Guido Villani for assistance during the underwater sampling and permission to use photos that enriched the manuscript. Thanks are also due to the diving center Centro SUB Pozzuoli (Guglielmo Fragale) for support field activities and Dr. Aurélie Tasiemski and Dr. Céline Boidin-Wichlacz for helping in sampling activities. We also thank the reviewers for the suggestions and comments. We are indebted to Dr. Jeroen Ingels (Florida State University) for useful discussions.

REFERENCES

Anderson, M., Gorley, R. N., and Clarke, R. K. (2008). *Permanova+ for Primer: Guide to Software and Statistical Methods: Primer-E Limited*, 1st Edn. Plymouth: PRIMER-E Ltd.

Anderson, M. J. (2001a). A new method for non-parametric multivariate analysis of variance. *Austral. Ecol.* 26, 32–46. doi: 10.1111/j.1442-9993.2001.01070.pp.x

Anderson, M. J. (2001b). Permutation tests for univariate or multivariate analysis of variance and regression. *Can. J. Fish. Aquat. Sci.* 58, 626–639. doi: 10.1139/f01-004

Anderson, M. J. (2004). *DISTLM v. 5: a FORTRAN Computer Program to Calculate a Distance-Based Multivariate Analysis for a Linear Model*. Auckland: University of Auckland.

Anderson, M. J., and Willis, T. J. (2003). Canonical analysis of principal coordinates: a useful method of constrained ordination for ecology.

Ecology 84, 511–525. doi: 10.1890/0012-9658(2003)084%5B0511:caopca%5D2.0.co;2

Arribas, L. P., Donnarumma, L., Palomo, M. G., and Scrosati, R. A. (2014). Intertidal mussels as ecosystem engineers: their associated invertebrate biodiversity under contrasting wave exposures. *Mar. Biodivers.* 44, 203–211. doi: 10.1007/s12526-014-0201-z

Benson, B. L. (1989). Airlift sampler: applications for hard substrata. *Bull. Mar. Sci.* 44, 752–756.

Bianchi, C. N., Dando, P. R., and Morri, C. (2011). Increased diversity of sessile epibenthos at subtidal hydrothermal vents: seven hypotheses based on observations at milos island Aegean Sea. *Adv. Oceanogr. Limnol.* 2, 1–31. doi: 10.1080/19475721.2011.565804

Blake, J. A. (2009). Redescription of capitella capitata (Fabricius) from west greenland and designation of a neotype (Polychaeta, Capitellidae). *Zoosymposia* 2, 55–80.

Bryan, G. W. (1976). *Some Aspects of Heavy Metal Tolerance in Aquatic Organisms*. Cambridge: Cambridge University Press.

Caldwell, R. S. (1975). *Hydrogen Sulfide Effects on Selected Larval and Adult Marine Invertebrates*. Corvallis, OR: Oregon State University.

Cardigos, F., Colaço, A., Dando, P. R., Ávila, S. P., Sarradin, P. M., Tempera, F., et al. (2005). Shallow water hydrothermal vent field fluids and communities of the D. João de Castro Seamount (Azores). *Chem. Geol.* 224, 153–168. doi: 10.1016/j.chemgeo.2005.07.019

Casoli, E., Bonifazi, A., Ardizzone, G., Gravina, M. F., Russo, G. F., Sandulli, R., et al. (2019). Comparative analysis of mollusc assemblages from different hard bottom habitats in the central tyrrhenian sea. *Diversity* 11:74. doi: 10.3390/d11050074

Chemello, R., and Russo, G. F. (1997). The molluscan taxocoene of photophilic algae from the island of lampedusa (strait of sicily, southern mediterranean). *Boll. Malacol.* 33, 95–104.

Chianese, E., Trimberio, G., and Riccio, A. (2019). PM2.5 and PM10 in the urban area of naples: chemical composition, chemical properties and influence of air masses origin. *J. Atmos. Chem. Inpress.* 76, 151–169. doi: 10.1007/s10874-019-09392-3

Cigliano, M., Gambi, M. C., Rodolfo-Metalpa, R., Patti, F. P., and Hall-Spencer, J. M. (2010). Effects of ocean acidification on invertebrate settlement at volcanic CO2 vents. *Mar. Biol.* 157, 2489–2502. doi: 10.1007/s00227-010-1513-6

Clarke, K. R., and Warwick, R. M. (2001). *Change in Marine Communities - an Approach to Statistical Analysis and Interpretation*, 2nd Edn. Plymouth: Primer-E Ldt.

Colognola, R., Masturzo, P., Russo, G. F., Scardi, M., Vlnci, D., and Fresi, E. (1986). Biometric and genetic analysis of the marine rissoid rissoa auriscalpium (Gastropoda, Prosobranchia) and its ecological implications. *Mar. Ecol.* 7, 265–285. doi: 10.1111/j.1439-0485.1986.tb00163.x

Dando, P. R. (2010). "Biological communities at marine shallow-water vent and seep sites," in *The Vent and Seep Biota*, ed. S. Kiel, (Dordrecht: Springer), 333–378. doi: 10.1007/978-90-481-9572-5_11

Dando, P. R., Aliani, S., Arab, H., Bianchi, C. N., Brehmer, M., Cocito, S., et al. (2000). Hydrothermal studies in the aegean sea. *Phys. Chem. Earth Part B Hydrol. Ocean. Atmos.* 25, 1–8. doi: 10.1016/S1464-1909(99)00112-4

Dando, P. R., Hughes, J. A., and Thiermann, F. (1995). Preliminary observations on biological communities at shallow hydrothermal vents in the aegean Sea. *Geol. Soc. London, Spec. Publ.* 87, 303–317. doi: 10.1144/GSL.SP.1995.087.01.23

Dando, P. R., Stüben, D., and Varnavas, S. P. (1999). Hydrothermalism in the mediterranean sea. *Prog. Oceanogr.* 44, 333–367. doi: 10.1016/S0079-6611(99)00032-4

Desprez, M. (2000). Physical and biological impact of marine aggregate extraction along the french coast of the eastern english channel: short-and long-term post-dredging restoration. *ICES J. Mar. Sci.* 57, 1428–1438. doi: 10.1006/jmsc.2000.0926

Di Napoli, R., Aiuppa, A., Sulli, A., Caliro, S., Chiodini, G., Acocella, V., et al. (2016). Hydrothermal fluid venting in the offshore sector of Campi Flegrei caldera: a geochemical, geophysical, and volcanological study. *Geochemistry. Geophys. Geosyst.* 17, 4153–4178. doi: 10.1002/2016GC006494

Doney, S. C., Fabry, V. J., Feely, R. A., and Kleypas, J. A. (2009). Ocean acidification: the other CO2 problem. *Ann. Rev. Mar. Sci.* 1, 169–192. doi: 10.1146/annurev.marine.010908.163834

Donnarumma, L., Lombardi, C., Cocito, S., and Gambi, M. C. (2014). Settlement pattern of *Posidonia oceanica* epibionts along a gradient of ocean acidification: an approach with mimics. *Mediterr. Mar. Sci.* 15, 498–509. doi: 10.12681/mms.677

Donnarumma, L., Sandulli, R., Appolloni, L., and Russo, G. F. (2018). Assessing molluscs functional diversity within different coastal habitats of marine protected areas. *Ecol. Quest.* 29, 35–51. doi: 10.12775/eq.2018.021

Dounas, C., and Koukouras, A. (1989). Sorne observations on the possible synonyrny of Eunice vittata (Delle Chiaje, 1825) and E. indica Kinberg, 1865 (*Annelida*, *Polychaeta*.). *Cah. Biol. Mar.* 30, 227–234.

Eleftheriou, A., and McIntyre, A. (eds) (2008). *Methods for the Study of Marine Benthos*, 3rd Edn. Hoboken, NJ: John Wiley & Sons.

Ellingsen, K. E. (2002). Soft-sediment benthic biodiversity. *Mar. Ecol. Prog. Ser.* 232, 15–27. doi: 10.3354/meps232015

Fabry, V. J., Seibel, B. A., Feely, R. A., and Orr, J. C. (2008). Impacts of ocean acidification on marine fauna and ecosystem processes. *ICES J. Mar. Sci.* 65, 414–432. doi: 10.1093/icesjms/fsn048

Fauchald, K., Granados-Barba, A., and Solís-Weiss, V. (2009). "Polychaeta (Annelida) of the gulf of mexico," in *Gulf of Mexico–Origins, Waters, and Biota. Biodiversity*, eds D. L. Felder, and D. K. Camp, (College Station, TX: Texas A&M University Press), 751–788.

Feder, H. M., Naidu, A. S., Jewett, S. C., Hameedi, J. M., Johnson, W. R., and Whitledge, T. E. (1994). The northeastern chukchi sea: benthos-environmental interactions. *Mar. Ecol. Prog. Ser.* 111, 171–190. doi: 10.3354/meps111171

Ferrero-Vicente, L. M., Marco-Méndez, C., Loya-Fernández, A., and Sánchez-Lizaso, J. L. (2013). Limiting factors on the distribution of shell/tube-dwelling sipunculans. *J. Exp. Mar. Bio. Ecol.* 446, 345–354. doi: 10.1016/j.jembe.2013.06.011

Fretter, V., and Graham, A. (1978). The prosobranch molluscs of britain and Denmark. Part 4 –Marine rissoacea. *J. Molluscan Stud.* suppl. 6, 153–241.

Gamenick, I., Abbiati, M., and Giere, O. (1998a). Field distribution and sulphide tolerance of *Capitella capitata* (*Annelida*: *Polychaeta*) around shallow water hydrothermal vents off milos (aegean sea). a new sibling species? *Mar. Biol.* 130, 447–453. doi: 10.1007/s002270050265

Gamenick, I., Vismann, B., Grieshaber, M. K., and Giere, O. (1998b). Ecophysiological differentiation of *Capitella capitata* (*Polychaeta*). Sibling species from different sulfidic habitats. *Mar. Ecol. Prog. Ser.* 175, 155–166. doi: 10.3354/meps175155

George, J. D., and Hartmann-Schröder, G. (1985). "Polychaetes: british amphinomida, spintherida and eunicida: keys and notes for the identification of the species," in *Synopses of the British Fauna*, eds M. Kermack, and R. S. K. Barnes, (London: Brill Archive), 1–221.

Grassle, J., and Grassle, J. F. (1976). Sibling species in the marine pollution indicator *Capitella* (*Polychaeta*). *Science* 192, 567–569. doi: 10.1126/science.1257794

Gray, J. S., Wu, R. S. S., and Ying, Y. O. (2002). Effects of hypoxia and organic enrichment on the coastal marine environment. *Mar. Ecol. Prog. Ser.* 238, 249–279. doi: 10.3354/meps238249

Gusso, C. C., Gravina, M. F., and Maggiore, F. R. (2001). Temporal variations in soft bottom benthic communities in central tyrrhenian sea (Italy). *Archo. Ocean. Limnol.* 22, 175–182.

Hall-Spencer, J. M., Rodolfo-Metalpa, R., Martin, S., Ransome, E., Fine, M., Turner, S. M., et al. (2008). Volcanic carbon dioxide vents show ecosystem effects of ocean acidification. *Nature* 454:96. doi: 10.1038/nature07051

Legendre, P., and Anderson, M. J. (1999). Distance-based redundancy analysis: testing multispecies responses in multicfacorial ecological experiments. *Ecol. Monogr.* 69, 1–24. doi: 10.1890/0012-9615(1999)069%5B0001:dbratm%5D2.0.co;2

Lloret, J., and Marín, A. (2009). The role of benthic macrophytes and their associated macroinvertebrate community in coastal lagoon resistance to eutrophication. *Mar. Poll. Bull.* 58, 1827–1834. doi: 10.1016/j.marpolbul.2009.08.001

Lucey, N. M., Lombardi, C., Florio, M., DeMarchi, L., Nannini, M., Rundle, S., et al. (2016). An in situ assessment of local adaptation in a calcifying polychaete from a shallow CO2 vent system. *Evol. Appl.* 9, 1054–1071. doi: 10.1111/eva.12400

Lutz, R. A., and Kennish, M. J. (1993). Ecology of deep-sea hydrothermal vent communities: a review. *Rev. Geophys.* 31, 211–242.

Martin, W., Baross, J., Kelley, D., and Russell, M. J. (2008). Hydrothermal vents and the origin of life. *Nat. Rev. Microbiol.* 6, 805–814. doi: 10.1038/nrmicro1991

Maugeri, T. L., Bianconi, G., Canganella, F., Danovaro, R., Gugliandolo, C., Italiano, F., et al. (2010). Shallow hydrothermal vents in the southern tyrrhenian sea. *Chem. Ecol.* 26, 285–298. doi: 10.1080/02757541003693250

Micheli, F., Peterson, C. H., Mullineaux, L. S., Fisher, C. R., Mills, S. W., Sancho, G., et al. (2002). Predation structures communities at deep-sea hydrothermal vents. *Ecol. Monogr.* 72, 365–382. doi: 10.1111/1462-2920.14806

Nygren, A. (2014). Cryptic polychaete diversity: a review. *Zool. Scr.* 43, 172–183. doi: 10.1111/zsc.12044

Parson, L. M., Walker, C. L., and Dixon, D. R. (1995). Hydrothermal vents and processes. *Geol. Soc. Spec. Publ.* 87, 1–2.

Passaro, S., Barra, M., Saggiomo, R., Di Giacomo, S., Leotta, A., Uhlen, H., et al. (2013). Multi-resolution morpho-bathymetric survey results at the Pozzuoli-Baia underwater archaeological site (Naples. Italy). *J. Archaeol. Sci.* 40, 1268–1278. doi: 10.1016/j.jas.2012.09.035

Purchon, R. D. (1977). *The Biology of the Mollusca*, 2nd Edn. Amsterdam: Elsevier.

Raghukumar, C., Mohandass, C., Cardigos, F., DeCosta, P. M., Santos, R. S., and Colaco, A. (2008). Assemblage of benthic diatoms and culturable heterotrophs in shallow-water hydrothermal vent of the D. Joao de Castro seamount, azores in the atlantic ocean. *Curr. Sci.* 95, 1715–1723.

Riera, R., Monterroso, Ó, and Núñez, J. (2012). Effects of granulometric gradient on macrofaunal assemblages in Los Cristianos harbour (tenerife, canary islands). arquipélago. *Life Mar. Sci.* 29, 33–41.

Rota, E., Perra, G., and Focardi, S. (2009). The European lancelet Branchiostoma lanceolatum (Pallas) as an indicator of environmental quality of tuscan archipelago (western mediterranean sea). *Chem. Ecol.* 25, 61–69. doi: 10.1080/02757540802641361

Schander, C., Rapp, H. T., Kongsrud, J. A., Bakken, T., Berge, J., Cochrane, S., et al. (2010). The fauna of hydrothermal vents on the mohn ridge (North Atlantic). *Mar. Biol. Res.* 6, 155–171. doi: 10.1080/17451000903147450

Schumacher, B. A. (2002). Methods for the Determination of Total Organic Carbon (TOC) in Soils and Sediments. Washington, DC: United States Environmental Protection Agency, National ESD (Exposure Research Laboratory).

Simboura, N., and Zenetos, A. (2002). Benthic indicators to use in ecological quality classification of mediterranean soft bottom ecosystems, including a new biotic index. *Mediterr. Mar. Sci.* 3, 77–112.

Southward, A. J., Southward, E. C., Dando, P. R., Hughes, J. A., Kennicutt, M. C., Herrera-Alcala, J., et al. (1997). Behaviour and feeding of the nassariid gastropod cyclope neritea, abundant at hydrothermal brine seeps off milos (aegean sea). *J. Mar. Biol. Assoc. U.K.* 77, 753–771. doi: 10.1017/s0025315400036171

Stevens, C. J., Juniper, S. K., Limén, H., Pond, D. W., Metaxas, A., and Gélinas, Y. (2015). Obligate hydrothermal vent fauna at East Diamante submarine volcano (mariana arc) exploit photosynthetic and chemosynthetic carbon sources. *Mar. Ecol. Prog. Ser.* 525, 25–39. doi: 10.3354/meps11229

Tarasov, V. G., Gebruk, A. V., Mironov, A. N., and Moskalev, L. I. (2005). Deep-sea and shallow-water hydrothermal vent communities: two different phenomena? *Chem. Geol.* 224, 5–39. doi: 10.1016/j.chemgeo.2005.07.021

Tarasov, V. G., Gebruk, A. V., Shulkin, V. M., Kamenev, G. M., Fadeev, V. I., Kosmynin, V. N., et al. (1999). Effect of shallow-water hydrothermal venting on the biota of matupi harbour (Rabaul Caldera, New Britain Island, Papua New Guinea). *Cont. Shelf Res.* 19, 79–116. doi: 10.1016/S0278-4343(98)00073-9

Tedesco, D., Allard, P., Sano, Y., Wakita, H., and Pece, R. (1990). Helium-3 in subaerial and submarine fumaroles of Campi Flegrei caldera, Italy. *Geochim. Cosmochim. Acta* 54, 1105–1116. doi: 10.1016/0016-7037(90)90442-N

Teixidó, N., Gambi, M. C., Parravacini, V., Kroeker, K., Micheli, F., Villéger, S., et al. (2018). Functional biodiversity loss along natural CO2 gradients. *Nat. Commun.* 9:5149. doi: 10.1038/s41467-018-07592-1

Terlizzi, A., Anderson, M. J., Fraschetti, S., and Benedetti-Cecchi, L. (2007). Scales of spatial variation in Mediterranean subtidal sessile assemblages at different depths. *Mar. Ecol. Prog. Ser.* 332, 25–39. doi: 10.3354/meps332025

Thiermann, F., Akoumianaki, I., Hughes, J. A., and Giere, O. (1997). Benthic fauna of a shallow-water gaseohydrothermal vent area in the aegean sea (Milos, Greece). *Mar. Biol.* 128, 149–159. doi: 10.1007/s002270050078

Thrush, S. F., Pridmore, R. D., Hewitt, J. E., and Cummings, V. J. (1991). Impact of ray feeding disturbances on sandflat macrobenthos: do communities dominated by polychaetes or shellfish respond differently? *Mar. Ecol. Prog. Ser.* 69, 245–252. doi: 10.3354/meps069245

Turner, L. M., Ricevuto, E., Massa Gallucci, A., Lorenti, M., Gambi, M. C., and Calosi, P. (2016). Metabolic responses to high pCO2 conditions at a CO2 vent site in juveniles of a marine isopod species assemblage. *Mar. Biol.* 163:211. doi: 10.1007/s00227-016-2984-x

Underwood, A. J. (1997). *Experiments in Ecology: Their Logical Design and Interpretation Using Analysis of Variance*. Cambridge: Cambridge University Press.

Van Dover, C. L., and Fry, B. (1989). Stable isotopic compositions of hydrothermal vent organisms. *Mar. Biol.* 102, 257–263. doi: 10.1007/BF00428287

Vaquer-Sunyer, R., and Duarte, C. M. (2010). Sulfide exposure accelerates hypoxia-driven mortality. *Limnol. Oceanogr.* 55, 1075–1082. doi: 10.4319/lo.2010.55.3.1075

Vaquer-Sunyer, R., and Duarte, C. M. (2011). Temperature effects on thresholds of hypoxia for marine organisms. *Glob. Chang. Biol.* 17, 1788–1797. doi: 10.1007/s11356-017-8908-6

Vismann, B. (1991). Sulfide tolerance: physiological mechanisms and ecological implications. *Ophelia* 34, 1–27. doi: 10.1080/00785326.1991.10429703

Wang, F., and Chapman, P. M. (1999). Biological implications of sulfide in sediment - a review focusing on sediment toxicity. *Environ. Toxicol. Chem.* 18, 2526–2532. doi: 10.1002/etc.5620181120

Washburn, T., Rhodes, A. C. E., and Montagna, P. A. (2016). Benthic taxa as potential indicators of a deep-sea oil spill. *Ecol. Indic.* 71, 587–597. doi: 10.1016/j.ecolind.2016.07.045

Wicks, L. C., and Roberts, M. J. (2012). "Benthic invertebrates in a high-CO2 world," in *Oceanography and Marine Biology - An Annual Review*, eds R. N. Gibson, R. J. A. Atkinson, J. D. M. Gordon, and R. N. Hughes, (Milton Park: Taylor & Francis), 127–188.

Woodin, S. A. N. N. (1978). Refuges, disturbance, and community structure: a marine soft-bottom example. *Ecology* 59, 274–284.

WoRMS Editorial Board, (2018). *World Register of Marine Species*. Available at: http://www.marinespecies.org at VLIZ (accessed June 19, 2018).

Yao, H., Dao, M., Imholt, T., Huang, J., Wheeler, K., Bonilla, A., et al. (2010). Protection mechanisms of the iron-plated armor of a deep-sea hydrothermal vent gastropod. *Proc. Natl. Acad. Sci. U.S.A.* 107, 987–992. doi: 10.1073/pnas.0912988107

Yoshida, M., Hamdi, H., Abdul Nasser, I., and Jedidi, N. (2002). Contamination of potentially toxic elements (PTEs) in bizerte lagoon bottom sediments, surface sediment and sediment repository. *Rpp Sepmcl.* 13–48.

Zhao, Q., Cheung, S. G., Shin, P. K. S., and Chiu, J. M. Y. (2011). Effects of starvation on the physiology and foraging behaviour of two subtidal nassariid scavengers. *J. Exp. Mar. Bio. Ecol.* 409, 53–61. doi: 10.1016/j.jembe.2011.08.003

Conflict of Interest: The authors declare that the research was conducted in the absence of any commercial or financial relationships that could be construed as a potential conflict of interest.

Copyright © 2019 Donnarumma, Appolloni, Chianese, Bruno, Baldrighi, Guglielmo, Russo, Zeppilli and Sandulli. This is an open-access article distributed under the terms of the Creative Commons Attribution License (CC BY). The use, distribution or reproduction in other forums is permitted, provided the original author(s) and the copyright owner(s) are credited and that the original publication in this journal is cited, in accordance with accepted academic practice. No use, distribution or reproduction is permitted which does not comply with these terms.

frontiers in Marine Science

PERSPECTIVE
published: 15 April 2020
doi: 10.3389/fmars.2020.00216

Metabolic Niches and Biodiversity: A Test Case in the Deep Sea Benthos

Craig R. McClain[1], Thomas J. Webb[2], Clifton C. Nunnally[1], S. River Dixon[3], Seth Finnegan[4] and James A. Nelson[3]*

[1] Louisiana Universities Marine Consortium (LUMCON), Chauvin, LA, United States, [2] Department of Animal and Plant Sciences, University of Sheffield, Sheffield, United Kingdom, [3] Department of Biology, University of Louisiana- Lafayette, Lafayette, LA, United States, [4] Department of Integrative Biology, University of California, Berkeley, Berkeley, CA, United States

The great anthropogenic alterations occurring to carbon availability in the oceans necessitate an understanding of the energy requirements of species and how changes in energy availability may impact biodiversity. The deep-sea floor is characterized naturally by extremely low availability of chemical energy and is particularly vulnerable to changes in carbon flux from surface waters. Because the energetic requirements of organisms impact nearly every aspect of their ecology and evolution, we hypothesize that species are adapted to specific levels of carbon availability and occupy a particular metabolic niche. We test this hypothesis in deep-sea, benthic invertebrates specifically examining how energetic demand, axes of the metabolic niche, and geographic range size vary over gradients of chemical energy availability. We find that benthic invertebrates with higher energetic expenditures, and ecologies associated with high energy demand, are located in areas with higher chemical energy availability. In addition, we find that range size and location of deep-sea, benthic species is determined by geographic patterns in chemical energy availability. Our findings indicate that species may be adapted to specific energy regimes, and the metabolic niche can potentially link scales from individuals to ecosystems as well as adaptation to patterns in biogeography and biodiversity.

Keywords: energetic, metabolism, adaptation, diversity, niche

OPEN ACCESS

Edited by:
Jeroen Ingels, Florida State University, United States

Reviewed by:
Michael Vecchione, National Oceanic and Atmospheric Administration (NOAA), United States
Ann Vanreusel, Ghent University, Belgium

****Correspondence:***
Craig R. McClain
cmcclain@lumcon.edu

Specialty section:
This article was submitted to Global Change and the Future Ocean, a section of the journal Frontiers in Marine Science

Received: *01 November 2019*
Accepted: *19 March 2020*
Published: *15 April 2020*

Citation:
McClain CR, Webb TJ, Nunnally CC, Dixon SR, Finnegan S and Nelson JA (2020) Metabolic Niches and Biodiversity: A Test Case in the Deep Sea Benthos. Front. Mar. Sci. 7:216. doi: 10.3389/fmars.2020.00216

INTRODUCTION

As demonstrated by several environmental indicators anthropogenic impacts on the environment continue to exhibit a long-term, post-industrial rise (Steffen et al., 2015). This human induced environmental degradation has led to significant declines in global biodiversity including increasing numbers of endangered species and decreasing abundances of key taxa (Lotze et al., 2006; Butchart et al., 2010). Alarmingly, this decline of species diversity in response to climate change is a factor of four greater in marine systems as compared to terrestrial systems (Blowes et al., 2018). Much research has been dedicated to alterations of the marine environment as

a function of several key parameters – including temperature, acidification, oxygen, and pollution – and how these have and will impact marine communities (Kennish, 1997; Harley et al., 2006; Vaquer-Sunyer and Duarte, 2008; Kordas et al., 2011; Doney et al., 2012). Much less research exists in characterizing how marine ecosystems will respond to the immense anthropogenic alterations to carbon cycling and availability, especially in the deep oceans, the largest habitat on Earth and the key in long-term sequestration of carbon.

We propose an eco-evolutionary adaptive theory of the metabolic niche (Wilson et al., 2011) where species are adapted to specific energy regimes which scale with biodiversity patterns. We hypothesize that the species observed in a locality are dependent on the energy content of that habitat. Here, we develop this hypothesis through a series of 10 linked propositions, from first principles of metabolic ecology through to biogeographic patterns in metabolic adaptation. For each of these propositions, we review current support and theory from a general eco-evolutionary viewpoint and specifically with a deep-sea perspective. The deep-sea benthos provides an ideal test system for metabolic hypotheses because the system is productivity limited, experiences little temperature variation, and has documented clines over productivity gradients (Gage and Tyler, 1991; Tittensor et al., 2011; McClain et al., 2012a; McClain and Barry, 2014; Woolley et al., 2016). The deep seafloor, which encompasses depths below 200 m, covers most of Earth and is an especially energy-deprived system (Gage and Tyler, 1991). Primary production is virtually absent in these dark depths. The carbon that sustains most deep-sea seafloor life is sequestered from sinking particulate organic carbon (POC) derived from primary production in the euphotic zone (Gage and Tyler, 1991). However, temperature is relatively constant over the deep seafloor varying between -1 and 4°C (Gage and Tyler, 1991), allowing us to examine the role of productivity largely independent of the role of temperature. Previous studies have also demonstrated that biodiversity patterns in the deep ocean are controlled primarily by productivity with a weaker or non-existent effect of temperature (Tittensor et al., 2011; McClain et al., 2012a; McClain and Barry, 2014; Woolley et al., 2016). For many of the propositions, we bring new data from deep-sea, benthic invertebrates to bear to quantify and specifically test the hypotheses.

PROPOSITION 1: LIFE REQUIRES ENERGY

Premise

Energy is the currency of life, intrinsically linked to ecological (Brown et al., 2004) and evolutionary (Van Valen, 1976; Bambach, 1993) processes and driving fitness through growth, maintenance, and reproduction (Van Valen, 1976). Four basic forms of energy affect biological systems – photosynthetically active radiation; thermal kinetic energy as indexed by temperature; mechanical energy in the form of movement of air, water, and earth; and chemical potential energy stored in reduced carbon compounds (Denny, 1999; Clarke and Gaston, 2006) – encompassing the fundamental axes which together form an organism's energetic niche.

Metabolic rate is the rate of chemical energy uptake, transformation, and allocation (Brown et al., 2004). In heterotrophs, this energy is obtained by oxidizing carbon compounds; the respiration rate of chemical energy is the metabolic rate (Brown et al., 2004). Thus, the energetic needs of an organism are its total organic carbon demand. We define carbon availability as the amount of organic carbon available for an organism to consume and in part can be viewed analogous to the more general term of food.

Here, we restrict our use of the term *energy* to chemical potential energy, or organic carbon, following the conventions of species-energy theory (Wright, 1983; Wright et al., 1993; Hurlbert, 2004, 2006). For terrestrial and shallow-water systems, productivity, e.g., net primary production, is often used as a metric for chemical energy. For the deep-sea benthos, organic carbon availability is often quantified as either POC flux or organic carbon in the sediment. Note that organic carbon may also arrive to the seafloor through large food parcels such as whale carcasses, macroalgae, jellyfish, and wood. However, these larger food falls are isolated and scarce both in time and space, due to the immense scale of ocean basins, so while they are locally important at certain times, background levels of organic carbon availability are more general drivers of deep-sea diversity. Promisingly, previous studies have demonstrated that macroecological patterns in the deep-sea benthos are highly correlated with POC flux (Tittensor et al., 2011; McClain et al., 2012a; McClain and Barry, 2014; Woolley et al., 2016). This suggests that POC represents a reasonable metric for understanding the chemical energy available to deep-sea benthic organisms.

Consequence

This basic requirement of energy can be quantified for each organism and potentially inform about biological patterns from the individual up to the ecosystem.

PROPOSITION 2: AGAINST A BACKDROP OF GLOBAL CHANGE IN ORGANIC CARBON AVAILABILITY, UNDERSTANDING THE ENERGETIC NEEDS OF ORGANISMS IS VITAL

Premise

In the oceans, the combination of global phytoplankton production declines over century to decadal timescales (Behrenfeld et al., 2006; Boyce et al., 2010), with more varied responses at regional and local scales (Harding and Perry, 1997; Boyce et al., 2010; McQuatters-Gollop et al., 2011; Rousseaux and Gregg, 2015), indicates significant heterogeneity of anthropogenic impacts and a major reworking of carbon cycling. This alteration of organic carbon availability is predicted to increase with continued anthropogenic disturbance (Chust et al., 2014; Bryndum-Buchholz et al., 2019) potentially leading to

15–30% decreases in biomass in some ocean basins and 20–80% increases in others (Bryndum-Buchholz et al., 2019).

Consequence

The metabolic niche and its relationship to biodiversity is important because of these immense anthropogenic alterations to carbon cycling and availability. Against this backdrop of global change in organic carbon availability, understanding how organisms respond to a changing energetic environment is critical. Changing organic carbon availability can affect aggregate properties of ecological communities such as the number of individuals and species (Wright, 1983; Wright et al., 1993; Brown et al., 2004), but the extent to which species with different carbon requirements and adaptations will vary in their responses to a novel energetic environment is not well known. This has consequences for how we expect ecological communities to be structured, and for predicting winners and losers as we progress into the Anthropocene.

PROPOSITION 3: THE DEEP-SEA BENTHOS IS PARTICULARLY VULNERABLE TO ALTERATIONS IN ORGANIC CARBON AVAILABILITY

Premise

As previously stated, below 200 m the oceans are chemical energy-deprived systems (Gage and Tyler, 1991; McClain et al., 2012a), with deep-sea floor communities reliant on primary production occurring in surface waters sinking in the form of POC (Gage and Tyler, 1991). This supply of chemical energy to the benthos varies as a function of depth because of remineralization and surface primary production, also often decreasing with distance from productive coastal regions (Gage and Tyler, 1991). On the abyssal plains, one of the largest habitats on Earth, with an average depth of 4.4 km, the downward flux of POC represents less than 1% of surface production (Lampitt and Anita, 1997) resulting in an extremely food-limited environment, albeit one with considerable energetic patchiness at a range of spatial scales. The decrease in environmental energy availability is mirrored by substantial decreases in biomass and abundance with depth (often used as a proxy for total energy availability) in benthic faunal groups ranging from bacteria to large mobile fish and invertebrates (Rex et al., 2006; Wei et al., 2010b; McClain et al., 2012a).

Consequence

Nearly every aspect of deep-sea benthic ecology and evolution is driven by this flux of carbon from the sea surface (Smith et al., 2008), and "[t]he presence and persistence of life itself on the ocean-floor can be viewed as a response to organic inputs" (Gooday, 2002). In contrast to shallower ecosystems (Tittensor et al., 2010), deep-sea diversity is primarily driven by patterns of chemical energy and not by other forms of energy such as thermal energy, indexed by temperature (Woolley et al., 2016). As noted by Smith et al. (2008) "Many aspects of ecosystem structure and function in the abyss are strongly modulated by the rate and nature of food flux to the seafloor. Climate change and human activities will alter patterns of sinking food flux to the deep ocean, substantially impacting the structure, function and biodiversity of abyssal ecosystems."

PROPOSITION 4: SUBSTANTIAL VARIATION EXISTS IN METABOLIC NEED, I.E., ENERGETIC NEEDS, ACROSS TAXA EVEN AFTER ACCOUNTING FOR TEMPERATURE AND BODY SIZE

Premise

Under the Metabolic Theory of Ecology (MTE) (Brown et al., 2004), energy is an allocated resource translated into work and mass and further allocated into the fitness-enhancing processes of survival, growth, and reproduction. The energy demand, i.e., the metabolic niche, of an organism in the MTE is largely set by first principles governing the distribution of materials and temperature-related kinetics as indexed by temperature and body size (Gillooly et al., 2001). Metabolic rate can be described by the power-law relationship between organismal size, temperature, and metabolic rate:

$$B = \beta_0 M^b e^{-E/kT}$$

where B is the metabolic rate, β_0 is a normalizing constant, M is mass, b is the scaling coefficient, T is temperature, E the activation energy of the respiratory complex, and k is Boltzmann's constant (Gillooly et al., 2001). Substantial variation–at least 1–2 orders of magnitude–exists in metabolic rates even when standardized for organismal mass and temperature (Glazier, 2005) even among deep-sea organisms (McClain et al., 2012a).

Data and Analysis

We analyze the global dataset of Brey et al. (2010) on relationships between mass, elemental composition and energy content for marine invertebrates to quantify the relationship between mass and respiration rate. We limited the dataset to include only benthic, marine, adult measurements. This includes data for 13,478 individuals from 444 species, 336 genera, 46 orders, 29 classes, and 14 phyla ranging in depths from 1 to 4,420 meters. Complete details on the construction of the database can be found in Brey et al. (2010). Original respiration and mass data from the literature included a wide array of measurement units. All of these were converted into respiration into the energy unit of Joules per day and all masses were converted from dry, ash free dry, wet, or carbon content into Joules. From the database, we analyze log10 of respiration rate (J) as a function of log10 of mass (J) and the inverse of temperature (°K) using a linear model in R Package (R Development Core Team, 2019). The general relationship was visualized utilizing ggplot (Wickham, 2009). Residuals from the linear model were further analyzed with ANOVA to test for significant

differences in the residuals among taxa. Residuals were visualized with ggridges (Wilke, 2018). We then test whether different phyla vary in their typical departure from this relationship by testing for significant differences in the residuals between phyla using ANOVA.

Consequence

Respiration rate is strongly and positively related to mass (**Figure 1**, $p < 0.0001$) across the 13,478 marine invertebrate individuals in our dataset. Even after correcting for mass and temperature, metabolic rate residuals exhibit considerable variation (**Figures 1**, **2**). Moreover, this variation is in part related to ecological and evolutionary differences in higher level taxa (**Figure 2**, ANOVA: $p < 0.0001$, $R^2 = 0.24$). This implies that the energetic need of organisms is set by factors beyond the first principles of distribution of materials and temperature-related kinetics (Gillooly et al., 2001). We thus propose an adaptive model of the metabolic niche where species are *adapted to specific energy regimes* to explain this residual variation.

PROPOSITION 5: THIS VARIATION IN METABOLIC NEED IS ADAPTIVE, I.E., SPECIES HAVE A METABOLIC NICHE

Premise

The metabolic niche represents a series of energetic tradeoffs within an organism that sets overall metabolic need, and is comprised of axes that govern the anatomy, physiology, and behaviors of an organism that increase or decrease these energetic costs. Under this model, we propose that species occur on a continuum of energetic need, from "high-energy taxa" (HET) to "low-energy taxa" (LET), and are thus adapted specifically for temporally and spatially varying levels of carbon availability.

Consequence

This variation in energetic need spans evolution across the tree of life (Uyeda et al., 2017). Major clades of vertebrates exhibit significant differences in scaling, suggesting fundamental evolutionary shifts in the adaptation of metabolic need (Uyeda et al., 2017), and comparative studies have revealed other generalities too, e.g., between endotherms and ectotherms (Nagy, 1987), trophic levels (Carbone et al., 2007), passerines and non-passerines (McNab, 2016), foraging (Childress, 1995), locomotory (Voight and Speakman, 2007; Shen et al., 2010) and predator avoidance strategies (McNab, 1986). Overall, this variation suggests that metabolic rates, while in part controlled by first-order principles, vary considerably within and across clades (Makarieva et al., 2008), and that this reflects trade-offs in energetic demand. Importantly, the links between metabolic rates and well-studied ecological traits or other well-understood mechanisms could be generalized to set up testable predictions in other groups and environmental settings.

PROPOSITION 6: A RELATIONSHIP EXISTS BETWEEN ENVIRONMENTAL AVAILABILITY OF CARBON AND METABOLIC NICHE

Premise

Given this variation in energy needs across the tree of life, we might also expect to observe a relationship between the environmental availability of carbon and the metabolic niche. However, previous research indicates that temperature- and mass-corrected basal metabolic rates do not appear to vary over carbon gradients (Childress, 1995). One possibility to reconcile our theory with this finding would be if basal metabolic rates themselves, as the lowest basic need of organism, were governed by fundamental first principles (Brown et al., 2004) and evolutionarily conserved. In this scenario, field metabolic rates or active metabolic rates indicating work and fitness beyond maintenance may more strongly map onto environmental availability of carbon.

Alternatively, total metabolic demand, accounting for differences in organismal mass, may vary with carbon availability, even if per unit mass metabolic rates do not. To restate, the primary ecological and evolutionary energetic response of species to changes in carbon availability is alterations in body size. Indeed, reductions in body size, and thus total metabolic demand, with declining POC are well documented in the deep sea (Thiel, 1975, 1979; Rex et al., 2006; Wei et al., 2010a; McClain et al., 2012b).

Data and Analysis

Allen (2008) compiled and taxonomically standardized bivalve data from samples collected with an epibenthic sledge during research cruises from 1962 to 1979. The dataset includes 204,068 individuals representing 527 bivalve species from 11 basins and 255 sites ranging in depth from 68 to 5875 m (McClain et al., 2012c). Species-level maximum body size (biovolume) was collected from the literature and biovolume was calculated as length*width^2 (details can be found in McClain et al., 2012b). Intraspecific variation in biovolume is much less than interspecific variation and the choice of using median or maximum body size in mollusks is unlikely to mask ecological patterns (McClain, 2004). Biovolume was converted to wet weight utilizing the conversions in Powell and Stanton (1985). Utilizing published scaling equations for bivalve families and orders (Vladimirova et al., 2003), we calculated metabolic rate (mW). Body size data was not available for all species, reducing the final analyzed dataset down to 475 bivalve species. We estimated POC flux (gC/m^2/yr) from Lutz et al. (2007) for each site. For each species, we calculated the mean POC across all station occurrences for that species. The Lutz et al. (2007) study uses empirically derived sediment trap POC flux estimates compared to remotely sensed estimates of net primary production and sea surface temperature. These data were used to develop an algorithm with coefficients predicting annual POC flux at a given depth from remotely sensed data. We analyzed the log10 of respiration rate (mW) as a function of log10 of POC

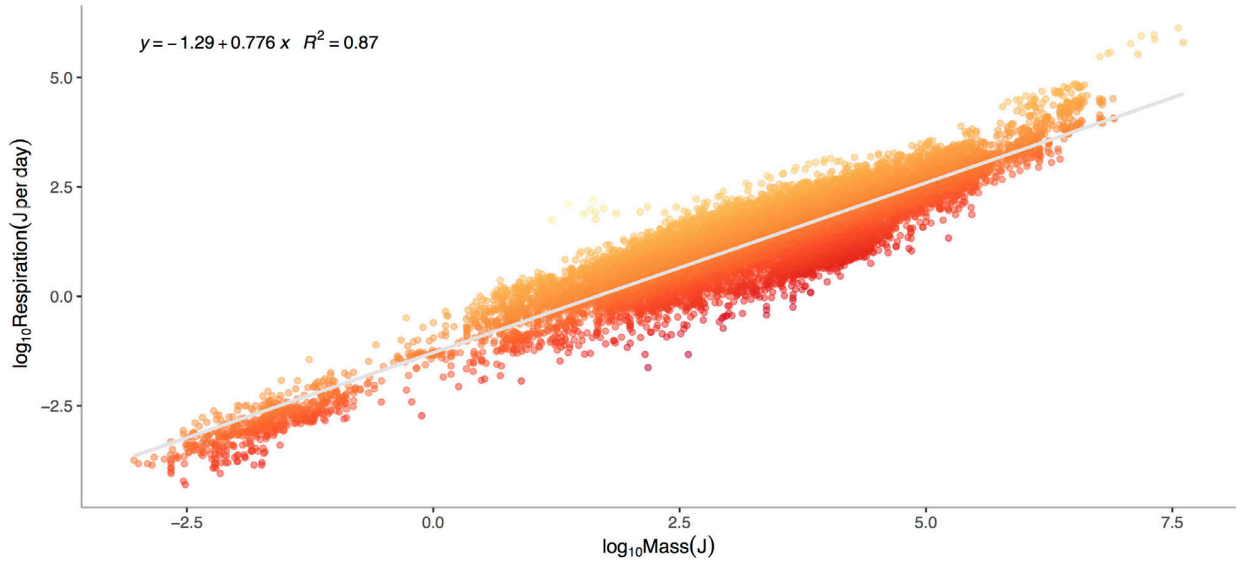

FIGURE 1 | Log_{10} Metabolic Rate (Joules per Day) verses Log_{10} Mass (Joules) for marine invertebrates. Data represent a global database from Brey et al. (2010) on relationships between mass, elemental composition and energy content for marine invertebrates. This includes data for 13,478 individuals from 444 species, 336 genera, 46 orders, 29 classes, and 14 phyla ranging in depths from 1 to 4,420 meters. Colors denote large negative (red) to large positive (orange) residuals of the relationship between respiration and mass.

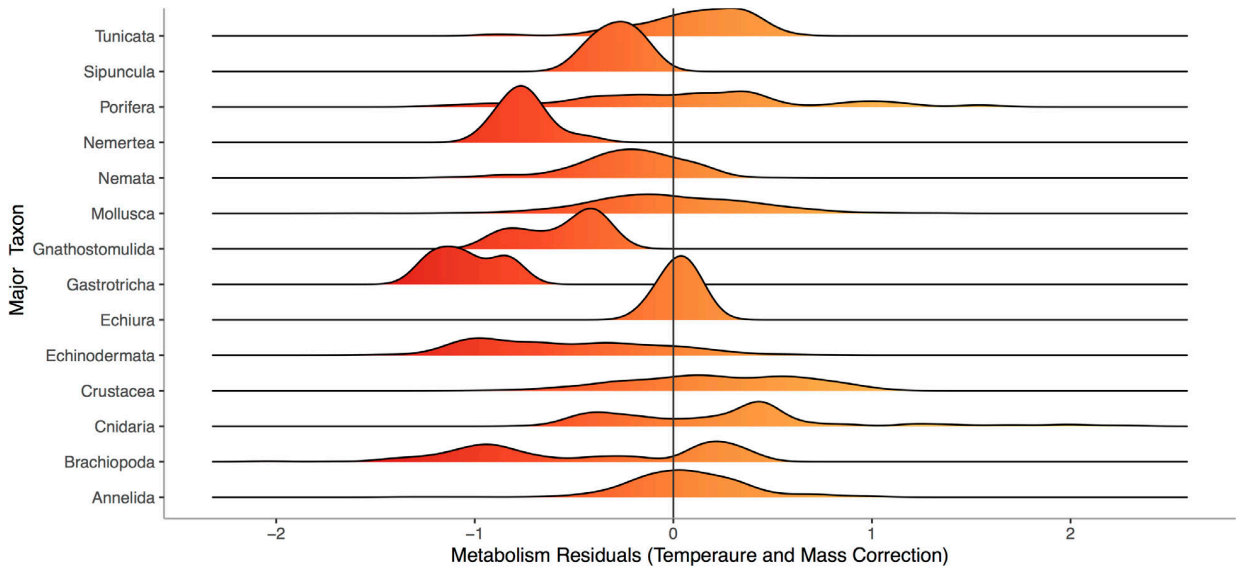

FIGURE 2 | Distribution of residuals for each of 14 phyla from a model fitting Log_{10} Metabolic Rate (Joules per Day) as a function of Log_{10} Mass (Joules) and 1/Temperature (°K), using data from the same 13,478 individuals from 444 species shown in **Figure 1**. Colors denote large negative (red) to large positive (orange) residuals of the relationship between respiration and mass.

flux and using a linear model in R Development Core Team (2019). The general relationship was visualized utilizing ggplot (Wickham, 2009).

Consequence

POC is a significant predictor of total bivalve metabolism ($p < 0.0001$) among 475 deep-sea bivalve species across the Atlantic Ocean (**Figure 3**). The intercepts ($p < 0.0001$) but not the slopes ($p = 0.0627$) of this relationship vary among bivalve orders. These results suggest that a species' total energetic demand, as set by body size, is concordant with energy available in the environment. Additional evolutionary history and ecology associated with higher taxonomic levels also sets additional energetic needs. Thus while body size is a major axis of the metabolic niche, different intrinsic factors of taxa define the other axes.

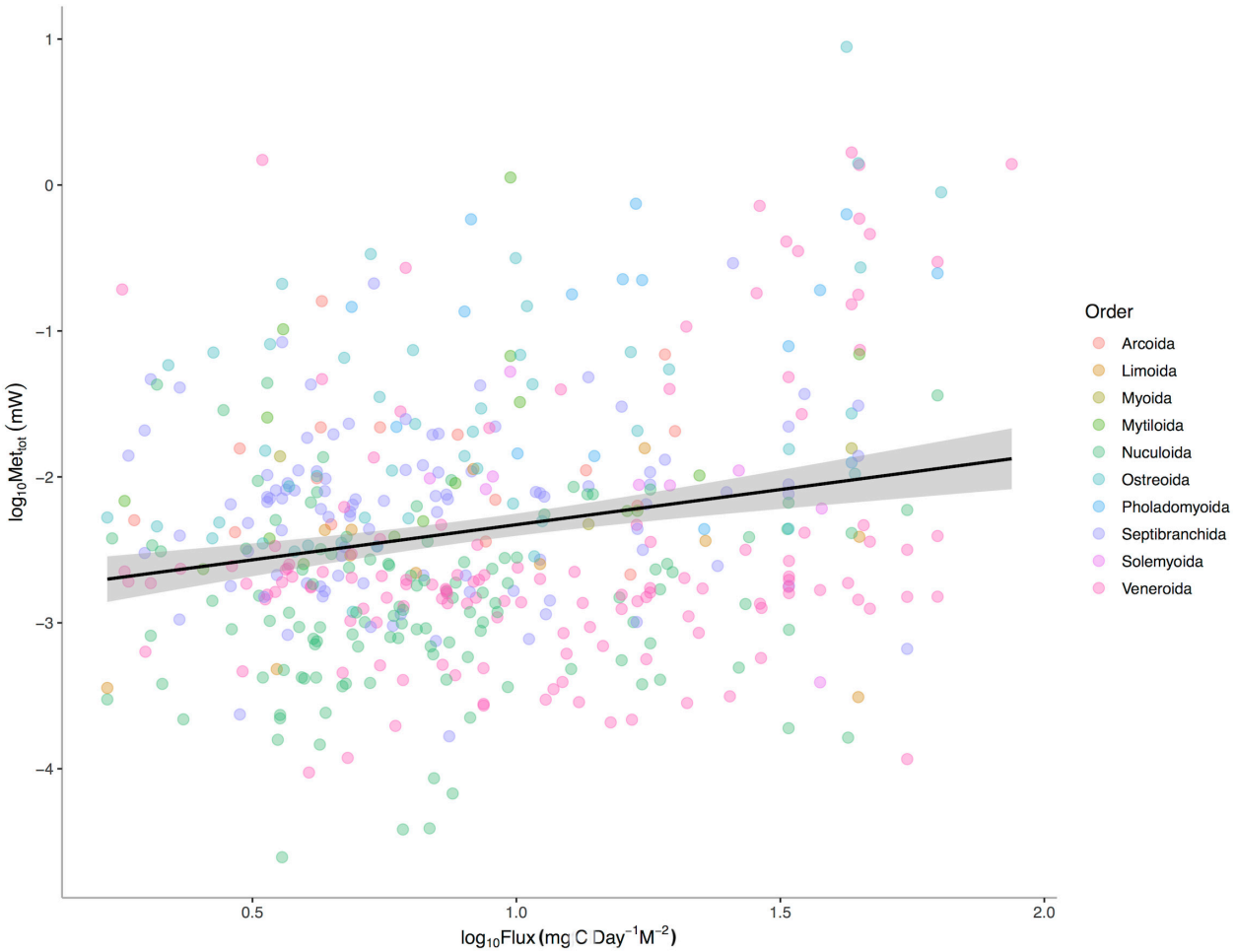

FIGURE 3 | Log_{10} Maximum Metabolic Rate (mW) verses Log_{10} Mean Standardized Carbon Flux (gC m^{-2} d^{-1}) for 475 species of deep-sea bivalves across the Atlantic Ocean. Black line represents linear regression for all species and gray area represents the 95% confidence interval around the linear fit.

PROPOSITION 7: THE METABOLIC NICHE IS THE SUM OF A SERIES OF ENERGETIC TRADEOFFS, THUS THE REPRESENTATION OF ECOLOGICAL TRAITS, AS SET BY THEIR METABOLIC REQUIREMENTS, SHOULD VARY WITH ENVIRONMENTAL AVAILABILITY OF CARBON

Premise

Energetic niche axes can be defined as specific functional traits that dictate overall energetic demand. Thus, quantifying the underlying functional traits and tradeoffs that impact the balance between metabolic intake and demand can be used to define the energetic niche. We can quantify these functional trait tradeoffs and begin to identify the traits of HET and LET, by either exploring how they impact metabolic demand or exploring how functional traits vary over a carbon energy gradient.

We know that energy demand is impacted by the functional traits of the organisms. For example, metabolic rates are higher in endotherms due to the increased costs of maintaining homeostasis (Nagy, 1987). Metabolic rates increase with increasing trophic level (McNab, 1986; Nagy, 1987) in vertebrates (Carbone et al., 2007) and invertebrates (Vladimirova, 2001; Vladimirova et al., 2003) alike, potentially reflecting the increased need for locomotor capacity and range to capture and search for resources at lower densities for carnivores versus herbivores (Tamburello et al., 2015). In the deep sea, temperature- and mass-corrected metabolic rates among species decline with depth in pelagic fish and crustaceans because the attenuation of light leads to a switch from visual-base foraging and a subsequent decline in need for locomotor capacity (Childress, 1995). Prior research indicates that at broad levels, physiological and trophic adaptations lead to a LET to HET spectrum.

A number of traits are known to co-vary with spatial clines in carbon availability. Metabolically expensive morphological characteristics, such as the production and maintenance of complex shells (McClain et al., 2004; McClain, 2005), may

be precluded in low energy environments. The environmental energy availability is also reflected in the trophic niches with, for example, suspension feeders and specialist carnivores declining in importance with decreasing carbon availability (Sokolova, 1960; Gage and Tyler, 1991). In some circumstances, lower carbon availability and resource competition may drive species to exploit and specialize on new carbon resources (Sanders, 1977), as observed in deep-sea polychetes (Jumars et al., 1990) and, anecdotally, in the occurrence of wood- and bone-eating deep-sea specialists (Turner, 1973; Rouse et al., 2004; Johnson et al., 2010). In general, as carbon availability increases, so too does the prevalence of direct development, while the prevalence of planktonic larval stages decreases (McClain et al., 2014). These findings suggest that some reproductive strategies are too energetically expensive at low carbon availabilities, or arise only when energy is available, and thus may be restricted to HET.

Data and Analysis

Methods and data are from McClain et al. (2018). Data, including carbon flux, were originally taken from McClain et al. (2012b). In brief, data on the taxonomy, maximum and minimum water depth in meters, maximum and minimum longitude, and maximum and minimum latitude were compiled for bivalves in the Northeast Pacific and Northwest Atlantic through an extensive search of the primary literature and online databases. The final dataset includes complete information for 1578 species from 75 families.

Over each species' biogeographic range, we estimated POC flux (gC/m2/yr) from Lutz et al. (2007) model (equal-area grid of 9 km resolution) as described above. These values were previously determined as part of another study (McClain et al., 2012b). For each species, McClain et al. (2012b) quantified the mean, median, and standard deviation of carbon flux over their known latitudinal and depth ranges. For the analyses here, we used mean carbon flux only as mean and median fluxes are highly correlated (Spearman's rho = 0.94, $p < 0.0001$). We created a range map for each species based on its latitudinal range. This range map was then overlain onto a bathymetry layer (GEBCO 08, 30 arc-second grid, September 2010 release)[1] and cropped to regions between the minimum and maximum reported depth. We assumed a species' range represents an elongated band with North/South limits set by maximum and minimum reported latitude. East/West limits were set by depth, instead of longitude, because North American coasts run approximately south to north with species occurring in depth bands along the continental margins. POC flux values were pulled for each cell within a species' biogeographic range as defined minimum and maximum latitude and depth.

We classified species according to a framework for ecological modes that is based on the first principles of functional morphology and developed by Bambach et al. (2007) and Bush et al. (2007). The ecological mode of a species is defined by three axes: tiering, motility, and feeding. Each axis consists of six categorical states. The tiering axis consists of pelagic, erect, surficial, semi-infaunal, shallow infaunal, and deep infaunal. The motility axis consists of freely motile/fast; freely motile/slow; facultatively motile/unattached; facultatively motile/attached; non-motile/unattached; and non-motile/attached. The feeding axis consists of suspension feeding, surficial deposit feeding, mining, grazing, predatory, and other (for feeding strategies that do not fit into the previous five feeding modes). Bush et al. (2007) provide a full description of this ecospace model. Ecological mode assignments were made at the genus level. Huber (2010) describes the life habits of individual bivalve families, and in the cases where genera within families are known to differ from one another, notes which genera differ and how they differ from other genera in the family. All ecological assignments were based on the life habits of the adult form. In the exceedingly rare cases where a genus occupied more than one ecological category for a given axis as an adult, the single ecological category that describes the majority of species in the genus was chosen. For the modern bivalve range dataset, we were able to assign ecological modes to 1,477 of 1,578 species by matching species to genera.

We conducted a correlation analysis of mean POC fluxes among ecological modes, to elucidate which modes were associated with HET and LET, comparing the mean POC values determined with the Atlantic data to those determined with the Pacific data using Spearman's *rho* statistic to estimate a rank-based measure of association. This allowed us to examine whether high-energy or low-energy ecological modes were consistently found in high- or low-energy settings using independent lists of species and independent ocean basins. We also tested whether the representation of ecological modes differs between the overall higher productivity Pacific Ocean and lower productivity Atlantic Ocean. For the Atlantic and Pacific oceans separately, we calculated the proportion of each species within each ecological mode. We then calculated the difference in the proportion of species within each ecological mode between the Atlantic and Pacific oceans and compare that to the mean carbon flux of the ecological mode. We predict that ecological modes more strongly tied to higher POC fluxes will occur at higher proportions in the Pacific compared to the Atlantic Ocean due to the overall higher productivity in the Pacific. We tested this relationship using a general linear regression model with mean POC flux of the ecological mode as the independent and the Atlantic/Pacific ratio of the proportion of species as the dependent variable. Linear models were performed in R Development Core Team (2019). The general relationship was visualized utilizing ggplot (Wickham, 2009).

Consequence

Ecological niche axes in modern bivalves over oceanic scales are correlated with the available environmental energy (McClain et al., 2018; **Figures 4**, **5**). More specifically, the basic functional traits of feeding mode, tiering level, and motility level are associated with their relative prevalence in low- or high-energy settings (McClain et al., 2018). The strong consistency between the rank orders of ecological modes based on carbon flux between the Atlantic and Pacific Oceans, observed across independent lists of endemic species, implies that the association between ecological mode and carbon flux is also not an artifact of indirect connections but, rather, a fundamental aspect of these ecological

[1] www.gebco.org

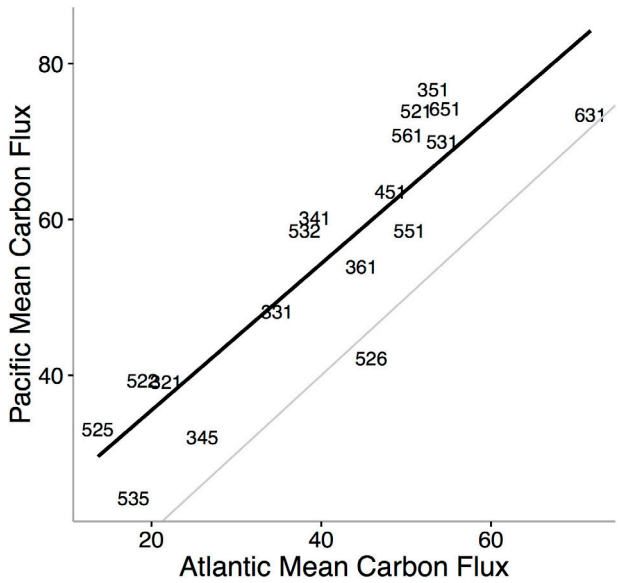

FIGURE 4 | Mean carbon flux of bivalve ecological modes in the Pacific Ocean versus the mean carbon flux of ecological modes in the Atlantic Ocean. Black line denotes the rank order correlation and the gray line represents the one-to-one value line. Numbers refer to unique functional combinations on three ecological mode axes: tiering, motility, and feeding. Each axis consists of six categorical states. The tiering axis consists of 1 pelagic, 2 erect, 3 surficial, 4 semi-infaunal, 5 shallow infaunal, and 6 deep infaunal. The motility axis consists of 1 freely motile/fast; 2 freely motile/slow; 3 facultatively motile/unattached; 4 facultatively motile/attached; 5 non-motile/unattached; and6 non-motile/attached. The feeding axis consists of 1 suspension feeding, 2 surficial deposit feeding, 3 mining, 4 grazing, 5 predatory, and 6 other (for feeding strategies that do not fit into the previous five feeding modes). Using independent values of mean carbon flux for ecological modes by restricting the analysis to species endemic to either the Atlantic or the Pacific, we find striking consistency in the ranking of carbon flux requirements in bivalve ecological modes. The finding that most ecological modes are typically associated with higher flux values in the Pacific Ocean is not surprising; the Pacific is on average more productive than the Atlantic (Marra et al., 1987; Lutz et al., 2007). From McClain et al. (2018).

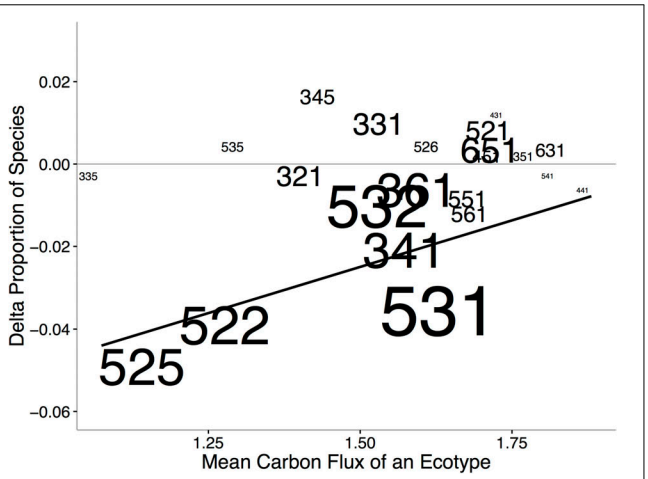

FIGURE 5 | Changes in the proportion of ecological modes between the Atlantic and Pacific Oceans verses the mean carbon flux of the ecological mode. Increases in values indicate increased representation in the Pacific and decreased representation in the Atlantic. Size of text indicates ecological-mode proportion in the data set. Numbers refer to unique functional combinations on three ecological mode axes, tiering, motility, and feeding (see **Figure 4** caption for details of numbers). We find that HET associated with higher POC fluxes occur in greater proportion in the Pacific Ocean and, conversely, LET occur in greater proportion in the Atlantic. From McClain et al. (2018). Dashed line represents in proportions in the Atlantic and Pacific Oceans. Solid line indicates significant regression line.

modes (**Figure 4**). Ecological differences among ocean basins, correlated with differences in POC, provide evidence that overall food availability at broad scales can shape the ecology of the regional to global biota (**Figure 5**). The differences in total carbon flux between the Atlantic and Pacific Ocean determine the relative proportion of specific bivalve ecologies (**Figure 5**). In the more productive Pacific, HET ecologies are numerically dominant, and conversely, in the less productive Atlantic, LET ecologies are numerically dominant (**Figure 5**).

In many cases, empirical results are surprising and contrary to theoretical predictions. Simultaneous hermaphroditism, predicted to increase with decreasing environmental carbon availability as low populations sizes would decrease the chance of finding a mate, actually show the opposite pattern in deep-sea mollusks (McClain et al., 2014). These kinds of counter-theory findings suggest that much work is required in order to elucidate patterns of functional tradeoffs and adaptation over energetic gradients. Emerging research does support the presence of certain metabolically expensive traits that can be tied to low-energy and high-energy taxa (LET vs. HET) such that their relative representations vary over energetic gradients. We analyzed the Atlantic deep-sea bivalve database with a general additive model (GAM) to examine how two common traits, suspension and deposit feeding, vary with POC flux. We find (**Figure 6**) that the proportion of species of suspension feeding increases ($p < 0.0001$, $R^2 = 0.19$) and deposit feeding decreases ($p = 0.0030$, $R^2 = 0.11$) with increasing POC flux. Suspension feeders require a continuous supply of suspended particulate matter at a density high enough to offset the energetic costs of filter feeding; thus, the link to regional carbon fluxes is predictable (McClain and Lundsten, 2015).

PROPOSITION 8: METABOLIC NICHE WIDTH INCREASES WITH INCREASING ENVIRONMENTAL AVAILABILITY OF CARBON

Premise

To the extent that biogeographic range is the realization of a species' niche (Slayter et al., 2013), processes controlling the metabolic niche should impact the size and placement of species distributions. For example, energetically expensive traits such as large body sizes may be confined to high energy regions (Fernández and Vrba, 2005; McClain et al., 2012b). In addition, within a given environmental setting

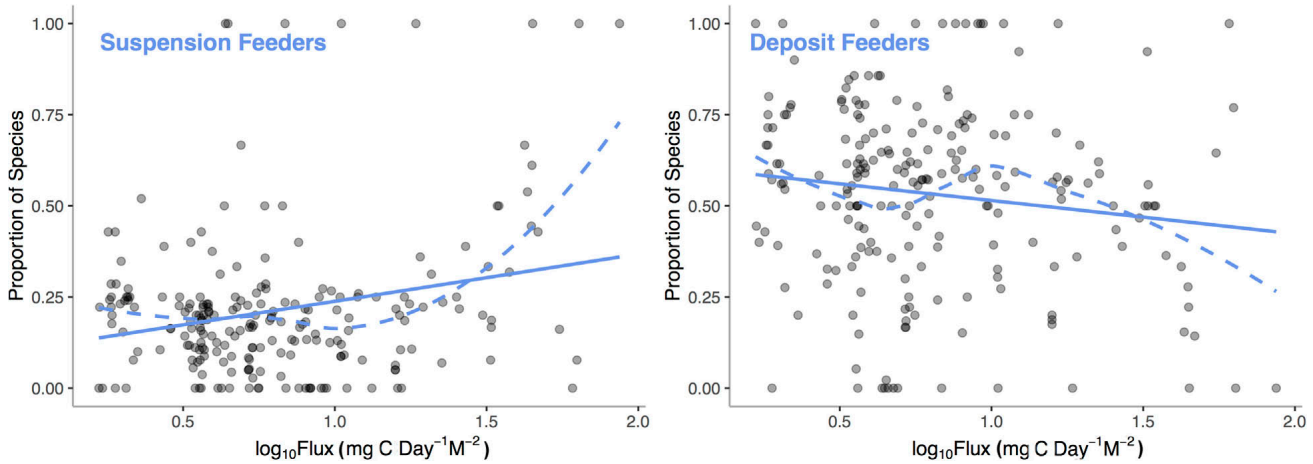

FIGURE 6 | Proportion of deep-sea, bivalve species that are suspension feeders and deposit feeders among sampling stations across the Atlantic Ocean verses Log_{10} Standardized Carbon Flux (gC m^{-2} d^{-1}) for the sampling station. Dashed line represent LOESS smooths and the solid lines represent general additive model fits.

HET are predicted to possess larger biogeographic ranges as home range sizes increase to incorporate the increased food resources required (McNab, 1963; Brown and Maurer, 1987). Energetics may also impact biogeographic range size because of the connections with niche breadth (Slatyer et al., 2013): higher energy availability can lead to smaller ranges because species become resource specialists (Sircom and Walde, 2010; Whitton et al., 2012). Range size is also impacted by the degree of environmental variability in both time and space. For instance, marine bivalves achieve broad geographic ranges across broad, contiguous isotherms (Jablonski et al., 2013; Tomasovych et al., 2015); widespread biogeographic ranges could also be constructed through large and homogenous chemical energetic landscapes. Environmental variables associated with habitat productivity, especially temperature and precipitation, are typically important predictors of species occurrence across taxonomic groups (Bradie and Leung, 2017), supporting the contention that the biogeographic ranges of many species are set, at least in part, by chemical energy availability.

Two different hypotheses relate niche width more generally to carbon availability: (1) Increased carbon availability increases the amount of a preferred resource allowing species to decrease their consumption of less optimal resources, i.e., specialization (Evans et al., 1999). Lower food availability may favor generalists, e.g., scavengers, so that any carbon resources can be utilized, expanding the niche. These hypotheses predict that niche width, or generalism, exhibits a negative relationship with carbon availability. (2) Alternatively, low carbon availability could favor specialization on previously underutilized carbon sources as energy sources become limited, leading to narrow niche widths (Sanders, 1977).

Measuring niche breadth directly is difficult. However, we can use geographic range as proxy, allowing us to test hypotheses. Geographic range is known to reflect niche width such that specialization is associated with smaller geographic ranges (Slayter et al., 2013).

Data and Analyses

We examine this relationship between geographic range size, as a proxy for niche width, and mean POC across the geographic range for gastropod species across the Atlantic Ocean. Data were compiled by McClain et al. (2018) in an extensive search of the primary literature and online databases resulting in complete information a 3,162 species from 100 families. Data include taxonomic information from subclass to species, synonymies, maximum and minimum water depth in meters, maximum and minimum longitude, and maximum and minimum latitude. Biogeographic range and POC were quantified for each gastropod species by the methods described in the Proposition 6 for bivalves. Total range size was calculated as the number of 1° by 1° cells assuming that a species occurs at all sites across its latitudinal and depth range. For the range size verses mean carbon flux, we utilized a GAM to account for potential non-linear effects. The full model also includes other known variants of range size including temperature, mean latitude, mean depth, and species biovolume. The GAM was implemented using the mgcv package in R (Wood, 2011).

Consequence

After accounting for temperature, body size, latitude and depth, we find a significant and positive relationship between geographic range size of Atlantic gastropods and mean POC ($p < 0.0001$, **Figure 7**). Increasing temperature, body size, depth, and latitude also correlated with increases in range size ($p < 0.0001$ for all independent factors) with the overall model accounting for 41.9% of the variation.

Lower carbon availabilities produce smaller geographic range sizes and potentially narrow niche widths. Increases in food availability correlate with larger ranges. This positive correlation is in contrast to most theories suggesting that higher carbon availability should lead to smaller ranges (Evans et al., 1999;

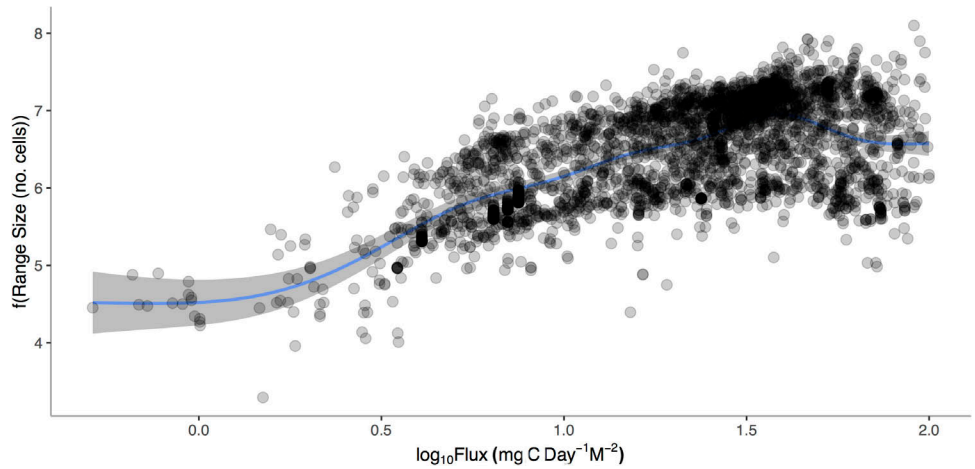

FIGURE 7 | Geographic range size (1°cells) of marine gastropods from the Atlantic Ocean verses Log_{10} Mean Carbon Flux (gC m^{-2} d^{-1}). General additive model relationship is shown for the conditional relationship once body size, mean depth, mean latitude, and temperature are accounted for.

Bonn et al., 2004; Sircom and Walde, 2010; Whitton et al., 2012). One possible reason for this result is that the analyses here control for a variety of other geographic, environmental, and biological factors correlated with body size. Thus, the negative pattern between productivity and range size may reflect other factors correlated with productivity. For example, body size increases with increasing productivity (McClain et al., 2012b). Sanders (1977) originally proposed that low productivity would favor specialization to consume previously underutilized carbon sources. Indeed, the low productivity encountered in the deep sea appears to select for specialization on exotic carbon sources (Van Dover, 2000; Braby et al., 2007; Bienhold et al., 2013).

PROPOSITION 9: IF METABOLIC NICHES, AND ENERGETIC REQUIREMENTS, VARY AMONG SPECIES THEN COMPOSITIONAL CHANGES ARE EXPECTED OVER SPATIAL OR TEMPORAL GRADIENTS OF ENERGY

Premise

Beta diversity (β-diversity) is "the extent of change in community composition, or degree of community differentiation, in relation to a complex-gradient of environment, or a pattern of environments" (Whittaker, 1960, p. 320). β-diversity patterns therefore emerge from the interaction between the environment and the varying metabolic niche requirements (indexed by biogeographic range and patchiness of occupancy within that range) of all species in an assemblage. If metabolic niches, and energetic requirements, do indeed vary among species then compositional changes are expected over spatial or temporal gradients of energy.

Consequence

In support of this, clines of β-diversity over energy gradients have been documented among bacteria (Zinger et al., 2011), invertebrates (McClain and Barry, 2010, 2014; McClain et al., 2011, 2012c, 2016; Andrew et al., 2012), and vertebrates (He and Zhang, 2009; Melo et al., 2009; Qian and Xiao, 2012), on land (He and Zhang, 2009; Melo et al., 2009; Andrew et al., 2012; Qian and Xiao, 2012) and in the ocean (McClain and Barry, 2010, 2014; McClain et al., 2011, 2012c, 2016; Zinger et al., 2011), with the rate of this turnover set by both niche width and the intensity of the environmental gradient in energy availability. At a taxonomic level, species or clades with comparatively higher metabolic demands should exhibit higher rates of turnover (Soininen et al., 2007a,b), because HET will be more sensitive to changes in environmental energy. Any reduction in energy should push HET increasingly near to their energetic minimum requirements. β-diversity does vary greatly among taxa with different body masses, trophic levels, and thermoregulation as predicted from energetic theory based on how these factors control metabolic demand (Soininen et al., 2007a,b).

Despite the overall paucity of energy, the deep seafloor supports high alpha diversity, which may be comparable to much more productive ecosystems such as coral reefs or tropical rainforests. This paradox of seemingly high diversity in a low-energy system is well treated in the deep-sea literature (McClain and Schlacher, 2015) but the most influential idea is the patch-mosaic hypothesis (Grassle and Sanders, 1973). Grassle posited that interactions between the spatially heterogeneous fall of POC and microscale topography such as burrows and mounds, or feeding trails of large mobile deposit feeders, create a mosaic of centimeter scale patches of high and low energy availability (Grassle, 1989) which – unlike in shallow water where patches are homogenized quickly (days to weeks) due to frequent bioturbation and currents – can persist for years (Etter and Mullineaux, 2001). Species are highly specialized in microhabitat preference which leads to an overall diverse mosaic

of assemblages, each with a unique set of species. To restate, species have a metabolic niche that contributes to high small-scale beta diversity increasing local alpha-diversity.

This patchiness is reflected in high species turnover at small scales (Etter and Mullineaux, 2001; Snelgrove and Smith, 2002), and experimental work enriching nutrients in deep-sea colonization trays has underlined the key role that energy plays, with species that are rare or absent in the background environment reaching high abundances in enriched patches (Levin and Smith, 1984; Snelgrove et al., 1992, 1994, 1996; Bernardino et al., 2010; McClain et al., 2011).

PROPOSITION 10: METABOLIC NICHES, AND ENERGETIC REQUIREMENTS, CAN BE USED TO MAKE SPECIFIC PREDICTIONS OF BIODIVERSITY PATTERNS OVER SPATIAL OR TEMPORAL GRADIENTS OF ENERGY

Premise

Increases in available carbon frequently translate into increases in species richness or alpha-diversity (Rosenzweig and Abramsky, 1993; Waide et al., 1999; Clarke and Gaston, 2006; Cusens et al., 2012), either linearly or as a unimodal relationship with richness peaking at intermediate levels of energy. Although a variety of mechanisms exist to explain the relationship between species richness and energy (Rosenzweig and Abramsky, 1993), here we explore only how understanding species metabolic niches may inform about diversity gradients. We envision two different scenarios for patterns of β- and a-diversity over gradients in energy availability in the context of the metabolic niche (**Figure 8**). These differ in whether β-diversity occurs because of the replacement of some species with others (species turnover) or because species loss leads to smaller communities forming ordered subsets of larger communities (nestedness) (Baselga, 2010, 2012). It is worth noting, across energy gradients there is evidence of both nestedness (Baselga et al., 2012; Brault et al., 2013; McClain et al., 2016; Stuart et al., 2016) and turnover (Andrew et al., 2012; Brault et al., 2013; Wagstaff et al., 2014). These two scenarios lead to different predictions of alpha-diversity over a productivity gradient as well.

PROPOSITION 10A: HIGH METABOLIC DEMAND TAXA ARE LOST FROM COMMUNITIES WHEN ENVIRONMENTAL ENERGY DROPS BELOW THEIR METABOLIC NEED

The first scenario predicts nestedness will occur as energy availability falls below the minimum metabolic requirement of certain taxa (**Figure 8**, top). At ecological scales, high-energy habitats offer more niches because more species can meet their minimum energetic requirements, and both LET and HET can persist. LET may survive on patches of low quality, quantity, or density of resources that are not monopolized by HET within these high-energy habitats, i.e., no competitive exclusion occurs. In low-energy habitats, HET are lost because minimum energetic requirements cannot be met. While empirical tests for this idea are lacking, the test is relatively straightforward – the diversity of interspecific metabolic rates should increase with greater energy availability.

If high-energy habitats support more energetic niches, species richness may increase at higher energy availability because species are able to specialize on preferred resources, e.g., a predator consuming a single prey species or a herbivore consuming a single plant, reducing competitive interactions and allowing for greater species coexistence (Evans et al., 2005). Again, empirical tests of this hypothesis are rare but easily conducted: the trophic niche, measured for instance as the variance in $\delta^{13}C$ (a measure of the variability in consumed carbon sources), and the variance in $\delta^{15}N$ (a measure of trophic specialization), should both decrease with increasing energy availability.

PROPOSITION 10B: LOW METABOLIC DEMAND TAXA ARE LOST FROM COMMUNITIES FROM COMPETITIVE EXCLUSION WHEN ENVIRONMENTAL ENERGY IS HIGH

In the second scenario, over a decreasing gradient of carbon availability, the expectation is for LET to replace HET, i.e., turnover (**Figure 8**, bottom). As before, the minimum metabolic demands of HET cannot be met when environmental energy declines, but this scenario additionally assumes that LET do not exist in higher energy availability habitats, because they are competitively excluded by HET that can monopolize resources. To restate, HETs with faster growth rates, population growth rates, increased mobility, and larger sizes may prove to be superior competitors to LETs in high energy environments. This is essentially the second half of the dynamic equilibrium model (Huston, 1979) and is in some aspects very similar to the resource ratio hypothesis in that it invokes competition under high energy availability (Tilman, 1982). The competitive exclusion of LET in high energy habitats predicts a unimodal relationship between α-diversity and energy availability, similar to the interaction competition hypothesis (Rosenzweig and Abramsky, 1993), where all increases in energy go to a competing taxon.

Data and Analyses

We analyze the Allen (2008) bivalve data as described in Proposition 6. We decomposed β-diversity over the POC gradient into two distinct components: species turnover and species loss leading to nestedness using the *betapart* package (Baselga et al., 2013) in R to decompose Sørensen's dissimilarity index $\beta_{SØR}$ into dissimilarity due to turnover measured as Simpson's index β_{SIM} and a new index of dissimilarity due to species loss leading to nestedness β_{NES}. We computed dissimilarity between pairs of sites against the difference in

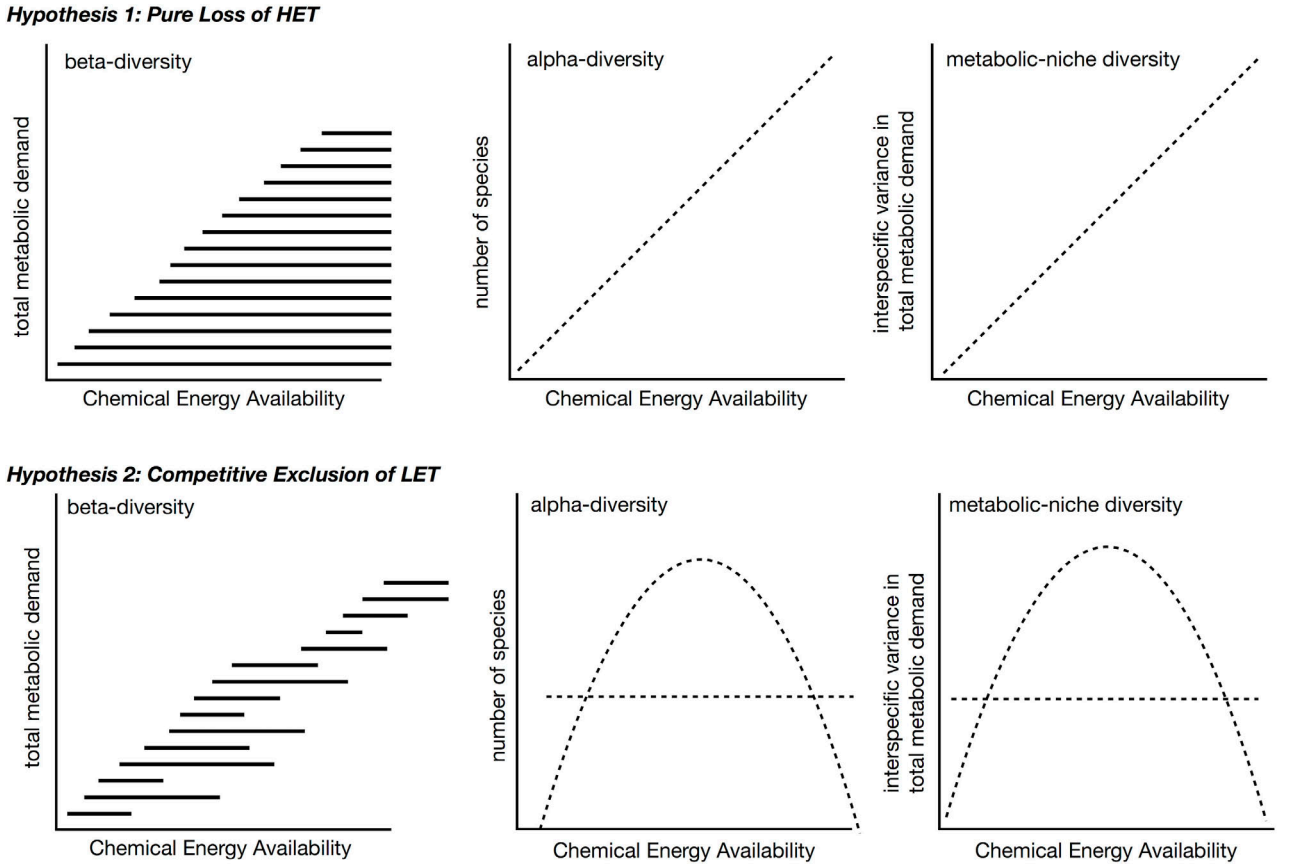

FIGURE 8 | Two hypotheses for beta- and alpha-diversity patterns in the context of metabolic niches. In both scenarios, high energy taxa (HET) are lost from communities as chemical energy availability decreases across a gradient. In the second hypothesis, high chemical energy availability LET are additionally outcompeted, e.g., due to slower populations rates, and are lost from these communities. The competitive exclusion in LET in second hypothesis leads to a unimodal species-energy relationship as opposed to a linear pattern. In both hypotheses, metabolic niche diversity, e.g., interspecific variation in metabolic rate, should mirror the species richness pattern.

depth for each pair (Baselga, 2010). We used a Mantel test with 1,000 replicates (Pearson correlation) to assess whether the components of β-diversity changed among sites along the gradient of POC flux.

Consequence

In our analysis of bivalves from the deep-sea of the Atlantic Ocean, we find that turnover (Mantel Test: $r = 0.1141, p < 0.0001$) rather than nestedness (Mantel Test: r = -0.258, p = 0.904) is prevalent (**Figure 9**) implying that both metabolic competition and limits are important in shaping compositional changes.

In the context of the two scenarios illustrated in **Figure 8**, turnover appears to be prevalent in deep-sea invertebrates over a depth gradient, implying LET are replacing HET and that LET are outcompeted at higher energy availabilities (Brault et al., 2013). Equally, in deep-sea canyons areas with increased POC support only a small subset of species, with the loss coming from competitive exclusion (McClain and Barry, 2010). At larger scales, patterns of taxonomic, functional, and phylogenetic beta-diversity are tied to POC (McClain et al., 2012c), implying that the changes in beta-diversity have an adaptive origin tied to species traits. From local to oceanic spatial scales, a pattern is emerging that the metabolic niche of deep-sea species and its relations to energy availability sets beta-diversity.

However at very low energy values, like those occurring on the abyssal plains, nestedness occurs, reflecting the loss of even LET when energy availability falls below minimum metabolic needs (Rex et al., 2005). Low-energy communities on deep-sea wood falls are also nested taxonomic subsets of high-energy communities (McClain et al., 2016). This switch from turnover to nestedness implies that at extreme energy limitation, evolutionary novelty and adaptation may not be possible; rather, a source-sink system emerges in which populations from higher energy availability regions of the deep sea sustain through emigration populations of abyssal low-energy sites mitigating Allee effects (Rex et al., 2005). This combination of nestedness and turnover is reflected in a general unimodal pattern of alpha-diversity which typically peaks at intermediate depths and levels of POC (Rex and Etter, 2010): in low-energy habitats, HET are lost because minimum energetic requirements cannot be met (Rex et al., 2005), whereas LETs may not be able to survive at the highest energy availabilities because they are outcompeted

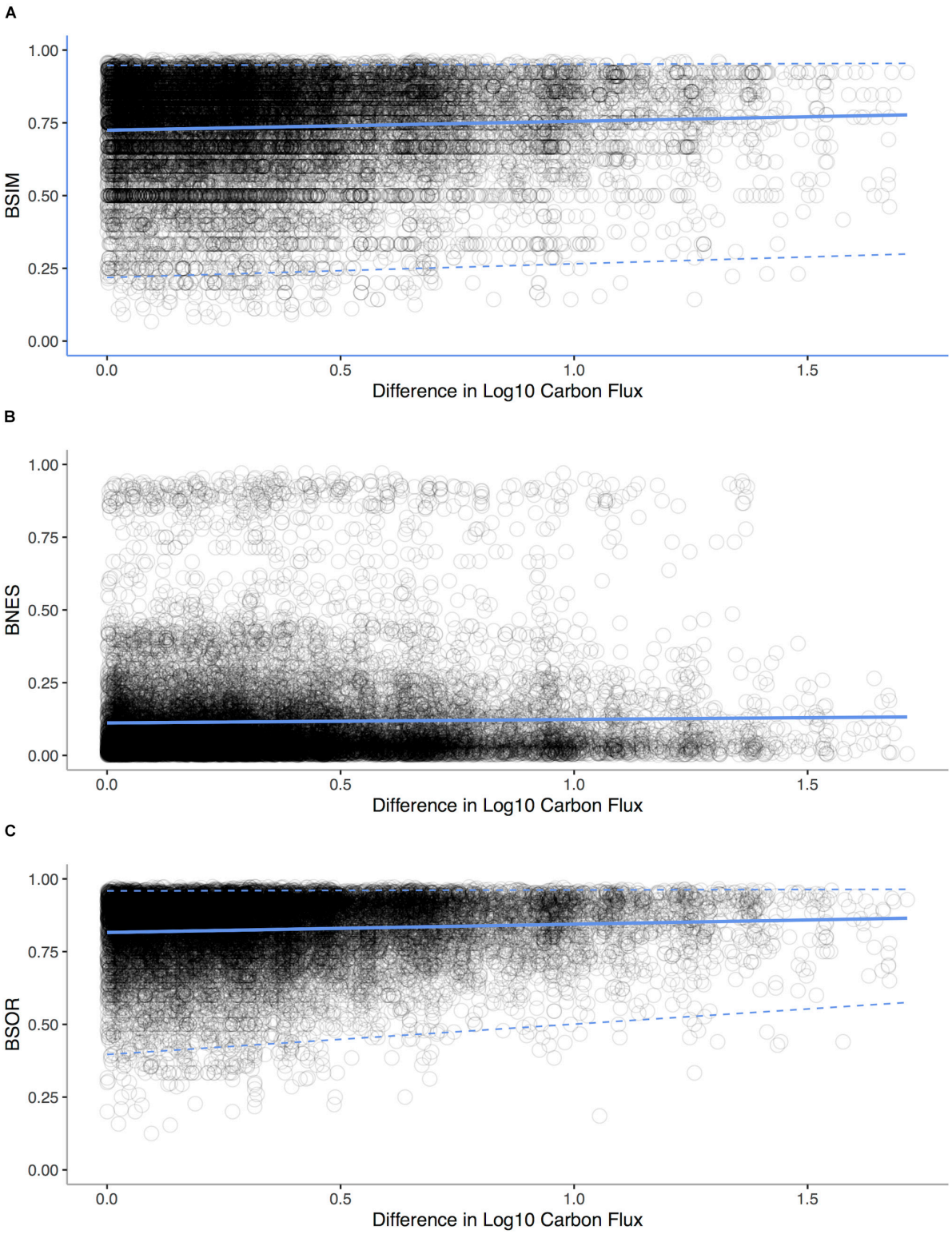

FIGURE 9 | Standard environmental distance-decay plots representing pairwise comparisons of bivalve community similarity verses differences in POC flux for each sampling station in the Atlantic Ocean. **(A)** Simpson's index β_{SIM} of dissimilarity due to turnover vs. difference in Log_{10} Carbon Flux (gC m^{-2} d^{-1}, Mantel statistic r: 0.08, $p < 0.0001$). **(B)** Dissimilarity due to species loss leading to nestedness β_{NES} verses Log_{10} Carbon Flux (Mantel statistic r: -0.03, $p = 0.904$). **(C)** Sørensen's dissimilarity index $\beta_{SØR}$ verses differences Log_{10} Carbon Flux (Mantel statistic r: 0.11, $p < 0.0001$). Regression lines (solid lines) and quantile regressions lines (1 and 99%, dashed lines) are shown.

by HETs that can monopolize resources, as observed in deep-sea canyons (McClain and Barry, 2010).

CONCLUSION

Van Valen (1976) stated that "Potential energy in the form of reduced carbon is the fuel of the fire of life. All other resources, even when regulatory, can be considered surrogates, when they are competed for." This perhaps represents an extreme view, but every aspect of an animal's existence requires carbon. We propose from this simple concept that understanding and quantifying the metabolic niche can potentially link scales from individuals to ecosystems and link adaptation to patterns in biogeography and biodiversity. Energy and the metabolic niche also allow for explicit links between ecological and evolutionary theory. Future avenues of research include addressing the following questions:

(1) Do intraspecific metabolic rates vary over energy gradients?
(2) What is the diversity of and energetic adaptations among organisms and how do these vary over energy gradients? Is a greater diversity of metabolic niches and adaptations afforded at greater energy availability?
(3) Do generalists or specialists prevail at high and low energy habitats?
(4) To what extent are range limits and biogeographic patterns set by the metabolic niche?
(5) Do patterns of α- and β-diversity differ among high and low energy taxa?
(6) Are low energy taxa competitively excluded at high energy availability?

We have outlined how the unique features of deep-sea benthos that make them an ideal testbed for many of these questions, but linking data on the occurrences and biological traits of species with their energetic environmental settings in a range of extreme systems, including deep-sea pelagic systems, will help to generalize the metabolic niche concept.

DATA AVAILABILITY STATEMENT

The datasets generated for this study are available on request to the corresponding author.

AUTHOR CONTRIBUTIONS

CM led writing, theory development, and analyses. SD, TW, and SF contributed to the analyses. All authors contributed to theory development, writing, and editing.

FUNDING

CM and CN were supported by NSF/OCE 1634586.

ACKNOWLEDGMENTS

This work and theory developed out of numerous conversations over the years with J. Payne, J. Nekola, J. Brown, A. Hulbert, M. Ernest, J. Barry, M. Rex, and countless others. We are indebted to them. D. McGlinn and M. Pennell, and their respective lab groups, provided friendly reviews and invaluable feedback.

REFERENCES

Allen, J. A. (2008). Bivalvia of the deep Atlantic. *Malacologia* 50, 57–173. doi: 10.4002/0076-2997-50.1.57

Andrew, M. E., Wulder, M. A., Coops, N. C., and Baillargeon, G. (2012). Beta-diversity gradients of butterflies along productivity axes. *Glob. Ecol. Biogeogr.* 21, 352–364. doi: 10.1111/j.1466-8238.2011.00676.x

Bambach, R. K. (1993). Seafood through time: changes in biomass, energetics, and productivity in the marine ecosystem. *Paleobiology* 19, 372–397. doi: 10.1017/s0094837300000336

Bambach, R. K., Bush, A. M., and Erwin, D. H. (2007). Autecology and the filling of ecospace: key metazoan radiations. *Paleontology* 50, 1–22. doi: 10.1111/j.1475-4983.2006.00611.x

Baselga, A. (2010). Partitioning the turnover and nestedness components of beta diversity. *Glob. Ecol. Biogeogr.* 19, 134–143. doi: 10.1111/j.1466-8238.2009.00490.x

Baselga, A. (2012). The relationship between species replacement, dissimilarity derived from nestedness, and nestedness. *Glob. Ecol. Biogeogr.* 21, 1223–1232. doi: 10.1111/j.1466-8238.2011.00756.x

Baselga, A., Gómez-Rodríguez, C., and Lobo, J. M. (2012). Historical legacies in world amphibian diversity revealed by the turnover and nestedness components of beta diversity. *PLoS One* 7:e32341. doi: 10.1371/journal.pone.0032341

Baselga, A., Orme, D., Villeger, S., Bortoli, J. D., and Leprieur, F. (2013). *Betapart: Partitioning Beta Diversity Into Turnover and Nestedness Components, Version R Package Version 1.3*.

Behrenfeld, M. J., O'malley, R. T., Siegel, D. A., Mcclain, C. R., Sarmiento, J. L., Feldman, G. C., et al. (2006). Climate-driven trends in contemporary ocean productivity. *Nature* 444, 752–755. doi: 10.1038/nature05317

Bernardino, A. F., Smith, C. R., Baco, A. R., Altamira, I., and Sumida, P. Y. G. (2010). Macrofaunal succession in sediments around kelp and woodfalls in the deep NE Pacific and community overlap with other reducing habitats. *Deep Sea Res. I* 57, 708–723. doi: 10.1016/j.dsr.2010.03.004

Bienhold, C., Risotva, P. P., Wenzhofer, F., Dittmar, T., and Boetius, A. (2013). How deep-sea wood falls sustain chemosynthetic life. *PLoS One* 8:e53590. doi: 10.1371/journal.pone.0053590

Blowes, S., Supp, S., Antao, L., Bates, A., Bruelheide, H., Chase, J., et al. (2018). Biodiversity trends are stronger in marine than terrestrial assemblages. *bioRxiv* [Preprint]. doi: 10.1101/457424

Bonn, A., Storch, D., and Gaston, K. J. (2004). Structure of the species–energy relationship. *Proc. R. Soc. B Biol. Sci.* 271, 1685–1691. doi: 10.1098/rspb.2004.2745

Boyce, D. G., Lewis, M. R., and Worm, B. (2010). Global phytoplankton decline over the past century. *Nature* 466, 591–596. doi: 10.1038/nature09268

Braby, C. E., Rouse, G. W., Johnson, S. B., Jones, W. J., and Vrijenhoek, R. C. (2007). Bathymetric and temporal variation among *Osedax* boneworms and associated megafauna on whale-falls in Monterey Bay, California. *Deep Sea Res. I* 54, 1773–1791. doi: 10.1016/j.dsr.2007.05.014

Bradie, J., and Leung, B. (2017). A quantitative synthesis of the importance of variables used in MaxEnt species distribution models. *J. Biogeogr.* 44, 1344–1361. doi: 10.1111/jbi.12894

Brault, S., Stuart, C., Wagstaff, M., Mcclain, C. R., Allen, J. A., and Rex, M. A. (2013). Contrasting patterns of α- and β-diversity in deep-sea bivalves of the

eastern and western North Atlantic. *Deep Sea Res. II* 92, 157–164. doi: 10.1016/j.dsr2.2013.01.018

Brey, T., Müller-Wiegmann, C., Zittier, Z. M., and Hagen, W. (2010). Body composition in aquatic organisms—a global data bank of relationships between mass, elemental composition and energy content. *J. Sea Res.* 64, 334–340. doi: 10.1016/j.seares.2010.05.002

Brown, J. H., Gillooly, J. F., Allen, A. P., Savage, V. M., and West, G. B. (2004). Toward a metabolic theory of ecology. *Ecology* 85, 1771–1789. doi: 10.1890/03-9000

Brown, J. H., and Maurer, B. A. (1987). Evolution of species assemblages : effects of energetic constraints and species dynamics on the diversification of the North-American Avifauna. *Am. Nat.* 130, 1–17. doi: 10.1086/284694

Bryndum-Buchholz, A., Tittensor, D. P., Blanchard, J. L., Cheung, W. W., Coll, M., Galbraith, E. D., et al. (2019). Twenty-first-century climate change impacts on marine animal biomass and ecosystem structure across ocean basins. *Glob. Chang. Biol.* 25, 459–472. doi: 10.1111/gcb.14512

Bush, A. M., Bambach, R. K., and Daley, G. M. (2007). Changes in theoretical ecospace utilization in marine fossil assemblages between the mid-Paleozoic and late Cenozoic. *Paleobiology* 33, 76–97. doi: 10.1666/06013.1

Butchart, S. H., Walpole, M., Collen, B., Van Strien, A., Scharlemann, J. P., Almond, R. E., et al. (2010). Global biodiversity: indicators of recent declines. *Science* 328, 1164–1168. doi: 10.1126/science.1187512

Carbone, C., Teacher, A., and Rowcliff, J. M. (2007). The cost of carnivory. *PLoS Biol.* 5:e22. doi: 10.1371/journal.pbio.0050022

Childress, J. J. (1995). Are there physiological and biochemical adaptations of metabolism in deep-sea animals? *Trends Ecol. Evol.* 10, 30–36. doi: 10.1016/s0169-5347(00)88957-0

Chust, G., Allen, J. I., Bopp, L., Schrum, C., Holt, J., Tsiaras, K., et al. (2014). Biomass changes and trophic amplification of plankton in a warmer ocean. *Glob. Chang. Biol.* 20, 2124–2139. doi: 10.1111/gcb.12562

Clarke, A., and Gaston, K. J. (2006). Climate, energy and diversity. *Proc. R. Soc. B Biol. Sci.* 273, 2257–2266.

Cusens, J., Wright, S. D., Mcbride, P. D., and Gillman, L. N. (2012). What is the form of the productivity–animal-species-richness relationship? A critical review and meta-analysis. *Ecology* 2012, 2241–2252. doi: 10.1890/11-1861.1

Denny, M. W. (1999). Are there mechanical limits to size in wave-swept organisms? *J. Exp. Biol.* 202, 3463–3467.

Doney, S. C., Ruckelshaus, M., Emmett Duffy, J., Barry, J. P., Chan, F., English, C. A., et al. (2012). Climate change impacts on marine ecosystems. *Annu. Rev. Mar. Sci.* 4, 11–37.

Etter, R. J., and Mullineaux, L. S. (2001). "Deep-sea communities," in *Marine Community Ecology*, eds M. D. Bertness, S. D. Gaines, and M. E. Hay (Sunderland, MA: Sinauer Associates, Inc), 367–394.

Evans, K. L., Greenwood, J. J. D., and Gaston, K. J. (2005). Dissecting the species-energy relationship. *Proc. Biol. Sci.* 272, 2155–2163. doi: 10.1098/rspb.2005.3209

Evans, K. L., Warren, P. H., and Gaston, K. J. (1999). Species–energy relationships at the macroecological scale: a review of the mechanisms. *Biol. Rev.* 80, 1–25. doi: 10.1017/s1464793104006517

Fernández, M. H., and Vrba, E. S. (2005). Body size, biomic specialization and range size of African large mammals. *J. Biogeogr.* 32, 1243–1256. doi: 10.1111/j.1365-2699.2005.01270.x

Gage, J. D., and Tyler, P. A. (1991). *Deep-Sea Biology: A Natural History of Organisms at the Deep-Sea Floor*. Cambridge: Cambridge University Press.

Gillooly, J. F., Brown, J. H., West, G. B., Savage, V. M., and Charnov, E. L. (2001). Effects of size and temperature on metabolic rate. *Science* 293, 2248–2251. doi: 10.1126/science.1061967

Glazier, D. S. (2005). Beyond the '3/4-power' law: variation in the intra- and interspecific scaling of metabolic rate in animals. *Biol. Rev.* 80, 611–662.

Gooday, A. J. (2002). Biological responses to seasonally varying fluxes of organic matter to the ocean floor: a review. *J. Oceanogr.* 58, 305–332.

Grassle, J. F. (1989). Species diversity in deep-sea communities. *Trends Ecol. Evol.* 4, 12–15. doi: 10.1016/0169-5347(89)90007-4

Grassle, J. F., and Sanders, H. L. (1973). Life histories and the role of disturbance. *Deep Sea Res.* 34, 313–341.

Harding, L. W. Jr., and Perry, E. S. (1997). Long-term increase of phytoplankton biomass in Chesapeake Bay, 1950-1994. *Mar. Ecol. Prog. Ser.* 157, 39–52. doi: 10.3354/meps157039

Harley, C. D., Randall Hughes, A., Hultgren, K. M., Miner, B. G., Sorte, C. J., Thornber, C. S., et al. (2006). The impacts of climate change in coastal marine systems. *Ecol. Lett.* 9, 228–241. doi: 10.1111/j.1461-0248.2005.00871.x

He, K., and Zhang, J. (2009). Testing the correlation between beta diversity and differences in productivity among global ecoregions, biomes, and biogeographical realms. *Ecol. Inform.* 4, 93–98. doi: 10.1016/j.ecoinf.2009.01.003

Huber, M. (2010). *Compendium of Bivalves. A Full-Color Guide to 3,300 of the World's Marine Bivalves. A Status on Bivalvia after 250 Years of Research*. Hackenheim: ConchBooks.

Hurlbert, A. H. (2004). Species-energy relationships and habitat complexity in bird communities. *Ecol. Lett.* 7, 714–720. doi: 10.1111/j.1461-0248.2004.00630.x

Hurlbert, A. H. (2006). Linking species–area and species–energy relationships in Drosophila microcosms. *Ecol. Lett.* 9, 287–294. doi: 10.1111/j.1461-0248.2005.00870.x

Huston, M. (1979). A general hypothesis of species diversity. *Am. Nat.* 113, 81–101. doi: 10.1086/283366

Jablonski, D., Belanger, C. L., Berke, S. K., Huang, S., Krug, A. Z., Roy, K., et al. (2013). Out of the tropics, but how? Fossils, bridge species, and thermal ranges in the dynamics of the marine latitudinal diversity gradient. *Proc. Natl. Acad. Sci. U.S.A.* 110, 10487–10494. doi: 10.1073/pnas.1308997110

Johnson, S. B., Waren, A., Lee, R. W., Kanyo, Y., Kaime, A., Davis, A., et al. (2010). *Rubyspira*, new genus and two new species of bone-eating deep-sea snails with ancient habits. *Biol. Bull.* 219, 166–177. doi: 10.1086/bblv219n2p166

Jumars, P. A., Mayer, L. M., Deming, J. W., Baross, J. A., and Wheatcroft, R. A. (1990). Deep-sea deposit-feeding strategies suggested by environmental and feeding constraints. *Philos. Trans. R. Soc. Lond. A* 331, 85–101. doi: 10.1098/rsta.1990.0058

Kennish, M. J. (1997). *Pollution Impacts on Marine Biotic Communities*. Boca Raton, FL: CRC Press.

Kordas, R. L., Harley, C. D., and O'Connor, M. I. (2011). Community ecology in a warming world: the influence of temperature on interspecific interactions in marine systems. *J. Exp. Mar. Biol. Ecol.* 400, 218–226. doi: 10.1016/j.jembe.2011.02.029

Lampitt, R. S., and Anita, A. N. (1997). Particle flux in the deep seas: regional characteristics and temporal variability. *Deep Sea Res. I* 44, 1377–1403. doi: 10.1016/s0967-0637(97)00020-4

Levin, L. A., and Smith, C. R. (1984). Response of background fauana to disturbance and enrichment in the deep sea: a sediment tray experiment. *Deep Sea Res.* 31, 1277–1285. doi: 10.1016/0198-0149(84)90001-3

Lotze, H. K., Lenihan, H. S., Bourque, B. J., Bradbury, R. H., Cooke, R. G., Kay, M. C., et al. (2006). Depletion, degradation, and recovery potential of estuaries and coastal seas. *Science* 312, 1806–1809. doi: 10.1126/science.1128035

Lutz, M. J., Caldiera, K., Dunbar, R. B., and Behrenfeld, M. J. (2007). Seasonal rhythms of net primary production and particulate organic carbon flux describes biological pump efficiency in the global ocean. *J. Geophys. Res.* 112:C10011.

Makarieva, A. M., Gorshkov, V. G., Li, B.-L., Chown, S. L., Reich, P. B., and Gavrilov, V. M. (2008). Mean mass-specific metabolic rates are strikingly similar across life's major domains: evidence for life's metabolic optimum. *Proc. Natl. Acad. Sci. U.S.A.* 105, 16995–16999. doi: 10.1073/pnas.0802148105

Marra, J., Weibe, P. H., Bishop, J. B., and Stepien, J. C. (1987). Primary production and grazing in the plankton of the Panama Bight. *Bull. Mar. Sci.* 40, 255–270.

McClain, C. R. (2004). Connecting species richness, abundance, and body size in deep-sea gastropods. *Glob. Ecol. Biogeogr.* 13, 327–334. doi: 10.1111/j.1466-822x.2004.00106.x

McClain, C. R. (2005). Bathymetric patterns of morphological disparity in deep-sea gastropods from the western North Atlantic Basin. *Evolution* 59, 1492–1499. doi: 10.1111/j.0014-3820.2005.tb01798.x

McClain, C. R., Allen, A. P., Tittensor, D. P., and Rex, M. A. (2012a). The energetics of life on the deep seafloor. *Proc. Natl. Acad. Sci. U.S.A.* 109, 5366–15371.

McClain, C. R., and Barry, J. P. (2010). Habitat heterogeneity, biogenic disturbance, and resource availability work in concert to regualte biodiversity in deep submarine canyons. *Ecology* 91, 964–976. doi: 10.1890/09-0087.1

McClain, C. R., and Barry, J. P. (2014). Beta-diversity on deep-sea wood falls reflects gradients in energy availability. *Biol. Lett.* 10:20140129. doi: 10.1098/rsbl.2014.0129

McClain, C. R., Barry, J. P., Eernisse, D., Horton, T., Judge, J., Kakui, K., et al. (2016). Multiple processes generate productivity-diversity relationships in experimental wood-fall communities. *Ecology* 97, 885–98.

McClain, C. R., Filler, R., and Auld, J. R. (2014). Does energy availaiblity predict gastropod reproductive strategies? *Proc. R. Soc. B Biol. Sci.* 281, 20140400. doi: 10.1098/rspb.2014.0400

McClain, C. R., Gullet, T., Jackson-Ricketts, J., and Unmack, P. J. (2012b). Increased energy promotes size-based niche availability in marine mollusks. *Evolution* 66, 2204–2215. doi: 10.1111/j.1558-5646.2012.01580.x

McClain, C. R., Heim, N. A., Knope, M. L., and Payne, J. L. (2018). Is biodiversity energy-limited or unbounded? A test in fossil and modern bivalves. *Paleobiology* 44, 385–401. doi: 10.1017/pab.2018.4

McClain, C. R., Johnson, N. A., and Rex, M. A. (2004). Morphological disparity as a biodiversity metric in lower bathyal and abyssal gastropod assemblages. *Evolution* 58, 338–348. doi: 10.1111/j.0014-3820.2004.tb01649.x

McClain, C. R., and Lundsten, L. (2015). Assemblage structure is related to slope and depth on a deep offshore Pacific seamount chain. *Mar. Ecol.* 36, 210–220. doi: 10.1111/maec.12136

McClain, C. R., Nekola, J. C., Kuhnz, L., and Barry, J. P. (2011). Local-scale turnover on the deep Pacific floor. *Mar. Ecol. Prog. Ser.* 442, 193–200. doi: 10.3354/meps08924

McClain, C. R., and Schlacher, T. (2015). On some hypotheses of diversity of animal life at great depths on the seafloor. *Mar. Ecol.* [Epub ahead of print].

McClain, C. R., Stegen, J. C., and Hurlbert, A. H. (2012c). Dispersal, niche dynamics, and oceanic patterns in beta-diversity in deep-sea bivalves. *Proc. R. Soc. B Biol. Sci.* 279, 1933–2002. doi: 10.1098/rspb.2011.2166

McNab, B. K. (1963). Bioenergetics and the derteminations of home range size. *Am. Nat.* 97, 133–140. doi: 10.1086/282264

McNab, B. K. (1986). The influence of food habits on the energetics of eutherian mammals. *Ecol. Monogr.* 56, 1–19. doi: 10.2307/2937268

McNab, B. K. (2016). Avian energetics: the passerine/non-passerine dichotomy. *Comp. Biochem. Physiol. Part A Mol. Integr. Physiol.* 191, 152–155. doi: 10.1016/j.cbpa.2015.10.005

McQuatters-Gollop, A., Reid, P. C., Edwards, M., Burkill, P. H., Castellani, C., Batten, S., et al. (2011). Is there a decline in marine phytoplankton? *Nature* 472, E6–E7.

Melo, A. S., Rangel, T. F. L. V. B., and Diniz-Filho, J. A. F. (2009). Environmental drivers of beta-diversity patterns in New-World birds and mammals. *Ecography* 32, 226–236. doi: 10.1111/j.1600-0587.2008.05502.x

Nagy, K. A. (1987). Field metabolic rate and food requirement scaling in mammals and birds. *Ecol. Monogr.* 57, 111–128. doi: 10.2307/1942620

Powell, E. N., and Stanton, R. J. (1985). Estimating biomass and energy-flow of mollusks in paleo-communities. *Paleontology* 28, 1–34.

Qian, H., and Xiao, M. (2012). Global patterns of the beta diversity–energy relationship in terrestrial vertebrates. *Acta Oecol.* 39, 67–71. doi: 10.1016/j.actao.2011.12.003

R Development Core Team, (ed.) (2019). *R: A Language and Environment for Statistical Computing*. Vienna, Austria: R Foundation for Statistical Computing.

Rex, M. A., and Etter, R. J. (2010). *Deep-Sea Biodiversity: Pattern and Scale*. Cambridge: Harvard University Press.

Rex, M. A., Etter, R. J., Morris, J. S., Crouse, J., Mcclain, C. R., Johnson, N. A., et al. (2006). Global bathymetric patterns of standing stock and body size in the deep-sea benthos. *Mar. Ecol. Prog. Ser.* 317, 1–8. doi: 10.3354/meps317001

Rex, M. A., Mcclain, C. R., Johnson, N. A., Etter, R. J., Allen, J. A., Bouchet, P., et al. (2005). A source-sink hypothesis for abyssal biodiversity. *Am. Nat.* 165, 163–178. doi: 10.1086/427226

Rosenzweig, M. L., and Abramsky, Z. (1993). "How are diversity and productivity related?" in *Species Diversity in Ecological Communities: Historical and Geographical Perspectives*, eds R. E. Ricklefs, and D. Schluter (Chicago, IL: University of Chicago Press), 52–65.

Rouse, G. W., Goffredi, S. K., and Vrijenhoek, R. (2004). Osedax: bone-eating marine worms with dwarf males. *Science* 305, 668–671. doi: 10.1126/science.1098650

Rousseaux, C. S., and Gregg, W. W. (2015). Recent decadal trends in global phytoplankton composition. *Glob. Biogeochem. Cycles* 29, 1674–1688. doi: 10.1080/2150704X.2017.1354263

Sanders, H. L. (1977). "Evolutionary ecology of the deep-sea benthos," in *The Changing Scenes in Natural Sciences: 1776-1976, Special Publication*, ed. C. E. Goulden (Philadelphia, PA: Academy of Natural Sciences).

Shen, Y.-Y., Liang, L., Zhu, Z.-H., Zhou, W.-P., Irwin, D., and Zhange, Y.-P. (2010). Adaptive evolution of energy metabolism genes and the origin of flight in bats. *Proc. Natl. Acad. Sci. U.S.A.* 107, 8666–8671. doi: 10.1073/pnas.0912613107

Sircom, J., and Walde, S. J. (2010). Niches and neutral processes contribute to the resource– diversity relationships of stream detritivores. *Freshw. Biol.* 2011, 877–888. doi: 10.1111/j.1365-2427.2010.02533.x

Slatyer, R. A., Hirst, M., and Sexton, J. P. (2013). Niche breadth predicts geographical range size: a general ecological pattern. *Ecol. Lett.* 16, 1104–1114. doi: 10.1111/ele.12140

Slayter, R. A., Hirst, M., and Sexton, J. P. (2013). Niche breadth predicts geographical range size: a general ecological pattern. *Ecol. Lett.* 16, 1104–1114. doi: 10.1111/ele.12140

Smith, C. R., De Leo, F. C., Bernardino, A. F., Sweetman, A. K., and Arbizu, P. M. (2008). Abyssal food limitation, ecosystem structure and climate change. *Trends Ecol. Evol.* 23, 518–528. doi: 10.1016/j.tree.2008.05.002

Snelgrove, P. V., and Smith, C. R. (2002). A riot of species in an environmental calm: the paradox of the species-rich deep-sea floor. *Oceanogr. Mar. Biol. Annu. Rev.* 40, 311–342. doi: 10.1201/9780203180594.ch6

Snelgrove, P. V. R., Grassle, J. F., and Petrecca, R. F. (1992). The role of food patches in maitaining high deep-sea diversity: field experiments with hydrodynamically unbiased colonization trays. *Limnol. Oceanogr.* 37, 1543–1550. doi: 10.4319/lo.1992.37.7.1543

Snelgrove, P. V. R., Grassle, J. F., and Petrecca, R. F. (1994). Macrofaunal response to artificial enrichments and depressions in a deep-sea habitat. *J. Mar. Sci.* 52, 345–369. doi: 10.1357/0022240943077082

Snelgrove, P. V. R., Grassle, J. F., and Petrecca, R. F. (1996). Experimental evidence for aging food patches as a factor contributing to high deep-sea macrofaunal diversity. *Limnol. Oceanogr.* 41, 605–614. doi: 10.4319/lo.1996.41.4.0605

Soininen, J., Lennon, J. J., and Hillebrand, H. (2007a). A multivariate analysis of beta diversity across organisms and environments. *Ecology* 88, 2830–2838. doi: 10.1890/06-1730.1

Soininen, J., Mcdonald, R., and Hillebrand, H. (2007b). The distance decay of similarity in ecological communties. *Ecography* 30, 3–12. doi: 10.1111/j.0906-7590.2007.04817.x

Sokolova, M. N. (1960). On the distribution of deep-water bottom animals in relation to their feeding habits and the character of sedimentation. *Deep Sea Res.* 6, 1–4. doi: 10.1016/0146-6313(59)90052-8

Steffen, W., Broadgate, W., Deutsch, L., Gaffney, O., and Ludwidg, C. (2015). The trajectory of the Anthropocene: the great acceleration. *Anthropocene Rev.* 2, 1–18. doi: 10.1038/s41586-018-0005-6

Stuart, C. T., Brault, S., Rowe, G. T., Wei, C.-L., Wagstaff, M., Mcclain, C. R., et al. (2016). Nestedness and species replacement along bathymetric gradients in the deep sea reflect productivity: a test with polychaete assemblages in the oligotrophic north-west Gulf of Mexico. *J. Biogeogr.* 44, 548–555. doi: 10.1111/jbi.12810

Tamburello, N., Cote, I. M., and Dulvy, N. K. (2015). Energy and the scaling of animal space use. *Am. Nat.* 186, 196–211. doi: 10.1086/682070

Thiel, H. (1975). The size structure of the deep-sea benthos. *Int. Rev. Gesamten Hyrdobiol.* 60, 575–606. doi: 10.1111/gcb.12480

Thiel, H. (1979). Structural aspects of the deep-sea benthos. *Ambio Spec. Rep.* 6, 25–31.

Tilman, D. (1982). *Resource Competition and Community Structure*. Princeton, NJ: Princeton University Press.

Tittensor, D. P., Mora, C., Jetz, W., Lotze, H. K., Berghe, E. V., and Worm, B. (2010). Global patterns and predictors of marine biodiveristy across taxa. *Nature* 466, 1098–1101. doi: 10.1038/nature09329

Tittensor, D. P., Rex, M. A., Stuart, C. T., Mcclain, C. R., and Smith, C. R. (2011). Species-energy relationships in deep-sea mollusks. *Biol. Lett.* 7, 718–722. doi: 10.1098/rsbl.2010.1174

Tomasovych, A., Jablonski, D., Berke, S. K., Krug, A. Z., and Valentine, J. W. (2015). Nonlinear thermal gradients shape broad-scale patterns in geographic range size and can reverse Rapoport's rule. *Glob. Ecol. Biogeogr.* 24, 157–167. doi: 10.1111/geb.12242

Turner, R. D. (1973). Wood-boring bivalves, opportunistic species in the deep sea. *Science* 180, 1377–1379. doi: 10.1126/science.180.4093.1377

Uyeda, J. C., Pennell, M. W., Miller, E. T., Maia, R., and Mcclain, C. R. (2017). The evolution of energetic scaling across the vertebrate tree of life. *Am. Nat.* 190, 185–199. doi: 10.1086/692326

Van Dover, C. L. (2000). *The Ecology of Deep-Sea Hydrothermal Vents*. Princeton, NJ: Princeton University Press.

Van Valen, L. (1976). Energy and evolution. *Evol. Theory* 1, 179–229.

Vaquer-Sunyer, R., and Duarte, C. M. (2008). Thresholds of hypoxia for marine biodiversity. *Proc. Natl. Acad. Sci. U.S.A.* 105, 15452–15457. doi: 10.1073/pnas.0803833105

Vladimirova, I. G. (2001). Standard metabolic rate in Gastropoda class. *Biol. Bull.* 28, 163–169.

Vladimirova, I. G., Kleimenov, S. Y., and Radzinskaya, L. I. (2003). The relation of energy metabolism and body weight in bivalves (Mollusca: Bivalvia). *Biol. Bull.* 30, 392–399.

Voight, C. C., and Speakman, J. R. (2007). Nectar-feeding bats fuel their high metabolism directly with exogenous carbohydrates. *Funct. Ecol.* 21, 913–921. doi: 10.1242/jeb.043505

Wagstaff, M. C., Howell, K. L., Bett, B. J., Billet, D. S. M., Brault, S., Stuart, C. T., et al. (2014). β-diversity of deep-sea holothurians and asteroids along a bathymetric gradient (NE Atlantic). *Mar. Ecol. Prog. Ser.* 508, 177–185. doi: 10.3354/meps10877

Waide, R. B., Willig, M. R., Steiner, C. F., Mittelbach, G. C., Gough, L., Dodson, S. I., et al. (1999). The relationship between productivity and species richness. *Annu. Rev. Ecol. Syst.* 30, 257–300.

Wei, C.-L., Rowe, G. T., Escobar-Briones, E., Boetius, A., Soltwedel, T., Caley, M. J., et al. (2010a). Global patterns and predictions of seafloor biomass using random forests. *PLoS One* 5:e15323. doi: 10.1371/journal.pone.0015323

Wei, C.-L., Rowe, G. T., Hubbard, G. F., Sheltema, A. H., Wilson, G. D. F., Petrescu, I., et al. (2010b). Bathymetric zonation of deep-sea macrofauna in relation to export of surface phytoplankton production. *Mar. Ecol. Prog. Ser.* 399, 1–14. doi: 10.3354/meps08388

Whittaker, R. H. (1960). Vegetation of the Siskiyou mountains, Oregan and California. *Ecol. Monogr.* 30, 279–338. doi: 10.2307/1943563

Whitton, F. S., Purvis, A., Orme, C. D. L., and Olalla-TaìRraga, M. A. (2012). Understanding global patterns in amphibian geographic range size: does Rapoport rule? *Glob. Ecol. Biogeogr.* 21, 179–190. doi: 10.1111/j.1466-8238.2011.00660.x

Wickham, H. (2009). *ggplot2: Elegant graphics for data analysis*. New York, NY: Springer.

Wilke, C. O. (2018). *ggridges: Ridgeline Plots in 'ggplot2*. Available at: https://CRAN.R-project.org/package=ggridges

Wilson, R. P., Mcmahon, C. R., Quintana, F., Frere, E., Scolaro, A., Hays, G. C., et al. (2011). N-dimensional animal energetic niches clarify behavioural options in a variable marine environment. *J. Exp. Biol.* 214, 646–656. doi: 10.1242/jeb.044859

Wood, S. N. (2011). Fast stable restricted maximum likelihood and marginal likelihood estimation of semiparametric generalized linear models. *J. R. Stat. Soc.* 73, 3–36. doi: 10.1111/j.1467-9868.2010.00749.x

Woolley, S. N. C., Titternsor, D. P., Dusntan, P. K., Guillera-Arroita, G., Lahoz-Monfrort, J. J., Wintle, B. A., et al. (2016). Deep-sea diversity patterns are shsaped by energy availability. *Nature* 533, 393–396. doi: 10.1038/nature17937

Wright, D. H. (1983). Species-energy theory: An extension of species-area theory. *Oikos* 41, 496–506.

Wright, D. H., Currie, D. J., and Maurer, B. A. (1993). "Energy supply and patterns of species richness on local and regional scales," in *Species Diversity in Ecological Communities: Historical and Geographical Perspectives*, eds R. E. Ricklefs, and D. Schluter (Chicago, IL: University of Chicago Press), 66–74.

Zinger, L., Amaral-Zettler, L. A., Fuhrman, J. A., Horner-Devine, M. C., Huse, S. M., Welch, D. B. M., et al. (2011). Global patterns of bacterial beta-diversity in seafloor and seawater ecosystems. *PLoS One* 6:e24570. doi: 10.1371/journal.pone.0024570

Conflict of Interest: The authors declare that the research was conducted in the absence of any commercial or financial relationships that could be construed as a potential conflict of interest.

Copyright © 2020 McClain, Webb, Nunnally, Dixon, Finnegan and Nelson. This is an open-access article distributed under the terms of the Creative Commons Attribution License (CC BY). The use, distribution or reproduction in other forums is permitted, provided the original author(s) and the copyright owner(s) are credited and that the original publication in this journal is cited, in accordance with accepted academic practice. No use, distribution or reproduction is permitted which does not comply with these terms.

frontiers in Marine Science

BRIEF RESEARCH REPORT
published: 24 April 2020
doi: 10.3389/fmars.2020.00200

Meiofauna Community in Soft Sediments at TAG and Snake Pit Hydrothermal Vent Fields

Adriana Spedicato, Nuria Sánchez, Lucie Pastor, Lenaick Menot and Daniela Zeppilli*

LEP, Ifremer Centre de Bretagne, Plouzané, France

The risk assessment of seafloor massive sulfide (SMS) mining on meiobenthic organisms, specifically on soft-sediment meiofauna, is impeded by a lack of knowledge on the biology and ecology of these communities. In this study, we investigated sediment samples taken in proximity of active vents at Trans-Atlantic Geotraverse (TAG) and Snake Pit, two hydrothermal vent fields of the Mid-Atlantic Ridge, in order to explore metazoan meiofauna, particularly nematode community, and its relation to organic carbon, total nitrogen, total sulfur, and dissolved oxygen. Organic carbon and nitrogen contents were low at both sites. High concentrations of total sulfur and low oxygen penetration were found at Snake Pit compared to TAG. Snake Pit showed approximately four times higher meiofauna and nematode density compared to TAG, as well as a dissimilar nematode community composition. We hypothesize that high sulfur concentrations at Snake Pit may support high microbial growth, which represents one of the main food source for nematodes. Moreover, TAG nematode community mostly consisted of persisters (K-strategists), whereas Snake Pit one was composed by both persisters (*Desmoscolecidae* family) and colonizers (r-strategists *Metalinhomoeus* and *Halomonhystera*), whose presence can be facilitated by the bioturbation effect of polychaetes observed on the sediment surface. Therefore, food availability, geochemical settings, and biotic interactions seem to drive the local meiofauna and nematode community. Our study also draws attention to the opportunity of including meiofauna and specifically nematodes in impact studies conducted in this area in order to assess and monitor the impact of SMS mining.

Keywords: meiobenthos, nematoda, Mid-Atlantic Ridge, seafloor massive sulfides, biodiversity

OPEN ACCESS

Edited by:
Paulina Martinetto, Institute of Marine and Coastal Research (IIMyC), Argentina

Reviewed by:
Sabine Gollner, Royal Netherlands Institute for Sea Research (NIOZ), Netherlands
Motohiro Shimanaga, Kumamoto University, Japan

****Correspondence:***
Adriana Spedicato
aspedica@ifremer.fr

Specialty section:
This article was submitted to Global Change and the Future Ocean, a section of the journal Frontiers in Marine Science

Received: *29 November 2019*
Accepted: *13 March 2020*
Published: *24 April 2020*

Citation:
Spedicato A, Sánchez N, Pastor L, Menot L and Zeppilli D (2020) Meiofauna Community in Soft Sediments at TAG and Snake Pit Hydrothermal Vent Fields. Front. Mar. Sci. 7:200. doi: 10.3389/fmars.2020.00200

INTRODUCTION

The demand for mineral raw materials is increasing nowadays as a result of constant population growth, rising living standards, urbanization, technological advance, and, more recently, the transition to a low-carbon economy (Murton et al., 2019). Therefore, alternative sources of minerals are currently being sought, such as deep-sea seafloor massive sulfide (SMS) (Boschen et al., 2013). Seafloor massive sulfide deposits form through hydrothermal vent activity, which generates areas of hard substrate enriched with high content of base metals (zinc, iron, lead, and copper), sulfides, and rare elements, such as gold, silver, cobalt, and platinum (Hoagland et al., 2010). Once the flow of chemically reduced hydrothermal fluid ceases, sulfide deposits are no longer hydrothermally active, thus becoming inactive (exinctSMS or eSMS) (Van Dover, 2019).

These deposits are likely accessible to future mining and are far more abundant than active ones, but their localization can be impeded by pelagic sediment, which slowly covers the deposits (Murton et al., 2019). For instance, according to Murton et al. (2019), the Trans-Atlantic Geotraverse (TAG) (**Figure 1**), which is one of the most studied hydrothermal sites of the Mid-Atlantic Ridge (MAR), is smeared with deposits that extend sub-seafloor and are actually larger than what previous studies estimated. Indeed, whereas Hannington et al. (1998) reported a deposit tonnage of 2.7 Mt, Murton et al. (2019) recently estimated TAG sulfides to be around 26 Mt. Thus, TAG has been defined as potentially more attractive for mining activities than it was believed so far. Moreover, SMS deposits located on a slow-spreading ridge, such as TAG and Snake Pit (**Figure 1**), are bigger, and their venting activity more stable, compared to fast-spreading ridges. They are thus more suitable sites for mining (Fouquet and Scott, 2009; Boschen et al., 2013).

Mining activities will directly affect benthic communities of the SMS deposits target areas mainly because of the removal of substrate that harbors the organisms, but also because of sediment turbidity and toxic plumes (Boschen et al., 2013). The risk assessment of eSMS mining is, however, impeded by a lack of knowledge on the biology and ecology of communities associated with eSMS, and particularly so for the soft-sediment communities (Van Dover, 2019). The few studies that sampled hydrothermal sediments or sediments in the vicinity of hydrothermal vents highlighted the patchiness of the distribution, as well as the heterogeneity in the structure and composition of meiofaunal and macrofaunal assemblages (Vanreusel et al., 1997; Levin et al., 2009). In the North Fiji Basin, Vanreusel et al. (1997) reported higher meiofauna densities in active than inactive hydrothermal sediments as well as a lower diversity and different nematode species in hydrothermal compared to background sediments. The hydrothermal sediments, sampled with a TV grab, were hardly quantitative, but it remains, to date, the best comparison of meiofaunal assemblages between hydrothermally active and inactive sediments.

During the BICOSE 2 cruise (Cambon-Bonavita, 2018), patches of sediment were quantitatively sampled at the periphery of TAG and Snake Pit, two hydrothermal vent fields of the MAR, with the aim of describing meiofauna communities and understanding the drivers of variations in community structure and composition in different geochemical contexts. The meiofauna and nematode assemblages were investigated in soft metalliferous sediments in relation with organic carbon (OC), total nitrogen (N), total sulfur (S), and dissolved oxygen (O_2).

MATERIALS AND METHODS

Study Sites

TAG (26°08′ N) and Snake Pit (23°23′ N) vent sites (**Figure 1**) are located on two different segments of the slow-spreading (22 mm/year) MAR (Kleinrock and Humphris, 1996) and are separated by a linear distance of about 300 km (Van Dover, 1995).

The TAG area holds several extinct SMS deposit and one high-temperature SMS deposit (i.e., TAG active mound) (Murton et al., 2019). Trans-Atlantic Geotraverse active mound is located at 3,670-m depth and 3 km east of the ridge axis. It consists in a 250-m diameter and 50-m-high deposit topped with black smoker

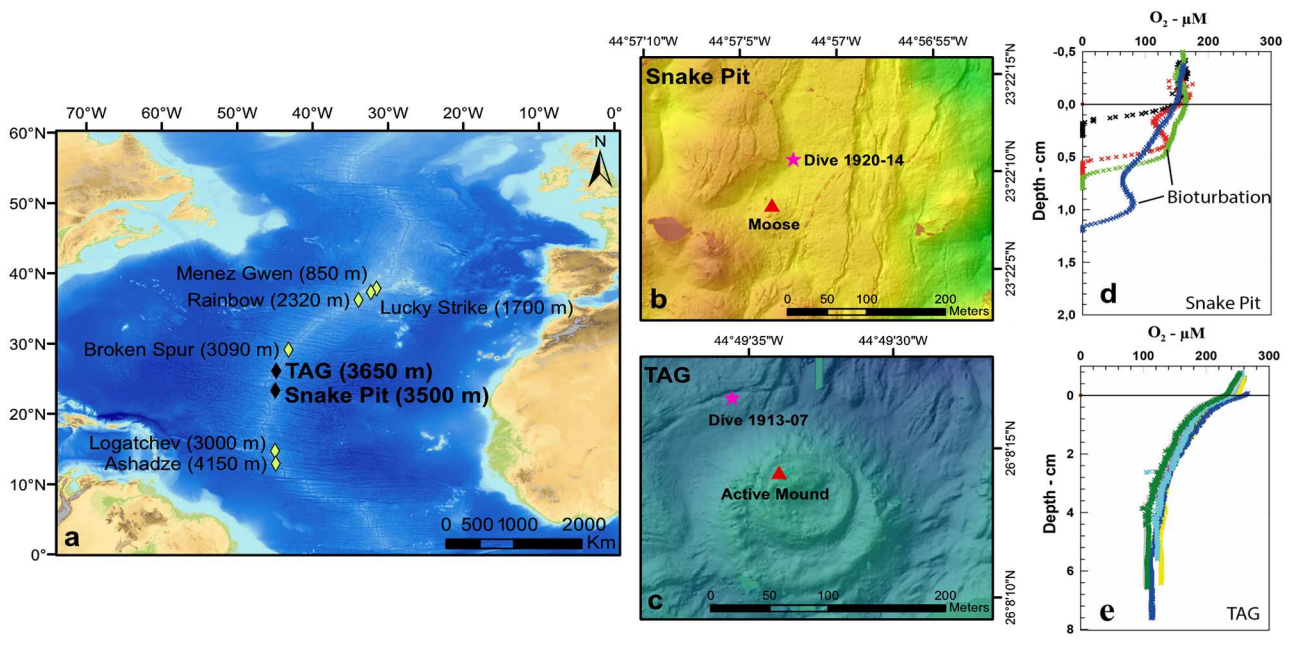

FIGURE 1 | Map of Trans-Atlantic Geotraverse (TAG) (26°08′ N) and Snake Pit (23°23′ N) vent fields in the Mid-Atlantic Ridge **(a)**; map of Snake Pit sampling site, pink star = dive 1920-14 **(b)**; map of TAG sampling site, pink star = dive 1913-07 (c), red triangle = nearest active mound **(b,c)**; Snake Pit oxygen profile and penetration depth with evidences of bioturbation **(d)**; TAG oxygen profile and penetration depth **(e)**.

chimneys (350°C) (Rona et al., 1986). Metalliferous red-brown oxide sediments have been observed up to 125 m away from the base of the deposit talus, specifically a 7-cm-thick layer of Fe-rich red-brown mud (20–40% Fe) overlying a 4-cm-thick layer of carbonate ooze (5–70% $CaCO_3$), which also contains up to 32% Fe (German, 1993). Trans-Atlantic Geotraverse active mound formed about 50,000 years ago and still shows hydrothermal activity (Lalou et al., 1990; German, 1993).

The Snake Pit vent field is located at the ridge axis at a water depth between 3,480 and 3,570 m, and it consists of three elongate parallel ridges (Thompson et al., 1988). The flat areas between the ridges are covered by metalliferous sediment composed of dark granular sulfides, mainly pyrrhotite, chalcopyrite, marcasite, and pyrite, and minor sphalerite (Thompson et al., 1988; Sudarikov and Galkin, 1995). Several small SMSs are known in the field, including the Beehive, Nail, Moose, Firtree, and the Cliff deposits. These mounds are 20–60 m in diameter and 20–25 m in height (Fouquet et al., 1993). High-temperature activity and related black smoker chimneys (325°-330°C) is restricted to the Beehive and Cliff hydrothermal sites (Fouquet et al., 1993).

Experimental Design, Sampling, and Processing

Samples were collected at the MAR during the BICOSE2 cruise (2018) on board the RV *Pourquoi Pas?*. Soft sediment samples were taken through the human-operated vehicle (HOV) Nautile during the dive 1913-07 for TAG and dive 1920-14 for Snake Pit, from January 27 to March 11, 2018 (**Figure 1**). These two sampling sites will thereafter be named TAG and Snake Pit for simplification. Trans-Atlantic Geotraverse sampling site was located 90 m to the northwest of the active mound. Snake Pit sampling site was located 70 m to the northeast of the black smoker "Moose." Four push cores (CT) (5.5-cm diameter, 24-cm^2 sampling area) were retrieved per site; three were used for meiofauna, and one was used for O_2 profiling and OC, N, and total S contents. Samples for meiofauna were sliced vertically on board according to depth in five layers of 1 cm each (0–1, 1–2, 2–3, 3–4, and 4–5 cm). Each layer was fixed in 4% formalin. The sediment core for geochemistry was first used for O_2 profiling and then sliced horizontally every centimeter. The sediment was kept frozen at −20°C until freeze dried, grinded, and analyzed back at the laboratory.

Meiofauna Identification

All samples were sieved on 1 mm, 300 µm, and 32 µm in order to separate fauna by body size. Meiofauna was extracted by Ludox centrifugation according to Heip et al. (1985) and then stained with fuchsine and fixed in 4% formalin. All meiobenthic animals retained in both 32- and 300-µm sieves were counted and classified to high taxonomic level under a stereomicroscope Olympus SZX16 (Olympus Corporation, Tokyo, Japan). All nematodes were mounted on permanent slides following the formalin–ethanol–glycerol technique described by Seinhorst (1959) and then identified at genus level with a Leica DM2500 LED microscope (Leica Microsystems GmbH, Wetzlar, Germany) according to Platt and Warwick (1988), WoRMS Editorial Board (2020), Bezerra et al. (2020), Bain et al. (2014).

Geochemical Data

Oxygen profiles were performed *ex situ* using Clark-type microelectrodes (Revsbech, 1989). The sediment core was kept at *in situ* temperature during profiling, and surface water was gently bubbled with an air diffusor to ensure a well-mixed overlying water. Linear calibration was achieved between an air-saturated seawater titrated using the Winkler technique (Grasshoff et al., 1983) and an O_2-free water obtained by adding sodium sulfite (Na_2SO_3). The averaged concentrations were then calculated for each layer in which meiofauna was retrieved (basically every cm down to 5 cm when O_2 was detected).

Total S, N, and carbon were determined using a TruMac CNS from LECO (LECO, St. Joseph, MI, USA) (Kowalenko, 2001). Total S and N were analyzed at 1,450°C using COMCAT (LECO, St. Joseph, MI, USA) as a combustion accelerator (Kowalenko, 2001). Organic carbon was measured at 1,350°C after removing carbonates overnight at a temperature of 60°C with 1 M HCl. Samples were then rinsed twice with Milli-Q water and dried before their introduction in the analyzer (Brodie et al., 2011 and references therein).

Statistical Analysis

Richness (number of taxonomic groups), density (number of individuals per 10 cm^2), and community composition for metazoan meiofauna were analyzed. For nematodes, richness (number of genera) and density (number of individuals per 10 cm^2) were considered. Kruskal–Wallis test was conducted to assess differences in richness and density between sites. Differences in meiofauna and nematode community composition between the two studied sites were tested using Ružička (abundance) matrix through permutational analysis of variance (PERMANOVA). Ružička index was calculated through the function "beta" of the R package vegan v. 2.2-1 (Oksanen, 2015), and PERMANOVA was performed using distance matrices calculated with the function "adonis" included in the R package vegan v. 2.2-1 (Oksanen, 2015). Principal component analysis (PCA) conducted by densities were performed to visualize community composition variations between sites using the Hellinger distance for data transformation, functions "rda" and "decostand" of the R package vegan v. 2.2-1 (Oksanen et al., 2018). Moreover, the Shannon diversity index (H') and the Pielou's evenness index (J) were calculated for both meiofauna and nematode with the software PRIMER v6 (PRIMER-e, Clarke and Gorley, Auckland, New Zealand) (Clarke and Gorley, 2006).

RESULTS

Visual Description of Sediment Cores

At Snake Pit, a thin layer of reddish sediments at the top of the core was draping darker brownish sediments. At the sediment surface, numerous hesionid polychaetes were observed crawling among tubes of ampharetid polychaetes.

The upper layer of the sediment core taken at TAG showed a reddish color, reflecting the typical TAG iron oxyhydroxide

minerals (German, 1993). No macrofauna was visually observed at the surface of the sediment during the dive.

Geochemical Setting

Oxygen concentration was decreasing with depth at both sites (**Table S1**, **Figure 1**). Oxygen penetration depth was 0.7 ± 0.5 cm at Snake Pit, with visual evidences for bioturbation (increases in O_2 concentrations at depth due to bioirrigation of burrows by polychaetes; **Figure 1**, **Table S1**), whereas O_2 concentration was still >100 μM at 7-cm depth at TAG, with no visible signs of bioturbation. The O_2 concentrations averaged per sediment layers (from 0 to 5 cm) are displayed in **Table S1**. Organic carbon contents were <0.5% at both sites, with values slightly decreasing with depth between 0 and 1 cm. Nitrogen contents were very low, ranging from 0.06 to 0.11% at Snake Pit and from 0.03 to 0.1% at TAG. Total S contents were 26 to 31% at Snake Pit and only 0.7 to 1.0% at TAG in the top 5 cm of the core.

Meiofauna Community Description and Composition

Snake Pit has the highest average meiofauna density (138 ± 34 ind/10 cm^2) compared to TAG (32 ± 16 ind/10 cm^2) (**Figure 2**), whereas the same taxonomic richness was observed at both sites (a total of 7 taxa per site) (**Table 1**). The highest meiofauna densities were found in the first 2 cm of sediment at both TAG (95%) and Snake Pit (97%), with a sharp decrease from the first to the second layer (from 90 to 6% at TAG and from 80% to 17% at Snake Pit). According to the Kruskal–Wallis test, the only statistically significant difference between TAG and Snake Pit was found in meiofauna density ($p = 0.049$). Nematodes account for 70% of the total meiofauna at TAG and for 62% at Snake Pit, thus being the highest density taxon, immediately followed by copepods and nauplii, together accounting for 27% at TAG and 34% at Snake Pit. Gastrotricha, Tantulocarida, Ostracoda, and Halacarida account each for <2%, whereas only at Snake Pit, polychaeta account for 3.4%. Only Nematoda were found in the deeper layers (3–5 cm) of TAG cores, whereas also Copepoda, Nauplii, and Ostracoda were present in those layers in Snake Pit samples (**Figure S1**). Moreover, Tantulocarida and Halacarida were exclusive taxa from TAG and Snake Pit, respectively (**Figure S1**). Permutational analysis of variance was conducted, but no statistically significant difference between sites was detected. Similarly, PCA did not identify a discrimination in taxa composition between the two sites (**Figure 3**). Both Shannon's diversity and Pielou's evenness indices were lower for TAG ($H' = 0.91$, $J = 0.47$) than for Snake Pit ($H' = 1.11$, $J = 0.57$) (**Table 1**).

Nematode Community Description and Composition

Nematodes were found mostly in the first 2 cm of sediment for both Snake Pit (97% of the total population) and TAG

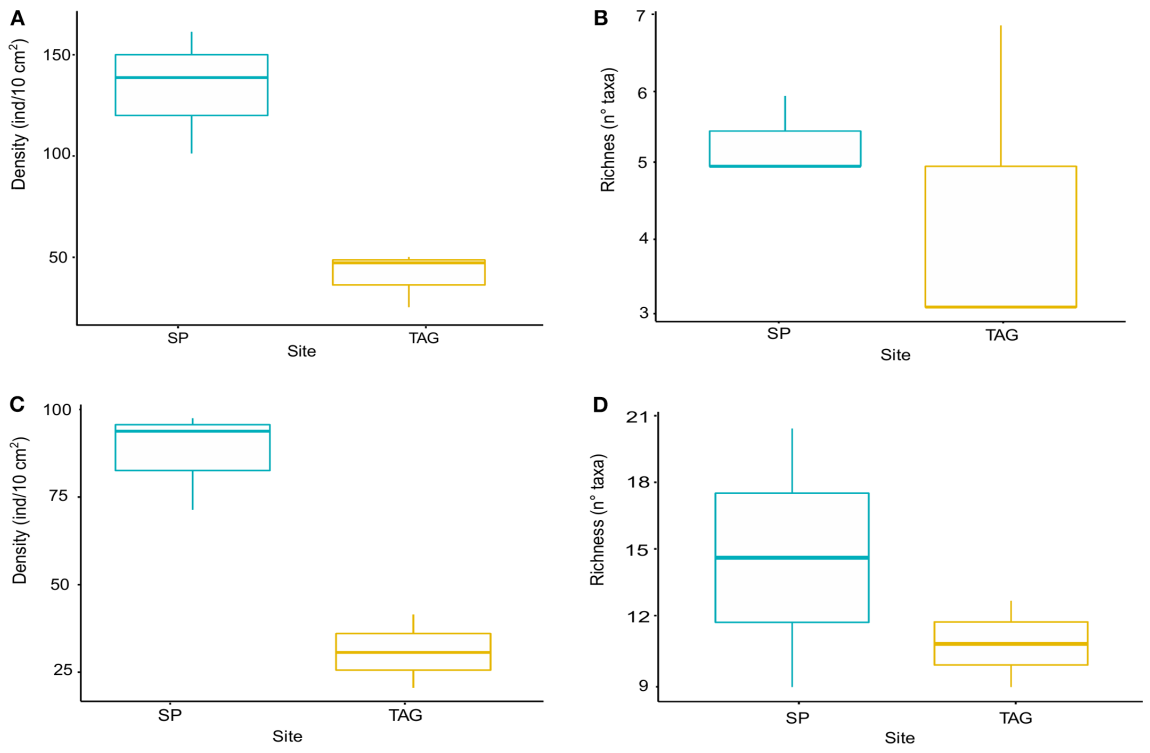

FIGURE 2 | Meiofauna density boxplot **(A)**, meiofauna richness boxplot **(B)**, nematode density boxplot **(C)**, nematode richness boxplot **(D)**. The boxplots represent the median value (horizontal thicker line within the box), the distributions of 50% of the data (the box), and the highest and lowest values of the distribution for both Snake Pit (in blue) and TAG (in yellow).

TABLE 1 | The density (ind/10 cm^2) per core of each meiofauna taxa and nematode genera is given for TAG (on the left) and for Snake Pit (on the right); total density and total abundance per core are also given, together with an average density, and average abundance per site.

	TAG					Snake pit			
	TB4	**TB8**	**TB12**	**TOT**		**T07**	**T10**	**T2**	**TOT**
	Density (ind/10 cm²)			**Avg**		**Density (ind/10 cm²)**			**Avg**
Nematoda	10.83	34.58	22.5	22.64	Nematoda	92.92	96.67	67.91	85.83
Copepoda	0.83	3.75	3.75	2.78	Copepoda	27.92	13.75	23.03	21.57
Nauplii	2.08	5.0	10.83	5.97	Nauplii	42.08	25.83	7.9	25.27
Bivalvia	0	0	0	0	Bivalvia	1.67	0	0	0.56
Gastrotricha	0	0	0.42	0.14	Gastrotricha	0	0	0	0
Polychaeta	0	0	0.83	0.28	Polychaeta	0	10	4.1	4.70
Ostracoda	0	0	1.25	0.42	Ostracoda	0	0	0.42	0.14
Halacarida	0	0	0	0	Halacarida	0.41	1.66	0	0.69
Tantulocarida	0	0	0.42	0.14	Tantulocarida	0	0	0	0
TOT Density	13.74	43.33	40	32.36	TOT Density	165	147.91	103.36	138.76
TOT Abundance	32	101	95	76	TOT Abundance	385	289	226	300
J′				0.47	J′				0.57
H′				0.91	H′				1.11
Acantholaimus	1.25	2.08	1.67	1.67	*Acantholaimus*	0	0	0	0
Anoplostoma	0	0	0	0	*Anoplostoma*	0	0.42	0	0.14
Amphymonistrella	0	0.42	0	0.14	*Amphymonistrella*	0	0	0	0
Camacolaimus	0	0	0	0	***Camacolaimus***	10	11.67	1.67	7.78
Cephalochaetosoma	0	0	0.42	0.14	*Cephalochaetosoma*	4.17	4.17	2.5	3.61
Chromadorella	0	2.91	4.17	2.36	*Chromadorella*	0	0	0	0
Chromadorina	0	0	0	0	*Chromadorina*	0	0.42	0	0.14
Cobbia	0.42	0	0	0.14	*Cobbia*	0	0	0	0
Cyatholaimus	0	0	0	0	*Cyatholaimus*	0	0.42	0	0.14
Daptonema	0	0	0	0	*Daptonema*	0	0.83	0	0.28
Desmodora	0	0	0	0	*Desmodora*	0	2.92	0	0.97
Desmoscolex	1.67	12.50	7.50	7.22	*Desmoscolex*	0	0	0	0
Dinetia	0	0	0	0	*Dinetia*	0	0.83	0	0.28
Diplopeltoides	0	0	0.42	0.14	*Diplopeltoides*	0	0	0	0
Dracogallus	0	0	0	0	*Dracogallus*	0	0.42	0	0.14
Eleutherolaimus	0	0	0	0	*Eleutherolaimus*	0	1.67	0	0.56
Epsilonema	0	0	0	0	*Epsilonema*	0.42	0.42	0	0.28
Euchromadora	0	0	0	0	*Euchromadora*	0.83	0.42	0.42	0.55
Leptolaimus	0	0	0	0	*Leptolaimus*	0	0	0.42	0.14
Halalaimus	1.25	1.67	0.83	1.25	*Halalaimus*	0	0	0	0
Halomonhystera	0	0	0	0	***Halomonhystera***	16.25	15.42	22.92	18.19
Megadesmolaimus	0	0	0	0	*Megadesmolaimus*	0.42	0.42	0	0.28
Metadesmolaimus	0	0	0	0	*Metadesmolaimus*	1.67	1	0	0.89
Metalinhomoeus	0	0	0	0	***Metalinhomoeus***	30.83	29.17	22.50	27.50
Microlaimus	2.08	8.75	3.33	4.72	*Microlaimus*	2.92	5	0.83	2.92
Molgolaimus	0.42	0	0	0.14	*Molgolaimus*	0	0	0	0
Oncholaimus	0	0	0.42	0.14	*Oncholaimus*	0	0	0	0
Prooncholaimus	0.83	1.25	1.67	1.25	*Prooncholaimus*	0	0	0	0
Pselionema	0	0.42	0	0.14	*Pselionema*	0	0	0	0
Retrotheristus	0	0.14	0	0	*Retrotheristus*	0	0	0	0
Oxystomina	0	0	0	0	*Oxystomina*	0.83	0	0	0.28
Sabatieria	0	0	0	0	*Sabatieria*	0	3.75	2.08	1.94
Syringolaimus	0.42	0	0	0.28	*Syringolaimus*	2.92	6.25	0.83	3.33

(Continued)

TABLE 1 | Continued

	TAG					Snake pit			
	TB4	**TB8**	**TB12**	**TOT**		**T07**	**T10**	**T2**	**TOT**
	Density (ind/10 cm²)			**Avg**		**Density (ind/10 cm²)**			**Avg**
Tricoma	0.42	0.83	0	0.63	*Tricoma*	0	0	0	0
Viscosia	0.42	0	0	0.14	*Viscosia*	0	0	0	0
Unidentified genus n°1	0	0	0	0	*Unidentified genus n°1*	0.42	0	0	0.14
Unidentified genus n°4	0	0.42	0	0.14	*Unidentified genus n°4*	0	0	0	0
Unidentified genus n°5	0.83	0	0	0.28	*Unidentified genus n°5*	0	0	0	0
Unident. genus(Chromadoridae)	0	0	0	0	*Unident. genus(Chromadoridae)*	0.42	0	0	0.14
Unident. genus(Comesomatidae)	0	0	0	0	*Unident. genus(Comesomatidae)*	0	0.42	0	0.14
TOT Density	10.83	34.58	22.50	22.64	TOT Density	72.08	86.01	54.17	70.75
TOT Abundance	26	80	54	53.33	TOT Abundance	223	232	163	206
J′				0.68	J′				0.59
H′				2.04	H′				1.92

The most abundant nematode genera per site are given in bold. The Pielou's evenness (J) and the Shannon index (H′) are given per site for both meiofauna and Nematoda.

(97%), with a sharper decrease from the first (94%) to the second (3%) cm at TAG than at Snake Pit (91% in the first cm, 6% in the second). Snake Pit has the highest average nematode density (86 ± 12 ind/10 cm^2) compared to TAG (22 ± 7 ind/10 cm^2) (**Figure 2**) and a slightly higher diversity (average of 14 genera, total of 24 genera) compared to TAG (average of 10 genera, total of 19 genera) (**Table 1**). According to the Kruskal–Wallis test, no statistically significant difference was found in terms of nematode diversity between the two sites, whereas the difference in nematode density is statistically significant ($p = 0.049$). The most abundant nematode genera at TAG are *Desmoscolex* (28% of the total density) and *Microlaimus* (18% of the total density), whereas at Snake Pit *Metalinhomoeus* accounts for 38% of the total density, and *Halomonhystera* accounts for 25% (**Table 1**). Three of the 24 and 19 genera observed at Snake Pit and TAG, respectively, were present at both sites: *Cephalochaetosoma*, *Microlaimus*, and *Syringolaimus*. Trans-Atlantic Geotraverse deeper layers (2–5 cm) host few nematodes: one specimen of *Chromadorella*, *Cobbia*, *Retrotheristus*, *Sabatieria*, and *Syringolaimus* (**Figure S2**). Snake Pit deeper layers (2–5 cm) host several nematode genera: two specimens of *Camacolaimus*, *Metalinhomoeus*, *Sabatieria*, and *Syringolaimus*; three of *Halomonhystera*; and only one of *Cephalochaetosoma* and *Desmodora* (**Figure S2**). Permutational analysis of variance analysis found a statistically significant difference in community composition between sites ($p = 0.001$; $F = 2.73$), which explains 13% of the variance. Moreover, PCA revealed a strong discrimination in genera composition between the two sites. Indeed, PC1 explains 78% of the variance, with *Metalinhomoeus* (score = 0.6) and *Halomonhystera* (score = 0.5) characterizing Snake Pit, whereas *Desmoscolex* (score = −0.5) typifies TAG (**Figure 3**). Both diversity and evenness indices were higher for TAG ($H' = 2.04$; $J = 0.68$) than for Snake Pit ($H' = 1.92$; $J = 0.59$) (**Table 1**).

DISCUSSION

The ecology of nematodes living in chemosynthetic environments has been reviewed by Vanreusel et al. (2010), who noted that the community structure was driven by the presence of soft substrate, geochemical settings, and the availability of food, whereas community composition was additionally driven by the spatial continuity of the habitat. In this study, sedimentation of particulate matter around the studied sites was mainly due to the erosion of ancient sulfides mounds and the settling of hydrothermal particles that precipitated within the plume. The solid phase composition shows a significant difference in total S, with a stronger influence of metalliferous sediment at Snake Pit (**Table S1**). Still, both sites exhibit similar and relatively low organic and N contents. Because O_2 is generally correlated to OC, with an increasing penetration depth when OC decreases (Wenzhöfer and Glud, 2002), one could have expected a similar O_2 penetration depth (OPD) between the sites. Nevertheless, while the OPD at TAG is what we expect from abyssal areas (i.e., several centimeters; Glud, 2008), the OPD at Snake Pit is much shallower, with evidences of bioturbation (**Figure 1**). This may have contributed to the observed differences in our nematodes community composition. While TAG nematode community is mostly composed by persisters with a K-type life strategy (low reproductive rates, low colonizing capability, and low levels of tolerance to disturbance) and no clear dominance pattern, Snake Pit community consists of both colonizers and persisters genera with a clear dominance of two taxa, *Metalinhomoeus* and *Halomonhystera*, representing together 63% of the total community. The dominance of these two tolerant genera and the presence of *Sabatieria* are consistent with the hypoxia of Snake Pit sediments. The two nematode genera *Metalinhomoeus* and *Sabatieria* are able to reach the deeper anoxic layers of Snake Pit sediments (5-cm depth) (**Figure S2**). *Metalinhomoeus* is one of the biggest and longest nematodes of our samples, a

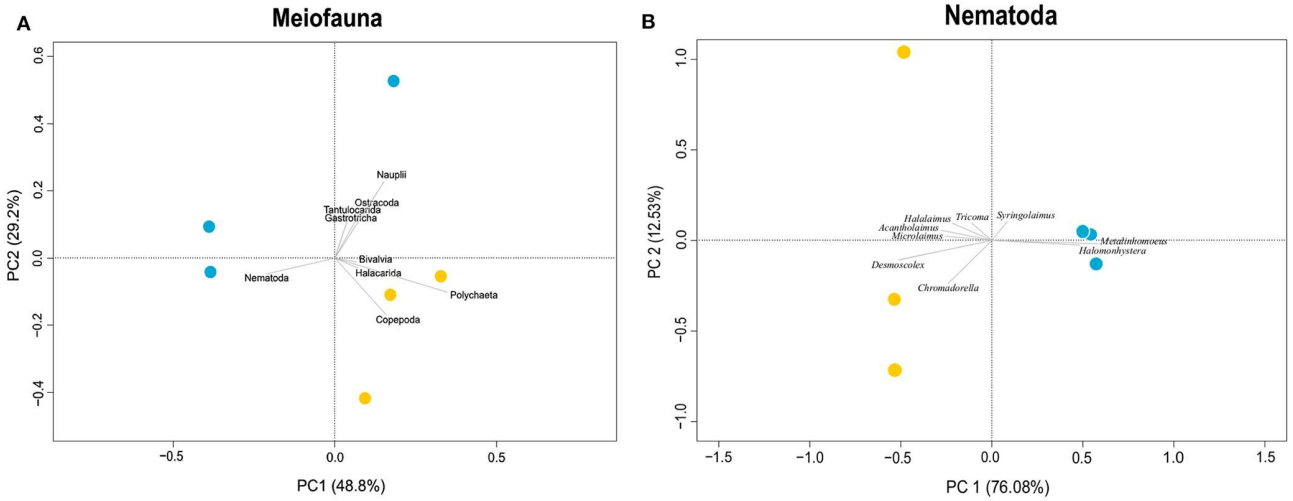

FIGURE 3 | Principal component analysis of meiofauna taxa composition **(A)** and nematode genera composition **(B)**. Blue dots indicate Snake Pit samples, whereas yellow dots indicate TAG samples. For meiofauna **(A)**, PC1 explains 76% of the variance, whereas PC2 explains 13%. For nematodes **(B)**, only the most representative genera are shown in the plot, and PC1 explains 76% of the variance, whereas PC2 explains 12%.

peculiar body shape of thiobiotic nematodes (deeper-living in the sediment) (Jensen, 1987). The pronounced body elongation and the increase in surface–volume ratio in thiobiotic species are an adaptive character related to low O_2 partial pressure (Vanreusel et al., 2010). The increased body length in suboxic or anoxic conditions reflects an increased mobility, which allows nematodes to move easily among sediment layers, passing quickly from depleted to well-oxygenated zones (Jensen, 1986, 1987). *Sabatieria* has already been described as a resistant genus to anoxic conditions, able to survive periods of anoxia of up to 7 weeks, and it is often the only remaining species in strongly anoxic conditions (Jensen, 1984; Modig and Ólafsson, 1998; Boyd et al., 2000; Wetzel et al., 2002; Steyaert et al., 2005, 2007). The ovoviviparous strategy observed in *Halomonhystera* as a response to stressful or toxic conditions (Walker and Tsui, 1968; Luc et al., 1979; Chen and Caswell-Chen, 2003) may also enhance their probability to survive and make them more tolerant than other meiofauna taxa (Polz et al., 1992; Thiermann et al., 2000; Bellec et al., 2018). In contrast to what Vanreusel et al. (1997) found at the Fiji basin, specialized nematode genera seem to have been able to invade the Snake Pit vent fields surrounding sediments, where they coexist with genera less tolerant to harsh conditions. The presence of the latter may be facilitated by the activity of polychaetes that were observed on the sediment surface, because polychaetes act as biodiffusors and bioturbators, mixing particles and pore water through the sediment layers (Reible et al., 1996).

The presence of numerous polychaetes and the higher density of meiofauna, together with the low OPD, would suggest an extra input of food sources at Snake Pit, despite the similar OC and N contents at both sites. Snake Pit sediments are characterized by sulfide-rich minerals, and Kato et al. (2018) suggested that chemolithoautotrophic bacteria may play a key role as primary producers in the sulfide deposits below the seafloor. This chemosynthetic system can be fueled by oxidized pyrite or pyrrhotite, which release Fe(II) and sulfide in oxygenated seawater (Schippers and Jorgensen, 2002). In these reactions, intermediate S species (ISS), such as elemental S, sulfite, and thiosulfate, are produced during electron transfer from sulfide to sulfate (Moses et al., 1987). Through the analysis of metagenome-assembled genomes from massive sulfide deposits, Kato et al. (2018) found that some yet-uncultivated bacteria are able to use sulfate or ISS as energy sources. Therefore, we hypothesize that high sedimentary S concentrations may result in an increase of bacterial density and, subsequently, in a raise of food inputs for the dominant meiofauna taxa, resulting in their flourishing (Van Gaever et al., 2009). Indeed, the most abundant nematode genera at Snake Pit (*Metalinhomoeus* and *Halomonhystera*) are nonselective deposit feeders (group 1B, Wieser, 1953), which can feed on bacteria as well (Moens and Vincx, 1997).

The observed differences in nematode community composition between TAG and Snake Pit could also be attributed to the distance between the sites (300 km) and the further separation due to the Kane Fracture Zone. As already suggested by Vanreusel et al. (1997), the dispersal ability of free-living nematodes is limited; thus, colonization of patchily distributed, and ephemeral hydrothermal vents comes from adjacent sediments rather than the long-range dispersal of a specialized fauna. In the Fiji basin indeed, the nematode genera composition was similar between vents and control sites with few dominating genera, of which *Monhystera* prevailed in the majority of samples (Vanreusel et al., 1997). However, this hypothesis will be further tested by a comparison with control sites in a future study.

At our sites, as the meiofauna community composition reflects the pattern reported in the literature for the deep sea, that is, nematodes as approximately 90% of the total abundance of meiofauna, it does not allow to determine a discrimination

between TAG and Snake Pit (Heip et al., 1985; Vanreusel et al., 2010; Zeppilli et al., 2014). Instead, nematodes show a genus-specific response to variable geochemical characteristics of metalliferous sediments. Thus, although meiofauna may be a powerful bioindicator of anthropogenic impacts (Zeppilli et al., 2015), a higher taxonomic resolution is needed to reveal the response of meiobenthic communities to the heterogeneity of their environments (Zekely et al., 2006; Gollner et al., 2010; Degen et al., 2012; Sarrazin et al., 2015). This heterogeneity should be taken into account when predicting the effect of a mining event on the structure of meiobenthic community, knowing that the reduction in habitat heterogeneity may permanently alter the structure of benthic communities (Zeppilli et al., 2015) and recolonization relies mainly on near vent sites (Vanreusel et al., 1997; Zekely et al., 2006).

CONCLUSION

The soft-sediment meiofauna and nematode communities showed four times higher densities at the Snake Pit than the TAG vent fields. The composition of the meiofauna at a low taxonomic resolution reflects the pattern reported in the literature for the deep sea (i.e., nematodes contributing for 90% of the total abundance of meiofauna) (Vanreusel et al., 2010 and references therein; Zeppilli et al., 2014), but differences in the Nematoda community composition at genus level revealed the influence of the surrounding environment. The geochemical settings (mostly O_2 and total S) and food availability are hypothesized to be the main drivers for the observed differences between the two study sites. Thus, our findings highlight the heterogeneity of hydrothermal sediments and the necessity of a high taxonomic resolution to reveal the response of meiofauna community to variations in biotic and abiotic factors and eventually mining impacts.

DATA AVAILABILITY STATEMENT

The datasets generated for this study are available on request to the corresponding author.

AUTHOR CONTRIBUTIONS

AS sorted meiofauna samples, identified the nematodes, and wrote the main body of the paper. NS designed the article, sorted meiofauna, ran the statistical analysis, and helped in nematodes identification. LP analyzed the cores for the geochemistry and contributed in defining the geochemical setting of the paper. LM designed the objectives of the study and the sampling strategy, supervised sampling on board during BICOSE2, and highly contributed to the statistical analysis. DZ was the chief of the project and contributed in the nematodes identification. Everybody contributed equally to the writing of the paper.

FUNDING

This work was supported by EQUINOR and IFREMER, which funded the postdoctoral fellowship of NS as part of the eCOREF project (Ecological connectivity and functional links between hydrothermal active and inactive sites in view of potential SMS mining in the deep-sea). We also thank Università Politecnica delle Marche and the Erasmus Traineeship Program for its contribution to AS first stay at Ifremer.

ACKNOWLEDGMENTS

We wish to thank all participants and the staff of the RV *Pourquoi Pas?*, the HOV Nautile crew and all scientists and students who participated in the BICOSE2 cruise (doi: 10.17600/18000004). We specially want to thank Dr. Marie-Anne Cambon-Bonavita, chief scientist of the cruise and Ewan Pelleter for his advice.

SUPPLEMENTARY MATERIAL

The Supplementary Material for this article can be found online at: https://www.frontiersin.org/articles/10.3389/fmars.2020.00200/full#supplementary-material

REFERENCES

Bain, O., Baldwin, J. G., Beveridge, I., Campinas Bezerra, T., Braeckman, U., Coomans, A., et al. (2014). *Nematoda*. Berlin; Boston, MA: De Gruyter. doi: 10.1515/9783110274257

Bellec, L., Cambon-Bonavita, M. A., Cueff-Gauchard, V., Durand, L., Gayet, N., and Zeppilli, D. (2018). A nematode of the mid-atlantic ridge hydrothermal vents harbors a possible symbiotic relationship. *Front Microbiol.* 9:2246. doi: 10.3389/fmicb.2018.02246

Bezerra, T. N., Decraemer, W., Eisendle-Flöckner, U., Hodda, M., Holovachov, O., Leduc, D., et al. (2020). *Nemys: World Database of Nematodes*. doi: 10.14284/366

Boschen, R. E., Rowden, A. A., Clark, M. R., and Gardner, J. P. A. (2013). Mining of deep-sea seafloor massive sulfides: a review of the deposits, their benthic communities, impacts from mining, regulatory frameworks and management strategies. *Ocean Coast. Manag.* 84, 54–67. doi: 10.1016/j.ocecoaman.2013.07.005

Boyd, S. E., Rees, H. L., and Richardson, C. A. (2000). Nematodes as sensitive indicators of change at dredged material disposal sites. *Estuar. Coast. Shelf Sci.* 51, 805–819. doi: 10.1006/ecss.2000.0722

Brodie, C. R., Leng, M. J., Casford, J. S. L., Kendrick, C. P., Lloyd, J. M., Yongqiang, Z., et al. (2011). Evidence for bias in C and N concentrations and δ13C composition of terrestrial and aquatic organic materials due to pre-analysis acid preparation methods. *Chem. Geol.* 282, 67–83. doi: 10.1016/j.chemgeo.2011.01.007

Cambon-Bonavita M.-A. (2018). *BICOSE 2 Cruise, RV Pourquoi Pas?* doi: 10.17600/18000004

Chen, J., and Caswell-Chen, E. P. (2003). Why Caenorhabditis elegans adults sacrifice their bodies to progeny. *Nematology* 5, 641–645. doi: 10.1163/156854103322683355

Clarke, K. R., and Gorley, R. N. (2006). PRIMER v6: *Prim. V6 User Manual/Tutorial*.

Degen, R., Riavitz, L., Gollner, S., Vanreusel, A., Plum, C., and Bright, M. (2012). Community study of tubeworm-associated epizooic meiobenthos from

deep-sea cold seeps and hot vents. *Mar. Ecol. Prog. Ser.* 468, 135–148. doi: 10.3354/meps09889

Fouquet, Y., and Scott, S. D. (2009). "SS: ocean mining: the science of seafloor massive sulfides (SMS) in the modern ocean - a new global resource for base and precious metals," in *Offshore Technology Conference*. doi: 10.4043/19849-MS

Fouquet, Y., Wafik, A., Cambon, P., Mevel, C., Meyer, G., and Gente, P. (1993). Tectonic setting and mineralogical and geochemical zonation in the snake pit sulfide deposit (mid-Atlantic ridge at 23°N). *Econ. Geol.* 88, 2018–2036. doi: 10.2113/gsecongeo.88.8.2018

German, C. R. (1993). A geochemical study of metalliferous sediment from the TAG hydrothermal mound, 26°08′N, Mid-Atlantic Ridge. *J. Geophys. Res.* 98, 9683–9692. doi: 10.1029/92JB01705

Glud, R. N. (2008). Oxygen dynamics of marine sediments. *Mar. Biol. Res.* 4, 243–289. doi: 10.1080/17451000801888726

Gollner, S., Riemer, B., Arbizu, P. M., le Bris, N., and Bright, M. (2010). Diversity of meiofauna from the 9°50′N east pacific rise across a gradient of hydrothermal fluid emissions. *PLoS ONE* 5:e12321. doi: 10.1371/journal.pone.0012321

Grasshoff, K., Ehrhardt, M., and Kremling, K. (1983). *Methods of Seawater Analysis, 2nd edn.* Weinheim: Verlag Chemie GmbH.

Hannington, M. D., Galley, A. G., Gerzig, P. M., and Petersen, S. (1998). Comparison of the TAG mound and stockwork complex with Cyprus-type massive sulfide deposits. *Proc. Ocean Drill. Progr. Sci. Results* 158, 389–415. doi: 10.2973/odp.proc.sr.158.217.1998

Heip, C., Vincx, M., and Vranken, G. (1985). The ecology of marine nematodes. *Oceanogr. Mar. Biol.* 23, 399–489.

Hoagland, P., Beaulieu, S., Tivey, M. A., Eggert, R. G., German, C., Glowka, L., et al. (2010). Deep-sea mining of seafloor massive sulfides. *Mar. Policy* 34, 728–732. doi: 10.1016/j.marpol.2009.12.001

Jensen, P. (1984). Ecology of benthic and epiphytic nematodes in brackish waters. *Hydrobiologia* 108, 201–217. doi: 10.1007/BF00006329

Jensen, P. (1986). Nematode fauna in the sulfide-rich brine seep and adjacent bottoms of the east flower garden northwestern gulf of mexico iv. *Ecol Aspects. Mar. Biol.* 92, 489–503. doi: 10.1007/BF00392509

Jensen, P. (1987). Differences in microhabitat, abundance, biomass and body size between oxybiotic and thiobiotic free-living marine nematodes. *Oecologia* 71, 564–567. doi: 10.1007/B.F.00379298

Kato, S., Shibuya, T., Takaki, Y., Hirai, M., Nunoura, T., and Suzuki, K. (2018). Genome-enabled metabolic reconstruction of dominant chemosynthetic colonizers in deep-sea massive sulfide deposits. *Environ. Microbiol.* 20, 862–877. doi: 10.1111/1462-2920.14032

Kleinrock, M. C., and Humphris, S. E. (1996). Structural asymmetry of the TAG rift valley: evidence from a near-bottom survey for episodic spreading. *Geophys. Res. Lett.* 23, 3439–3442. doi: 10.1029/96GL03073

Kowalenko, C. G. (2001). Assessment of Leco CNS-2000 analyzer for simultaneously measuring total carbon, nitrogen, and sulphur in soil. *Commun. Soil Sci. Plant Anal.* 32, 2065–2078. doi: 10.1081/CSS-120000269

Lalou, C., Thompson, G., Arnold, M., Brichet, E., Druffel, E., and Rona, P. A. (1990). Geochronology of TAG and Snake Pit hydrothermal fields; MAR - Witness to a long ans complex hydrothermal history. *Earth Planet. Sci. Lett.* 97, 113–128. doi: 10.1016/0012-821X(90)90103-5

Levin, L. A., Mendoza, G. F., Konotchick, T., and Lee, R. (2009). Macrobenthos community structure and trophic relationships within active and inactive Pacific hydrothermal sediments. *Deep. Res. Part II Top. Stud. Oceanogr.* 56, 1632–1648. doi: 10.1016/j.dsr2.2009.05.010

Luc, M., Taylor, D. P., and Netscher, C. (1979). On endotokia matricida and intra-uterine development and hatching in nematodes. *Nematologica* 25, 268–274. doi: 10.1163/187529279X00299

Modig, H., and Ólafsson, E. (1998). Responses of Baltic benthic invertebrates to hypoxic events. *J. Exp. Mar. Bio. Ecol.* 229, 133–148. doi: 10.1016/S0022-0981(98)00043-4

Moens, T., and Vincx, M. (1997). Observations on the feeding ecology of estuarine nematodes. *J. Mar. Biol. Ass. U.K.* 77, 211–227. doi: 10.1017/S0025315400033889

Moses, C. O., Kirk Nordstrom, D., Herman, J. S., and Mills, A. L. (1987). Aqueous pyrite oxidation by dissolved oxygen and by ferric iron. *Geochim. Cosmochim. Acta* 51, 1561–1571. doi: 10.1016/0016-7037(87)90337-1

Murton, B. J., Lehrmann, B., Dutrieux, A. M., Martins, S., de la Iglesia, A. G., Stobbs, I. J., et al. (2019). Geological fate of seafloor massive sulphides at the TAG hydrothermal field (Mid-Atlantic Ridge). *Ore Geol. Rev.* 107, 903–925. doi: 10.1016/j.oregeorev.2019.03.005

Oksanen, J. (2015). *Vegan: Community Ecology Package.* R package version 2.4-3. Available online at: https://CRAN.R-project.org/package=vegan. (accessed February 28, 2020).

Oksanen, J., Blanchet, F. G., Friendly, M., Kindt, R., Legendre, P., McGlinn, D., et al. (2018). *vegan: Community Ecology Package.* R package version 2.5-2. *CRAN R.*

Platt, H. M., and Warwick, R. M. (1988). *Free-Living Marine Nematodes, Part II British Chromadorids*. Netherlands: Brill, Leiden.

Polz, M., Felbeck, H., Novak, R., Nebelsick, M., and Ott, J. A. (1992). Chemoautotrophic, sulfur-oxidizing symbiotic bacteria on marine nematodes: morphological and biochemical characterization. *Microb. Ecol.* 24, 313–329. doi: 10.1007/BF00167789

Reible, D. D., Popov, V., Valsaraj, K. T., Thibodeaux, L. J., Lin, F., Dikshit, M., et al. (1996). Contaminant fluxes from sediment due to Tubificid oligochaete bioturbation. *Water Res.* 30, 704–714. doi: 10.1016/0043-1354(95)00187-5

Revsbech, N. P. (1989). An oxygen microsensor with a guard cathode. *Limnol. Oceanogr.* 34, 474–478. doi: 10.4319/lo.1989.34.2.0474

Rona, P. A., Klinkhammer, G., Nelsen, T. A., Trefry, J. H., and Elderfield, H. (1986). Black smokers, massive sulphides and vent biota at the Mid-Atlantic ridge. *Nature* 321, 33–37. doi: 10.1038/321033a0

Sarrazin, J., Legendre, P., de Busserolles, F., Fabri, M. C., Guilini, K., Ivanenko, V. N., et al. (2015). Biodiversity patterns, environmental drivers and indicator species on a high-temperature hydrothermal edifice, Mid-Atlantic Ridge. *Deep. Res. Part II Top. Stud. Oceanogr.* 121, 177–191. doi: 10.1016/j.dsr2.2015.04.013

Schippers, A., and Jorgensen, B. B. (2002). Biogeochemistry of pyrite and iron sulfide oxidation in marine sediments. *Geochim. Cosmochim. Acta* 66, 85–92. doi: 10.1016/S0016-7037(01)00745-1

Seinhorst, J. W. (1959). A rapid method for the transfer of nematodes from fixative to anhydrous glycerin. *Nematologica* 4, 67–69. doi: 10.1163/187529259X00381

Steyaert, M., Moodley, L., Nadong, T., Moens, T., Soetaert, K., and Vincx, M. (2007). Responses of intertidal nematodes to short-term anoxic events. *J. Exp. Mar. Bio. Ecol.* 345, 175–184. doi: 10.1016/j.jembe.2007.03.001

Steyaert, M., Moodley, L., Vanaverbeke, J., Vandewiele, S., and Vincx, M. (2005). Laboratory experiments on the infaunal activity of intertidal nematodes. *Hydrobiologia* 140, 217–223. doi: 10.1007/s10750-004-7145-4

Sudarikov, S. M., and Galkin, S. V. (1995). Geochemistry of the Snake Pit vent field and its implications for vent and non-vent fauna. *Geol. Soc. Spec. Publ.* 87, 319–327. doi: 10.1144/GSL.SP.1995.087.01.24

Thiermann, F., Vismann, B., and Giere, O. (2000). Sulphide tolerance of the marine nematode Oncholaimus campylocercoides - A result of internal sulphur formation? *Mar. Ecol. Prog. Ser.* 193, 251–259. doi: 10.3354/meps193251

Thompson, G., Humphris, S. E., Schroeder, B., Sulanowska, M., and Rona, P. A. (1988). Active vents and massive sulfides at 26°N (TAG) and 23°N (Snake Pit) on the Mid-Atlantic Ridge. *Can. Mineral.* 26, 697–711.

Van Dover, C. L. (1995). Ecology of Mid-Atlantic Ridge hydrothermal vents. *Geol. Soc. London Spec. Publ.* 87, 257–294. doi: 10.1144/GSL.SP.1995.087.01.21

Van Dover, C. L. (2019). Inactive sulfide ecosystems in the deep sea: a review. *Front. Mar. Sci.* 6:461. doi: 10.3389/fmars.2019.00461

Van Gaever, S., Olu, K., Derycke, S., and Vanreusel, A. (2009). Metazoan meiofaunal communities at cold seeps along the Norwegian margin: Influence of habitat heterogeneity and evidence for connection with shallow-water habitats. *Deep. Res. Part I Oceanogr. Res. Pap.* 56, 772–785. doi: 10.1016/j.dsr.2008.12.015

Vanreusel, A., de Groote, A., Gollner, S., and Bright, M. (2010). Ecology and biogeography of free-living nematodes associated with chemosynthetic environments in the deep sea: a review. *PLoS ONE* 5:e12449. doi: 10.1371/journal.pone.0012449

Vanreusel, A., Van Den Bossche, I., and Thiermann, F. (1997). Free-living marine nematodes from hydrothermal sediments: Similarities with communities from diverse reduced habitats. *Mar. Ecol. Prog. Ser.* 157, 207–219. doi: 10.3354/meps157207

Walker, J. T., and Tsui, R. K. (1968). Induction of ovoviviparity in rhabditis by sulfur dioxide. *Nematologica* 14, 148–149. doi: 10.1163/187529268X00769

Wenzhöfer, F., and Glud, R. N. (2002). Benthic carbon mineralization in the Atlantic: a synthesis based on in situ data from the last decade. *Deep-Sea Res. I* 49, 1255–1279. doi: 10.1016/S0967-0637(02)00025-0

Wetzel, M. A., Weber, A., and Giere, O. (2002). Re-colonization of anoxic/sulfidic sediments by marine nematodes after experimental removal of macroalgal cover. *Mar. Biol.* 141, 679–689. doi: 10.1007/s00227-002-0863-0

Wieser, W. (1953). Die beziehung zwischen mundhohlengestalt, ernahrungsweise und vorkommen be1 fre lebenden marmen nernatoden. *Ark. Zool.* 4, 439–484.

WoRMS Editorial Board (2020). *World Register of Marine Species.* doi: 10.14284/170

Zekely, J., Van Dover, C. L., Nemeschkal, H. L., and Bright, M. (2006). Hydrothermal vent meiobenthos associated with mytilid mussel aggregations from the Mid-Atlantic Ridge and the East Pacific Rise. *Deep. Res. Part I Oceanogr. Res. Pap.* 53, 1363–1378. doi: 10.1016/j.dsr.2006.05.010

Zeppilli, D., Bongiorni, L., Santos, R. S., and Vanreusel, A. (2014). Changes in nematode communities in different physiographic sites of the Condor Seamount (North-East Atlantic Ocean) and adjacent sediments. *PLoS ONE* 9:115601. doi: 10.1371/journal.pone.0115601

Zeppilli, D., Sarrazin, J., Leduc, D., Arbizu, P. M., Fontaneto, D., Fontanier, C., et al. (2015). Is the meiofauna a good indicator for climate change and anthropogenic impacts? *Mar. Biodivers.* 45, 505–535. doi: 10.1007/s12526-015-0359-z

Conflict of Interest: The authors declare that the research was conducted in the absence of any commercial or financial relationships that could be construed as a potential conflict of interest.

Copyright © 2020 Spedicato, Sánchez, Pastor, Menot and Zeppilli. This is an open-access article distributed under the terms of the Creative Commons Attribution License (CC BY). The use, distribution or reproduction in other forums is permitted, provided the original author(s) and the copyright owner(s) are credited and that the original publication in this journal is cited, in accordance with accepted academic practice. No use, distribution or reproduction is permitted which does not comply with these terms.

frontiers in Marine Science

REVIEW
published: 21 May 2020
doi: 10.3389/fmars.2020.00244

Cold Seeps in a Warming Arctic: Insights for Benthic Ecology

Emmelie K. L. Åström[1†], Arunima Sen[2†], Michael L. Carroll[3] and JoLynn Carroll[3,4]*

[1] Department of Arctic and Marine Biology, UiT – The Arctic University of Norway, Tromsø, Norway, [2] Faculty of Bioscience and Aquaculture, Nord University, Bodø, Norway, [3] Akvaplan-niva, FRAM – High North Research Centre for Climate and the Environment, Tromsø, Norway, [4] Department of Geosciences, UiT – The Arctic University of Norway, Tromsø, Norway

Cold-seep benthic communities in the Arctic exist at the nexus of two extreme environments; one reflecting the harsh physical extremes of the Arctic environment and another reflecting the chemical extremes and strong environmental gradients associated with seafloor seepage of methane and toxic sulfide-enriched sediments. Recent ecological investigations of cold seeps at numerous locations on the margins of the Arctic Ocean basin reveal that seabed seepage of reduced gas and fluids strongly influence benthic communities and associated marine ecosystems. These Arctic seep communities are mostly different from both conventional Arctic benthic communities as well as cold-seep systems elsewhere in the world. They are characterized by a lack of large specialized chemo-obligate polychetes and mollusks often seen at non-Arctic seeps, but, nonetheless, have substantially higher benthic abundance and biomass compared to adjacent Arctic areas lacking seeps. Arctic seep communities are dominated by expansive tufts or meadows of siboglinid polychetes, which can reach densities up to $>3 \times 10^5$ ind.m^{-2}. The enhanced autochthonous chemosynthetic production, combined with reef-like structures from methane-derived authigenic carbonates, provides a rich and complex local habitat that results in aggregations of non-seep specialized fauna from multiple trophic levels, including several commercial species. Cold seeps are far more widespread in the Arctic than thought even a few years ago. They exhibit *in situ* benthic chemosynthetic production cycles that operate on different spatial and temporal cycles than the sunlight-driven counterpart of photosynthetic production in the ocean's surface. These systems can act as a spatio-temporal bridge for benthic communities and associated ecosystems that may otherwise suffer from a lack of consistency in food quality from the surface ocean during seasons of low production. As climate change impacts accelerate in Arctic marginal seas, photosynthetic primary production cycles are being modified, including in terms of changes in the timing, magnitude, and quality of photosynthetic carbon, whose delivery to the seabed fuels benthic communities. Furthermore, an increased northward expansion of species is expected as a consequence of warming seas. This may have implications for dispersal and evolution of both chemosymbiotic species as well as for background taxa in the entire realm of the Arctic Ocean basin and fringing seas.

Keywords: authigenic carbonates, chemosynthesis, commercial species, methane seepage, trophic structure

OPEN ACCESS

Edited by:
Jeroen Ingels,
Florida State University, United States

Reviewed by:
Clara Rodrigues,
University of Aveiro, Portugal
Cindy Lee Van Dover,
Nicholas School of the Environment,
United States

****Correspondence:***
Emmelie K. L. Åström
emmelie.k.astrom@uit.no

[†] These authors have contributed equally to this work

Specialty section:
This article was submitted to Global Change and the Future Ocean, a section of the journal Frontiers in Marine Science

Received: *30 November 2019*
Accepted: *27 March 2020*
Published: *21 May 2020*

Citation:
Åström EKL, Sen A, Carroll ML and Carroll J (2020) Cold Seeps in a Warming Arctic: Insights for Benthic Ecology. Front. Mar. Sci. 7:244. doi: 10.3389/fmars.2020.00244

INTRODUCTION

Photosynthesis is the main pathway of organic material production in the world's oceans. Since this process relies on energy from sunlight, it is only spatially and temporally possible where and when there is enough light in the water column to stimulate photosynthetic activity (Harrison and Platt, 1986; Duarte and Cebrián, 1996). Generally, photic zones terminate at a maximum of 200 m water depth, and outside the tropics, photosynthetic production is highly seasonal (Sakshaug and Slagstad, 1991; Moran et al., 2012). Organisms living on the ocean floor outside the coastal zone largely rely on organic material sinking from the photic zone to the seabed, and the quality and quantity of organic material reaching the seafloor is correlated with water depth (Southward and Southward, 1982; Gage and Tyler, 1991; Morata et al., 2008). However, photosynthetic organisms and their carbon fixation activities in surface waters do not represent the entirety of the food supply to the benthos. Other sources of food are zooplankton and fecal pellets that become available to the benthos via pelagic–benthic coupling processes (Graf, 1989; Grebmeier and Barry, 1991). In benthic deep-sea systems, inorganic carbon fixed via prokaryotes (so-called "dark fixation") may also provide significant carbon sources (Molari et al., 2013; Sweetman et al., 2019). Occasionally, large pulses of food arrive at the bottom of the ocean in the form of carcasses of large animals such as whale/shark falls, or mass mortality of jellyfish (e.g., Smith and Baco, 2003; Higgs et al., 2014; Dunlop et al., 2018) or even from terrestrial sources by wood-falls or large inputs of sediment (e.g., Dando et al., 1992; Bienhold et al., 2013; Holding et al., 2017; Sen et al., 2017).

Nonetheless, food availability on the seafloor is closely tied to photosynthetic primary production in surface waters (Rice et al., 1986 Renaud et al., 2008; Morata et al., 2013). This pelagic–benthic coupling means that temporal and spatial patterns in surficial primary production regulates benthic food availability (Gooday et al., 1990; Wassmann et al., 2006; Morata et al., 2008). The most common manifestation of variable food input to the seafloor as a result of surface conditions is seasonality: benthic systems tend to be more food limited during the winter months when daylight is limited (Renaud et al., 2007; Ambrose et al., 2012; Morata et al., 2013). In polar regions, this seasonal disparity is particularly pronounced due to the phenomena of midnight sun and polar night (the absence of setting or rising of the sun above the horizon, respectively) (Berge et al., 2015). Summer biological blooms in polar regions are, furthermore, not limited to phytoplankton. Sea ice allows for the proliferation of ice algae during periods of unrestricted sunlight (Hegseth, 1998; McMahon et al., 2006; Søreide et al., 2006). The simultaneous presence of phytoplankton blooms and melting sea ice during Arctic spring and early summer results in a peak in both the quantity and quality of food supply to the benthos (Ambrose and Renaud, 1997; Wassmann et al., 2006; Renaud et al., 2008).

Cold seeps are locations on the seafloor where reduced compounds from subsurface hydrocarbon reserves enrich sediment fluids or emanate freely as gas from the seabed. Methane is often the predominant gas seeping up from sub-seabed reservoirs, however, fractions of heavier hydrocarbons can also occur (MacDonald, 1990; Hovland and Svensen, 2006; Andreassen et al., 2017). A consortium of sediment microbes oxidizes methane anaerobically through a process known as the anaerobic oxidation of methane (AOM) (Boetius et al., 2000). Sulfate reduction takes place concomitantly in this process, thereby generating another reduced compound, hydrogen sulfide. The enrichment of sediment porewater in compounds such as methane and sulfide provides the setting for chemosynthesis or the fixation of carbon by microbes with reduced compounds as the energy source. Chemosynthetic microbes can either be free living or reside within or on organisms with which they form a symbiotic relationship. Together, such autochthonous primary production at the seabed forms the base of a food chain and an ecosystem that revolves around chemical-based autotrophic processes (Fisher, 1996; Sibuet and Olu, 1998; Levin, 2005; Becker et al., 2013). Cold-seep systems, thus, function largely outside the paradigm of conventional benthic systems that rely on food supplied from the pelagic zone. They typically exhibit an uncharacteristically high biomass and abundance of organisms due to local energy sources and food production (Sibuet and Olu, 1998; Levin et al., 2016). However, sulfide that is produced as a result of seabed methane seepage and microbial activity is lethal even in low concentrations for most organisms because of its negative effect on oxidative respiration (Vismann, 1991; Bagarinao, 1992). Thus, despite high biomass at cold seeps, the presence of sulfide may limit biodiversity at seeps in comparison to non-reducing environments (Sibuet and Olu, 1998; Levin et al., 2003).

Until recently, Arctic seep-ecology research was nearly exclusively limited to the study of the Håkon Mosby mud volcano (HMMV) in the south-west Barents Sea at 72°N, 14°E (**Figure 1**). Concentrated efforts at HMMV proved insightful in understanding various aspects of this Arctic cold-seep system (e.g., Hjelsteun et al., 1999; Gebruk et al., 2003; Niemann et al., 2006; Jerosch et al., 2007; Decker et al., 2012). Yet, to extrapolate to larger scale processes and broader contexts requires investigation of multiple locations. In this review, we reveal how Arctic seep studies have progressed from merely viewing HMMV as a single anomaly to a more comprehensive understanding of Arctic seep ecology. We also discuss how Arctic seeps differ from seep ecology in lower latitudes.

The world's oceans are in constant interaction of large-scale oceanographic and chemical processes, mitigating causes of climate changes through uptake of atmospheric CO_2, other greenhouse gas equivalents, and excess heat. Consequences of such processes are warmer oceans affecting circulation and mixing, solubility of gases (i.e., reduced oxygen levels), changes in productivity, and ocean acidification (Levin and Bris, 2015; IPCC, 2018; Mora et al., 2018). The Arctic is no exception to these impacts; in fact, warming at the poles is occurring faster than elsewhere on Earth (Comiso and Hall, 2014), and the region is subjected to unprecedented changes as a result of the continuing rise of atmospheric greenhouse gases (IPCC, 2018). Even if global actions to reduce emissions are implemented immediately, climate change impacts will continue for at least the next few decades due to the time lag of effects (Steffen et al., 2018). It is, therefore, relevant and timely to examine Arctic seeps within the context of climate change.

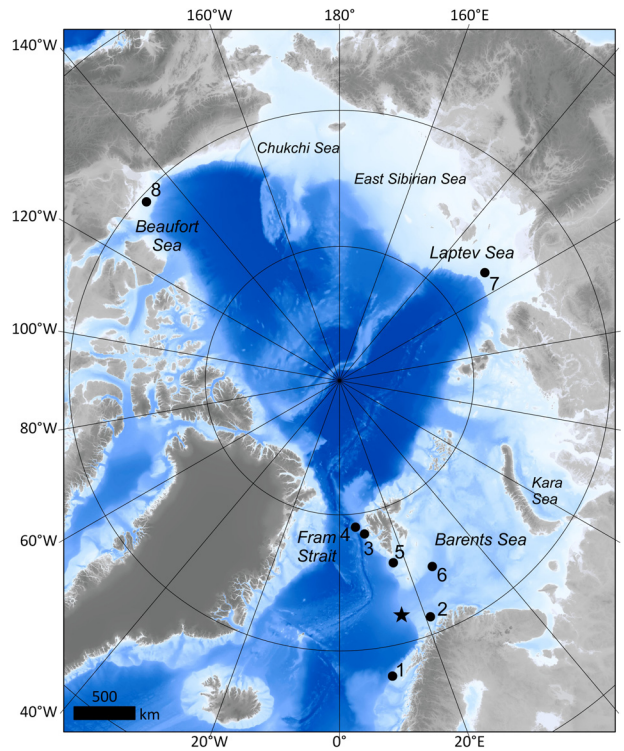

FIGURE 1 | The Arctic and major seas. Seep sites discussed in this review are marked with black circles. Water depths of seep locations are presented in parentheses after the site name. The star marks the location of the Håkon Mosby mud volcano (HMMV) (1,250 m). 1: Lofoten canyons (750–800 m), 2: Svanfjell seep (380 m), 3: Prins Karls Forland (80–350 m), 4: Vestnesa Ridge (1,200 m), 5: Storfjordrenna seep and gas hydrate mounds/pingos (350–390 m), 6: Bjørnøyrenna seep and craters (330–360 m), 7: Laptev Sea (70 m), 8: Beaufort Sea mud volcanoes (280–740 m). Bathymetry for this map was obtained from IBCAO (Jakobsson et al., 2012).

In this review, we specifically focus on macrofaunal and megafaunal communities, i.e., taxa $\geq$ 0.5 cm and taxa visible with the naked eye from seafloor images (cm scale and larger) (e.g., Bowden et al., 2013; Amon et al., 2017; Sen et al., 2018a). Microbiology and meiofaunal communities are referred to only within the context of the ecology of larger animals. We discuss taxa and species inhabiting cold seeps using the following terminology: "Obligate chemosymbiotrophic" species reliant on nutritional chemosymbiosis; "obligate seep" species only present at seeps, "background" species occurring at seeps and non-seep sites, not matching the abovementioned criteria. Characteristically for many seeps worldwide are three groups of taxa: vestimentiferan siboglinids, vesicomyid clams, and bathymodioline mussels. We refer to these taxa as "hallmark seep" taxa. The geographical focus of this review is "the Arctic," and we discuss the Arctic as the area above the Arctic Circle (66°33′N). We are aware that there are many different ways of defining the Arctic (Artcic Monitoring and Assessment Programme [AMAP], 1998), however, using the Arctic Circle makes this definition easily identifiable. Furthermore, this definition is biologically relevant due to the phenomena of midnight sun and polar night, which are strongly coupled to annual biological production cycles.

PAST ARCTIC COLD-SEEP INVESTIGATIONS

The Håkon Mosby Mud Volcano (HMMV)

The Håkon Mosby Mud volcano is a large, circular-shaped (1–2 km) mud volcano, located at 72°N at a water depth of about 1,250 m (**Figure 1**). Since its discovery in 1989, HMMV stood out as an unusual cold-seep system in the world's oceans (Vogt et al., 1997). It lacks an association with either salt or plate tectonics, which are two of the primary means of providing migration conduits for seepage of gas-enriched fluids from within the seabed (Vogt et al., 1997). Additionally, the site is located within the Arctic and appears to have developed within glacial sediments. These unusual features prompted numerous scientific campaigns across various disciplines including geophysics, biogeochemistry, microbiology, and ecology to be carried out at HMMV (e.g., Vogt et al., 1997; Hjelsteun et al., 1999; Gebruk et al., 2003; Niemann et al., 2006; Jerosch et al., 2007; Lösekann et al., 2007; Decker et al., 2012; Rybakova et al., 2013). These studies provided the first insight into the structure and functioning of an Arctic cold-seep system.

Distinct habitats and species assemblages radiate concentrically from a central, visually uninhabited zone of fluid expulsion of HMMV (Gebruk et al., 2003; Jerosch et al., 2007; Rybakova et al., 2013). The zone just outward of the central zone is covered in mosaics of bacterial mats of various thicknesses. The most dominant forms among the mats are filamentous bacteria resembling sulfur-oxidizing strains such as *Beggiatoa* (Pimenov et al., 2000; Gebruk et al., 2003). Beyond the bacterial mats, there are zones dominated by siboglinid worms of two species: the moniliferan *Sclerolinum contortum* and the frenulate *Oligobrachia haakonmosbiensis* (Smirnov, 2008, 2014) (**Figure 2**). Though both species occur in high densities, forming large (up to meter square) tufts, *S. contortum* is the dominant species (biomass 435 g m^{-2} vs. 350 g m^{-2}) (Gebruk et al., 2003).

The outermost zone is characterized by ophiuroids and a lack of chemosynthesis-based community members such as bacterial mats and siboglinid worms (Rybakova et al., 2013). In total, 80 in faunal and epifaunal taxa have been recorded at HMMV (Gebruk et al., 2003; Decker et al., 2012; Rybakova et al., 2013). Biomass is higher within the mud volcano compared to the outside and background benthos, while taxonomic richness does not differ significantly between inside and outside of the volcano (**Figure 3**; Rybakova et al., 2013). Gebruk et al. (2003) also noted that the background fauna (animals inhabiting the seafloor beyond the seep-influenced area) appeared to be considerably "poorer," particularly with respect to biomass.

The ambient water around HMMV is characterized by subzero temperatures (De Beer et al., 2006; Portnova et al., 2011); however, sediment and fluid release at the mud volcano is accompanied by considerable heat release in the center (up to 40°C at 0.5 m below sediment surface) (Kaul et al., 2006; Feseker et al., 2008). The extent of heat, fluid, and mud

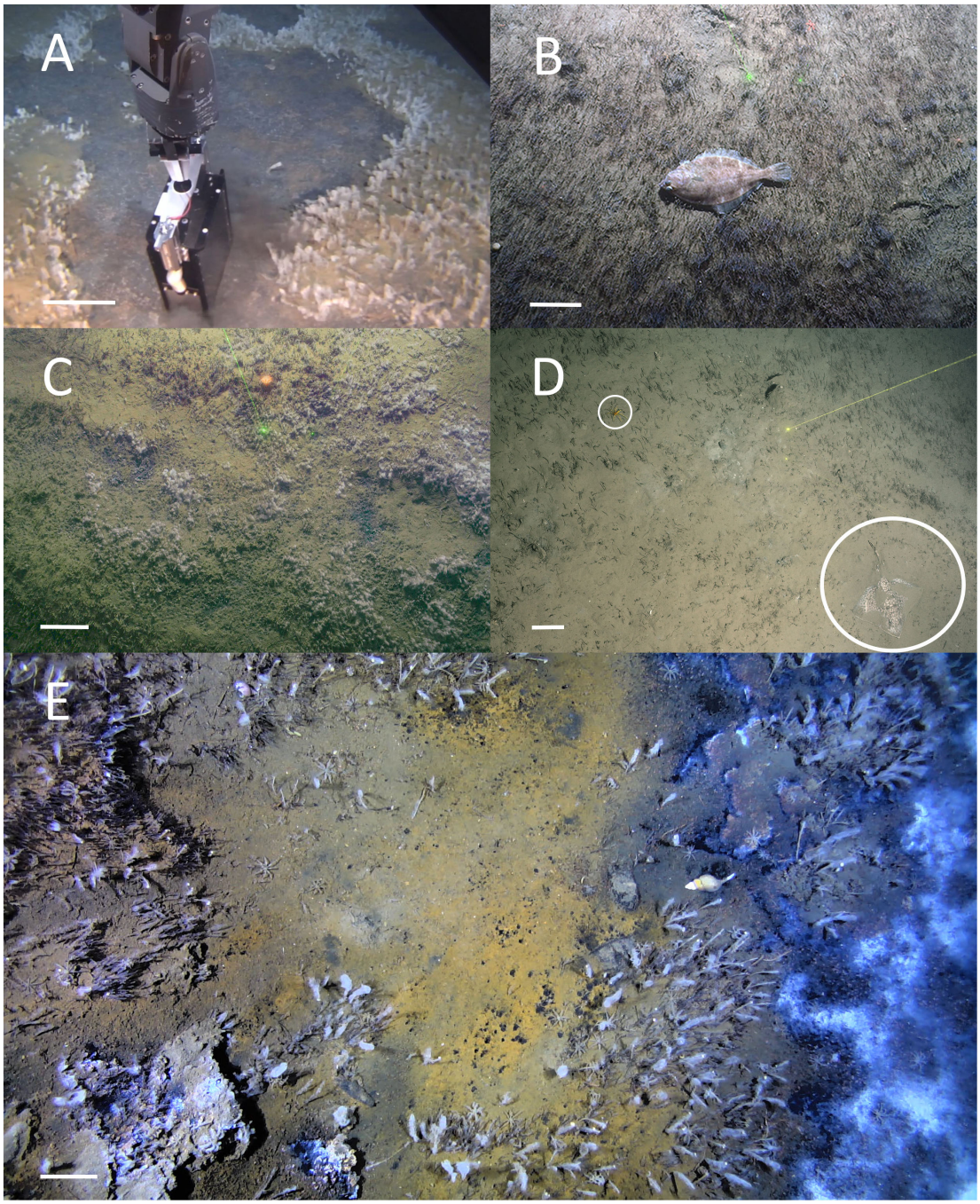

FIGURE 2 | Tufts of siboglinids (mainly *Oligobrachia* spp.) from different Arctic cold-seep locations. From top left to right: **(A)** A large siboglinid field covered by filamentous bacteria in the "Bjørnøyrenna crater seep" Barents Sea (330 m) from Åström et al. (2019). **(B)** An American plaice (*Hippoglossoides platessoides*) in a dense meadow of siboglinids at the Storfjordrenna gas hydrate mounds/pingos, (380 m), from Åström et al. (2016). **(C)** Siboglinids and filamentous bacteria at the Storfjordrenna seep field (350 m), note also the bright orange anemone in the top middle, from Åström et al. (2019). **(D)** Siboglinid tufts at the deep Vestnesa seep (Fram Strait, 1,200 m); encircled is a half-buried Arctic skate (*Amblyraja hyperborea*) and a sea spider (*Colossendeis* sp.), from Åström et al. (2018). **(E)** Carbonate outcrops, microbial mats, and filamentous bacteria covering siboglinid tubes at the Lofoten canyon seeps (750 m); note the many sea spiders (*Nymphon hirtipes*) at the bottom, from Sen et al. (2019b). Scale bars indicate 20 cm.

release follows a concentric pattern where the greatest mud and fluid expulsion rates occur in the central zone, while the outer zones are less dynamic. Seepage of heated methane-rich porewater from deep sediments below HMMV causes unstable sediments as oversaturated mud is expulsed to the seafloor surface. The temperature variability in the surface sediments

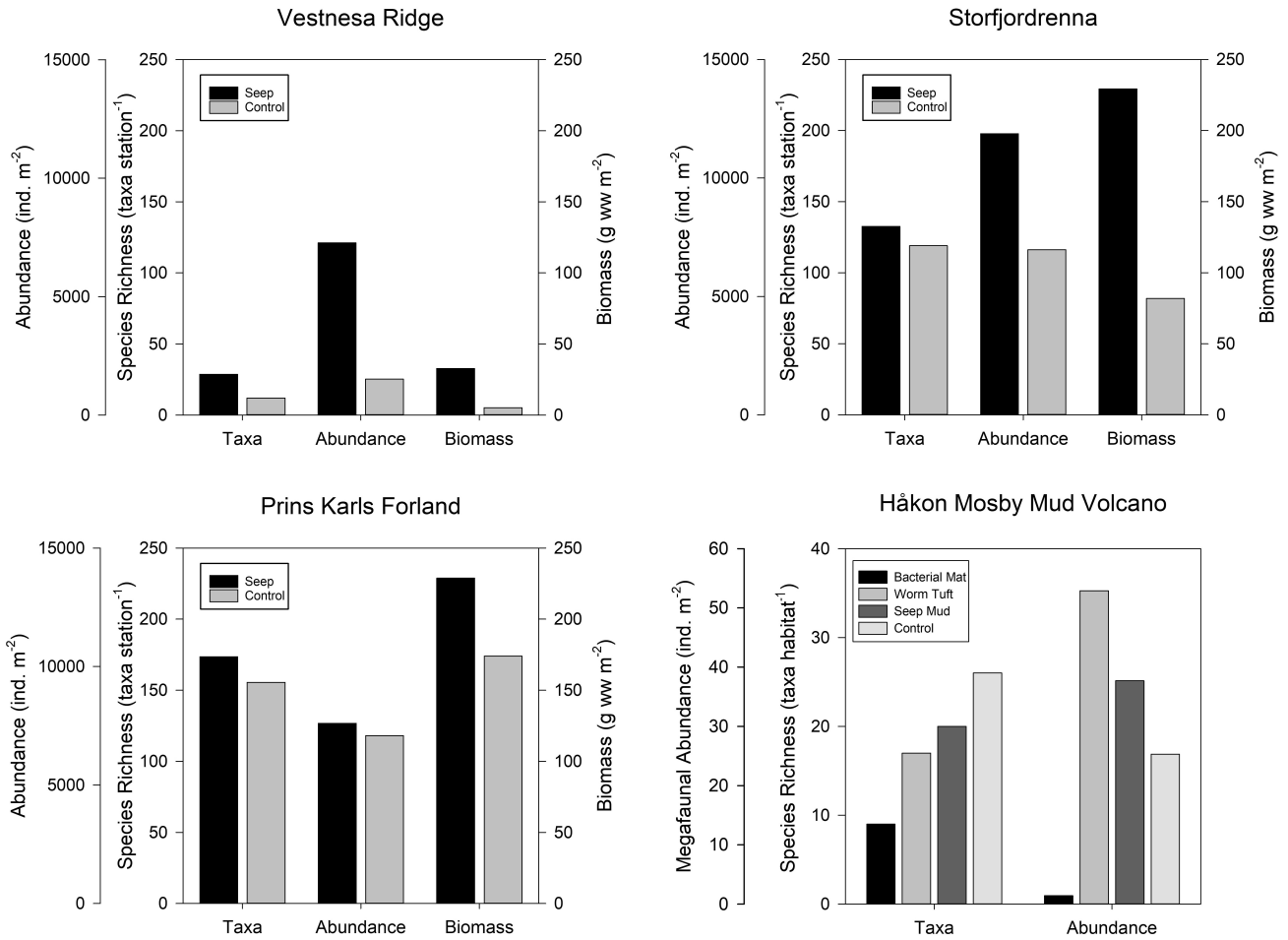

FIGURE 3 | Community faunal parameters [species richness, abundance (density), and biomass] at cold seeps and control areas from four regions in the Arctic where quantitative faunal data are available. Vestnesa Ridge, Storfjordrenna seep, and Prins Karls Forland document macrofaunal infauna, while the Håkon Mosby Mud Volcano is mobile megafauna. Data are compiled from the following sources: Vestnesa Ridge (1,200 m) – Åström et al. (2018), Storfjordrenna (350–390 m) – Åström et al. (2016, 2019), Prins Karls Forland (85–350 m) – Åström et al. (2016), Håkon Mosby Mud Volcano (1,250 m) – Rybakova et al. (2013).

(-0.8 to + 25°C) (Kaul et al., 2006) at HMMV suggests dynamic systems with frequent eruptions and fluid flows in the center (Feseker et al., 2008). Such unstable sediments likely cause the observed faunally devoid area in the central zone (Gebruk et al., 2003; Van Gaever et al., 2006; Decker et al., 2012). High temperature has also been hypothesized as a possible cause of the conspicuous absence of fauna in addition to microbial mats (Gebruk et al., 2003; Decker et al., 2012). Indeed, the heat anomalies detected in the central zone (40°C) are some of the highest recorded at any cold-seep site (Feseker et al., 2008). High sulfide concentrations accompany the release of heat, which, together with the instability of the environment, may further hinder settlement and colonization of animals (Heyl et al., 2007; Rybakova et al., 2013; Feseker et al., 2014).

Distinctive Ecological Features of HMMV

Key ecological features of HMMV are an elevated biomass and a difference in faunal composition relative to the surrounding seafloor. This parallels what has been observed at seeps in other locations: seeps are known as biomass-rich "hotspots" (Carney, 1994; Weaver et al., 2004) on the seafloor, and community composition tends to differ substantially from the surrounding benthos due to the presence of obligate seep and chemosymbiotrophic fauna as well as opportunistic and vagrant background species (Levin et al., 2016). Local chemosynthesis-based primary production is usually cited to account for this trend since it provides an additional food-source to deep-sea seabed habitats. At HMMV, chemosynthetically derived carbon can be detected in the benthic food web and contributes significantly to the diet of some taxa such as *Alvania* gastropods, capitellid polychetes, amphipods, and pantopods (sea spiders) (Decker and Olu, 2012). Nonetheless, HMMV displays some characteristics that stand apart from cold seeps in other parts of the world.

Most striking is the absence of characteristic faunal groups associated with cold-seep ecosystems, e.g., vesicomyid clams, vestimentiferan worms, and bathymodioline mussels (hallmark

seep fauna). These taxa tend to dominate seep systems and account for a large part of the biomass at cold seeps, presumably due to their ability to derive nutrition from seep fluids through endosymbiotic, chemosynthetic bacteria. The absence of such hallmark seep species at HMMV is particularly intriguing since these groups are known from North Atlantic locations both along the European and North American margin (e.g., Mayer et al., 1988; Rodrigues et al., 2013; Skarke et al., 2014) including marginal seas such as the Mediterranean (Olu-Le Roy et al., 2004; Loher et al., 2018).

Second, the taxonomic inventory of HMMV appears to consist entirely of background fauna (no obligate seep taxa) and two chemosymbiotrophic taxa (*Sclerolinum* moniliferans and *Oligobrachia* frenulates) (**Figure 2**) (Rybakova et al., 2013; Georgieva et al., 2015). Seeps tend to host taxa that are found only at seeps due to the toxicity of sulfide (Black et al., 1997; Schulze and Halanych, 2003). Even though these taxa are not the exclusive residents of seeps, they, nonetheless, make up at least some part of seep communities worldwide. Exceptions are shallow-water seeps (less than 200 m water depth) where greater availability of photosynthetic material at these locations and/or increased available substrate have been hypothesized to select against chemosymbiotic species and subsequently, seep obligate taxa (Sahling et al., 2003; Tarasov et al., 2005; Dando, 2010). At the time, the overall lack of obligate seep fauna at HMMV was considered the exception to the concept of deep-seep systems hosting specialized seep communities.

Third, HMMV does not appear to host a lower macrofaunal diversity community than the surrounding non-seep seafloor. Toxic sulfide is often considered the reason for low diversity and the presence of specialized taxa at seeps (Levin et al., 2003; Heyl et al., 2007). However, Rybakova et al. (2013) found that the HMMV community exhibited more diverse faunal assemblages than the surrounding seafloor community (**Figure 3**). Therefore, HMMV appears to attract and host a high number of background benthic species from the surrounding seafloor in contrast to non-Arctic seeps.

While these ecological characteristics at HMMV distinguished it from seep systems in other parts of the world, it was unknown at the time whether HMMV was simply a rarity or whether it was representative of Arctic seeps in general. Answering this question necessitated examining additional Arctic seeps. Such investigations were, however, not conducted until recently.

RECENT ARCTIC COLD-SEEP INVESTIGATIONS

Sources of Seafloor Seepage in the Arctic

Seafloor hydrocarbon seepage may occur because of migration of gas and fluids from sub-seabed reservoirs to the sediment surface. In the Arctic, though, a major contributor to seafloor seepage is the presence of subsurface gas hydrate reserves. Gas hydrates are frozen water structures (ice) within which gas molecules (usually methane) are trapped or "caged" (Koh and Sloan, 2007). These solid pieces of ice and gas are stable in sediments with high pressure and low temperature, a zone referred to as the Gas Hydrate Stability Zone (GHSZ) (Sloan, 1998). In most of the world's oceans, conditions for maintaining the GHSZ (i.e., high pressure and low temperature) are met only in deep-water slope sediments and continental margins (Weaver and Stewart, 1982; Kvenvolden et al., 1993). Cold conditions in the Arctic, however, allow gas hydrates to be present in sediment at relatively shallow water depths (Kvenvolden et al., 1993). The Arctic Ocean is surrounded by continents with large, relatively shallow shelves and continental margins, and at these circumpolar margins, large quantities of hydrocarbon reservoirs and gas hydrates are expected to exist in the sediment because of the Arctic's glacial history, hydrostatic pressure, and thermal gradients (Shakhova et al., 2010; Stranne et al., 2016; Andreassen et al., 2017). In short, the Arctic may hold substantial quantities of gas hydrates because of cold conditions and widespread, glacially influenced shelves, and therefore, there is a high potential for the development of seep ecosystems.

Subsequently, there is evidence for seeps being abundant in the Arctic. Large-scale bathymetric features such as mud volcanoes and pockmarks are present both at North American and European continental margins. Pockmarks, which commonly form due to the collapse of oversaturated gas or fluid-filled pore-spaces in sediments, are markers of past or present gas seepage from the seabed. They are common along the North Sea – Norwegian margin and the southern Barents Sea, and are sometimes observed in high densities, extending over several hundred km^{-2} (Hovland and Svensen, 2006; Chand et al., 2009; Rise et al., 2014). Seeps have also been identified along the Norwegian continental margin and the Western Svalbard shelf (Solheim and Elverhøi, 1993; Vogt et al., 1994, 1997; Lammers et al., 1995). In the Kara Sea, there are numerous locations where hydro acoustic gas flares have been documented (Portnov et al., 2013; Serov et al., 2015), and a large part of the Siberian shelves are predicted to hold substantial amounts of gas hydrates in the seabed (Stranne et al., 2016). Methane and gas hydrates are also believed to be present along the Alaskan, Canadian, and Greenland continental margins (Weaver and Stewart, 1982; Kvenvolden et al., 1993).

If either the temperature or the pressure criteria for the maintenance of gas hydrates is breached, large-scale dissociation of gas hydrates can occur. As a result, the limits of the GHSZ in the Arctic have in the past been closely linked to the glacial history of Arctic shelves (Shakhova et al., 2010; Stranne et al., 2016; Andreassen et al., 2017). Periods characterized by gas hydrate dissociation have shaped regions of the Arctic seafloor bathymetry, due to releases, some even catastrophic, creating structures such as mounds or blow-out craters on the seafloor (Andreassen et al., 2017; Serov et al., 2017). Warming conditions in the Arctic have, furthermore, raised concerns of gas hydrate dissociation in current times: shallow water gas hydrates, for example, could quickly lose stability with rising temperatures. Methane is a much more potent greenhouse gas than CO_2, so methane reaching the atmosphere may have a disproportionate impact on the planet's climate. The potential for the vast Arctic gas hydrate reserves to destabilize and expel large quantities

of methane into the atmosphere is one of the reasons for an increase in Arctic seep research in recent years (Shakhova et al., 2010). Results, to date, indicate little evidence supporting a doomsday scenario of a massive efflux of a potent greenhouse gas from the ocean to the atmosphere (Berchet et al., 2016; James et al., 2016; Myhre et al., 2016), but such studies opened up the opportunity to conduct biological research at a number of Arctic seep sites.

We concentrate on the findings from eight locations in addition to HMMV where biological studies have been conducted (**Figure 1**). These recent investigations serve as the rationale for this review and the basis for this synthesis of the current state of knowledge on the biology and ecology of Arctic seeps.

Arctic Seep Sites

Lofoten Canyons (750–800 m Water Depth)

Offshore northern Norway and the Lofoten islands, more than 15 canyons are located on the continental slope at about 68°N (**Figure 1**). Some are deeply incised into the Cenozoic sedimentary succession (Rise et al., 2013). The two smallest canyons, approximately 2 km in length and up to 50 m deep, are located in water depths of about 750 m and were discovered to host cold-seep communities (Bellec, 2015). No free gas (bubbling of gas from the seafloor) has been observed at this location; however, sediment porewater fluids are enriched in dissolved gases of reduced compounds. Isotope analyses of porewater fluids indicate that dissolved methane is of biogenic origin, although the actual sources are still being investigated (Hong et al., 2019). In addition to methane seepage at the canyons, there is a freshwater discharge from submarine groundwater reservoirs, which is suggested to considerably influence the local circulation and ocean chemistry in the area (Hong et al., 2019).

Svanefjell (380 m Water Depth)

North of the Lofoten canyons, at about 72°N on the Norwegian continental shelf, lies the Svanefjell seep site at about 380 m water depth (**Figure 1**; Sen et al., 2019a). The surroundings of the Svanfjell seep consists of numerous seafloor pockmarks between 30 and 50 m in diameter (Rise et al., 2014; Sen et al., 2019a). Gas flares have been detected rising into the water column from a number of the pockmarks through multibeam surveys of the area, and seismic profiles of the sediment reveal anomalies that are indicative of subsurface hydrocarbon reserves.

Prins Karls Forland (PKF) (80–350 m Water Depth)

Prins Karls Forland is located on the shelf west of Svalbard (78°N) (**Figure 1**), where extensive gas seepage has been reported in the form of hydro-acoustically detected bubble plumes in water depths between 80 and 400 m (Berndt et al., 2014; Sahling et al., 2014; Åström et al., 2016). Additionally, high concentrations of methane have been detected in the water column at these locations (Berndt et al., 2014; Myhre et al., 2016; Pohlman et al., 2017). A cluster of sites exhibiting strong seafloor seepage at about 400 m water depth along the Prins Karls Forland shelf aligns with the predicted upper border of the GHSZ (∼400 m) (Portnov et al., 2016; Mau et al., 2017). Moreover, there is abundant seepage activity at considerably shallower depths at the Forland moraine complex (>80 m), and this shallower cluster of seeps is thought to be caused by gas migrating from deeper reservoirs through sub-seabed faults (Berndt et al., 2014; Sahling et al., 2014; Portnov et al., 2016).

Vestnesa Ridge (1,200 m Water Depth)

Northwest of PKF on the continental slope in the Fram Strait at 79°N lies Vestnesa Ridge (**Figure 1**), a ∼100 km long ultraslow spreading sediment-drift ridge (Johnson et al., 2015) at ∼1,200 m water depth. Along the ridge are numerous pockmarks associated with sub-seabed methane hydrate reservoirs (Vogt et al., 1994; Bünz et al., 2012). The sub-surface gas at these pockmarks is of both microbial and abiotic/thermogenic (Johnson et al., 2015). Multiple methane bubble plumes have been acoustically detected in geophysical surveys in the water column along the ridge, rising up to 800 m above the seafloor (Bünz et al., 2012).

The Storfjordrenna Seep and Storfjordrenna Pingos/Gas Hydrate Mounds (350–390 m Water Depth)

Prins Karls Forland and Vestnesa represent the western edge of one of the most well known and well studied of the Arctic seas, the Barents Sea. The bathymetry of the Barents Sea is largely influenced by the glacial history of northern margins and the coverage of the Barents Sea Ice Sheet (BSIS), and its deglaciation starting approximately 20,000 years BP (Rasmussen et al., 2007; Ingólfsson and Landvik, 2013; Patton et al., 2017). The present day average water depth of the Barents Sea is ∼230 m, and the shelf is characterized by extensive post-glacial features such as, troughs, plow marks, and mega-scale lineations (Patton et al., 2017). Located in the western Barents Sea and south of the Svalbard archipelago, Storfjordrenna is one of the larger troughs (∼250 km long). In the mouth of the trough, there are several locations of active methane seepage that align with the upper predicted limit of the GHSZ (∼350–400 m water depth) (**Figure 1**; Åström et al., 2016; Mau et al., 2017; Serov et al., 2017). One of these active methane seep sites is referred to simply as the "Storfjordrenna seep" (SR), located close to a glacial grounding zone wedge at approximately 350 m water depth (75°N). A few tens of kilometers north of the Storfjordrenna seep and within Storfjordrenna, is another area of highly active methane seepage located in similar water depths, at 76°N. This site is characterized by a cluster of several gas hydrate bearing mounds, or submarine "pingos," which individually are a few hundred meters in diameter and rise approximately 10–15 m above the seabed (Hong et al., 2017; Serov et al., 2017). Seepage, identified by hydroacoustic flares has been observed from the tops of these pingos, with some flares reaching hundreds of meters above the seabed. This site is referred to as the Storfjordrenna pingo site or Storfjordrenna gas hydrate mound site.

Bjørnøyrenna Flare Area and Bjørnøyrenna Craters (330–360 m Water Depth)

Bjørnøyrenna is another large trough located south-east of Storfjordrenna, moving into the central Barents Sea. Within this trough, a large area (∼440 km^2) with hundreds of seafloor

depressions, craters, and crater–mound complexes is present at about 74°N (**Figure 1**; Solheim and Elverhøi, 1993). These craters and mounds are thought to be the result of massive blowouts of sub-surface gas deposits and subglacial gas hydrates during the deglaciation of the BSIS (Andreassen et al., 2017). The craters vary from approximately 100 m up to 1 km in diameter and are up to 30 m deep, whereas mounds rise up to 20 m above the seabed. Several of the craters and mounds are associated with methane seepage from the seabed (Andreassen et al., 2017), and the seafloor inside and around the craters and mounds is strikingly characterized by large angular blocks (Solheim and Elverhøi, 1993). This area, as a whole, is referred to as the Bjørnøyrenna crater area (e.g., Åström et al., 2016, 2019; Sen et al., 2018b; Ofstad et al., 2020).

Laptev Sea Seep (70 m Water Depth)

Along the Siberian Arctic, both terrestrial and sub-seabed permafrost layers in the ground are relics of past glacial history, and such features can store large quantities of methane gas and hydrates. In the Laptev Sea, located between the two marginal seas along the Siberian shelf, the Kara Sea and the East Siberian Sea, sub-seabed permafrost layers are estimated to reach 20–60 m down into the seabed. The second largest river in the Siberian Arctic, the Lena River, terminates into the Laptev Sea, and the river-delta system contributes large amounts of freshwater and suspended matter from the river catchment area. North of this river delta and at about 70 m water depth, a methane-seep site was recently discovered at 76.5°N, 127°E (**Figure 1**). This site represents one of the shallowest known seep sites in the Arctic (Demina and Galkin, 2018).

Beaufort Sea Mud Volcanoes (280–740 m Water Depth)

Most of the recent investigations of Arctic seeps have been carried out in the European Arctic and particularly within the Barents Sea. However, some biological data exist on seep systems in the North American Arctic. A number of mud volcanoes have been described and examined at water depths ranging from 282 to 740 m on the Canadian shelf and extending down to the slope, offshore the outflow of the Mackenzie River (**Figure 1**; Paull et al., 2007, 2015). These mud volcanoes are about 600 m to 1 km in diameter and rise up to 30 m above the seafloor. Coring into the shelf revealed the presence of ice-bonded permafrost and methane hydrates hundreds of meters to over a kilometer below the sediment surface. Though multiple mud volcanoes have been recorded and investigated in this region, one, at about 420 m water depth, has been targeted for biological studies (Paull et al., 2015; Lee D. H. et al., 2019, Lee Y. M. et al., 2019).

ENERGY SOURCES AND TROPHIC PATHWAYS AT ARCTIC SEEPS

Chemosynthesis-Based Primary Production

The seepage of methane from subsurface hydrocarbon reserves results in methane-enriched fluids emanating from the seabed at cold seeps. As methane seeps upward from subsurface sediment reserves, sulfate migrates downward in the sediment from the overlying water column. These two compounds are oxidized and reduced, respectively, in a tightly coupled, microbially driven process termed AOM (Boetius et al., 2000; Cavanaugh et al., 2006). This process releases hydrogen sulfide, which is why this compound, along with methane, is abundant in sediment porewater at seep locations. Both methane and hydrogen sulfide are reduced compounds; therefore, the energy release that accompanies their oxidation can be utilized by microbes for carbon fixation via chemosynthesis. A key difference between sulfur oxidizing and methane oxidizing chemosynthetic microbes is their inorganic carbon source. The former relies mostly on either dissolved inorganic carbon in seawater or in sediment porewater. In contrast, methane is an organic compound that provides microbes with both energy and inorganic carbon in a single source. Chemosynthetic microbes can either be free living or reside within or on organisms with which they form a symbiotic relationship. Together, they form the base of a food chain and an ecosystem that revolves around chemical-based autotrophic processes (Fisher, 1996; Sibuet and Olu, 1998; Levin, 2005; Becker et al., 2013).

When chemosynthetic bacteria form close symbiotic associations with animals, those animals essentially function as primary consumers within cold-seep ecosystems. At Arctic seeps, siboglinid worms (*Oligobrachia* frenulates and the moniliferan *Sclerolinum contortum* at HMMV, only the former at other sites) are the dominant species and the only confirmed chemosynthesis-based macrofauna and, thus, key players in the food web (Decker and Olu, 2012; Åström et al., 2019; Sen et al., 2019b). They form extensive tufts (sometimes grass like meadows) at Arctic seeps that are clearly visible in images (**Figure 2**). Though the frenulates (and moniliferans in the case of HMMV) represent the entirety of the macrofaunal chemosynthesis-based community presently known at Arctic seeps, small thyasirids (maximum 5 mm length) are also highly abundant at Arctic seeps (Åström et al., 2016, 2019). The family of Thyasiridae bivalves includes chemosymbiotrophic species associated with sulfur-oxidizing symbionts (Dufour, 2005; Dufour and Felbeck, 2006; Duperron et al., 2013), and a high abundance of thyasirids at seep sites is suggestive of these bivalves harboring chemosynthetic symbionts. Furthermore, thyasirids are extremely flexible regarding the nature of their symbiotic associations and exhibit a wide range of different dietary adaptations, from microbial syntrophy and chemosymbiosis to mixotrophy and heterotrophy (Dando and Spiro, 1993; Dufour, 2005; Taylor and Glover, 2010; Duperron et al., 2013). The two most abundant thyasirid species at Arctic seeps are *Mendicula* cf. *pygmaea* and *Thyasira gouldi* where the former is highly abundant both at Arctic seeps (up to 2,500 ind. m^{-2}) and at non-seep, background locations (up to 2,125 ind. m^{-2}) (Åström et al., 2019). Neither *M.* cf. *pygmaea* and *T. gouldi* are obligately chemosymbiotic (Oliver and Killeen, 2002; Dufour, 2005; Taylor and Glover, 2010), and it has not yet been possible to determine whether the populations of these thyasirids at Arctic seeps are symbiotic. Similarly,

Sen et al. (2018a) suggested that *Thenea* sponges, which were abundant at the Storfjordrenna pingo/mound site, might contain chemosynthetic microbial symbionts. Thus, though carbon fixation and symbiotic chemosynthesis-based primary production is only presently confirmed for siboglinids, there are hints that this might also occur in more taxonomic groups.

Microbial Grazing and Secondary Consumption

Chemosynthetic microbes are not limited to symbiotic associations with animals. They can also be free living at the sediment surface, rocks, and carbonate crusts, or on top of other organisms (Cavanaugh et al., 2006). These strains can thrive at seep conditions to the extent that they form thick, clearly visible mats on the sediment surface (Boetius et al., 2000; Grünke et al., 2012). From a community perspective, such mats provide another pathway to chemosynthetically fixed carbon and organic material since organisms can actively graze microbial mats and sediment (i.e., microbial grazers). At Arctic seeps, this trophic level of microbial grazers appears to be represented most clearly by small (mm)-sized gastropods. At HMMV, the Lofoten canyons, and Vestnesa, rissoid snails (*Alvania* sp.) constitute this group (Gebruk et al., 2003; Decker et al., 2012; Sen et al., 2019b), whereas at the Bjørnøyrenna crater site, *Hyalogyrina* snails occupy this niche (Åström et al., 2019). Rissoids (the genus *Alvania*) have been recorded at non-chemosynthetic habitats in polar areas (Coyle et al., 2007; Meyer et al., 2013), whereas *Hyalogyrina* has only been reported from reducing environments such as wood-falls, vents, seeps, and whale falls (Marshall, 1988; Braby et al., 2007; Sasaki et al., 2010). At HMMV, Decker and Olu (2012) reported carbon isotope values as low as −46.6‰ in *Alvania* sp. located in microbial mats, while snails in the adjacent sediment had heavier values, of about −40.2‰. Both of these values are suggestive of chemosynthesis-based carbon (CBC) in their diets, and indeed, it was estimated based on a two-source food web model that 21–66% of the carbon uptake of these snails is from CBC (Decker and Olu, 2012). Carbon isotopic signatures of *Hyalogyrina* gastropods among mats of filamentous bacteria at Bjørnøyrenna crater seeps ($\delta^{13}C$ = −23.8‰) (Åström et al., 2019) were heavier than in the alvanids at HMMV, but were also indicative of partial uptake of CBC in their diet (4.8–21.7%) based on a two-source food web model using local end-member values. In addition, these snails are highly abundant at Arctic seeps, particularly among microbial mats, which further suggests that they are grazing on the mats to a certain extent. In addition to small gastropods, other species and faunal groups likely graze on microbial mats as well, such as other mollusks and small polychetes (Levin et al., 2017). However, the link between chemosymbiotic primary producers (microbial associations) and primary consumers at cold seeps (i.e., small microbial mat grazers) is not well represented in seep food-web studies, so far, presumably because organisms in the latter niche are difficult to collect.

More conspicuous members of microbial mat grazers are large crustaceans that have been observed among microbial mats at certain Arctic seeps. For example, at the Storfjordrenna pingo/mound site, snow crabs (*Chionoecetes opilio)* were seen among mats in positions that suggest they are actively feeding on the bacteria (Sen et al., 2018a). Microbial grazing by crabs is known from seeps at the Costa Rica Subduction Zone where lithoid crabs intensely graze mats of *Epsilon proteobacteria*, and from seeps along the North American west coast, where tanner crabs *(Chionoecetes tanneri)* have been observed feeding on microbial mats (Niemann et al., 2013; Seabrook et al., 2019). For both species, compound-specific stable isotope analysis revealed that there was a partial microbial (and ultimately chemosynthesis based) input into their diet (Niemann et al., 2013; Seabrook et al., 2019). At seeps along the North American east coast, Turner et al. (2020) analyzed red crabs (*Chaceon quinquedens*) using bulk stable isotope analysis of carbon, and it was suggested that free-living chemsoymbiotic bacteria contributed to the crab's chemosynthetically derived nutrition in addition to bathymodiolin mussels. Hence, it is likely that chemosynthesis-based carbon may play a role in the diets of snow crabs in areas where their distribution overlaps with that of cold seeps.

Secondary and higher-order consumers at Arctic seeps are diverse and represent various taxonomic groups (Decker and Olu, 2012; Sen et al., 2018a; Åström et al., 2019). Within the seep environment, some of these taxa appear to display specific preferences for seep-associated habitats such as microbial mats, siboglinid tufts, and methane-derived authigenic carbonates, i.e., carbonate outcrops (carbonate precipitates that form due to AOM). Pycnogonids (*Nymphon hirtipes*) were documented at the Lofoten canyon site (overall abundance for the canyons ∼35 ind.m^{-2}), and they were concomitantly observed among microbial mats and siboglinid tufts (Sen et al., 2019b). In addition to *N. hirtipes*, other pycnogonids (*Colossendeis* sp.) have been documented in association with siboglinid tufts and carbonate outcrops at both Vestnesa seeps and the Storfjordrenna pingos/mounds, where they occur in higher densities in contrast to areas where such features are absent (Åström et al., 2018; Sen et al., 2018a). The northern shrimp *Pandalus borealis* has been observed aggregating among siboglinid tufts and microbial mats at several of the seeps in the Barents Sea (Sen et al., 2018a; Åström et al., 2019). From the perspective of both predators and scavengers, microbial mats and siboglinid tufts represent potential food-rich locations due to the presence of associated animals (Decker and Olu, 2012; Sen et al., 2018a; Åström et al., 2019). Individual siboglinid tubes have been seen to host a diverse array of fauna, from single-celled epibenthic foraminifera (*Cibicidoides*), to predatory caprellids and small polychetes (Decker et al., 2012; Sen et al., 2018a,b; Åström et al., 2019). Furthermore, worm tufts are sometimes overgrown by filamentous bacteria (**Figures 2A,C,E**; Sen et al., 2018b; Åström et al., 2019). Whether the animals associated with the tufts utilize them as substrate, refuges for hiding and/or resting (i.e., attracted by the seafloor heterogeneity that the tufts provide), or whether the tufts serve as feeding grounds for motile predators is an intriguing question. It is evident, however, that both

siboglinid tufts and microbial mats attract certain organisms (from meiofauna to megafauna) at the Arctic seeps (Decker et al., 2012; Åström et al., 2018, 2019; Sen et al., 2018a, 2019b).

Chemosynthesis-based carbon (CBC) has also been found as a source of nutrition in predators at Arctic seeps. Carbon signatures ($\delta^{13}C = -31.4‰$) in predatory polychaetes (*Nephtys* sp.) suggest that CBC comprises up to 28% to 41% of their diet at Bjørnøyrenna crater seeps based on a two-source food web model (Åström et al., 2019). Likewise, carbon signatures ($\delta^{13}C = -29.1‰$) in *Scoletoma fragilis* from the Storfjordrenna gas hydrate mounds indicate partial input of CBC (18–32%) with the same two-source model (Åström et al., 2019). At HMMV, Gebruk et al. (2003) found depleted carbon isotope signals ($\delta^{13}C = -44.9‰$) in caprellids, indicating CBC in their diets. Moreover, they suggested that eelpouts (*Lycodes* sp.) prey directly on siboglinids based on depleted carbon isotopic signals in tissue ($\delta^{13}C = -51.9‰$) and stomach contents that included fragments of frenulate tubes. In addition to the reports at HMMV from Gebruk et al. (2003), Decker and Olu (2012) noted as well depleted carbon isotope signals in samples from sea spiders and amphipods, indicating substantial input of CBC (41–77%) for these taxa. There are a few studies of animal tissues at seep locations that detect chemosynthesis-based carbon beyond obligate chemosymbiotrophic animals and primary consumers (e.g., MacAvoy et al., 2003; Becker et al., 2013; Zapata-Hernández et al., 2014; Portail et al., 2016). Indeed, even at Arctic seeps, most of the assessed organisms have carbon isotopic signatures that indicate that most nutrition originates from photosynthetically derived carbon (Decker and Olu, 2012; Åström et al., 2019). Nevertheless, chemosynthetically derived carbon is detectable up the food chain at Arctic seeps (Gebruk et al., 2003; Decker and Olu, 2012; Åström et al., 2019). Advances in the use of bulk stable isotope analyses, combined with the application of compound-specific isotope and fatty acid analyses, have revealed new insights in benthic food webs (Reeburgh, 2007; Niemann et al., 2013; Seabrook et al., 2019) and could, thus, reveal new information about food web interactions, Arctic seep benthos, and carbon-source utilization.

KEY ECOLOGICAL ASPECTS OF ARCTIC SEEPS

Siboglinids at Arctic Seeps

In contrast with lower latitude seeps, there is an absence of hallmark chemosymbiotic species at Arctic seeps, such as vestimentiferan worms, vesicomyid clams, and bathymodioline mussels. At all Arctic seeps studied to date, chemosynthesis-based symbioses between macro/megafaunal taxa and bacteria are restricted to the siboglinid clade. At HMMV, both moniliferans and frenulates are present, with the former being the more abundant of the two (Gebruk et al., 2003). At other Arctic seeps, obligate chemosymbiotrophic fauna are restricted to frenulates and, specifically, to a complex of closely related *Oligobrachia* frenulates. Currently, across all Arctic seep sites, three morphologically cryptic species have been identified based on mitochondrial COI sequences: *O. haakonmosbiensis* (present at HMMV, the Lofoten canyons and Vestnesa), *Oligobrachia* sp. CPL-clade (present at Storfjordrenna pingos/mounds, Bjørnøyrenna craters, Laptev Sea, and the Beaufort Sea mud volcanoes) and a third, unnamed *Oligobrachia* species found at Vestnesa (Sen et al., 2018b, 2020; Lee Y. M. et al., 2019). Collections in the Bjørnøyrenna flare area have additionally revealed other frenulates, but no descriptions or identifications have been made for them (Åström et al., 2016, 2019). Therefore, among the multiple seep sites studied across the Arctic, merely three *Oligobrachia* frenulates and one moniliferan species have been confirmed to constitute the chemosynthesis-based megafauna, and dominant biomass (**Table 1**). This is a distinctive and highly visible feature of Arctic seeps and one that sets them apart from cold seeps in other parts of the world.

A notable deviation from the generalized Arctic seep community pattern of chemosynthesis-based siboglinids and background benthic species are the shallow water seeps (∼80 m water depth) at Prins Karls Forland (PKF). No siboglinid worms have been observed at these sites, and overall community composition is different, characterized by high abundances and biomass of bivalves and echinoderms in relation to other Arctic seeps (Paull et al., 2015; Åström et al., 2016, 2019; Demina and Galkin, 2018). Shallow water sites tend to have fewer specialist species and chemosymbiotic taxa compared to deeper water seeps (Tarasov et al., 2005; Dando, 2010). Increased predatory pressure and higher input of photosynthetic material have been hypothesized to drive this difference and select against a dominance by specialist fauna and chemosynthesis-based taxa (Sahling et al., 2003; Dando, 2010). Despite a highly limited overall chemosymbiotic faunal inventory at Arctic seeps, this is, nonetheless, a reasonable explanation for the absence of siboglinid worms at shallow PKF seeps. Indeed, single records of siboglinids have been recovered from samples taken at deeper sites (240 m) at PKF (Åström et al., 2016). Oceanographic conditions at PKF, including high-velocity currents and sedimentary properties (gravelly, stony sediment versus soft-bottom sediments) could also account for the differences in PKF relative to other Arctic seeps. Detailed ecological assessments of all PKF sites where seepage is confirmed have not been conducted. Therefore, it is difficult to make comparisons with other Arctic seep sites and even along a depth gradient of the PKF shelf. In contrast to PKF, the shallow (70 m) Laptev Sea site shares a number of characteristic fauna with other Arctic seeps, including the high dominance of siboglinid worms (Åström et al., 2016; Demina and Galkin, 2018). Hence, for the Laptev Sea seep, depth alone is not an environmental barrier to exclude the presence of siboglinids (Demina and Galkin, 2018; Savvichev et al., 2018).

High Taxonomic Richness of Background Fauna

Arctic seeps often exhibit relatively higher taxonomic richness than the nearby surrounding non-seep benthos (Åström et al., 2018; Sen et al., 2018a, 2019a). Biomass and abundance are also higher at Arctic seeps compared to non-seep locations in similar areas (Carroll et al., 2008; Cochrane et al., 2012;

TABLE 1 | (A) Modern symbiotrophic taxa identified at Arctic cold seeps; locations where taxa are present are marked as "x." **(B)** Recent fossil (records younger than ~20,000 years B.P.) of chemosymbiotic taxa identified from Arctic cold seep sediments.

			Location	**North**	**Atlantic**			**Barents sea**		**Siberian shelf**	**Beaufort sea**	**Arctic ocean**	
			Taxa	**HMVV**	**Lofoten**	**Vestnesa ridge**	**West svalbard shelf (PKF)**	**Storfjordrenna Seep field, mounds/ pingos**	**Bjørnøy-renna Craters**	**Laptev sea**	**Mud volcanoes**	**Gakkel ridge**	**References**
A													
	Polychatea	Siboglinidae	*Sclerolinum contortum*	x									Pimenov et al., 2000
			Oligobrachia haakonmosbiensis	x	x	x							Pimenov et al., 2000
			Oligobrachia sp.1 (CPL-clade)					x	x	x	x		Sen et al., 2018b
			Oligobrachia sp.2			x							Sen et al., 2020
			**Polybrachia* sp.						x				Åström et al., 2019
			**Diplobrachia* sp.						x				Åström et al., 2019
	Mollusca	Thysiridae	*Thyasira gouldi*					x					Åström et al., 2016, 2019
B													
	Mollusca	Solemyidae	*Acharax svalbardensis*			x							Hansen et al., 2020
		Vesicomyidae	*Archivesica arctica*			x						x	Sirenko et al., 2004; Hansen et al., 2017
			Isorropodon nyeggaensis			x							Ambrose et al., 2015; Hansen et al., 2017
		Thyasiridae	*Rhachothyas kolgae*			x	x						Thomsen, 2019; Åström et al., 2017
			Thyasira capitanea					x					Carroll et al., 2016; Åström et al., 2017

**Species with unsatisfactory taxonomic identification.*

Åström et al., 2019; **Figure 3**). The relatively high taxonomic richness of Arctic seeps in relation to background, non-seep locations is likely linked to the cold-seep communities being composed almost entirely of background fauna (i.e., no obligate seep taxa) that are typical for the Arctic region. With limited exceptions, including some of the *Oligobrachia* species that might potentially be obligate to seeps and some *Alvania* snails that have been suggested to possibly exclusively inhabit seep systems (Decker and Olu, 2012), taxa inhabiting Arctic seeps are extensions of the larger community of background Arctic benthos. This is a distinctive feature of Arctic seeps that contrasts with those at lower latitudes where seeps support a subset of the benthos taxa dominated by obligate seep or chemosymbiotrophic taxa. Arctic seeps, however, do not appear to host obligate seep fauna, and instead, are richly populated by diverse assemblages of benthic taxa at higher densities and abundances than the surrounding seafloor.

The Role of Carbonate Structures at Seeps

A key feature of many cold-seep systems is methane-derived authigenic carbonate outcrops. These features precipitate due to the AOM-sulfate reduction reactions that occur in the sediment. At cold seeps, carbonate outcrops generate complex spatial patterns on the seafloor (Cordes et al., 2010; Levin et al., 2017), and the 3D structures of carbonates provide refuges for organisms to hide or escape from predation (Levin et al., 2017; Åström et al., 2018). Carbonate outcrops contribute to enhanced biomass and megafaunal diversity of Arctic cold seeps. Several motile megafaunal taxa, such as red rockfish, eelpouts, wolfish and sea spiders, were commonly observed in and among the carbonate structures (Åström et al., 2018; Sen et al., 2019a), and the carbonates provide extensive hard surfaces for various sessile hard-bottom background species in a predominantly soft-bottom seafloor (Åström et al., 2018; Sen et al., 2018a; **Figure 4**). Ice rafted debris (drop stones) from icebergs and glacial deposits, which are randomly located on the Arctic seafloor, have been recorded to function as islands within Arctic soft-bottom habitats (Soltwedel et al., 2009; Schulz et al., 2010). In comparison to drop stones, carbonates provide much larger habitat areas and volumes. Furthermore, carbonate outcrops in combination with other large bathymetric features, such as pockmarks and mounds, can create refuges for sensitive, slow-growing hard-bottom fauna (e.g., corals and sponges), especially in areas with intense trawling activities (Webb et al., 2009; MacDonald et al., 2010; Clark et al., 2016). The habitat complexity and physical structures that carbonates provide at seeps cause a so-called "reef-effect" (Stone et al., 1979) where background motile organisms can aggregate regardless of seepage (Hovland, 2008; MacDonald et al., 2010). Since carbonates persist after seepage ceases, the effect of seeps on the seafloor can outlive the seep itself (Bowden et al., 2013; Levin et al., 2016). This is demonstrated by the Svanfjell seep site in the southern Barents Sea, where low levels of seepage activity suggest a senescent stage and limited chemosymbiotic-based production. Nonetheless, taxonomic richness and abundance are still considerably higher at the seep compared to the adjacent non-seep seafloor and appears to be linked to carbonate availability at the seep location (Sen et al., 2019a). Thus active, senescent, and even inactive seeps function as locations where benthic animals aggregate on the Arctic seafloor (Bowden et al., 2013; Sen et al., 2019a). These effects of carbonates are not unique to Arctic seeps (Bowden et al., 2013; Levin et al., 2016, 2017); for example, seep-derived carbonates have been documented to enhance the settlement of large reef-building animals such as cold water corals (Cordes et al., 2006, 2008; Becker et al., 2009). In the Arctic, though, this has particularly important implications, since Arctic seeps function as local diversity and biomass "hotspots" for Arctic benthos, and not only attract a specialized subset of taxa. Accordingly, this is another important consideration for ecosystem management because it means that seep locations, regardless of activity, have the potential to lead to increased benthic diversity and biomass on the Arctic seafloor (Webb et al., 2009; Åström et al., 2018; Sen et al., 2018a, 2019a).

Similarity of Seep Communities Across Geographic Regions

Despite a lack of obligate seep species, Arctic seep communities stand out as distinct from the surrounding benthic communities. Species composition alone does not contribute toward Arctic seep communities being different from background communities. It is the number of species present and the abundances of respective individual taxa that distinguish Arctic seeps from other non-seep locations. The influence of seepage to benthos is so distinctive that benthic communities at strongly influenced seep locations separated across large geographic areas are more similar to each other than to non-seep communities within the same geographic area (Åström et al., 2019). For example, seep-community composition and structure at the Barents Sea differ significantly from PKF seeps at W. Svalbard seep communities despite intense and active seepage at both locations (Sahling et al., 2014; Andreassen et al., 2017; Serov et al., 2017). At PKF seeps, the seep community is composed of background species and characterized by high densities of ophiuroids and high biomass of mollusks and various epifauna. In contrast, to Barents Sea seeps (pingos, mounds, and craters), host thousands of individuals of siboglinids and small thyasirid bivalves (Åström et al., 2016). The disparity in the community structure has been attributed mainly to differences in the oceanographic settings among the regions and depth; hence, significant differences in faunal composition is expected (Åström et al., 2016). However, within the Barents Sea, the distinct characteristics of Arctic seep communities override such large-scale geographic patterns. Storfjordrenna and Bjørnøyrenna sites are both located in the Barents Sea, south of Svalbard, yet their "background" benthic communities are distinct from one another despite similar water depths and sediment properties (Carroll et al., 2008; Cochrane et al., 2012; Åström et al., 2019). Conversely, the seep characteristics of Storfjordrenna and Bjørnøyrenna cold seeps are highly similar to each other, and strongly influenced seep locations are dominated by siboglinids and thyasirids.

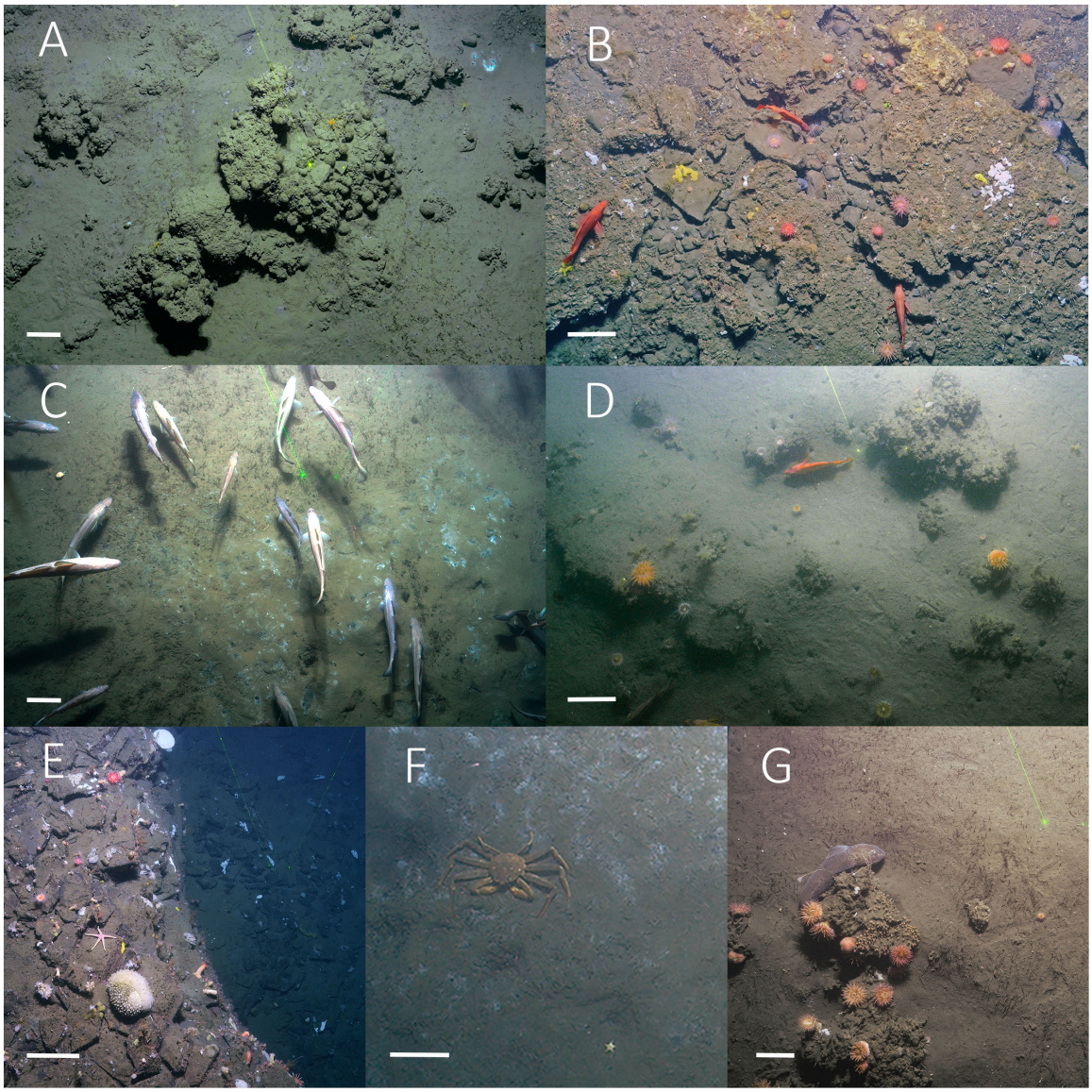

FIGURE 4 | Arctic seep habitats; heterogeneity, carbonate outcrops, and commercial species, from top left to right. **(A)** Carbonate outcrops, siboglinid tufts, and microbial mats at the Vestnesa seep (1,200 m) from Åström et al. (2018). **(B)** At the Prins Karls Forland shelf (240 m); large carbonate outcrops and glacial debris provide hard surfaces for epifauna and a varied habitat for Red rock-fish (*Sebastes* sp.) and spotted wolffish (*Anarhichas minor*), from Åström (2018). **(C)** A school of cod (*Gadhus morhua*) swimming over mats of microbes and siboglinids at the Storfjordrenna gas hydrate mounds/pingos (380 m), from Åström (2018). **(D)** Red rock-fish (*Sebastes* sp.) and carbonate outcrops at Storfjordrenna seep field (350 m), from Åström et al. (2019). **(E)** Epifaunal organisms on a rocky slope into one of the craters at the Bjørnøyrenna crater seeps (330 m), from Åström et al. (2019). **(F)** A snow crab feeding in a microbial mat at Storfjordrenna gas hydrate mounds/pingos (380 m), from Sen et al. (2018a). **(G)** A spotted wolffish (*A. minor*) carbonate crust with epifaunal anemones, hydroids, and solitary corals surrounded by siboglinid tufts at Storfjordrenna gas hydrate mounds/pingos (380 m), from Åström et al. (2019). Scale bars indicate 20 cm.

The Bjørnøyrenna crater seeps and the Storfjordrenna seep communities are separated by a distance over 300 km, yet the communities are regulated by a seepage signal strong enough to override faunal and biogeographical aspects within the Barents Sea. These distant seep communities, hence, are more similar to each other than they are to background benthic communities located just meters away from the impact of seepage (Åström et al., 2019).

Presence of Commercial Species

A noteworthy aspect of Arctic seep communities is the prevalence of several commercially important taxa. The Northern shrimp (*Pandalus borealis*), and fish such as Atlantic cod (*Gadus morhua*), saithe (*Pollachius virens*), haddock (*Melanogrammus aeglefinus*), Greenland halibut (*Reinhardtius hippoglossides*), red rockfish (*Sebastes* sp.), wolffish (*Anarhichas*), and even snow crabs (*Chionoecetes opilio*) have been recorded at Arctic seep

sites (Åström et al., 2018, 2019; Sen et al., 2018a). Shrimp and cod are particularly numerous, especially at shelf seep sites (Sen et al., 2018a). Commercially harvested species have been recorded from cold seeps around the world (Bowden et al., 2013; Niemann et al., 2013; Zapata-Hernández et al., 2014; Higgs et al., 2016; Seabrook et al., 2019; Turner et al., 2020), but more often, single or few commercial species tend to be associated with a specific seep site or region. In the Arctic, multiple commercial species occur and overlap at individual seep locations (**Figure 4**). We suggest that the large-scale heterogeneity caused by the carbonate rocks (the "reef effect") (Stone et al., 1979) is one reason for the high occurrence of individuals (Åström et al., 2018). Second, it is likely that these large motile and predatory organisms exploit the seeps because of localized and ample food resources. We, furthermore, suggest that the presence of multiple commercially important species co-occurring at the seeps, first and foremost at the shelves, is a consequence of the relatively shallow depths of the seeps and the rich and productive fishing grounds on the Barents Sea shelf (Kjesbu et al., 2014; Haug et al., 2017). It remains, however, unclear to what extent Arctic seeps contribute toward the maintenance of commercial stocks that inhabit the Arctic marginal seas.

Arctic Seeps Can Function as Nursery Grounds

The Lofoten canyon seep site was discovered to function as an egg case nursery for the Arctic skate, *Amblyraja hyperborea* (Sen et al., 2019b). The canyon setting alone was ruled out as the primary reason behind the Lofoten canyons serving as an egg case nursery ground. Egg cases were highly concentrated among seep locations and were notably rare or absent in areas with no visual evidence of seepage (presence of microbial mats or worm tufts). Surprisingly, egg cases were not associated with carbonate rocks, an observation that contrasts with observations at the Concepción seep offshore Chile, which is the only other seep recorded as being used as a skate egg case nursery ground (Treude et al., 2011). Ambient bottom water temperatures at the Lofoten canyons are lower than 0°C; therefore, a likely explanation is that seepage-related heat releases allow for the site to serve as a natural incubator for egg cases. Though seeps have earned the "cold" moniker because they do not exhibit the boiling temperatures of hydrothermal vents, they are neither particularly cold nor colder than the surrounding seafloor. In fact, the opposite is true: "cold seeps" can be slightly warmer than the background ambient bottom waters, albeit the temperature difference is small, typically less than 1°C (Sibuet and Olu, 1998). The link between temperature increase and nursery habitats has also been observed at low-temperature zones of a Galapagos hydrothermal vent, suggested to function as natural incubators for egg cases of deep water skates (Salinas-De-León et al., 2018). Ambient water temperature at the vent site was measured to ∼2.76°C, and the largest number of skate egg cases was observed in bottom water temperatures where there was an increase of ∼0.25°C. Such temperature anomalies closely match the low-scale temperature anomalies of seeps, which, in subzero conditions, are particularly relevant, first, because they would result in positive bottom water temperatures, and second, because even small increases in temperatures have been modeled to decrease the long incubation times of deep-water skates (Berestovskii, 1994; Hoff, 2010). Therefore, it is possible that the attraction of the Lofoten canyon seep site as a place for Arctic skates to deposit their egg cases might be the slightly warmer environment relative to the surrounding conditions. There are, furthermore, numerous reports of skates from HMMV (Rybakova et al., 2013), although whether this site also functions as an egg case nursery ground for skates is yet to be determined. Nonetheless, the ability for seeps to provide some degree of temperature increase could potentially benefit Arctic benthic fauna, especially for species with long incubation times, in ways previously not considered, such as serving as skate egg case nurseries.

Another hypothesis for high densities of elasmobranch egg cases and other egg-brooding deep-sea fauna in habitats such as seeps and vents, in addition to the higher bottom water temperatures, is the potential increase in available food resources and structures for shelter to hatched juveniles (Drazen et al., 2003; Treude et al., 2011; Turner et al., 2020). For the management of deep-sea ecosystems, in particular, for vulnerable species with long maturation and incubation times, deep-sea nursing habitats could be of high relevance for long-term monitoring and conservation (Drazen et al., 2003; Clark et al., 2016; Da Ros et al., 2019).

ARCTIC SEEPS: IMPLICATIONS FOR ARCTIC ECOLOGY

The ecological features discussed above have several implications for seep and Arctic research. The absence of living chemosymbiotic megafauna (e.g., hallmark taxa), the lack of obligate seep taxa, and the high diversity in addition to high biomass and abundance of Arctic seeps compared to background communities are features that are shared across Arctic seeps, though, different from seeps in other parts of the world. Therefore, Arctic seeps deviate from generalizations of cold-seep ecosystems and represent a novel aspect of seep ecological understanding (Sibuet and Olu, 1998; Vanreusel et al., 2009; Levin et al., 2016). The theoretical importance of Arctic seeps is not limited to seep or chemosynthesis-based research; it is also highly relevant to Arctic ecology. For example, the role of Arctic seeps as seafloor oases for a large variety of benthic species, not just for a small group of specialized animals, means that seeps impact the benthos in various ways and across different scales (Bowden et al., 2013; Levin et al., 2016). Simple differences in community structure to larger-scale processes such as food production, carbon transfer, storage, carbon cycling, etc., are all likely to be connected to seeps and need to be considered in the ecology of the Arctic (**Figure 5**). Furthermore, the presence of numerous commercial species means that Arctic seeps could also be important from a management perspective. In short, studies from these multiple Arctic seep sites indicate the importance of seeps for Arctic biology and ecology. We discuss below some of the implications of these results, and some questions that arise

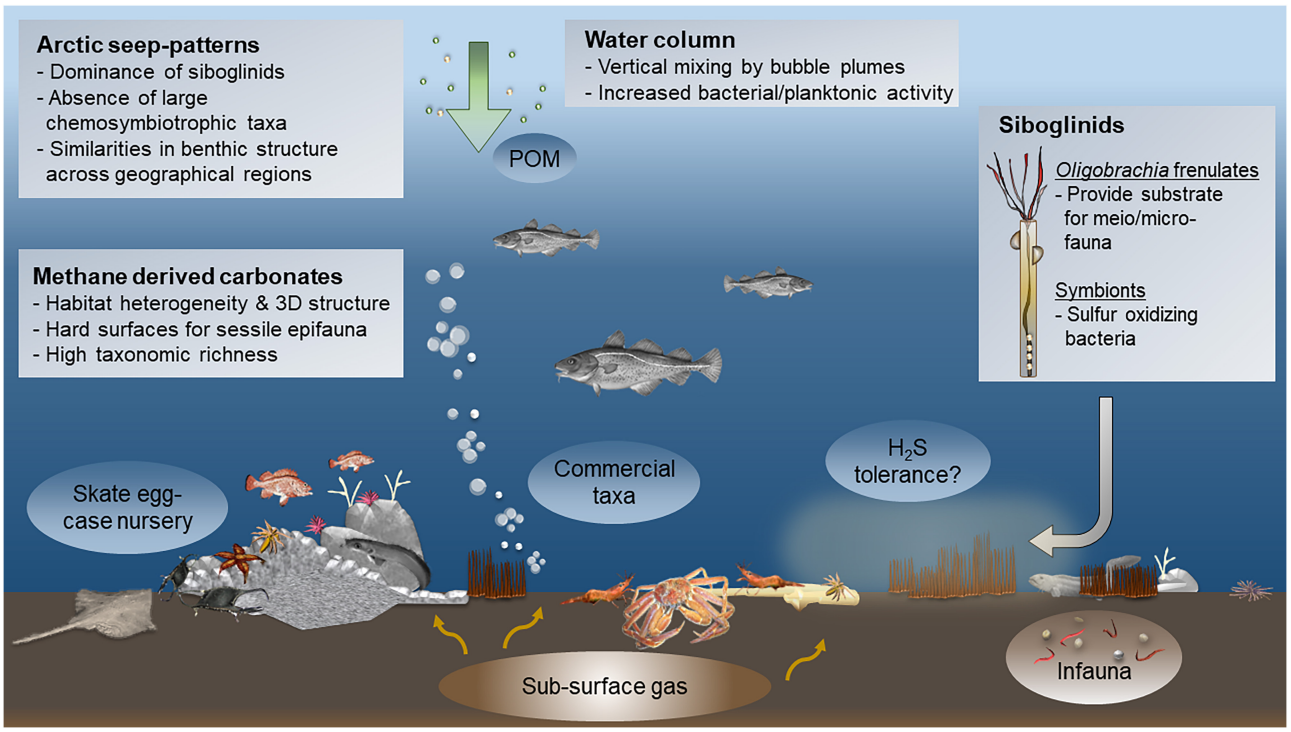

FIGURE 5 | Graphic representation of the key elements of Arctic seeps; a schematic overview of community patterns and characteristics found in Arctic seep habitats. Note that not all patterns are necessarily observed within one single cold-seep site. POM - particulate organic matter.

both from a theoretical perspective, as well as with respect to the Arctic and its future.

How Do Seeps Fit Within the Highly Seasonal Arctic Paradigm?

Marine ecosystems in the high Arctic are driven by several processes that are absent outside the polar realm. The presence of sea ice during all or part of the year and intense seasonality in physicochemical features leads to strongly episodic production of organic material, with intense seasonal blooms of primary production in the euphotic zone interrupting extended periods of little or no new production (e.g., Wassmann et al., 2006). Benthic consumers are adapted to this feast-or-famine pattern through pelagic–benthic coupling and vertical transport of organic matter, with seabed community composition and ecological functioning reflecting the spatial and temporal dynamics of organic matter on the surface of the Arctic Ocean, as mitigated through consumers in the pelagic zone (Ambrose and Renaud, 1997; Renaud et al., 2008; Smith et al., 2012).

Chemosynthetic production associated with cold seeps occurs on different spatial and temporal scales than Arctic photosynthetic processes (Jerosch et al., 2007; Bowden et al., 2013; Campanyà-Llovet and Snelgrove, 2018). Such autochthonous production is largely independent of the vagrancies and seasonal cycles of the photosynthetic production at the surface ocean. To the extent that organic matter derived from chemosynthetic production makes its way out of the microbes and chemosymbiotic species to the community at large, this pathway provides a more temporally consistent supply of food resources throughout the year. Further, since locally produced at the seabed, chemosynthetic-based organic matter is not first available to the pelagic grazers (i.e., zooplankton and other planktonic grazers), whose efficiency at consuming and reprocessing surface production often leads to degraded organic material by the time it reaches the seabed. Hence, the chemosynthetic *in situ* sea bed production can have high relevance especially in systems with low photoautotrophic primary production (oligotrophy) (Carlier et al., 2010). Chemosynthesis-based production bypasses this pelagic filter and, therefore, provides a more-or-less temporally steady source of high-quality unprocessed food for the benthic community that can mitigate the seasonal fluctuations of food availability to Arctic benthic communities.

Are Populations of Hallmark Chemosymbiotic Seep Taxa Absent at Arctic Seeps?

A distinct feature of Arctic seeps is the absence of the hallmark chemosymbiotic species (e.g., vesicomyid clams, vestimentiferan worms, and bathymodioline mussels). No evidence has yet been found for the latter two groups at Arctic seeps in recent geological time (Hryniewicz et al., 2019). Vesicomyid shells have, however, been recovered from several Arctic seep locations (Hansen et al., 2017 and references herein) (**Table 1**). Dating of vesicomyid

shells suggest that these chemosymbiotic bivalves disappeared from Arctic seeps approximately 15,000 years ago (Ambrose et al., 2015; Hansen et al., 2017, 2020). Since carbonates with preserved remains of frenulate tubes from Arctic seep sites have been dated to a minimum of 20,000 years old (Hong et al., 2019), the chemosymbiotic megafaunal communities of Arctic seeps in the past likely consisted of large bivalves along with siboglinids.

It is possible that an event occurred ∼15,000 years ago that led to the disappearance of large chemosymbiotic bivalves (including also solemyids and thyasirids in addition to vesicomyids) from Arctic seeps, leaving siboglinids unaffected (Ambrose et al., 2015; Hansen et al., 2017, 2020). A massive destabilization of gas hydrates triggered by deglaciation, accompanied by decreasing pressure at the seabed, could have resulted in the widespread release of gases. Such events are considered to have been responsible for topographical changes to the Arctic seafloor, including the creation of the blowout craters at Bjørnøyrenna and at the mound/pingos in Storfjordrenna (Andreassen et al., 2017; Serov et al., 2017). A problematic aspect of this hypothesis is the idea that these bivalves would be more vulnerable to such disturbances than the siboglinids, despite some groups such as vesicomyids, having behavioral adaptations for dealing with disruptions such as reorienting themselves in the sediment (Krylova and Von Cosel, 2011).

Another explanation for the absence of large chemosymbiotic bivalves could be the thermal barrier of low-bottom water temperatures in the Arctic. One hypothesis is that chemosymbiotic bivalves (vesicomyids and solemyids) colonized Arctic deep-water seeps during the Heinrich Stadial (HS1), after the most recent glacial period (Hansen et al., 2017, 2020). During this period of time, Arctic surface waters were generally colder, however, bottom water temperature was up to 2°C warmer than today (Rasmussen et al., 2007). When bottom water temperature decreased, resulting in negative bottom sea temperatures that persist at seeps today on the Arctic continental slope, this presumably caused an extinction of distinct chemosymbiotic vesicomyids and solemyids (Sztybor and Rasmussen, 2016; Hansen et al., 2017). This explanation does, however, fail to account for the perceived absence of large chemosymbiotic bivalves from seep sites on the shelf today, where temperatures are low, but nonetheless above 0°C (Åström et al., 2016, 2019; Hong et al., 2017). Vesicomyids have also been found at deep-water sites around the world where temperatures reach only a few degrees above freezing (Fisher, 1990; Taylor and Glover, 2010; Sen et al., 2017).

While it is currently impossible to pinpoint what factor(s) contributed to the disappearance of the large chemosymbiotic bivalves from Arctic seeps, their absence suggests that either the conditions that led to their extinction in the first place persist today, or barriers exist that have prevented recolonization. Since relatively warm, Atlantic water makes its way up past Svalbard and mixes with cold, Arctic water between Svalbard and mainland Norway (Loeng, 1991), dispersal, at least from the Atlantic to the Arctic, should not be limiting. Furthermore, Atlantic water inflow appears to be effective in transporting other species observed at Arctic seeps, namely, *Oligobrachia* worms (Sen et al., 2020). Additionally, the small thyasirids that have been collected from Arctic seeps today are also known to be present further south in the Atlantic (Oliver and Killeen, 2002; Decker et al., 2012; Åström et al., 2017).

Alternatively, some of these taxa might have re-populated Arctic seeps or never went extinct at all. A few shells of the large, presumably chemosymbiotic, species of thyasirids recovered from Storfjordrenna seeps reveal relatively modern and young ages (in comparison to the other large bivalves mentioned above), of about 500–1,300 years before present (Carroll et al., 2016; Åström et al., 2017). Therefore, certain taxa could have been present until just recently, and the question even arises as to whether they are currently present at Arctic seeps but have simply not yet been collected alive.

Are Seeps Stepping Stones for Arctic Benthic Dispersal?

At cold seeps, methane plays a key role in the process of chemosynthesis, although sulfide functions as the critical compound in shaping the benthic community. Sulfide is toxic to oxygen-breathing life forms (Vismann, 1991; Fisher and Childress, 1992), and tolerance to sulfide exposure requires special binding proteins that have evolved in animals specialized for a life in sulfide-rich habitats (Terwilliger, 1998). For motile animals, sulfide toxicity can be avoided by moving away from the most sulfidic areas while remaining in the seep vicinity. This behavioral strategy is not uncommon and is a possible explanation that no seep system in the world is populated solely by obligate seep species. As a result, vagrant, opportunistic background species are common residents around seeps (Bowden et al., 2013; Zapata-Hernández et al., 2014; Levin et al., 2016).

Less motile benthic animals populating Arctic seep sites may have acquired necessary physiological adaptations to protect them from the toxic effects of sulfide. Adaptations for prolonged sulfide exposure are, however, costly and, therefore, unexpected in background, non-seep obligate species (Sen et al., 2019b). Conversely, Arctic seasonality and the resulting episodic input of photosynthetic food to the benthic realm may have selected for adaptations in dealing with sulfide that are normally found in species endemic to, or specialized for, reducing environments (Sen et al., 2019b). This would infer an advantage in allowing them to utilize a food resource that is stable throughout the year (Åström et al., 2018). However, many Arctic seeps are relatively young in evolutionary terms, given the past glacial history of the Arctic and the Northern hemisphere (Stokes et al., 2015; Patton et al., 2017). The most recent deglaciation of the Arctic ice sheets started approximately 20,000 years cal. BP (Rasmussen et al., 2007; Patton et al., 2017; Margold et al., 2018), and a large part of the Arctic was not ice free until several thousand years later (Ingólfsson and Landvik, 2013; Andreassen et al., 2017; Margold et al., 2018). This is a short time frame for organisms to evolve both to the extremes of an Arctic environment and to cope with the presence of sulfide at seep habitats.

Given the ecological patterns of Arctic cold seeps, most benthic taxa found at seep sites in the Arctic are species that commonly occur at Arctic non-seep habitats (i.e., background fauna). Only a small subset of the species at Arctic cold seeps

are chemosymbiotrophic or organisms recognized from other reduced or chemosynthetic habitats (Decker and Olu, 2012; Sen et al., 2018a; Åström et al., 2019). For chemosymbiotic species, seeps can function as stepping stones by linking the dispersal of chemosynthetic fauna from source populations at lower latitudes to locations of reduced habitats, seeps, and vents bordering the northern polar region (e.g., Mayer et al., 1988; Sahling et al., 2003; Kiel, 2016; Åström et al., 2017; Sen et al., 2020). In addition, reduced environments associated with large food falls can increase the connectivity between vents and seeps and serve as provisory habitats allowing a northward or circumpolar expansion of taxa (Georgieva et al., 2015; Smith et al., 2015). However, seeps may not only provide gateways of dispersal and connectivity for chemsoymbiotic taxa; the ample resources at seeps could also serve for background, migrating taxa. One sub-Arctic species that has rapidly expanded its geographical range in the Arctic is the snow crab (*Chionoecetes opilio*). In 1996, it was first documented in the Barents Sea (Kuzmin et al., 1998; Alvsvåg et al., 2009) and has since spread further west and north. Its current distribution reaches as far as northern Svalbard fjords and is currently an established and commercially harvested species in the Barents Sea system (Jørgensen et al., 2019). Snow crabs have been documented at cold seeps in the western Barents Sea where images indicate that they can feed on bacterial mats (Sen et al., 2018a). The presence of snow crabs at seeps and their observed behavior may imply that they are benefiting from resources provided by the seep. The motile snow crab is a typical example of an animal expanding its geographical boundary, while exploiting resources (food) at the seep habitat. Consequently, despite Arctic seeps being extreme habitats, they might play an important role in dispersal and connectivity of various Arctic biota.

How Might Climate Change Influence Arctic Seeps?

Key elements of photosynthetic primary production cycles will be affected as the Arctic warms, sea ice melts, and water mass and nutrient distributions change. This includes changes in the timing and location of surface blooms, the species that drive the blooms, and the match of such photosynthetic primary production to pelagic and benthic consumers (Stenseth and Mysterud, 2002; Wassmann et al., 2006) all with impacts on the availability of organic detritus at the seabed, which fuels benthic communities. Carroll and Carroll (2003) hypothesized that a warmer Arctic with less sea ice may favor pelagic communities at the expense of the benthos, due to the loss of sea-ice algal production. Sea-ice algae has been shown to play a crucial role in the export of organic matter to benthos (i.e., sympagic–benthic coupling) (McMahon et al., 2006; Sun et al., 2007), as large pieces of ice algae could bypass the pelagic filter (Boetius et al., 2013). Cold-seep communities may locally mitigate such a phenomenon by supporting benthic communities when surface-based organic matter is lacking or of poor quality. The existence of seep-related production may locally have a profound impact on the community structure, ecological interactions, and secondary production of the benthos as well as its coupling with the surface ocean (Pohlman et al., 2017; Åström et al., 2018, 2019; Ofstad et al., 2020). In this way, cold seeps can act as productive hotspots in the Arctic and function as a temporal bridge for benthic communities and associated ecosystems that may otherwise suffer from a lack of consistency in food quality from the surface ocean (McMahon et al., 2006). Indeed, by the combination of enhanced *in situ* organic material production, heterogeneous habitats from the carbonate outcrops, and function as stepping stones for dispersal of species (Smith et al., 2015), the entire vicinity of Arctic cold-seep habitats serve as an oasis for background species in contrast to non-seep locations sharing similar environmental characteristics (Åström et al., 2018).

As the Arctic warms at rates well above the world average, boreal and sub-arctic species are expanding their ranges northward, interacting with, and possibly even displacing, Arctic-adapted species (Fossheim et al., 2015; Frainer et al., 2017; Haug et al., 2017). Whether continued warming and the concomitant biogeographic changes predicted for pelagic and benthic systems will be valid for cold seeps as well is an open question. Cold seeps could act as refuges for Arctic-adapted species otherwise facing variability in the timing and quality of surface-based primary production outside the ranges previously experienced. Conversely, the reduction in the temporal variability in food supply at seeps may favor boreal and temperate species at the expense of Arctic-adapted benthic species that are used in highly episodic food inputs and sub-zero temperatures. Combined with warming sea temperatures, the functional adaptations of the more southerly species may infer a competitive advantage and favor their replacement of Arctic species. Even if Arctic seeps do not experience widespread replacements of boreal species, there is also a possibility of species replacements among Arctic species. If Arctic species are predisposed for dealing with seep conditions, then species whose ranges might be increasing either naturally, or due to human activities, could start colonizing and settling successfully at seeps outside their prior ranges, which could affect local community structures and dynamics.

Another consequence of climate warming is deoxygenation of marine systems as a result of increased pelagic stratification and decreased solubility of gases (Gruber, 2011). Moving from a sea ice-dominated system toward a more open-ocean Arctic combined with changes in seasonal primary production patterns, could lead to a trophic mis-match in pelagic–benthic coupling and eventually increase the input of organic matter degradation and oxygen consumption at the seafloor (Renaud et al., 2007; Sweetman et al., 2017; Durant et al., 2019). Hypoxic seafloor conditions can cause devoid areas, empty of larger life forms, and it is essential to maintain oxygen concentration above crucial levels in order to sustain seep faunal communities (Diaz, 2001; Vaquer-Sunyer and Duarte, 2010). Oxygen is also required for symbionts to carry out the sulfide and methane oxidation processes (Cavanaugh et al., 2006; Dubilier et al., 2008). If seafloor deoxygenation becomes a problem in the Arctic, particularly in enclosed water basins, fjords and estuaries, Diaz (2001) and Liira et al. (2019), one can speculate that organisms inhabiting seeps may have an advantage over others in less oxygenated systems (Pearson and Rosenberg, 1978, Levin et al., 2003; Sweetman et al., 2017). Some organisms, incapable of large-scale movements

in and out of habitats can avoid hypoxia by modulating the surroundings to enhance oxygen circulation (i.e., re-working sediment or modulate their position in the sediment–water interface) (Hourdez and Lallier, 2007; Dando et al., 2008; Guillon et al., 2017). Others already have physiological adaptations to cope with such conditions such as increased gill size or oxygen-binding proteins (e.g., Hourdez and Lallier, 2007; Tobler et al., 2016). High densities of taxa that are known to inhabit locations with high organic matter degradation or low-oxygen habitats, at seeps compared to background sediments (Levin et al., 2003; Åström et al., 2016) could potentially indicate that these species may have a better ability to handle deoxygenation as a consequence of a warmer Arctic (Olsen et al., 2007; Norkko et al., 2019).

To summarize, cold seeps in the Arctic serve multiple ecological functions and provide critical ecosystem services (**Figure 5**). Recently, the Norwegian Environmental Agency recognized cold-seep habitats in the Norwegian marine sector as areas of special interest and vulnerable habitats with high conservation value (Miljødirektoratet, 2019). This recognition of cold-seep habitats, providing substrate and heterogeneity, alternative food resources, and possibly functioning as gateways for dispersal and connectivity of benthic taxa, including commercial species, clearly highlights the key role that Arctic cold seeps serve to the wider marine ecotone.

CONCLUSION

The physical extremes of the Arctic environment and the chemical extremes and strong environmental gradients of cold-seep systems are two primary drivers that interact in the Arctic, forming benthic communities that are distinct from not only adjacent Arctic benthic communities but also from lower-latitude seep communities.

Arctic cold seeps are conspicuously lacking in large and charismatic obligate chemosymbiotrophic faunal species that are characteristics of lower-latitude seeps. The dominant and distinct chemosymbiotic fauna at Arctic seeps is largely limited to *Oligobrachia* frenulates (with the addition of the moniliferan, *S. contortum* at HMMV). These frenulates, however, form incredibly dense tufts that are a defining biological feature of Arctic cold seeps. They alter the sediment stability, biogeochemistry, and are likely a key link between chemosynthetic and heterotrophic fauna.

Arctic seep communities support different community structure characteristics and have far-reaching trophic effects, as both diversity, abundance, and biomass are higher at Arctic seeps than at background communities (Levin et al., 2016). Importantly, this enhanced diversity and high abundance and biomass consists mainly of background, benthic species, and specific seep obligate fauna are almost entirely lacking.

The interaction of the few obligate chemosymbiotrophic species with the larger background benthic community is one of the key features of Arctic seep systems. It is the combination of autochthonous production and enhancement of the seabed heterogeneity that provides a dual basis for seeps' ability to attract and accumulate biomass and diversity in a food and substrate-limited biome. The temporal consistency of chemosynthetic-based production is largely independent of the intense seasonality of the phytosynthetic-based production cycle, providing organic matter to the benthos in the larger parts of the year when it would otherwise be low. Arctic seeps, therefore, function as local diversity and biomass hotspots on the seafloor. These hotspots may also serve as geographic stepping stones for dispersal of both chemosynthetic and background species in the larger Arctic Ocean basin.

These features highlight the role of Arctic seeps and demonstrate important baseline insights both to science and to society. Since Arctic seep research is still fairly new, and these findings are known mostly to a niche audience, seeps have not yet been included in policy making or in modeling outcomes of a warming Arctic. It is clear, though, that these habitats are an important ecosystem resource of relevance for conservation and with broader implications for marine ecosystem functioning in the age of global climate change (Renaud et al., 2015; Haug et al., 2017). Recently, they have been granted the status of particularly valuable and vulnerable habitats by the Norwegian government (Miljødirektoratet, 2019).

FUTURE DIRECTIONS

Despite notable gains in the understanding of Arctic seep systems acquired through recent studies, significant gaps remain. Most Arctic seep research has been conducted in the European Arctic, particularly in Nordic waters, and large parts of the Arctic, despite seeps being present, have not been studied from a biological perspective. Furthermore, seeps fringing but outside the Arctic Circle (e.g., the North Atlantic–Norwegian Sea, Sea of Okhotsk, North Atlantic east, and west coast) have yet to be sufficiently studied (Sahling et al., 2003; Vaughn Barrie et al., 2011; Decker et al., 2012; Skarke et al., 2014). This is of importance since these locations experience some of the extreme phenomena that appear to drive current and past processes at Arctic seeps. Indeed, some of these seep sites also appear to share the community structure seen at Arctic seeps (Sahling et al., 2003; Krylova et al., 2011; Decker and Olu, 2012; Decker et al., 2012; Hansen et al., 2020).

Most biological seep studies address the impact of seeps on the Arctic benthos. However, Vinogradov and Semenova (2000) described the peculiarities of the mesoplankton distribution above HMMV, and Ofstad et al. (2020) measured different pelagic foraminifera and pteropod communities above Barents Sea seep sites. Furthermore, Pohlman et al. (2017) suggest that high methane concentrations and nearshore upwelling stimulate consumption of CO_2 by photosynthetic phytoplankton at the shallow PKF seeps. Seasonal ecological studies at Arctic seeps are also lacking, despite the role of seasonality as a key driver of Arctic biological cycles, and the intriguing possibility that chemosynthetic production cycles can have strong effects mitigating such seasonality. Additionally, the investigation of specific trophic linkages between high-trophic level marine resources, their prey, and Arctic seep systems remains in its early stages. Finally, a focus on better understanding the ecosystem

services associated with these unique habitats, specifically in an Arctic context, will provide stakeholders a basis of information to assess the possible conservation value of Arctic cold seeps.

With further investigation, we may begin to merge chemosynthesis-based systems in the Arctic and include them as an integral part of the Arctic marine ecosystem. Arctic vent communities seem to be more like Arctic seep communities than Atlantic vents. They share characteristics such as a lack of hallmark species and large symbiotrophic animals and are also mainly comprised of non-specialist, background species (Sweetman et al., 2013). Large "clouds" of planktonic animals have been observed above Arctic vent sites (Schander et al., 2010); therefore, the effects of vents might resemble those of Arctic seeps. The merging of seeps and vents into a single compartment may provide a basis for understanding processes at other Arctic systems where chemosymbiotrophic animals are observed, such as fjords, and generating new ecological perspectives and insights for the larger Arctic ecosystem.

AUTHOR CONTRIBUTIONS

JC: manuscript initialization. EÅ and AS: conceptualization. AS and EÅ: drafting the manuscript. AS, EÅ, and MC: visualization. All authors: writing, revisions, and edits.

FUNDING

EÅ was a post-doctoral scholar funded by VISTA – a basic research program in collaboration between The Norwegian Academy of Science and Letters and Equinor (#6172). AS was a post-doctoral scholar at Nord University (Bodø, Norway). JC and MC contributions to this manuscript were funded by the Research Council of Norway (RCN #228107). The publication charges for this article have been funded by a grant from the publication fund of UiT – The Arctic University of Norway.

ACKNOWLEDGMENTS

We thank Dr. Bodil Bluhm, Dr. Henning Reis, and Dr. Paul Renaud for their support and guidance during the development of this publication. We are also grateful to Dr. Eve Southward and Dr. Paul Dando for sharing their knowledge on siboglinids and geochemistry through extensive discussions over the past few years. Part of the ecological research at the sites described in section 3.2.1 to 3.2.6 has been enabled through CAGE – The Center for Arctic Gas Hydrate, Environment and Climate, UiT – The Arctic University of Norway. Thanks to the two reviewers who helped refine the final manuscript.

REFERENCES

Alvsvåg, J., Agnalt, A.-L., and Jørstad, K. E. (2009). Evidence for a permanent establishment of the snow crab (*Chionoecetes opilio*) in the Barents Sea. *Biol. Invasions* 11, 587–595.

Ambrose, W. G. J., Panieri, G., Schneider, A., Plaza-Faverola, A., Carroll, M. L., Åström, E. K. L., et al. (2015). Bivalve shell horizons in seafloor pockmarks of the last glacial-interglacial transition: a thousand years of methane emissions in the Arctic Ocean. *Geochemistry, Geophys. Geosystems* 16, 4108–4129. doi: 10.1002/2015GC005980

Ambrose, W. G. J., and Renaud, P. E. (1997). Does a pulsed food supply to the benthos affect polychaete recruitment patterns in the Northeast Water Polynya? *J. Mar. Syst.* 10, 483–495.

Ambrose, W. G. J., Renaud, P. E., Locke, V., Cottier, F. R., Berge, J., Carroll, M. L., et al. (2012). Growth line deposition and variability in growth of two circumpolar bivalves (*Serripes groenlandicus*, and *Clinocardium ciliatum*). *Polar Biol.* 35, 345–354.

Amon, D. J., Gobin, J., Van Dover, C. L., Levin, L. A., Marsh, L., and Raineault, N. A. (2017). Characterization of methane-seep communities in a deep-sea area designated for oil and natural gas exploitation off trinidad and tobago. *Front. Mar. Sci.* 4:342. doi: 10.3389/fmars.2017.00342

Andreassen, K., Hubbard, A., Winsborrow, M., Patton, H., Vadakkepuliyambatta, S., Plaza-Faverola, A., et al. (2017). Massive blow-out craters formed by hydrate-controlled methane expulsion from the Arctic seafloor. *Science* 356, 948–953. doi: 10.1126/science.aal4500

Artcic Monitoring and Assessment Programme [AMAP], (1998). *AMAP Assessment Report: Arctic Pollution Issues.* Norway: Arctic Monitoring and Assessment Programme, xii+859.

Åström, E. K., Carroll, M., Sen, A., Niemann, H., Ambrose, W., Lehmann, M., et al. (2019). Chemosynthesis influences food web and community structure in high-Arctic benthos. *Mar. Ecol. Prog. Ser.* 629, 19–42. doi: 10.3354/meps13101

Åström, E. K. L. (2018). *Benthic Communities At High-Arctic Cold Seeps: Faunal Response To Methane Seepage In Svalbard*. Ph. D. thesis, UiT-The Arctic University of Norway, Tromsø.

Åström, E. K. L., Carroll, M. L., Ambrose, W. G., Sen, A., Silyakova, A., and Carroll, J. (2018). Methane cold seeps as biological oases in the high-Arctic deep sea. *Limnol. Oceanogr.* 63, S209–S231. doi: 10.1002/lno.10732

Åström, E. K. L., Carroll, M. L., Ambrose, W. G. J., and Carroll, J. (2016). Arctic cold seeps in marine methane hydrate environments : impacts on shelf macrobenthic community structure offshore Svalbard. *Mar. Ecol. Prog. Ser.* 552, 1–18. doi: 10.3354/meps11773

Åström, E. K. L., Oliver, P. G., and Carroll, M. L. (2017). A new genus and two new species of *Thyasiridae* associated with methane seeps off Svalbard. Arctic Ocean. *Mar. Biol. Res.* 13, 402–416. doi: 10.1080/17451000.2016.1272699

Bagarinao, T. (1992). Sulfide as an environmental factor and toxicant: tolerance and adaptations in aquatic organisms. *Aquat. Toxicol.* 24, 21–62. doi: 10.1016/0166-445X(92)90015-F

Becker, E. L., Cordes, E. E., Macko, S. A., and Fisher, C. R. (2009). Importance of seep primary production to *Lophelia pertusa* and associated fauna in the Gulf of Mexico. *Deep Sea Res. Part I Oceanogr. Res. Pap.* 56, 786–800. doi: 10.1016/j.dsr.2008.12.006

Becker, E. L., Cordes, E. E., Macko, S. A., Lee, R. W., and Fisher, C. R. (2013). Using stable isotope compositions of animal tissues to infer trophic interactions in gulf of mexico lower slope seep communities. *PLoS One* 8:e74459. doi: 10.1371/journal.pone.0074459

Bellec, V. (2015). "The deep sea off lofoten, vesterålen and troms," in *The Norwegian Sea Floor - New Knowledge From MAREANO for Ecosystem-Based Management*, eds H. Bhul-Mortenssen, and T. Thorsnes, (Berlin: Springer), 61–79.

Berchet, A., Bousquet, P., Pison, I., Locatelli, R., Chevallier, F., Paris, J. D., et al. (2016). Atmospheric constraints on the methane emissions from the East Siberian Shelf. *Atmos. Chem. Phys.* 16, 4147–4157.

Berestovskii, E. G. (1994). Reproductive biology of skates of the family Rajidae in the seas of the far north. *J. Ichthyol. Ikhtiologii.* 34:2.

Berge, J., Renaud, P. E., Darnis, G., Cottier, F., Last, K., Gabrielsen, T. M., et al. (2015). In the dark: a review of ecosystem processes during the Arctic polar night. *Prog. Oceanogr.* 139, 258–271. doi: 10.1016/j.pocean.2015.08.005

Berndt, C., Feseker, T., Treude, T., Krastel, S., Liebetrau, V., Niemann, H., et al. (2014). Temporal constraints on hydrate-controlled methane seepage off svalbard. *Science* 343, 284–287. doi: 10.1126/science.1246298

Bienhold, C., Pop Ristova, P., Wenzhöfer, F., Dittmar, T., and Boetius, A. (2013). How deep-sea wood falls sustain chemosynthetic life. *PLoS One* 8:53590. doi: 10.1371/journal.pone.0053590

Black, M. B., Halanych, K. M., Maas, P. A. Y., Hoeh, W. R., Hashimoto, J., Desbruyères, D., et al. (1997). Molecular systematics of vestimentiferan tubeworms from hydrothermal vents and cold-water seeps. *Mar. Biol.* 130, 141–149. doi: 10.1007/s002270050233

Boetius, A., Albrecht, S., Bakker, K., Bienhold, C., Felden, J., Fernandez-Mendez, M., et al. (2013). Export of algal biomass from the melting arctic sea ice. *Science* 339, 1430–1432. doi: 10.1126/science.1231346

Boetius, A., Ravenschlag, K., Schubert, C. J., Rickert, D., Widdel, F., Gleeske, A., et al. (2000). A marine microbial consortium apparently mediating AOM. *Nature* 407, 623–626. doi: 10.1038/35036572

Bowden, D. A., Rowden, A. A., Thurber, A. R., Baco, A. R., Levin, L. A., and Smith, C. R. (2013). Cold Seep epifaunal communities on the hikurangi margin, new zealand: composition, succession, and vulnerability to human activities. *PLoS One* 8:e76869. doi: 10.1371/journal.pone.0076869

Braby, C. E., Rouse, G. W., Johnson, S. B., Jones, W. J., and Vrijenhoek, R. C. (2007). Bathymetric and temporal variation among Osedax boneworms and associated megafauna on whale-falls in Monterey Bay, California. *Deep Sea Res. Part I Oceanogr. Res. Pap.* 54, 1773–1791. doi: 10.1016/j.dsr.2007.05.014

Bünz, S., Polyanov, S., Vadakkepuliyambatta, S., Consolaro, C., and Mienert, J. (2012). Active gas venting through hydrate-bearing sediments on the vestnesa ridge, offshore w-svalbard. *Mar. Geol.* 332–334, 189–197. doi: 10.1016/j.margeo.2012.09.012

Campanyà-Llovet, N., and Snelgrove, P. V. R. (2018). Fine-scale infaunal community and food web patch mosaics from Barkley methane hydrates (British Columbia, Canada): the role of food quality. *Deep Sea Res. Part I Oceanogr. Res. Pap.* 140, 186–195. doi: 10.1016/j.dsr.2018.06.009

Carlier, A., Ritt, B., Rodrigues, C. F., Sarrazin, J., Olu, K., Grall, J., et al. (2010). Heterogeneous energetic pathways and carbon sources on deep eastern Mediterranean cold seep communities. *Mar. Biol.* 157, 2545–2565.

Carney, R. S. (1994). Consideration of the oasis analogy for chemosynthetic communities at Gulf of Mexico hydrocarbon vents. *Geo. Mar. Lett.* 14, 149–159. doi: 10.1007/BF01203726

Carroll, M. L., Åström, E. K. L., Ambrose, W. G. J., Locke, W., Oliver, G. P., Hong, W.-L., et al. (2016). "Shell growth and environmental control of methanophyllic Thyasirid bivalves from Svalbard cold seeps," in *Proceedings of the EGU General Assembly Conference Abstracts EGU General Assembly Conference Abstracts*, Vienna.

Carroll, M. L., and Carroll, J. (2003). "The Arctic Seas," in *Biogeochemistry of Marine Systems*, eds K. Black, and G. Shimmield, (Oxford: Blackwell Publishing), 127–156.

Carroll, M. L., Denisenko, S. G., Renaud, P. E., and Ambrose, W. G. J. (2008). Benthic infauna of the seasonally ice-covered western Barents Sea: patterns and relationships to environmental forcing. *Deep. Res. Part II Top. Stud. Oceanogr.* 55, 2340–2351. doi: 10.1016/j.dsr2.2008.05.022

Cavanaugh, C. M., McKiness, Z. P., Newton, I. L. G., and Stewart, F. J. (2006). "Marine Chemosynthetic Symbioses," in *The Prokaryotes*, eds M. Dworkin, S. Falkow, E. Rosenberg, K.-H. Schleifer, and E. Stackebrandt, (New York, NY: Springer), 475–507. doi: 10.1007/0-387-30741-9_18

Chand, S., Rise, L., Ottesen, D., Dolan, M. F. J., Bellec, V., and Bøe, R. (2009). Pockmark-like depressions near the goliat hydrocarbon field, barents sea: morphology and genesis. *Mar. Pet. Geol.* 26, 1035–1042.

Clark, M. R., Althaus, F., Schlacher, T. A., Williams, A., Bowden, D. A., and Rowden, A. A. (2016). The impacts of deep-sea fisheries on Benthic communities: a review. *ICES J. Mar. Sci. J. Du Cons.* 73, i51–i69.

Cochrane, S. K. J., Pearson, T. H., Greenacre, M., Costelloe, J., Ellingsen, I. H., Dahle, S., et al. (2012). Benthic fauna and functional traits along a Polar front transect in the Barents sea - advancing tools for ecosystem-scale assessments. *J. Mar. Syst.* 94, 204–217. doi: 10.1016/j.jmarsys.2011.12.001

Comiso, J. C., and Hall, D. K. (2014). Climate trends in the Arctic as observed from space. *Wiley Interdiscip. Rev. Clim. Chang.* 5, 389–409. doi: 10.1002/wcc.277

Cordes, E. E., Bergquist, D. C., Predmore, B. L., Jones, C., Deines, P., Telesnicki, G., et al. (2006). Alternate unstable states: convergent paths of succession in hydrocarbon-seep tubeworm-associated communities. *J. Exp. Mar. Bio. Ecol.* 339, 159–176. doi: 10.1016/j.jembe.2006.07.017

Cordes, E. E., Cunha, M. R., Galéron, J., Mora, C., Olu-Le Roy, K., Sibuet, M., et al. (2010). The influence of geological, geochemical, and biogenic habitat heterogeneity on seep biodiversity. *Mar. Ecol.* 31, 51–65. doi: 10.1111/j.1439-0485.2009.00334.x

Cordes, E. E., McGinley, M. P., Podowski, E. L., Becker, E. L., Lessard-Pilon, S., Viada, S. T., et al. (2008). Coral communities of the deep Gulf of Mexico. *Deep Sea Res. Part I Oceanogr. Res. Pap.* 55, 777–787. doi: 10.1016/j.dsr.2008.03.005

Coyle, K. O., Konar, B., Blanchard, A., Highsmith, R. C., Carroll, J., Carroll, M. L., et al. (2007). Potential effects of temperature on the benthic infaunal community on the southeastern Bering Sea shelf: possible impacts of climate change. *Deep. Res. Part II Top. Stud. Oceanogr.* 54, 2885–2905. doi: 10.1016/j.dsr2.2007.08.025

Da Ros, Z., Dell'Anno, A., Morato, T., Sweetman, A. K., Carreiro-Silva, M., Smith, C. J., et al. (2019). The deep sea: the new frontier for ecological restoration. *Mar. Policy* 108:103642. doi: 10.1016/j.marpol.2019.103642

Dando, P. R. (2010). "Biological communities at marine shallow-water vent and seep sites," in *The Vent and Seep Biota Topics in Geobiology*, ed. S. Kiel, (Dordrecht: Springer), 333–378. doi: 10.1007/978-90-481-9572-5

Dando, P. R., Southward, A. F., Southward, E. C., Dixon, D. R., and Crawford, A. (1992). Shipwrecked tube worms. *Nature* 356, 667–667. doi: 10.1038/356667a0

Dando, P. R., Southward, A. J., Southward, E. C., Lamont, P., and Harvey, R. (2008). Interactions between sediment chemistry and frenulate pogonophores (Annelida) in the north-east Atlantic. *Deep. Res. Part I Oceanogr. Res. Pap.* 55, 966–996. doi: 10.1016/j.dsr.2008.04.002

Dando, P. R., and Spiro, B. (1993). Varying nutritional dependence of the thyasirid bivalves Thyasira sarsi and T. equalis on chemoautotrophic symbiotic bacteria, demonstrated by isotope ratios of tissue carbon and shell carbonate. *Mar. Ecol. Prog. Ser.* 92, 151–158. doi: 10.3354/meps092151

De Beer, D., Sauter, E., Niemann, H., Kaul, N., Foucher, J. P., Witte, U., et al. (2006). In situ fluxes and zonation of microbial activity in surface sediments of the Håkon Mosby Mud Volcano. *Limnol. Oceanogr.* 51, 1315–1331. doi: 10.4319/lo.2006.51.3.1315

Decker, C., Morineaux, M., Van Gaever, S., Caprais, J.-C. C., Lichtschlag, A., Gauthier, O., et al. (2012). Habitat heterogeneity influences cold-seep macrofaunal communities within and among seeps along the Norwegian margin. Part 1: macrofaunal community structure. *Mar. Ecol.* 33, 205–230. doi: 10.1111/j.1439-0485.2011.00503.x

Decker, C., and Olu, K. (2012). Habitat heterogeneity influences cold-seep macrofaunal communities within and among seeps along the Norwegian margin - Part 2: contribution of chemosynthesis and nutritional patterns. *Mar. Ecol.* 33, 231–245. doi: 10.1111/j.1439-0485.2011.00486.x

Demina, L. L., and Galkin, S. V. (2018). Ecology of the bottom fauna and bioaccumulation of trace metals along the Lena River–Laptev Sea transect. *Environ. Earth Sci.* 77:43. doi: 10.1007/s12665-018-7231-y

Diaz, R. J. (2001). Overview of hypoxia around the world. *J. Environ. Qual.* 30, 275–281.

Drazen, J. C., Goffredi, S. K., Schlining, B., and Stakes, D. S. (2003). Aggregations of egg-brooding deep-sea fish and cephalopods on the gorda escarpment: a reproductive hot spot. *Biol. Bull.* 205, 1–7. doi: 10.2307/1543439

Duarte, C. M., and Cebrián, J. (1996). The fate of marine autotrophic production. *Limnol. Oceanogr.* 41, 1758–1766. doi: 10.4319/lo.1996.41.8.1758

Dubilier, N., Bergin, C., and Lott, C. (2008). Symbiotic diversity in marine animals: the art of harnessing chemosynthesis. *Nat. Rev. Microbiol.* 6, 725–740. doi: 10.1038/nrmicro1992

Dufour, S. C. (2005). Gill anatomy and the evolution of symbiosis in the bivalve family thyasiridae. *Biol. Bull.* 208, 200–212. doi: 10.2307/3593152

Dufour, S. C., and Felbeck, H. (2006). Symbiont abundance in thyasirids (Bivalvia) is related to particulate food and sulphide availability. *Mar. Ecol. Prog. Ser.* 320, 185–194. doi: 10.3354/meps320185

Dunlop, K. M., Jones, D. O. B., and Sweetman, A. K. (2018). Scavenging processes on jellyfish carcasses across a fjord depth gradient. *Limnol. Oceanogr.* 63, 1146–1155. doi: 10.1002/lno.10760

Duperron, S., Gaudron, S. M., Rodrigues, C. F., Cunha, M. R., Decker, C., and Olu, K. (2013). An overview of chemosynthetic symbioses in bivalves from the North Atlantic and Mediterranean Sea. *Biogeosciences* 10, 3241–3267. doi: 10.5194/bg-10-3241-2013

Durant, J. M., Molinero, J. C., Ottersen, G., Reygondeau, G., Stige, L. C., and Langangen, O. (2019). Contrasting effects of rising temperatures on trophic interactions in marine ecosystems. *Sci. Rep.* 9:15213. doi: 10.1038/s41598-019-51607-w

Feseker, T., Boetius, A., Wenzhöfer, F., Blandin, J., Olu, K., Yoerger, D. R., et al. (2014). Eruption of a deep-sea mud volcano triggers rapid sediment movement. *Nat. Commun.* 5, 1–8. doi: 10.1038/ncomms6385

Feseker, T., Foucher, J.-P., and Harmegnies, F. (2008). Fluid flow or mud eruptions? Sediment temperature distributions on Håkon Mosby mud volcano, SW Barents Sea slope. *Mar. Geol.* 247, 194–207. doi: 10.1016/j.margeo.2007.09.005

Fisher, C. R. (1990). Chemoautotrophic and methanotrophic symbiosis in marine invertebrates. *Rev. Aquat. Sci* 2, 399–436.

Fisher, C. R. (1996). "Ecophysiology of primary production at deep-sea vents and seeps," in *Deep-Sea and Extreme Shallow-Water Habitats: Affinities and Adaptations—Biosyste- matics and Ecology Series*, eds F. Uiblein, J. Ott, and M. Stachowtisch, (Berlin: Springer), 313–336.

Fisher, C. R., and Childress, J. J. (1992). Organic carbon transfer from methanotrophic symbionts to the host hydrocarbon-seep mussel. *Symbiosis* 12, 221–235.

Fossheim, M., Primicerio, R., Johannesen, E., Ingvaldsen, R. B., Aschan, M. M., and Dolgov, A. V. (2015). Recent warming leads to a rapid borealization of fish communities in the Arctic. *Nat. Clim. Chang.* 5, 673–677. doi: 10.1038/nclimate2647

Frainer, A., Primicerio, R., Kortsch, S., Aune, M., Dolgov, A. V., Fossheim, M., et al. (2017). Climate-driven changes in functional biogeography of Arctic marine fish communities. *Proc. Natl. Acad. Sci.* 114, 12202–12207. doi: 10.1073/pnas.1706080114

Gage, J. D., and Tyler, P. A. (1991). *Deep-Sea Biology: A Natural History Of Organisms At The Deep-Sea Floor*. Cambridge: Cambridge University Press.

Gebruk, A. V., Krylova, E. M., Lein, A. Y., Vinogradov, G. M., Anderson, E., Pimenov, N. V., et al. (2003). Methane seep community of the Håkon Mosby mud volcano (the Norwegian Sea): composition and trophic aspects. *Sarsia* 88, 394–403. doi: 10.1080/00364820310003190

Georgieva, M. N., Wiklund, H., Bell, J. B., Eilertsen, M. H., Mills, R. A., Little, C. T. S., et al. (2015). A chemosynthetic weed: the tubeworm *Sclerolinum contortum* is a bipolar, cosmopolitan species. *BMC Evol. Biol.* 15:280. doi: 10.1186/s12862-015-0559-y

Gooday, A. J., Turley, C. M., and Allen, J. A. (1990). Responses by benthic organisms to inputs of organic material to the ocean floor: a review [and Discussion}. *Philos. Trans. R. Soc.* 331:119.

Graf, G. (1989). Benthic-pelagic coupling in a deep-sea benthic community. *Nature* 341, 437–439. doi: 10.1038/341437a0

Grebmeier, J. M., and Barry, J. P. (1991). The influence of oceanographic processes on pelagic-benthic coupling in polar regions : a benthic perspective. *J. Mar. Syst.* 2, 495–518.

Gruber, N. (2011). Warming up, turning sour, losing breath: ocean biogeochemistry under global change. *Philos. Trans. R. Soc. A Math. Phys. Eng. Sci.* 369, 1980–1996. doi: 10.1098/rsta.2011.0003

Grünke, S., Lichtschlag, A., De Beer, D., Felden, J., Salman, V., Ramette, A., et al. (2012). Mats of psychrophilic thiotrophic bacteria associated with cold seeps of the Barents Sea. *Biogeosciences* 9, 2947–2960. doi: 10.5194/bg-9-2947-2012

Guillon, E., Menot, L., Decker, C., Krylova, E., and Olu, K. (2017). The vesicomyid bivalve habitat at cold seeps supports heterogeneous and dynamic macrofaunal assemblages. *Deep. Res. Part I Oceanogr. Res. Pap.* 120, 1–13. doi: 10.1016/j.dsr.2016.12.008

Hansen, J., Ezat, M. M., Åström, E. K. L., and Rasmussen, T. L. (2020). New late pleistocene species of acharax from arctic methane seeps off svalbard. *J. Syst. Palaeontol.* 18, 197–212. doi: 10.1080/14772019.2019.1594420

Hansen, J., Hoff, U., Sztybor, K., and Rasmussen, T. L. (2017). Taxonomy and palaeoecology of two Late Pleistocene species of vesicomyid bivalves from cold methane seeps at Svalbard (79°N). *J. Molluscan Stud.* 83, 270–279. doi: 10.1093/mollus/eyx014

Harrison, W. G., and Platt, T. (1986). Photosynthesis-irradiance relationships in polar and temperate phytoplankton populations. *Polar Biol.* 5, 153–164. doi: 10.1007/BF00441695

Haug, T., Bogstad, B., Chierici, M., Gjøsaeter, H., Hallfredsson, E. H., Høines, A. S., et al. (2017). Future harvest of living resources in the Arctic Ocean north of the Nordic and Barents Seas: a review of possibilities and constraints. *Fish. Res.* 188, 38–57. doi: 10.1016/j.fishres.2016.12.002

Hegseth, E. N. (1998). Primary production of the northern Barents Sea. *Polar Res.* 17, 113–123. doi: 10.1111/j.1751-8369.1998.tb00266.x

Heyl, T. P., Gilhooly, W. P., Chambers, R. M., Gilchrist, G. W., Macko, S. A., Ruppel, C. D., et al. (2007). Characteristics of vesicomyid clams and their environment at the Blake Ridge cold seep, South Carolina, USA. *Mar. Ecol. Prog. Ser.* 339, 169–184. doi: 10.3354/meps339169

Higgs, N. D., Gates, A. R., and Jones, D. O. B. (2014). Fish food in the deep sea: revisiting the role of large food-falls. *PLoS One* 9:96016. doi: 10.1371/journal.pone.0096016

Higgs, N. D., Newton, J., and Attrill, M. J. (2016). Caribbean spiny lobster fishery is underpinned by trophic subsidies from chemosynthetic primary production. *Curr. Biol.* 26, 3393–3398. doi: 10.1016/j.cub.2016.10.034

Hjelsteun, B. O., Eldholm, O., Faleide, J. I., and Vogt, P. (1999). Regional settings of hakon mosby mud volcano, SE Barents Sea margin. *Geo-Marine Lett.* 19, 22–28. doi: 10.1007/s003670050089

Hoff, G. R. (2010). Identification of skate nursery habitat in the eastern Bering Sea. *Mar. Ecol. Prog. Ser.* 403, 243–254. doi: 10.3354/meps08424

Holding, J. M., Duarte, C. M., Delgado-Huertas, A., Soetaert, K., Vonk, J. E., Agustí, S., et al. (2017). Autochthonous and allochthonous contributions of organic carbon to microbial food webs in Svalbard fjords. *Limnol. Oceanogr.* 62, 1307–1323. doi: 10.1002/lno.10526

Hong, W.-L., Lepland, A., Himmler, T., Kim, J., Chand, S., Sahy, D., et al. (2019). Discharge of meteoric water in the eastern norwegian sea since the last glacial period. *Geophys. Res. Lett.* 46, 8194–8204. doi: 10.1029/2019gl084237

Hong, W.-L., Torres, M. E., Carroll, J., Crémière, A., Panieri, G., Yao, H., et al. (2017). Seepage from an arctic shallow marine gas hydrate reservoir is insensitive to momentary ocean warming. *Nat. Commun.* 8:15745. doi: 10.1038/ncomms15745

Hourdez, S., and Lallier, F. H. (2007). Adaptations to hypoxia in hydrothermal-vent and cold-seep invertebrates. *Rev. Environ. Sci. Biotechnol.* 6, 143–159. doi: 10.1007/s11157-006-9110-9113

Hovland, M. (2008). *Deep-water Coral Reefs: Unique Biodiversity*. Chichester, UK: Hotspots Praxis Publishing (Springer), 278.

Hovland, M., and Svensen, H. (2006). Submarine pingoes: indicators of shallow gas hydrates in a pockmark at Nyegga, Norwegian Sea. *Mar. Geol.* 228, 15–23. doi: 10.1016/j.margeo.2005.12.005

Hryniewicz, K., Amano, K., Bitner, M., Hagström, J., Kiel, S., Klompmaker, A., et al. (2019). A late Paleocene fauna from shallow-water chemosynthesis-based ecosystems, Spitsbergen, Svalbard. *Acta Palaeontol. Pol.* 64:554. doi: 10.4202/app.00554.2018

Ingólfsson, Ó, and Landvik, J. Y. (2013). The svalbard-barents sea ice-sheet - historical, current and future perspectives. *Quat. Sci. Rev.* 64, 33–60. doi: 10.1016/j.quascirev.2012.11.034

IPCC, (2018). *Global Warming of 1.5°C: An IPCC Special Report on the Impacts of Global Warming of 1.5°C Above Pre-industrial Levels and Related Global Greenhouse Gas Emission Pathways, in the Context of Strengthening the Global Response to the Threat of Climate Chang*. Geneva: Intergovernmental Panel on Climate Change.

Jakobsson, M., Mayer, L., Coakley, B., Dowdeswell, J. A., Forbes, S., Fridman, B., et al. (2012). The international bathymetric chart of the arctic ocean (IBCAO) version 3.0. *Geophys. Res. Lett.* 39:219. doi: 10.1029/2012GL052219

James, R. H., Bousquet, P., Bussmann, I., Haeckel, M., Kipfer, R., Leifer, I., et al. (2016). Effects of climate change on methane emissions from seafloor sediments in the Arctic Ocean: a review. *Limnol. Oceanogr.* 61, S283–S299. doi: 10.1002/lno.10307

Jerosch, K., Schlüter, M., Foucher, J.-P. P., Allais, A.-G. G., Klages, M., Edy, C., et al. (2007). Spatial distribution of mud flows, chemoautotrophic communities, and biogeochemical habitats at Håkon Mosby Mud Volcano. *Mar. Geol.* 243, 1–17. doi: 10.1016/j.margeo.2007.03.010

Johnson, J. E., Mienert, J., Plaza-Faverola, A., Vadakkepuliyambatta, S., Knies, J., Bünz, S., et al. (2015). Abiotic methane from ultraslow-spreading ridges can charge Arctic gas hydrates. *Geology* 43, 371–374. doi: 10.1130/G36440.1

Jørgensen, L. L., Primicerio, R., Ingvaldsen, R. B., Fossheim, M., Strelkova, N., Thangstad, T. H., et al. (2019). Impact of multiple stressors on sea bed fauna in a warming Arctic. *Mar. Ecol. Prog. Ser.* 608, 1–12. doi: 10.3354/meps12803

Kaul, N., Foucher, J. P., and Heesemann, M. (2006). Estimating mud expulsion rates from temperature measurements on Håkon Mosby Mud Volcano, SW Barents Sea. *Mar. Geol.* 229, 1–14. doi: 10.1016/j.margeo.2006.02.004

Kiel, S. (2016). A biogeographic network reveals evolutionary links between deep-sea hydrothermal vent and methane seep faunas. *Proc. R. Soc. B Biol. Sci.* 283:20162337. doi: 10.1098/rspb.2016.2337

Kjesbu, O. S., Bogstad, B., Devine, J. A., Gjøsaeter, H., Howell, D., Ingvaldsen, R. B., et al. (2014). Synergies between climate and management for Atlantic cod fisheries at high latitudes. *Proc. Natl. Acad. Sci.* 111, 3478–3483. doi: 10.1073/pnas.1316342111

Koh, C. A., and Sloan, E. D. (2007). Natural gas hydrates: recent advances and challenges in energy and environmental applications. *AIChE J.* 53, 1636–1643. doi: 10.1002/aic.11219

Krylova, E. M., Gebruk, A. V., Portnova, D. A., Todt, C., and Haflidason, H. (2011). New species of the genus Isorropodon (Bivalvia: Vesicomyidae: Pliocardiinae) from cold methane seeps at Nyegga (Norwegian Sea, Vøring Plateau, Storrega Slide). *J. Mar. Biol. Assoc. U. K.* 91, 1135–1144. doi: 10.1017/S002531541100004X

Krylova, E. M., and Von Cosel, R. (2011). A new genus of large vesicomyidae (Mollusca, Bivalvia, Vesicomyidae, Pliocardiinae) from the Congo margin, with the first record of the subfamily Pliocardiinae in the Bay of Biscay (northeastern Atlantic). *Zoosystema* 33, 83–99.

Kuzmin, S. A., Akhtarin, S. M., and Menis, D. T. (1998). The first findings of snow crab *Chionoecetes opilio* (Decapoda, Majidae) in the Barents Sea. *Zool. J.* 40, 490–492.

Kvenvolden, K. A., Ginsburg, G. D., and Soloviev, V. A. (1993). Worldwide distribution of subaquatic gas hydrates. *Geo. Mar. Lett.* 13, 32–40. doi: 10.1007/BF01204390

Lammers, S., Suess, E., and Hovland, M. (1995). A large methane plume east of Bear Island (Barents Sea): implications for the marine methane cycle. *Geol. Rundschau.* 84, 59–66. doi: 10.1007/BF00192242

Lee, D. H., Kim, J. H., Lee, Y. M., Jin, Y. K., Paull, C., Kim, D., et al. (2019). Chemosynthetic bacterial signatures in Frenulata tubeworm *Oligobrachia* sp. In an active mud volcano of the Canadian Beaufort Sea. *Mar. Ecol. Prog. Ser.* 628, 95–104. doi: 10.3354/meps13084

Lee, Y. M., Noh, H.-J., Lee, D.-H., Kim, J.-H., Jin, Y. K., and Paull, C. (2019). Bacterial endosymbiont of *Oligobrachia* sp. (Frenulata) from an active mud volcano in the Canadian Beaufort Sea. *Polar Biol.* 42, 2305–2312. doi: 10.1007/s00300-019-02599-w

Levin, L. (2005). "Ecology of cold seep sediments: interactions of fauna with flow, chemistry and microbes," in *Oceanography and Marine Biology - an Annual Review*, eds R. Gibson, R. Atkinson, and J. Gordon, (Berlin: Springer), 1–46. doi: 10.1201/9781420037449.ch1

Levin, L., Ziebis, W., Mendoza, G., Growney, V., Tryon, M., Brown, K., et al. (2003). Spatial heterogeneity of macrofauna at northern California methane seeps: influence of sulfide concentration and fluid flow. *Mar. Ecol. Prog. Ser.* 265, 123–139. doi: 10.3354/meps265123

Levin, L. A., Baco, A. R., Bowden, D., Colaço, A., Cordes, E., Cunha, M. R., et al. (2016). Hydrothermal vents and methane seeps: rethinking the sphere of influence. *Front. Mar. Sci.* 3:72. doi: 10.3389/fmars.2016.00072

Levin, L. A., and Bris, N. L. (2015). The deep ocean under climate change. *Science* 350, 766–768. doi: 10.1126/science.aad0126

Levin, L. A., Mendoza, G. F., and Grupe, B. M. (2017). Methane seepage effects on biodiversity and biological traits of macrofauna inhabiting authigenic carbonates. *Deep Sea Res. Part II Top. Stud. Oceanogr.* 137, 26–41. doi: 10.1016/j.dsr2.2016.05.021

Liira, M., Noormets, R., Sepp, H., Kekišev, O., Maddison, M., and Olaussen, S. (2019). Sediment geochemical study of hydrocarbon seeps in Isfjorden and Mohnbukta : a comparison between western and eastern. *Arktos* 5, 49–62. doi: 10.1007/s41063-019-00067-67

Loeng, H. (1991). Features of the physical oceanograpic conditions of the Barents Sea. *Polar Res.* 10, 5–18. doi: 10.1111/j.1751-8369.1991.tb00630.x

Loher, M., Marcon, Y., Pape, T., Römer, M., Wintersteller, P., dos Santos Ferreira, C., et al. (2018). Seafloor sealing, doming, and collapse associated with gas seeps and authigenic carbonate structures at Venere mud volcano, Central Mediterranean. *Deep Sea Res. Part I Oceanogr. Res. Pap.* 137, 76–96. doi: 10.1016/j.dsr.2018.04.006

Lösekann, T., Knittel, K., Nadalig, T., Fuchs, B., Niemann, H., Boetius, A., et al. (2007). Diversity and abundance of aerobic and anaerobic methane oxidizers at the Haakon Mosby Mud Volcano, Barents Sea. *Appl. Environ. Microbiol.* 73, 3348–3362. doi: 10.1128/AEM.00016-17

MacAvoy, S. E., Macko, S. A., and Carney, R. S. (2003). Links between chemosynthetic production and mobile predators on the Louisiana continental slope: Stable carbon isotopes of specific fatty acids. *Chem. Geol.* 201, 229–237.

MacDonald, G. J. (1990). Role of methane clathrates in past and future climates. *Clim. Change* 16, 247–281. doi: 10.1007/BF00144504

MacDonald, I. R., Smith, M., and Huffer, F. W. (2010). Community structure comparisons of lower slope hydrocarbon seeps, northern Gulf of Mexico. *Deep. Res. Part II Top. Stud. Oceanogr.* 57, 1904–1915. doi: 10.1016/j.dsr2.2010.09.002

Margold, M., Stokes, C. R., and Clark, C. D. (2018). Reconciling records of ice streaming and ice margin retreat to produce a palaeogeographic reconstruction of the deglaciation of the *Laurentide* Ice Sheet. *Quat. Sci. Rev.* 189, 1–30. doi: 10.1016/j.quascirev.2018.03.013

Marshall, B. A. (1988). Skeneidae, Vitrinellidae and Orbitestellidae (Mollusca: Gastropoda) associated with biogenic substrata from bathyal depths off New Zealand and New South Wales. *J. Nat. Hist.* 22, 949–1004. doi: 10.1080/00222938800770631

Mau, S., Römer, M., Torres, M. E., Bussmann, I., Pape, T., Damm, E., et al. (2017). Widespread methane seepage along the continental margin off Svalbard-from Bjørnøya to Kongsfjorden. *Sci. Rep.* 7:42997. doi: 10.1038/srep42997

Mayer, L. A., Shor, A. N., Clarke, J. H., and Piper, D. J. W. (1988). Dense biological communities at 3850 m on the laurentian fan and their relationship to the deposits o f the 1929 G r and Banksearthquake. *Deep Sea Res. Part A Oceanogr. Res. Pap.* 35, 1235–1246.

McMahon, K. W., Ambrose, W. G. J., Johnson, B. J., Sun, M.-Y., Lopez, G. R., Clough, L. M., et al. (2006). Benthic community responses to ice algae and phytoplankton in Ny Alesund. *Svalbard. Mar. Ecol. Prog. Ser.* 310, 1–14. doi: 10.3354/meps310001

Meyer, K. S., Bergmann, M., and Soltwedel, T. (2013). Interannual variation in the epibenthic megafauna at the shallowest station of the HAUSGARTEN observatory (79° N, 6° E). *Biogeosciences* 10, 3479–3492. doi: 10.5194/bg-10-3479-2013

Miljødirektoratet, (2019). Saerlig Verdifulle Og Sårbare Områder - Faggrunnlag For Revisjon Og Oppdatering Av Forvaltningsplanene For Norske Havområder M-1303/2019. Available at: https://www.miljodirektoratet.no/globalassets/publikasjoner/m1303/m1303.pdf (accessed November 4, 2019).

Molari, M., Manini, E., and Dell'Anno, A. (2013). Dark inorganic carbon fixation sustains the functioning of benthic deep-sea ecosystems. *Global Biogeochem. Cycles* 27, 212–221. doi: 10.1002/gbc.20030

Mora, C., Spirandelli, D., Franklin, E. C., Lynham, J., Kantar, M. B., Miles, W., et al. (2018). Broad threat to humanity from cumulative climate hazards intensified by greenhouse gas emissions. *Nat. Clim. Chang.* 8, 1062–1071. doi: 10.1038/s41558-018-0315-316

Moran, S. B., Lomas, M. W., Kelly, R. P., Gradinger, R., Iken, K., and Mathis, J. T. (2012). Seasonal succession of net primary productivity, particulate organic carbon export, and autotrophic community composition in the eastern Bering Sea. *Deep. Res. Part II Top. Stud. Oceanogr.* 6, 84–97. doi: 10.1016/j.dsr2.2012.02.011

Morata, N., Michaud, E., and Włodarska-Kowalczuk, M. (2013). Impact of early food input on the arctic benthos activities during the polar night. *Polar Biol.* 38, 99–114. doi: 10.1007/s00300-013-1414-1415

Morata, N., Renaud, P. E., Brugel, S., Hobson, K. A., and Johnson, B. J. (2008). Spatial and seasonal variations in the pelagic- benthic coupling of the southeastern Beaufort Sea revealed by sedimentary biomarkers. *Mar. Ecol. Prog. Ser.* 371, 47–63. doi: 10.3354/meps07677

Myhre, C. L., Ferré, B., Platt, S. M., Silyakova, A., Hermansen, O., Allen, G., et al. (2016). Extensive release of methane from Arctic seabed west of Svalbard

during summer 2014 does not influence the atmosphere. *Geophys. Res. Lett.* 43, 4624–4631. doi: 10.1002/2016GL068999.Received

Niemann, H., Linke, P., Knittel, K., MacPherson, E., Boetius, A., Brückmann, W., et al. (2013). Methane-carbon flow into the benthic food web at cold seeps – a case study from the costa rica subduction zone. *PLoS One* 8:e74894. doi: 10.1371/journal.pone.0074894

Niemann, H., Lösekann, T., de Beer, D., Elvert, M., Nadalig, T., Knittel, K., et al. (2006). Novel microbial communities of the Haakon Mosby mud volcano and their role as a methane sink. *Nature* 443, 854–858. doi: 10.1038/nature05227

Norkko, J., Pilditch, C. A., Gammal, J., Rosenberg, R., Enemar, A., Magnusson, M., et al. (2019). Ecosystem functioning along gradients of increasing hypoxia and changing soft-sediment community types. *J. Sea Res.* 153, 101781.

Ofstad, S., Meilland, J., Zamelczyk, K., Chierici, M., Fransson, A., Gründger, F., et al. (2020). Development, Productivity, and Seasonality of Living Planktonic Foraminiferal Faunas and Limacina helicina in an Area of Intense Methane Seepage in the Barents Sea. *J. Geophys. Res. Biogeosciences* 125, 1–24. doi: 10.1029/2019JG005387

Oliver, P. G., and Killeen, I. J. (2002). *The Thyasiridae (Mollusca: Bivalvia) Of The British Continental Shelf And North Sea Oil Fields: An Identification Manual*. Cardiff, CF: National Museums & Galleries of Wales.

Olsen, G. H., Carroll, M. L., Renaud, P. E., Ambrose, W. G. J., Olssøn, R., and Carroll, J. (2007). Benthic community response to petroleum-associated components in arctic versus temperate marine sediments. *Mar. Biol.* 151, 2167–2176. doi: 10.1007/s00227-007-0650-z

Olu-Le Roy, K., Sibuet, M., Fiala-Médioni, A., Gofas, S., Salas, C., Mariotti, A., et al. (2004). Cold seep communities in the deep eastern Mediterranean Sea: composition, symbiosis and spatial distribution on mud volcanoes. *Deep. Res. Part I Oceanogr. Res. Pap.* 51, 1915–1936. doi: 10.1016/j.dsr.2004.07.004

Patton, H., Hubbard, A., Andreassen, K., Auriac, A., Whitehouse, P. L., Stroeven, A. P., et al. (2017). Deglaciation of the eurasian ice sheet complex. *Quat. Sci. Rev.* 169, 148–172. doi: 10.1016/j.quascirev.2017.05.019

Paull, C. K., Dallimore, S. R., Caress, D. W., Gwiazda, R., Melling, H., Riedel, M., et al. (2015). Active mud volcanoes on the continental slope of the Canadian Beaufort Sea. *Geochem. Geophys. Geosyst.* 16, 3160–3181. doi: 10.1002/2015GC005928

Paull, C. K., Ussler, W., Dallimore, S. R., Blasco, S. M., Lorenson, T. D., Melling, H., et al. (2007). Origin of pingo-like features on the Beaufort Sea shelf and their possible relationship to decomposing methane gas hydrates. *Geophys. Res. Lett.* 34, 1–5. doi: 10.1029/2006GL027977

Pearson, T., and Rosenberg, R. (1978). Macrobenthic succession in relation to organic enrichment and pollution of the marine environment. *Ocean Mar. Biol. Annu. Rev.* 16, 229–311. doi: 10.1016/j.marpolbul.2006.09.008

Pimenov, N. V., Savvichev, A., Rusanov, I. I, Lein, A. Y., and Ivanov, M. V. (2000). Microbiological processes of the carbon and sulfur cycle in cold methane seeps in the North Atlantic. *Mikrobiologiia* 69, 831–843. doi: 10.1023/A:1026666527034

Pohlman, J. W., Greinert, J., Ruppel, C., Silyakova, A., Vielstädte, L., Casso, M., et al. (2017). Enhanced CO 2 uptake at a shallow arctic ocean seep field overwhelms the positive warming potential of emitted methane. *Proc. Natl. Acad. Sci. U.S.A.* 114, 5355–5360. doi: 10.1073/pnas.1618926114

Portail, M., Olu, K., Dubois, S. F., Escobar-Briones, E., Gelinas, Y., Menot, L., et al. (2016). Food-web complexity in guaymas basin hydrothermal vents and cold seeps. *PLoS One* 11:e0162263. doi: 10.1371/journal.pone.0162263

Portnov, A., Smith, A. J., Mienert, J., Cherkashov, G., Rekant, P., Semenov, P., et al. (2013). Offshore permafrost decay and massive seabed methane escape in water depths >20 m at the South Kara Sea shelf. *Geophys. Res. Lett.* 40, 3962–3967. doi: 10.1002/grl.50735

Portnov, A., Vadakkepuliyambatta, S., Mienert, J., and Hubbard, A. (2016). Ice-sheet-driven methane storage and release in the Arctic. *Nat. Commun.* 7:10314. doi: 10.1038/ncomms10314

Portnova, D., Mokievsky, V., and Soltwedel, T. (2011). Nematode species distribution patterns at the Håkon Mosby Mud Volcano (Norwegian Sea). *Mar. Ecol.* 32, 24–41. doi: 10.1111/j.1439-0485.2010.00403.x

Rasmussen, T. L., Thomsen, E., Ślubowska, M. A., Jessen, S., Solheim, A., and Koç, N. (2007). Paleoceanographic evolution of the SW Svalbard margin (76°N) since 20,000 14C yr BP. *Quat. Res.* 67, 100–114. doi: 10.1016/j.yqres.2006.07.002

Reeburgh, W. S. (2007). Oceanic methane biogeochemistry. *Chem. Rev.* 107, 486–513. doi: 10.1021/cr050362v

Renaud, P. E., Morata, N., Carroll, M. L., Denisenko, S. G., and Reigstad, M. (2008). Pelagic–benthic coupling in the western Barents Sea: processes and time scales. *Deep. Res. Part II Top. Stud. Oceanogr.* 55, 2372–2380. doi: 10.1016/j.dsr2.2008.05.017

Renaud, P. E., Riedel, A., Michel, C., Morata, N., Gosselin, M., Juul-Pedersen, T., et al. (2007). Seasonal variation in benthic community oxygen demand: a response to an ice algal bloom in the Beaufort Sea. *Canadian Arctic? J. Mar. Syst.* 67, 1–12. doi: 10.1016/j.jmarsys.2006.07.006

Renaud, P. E., Sejr, M. K., Bluhm, B. A., Sirenko, B., and Ellingsen, I. H. (2015). The future of Arctic benthos: expansion, invasion, and biodiversity. *Prog. Oceanogr.* 139, 244–257. doi: 10.1016/j.pocean.2015.07.007

Rice, A. L., Billett, D. S. M., Fry, J., John, A. W. G., Lampitt, R. S., Mantoura, R. F. C., et al. (1986). Seasonal deposition of phytodetritus to the deep-sea floor. *Proc. R. Soc. Edinburgh. Sect. B. Biol. Sci.* 88, 265–279. doi: 10.1017/S0269727000004590

Rise, L., Bellec, V. K., Ch, S., and Bøe, R. (2014). Pockmarks in the southwestern Barents Sea and Finnmark fjords. *Nor. Geol. Tidsskr.* 94, 263–282.

Rise, L., Bøe, R., Riis, F., Bellec, V. K., Laberg, J. S., Eidvin, T., et al. (2013). The Lofoten-Vesterålen continental margin, North Norway: canyons and mass-movement activity. *Mar. Pet. Geol.* 45, 134–149. doi: 10.1016/j.marpetgeo.2013.04.021

Rodrigues, C. F., Hilario, A., and Cunha, M. R. (2013). Chemosymbiotic species from the Gulf of Cadiz (NE Atlantic): distribution, life styles and nutritional patterns. *Biogeosciences* 10, 2569–2581. doi: 10.5194/bg-10-2569-2013

Rybakova, E., Galkin, S., Bergmann, M., Soltwedel, T., and Gebruk, A. (2013). Density and distribution of megafauna at the Håkon Mosby mud volcano (the Barents Sea) based on image analysis. *Biogeosciences* 10, 3359–3374. doi: 10.5194/bg-10-3359-2013

Sahling, H., Galkin, S. V., Salyuk, A., Greinert, J., Foerstel, H., Piepenburg, D., et al. (2003). Depth-related structure and ecological significance of cold-seep communities—a case study from the Sea of Okhotsk. *Deep Sea Res. Part I Oceanogr. Res. Pap.* 50, 1391–1409. doi: 10.1016/j.dsr.2003.08.004

Sahling, H., Römer, M., Pape, T., Bergès, B., dos Santos Fereirra, C., Boelmann, J., et al. (2014). Gas emissions at the continental margin west of Svalbard: mapping, sampling, and quantification. *Biogeosciences* 11, 6029–6046. doi: 10.5194/bg-11-6029-2014

Sakshaug, E., and Slagstad, D. (1991). Light and productivity of phytoplankton in polar marine ecosystems: a physiological view. *Polar Res.* 10, 69–86. doi: 10.3402/polar.v10i1.6729

Salinas-De-León, P., Phillips, B., Ebert, D., Shivji, M., Cerutti-Pereyra, F., Ruck, C., et al. (2018). Deep-sea hydrothermal vents as natural egg-case incubators at the Galapagos Rift. *Sci. Rep.* 8, 1–7. doi: 10.1038/s41598-018-20046-20044

Sasaki, T., Warén, A., Kano, Y., Okutani, T., and Fujikura, K. (2010). "Gastropods from recent hot vents and cold seeps: systematics, diversity and life strategies," in *The Vent and Seep Biota*, ed. S. Kiel, (Berlin: Springer), 169–254. doi: 10.1007/978-90-481-9572-5_7

Savvichev, A. S., Kadnikov, V. V., Kravchishina, M. D., Galkin, S. V., Novigatskii, A. N., Sigalevich, P. A., et al. (2018). Methane as an organic matter source and the trophic basis of a laptev sea cold seep microbial community. *Geomicrobiol. J.* 35, 411–423. doi: 10.1080/01490451.2017.1382612

Schander, C., Rapp, H. T., Kongsrud, J. A., Bakken, T., Berge, J., Cochrane, S., et al. (2010). The fauna of hydrothermal vents on the Mohn Ridge (North Atlantic). *Mar. Biol. Res.* 6, 155–171. doi: 10.1080/17451000903147450

Schulz, M., Bergmann, M., von Juterzenka, K., and Soltwedel, T. (2010). Colonisation of hard substrata along a channel system in the deep Greenland Sea. *Polar Biol.* 33, 1359–1369. doi: 10.1007/s00300-010-0825-829

Schulze, A., and Halanych, K. M. (2003). Siboglinid evolution shaped by habitat preference and sulfide tolerance. *Hydrobiologia* 496, 199–205. doi: 10.1023/A:1026192715095

Seabrook, S., De Leo, F. C., and Thurber, A. R. (2019). Flipping for food: the use of a methane seep by tanner crabs (*Chionoecetes tanneri*). *Front. Mar. Sci.* 6:43. doi: 10.3389/fmars.2019.00043

Sen, A., Åström, E. K. L., Hong, W.-L., Portnov, A., Waage, M., Serov, P., et al. (2018a). Geophysical and geochemical controls on the megafaunal community of a high Arctic cold seep. *Biogeosciences* 15, 4533–4559. doi: 10.5194/bg-15-4533-2018

Sen, A., Duperron, S., Hourdez, S., Piquet, B., Léger, N., Gebruk, A., et al. (2018b). Cryptic frenulates are the dominant chemosymbiotrophic fauna at Arctic and high latitude Atlantic cold seeps. *PLoS One* 13:e0209273. doi: 10.1371/journal.pone.0209273

Sen, A., Chitkara, C., Hong, W.-L., Lepland, A., Cochrane, S., di Primio, R., et al. (2019a). Image based quantitative comparisons indicate heightened megabenthos diversity and abundance at a site of weak hydrocarbon seepage in the southwestern Barents Sea. *PeerJ* 7:e7398. doi: 10.7717/peerj.7398

Sen, A., Himmler, T., Hong, W. L., Chitkara, C., Lee, R. W., Ferré, B., et al. (2019b). Atypical biological features of a new cold seep site on the Lofoten-Vesterålen continental margin (northern Norway). *Sci. Rep.* 9:1762. doi: 10.1038/s41598-018-38070-38079

Sen, A., Dennielou, B., Tourolle, J., Arnaubec, A., Rabouille, C., and Olu, K. (2017). Fauna and habitat types driven by turbidity currents in the lobe complex of the Congo deep-sea fan. *Deep. Res. Part II Top. Stud. Oceanogr.* 142, 167–179. doi: 10.1016/j.dsr2.2017.05.009

Sen, A., Didriksen, A., Hourdez, S., Svenning, M. M., and Rasmussen, T. L. (2020). Frenulate siboglinids at high Arctic methane seeps and insight into high latitude frenulate distribution. *Ecol. Evol.* 10, 1339–1351. doi: 10.1002/ece3.5988

Serov, P., Portnov, A., Mienert, J., Semenov, P., and Ilatovskaya, P. (2015). Methane release from pingo-like features across the South Kara Sea shelf, an area of thawing offshore permafrost. *J. Geophys. Res. Earth Surf.* 120, 1515–1529. doi: 10.1002/2015JF003467

Serov, P., Vadakkepuliyambatta, S., Mienert, J., Patton, H., Portnov, A., Silyakova, A., et al. (2017). Postglacial response of Arctic Ocean gas hydrates to climatic amelioration. *Proc. Natl. Acad. Sci.* 114, 6215–6220. doi: 10.1073/pnas.1619288114

Shakhova, N., Semiletov, I., Leifer, I., Salyuk, A., Rekant, P., and Kosmach, D. (2010). Geochemical and geophysical evidence of methane release over the East Siberian Arctic Shelf. *J. Geophys. Res.* 115:C08007. doi: 10.1029/2009JC005602

Sibuet, M., and Olu, K. (1998). Biogeography, biodiversity and fluid dependence of deep-sea cold-seep communities at active and passive margins. *Deep Sea Res. Part II Top. Stud. Oceanogr.* 45, 517–567. doi: 10.1016/S0967-0645(97)00074-X

Sirenko, B., Denisenko, S., Deubel, H., and Rachor, E. (2004). Deep water communities of the laptev sea and adjacent parts of the arctic ocean. fauna ecosyst. laptev sea adjac. *Deep waters Arctic. Part I. St.-petersbg.* 54, 28–73.

Skarke, A., Ruppel, C., Kodis, M., Brothers, D., and Lobecker, E. (2014). Widespread methane leakage from the sea floor on the northern US Atlantic margin. *Nat. Geosci.* 7, 657–661.

Sloan, E. D. (1998). Gas hydrates: review of physical/chemical properties. *Energy Fuels* 12, 191–196. doi: 10.1021/ef970164

Smirnov, R. V. (2008). Morphological characters and classification of the subclass monilifera (Pogonophora) and the problem of evolution of the bridle in pogonophorans. *Russ. J. Mar. Biol.* 34, 359–368. doi: 10.1134/S1063074008060035

Smirnov, R. V. (2014). A revision of the Oligobrachiidae (Annelida: Pogonophora), with notes on the morphology and distribution of *Oligobrachia haakonmosbiensis* Smirnov. *Mar. Biol. Res.* 10, 972–982. doi: 10.1080/17451000.2013.872799

Smith, C. R., and Baco, A. R. (2003). Ecology of whale falls at the deep-sea floor. *Oceanogr. Mar. Biol. Vol* 41, 311–354.

Smith, C. R., De Master, D. J., Thomas, C., Sršen, P., Grange, L., Evrard, V., et al. (2012). Pelagic-benthic coupling, food banks, and climate change on the west Antarctic Peninsula shelf. *Oceanography* 25, 189–201. doi: 10.5670/oceanog.2012.94

Smith, C. R., Glover, A. G., Treude, T., Higgs, N. D., and Amon, D. J. (2015). Whale-fall ecosystems: recent insights into ecology, paleoecology, and evolution. *Ann. Rev. Mar. Sci.* 7, 571–596. doi: 10.1146/annurev-marine-010213-135144

Solheim, A., and Elverhøi, A. (1993). Gas-related sea floor craters in the Barents Sea. *Geo. Mar. Lett.* 13, 235–243. doi: 10.1007/BF01207753

Soltwedel, T., Jaeckisch, N., Ritter, N., Hasemann, C., Bergmann, M., and Klages, M. (2009). Bathymetric patterns of megafaunal assemblages from the arctic deep-sea observatory HAUSGARTEN. *Deep. Res. Part I Oceanogr. Res. Pap.* 56, 1856–1872. doi: 10.1016/j.dsr.2009.05.012

Søreide, J. E., Hop, H., Carroll, M. L., Falk-Petersen, S., and Hegseth, E. N. (2006). Seasonal food web structures and sympagic–pelagic coupling in the European Arctic revealed by stable isotopes and a two-source food web model. *Prog. Oceanogr.* 71, 59–87. doi: 10.1016/j.pocean.2006.06.001

Southward, A. J., and Southward, E. C. (1982). The role of dissolved organic matter in the nutrition of deep-sea Benthos. *Am. Zool.* 22, 647–658.

Steffen, W., Rockström, J., Richardson, K., Lenton, T. M., Folke, C., Liverman, D., et al. (2018). Trajectories of the earth system in the anthropocene. *Proc. Natl. Acad. Sci. U.S.A.* 115, 8252–8259. doi: 10.1073/pnas.1810141115

Stenseth, N. C., and Mysterud, A. (2002). Climate, changing phenology, and other life history traits: Nonlinearity and match-mismatch to the environment. *Proc. Natl. Acad. Sci. U.S.A.* 99, 13379–13381. doi: 10.1073/pnas.212519399

Stokes, C. R., Tarasov, L., Blomdin, R., Cronin, T. M., Fisher, T. G., Gyllencreutz, R., et al. (2015). On the reconstruction of palaeo-ice sheets: recent advances and future challenges. *Quat. Sci. Rev.* 125, 15–49. doi: 10.1016/j.quascirev.2015.07.016

Stone, R. B., Pratt, H. L., Parker, R. O., and Davis, G. E. (1979). A comparison of fish populations on an artificial and natural reef in the florida Keys. *Mar. Fish. Rev.* 41, 1–11.

Stranne, C., O'Regan, M., Dickens, G. R., Crill, P., Miller, C., Preto, P., et al. (2016). Dynamic simulations of potential methane release from East Siberian continental slope sediments. *Geochem. Geophys. Geosyst.* 17, 872–886.

Sun, M., Carroll, M. L., Ambrose, W. G. J., Clough, L. M., Zou, L., and Lopez, G. R. (2007). Rapid consumption of phytoplankton and ice algae by Arctic soft-sediment benthic communities : evidence using natural and 13 C-labeled food materials. *J. Mar. Res.* 65, 561–588.

Sweetman, A., Levin, L., Rapp, H., and Schander, C. (2013). Faunal trophic structure at hydrothermal vents on the southern Mohn's Ridge, Arctic Ocean. *Mar. Ecol. Prog. Ser.* 473, 115–131. doi: 10.3354/meps10050

Sweetman, A. K., Smith, C. R., Shulse, C. N., Maillot, B., Lindh, M., Church, M. J., et al. (2019). Key role of bacteria in the short-term cycling of carbon at the abyssal seafloor in a low particulate organic carbon flux region of the eastern Pacific Ocean. *Limnol. Oceanogr.* 64, 694–713. doi: 10.1002/lno.11069

Sweetman, A. K., Thurber, A. R., Smith, C. R., Levin, L. A., Mora, C., Wei, C.-L., et al. (2017). Major impacts of climate change on deep-sea benthic ecosystems. *Elem. Sci. Anth.* 5:4. doi: 10.1525/elementa.203

Sztybor, K., and Rasmussen, T. L. (2016). Diagenetic disturbances of marine sedimentary records from methane- influenced environments in the Fram Strait as indications of variation in seep intensity during the last 35 000 years. *Boreas* 46, 212–228. doi: 10.1111/bor.12202

Tarasov, V. G., Gebruk, A. V., Mironov, A. N., and Moskalev, L. I. (2005). Deep-sea and shallow-water hydrothermal vent communities: two different phenomena? *Chem. Geol.* 224, 5–39. doi: 10.1016/j.chemgeo.2005.07.021

Taylor, J. D., and Glover, E. A. (2010). "Chemosymbiotic bivalves," in *The Vent and Seep Biota*, ed. S. Kiel, (Göttingen: Springer), 107–135.

Terwilliger, N. B. (1998). Functional adaptations of oxygen-transport proteins. *J. Exp. Biol.* 201, 1085–1098.

Thomsen, E., Lander Rasmussen, T., Sztybor, K., Hanken, N.-M., Secher Tendal, O., and Uchman, A. (2019). Cold-seep fossil macrofaunal assemblages from Vestnesa Ridge, eastern Fram Strait, during the past 45 000 years. *Polar Res.* 38. doi: 10.33265/polar.v38.3310

Tobler, M., Passow, C. N., Greenway, R., Kelley, J. L., and Shaw, J. H. (2016). The evolutionary ecology of animals inhabiting hydrogen sulfide – rich environments. *Annu. Rev. Ecol. Evol. Syst.* 47, 239–262. doi: 10.1146/annurev-ecolsys-121415-132418

Treude, T., Kiel, S., Linke, P., Peckmann, J., and Goedert, J. L. (2011). Elasmobranch egg capsules associated with modern and ancient cold seeps: a nursery for marine deep-water predators. *Mar. Ecol. Prog. Ser.* 437, 175–181. doi: 10.3354/meps09305

Turner, P. J., Ball, B., Diana, Z., Fariñas-Bermejo, A., Grace, I., McVeigh, D., et al. (2020). Methane Seeps on the US atlantic margin and their potential importance to populations of the commercially valuable deep-sea red crab, *Chaceon quinquedens*. *Front. Mar. Sci.* 7:75. doi: 10.3389/fmars.2020.00075

Van Gaever, S., Moodley, L., de Beer, D., and Vanreusel, A. (2006). Meiobenthos at the Arctic Håkon Mosby Mud Volcano, with a parental-caring nematode thriving in sulphide-rich sediments. *Mar. Ecol. Prog. Ser.* 321, 143–155. doi: 10.3354/meps321143

Vanreusel, A., Andersen, A., Boetius, A., Connelly, D., Cunha, M. R., Decker, C., et al. (2009). Biodiversity of cold seep ecosystems along the European margins. *Oceanography* 22, 110–127.

Vaquer-Sunyer, R., and Duarte, C. M. (2010). Sulfide exposure accelerates hypoxia-driven mortality. *Limnol. Oceanogr.* 55, 1075–1082. doi: 10.4319/lo.2010.55.3.1075

Vaughn Barrie, J., Cook, S., and Conway, K. W. (2011). Cold seeps and benthic habitat on the Pacific margin of Canada. *Cont. Shelf Res.* 31, 85–92. doi: 10.1016/j.csr.2010.02.013

Vinogradov, G. M., and Semenova, T. N. (2000). Some peculiarities of the vertical distribution of mesoplankton in the Norwegian-Greenland Basin. *Oceanology* 40, 370–377.

Vismann, B. (1991). Sulfide tolerance: physiological mechanisms and ecological implications. *Ophelia* 34, 1–27.

Vogt, P., Crane, K., Sundvor, E., Max, M. D., and Pfirman, S. L. (1994). Methane-generated(?) pockmarks on young, thickly sedimented oceanic crust in the arctic: vestnesa ridge, fram strait. *Geology* 22, 255–258.

Vogt, P. R., Cherkashev, G., Ginsburg, G., Ivanov, G., Milkov, A., Crane, K., et al. (1997). Haakon Mosby mud volcano provides unusual example of venting. *EOS Trans. Am. Geophys. Union* 78, 549–557.

Wassmann, P., Reigstad, M., Haug, T., Rudels, B., Carroll, M. L., Hop, H., et al. (2006). Food webs and carbon flux in the Barents Sea. *Prog. Oceanogr.* 71, 232–287. doi: 10.1016/j.pocean.2006.10.003

Weaver, J. S., and Stewart, J. M. (1982). "In situ hydrates under the Beaufort Sea shelf," in *Proceedings of the 4th International Conferences on Permafrost*, Ottawa, 312–319.

Weaver, P. P. E., Billett, D. S. M., Boetius, A., Danovaro, R., Freiwald, A., and Sibuet, M. (2004). Hotspot ecosystem research on Europe's deep-ocean margins. *Oceanography* 17, 132–143. doi: 10.5670/oceanog.2004.10

Webb, K., Barnes, D. K. A., and Planke, S. (2009). Pockmarks: refuges for marine benthic biodiversity. *Limnol. Oceanogr.* 54, 1776–1788. doi: 10.4319/lo.2009.54.5.1776

Zapata-Hernández, G., Sellanes, J., Thurber, A. R., Levin, L. A., Chazalon, F., and Linke, P. (2014). New insights on the trophic ecology of bathyal communities from the methane seep area off Concepción, Chile (∼36° S). *Mar. Ecol.* 35, 1–21. doi: 10.1111/maec.12051

Conflict of Interest: The authors declare that the research was conducted in the absence of any commercial or financial relationships that could be construed as a potential conflict of interest.

Copyright © 2020 Åström, Sen, Carroll and Carroll. This is an open-access article distributed under the terms of the Creative Commons Attribution License (CC BY). The use, distribution or reproduction in other forums is permitted, provided the original author(s) and the copyright owner(s) are credited and that the original publication in this journal is cited, in accordance with accepted academic practice. No use, distribution or reproduction is permitted which does not comply with these terms.

frontiers in Marine Science

ORIGINAL RESEARCH
published: 09 June 2020
doi: 10.3389/fmars.2020.00393

Drivers of Megabenthic Community Structure in One of the World's Deepest Silled-Fjords, Sognefjord (Western Norway)

Heidi K. Meyer[1], Emyr M. Roberts[1], Furu Mienis[2] and Hans T. Rapp[1,3†]*

[1] Department of Biological Sciences and K.G. Jebsen Centre for Deep-Sea Research, University of Bergen, Bergen, Norway, [2] Department of Ocean Systems, Royal Netherlands Institute for Sea Research and Utrecht University, Den Burg, Netherlands, [3] NORCE, Norwegian Research Centre, NORCE Environment, Bergen, Norway

The Sognefjord is the longest (205 km) and deepest (1308 m) fjord in Norway, and the second-longest in the world. Coast-fjord exchange in Sognefjord is limited by a seaward sill at 170 m water depth, which causes a clear stratification between water masses as the dense oxygen-poor basin water mixes slowly with the well-oxygenated water directly above from the coastal ocean. Due to the homogeneity and limited variability in the deep-water, the deep slopes of Sognefjord represent the ideal setting to study how abiotic factors influence the deep-water benthic community structure. During the summer of 2017, two remotely operated vehicle (ROV) video transects were performed to compare the megabenthic community behind the sill (water depth: 1230 to 55 m; transect length: 1.39 km; distance from sill: ∼17 km) and within the central fjord (water depth: 1155–85 m; transect length: 2.43 km; distance from sill: ∼79 km). Accompanying conductivity–temperature–depth (CTD) deployments were made to measure the *in situ* abiotic factors and nutrient concentrations at each transect location, while the substrate characteristics (percent cover of soft and hard exposed substrate) were documented from the video footage. Here, Sognefjord's megabenthic community composition, distribution, and species richness were analyzed in relation to abiotic factors (e.g., depth, salinity, dissolved oxygen, chlorophyll *a* concentration, and percent cover of hard and soft substrata) within the fjord. Basin communities were homogeneous and characterized by sponges, echinoderms, and crustaceans, whereas the shallower regions were dominated by mobile scavengers. Contrary to other fjord-based studies, species richness and diversity were stable in the fjord basin and decreased with proximity to the sill, decreasing water depth, and at the boundary between intermediate and basin water. The findings demonstrate that highly stratified fjords support stable communities in their basins; however, further research is needed to investigate the influence water mass dynamics have on silled-fjord megafauna communities.

Keywords: fjord fauna, glass sponges, megafauna, Sognefjord, Norwegian fjords, remotely operated vehicles, extreme habitats

OPEN ACCESS

Edited by:
Thomas Wernberg, University of Western Australia, Australia

Reviewed by:
Giorgio Bavestrello, University of Genoa, Italy
Torstein Pedersen, UiT The Arctic University of Norway, Norway

****Correspondence:***
Heidi K. Meyer
Heidi.Meyer@uib.no

† Deceased

Specialty section:
This article was submitted to Global Change and the Future Ocean, a section of the journal Frontiers in Marine Science

Received: *13 December 2019*
Accepted: *07 May 2020*
Published: *09 June 2020*

Citation:
Meyer HK, Roberts EM, Mienis F and Rapp HT (2020) Drivers of Megabenthic Community Structure in One of the World's Deepest Silled-Fjords, Sognefjord (Western Norway). Front. Mar. Sci. 7:393. doi: 10.3389/fmars.2020.00393

INTRODUCTION

Deep fjords are valuable study areas because they allow easy access to habitats that share similarities with continental shelf or deep-sea communities found in the open ocean (Bernd, 1993; Sweetman and Witte, 2008; Storesund et al., 2017). Their accessibility allows researchers to study the influence of abiotic factors on the shelf or deep-sea community ecology whilst reducing the limitations of cost and transportation that is often problematic for deep-sea research.

It is well documented that fjord communities are influenced by both the coast-fjord and/or depth gradients (Buhl-Mortensen and Høisaeter, 1993; Holte et al., 2004; Włodarska-Kowalczuk and Pearson, 2004; Storesund et al., 2017; Molina et al., 2019). The interaction between the ocean water and the fjord system helps carry seawater into the fjord, which aids in the distribution of fauna, organic nutrients, and inorganic material (Buhl-Mortensen and Høisaeter, 1993; Holte et al., 2004). However, within silled-fjords, the exchange of seawater between the coastal and fjord systems is reduced. The sill height, fjord topography, and freshwater input influences the transport of nutrients, pelagic larvae, organic matter, and dissolved oxygen, where benthic communities toward the inner fjord regions are negatively impacted due to the decreased access to resources (e.g., dissolved oxygen, organic carbon, nutrients) (Buhl-Mortensen and Høisaeter, 1993; Blanchard et al., 2010; Storesund et al., 2017). Density stratification between upper and bottom water masses is often observed and the inner basin(s) below the sill depth becomes isolated from the adjacent coastal system. This stratification leads to relatively stable temperatures and salinities within the basins (Renaud et al., 2007; Drewnik et al., 2016; Molina et al., 2019). With limited mixing within the water column, dissolved oxygen levels tend to decrease with depth, distance from the sill, and over time until a renewal event occurs, whereby more oxygenated ocean water mixes with fjord water. In general, faunal diversity and species richness is seen to decrease with increasing distance from the coastal regions and increasing water depth (Buhl-Mortensen and Høisaeter, 1993; Holte et al., 2004; Molina et al., 2019).

Deep-water stagnation is thought have a major influence on fjord basin communities, where lower oxygen concentrations can negatively impact the community structure and species composition (Blanchard et al., 2010; Molina et al., 2019), resulting in lower species richness with lower oxygen levels (Buhl-Mortensen and Høisaeter, 1993). In periods of hypoxic and anoxic conditions, where the oxygen concentration is <2.1 mL L^{-1}, defaunation of macrofauna and changes in faunal assemblages have been observed within the basin (Holte et al., 2005; Molina et al., 2019). In extreme cases of deoxygenation and strong stratification, a rise of acidification within fjord basins can occur (Jantzen et al., 2013), particularly if water exchange with adjacent coastal systems is insufficient.

Sognefjord is Norway's longest and deepest fjord. It is host to numerous towns and villages and has become a sought-out destination for many cruise ships, where thousands of tourists visit the fjord each year. There is concern on how these anthropogenic influences impact the fjord's marine habitat (Manzetti and Stenersen, 2010). Numerous studies in recent years have been conducted primarily on the microbial community (Poremba and Jeskulke, 1995; Storesund et al., 2017) or the influence of phytodetrital pulses on the macrofaunal community (Witte et al., 2003). Despite the accessibility of Sognefjord, the epibenthic megafauna community has been poorly studied, especially in recent years (Bernd, 1993). Bernd (1993) found that the central fjord and shallower adjacent side-fjord, Høyangsfjord, were primarily dominated by soft-bottom dwelling burrowing decapods (*Munida sarsi* and *Munida tenuimana*), holothurians (*Bathyplotes natans* and *Parastichopus tremulus*), and anthozoans. Høyangsfjord was found to have a lower megafaunal density compared to the main fjord. However, besides depth and general observations of substrate type, no thorough analysis was conducted on the influence of abiotic variables on the megafaunal community, especially over a horizontal or vertical gradient. In recent years several expeditions by the University of Bergen and the Institute for Marine Research in Norway, have taken place in the main- as well as the side-fjords, and knowledge about the fauna and benthic communities in Sognefjord is expected to increase rapidly when new data are made available over the coming years (Buhl-Mortensen et al., 2017; H. Glenner, personal communication).

In the present study, we used visual data collected with the remotely operated vehicle (ROV) *AEgir 6000* to investigate the benthic megafaunal community diversity and distribution in Sognefjord and the influence of abiotic variables on the community structure at two locations in the fjord. It is expected that the communities would be less diverse and dense with increasing distance from the sill due to the extremely stable conditions identified by Storesund et al. (2017) (see the section "Study Area" for site description). For this study, we had three main objectives: (1) characterize the benthic community structure based on their depth and distance from the sill, (2) detect any response in community structure and diversity to changes in water mass characteristics above and below the sill, and (3) examine the relationships between environmental conditions and community composition and diversity (using generalized linear models, or GLMs).

MATERIALS AND METHODS

Study Area

Sognefjord is located on the western Norwegian coast, extends to about 205 km and has a maximum water depth of 1308 m (Poremba and Jeskulke, 1995; Storesund et al., 2017). The fjord has a 3-layer water column structure (Svendsen, 2006; Storesund et al., 2017): the top layer is brackish water (salinity $\leq$ 33 psu), formed by the mixture of freshwater runoff and seawater, and moves out of the fjord; the intermediate layer (salinity between 33 and 35 psu) is well-oxygenated, owing to exchanges with the Norwegian Coastal Current above the sill depth, and hosts compensatory flows that may be in-fjord or out-fjord; and the bottom, or basin, water below the sill depth (salinity $>$ 35 psu after deep-water renewal) originates from Atlantic water and becomes gradually less dense between renewal events because

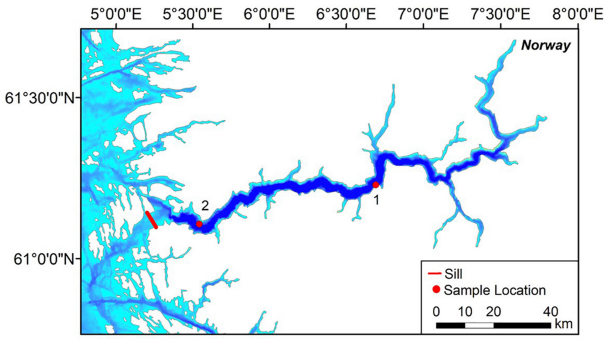

FIGURE 1 | Location of the two *AEgir 6000* transects in Sognefjord, Norway. Digital bathymetry with a resolution of 1/16 × 1/16 arc min was extracted from EMODnet Bathymetry Consortium (2018). ArcGIS (version 10.4; Environmental Systems Research Institute [ESRI], 2016) was used to map the transects.

of diffusion and mixing with the layer above, driven by tidal forcing. Whilst the shallow sill (170 m) at the mouth of the fjord allows for some exchange of water between the fjord system and the adjacent coastal water, the mixing is fairly reduced and strong stratification occurs because of the influx of terrestrial runoff (Storesund et al., 2017). Renewal of the basin water occurs approximately every 8 years (Buhl-Mortensen et al., 2020).

Conditions within the fjord basin below sill depth are fairly stable and homogeneous. Water temperature is consistently around 7.4°C and the salinity is generally greater than 35.0 psu (Witte et al., 2003; Storesund et al., 2017). Oxygen concentrations have been found to decrease with increasing distance from the sill and with depth, where Storesund et al. (2017) found the inner fjord and lower basin water to have oxygen concentrations below 4.5 mL L^{-1} in May and November 2012.

Data Collection

Two video transects were performed with the work-class ROV *Ægir 6000* in Sognefjord in July 2017 during a SponGES cruise with the R.V. *G.O. Sars* (**Figure 1**). Dive 1 (D1) was conducted within the central fjord (1155 – 85 m; 61° 6′ N, 6° 39′ E) and Dive 2 (D2) was located near the sill (1230 – 55 m; 61° 3′ N, 5° 22′ E), respectively. D1 and D2 had approximate transect lengths of 2.43 km and 1.39 km, and were located approximately 79 km and 17 km away from the sill, respectively. The approximate fjord side slopes for D1 and D2 are 43° and 44° inclined to the horizontal plane. Physical samples were collected by the ROV during the transects to help confirm identifications of fauna.

One ship-based conductivity–temperature–depth (CTD) sensor package cast was conducted for each transect to profile temperature (°C), salinity (psu), dissolved oxygen (mL L^{-1}) and chlorophyll *a* concentration (μg L^{-1}) throughout the water column. The bottom depths of the CTD casts corresponding to D1 and D2 were 1017 m and 1223 m, respectively. In addition, water samples were collected (using a rosette water sampler, on which the CTD package was mounted) from the different water masses for nutrient analysis. From the video footage, the percent cover of exposed hard substrate and soft sediment was estimated for each image analyzed.

Nutrient Content Analysis

Seawater samples for the analysis of inorganic dissolved nutrients (Si, PO_4, NH_4, NO_3, and NO_2) were collected with the CTD-rosette from selected depths. Sample depths were selected based on the profile of the CTD downcast, whereby samples were collected from five different depths. Subsamples were collected in 50 mL syringes, which were rinsed three times with water from the niskin bottles of the CTD rosette before being filled. After sampling on deck, samples were filtered through 0.2 μm filters and instantly sub-sampled into two vials, one of which was used for samples of ortho-phosphate (PO_4), ammonium (NH_4), nitrate (NO_3), and nitrite (NO_2), stored at −20°C and the other for silicate (Si), stored at 4°C. Nutrients were analyzed at NIOZ with a QuAAtro Gas Segmented Continuous Flow Analyzer. Measurements were made simultaneously on four channels for PO_4 (Murphy and Riley, 1962), NH_4 (Helder and De Vries, 1979), NO_2, and NO_3 (Grasshoff et al., 1983). Si was measured during a separate run (Strickland and Parsons, 1968). All measurements were calibrated with standards diluted in low nutrient seawater. For a detailed description of the sampling procedure we refer to Roberts et al. (2018).

Video Annotation

Still images were extracted from the videos approximately every 30 s to ensure there was no spatial overlap between images during analysis. Due to fluctuations in ROV altitude and changes in turbidity or topography, some areas of the transects were not suitable for analysis. Images were excluded if they contained any of the following characteristics: (1) image area obscured by part of the ROV or suspended material, (2) ROV was collecting physical specimens, (3) ROV was too far from the substrate (>10 m), (4) camera angle was not seabed-facing, (5) image contained poor light visibility, (6) image was blurred, and (7) overlapping image area. Videos were rescanned during image annotation to help identify individuals that were difficult to decipher in the stills alone, and in some cases, new stills were extracted if a more suitable image was present ±5 s from the original still. This was mostly the case for images that were blurred or contained poor light visibility and more suitable images of the same area were available within 5 s of the original image extracted. Parallel lasers of known separation (which project spots onto the seabed in order to determine image scale) were only active for the first hour of D1. It was therefore not possible to determine area (m^2) and density (individuals m^{-2}) for the survey and megafauna were enumerated based on individuals per image.

ImageJ (version 1.52) was used to annotate the extracted imagery. A virtual grid with 496 cells was overlaid on each image in ImageJ. The grid size was selected because the cells completely overlapped the images. Percent cover of substrate type was estimated by counting the number of grid cells that contained that particular substrate type, then calculating the percentage of the total number of grid cells represented by that value. The grid resolution was selected such that the cells were small enough to minimize the number containing multiple substrate types as

a proportion of total number of cells (and thereby increase the precision in the percent cover estimates) and large enough that the gridlines were not so dense as to obscure the fauna present in the image. In cases where cells contained multiple substrate types, the cell was characterized as the substrate that covered more than half of the cell. All epibenthic megafauna individuals that were easily visible within the imagery were counted and identified to the lowest taxonomic level. Due to fluctuations in altitude during video transects, some fauna had to be identified based on gross morphology (e.g., white sponge 1, yellow sponge 2, etc.). Taxa were classified as rare if represented by three or less individuals.

Statistical Analysis

Data Preparation

Based on the description of the Sognefjord water mass structure by Storesund et al. (2017), the biotic and abiotic data were assigned to three depth zones to identify any depth-related changes in the benthic community structure: "Above Sill" ($\leq$170 m), "Intermediate" (>170 to $\leq$300 m), and "Basin" (>300 m). No data from the surface brackish top-layer (1–10 m) was included. Due to differences in sampling frequency between the CTD profiling and image annotation, the abiotic variables were interpolated at 10 m depth intervals in Rstudio (version 1.2.5; RStudio Team, 2019). Nutrient composition was sampled with low frequency and was thereby excluded from statistical analysis. The megafauna abundances were summed into 10 m depth intervals. To account for missing data in the biotic dataset, certain depth intervals were removed from the abiotic dataset prior to statistical analysis. All multivariate statistical analysis was conducted in Primer (version 7) unless otherwise specified.

Environmental Variables

The environmental variables of D1 (central) and D2 (near-sill) were plotted against each other (e.g., temperatures from D1 vs. temperatures, at corresponding depths, from D2) to identify any notable differences in abiotic conditions between dives (**Supplementary Figure S1**). Furthermore, a correlation matrix was generated in Rstudio with package "corrplot" (version 0.84; Wei and Simko, 2017) to identify which abiotic variables were correlated (**Supplementary Figure S2**). Temperature had a strong negative correlation with salinity and positive correlation with dissolved oxygen (rho > 0.9), and was thereby dropped from further analysis. While depth was significantly correlated with the majority of the abiotic variables (p-value < 0.05) and had a moderately strong positive correlation with salinity and negative correlation with dissolved oxygen (rho > 0.7), it was selected to remain since it often acts as a proxy for other abiotic variables that were not measured in the present study. The remaining variables were normalized in Primer prior to multivariate analysis due to the different units used for each variable. A principal component analysis (PCA) of the selected abiotic variables was used to examine the environmental conditions within each depth zone per dive.

Community Composition and Diversity

Due to the lack of lasers throughout most of the dives, the abundances were converted to presence-absence data. A Sørensen similarity matrix between the two dives was calculated on the presence-absence dataset. Non-metric multidimensional scaling (nMDS) plots were constructed for each dive to identify differences between the community structure within each depth zone. An analysis of similarities (ANOSIM) was generated to identify significant differences between the depth zones and dives. SIMPER was used to determine which taxa were considered indicator organisms for each depth zone.

Diversity indices such as species richness and Shannon-Wiener diversity were calculated from the megafauna presence-absence data for the depth zones in both dives to compare the changes in species richness and diversity over the vertical and horizontal gradients. In SPSS (version 25), a Levene's test of homogeneity of variances was used to determine if the diversity indices were homogeneous prior to running a one-way analysis of variance (ANOVA) to determine if there were significant differences for each index. A Tukey honestly significant difference (HSD) *post hoc* test on the diversity indices was used to identify which depth zones were significantly different for each dive.

To examine which environmental variables best explained the variance in species richness and Shannon-Wiener diversity indices, GLMs were generated in Rstudio. The residual deviance was larger than the residual degrees of freedom, therefore a quasi-Poisson error was fitted to the GLMs to account for overdispersion (Zuur et al., 2009). Depth, salinity, dissolved oxygen, chlorophyll *a*, percent cover of exposed hard substrate and soft sediment were included in the GLMs.

RESULTS

Environmental Conditions

In general, the water was slightly warmer, more saline, and more oxygenated in the water column below the sill at D2 (near-sill), relative to the same depths in D1 (central). The top layer of water was made up of warm brackish water (**Figure 2**), and a sub-surface chlorophyll maximum occurred at the halocline between the brackish surface water and intermediate water (approximately at 20 to 30 m). At approximately 80 to 100 m, dissolved oxygen decreased. Dissolved oxygen levels recovered in the intermediate water just below the sill depth. There was a gradual transition between the intermediate water mass and basin water until about 300 m, where a drop in temperature and dissolved oxygen levels occurred. The basin water was fairly homogeneous and there was not much difference in the water properties between the dives, where temperature was around 7.5°C, salinity at 35.06 psu, and dissolved oxygen around 4.2 mL L^{-1}. D1 was frequently covered in soft sediment with exposed hard substrate patches throughout the transect, whereas D2 had distinct regions of solely soft sediment (e.g., bottom of fjord basin) and exposed hard substrate (e.g., along slopes and cliffs). Within the Intermediate Zone, small boulders and rocks became more frequent, and the sediment type became more coarse.

Inorganic nutrient concentrations increased with depth (**Table 1**), showing highest concentrations below 450 m water depth, while lowest concentrations were measured in surface

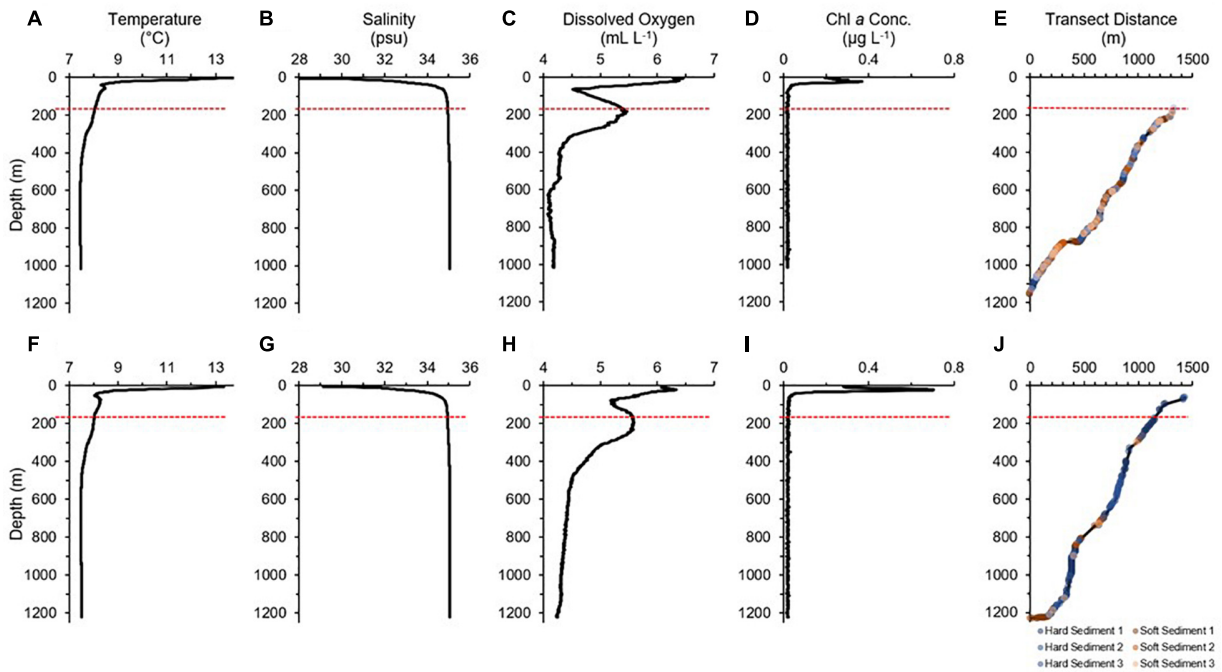

FIGURE 2 | CTD profiles and substrate type for Dive 1 **(A–E)** and Dive 2 **(F–J)** in Sognefjord, Norway. Red dashed line indicates the approximate sill depth (170 m). In **(E,J)**, sediment type 1 to 3 correspond with percent cover, where 1 = 100–91%; 2 = 90–71%; 3 = 70–51%.

TABLE 1 | Concentration of nutrients over depth for Dive 1 (central) and Dive 2 (near-sill) in Sognefjord, Norway.

Dive	*Depth (m)*	*Si* (µmol L(1L-1))	PO_4 ($\mu mol\ L^{-1}$)	NH_4 ($\mu mol\ L^{-1}$)	NO_3 ($\mu mol\ L^{-1}$)	NO_2 ($\mu mol\ L^{-1}$)
1	1028	16.67	1.158	0.202	14.87	0.034
	799	16.85	1.161	0.139	15.05	0.017
	500	14.63	1.114	0.135	14.95	0.019
	150	6.223	0.778	0.153	11.11	0.108
	6	0.153	0.046	0.139	0.135	0.066
2	1237	16.78	1.144	0.221	14.41	0.077
	800	14.52	1.091	0.173	14.39	0.028
	500	13.49	1.07	0.172	14.04	0.034
	150	5.46	0.726	0.112	10.48	0.021
	10	0.097	0.033	0.119	0.073	0.036

waters at both sites. Nutrient concentrations did not show large differences between the two sites.

In D1, from the suspended particulates observed in the video footage, predominately vertical settling appeared to occur. In these regions, sessile fauna and vertical rock walls were covered with a fine layer of particulate matter. However, D2 had higher observed turbidity throughout the dive compared to D1, with the settling of particulate matter apparent and some evidence of horizontal flow based on the position of the feeding apparatus of filter feeders and particulate direction changes.

In the PCA ordination, the first two principal components (PC) represented approximately 76% of the environmental variability within the two dives combined (47.1% and 28.6% for PC1 and PC2, respectively) (**Figure 3**). The PCA ordination showed that the images within the Basin Zones of both D1 and D2 were clearly distinguishable from the Intermediate and Above Sill Zones along the axes of PC1 and PC2. Dissolved oxygen (Eigenvector = 0.503), salinity (Eigenvector = −0.498), and depth (Eigenvector = −0.490) had the strongest influence on PC1. Percent cover of soft sediment (Eigenvector = −0.623) and exposed hard substrate (Eigenvector = 0.613) most strongly influenced PC2.

Sognefjord Megafauna Composition

In total, D1 had 79 taxa with a total of 11557 individuals and D2 had 89 taxa with a total of 10615 individuals (**Table 2**). After rare taxa were excluded from the dataset, there was a total of 22105 individuals and 72 taxa identified within 511 images, where D1 had 11528 individuals and 57 taxa and D2 had 10577 individuals and 63 taxa. Porifera made up the majority of the taxa (24),

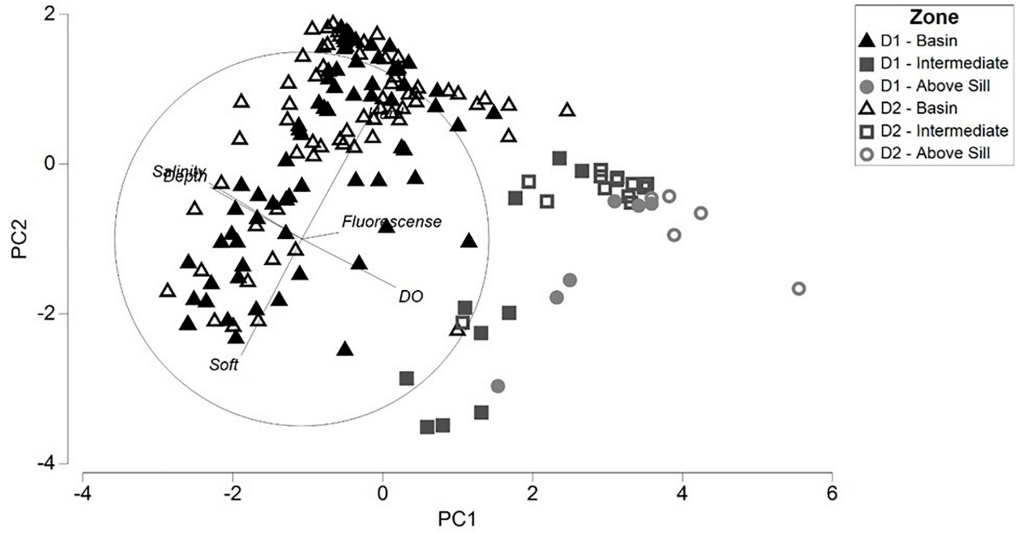

FIGURE 3 | Principal component plot of the abiotic variables for the depth zones within Dive 1 (closed) and Dive 2 (open), with the direction of the respective abiotic variables and their component score influence.

followed by Echinodermata (16), and Cnidaria (10). The Above Sill Zone for both D1 and D2 had the lowest total abundances and number of species compared to the other zones.

The top 10 most abundant taxa for D1 were White Encrusting Sponge 1, *Psolus squamatus* (O.F. Müller, 1776), *Hymedesmia* sp., Brachiopoda 1, *Munida tenuimana* Sars, 1872, *Gracilechinus acutus* (Lamarck, 1816), *Polymastia nivea* (Hansen, 1885), *Gracilechinus elegans* (Düben & Koren, 1844), Yellow Encrusting Sponge 1, and *Stylocordyla borealis* (Lovén, 1868). For D2, the top 10 most abundant taxa were the White Encrusting Sponge 1, Echinoidea 1, *P. squamatus*, *Hymedesmia* sp., *G. acutus*, *M. tenuimana*, Yellow Encrusting Sponge 1, *G. elegans*, *Acesta excavata* (Fabricius, 1779), and *Phakellia* spp.

Community Trends and Observations

Within the Basin Zone, exposed hard substrate was often covered with polychaete tubes, the bivalve *A. excavata*, cnidarians, and encrusting sponges (**Figure 4**). *Acesta excavata* was present in high densities when observed on vertical rocky walls, often with juveniles and dense accumulations of encrusting polychaetes nearby. The octocoral *Anthomastus grandiflorus* (Verril, 1878) (**Figure 4b**) and large glass sponges *Asconema* aff. *foliatum* (Fristedt, 1887) (**Figure 4e**) occurred only on vertical rock walls. In D1, *A.* aff. *foliatum* was covered by a fine layer of suspended particulate matter (**Figure 4e**).

Soft bottom areas were characterized by the enigmatic asteroid *Hymenodiscus coronata* (Sars, 1871), *M. tenuimana*, *Bathyplotes natans* (Sars, 1868), *Mesothuria intestinalis* (Ascanius, 1805), *Psilaster andromeda* (Müller & Troschel, 1842), small patches of *Kophobelemnon stelliferum* (Müller, 1776) and carnivorous sponges, and in rare cases, *Virgularia mirabilis* (Müller, 1776). Signs of lebensspuren such as burrows containing *M. tenuimana* within or nearby were observed throughout both dives (**Figures 4n,p**).

In regions with mixed substrate types (e.g., exposed hard substrate and soft sediment), *Psolus squamatus* was often observed concentrated at breaks in the slope or protruding surfaces. *Phakellia* spp., *Phakellia ventilabrum* (Linnaeus, 1767), and *Axinella infundibuliformis* (Linnaeus, 1759) were commonly positioned along slopes, aligned with the direction of observed horizontal particle flow (**Figure 4m**). Large anemones like *Bolocera tuediae* (Johnston, 1832) were observed residing on exposed hard substrate walls with soft sediment surrounding the substrate.

In the Intermediate and Above Sill Zone of D2, it should also be noted that there was a sudden occurrence of Echinoidea 1 in large quantities (max. 859 individuals per image) from 240 m to 60 m water depth (**Figure 4u**). For D2, the Above Sill Zone had a higher proportion of echinoderms present (**Figures 4v,y**). Numerous fish species, including *Chimaera monstrosa* (Linnaeus, 1758), *Sebastes viviparus* (Krøyer, 1845) (**Figure 4v**), and *Coryphaenoides rupestris* (Gunnerus, 1765), were observed within the upper regions of D1 and D2. Anthropogenic waste was found in the D1 Above Sill Zone (**Figure 4w**).

Community Structure

The community composition of the non-rare taxa showed significant differences between the depth zones and dives (ANOSIM Global R: 0.261, $p = 0.001$) (**Figure 5**). For D1, the nMDS plots and pairwise ANOSIM test indicated that the Basin and Intermediate Zones shared a similar community composition ($p > 0.05$). All other zones showed significant differences in community composition.

The SIMPER analysis revealed that for both dives, all zones except for D2-Above Sill had *P. squamatus*, *Hymedesmia* sp., and White Encrusting Sponge 1 within the top five contributing taxa (**Table 3**). Taxa from the Echinodermata were more common in D2 than D1. For both dives, the Basin and Above Sill

TABLE 2 | The presence (x) of all megafauna within each depth zone for Dive 1 (left) and Dive 2 (right) in Sognefjord, Norway.

				D1				*D2*			
Phylum	***Class (subclass*)***	***Taxon***	**Figure 4 *plate #***	***Basin***	***Intermediate***	***Above sill***	***Total %***	***Basin***	***Intermediate***	***Above sill***	***Total %***
Annelida	Echiura*	*Bonellia viridis* (Rolando, 1822)*	j	x			0.03				
		Maxmuelleria faex (Selenka, 1885)		x			0.17	x	x		0.16
	Sedentaria*	Serpulidae 1		x	x	x	0.36	x			0.22
		Serpulidae 2**	g					x			0.05
		Serpulidae 3**						x			0.01
	Undetermined	**Polychaeta 1***		x			0.03				
Arthropoda	Malacostraca	*Munida tenuimana* Sars, 1872	b, n, o, p	x	x		3.89	x			3.16
		Decapod 1	g	x	x		0.43	x			0.24
		Decapod 2		x			0.09		x		0.01
		Decapod 3**						x	x		0.21
		Decapod 4**						x			0.05
		Decapod 5*		x	x		0.03				
		Decapod 6		x	x		0.13	x			0.01
Brachiopoda		Brachiopoda 1	i	x	x		8.85	x			0.53
Chordata	Ascidiacea	Ascidiacea 1*		x			0.08				
	Holocephali	***Chimaera monstrosa* (Linnaeus, 1758)**		x			0.01		x		0.02
	Actinopterygii	***Sebastes viviparus* (Krøyer, 1845)****	v						x		0.02
		Coryphaenoides rupestris* (Gunnerus, 1765)*						x			0.01
	Undetermined	**Pisces 1***		x			0.01				
		Pisces 2*			x		0.01				
		Pisces 3**	x							x	0.01
		Pisces 4**								x	0.02
Cnidaria	Hexacorallia*	*Bolocera tuediae* (Johnston, 1832)		x	x		0.34	x	x		0.18
		Sagartia sp.	k	x	x		0.86	x			0.75
		Protanthea simplex* (Carlgren, 1891)*						x			0.01
		Actiniaria 1	h, s	x	x	x	0.35		x		0.07
		Actiniaria 2*		x			0.11				
		Actiniaria 3**						x	x		0.84
		Actiniaria 4**						x			0.04
		Actiniaria 5**								x	0.05
		Actiniaria 6**						x			0.12
	Octocorallia*	*Anthomastus grandiflorus* (Verrill, 1878)	b	x			0.29	x			0.34
		Kophobelemnon stelliferum (Müller, 1776)	q	x			0.08	x	x		0.03
		Virgularia mirabilis* (Müller, 1776)	r	x			0.01				
		Octocorallia 1**						x			0.02
		Octocorallia 2**						x			0.02
		Octocorallia 3*		x			0.02				
Echinodermata	Asteroidea	*Ctenodiscus crispatus* (Bruzelius, 1805)*		x	x	x	0.04				
		Henricia spp.		x	x	x	0.06	x	x	x	0.44
		Hymenodiscus coronata (Sars, 1871)	o	x			0.17	x			0.34

(Continued)

TABLE 2 | Continued

				D1				D2			
Phylum	***Class (subclass*)***	***Taxon***	**Figure 4 *plate #***	***Basin***	***Intermediate***	***Above sill***	***Total %***	***Basin***	***Intermediate***	***Above sill***	***Total %***
		Poraniomorpha (Poraniomorpha) hispida* (M. Sars, 1872)*	f					x			0.01
		Pseudarchaster parellii (Düben & Koren, 1846)**							x	x	0.07
		Psilaster andromeda (Müller & Troschel, 1842)		x	x		0.04	x			0.01
		Pteraster militaris (O.F. Müller, 1776)		x	x	x	0.15	x	x	x	0.09
		Pteraster* sp.*						x			0.01
		Asteroidea 1	c	x			0.02	x			0.02
		Asteroidea 2**						x	x		0.02
		Asteroidea 3	i	x			0.01	x			0.02
		Asteroidea 4				x	0.01	x	x		0.02
		Asteroidea 5**						x		x	0.02
	Echinoidea	*Gracilechinus acutus* (Lamarck, 1816)	t, v, y	x	x	x	2.30	x	x	x	5.62
		Gracilechinus elegans (Düben & Koren, 1844)	s, x	x	x	x	1.83	x	x	x	1.26
		Echinoidea 1**	u					x	x	x	21.35
	Holothuroidea	*Bathyplotes natans* (M. Sars, 1868)		x			0.48	x			0.06
		Mesothuria intestinalis (Ascanius, 1805)		x	x		0.53	x			0.14
		Parastichopus tremulus (Gunnerus, 1767)	l, p, y	x	x	x	0.54	x	x	x	0.67
		Psolus squamatus (O.F. Müller, 1776)	e, j, m	x	x	x	23.09	x	x	x	19.31
	Ophiuroidea	*Ophiura albida* (Forbes, 1839)	g	x			0.02	x			0.03
		Ophiuroidea 1		x	x		0.37	x	x		0.18
		Ophiuroidea 2*		x			0.01				
		Ophiuroidea 3		x			0.01	x			0.01
Mollusca	Bivalvia	*Acesta excavata* (Fabricius, 1779)	d	x			0.11	x			1.27
	Polyplacophora	Polyplacophora 1*		x			0.01				
		Polyplacophora 2**						x			0.01
Porifera	Demospongiae	*Axinella infundibuliformis* (Linnaeus, 1759)	f	x		x	0.22	x	x		0.24
		Axinella rugosa (Bowerbank, 1866)		x	x		0.16	x			0.08
		Haliclona (Haliclona) urceolus (Rathke & Vahl, 1806)	t	x	x		0.90	x			0.25
		Hexadella dedritifera (Topsent, 1913)	g	x		x	0.01	x	x		0.84
		Hymedesmia sp.	g	x	x	x	11.34	x	x	x	7.98
		Phakellia ventilabrum (Linnaeus, 1767)	x	x	x	x	0.62	x	x		0.13
		Phakellia spp.	s, w	x	x	x	0.50	x			1.06
		Polymastia nivea (Hansen, 1885)		x	x	x	2.14	x	x		0.59
		Stryphnus fortis* (Vosmaer, 1885)		x			0.01				
		Stylocordyla borealis (Lovén, 1868)		x	x		0.97	X			0.14
		Thenea sp.*		x			0.02				
		Carnivorous Sponge 1*		x			0.04				
	Hexactinellida	*Asconema* aff. *foliatum* (Fristedt, 1887)	e	x			0.01	x			0.04
	Undetermined	**Orange Encrusting Sponge 1****						x			0.03
		White Encrusting Sponge 1	b, g	x	x	x	32.21	x	x	x	26.66
		Yellow Encrusting Sponge 1	g	x	x	x	1.48	x	x	x	2.26

(Continued)

TABLE 2 | Continued

				D1				D2			
Phylum	***Class (subclass*)***	***Taxon***	**Figure 4 *plate #***	***Basin***	***Intermediate***	***Above sill***	***Total %***	***Basin***	***Intermediate***	***Above sill***	***Total %***
		Brown Globular Sponge 1		x	x		0.09		x		0.01
		White Globular Sponge 1		x	x		0.17	x			0.06
		White Globular Sponge 2		x			0.03	x			0.03
		White Globular Sponge 3**						x			0.14
		Infundibuliform Sponge 1		x			0.02	x			0.02
		Infundibuliform Sponge 2		x	x		0.41	x			0.14
		Infundibuliform Sponge 3		x	x		0.03	x			0.03
		Infundibuliform Sponge 4**						x			0.01
		White Massive Sponge 1		x	x	x	0.72		x		0.03
		White Massive Sponge 2		x			0.12	x			0.05
		White Massive Sponge 3**						x			0.05
		Yellow Massive Sponge 1**						x			0.04
		Stalked Sponge 1		x	x		0.73	x			0.11
		White Verrucose Sponge 1**	a					x			0.08
		Indet Sponge 1*			x		0.01				
		Indet Sponge 2*		x			0.02				
		Indet Sponge 3*		x			0.02				
		Indet Sponge 4*		x			0.01				
Other		Unidentified 1*		x			0.13				
		Unidentified 2		x			0.04	x			0.01
		Unidentified 3		x		x	0.07	x			0.03
		Unidentified 4*		x			0.07				
		Unidentified 5*		x	x		0.54				
		Unidentified 6		x			0.05	x			0.31
		Unidentified 7**						x			0.14
		Unidentified 8**						x			0.06
		Unidentified 9*		x			0.01				
		Unidentified 10*		x			0.02				
		Unidentified 11*		x		x	0.03				
		Unidentified 12**						x			0.01
		Unidentified 13**						x			0.03
		Unidentified 14**						x			0.01
		Unidentified 15**						x			0.02
		Unidentified 16**						x			0.01
		Total abundance		9676	1449	432	11557	6837	3191	587	10615
		Total number of species		76	37	21	79	79	28	15	89
		Total number of images		275	32	13	320	165	18	8	191

*Total percentage (%) is the percentage of total abundance for each respective taxon. Asterisks denotes morphotaxa that were only observed within one dive, where * = Dive 1 and ** = Dive 2. Highlighted taxa are rare (<3 individuals) and dropped from statistical analyses.* ***Figure 4*** *plate reference indicates which* ***Figure 4*** *image plate that particular taxa can be found within. Bolded taxa are rare (<3 individuals) and dropped from statistical analyses.*

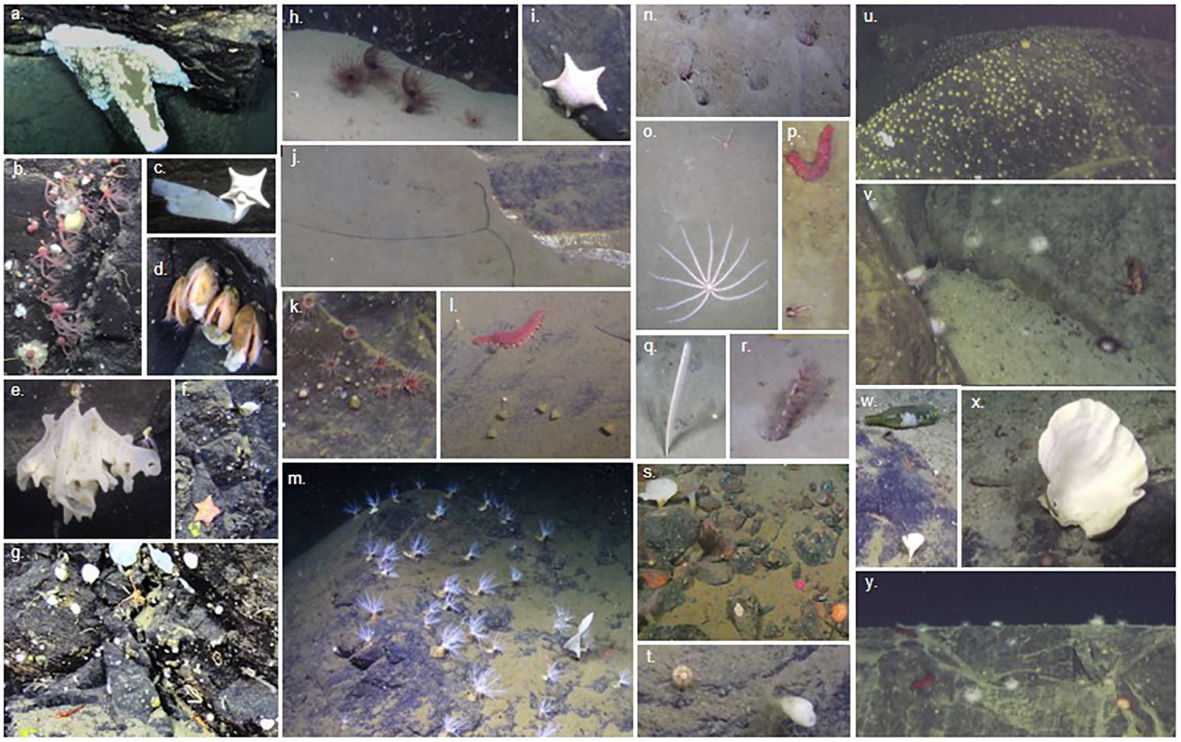

FIGURE 4 | Example of taxa and megafauna communities observed in Sognefjord, Norway. Panels **(a–g)** represents Basin Zone taxa on exposed hard substrate. Panels **(h–m)** displays Basin taxa in environments with both hard and soft substrate present. Panels **(n–r)** shows taxa common in soft sediment habitats. Panels **(s–u)** displays taxa within the Intermediate Zone. Panels **(v–y)** shows the Above Sill Zone. Refer to **Table 2** for the taxa identifications.

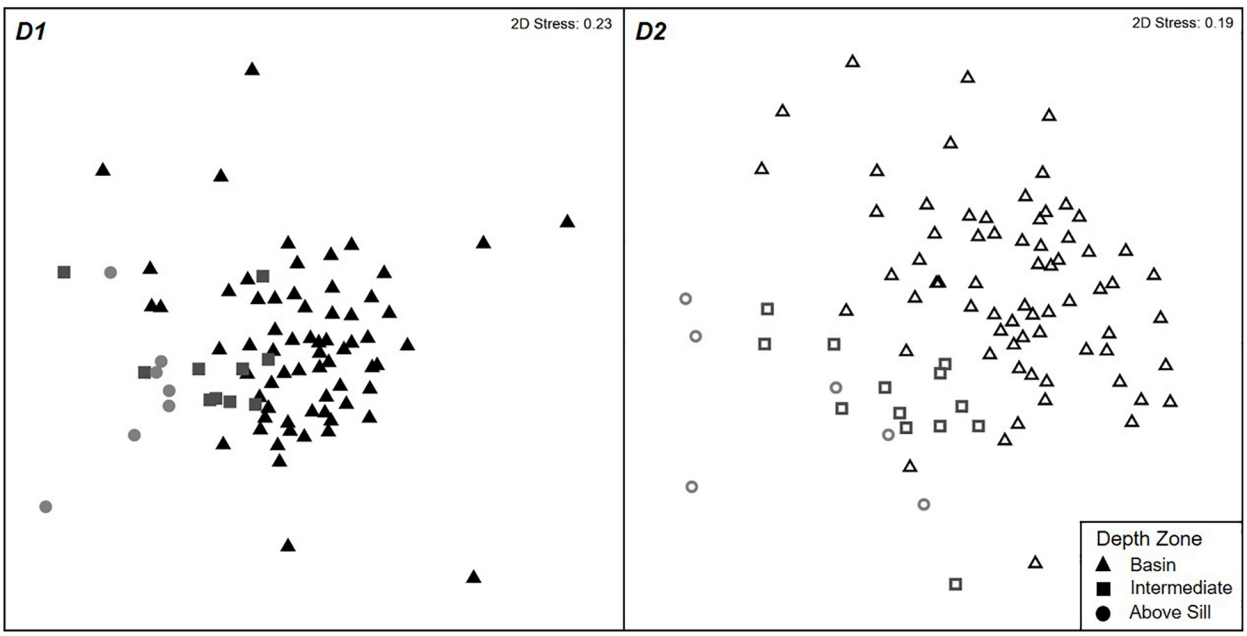

FIGURE 5 | Non-metric MDS ordination plots visualizing the Sørensen resemblances of the megafauna presence-absence data at different depth zones between Dive 1 (stress = 0.23; left) and Dive 2 (stress = 0.19; right). The distance between the points relates to the similarity of community composition at each depth, whereby the closer the points the more similar the community.

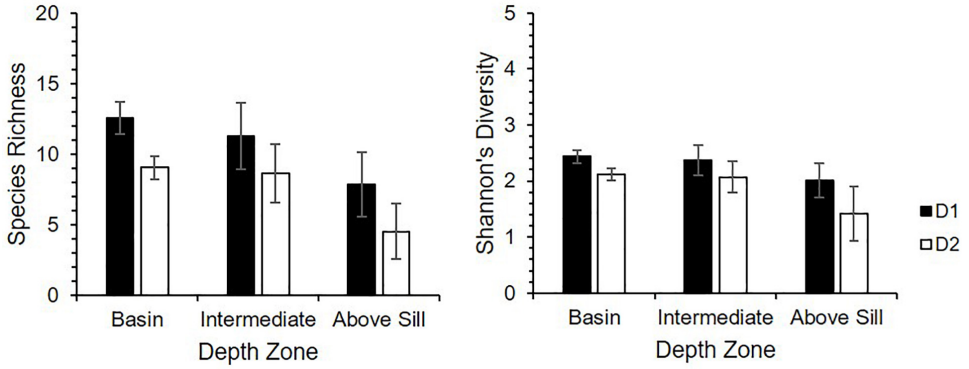

FIGURE 6 | Averaged diversity indices (species richness and Shannon-Wiener diversity index) per depth zone of the Dive 1 (D1; closed) and Dive 2 (D2; open) presence-absence community data in relation to the three depth zones in Sognefjord, Norway. Error bars represent 95% confidence intervals.

Zones had the largest difference in community composition (SIMPER, D1: Average dissimilarity = 63.03%; D2: Average dissimilarity = 78.87%). *Munida tenuimana*, *Parastichopus tremulus* (Gunnerus, 1767), Brachiopoda 1, *G. elegans*, and *Pteraster militaris* (O.F. Müller, 1776) contributed most to the differences between the Basin and Above Sill communities for D1. For D2, *M. tenuimana*, *P. squamatus*, *G. acutus*, *Hymedesmia* sp., and White Encrusting Sponge 1 contributed most to the differences between the two zones.

Diversity of Sognefjord's Megafauna Community

The diversity indices for the D2 (near-sill) zones were consistently lower than those of the corresponding zones in D1 (central) (**Figure 6**). For both dives, the diversity indices for the Above Sill Zones were lower than those of the deeper zones. The diversity indices all passed the Levene's test of homogeneity ($p > 0.05$), and the one-way ANOVA indicated that there were significant differences ($p < 0.001$) in the indices for D1 and D2 and their respective depth zones. The species richness and diversity were statistically significantly different between the D1 and D2 respective Basin Zones (Tukey HSD: $p < 0.01$). There was a significant difference in species richness between the Basin and Above Sill Zones for D1 (Tukey HSD: $p = 0.03$) and trend toward significant difference between the Basin and Above Sill Zones for D2 (Tukey HSD: $p = 0.069$). For the Shannon-Wiener diversity index, there was a significant difference between the Basin and Above Sill Zones for D2 (Tukey HSD: $p = 0.005$), and a significant difference between the Intermediate and Above Sill Zones (Tukey HSD: $p = 0.047$).

Environmental Influence on the Megafauna Community

Salinity and dissolved oxygen were the most influential variables on the diversity indices when considered separately, as revealed by GLMs (**Table 4** and **Supplementary Figure S3**), and depth had little influence alone. For species richness, the combination of depth and dissolved oxygen explained 10.85% of the deviance within the dataset. For diversity, the combination of depth, salinity, and dissolved oxygen explained 19.01% of the deviance in the dataset.

DISCUSSION

The present study provides a more recent overview of the Sognefjord megabenthic community composition than Bernd (1993) and focuses on the abiotic conditions more than was recently published by Buhl-Mortensen et al. (2017, 2020). The observations were similar to the findings from Bernd, where the deeper regions were characterized by sponges, holothurians and *Munida tenuimana*; however, in addition to sponges and holothurians, the shallower regions, particularly above the sill, had a higher abundance of urchins and anemones present.

Sognefjord shares some of the same fauna elements found in Hardangerfjord (Buhl-Mortensen and Buhl-Mortensen, 2014; Buhl-Mortensen et al., 2020). Both fjords are dominated by *Munida* sp., *Parastichopus tremulus*, *Psolus squamatus*, and *Phakellia* species. However, as stated by Buhl-Mortensen et al. (2020), and as was observed in this study, many of the taxa observed in Sognefjord are not present in Hardangerfjord.

As is common for fjord systems, many of the taxa observed are continental slope or deep-water species. For example, *Anthomastus grandiflorus* (Verril, 1878), which is considered a deep-sea species with a distribution of 457–1760 m (Molodtsova et al., 2008), was observed in small clusters on vertical rock walls at depths below 540 m, and *Kophobelemnon stelliferum* and *Virgularia mirabilis* (Müller, 1776) were both observed in low quantities in soft bottom regions at depths below 630 and 500 m, respectively. *Coryphaenoides rupestris* was observed in the Basin Zone of D2, a deep-water fish that has been found to have isolated subpopulations within Sognefjord (Delaval et al., 2018). A peculiar finding was the presence of very large specimens (up to 140 cm long) of the hexactinellid (glass) sponge *Asconema* aff. *foliatum* on vertical cliffs below 800 m depth at both dive sites, representing a group of species normally confined to deep and cold waters on the outer shelf off Northern Norway, or along the Reykjanes or Arctic Mid-Ocean Ridges (e.g., Tabachnick and Menshenina, 2007; Maldonado et al., 2016; Roberts et al., 2018).

TABLE 3 | Taxa responsible for the differences in the top 10 highest contributing megafauna within each zone identified in the similarity percentage analysis (SIMPER) for Dive 1 (Left) and Dive 2 (Right).

D1	*Morphotaxa*	*Sim/SD*	*%*	*Cumulative %*	*D2*	*Morphotaxa*	*Sim/SD*	*%*	*Cumulative %*
	Basin								
	*Psolus squamatus**	**1.99**	15.3	15.3		*Psolus squamatus**	**1.64**	20.2	20.2
	White Encrusting Sponge 1*	**1.78**	13.7	29.0		White Encrusting Sponge 1*	1.39	18.0	38.2
	*Munida tenuimana**	**1.67**	13.3	42.3		*Hymedesmia* sp.*	1.42	17.6	55.7
	Hymedesmia sp.*	**1.68**	12.3	54.6		*Munida tenuimana**	1.15	17.3	73.0
	Brachiopoda 1	0.91	7.8	62.4		Yellow Encrusting Sponge 1*	0.53	5.2	78.2
	Yellow Encrusting Sponge 1*	0.65	4.5	67.0		*Phakellia* spp.*	0.47	4.4	82.6
	Phakellia spp.*	0.63	4.5	71.5		*Gracilechinus acutus*	0.38	3.7	86.3
	Stylocordyla borealis	0.60	4.1	75.5		*Parastichopus tremulus*	0.23	1.6	87.9
	Haliclona (Haliclona) urceolus	0.56	3.6	79.2		Decapod 1	0.26	1.5	89.5
	Polymastia nivea	0.49	3.0	82.2		*Gracilechinus elegans*	0.26	1.5	91.0
	Intermediate								
	*Psolus squamatus**	**4.48**	16.6	16.6		*Parastichopus tremulus*	**1.99**	18.8	18.8
	White Encrusting Sponge 1*	**4.48**	16.6	33.1		White Encrusting Sponge 1*	1.4	15.2	34.1
	*Gracilechinus elegans**	**1.76**	13.4	46.5		*Gracilechinus acutus**	1.08	13.4	47.4
	Hymedesmia sp.*	**1.92**	12.0	58.5		*Psolus squamatus**	1.08	12.9	60.3
	Yellow Encrusting Sponge 1*	1.25	9.0	67.5		*Bolocera tuediae*	0.88	10.9	71.3
	Phakellia spp.	0.91	7.0	74.5		*Gracilechinus elegans**	0.87	9.7	81.0
	*Gracilechinus acutus**	0.91	6.8	81.3		*Hymedesmia* sp.*	0.73	6.8	87.7
	Polymastia nivea	0.69	4.8	86.1		Yellow Encrusting Sponge 1*	0.48	3.7	91.4
	Parastichopus tremulus	0.52	3.4	89.5		Echinoidea 1	0.36	3.5	94.9
	Haliclona (Haliclona) urceolus	0.53	3.2	92.6		Ophiuroidea 1	0.2	0.9	95.8
	Above Sill								
	White Encrusting Sponge 1*	**4.72**	23.4	23.4		*Gracilechinus acutus*	**3.55**	51.9	51.9
	Hymedesmia sp.*	**1.44**	16.0	39.4		Echinoidea 1	0.78	16.1	68.0
	*Parastichopus tremulus**	**1.46**	15.6	54.9		*Parastichopus tremulus**	0.46	12.7	80.7
	Gracilechinus elegans	**1.46**	15.6	70.5		Actiniaria 5	0.48	7.8	88.5
	Psolus squamatus	0.91	9.8	80.3		*Henricia* spp.	0.26	4.2	92.7
	Pteraster militaris	0.61	5.9	86.2		White Encrusting Sponge 1*	0.26	2.7	95.3
	Yellow Encrusting Sponge 1*	0.61	5.9	92.1		Yellow Encrusting Sponge 1*	0.26	2.4	97.8
	Phakellia spp.	0.62	5.2	97.2		*Hymedesmia* sp.*	0.26	2.2	100.0
	White Massive Sponge 1	0.22	1.1	98.4					
	Polymastia nivea	0.22	0.8	99.2					

Bolded taxa have the highest similarity (SIM)/standard deviation values (< 1.5). Asterisks (*) indicate taxa that were present in the respective depth zone for both dives.

Now we address each of this study's objectives in turn.

Community Patterns With Depth and Distance From the Sill

In general, much of the same taxa composition was observed in both dives for depth zones below the sill depth. The largest difference in megabenthic community composition was found between the deepest and shallowest zones for both dives, and similar trends have been observed in other surveys (Starmans et al., 1999; Sswat et al., 2015; Molina et al., 2019). In the present study, the Basin Zone was characterized more by sessile fauna (e.g., *P. squamatus, Acesta excavata, Hymenodiscus coronata*, and sponges) and *M. tenuimana*, whereas the Above Sill Zone was more dominated by echinoderms and anemones.

Contrary to numerous fjord and shelf-based studies (Buhl-Mortensen and Høisaeter, 1993; Holte et al., 2004; Webb et al., 2009; Włodarska-Kowalczuk et al., 2012; Sswat et al., 2015; Gasbarro et al., 2018; Molina et al., 2019), we find that communities at the shallowest depths (Above Sill Zone) and in closer proximity to the sill (D2) have the lowest number of species and diversity. Buhl-Mortensen et al. (2017, 2020) observed a similar trend in relation to the proximity to sill, where the outer region in Sognefjord had lower species richness compared to the middle region (Buhl-Mortensen et al., 2017, 2020). However, Buhl-Mortensen et al. (2020) observed a trend of decreasing species richness with increasing depth, which was not observed in the present study. The trends observed in the present study are more consistent with shelf community patterns observed by Starmans et al. (1999), where shallower regions contained a lower number of highly abundant taxa than the deeper stations and diversity increased with increasing water depth. This reduction in species richness and diversity in D2 (near-sill) and the areas above the sill could be driven by changes in water mass characteristics or increased physical stress on the

TABLE 4 | Summary statistics of the generalized linear models (GLMs) fitted to species richness and Shannon-Wiener diversity (Poisson distribution, quasi-Poisson error).

Diversity index	*Variable*	*Explained deviance*	*Residual deviance*	*% Explained*	*Pr(>|t|)*
Total number of species	Null		320.65		
	Depth (m)	0.99	319.66	0.31	0.461
	Salinity (psu)	14.75	305.90	4.60	0.006
	Dissolved oxygen (mL L^{-1})	22.13	298.52	6.90	0.001
	Chlorophyll *a* concentration (μg L^{-1})	0.00	320.65	0.00	0.980
	Exposed hard substrate (%)	5.31	315.34	1.66	0.089
	Soft sediment (%)	2.43	318.22	0.76	0.245
	Silicon (μmol L^{-1})	1.43	319.22	0.45	1.245
	Phosphate (μmol L^{-1})	0.43	320.22	0.13	2.245
	Ammonium (μmol L^{-1})	−0.57	321.22	−0.18	3.245
	Nitrate (μmol L^{-1})	−1.57	322.22	−0.49	4.245
	Nitrogen dioxide (μmol L^{-1})	−2.57	323.22	−0.80	5.245
	Best combination				
	Depth + dissolved oxygen	34.78	285.87	10.85	
Shannon-Wiener diversity	Null		21.09		
	Depth (m)	0.08	21.01	0.38	0.396
	Salinity (psu)	0.98	20.11	4.65	0.003
	Dissolved oxygen (mL L^{-1}	1.05	20.03	4.99	0.002
	Chlorophyll *a* concentration (μg L^{-1})	0.00	21.08	0.01	0.865
	Exposed hard substrate (%)	0.41	20.68	1.95	0.056
	Soft sediment (%)	0.02	21.07	0.08	0.712
	Silicon (μmol L^{-1})	1.43	319.22	0.45	1.245
	Phosphate (μmol L^{-1})	0.43	320.22	0.13	2.245
	Ammonium (μmol L^{-1})	−0.57	321.22	−0.18	3.245
	Nitrate (μmol L^{-1})	−1.57	322.22	−0.49	4.245
	Nitrogen dioxide (μmol L^{-1})	−2.57	323.22	−0.80	5.245
	Best combination				
	Depth + salinity + dissolved oxygen	2.07	19.01	9.83	

Percentage (%) explained is the percentage of null deviance in the data explained by the model.

benthic communities as the environmental conditions become less stable (Starmans et al., 1999; Jones et al., 2007).

Influence of Water Mass Properties and Sill Depth

The basin waters of both dives were fairly homogeneous (Storesund et al., 2017) and likely contributed to the homogeneity observed in the species composition in the deeper regions. Water mass properties (e.g., temperature, salinity, dissolved oxygen) play a significant role in megabenthic community composition (Buhl-Mortensen and Høisaeter, 1993; Williams et al., 2010: Meyer et al., 2015), which appears to be the case for Sognefjord as well. The changes in species composition appear to gradually occur around the transition between the basin and intermediate water masses, which is at approximately 300 m (Storesund et al., 2017), and more clearly near the sill depth. Studies have shown that sills affect water mass dynamics in ways that are critical to the structuring of benthic communities (Strømgren, 1970; Rüggeberg et al., 2011).

As Buhl-Mortensen and Høisaeter (1993) stated, the environment in fjord basins is influenced by the sill depth. With shallow sills, organic matter becomes trapped within the inner fjord below the sill depth and is not flushed out readily by the adjacent coastal water (Klitgaard-Kristensen and Buhl-Mortensen, 1999). As such, it is possible that organic input from renewal events and terrestrial sources (e.g., rivers, runoff, snowmelt, etc.) accumulates and has longer residence times in fjord basins (relative to shallower waters), providing food and nutrients to the benthic fauna below the sill depth. In a recent study of the Sognefjord by Buhl-Mortensen et al. (2020), the authors observed continuous detritus cover on sloping bedrocks at depths greater than 400 m and terrestrial organic material mixed in with the basin's soft sediment. The observed higher species richness and presence of deposit-feeding holothurians (*Bathyplotes natans* and *Mesothuria intestinalis*) and suspension-feeding *Hymenodiscus coronata* in the Basin Zone's soft bottom regions indicate availability of organic matter to the basin floor (Roberts and Moore, 1997; Flach et al., 1998; Amaro et al., 2015).

The vertical-falling particulate matter along the rocky walls observed in D1 is likely an important food source for many of the filter- and suspension-feeders (e.g., encrusting sponges, *Asconema* aff. *foliatum*, encrusting polychaetes, and *Acesta exacta*) residing on the vertical rock walls or under overhangs. Areas of flow acceleration owing to irregular topography (e.g., ridges, peaks, and other elevated substrate) experience increased

particle fluxes and are also likely important for suspension feeders (e.g., *Psolus squamatus*, *Phakellia* spp., *Phakellia ventilabrum*, and *Axinella infundibuliformis*) (Flach et al., 1998; Buhl-Mortensen et al., 2020). As is common in fjord environments, it is likely that the quality of food is lower in the basin and inner fjord compared to regions nearer to the sill (Klitgaard-Kristensen and Buhl-Mortensen, 1999). However, the higher species richness and presence of suspension- and deposit-feeders within the basin suggests the fauna may be adapted to the low quality of food, or that this is compensated by the stability of the basin environment. It is clear that a more rigorous study should be conducted to quantify and assess the quality of the organic matter supplied to the basin communities.

Environmental Dynamics

Depth, salinity, and dissolved oxygen were highlighted as important variables for the diversity indices. Depth acts as a proxy for other factors and it is likely that parameters which were not accounted for in the present study (e.g., food availability, particulate organic matter, localized hydrodynamics, pollution) are also influencing the patterns observed (Jones et al., 2007; Webb et al., 2009; Williams et al., 2010). Dissolved oxygen and percentage cover of substrate type varied most between the two dives, both of which are known to be critical for many benthic habitats (Holte et al., 2005; Williams et al., 2010; Sswat et al., 2015). The availability of hard substrate is important for sessile invertebrates (Williams et al., 2010; Buhl-Mortensen et al., 2012), and in this study, regions with exposed hard substrate were often covered with sponges, serpulid worm tubes, bivalves, and holothurians, similar to observations made by Gasbarro et al. (2018). However, for the Sognefjord megafauna community, there was not much difference in diversity and species richness between percent cover of hard substrate, soft bottom or mixed substrates. Therefore, it is possible that other factors like environmental dynamics or food availability is driving the patterns observed.

The megafauna communities at the mouth of the fjord (D2) showed lower diversity and species richness compared to central fjord (D1) communities. The central fjord environment is more stable than that of the fjord mouth, which is subjected to greater temporal variability (Storesund et al., 2017) due to exchange with the coastal ocean. Differences between the two dives are likely to be largely a result of horizontal environmental gradients along the fjord set up by biogeochemical and physical processes. For example, dissolved oxygen concentrations at the interface between the basin and intermediate water and at the sill depth differed slightly between dives (**Supplementary Figure S1**), the water being more oxygenated toward the sill (D2) because of the influence of coastal water. Dissolved oxygen concentrations at these depths are likely diminished with distance up-fjord by diffusion to and entrainment of vertically adjacent, less oxygenated waters and by the cumulative effects of (bacterial) respiration with distance from the sill (Storesund et al., 2017).

Areas with high environmental disturbance are characterized by an increase in mobile species, decrease in sessile fauna, and overall lower diversity (Włodarska-Kowalczuk et al., 2005; Jones et al., 2006; Webb et al., 2009; Hughes et al., 2010; Włodarska-Kowalczuk et al., 2012), as was observed in D2 and regions above the sill depth. The higher turbidity observed in D2 may have impacted the fjord benthic communities. Sessile suspension-feeding invertebrates are at a risk of smothering in areas with high quantities of suspended material in the water column (Jones et al., 2006; Kutti et al., 2015; Meyer et al., 2015). Fauna that are not limited by such conditions can persist (Rygg, 1985; Włodarska-Kowalczuk et al., 2005, 2012; Gasbarro et al., 2018), sometimes in high abundances, which could contribute to the increased abundance of echinoderms and reduced occurrences of sponges and sessile holothurians in the shallower regions of the fjord. Buhl-Mortensen et al. (2020) also noted that the shallower and silled regions of the fjord have relatively strong currents, whereas, the bottom currents in the basin were weak. This supports the general picture of gradients in environmental variability and stress within the fjord.

Future Implications

The environmental conditions in Sognefjord are affected by anthropogenic influences, such as cruise ships, fish farms, hydroelectric stations, and pollution (Manzetti and Stenersen, 2010). There is limited information concerning how such influences impact the Sognefjord community, though fish stocks have seen a considerable reduction (see Manzetti and Stenersen, 2010) and the shellfish community showed increased diarrhetic shellfish poisoning toxins with increased distance into the fjord (Ramstad et al., 2001).

A study by Rygg (1985) found that fjords with high pollutant concentrations were characterized by opportunistic species. Additional organic input from anthropogenic sources like fish farming or nutrient runoff may lead to hypoxic conditions in the fjord basin (Levin et al., 2009; Johansen et al., 2018). Johansen et al. (2018) predicted that increased organic matter within Norwegian fjord basins will lead to a dominance of deposit feeders, while the presence of suspension feeders will decline. Similar to the findings of Rygg (1985), Johansen et al. (2018) also found a shift in the community structure toward opportunistic species as a result of oxygen depletion and increased temperatures. Coastal water temperatures have been rising (Aure, 2016), which has led to increased temperatures within fjord basins (Johansen et al., 2018), resulting in changes in stratification and reduced oxygen supply. Long-time series temperature and organic input data are not readily available for Sognefjord, but if its environmental conditions follow the trajectories of other Norwegian fjords it is possible to predict a similar shift toward more opportunistic species. The present study does not include any temporal replication and the impact and future implications of anthropogenic-derived environmental change on the system is largely unknown and requires more research.

CONCLUSION

This study provides a recent overview of Sognefjord's megabenthic community near the sill of the fjord and the central fjord. Megafauna community composition was homogeneous within the fjord basin; however, species richness and diversity declined with proximity to the sill and with decreasing

water depth, particularly at the boundary between basin and intermediate water and at the sill depth. The fjord basin was characterized by *Psolus squamatus*, *Munida tenuimana*, *Phakellia* sp., *Acesta excavata*, and encrusting sponges. At shallower depths, the fjord was dominated by echinoderms, particularly in the dive closest to the sill. It is clear that more research is needed to understand the influence of shallow sills and water mass structure on fjord communities, as this study shows these features are important to Sognefjord's megabenthic communities. The clear stratification occurring between the basin water and intermediate water within Sognefjord would make it well suited for future surveys designed to monitor a wider range of environmental conditions or to understand future scenarios with stratification changes or deoxygenation.

DATA AVAILABILITY STATEMENT

The datasets generated for this study can be found at PANGAEA: https://doi.pangaea.de/10.1594/PANGAEA.914801.

AUTHOR CONTRIBUTIONS

HR, ER, and FM collected the video footage, CTD casts, and nutrient data for the study. HM annotated the video footage. HR provided fauna identifications. ER interpreted the *in situ* abiotic conditions and calculated the slope and distance from the sill for the transects. HM performed the statistical analysis. FM provided the sampling design, analysis and description for the nutrient contents. HM wrote the manuscript. All the authors read, edited, and approved the final manuscript.

FUNDING

The work leading to this publication has received funding from the European Union's Horizon 2020 Research and Innovation Programme through the SponGES project (Grant Agreement No. 679849). This document reflects only the authors' view and the Executive Agency for Small and Medium-sized Enterprises (EASME) is not responsible for any use that may be made of the information it contains. FM is supported by the Innovational Research Incentives Scheme of the Netherlands Organisation for Scientific Research (NWOVIDI Grant No. 016.161.360).

ACKNOWLEDGMENTS

The video footage and CTD casts were collected in 2017 on the RV *G.O. Sars* during a SponGES cruise, therefore, the crew of the RV *G.O. Sars* and the ROV *AEgir 6000* as well as participating SponGES team are thanked for their contribution to this project. EMODnet Bathymetry Consortium (2018) is acknowledged for the use of high-resolution bathymetry map for Sognefjord. The work presented here is dedicated to the memory of our friend and mentor HR, who spent his life improving global understanding of deep-sea sponges.

SUPPLEMENTARY MATERIAL

The Supplementary Material for this article can be found online at: https://www.frontiersin.org/articles/10.3389/fmars.2020.00393/full#supplementary-material

REFERENCES

Amaro, T., de Stigter, H., Lavaleye, M., and Duineveld, G. (2015). Organic matter enrichment in the whittard channel; its origin and possible effects on benthic megafauna. *Deep Sea Res. Part I Oceanogr. Res. Pap.* 102, 90–100. doi: 10.1016/j.dsr.2015.04.014

Aure, J. (2016). *Kystklima. Havforskningsrapporten-2016. Fisken Havet Særnummer 1-2016*. Bergen: Institute of Marine Research.

Bernd, C. (1993). A television and photographic survey of megafaunal abundance in Central Sognefjorden, Western Norway. *Sarsia* 78, 1–8. doi: 10.1080/00364827.1993.10413515

Blanchard, A. L., Feder, H. M., and Hoberg, M. K. (2010). Temporal variability of benthic communities in an Alaskan glacial fjord, 1971-2007. *Mar. Environ. Res.* 69, 95–107. doi: 10.1016/j.marenvres.2009.08.005

Buhl-Mortensen, L., Buhl-Mortensen, P., Dolan, M. F. J., Dannheim, J., Bellec, V., and Holte, B. (2012). Habitat complexity and bottom fauna composition at different scales on the continental shelf and slope of northern Norway. *Hydrobiologia* 685, 191–219. doi: 10.1007/s10750-011-0988-986

Buhl-Mortensen, L., Buhl-Mortensen, P., Glenner, H., and Båmstedt, U. (2017). Dyphavshabitater langt inn i landet: nye undersøkelser av havbunnen i sognefjorden. *Naturen* 6, 246–251.

Buhl-Mortensen, L., Buhl-Mortensen, P., Glenner, H., Båmstedt, U., and Bakkeplass, K. (2020). Chapter 19 -The inland deep sea - benthic biotopes in the Sognefjord. *Seafloor Geomorphol. Benthic Habit.* 5, 355–372. doi: 10.1016/B978-0-12-814960-7.00019-11

Buhl-Mortensen, L., and Høisaeter, T. (1993). Mollusc fauna along an offshore-fjord gradient. *Mar. Ecol. Prog. Ser.* 97, 209–224. doi: 10.3354/meps097209

Buhl-Mortensen, P., and Buhl-Mortensen, L. (2014). Diverse and vulnerable deep-water biotopes in the Hardangerfjord. *Mar. Biol. Res.* 10, 253–273. doi: 10.1080/17451000.2013.810759

Delaval, A., Dahle, G., Knutsen, H., Devine, J., and Salvanes, A. G. V. (2018). Norwegian fjords contain sub-populations of roundnose grenadier, Coryphaenoides rupestris, a deep-water fish. *Mar. Ecol. Prog. Ser.* 586, 181–192. doi: 10.3354/meps12400

Drewnik, A., Wêsławski, J. M., Włodarska-Kowalczuk, M., Łącka, M., Promińska, A., Zaborska, A., et al. (2016). From the worm's point of view. I: environmental settings of benthic ecosystems in Arctic fjord (Hornsund, Spitsbergen). *Polar Biol.* 39, 1411–1424. doi: 10.1007/s00300-015-1867-1869

EMODnet Bathymetry Consortium (2018). *EMODnet Digital Bathymetry (2018).* Available online at: https://www.emodnet-bathymetry.eu/data-products/acknowledgement-in-publications

Environmental Systems Research Institute [ESRI], (2016). *ArcGIS Release 10.4*. Redlands, CA: ESRI.

Flach, E., Lavaleye, M., de Stigter, H., and Thomsen, L. (1998). Feeding types of benthic community and particle transport across the N.W. European continental margin (Goban Spur). *Prog. Oceanogr.* 42, 209–231. doi: 10.1016/S0079-6611(98)00035-34

Gasbarro, R., Wan, D., and Tunnicliffe, V. (2018). Composition and functional diversity of macrofaunal assemblages on vertical walls of a deep northeast Pacific fjord. *Mar. Ecol. Prog. Ser.* 597, 47–64. doi: 10.3354/meps12599

Grasshoff, K., Erhardt, M., and Kremling, K. V. (1983). *Methods of Seawater Analysis*. Weinheim: John Wiley & Sons.

Helder, W., and De Vries, R. T. P. (1979). An automatic phenol-hypochlorite method for determination of ammonia in sea- and brackish waters. *Neth. J. Sea Res.* 13, 154–160. doi: 10.1016/0077-7579(79)90038-90033

Holte, B., Oug, E., and Cochrane, S. (2004). Depth-related benthic macrofaunal biodiversity patterns in three undisturbed north Norwegian fjords. *Sarsia* 89, 91–101. doi: 10.1080/00364820410003496

Holte, B., Oug, E., and Dahle, S. (2005). Soft-bottom fauna and oxygen minima in sub-arctic north Norwegian sill basins. *Mar. Biol. Res.* 1, 85–96. doi: 10.1080/17451000510019033

Hughes, S. J. M., Jones, D. O. B., Hauton, C., Gates, A. R., and Hawkins, L. E. (2010). An assessment of drilling disturbance on *Echinus acutus* var. *norvegicus* based on in-situ observations and experiments using a remotely operated vehicle (ROV). *J. Exp. Mar. Bio. Ecol.* 395, 37–47. doi: 10.1016/j.jembe.2010.08.012

Jantzen, C., Haussermann, V., Forsterra, G., Laudien, J., Ardelan, M., Maier, S., et al. (2013). Occurrence of a cold-water coral along natural pH gradients (Patagonia, Chile). *Mar. Biol.* 160, 2597–2607. doi: 10.1007/s00227-013-2254-2250

Johansen, P.-O., Isaksen, T. E., Bye-Ingebrigtsen, E., Haave, M., Dahlgren, T. G., Kvalø, S. E., et al. (2018). Temporal changes in benthic macrofauna on the west coast of Norway resulting from human activities. *Mar. Pollut. Bull.* 128, 483–495. doi: 10.1016/j.marpolbul.2018.01.063

Jones, D. O. B., Bett, B. J., and Tyler, P. A. (2007). Depth-related changes in the arctic epibenthic megafaunal assemblages of Kangerdlugssuaq, East Greenland. *Mar. Biol. Res.* 3, 191–204. doi: 10.1080/17451000701455287

Jones, D. O. B., Hudson, I. R., and Bett, B. J. (2006). Effects of physical disturbance on the cold-water megafaunal communities of the Faroe-Shetland Channel. *Mar. Ecol. Prog. Ser.* 319, 43–54. doi: 10.3354/meps319043

Klitgaard-Kristensen, D., and Buhl-Mortensen, L. (1999). Benthic foraminifera along an offs.hore-fjord gradient: a comparison with amphipods and molluscs. *J. Nat. Hist.* 33, 317–350. doi: 10.1080/002229399300281

Kutti, T., Bannister, R. J., Fossa, J. H., Krogness, C. M., Tjensvoll, I., and Sovik, G. (2015). Metabolic responses of the deep-water sponge *Geodia barretti* to suspended bottom sediment, simulated mine tailings and drill cuttings. *J. Exp. Mar. Biol. Ecol.* 473, 64–72. doi: 10.1016/j.jembe.2015.07.017

Levin, L. A., Ekau, W., Gooday, A. J., Jorissen, F., Middelburg, J. J., Naqvi, S. W. A., et al. (2009). Effects of natural and human-induced hypoxia on coastal benthos. *Biogeosciences* 6, 2063–2098. doi: 10.5194/bg-6-2063-2009

Maldonado, M., Aguilar, R., Bannister, R. J., Bell, J. J., Conway, K. W., Dayton, P. K., et al. (2016). "Sponge grounds as key marine habitats: a synthetic review of types, structure, functional roles, and conservation concerns," in *Marine Animal Forests: the Ecology of Benthic Biodiversity Hotspots*, eds S. Rossi, L. Bramanti, A. Gori, and C. Orejas. (Springer: Switzerland), 1–39.

Manzetti, S., and Stenersen, J. H. V. (2010). A critical view of the environmental condition of the Sognefjord. *Mar. Pollut. Bull.* 60, 2167–2174. doi: 10.1016/j.marpolbul.2010.09.019

Meyer, K. S., Sweetman, A. K., Young, C. M., and Renaud, P. E. (2015). Environmental factors structuring Arctic megabenthos – a case study from a shelf and two fjords. *Front. Mar. Sci.* 2:22. doi: 10.3389/fmars.2015.00022

Molina, E. J., Silberberger, M. J., Kokarev, V., and Reiss, H. (2019). Environmental drivers of benthic community structure in a deep sub-arctic fjord system. *Estuar. Coast. Shelf Sci.* 225:106239. doi: 10.1016/j.ecss.2019.05.021

Molodtsova, T. N., Sanamyan, N. P., and Keller, N. B. (2008). Anthozoa from the northern mid-atlantic ridge and charlie-gibbs fracture zone. *Mar. Biol. Res.* 4, 112–130. doi: 10.1080/17451000701821744

Murphy, J., and Riley, J. P. (1962). A modified single solution method for the determination of phosphate in natural waters. *Anal. Chim. Acta* 27, 31–36. doi: 10.1016/S0003-2670(00)88444-88445

Poremba, K., and Jeskulke, K. (1995). Microbial activity in the sediment of the Sognefjord (Norway). Helgoländ. Meeresuntersuchun. 49, 169-176.

RStudio Team (2019). *RStudio: Integrated Development.* Boston: R. RStudio, Inc. Available online at: http://www.rstudio.com/

Ramstad, H., Hovgaard, P., Yasumoto, T., Larsen, S., and Aune, T. (2001). Monthly variations in diarrhetic toxins and yessotoxin in shellfish from coast to inner part of the Sognefjord, Norway. *Toxicon.* 39, 1035–1043. doi: 10.1016/S0041-0101(00)00243-249

Renaud, P. E., Włodarska-Kowalczuk, M., Trannum, H., Holte, B., Wêsławski, J. M., Cochrane, S., et al. (2007). Multidecadal stability of benthic community structure in a high-Arctic glacial fjord (van Mijenfjord, Spitsbergen). *Polar Biol.* 30, 295–305. doi: 10.1007/s00300-006-0183-189

Roberts, D., and Moore, H. M. (1997). Tentacular diversity in deep-sea deposit-feeding holothurians: implications for biodiversity in the deep sea. *Biodivers. Conserv.* 6, 1487–1505. doi: 10.2307/1543510

Roberts, E. M., Mienis, F., Rapp, H. T., Hanz, U., Meyer, H. K., and Davies, A. J. (2018). Oceanographic setting and short-timescale environmental variability at an Arctic seamount sponge ground. *Deep Sea Res. Part I Oceanogr. Res. Pap.* 138, 98–113. doi: 10.1016/j.dsr.2018.06.007

Rüggeberg, A., Flögel, S., Dullo, W.-C., Hissmann, K., and Freiwald, A. (2011). Water mass characteristics and sill dynamics in a subpolar cold-water coral reef setting at Stjernsund, northern Norway. *Mar. Geol.* 282, 5–12. doi: 10.1016/j.margeo.2010.05.009

Rygg, B. (1985). Distribution of species along pollution-induced diversity gradients in benthic communities in Norwegian fjords. *Mar. Pollut. Bull.* 16, 469–474. doi: 10.1016/0025-326X(85)90378-90379

Sswat, M., Gulliksen, B., Menn, I., Sweetman, A. K., and Piepenburg, D. (2015). Distribution and composition of the epibenthic megafauna north of Svalbard (Arctic). *Polar Biol.* 38, 861–877. doi: 10.1007/s00300-015-1645-1648

Starmans, A., Gutt, J., and Arntz, W. E. (1999). Mega-epibenthic communities in Arctic and Antarctic shelf areas. *Mar. Biol.* 135, 269–280. doi: 10.1007/s002270050624

Storesund, J. E., Sandaa, R. A., Thingstad, T. F., Asplin, L., Albretsen, J., and Erga, S. R. (2017). Linking bacterial community structure to advection and environmental impact along a coast-fjord gradient of the Sognefjord, western Norway. *Prog. Oceanogr.* 159, 13–30. doi: 10.1016/j.pocean.2017.09.002

Strickland, J. D. H., and Parsons, T. R. (1968). A practical handbook of seawater analysis. *Bull. Fish. Res. Board Canada* 167, 1–31.

Strømgren, T. (1970). Emergence of *Paramuricea placomus* (L.) and *Primnoa resedaeformis* (Gunn.) in the inner part of *Trondheimsfjord* (West coast of Norway). *K. Norske Vidensk. Selsk. Skr.* 70, 1–5.

Svendsen, S. W. (2006). *Stratification and Circulation in Sognefjorden*. Master's thesis, University of Bergen, Bergen.

Sweetman, A. K., and Witte, U. (2008). Macrofaunal response to phytodetritus in a bathyal Norwegian fjord. *Deep Sea Res. Part I Oceanogr. Res. Pap.* 55, 1503–1514. doi: 10.1016/j.dsr.2008.06.004

Tabachnick, K. R., and Menshenina, L. L. (2007). Revision of the genus *Asconema* (Porifera : Hexactinellida : Rossellidae). *J. Mar. Biol. Assoc. U. K.* 87, 1403–1429.

Webb, K. E., Barnes, D. K. A., and Gray, J. S. (2009). Benthic ecology of pockmarks in the Inner Oslofjord, Norway. *Mar. Ecol. Prog. Ser.* 387, 15–25. doi: 10.3354/meps08079

Wei, T., and Simko, V. (2017). *R Package "Corrplot": Visualization of a Correlation Matrix (Version 0.84)*. Available online at: https://github.com/taiyun/corrplot

Williams, A., Althaus, F., Dunstan, P. K., Poore, G. C. B., Bax, N. J., Kloser, R. J., et al. (2010). Scales of habitat heterogeneity and megabenthos biodiversity on an extensive Australian continental margin (100-1100-m depths). *Mar. Ecol.* 31, 222–236. doi: 10.1111/j.1439-0485.2009.00355.x

Witte, U., Aberle, N., Sand, M., and Wenzhöfer, F. (2003). Rapid response of a deep-sea benthic community to POM enrichment: an in situ experimental study. *Mar. Ecol. Prog. Ser.* 251, 27–36. doi: 10.3354/meps251027

Włodarska-Kowalczuk, M., and Pearson, T. H. (2004). Soft-bottom macrobenthic faunal associations and factors affecting species distributions in an Arctic glacial fjord (Kongsfjord, Spitsbergen). *Polar Biol.* 27, 155–167. doi: 10.1007/s00300-003-0568-y

Włodarska-Kowalczuk, M., Pearson, T. H., and Kendall, M. A. (2005). Benthic response to chronic natural physical disturbance by glacial sedimentation in an Arctic fjord. *Mar. Ecol. Prog. Ser.* 303, 31–41.

Włodarska-Kowalczuk, M., Renaud, P. E., W?sławski, J. M., Cochrane, S. K. J., and Denisenko, S. G. (2012). Species diversity, functional complexity and rarity in Arctic fjordic versus open shelf benthic systems. *Mar. Ecol. Prog. Ser.* 463, 73–87. doi: 10.3354/meps09858

Zuur, A. F., Ieno, E. N., Walker, N. J., Saveliev, A. A., and Smith, G. M. (2009). *Mixed Effect Models and Extensions in Ecology with R. Statistics for Biology and Health*. New York, NY: Springer.

Conflict of Interest: The authors declare that the research was conducted in the absence of any commercial or financial relationships that could be construed as a potential conflict of interest.

Copyright © 2020 Meyer, Roberts, Mienis and Rapp. This is an open-access article distributed under the terms of the Creative Commons Attribution License (CC BY). The use, distribution or reproduction in other forums is permitted, provided the original author(s) and the copyright owner(s) are credited and that the original publication in this journal is cited, in accordance with accepted academic practice. No use, distribution or reproduction is permitted which does not comply with these terms.

frontiers in Marine Science

ORIGINAL RESEARCH
published: 16 June 2020
doi: 10.3389/fmars.2020.00443

A New Species of *Osedax* (Siboglinidae: Annelida) From Colonization Experiments in the Arctic Deep Sea

Mari Heggernes Eilertsen[1,2,3], Thomas G. Dahlgren[4,5,6] and Hans Tore Rapp[1,3,4†]*

[1] Department of Biological Sciences, University of Bergen, Bergen, Norway, [2] Department of Earth Sciences, University of Bergen, Bergen, Norway, [3] K. G. Jebsen Centre for Deep-Sea Research, University of Bergen, Bergen, Norway, [4] NORCE Norwegian Research Centre, Bergen, Norway, [5] Department of Marine Sciences, University of Gothenburg, Gothenburg, Sweden, [6] Gothenburg Global Biodiversity Centre, Gothenburg, Sweden

Large parcels of organic matter in the deep sea, such as whale carcasses, harbor a very specialized fauna, most famously the bone-eating worms in the genus *Osedax* (Annelida, Siboglinidae). Although *Osedax* was first described only 15 years ago, there are already 26 described species from the Pacific, Atlantic, and Southern Oceans. The high discovery rate of new *Osedax* species indicates that there is still a lot of undescribed diversity. In this study we describe the most northerly species of *Osedax* to date, *Osedax fenrisi* sp. nov. from 73°N on the Arctic Mid-Ocean Ridge. We also present an updated molecular phylogeny of *Osedax* based on cytochrome oxidase subunit I and 18S rRNA, including all described species in the genus. The molecular results support that *O. fenrisi* sp. nov. is distinct from the previously known species of *Osedax*. Both morphological characters and the molecular phylogeny support the placement of *O. fenrisi* sp. nov. in clade V. The most striking morphological character shared with other described species in this clade (*Osedax rubiplumus*, *Osedax roseus*, and *Osedax bryani*) is the presence of long pinnules inserted on the outside of the palps. Nomenclatural act recorded in Zoobank. LSID: E55A5C87-0CB6-4146-B3D9-7E3B19B68628.

Keywords: deep sea, *Osedax*, organic falls, phylogeny, Siboglinidae

OPEN ACCESS

Edited by:
Andrew Kvassnes Sweetman, Heriot-Watt University, United Kingdom

Reviewed by:
Paulo Yukio Gomes Sumida, University of São Paulo, Brazil
Robert C. Vrijenhoek, Monterey Bay Aquarium Research Institute (MBARI), United States

****Correspondence:***
Mari Heggernes Eilertsen
Mari.eilertsen@uib.no

†This article is dedicated to the memory of Professor Hans Tore Rapp who passed away on the 7th of March 2020

Specialty section:
This article was submitted to Global Change and the Future Ocean, a section of the journal Frontiers in Marine Science

Received: *01 December 2019*
Accepted: *20 May 2020*
Published: *16 June 2020*

Citation:
Eilertsen MH, Dahlgren TG and Rapp HT (2020) A New Species of Osedax (Siboglinidae: Annelida) From Colonization Experiments in the Arctic Deep Sea. Front. Mar. Sci. 7:443. doi: 10.3389/fmars.2020.00443

INTRODUCTION

Large parcels of organic matter in the deep sea such as whale carcasses or sunken wood logs provide nutrients both for opportunistic scavengers and a more specialized fauna (Smith and Baco, 2003; Bienhold et al., 2013). The most famous of the organic fall specialists is probably the bone-eating worms in the genus *Osedax* (Rouse et al., 2004). *Osedax* belongs to the annelid family Siboglinidae, which is characterized by adult worms lacking a functional digestive system, and instead relying on bacterial symbionts for nutrients (Schulze and Halanych, 2003). Siboglinids are found in reducing habitats such as organically enriched sediments, organic falls, cold seeps and hydrothermal vents, and most of the siboglinid taxa have chemoautotrophic symbionts that rely on sulfide or methane (Hilário et al., 2011). Within the siboglinids, *Osedax* is unique in having heterotrophic symbionts, which live in the posterior root-like extensions that protrude into the bone substratum and probably utilize collagen from the bones (Goffredi et al., 2005, 2007). Colonization experiments have demonstrated that *Osedax* are not limited to inhabiting the bones of marine mammals such as

whales and seals, some species can also inhabit bones from turtles, birds, teleosts or from terrestrial mammals such as cows and pigs (Glover et al., 2008; Jones et al., 2008; Rouse et al., 2011, 2018).

Although *Osedax* was first described only 15 years ago (Rouse et al., 2004), there are already 26 described species and an additional 9 unnamed OTUs (Rouse et al., 2018; Fujiwara et al., 2019). The Monterey Bay in California, from where the first *Osedax* species was described, has the highest documented diversity with 18 named species (Rouse et al., 2018). Research on natural organic falls and colonization experiments in other oceans has, however, lead to the discovery of new *Osedax* species in most of the world oceans, and at depths from 10–4204 m (e.g., Glover et al., 2005, 2013; Fujikura et al., 2006). The continued high discovery rate of new *Osedax* species would indicate that more undescribed diversity remains, and that the high diversity observed along the California margin is a product of the intensity of deep-sea research in this region.

The co-occurrence of many species of *Osedax* in the Monterey Bay area, where the diversity of *Osedax* is best explored, could be partly explained by depth segregation. It appears that most species are restricted to a certain depth range, and many species are only known from a single depth (Rouse et al., 2018). It has been suggested that the Antarctic species of *Osedax* have a more eurybathic distribution due to the lack of strong temperature clines through the water column (Amon et al., 2014). However, depth ranges of over 1000 m are also known in three species from Monterey Bay (Lundsten et al., 2010), so the ability of some species to occupy wide depth ranges is not unique to the Antarctic. In addition to a species turnover with depth, some species are segregated by stage of decomposition of the bones, with early colonizers being replaced by other species after some time (Rouse et al., 2018).

Compared to the Pacific and the Antarctic, organic fall fauna from the Atlantic and Arctic are not very well known. The only described species of *Osedax* in the North Atlantic, *Osedax mucofloris,* was originally described from 125 m depth in a fjord on the west coast of Sweden (Glover et al., 2005), and has subsequently been reported from a similar depth on the west coast of Norway (Schander et al., 2010) and from 1000 m depth in the Setubal Canyon, off Portugal (Hilario et al., 2015). One new species of *Osedax* and four OTUs were recently recorded from the deep southwest Atlantic (4204 m depth off Brazil; Fujiwara et al., 2019; Shimabukuro and Sumida, 2019). In addition, there are two undescribed putative species: one from the Setubal Canyon off Portugal (1000 m depth; Hilario et al., 2015) and one from the Mediterranean (53 m depth; Taboada et al., 2015). The most northerly species of *Osedax*, *O. mucofloris*, has not been recorded further north than 60°N (Schander et al., 2010), and thus there are no species of *Osedax* previously known from within the Arctic circle.

Here we report on findings of a new species of *Osedax* from colonization experiments on the Arctic Mid-Ocean Ridge at 73° N and 2340 m depth, near the Loki's Castle Vent Field (LCVF). To assess the phylogenetic position of the new species, we performed a phylogenetic analysis based on cytochrome oxidase subunit I (COI) and 18S rRNA (18S), including all described species of *Osedax* and known OTUs available in GenBank.

MATERIALS AND METHODS

Colonization Experiment

The colonization experiments were deployed and retrieved during the K. G. Jebsen Centre for Deep-Sea Research cruises to the Arctic mid-Ocean Ridge on the RV G. O. Sars in 2017 and 2018. Dried cow bones bought from a pet shop were used as substratum for the colonization experiment. The bones were enclosed in cages with holes of 4 mm in diameter to prevent them from being picked up and moved by larger animals, and to retain animals that had colonized the bones during retrieval of the experiments. Two bones, each in a separate cage, were deployed on (10.07.2017) on a sedimented plain at 2341 m depth near the LCVF using the ROV Ægir 6000. Although in close proximity to the active hydrothermal vent field, the sediments where the experiments were deployed were passive, without any signs of venting fluid or bacterial mats. The experiments were collected by ROV 1 year later (22.07.2018) at 73°34′01.6″N 8°09′31.7″E (experiment CB1) and at 73°34′01.2″N 8°09′29.9″E (experiment CB2). The bones were densely colonized by *Osedax fenrisi* sp. nov., and over 100 specimens were collected. The worms were carefully removed from the bones and fixed in 96% ethanol, RNA later or formalin, and some specimens were flash frozen in liquid nitrogen and stored at −80°C.

Morphological Analyses

In the lab, fixed specimens were examined using dissecting and compound microscopes. Scanning electron microscopy (SEM) using a Zeiss Supra 55VP was applied on two specimens that were critical point dried and mounted on stubs following a preparation of graded ethanol dehydration.

Molecular Analyses

For phylogenetic analysis the mitochondrial marker COI and the nuclear small ribosomal subunit 18S were sequenced. Tissue for DNA extraction was sampled from the palps of the worms. DNA was extracted using the Qiagen DNeasy Blood and Tissue kit, following the manufacturers protocol. PCR and sequencing primers can be found in **Table 1**. PCR reactions were run with TaKaRa taq and PCR protocols were as follows: COI – 4 min at 96°C, 45 cycles of 30 s at 95°C, 30 s at 48°C, and 1 min at 72°C, and finally 7 min at 72°C. 18S – 3 min at 94°C, 35 cycles with 1 min at 94°C, 1.5 min at 42°C, and 2 min at 72°C, and finally 7 min at 72°C. Quality and quantity of amplicons were assessed by gel electrophoresis imaging using a FastRuler DNA Ladder (Life Technologies) and GeneSnap and GeneTools (SynGene) for image capture and band quantification. Successful PCRs were purified using Exonuclease 1 (EXO, 10 U mL^{-1}) and Shrimp 90 Alkaline Phosphatase (SAP, 10 U mL^{-1}, USB Europe, Germany) in 10 μL reactions (0.1 mL EXO, 1 μL SAP, 0.9 μL ddH 2O, and 8 μL PCR product). Samples were incubated at 37°C for 15 min followed by an inactivation step at 80°C for 15 min. The purified PCR products were sequenced using BigDye v3.1 (Life Technologies) and run on an Automatic Sequencer 3730XL

TABLE 1 | PCR and sequencing primers.

Marker	Primer name	Sequence 5′-3′	Source
COI	OsCOI (F)	AATTATTCGAATTGAATTAGG	Glover et al., 2005
	OsCOI (R)	AATCAAAATAGGTGTTGGAATAG	–
18S	18e (F)	CTGGTTGATCCTGCCAGT	Hillis and Dixon, 1991
	18L (R)	GAATTACCGCGGCTGCTGGCACC	Halanych et al., 1995
	18F509 (F)	CCCCGTAATTGGAATGAGTACA	Struck et al., 2002
	18R (R)	GTCCCCTTCCGCAATTYCTTTAAG	Passamaneck et al., 2004
	18F997 (F)	TTCGAAGACGATCAGATACCG	Struck et al., 2002
	18R1843 (R)	GGATCCAAGCTTGATCCTTCTGCAGG TTCACCTAC	Struck et al., 2005, modified from Cohen et al., 1998

at the sequencing facility of the Institute of Molecular Biology, University of Bergen.

Forward and reverse sequences were assembled in Geneious (Biomatters Ltd.) and checked for contamination using BLAST (Altschul et al., 1990). Sequences of 35 known species of *Osedax* (26 described species and 9 undescribed putative species) and sequences of *Sclerolinum brattstromi* as an outgroup were downloaded from Genbank. The dataset was based on the phylogenetic dataset in Rouse et al. (2018), with some additional sequences of newly described species and OTUs added. For species with very wide distributions, one specimen from each region was included, and also two specimens of the new species. For Genbank accession numbers see **Table 2**. For the four OTUs and specimens of *Osedax frankpressi* recorded from the South-West Atlantic (Shimabukuro and Sumida, 2019), only sequences of COI were available. An initial attempt was made to include these in the combined analysis of COI + 18S with 18S as missing data, but this resulted in a poorly supported tree. Thus, these sequences were only included in the single-gene analysis of COI.

Sequences were aligned in Geneious using the MUSCLE algorithm for COI (Edgar, 2004), and MAFFT for 18S (Katoh and Standley, 2013). Alignments were trimmed and missing data at the ends were coded with question marks. Pairwise p-distances for COI were calculated in Geneious and can be found in **Supplementary Table 1**. Substitution saturation was tested for the first, second and third codon position of COI using the Xia method implemented in DAMBE6 (Xia and Lemey, 2009), which indicated high levels of saturation in the third codon position. This position was thus excluded from the alignment for the combined analysis with 18S. Single-gene analysis of COI was performed both with and without the third codon position.

The best partition scheme and substitution models were identified using Partition Finder v2.1.1 with the greedy algorithm and PhyML (Guindon et al., 2010; Lanfear et al., 2016). The best partition scheme was found to be one with the first and second codon position of COI as separate partitions, and 18S as one partition. For the first codon position of COI the SYM + G model was selected, GTR + I for the second codon position and GTR + I + G for 18S. The datasets were analyzed by Bayesian Inference in MrBayes v.3.2.7a (Ronquist and Huelsenbeck, 2003) and by Maximum Likelihood in RAxML v.8.2.10 (Stamatakis, 2014). The MrBayes analysis was run for 10 million generations for the analysis of the concatenated dataset, and 3 million generations for the single-gene analyses. Tracer v1.5 was used to check for convergence, and to determine the burnin, which was set to 10%. The RAxML analyses were run with the GTRGAMMA model and the program was allowed to halt bootstrapping automatically. All phylogenetic analyses were run on the CIPRES Science Gateway (Miller et al., 2010). The trees were converted to graphics using FigTree v1.4.0 (Rambaut, 2012) and final adjustments were made in Adobe Illustrator v24.1 (Adobe Systems, San Jose, CA, United States).

RESULTS

Morphological Description

Annelida Lamarck, 1809, Siboglinidae Caullery, 1914.

O. fenrisi sp. nov. Eilertsen, Dahlgren and Rapp, 2020 (**Figures 1A–F**).

Material Examined

Holotype: ZMBN 136747, Female, fixed in formalin preserved in ethanol, collected with ROV Ægir 6000 from cow bone at 2340 m depth at 73°34′01.6″N 8°09′31.7″E (experiment CB1) on 22.07.2018. Paratypes: ZMBN 136748, Females (2), fixed in formalin preserved in ethanol, collected with ROV Ægir 6000 from cow bone at 2340 m depth at 73°34′01.2″N 8°09′29.9″E (experiment CB2) on July 22, 2018.

Diagnosis and Description

Holotype female; preserved trunk 2.4 mm long, 0.3 mm wide; crown of palps 1.7 mm long. Pinnules long, some extending up to half the length of the palps, inserted dorsally, with a distal bulb or knob (**Figure 1C**). Oviduct short, emerging from the rim of the trunk, extending between the base of the dorsal palps a quarter of the length of palps (**Figure 1A**). Trunk with inconspicuous collar on anterior margin, thicker on the ventral side (opposite the oviduct) including a "bump" (**Figures 1C,D**). No demarcation of upper and lower trunk. Live specimen with red palps (**Figure 1B**). Color of trunk pale or white (**Figure 1B**). Color of the collar not observed. Preserved specimens without pigmentation. Tube cylindrical and not very gelatinous (**Figure 1B**). Root structure bulbous (**Figure 1E**). Ovisac an ellipsoidal mass (**Figure 1F**). Males not observed in 10 preserved specimens investigated with dissecting microscope.

Distribution

Known from LCVF at 2340 m depth in cow bone.

TABLE 2 | Specimens included in the phylogenetic analyses with GenBank vouchers.

Species (or putative species)	Locality	COI	18S
Sclerolinum brattstromi	–	FJ347644	FJ347680
Osedax antarcticus	Bransfield Strait, Antarctica	KF444422	KF444420
Osedax braziliensis	SW Atlantic, off Brazil	LC381421	LC381424
Osedax bryani	Monterey Bay, California	JX280609	KP119593
Osedax crouchi	East Scotia Sea, Antarctica	KJ598038	KJ598035
Osedax deceptionensis	Bransfield Strait, Antarctica	KF444428	KF444421
Osedax docricketts	Monterey Bay, California	FJ347626	FJ347688
–	Sagami Bay, Japan	FM998107	FM995540
Osedax fenrisi sp. nov.	Arctic Mid-Ocean Ridge	MT556178	MT556473
–	Arctic Mid-Ocean Ridge	MT556179	MT556474
Osedax frankpressi	Monterey Bay, California	FJ347607	FJ347682
–	SW Atlantic, off Brazil	MH616017	
Osedax jabba	Monterey Bay, California	FJ347638	FJ347693
Osedax japonicus	Cape Nomamisaki, Japan	FM998111	FM995535
Osedax knutei	Monterey Bay, California	FJ347635	FJ347692
Osedax lehmani	Monterey Bay, California	DQ996635	FJ347689
Osedax lonnyi	Monterey Bay, California	FJ347643	FJ347695
Osedax mucofloris	Kosterfjord, Sweden	AY827562	AY941263
Osedax nordenskjoeldi	Bransfield Strait, Antarctica	KJ598039	KJ598036
Osedax packardorum	Monterey Bay, California	FJ347629	FJ347690
Osedax priapus	Monterey Bay, California	KP119564	KP119594
Osedax randyi	Monterey Bay, California	FJ347615	FJ347684
–	Sagami Bay, Japan	FM998109	FM995542
Osedax rogersi	East Scotia Sea, Antarctica	KJ598040	KJ598037
Osedax roseus	Monterey Bay, California	FJ347609	FJ347683
Osedax rubiplumus	Monterey Bay, California	EU852488	FJ347681
–	Longqi vent field, Indian Ocean	MN699849	MN699853
Osedax ryderi	Monterey Bay, California	KP119563	KP119597
Osedax sigridae	Monterey Bay, California	FJ347642	FJ347694
Osedax talkovici	Monterey Bay, California	FJ347621	FJ347685
Osedax tiburon	Monterey Bay, California	FJ347624	FJ347694
Osedax ventana	Monterey Bay, California	EU236218	FJ347686
Osedax westernflyer	Monterey Bay, California	FJ347631	FJ347691
–	Sagami Bay, Japan	FM998110	FM995534
Osedax sp. "BioSuOr-1"	SW Atlantic, off Brazil	MH616036	
Osedax sp. "BioSuOr-2"	SW Atlantic, off Brazil	MH616081	
Osedax sp. "BioSuOr-3"	SW Atlantic, off Brazil	MH616075	
Osedax sp. "BioSuOr-4"	SW Atlantic, off Brazil	MH616012	
Osedax sp. "MB16"	Monterey Bay, California	JX280613	KP119592
Osedax sp. "Mediterreana"	Mediterranean Sea	KT860548	KT860550
Osedax sp. "Sagami 3"	Sagami Bay, Japan	FM998081	FM995537
Osedax sp. "Sagami 4"	Sagami Bay, Japan	FM998082	FM995541
Osedax sp. "Sagami 5"	Sagami Bay, Japan	FM998083	FM995539

Placeholder names for undescribed OTUs are shown in quotation marks. Repeated species names are indicated with a dash (–).

Etymology

This species is named after the Fenris wolf, son of the Norse god Loki, for whom the vent field where the species was discovered is named.

Remarks

Osedax fenrisi sp. nov. is part of *Osedax* clade V and is sister taxon to the *O. rubiplumus*, *O. roseus*, *O.* "sagami 3," and *O.* "sagami 4" clade (**Figure 2**). *O. fenrisi* sp. nov. has palps with long pinnules inserted dorsally as in *O. bryani*. Like other *Osedax* in clade V, *O. fenrisi* sp. nov. has an oviduct that extend beyond the trunk into the crown. However, in *O. fenrisi* sp. nov. it is relatively short and like in *Osedax randyi* and *Osedax braziliensis* not extending beyond half the length of the palps. A weak collar present at crown base similar to *O. roseus,* including a bump that is less pronounced than in *O. braziliensis*. The root structure is bulbous but branched, while in *O. rubiplumus* and *O. roseus* the root is long. No comparable morphological data currently available for *O.* "sagami 3" or *O.* "sagami 4."

A peculiar observation and apparently unique (among known *Osedax*) is that the tubes are inhabited by a small nematode in very high abundancies. However, similar observations have been made in other polychaetes from the Loki's Castle, where the nematode abundances were particularly high in *Nicomache lokii* (Kongsrud and Rapp, 2012).

Molecular Results

The COI sequences of *O. fenrisi* sp. nov. were 0.4% different from each other (2 bp difference), and 14.6–14.8% different from the most closely related species (*Osedax* sp. "Sagami 4"). A complete matrix of pairwise uncorrected p-distances can be found in **Supplementary Table 1**. The gene-trees for COI (including third codon position) and 18S can be found in **Supplementary Figures 1, 2**. The phylogenetic analyses of COI with and without the third codon position included yielded a similar topology, but with lower support when the third codon position was excluded. In general, the COI gene-tree is very poorly resolved (**Supplementary Figure 1**).

The phylogenetic analysis of the concatenated dataset of COI and 18S recovered the same well supported clades (clade I–V, see **Figure 2**) as described by Vrijenhoek et al. (2009), and with *Osedax deceptionensis* recovered as sister to clades I and II (clade VI; Amon et al., 2014; Rouse et al., 2018). *O. fenrisi* sp. nov. is recovered within clade V with high support (**Figure 2**). *O. mucofloris*, the only species previously known from the North Atlantic, is recovered within clade IV, which is the sister clade to clade V.

DISCUSSION

In the present study, we described the most northerly species of *Osedax* to date, and confirmed the presence of *Osedax* in the Arctic. The molecular results supported that *O. fenrisi* sp. nov. was distinct from the previously known species of *Osedax*. Both morphological characters and the molecular phylogeny supported the placement of *O. fenrisi* sp. nov. in clade V. The most striking morphological character shared with other described species in this clade (*O. rubiplumus*, *O. Roseus*, and *O. bryani*) is the presence of long pinnules inserted dorsally on the palps. Males were not observed in the investigated material. This is most likely due to the small size of males, and that

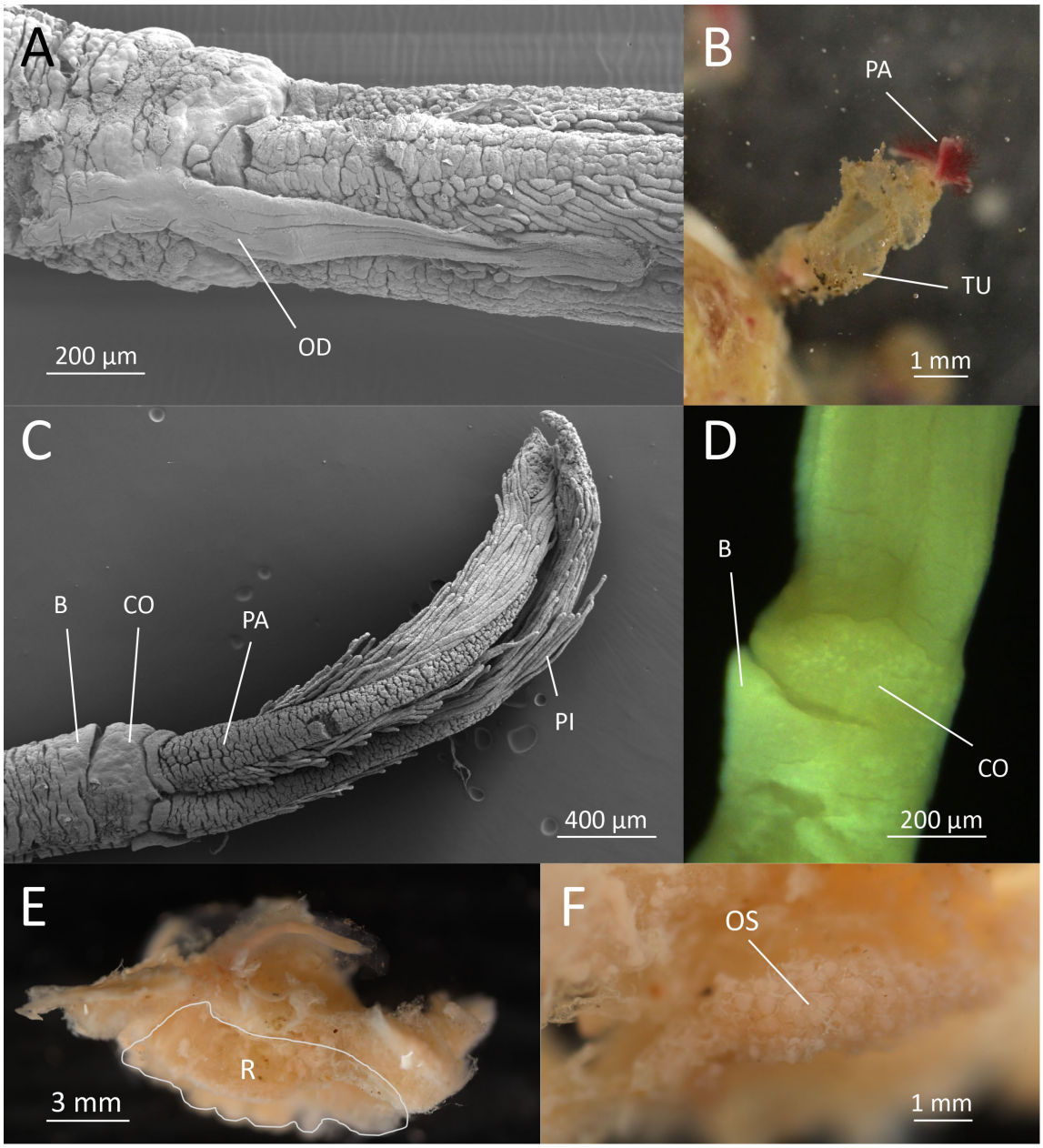

FIGURE 1 | *Osedax fenrisi* sp. nov. **(A)** SEM. Dorsal view. Oviduct (OD) extending between the dorsal most palps. **(B)** Live image from tank. Red palps (PA) extending out from mucous tube (TU). **(C)** SEM. Lateral view. Ventral collar (CO) visible with a small bump (B). **(D)** Light microscopy. Ventral view. Bump (B) visible on the lower rim of collar (CO). **(E)** Formalin fixed female dissected out of bone with attached bone material. The root tissue is indicated (R). **(F)** Ovisac (OS) in formalin fixed root tissue.

they are difficult to observe in preserved specimens. The OTU "BioSuOr 4" from the South-West Atlantic also most likely belongs to clade V, based on the presence of pinnules and a phylogenetic association with species in clade V (Shimabukuro and Sumida, 2019; see also **Supplementary Figure 1**). However, the lack of sequence data for other genes in addition to COI for this OTU, and other OTUs from the South-West Atlantic, prevents confident placement of these OTUs in the phylogeny of *Osedax*. The low resolution of the COI gene-tree (see **Supplementary Figure 1**) shows that although COI works well as a barcoding gene in *Osedax*, it has limited use as a phylogenetic marker. The phylogeny presented here based on COI and 18S mainly shows the same topology as previous phylogenies based on more markers (e.g., Rouse et al., 2018), but with some minor differences in the relationships between species within clades II and V. To produce a robust phylogeny of the genus including the new species would require a higher number of independent genetic markers, but that was outside the scope of this article.

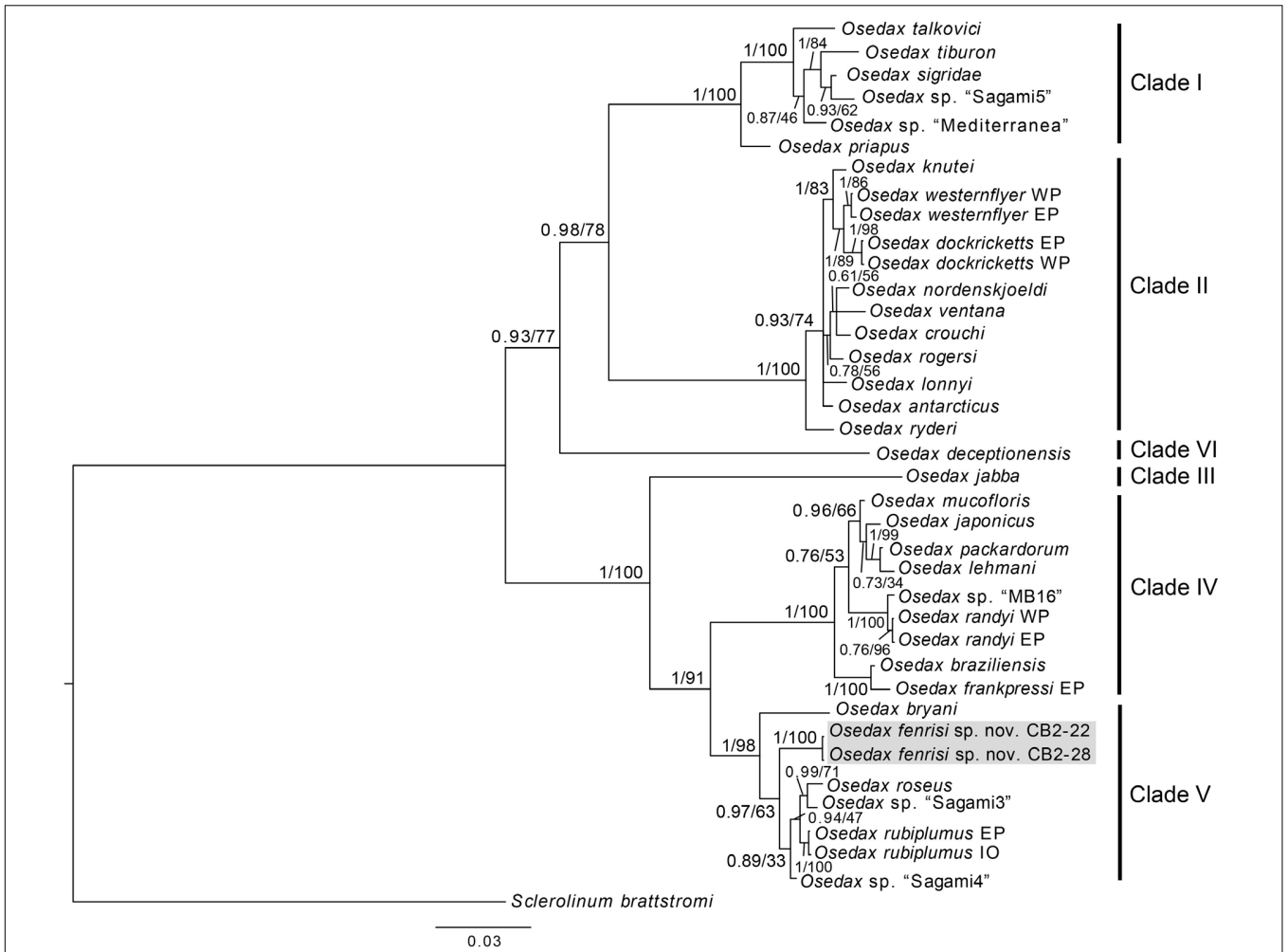

FIGURE 2 | Phylogenetic reconstruction based on the concatenated dataset of COI and 18S. The tree is the summary tree from the MrBayes analysis, and node support values are given as PP/BS. For nodes that were not recovered in the tree from the maximum likelihood analysis, support is denoted as a hyphen (-). Placeholder names for undescribed OTUs are shown in quotation marks, while for species with more than one specimen is included, the region of the specimens is indicated following the species name (EP, East Pacific; WP, West Pacific; At, Atlantic; IO, Indian Ocean).

The North-Atlantic species *O. mucofloris* was not found on the deployed bones. This could indicate that the experiments were outside of either the geographic range or the depth range of *O. mucofloris*. Several *Osedax* species are known to have wide geographic distributions, for example there are five species that have a trans-Pacific distribution (Rouse et al., 2018), a range of over 8000 km. Recently, two species have also been recorded from multiple oceans; *O. rubiplumus* from the Pacific, Antarctic, and Indian Oceans (Zhou et al., 2020), and *O. frankpressi* from the Pacific and the Atlantic Oceans (Shimabukuro and Sumida, 2019). *O. mucofloris* is known from the coast of Sweden, Norway and from the Setubal Canyon off Portugal (Glover et al., 2005; Dahlgren et al., 2006; Schander et al., 2010; Hilario et al., 2015), which is also a sizeable range. Therefore, it seems unlikely that distance alone could limit *O. mucofloris* from colonizing the deployed bones. The known depth range of *O. mucofloris* is 30–1000 m, which means that the Arctic bone deployments were over 1000 m outside the known depth range of *O. mucofloris*. However, it is more likely that the distribution is regulated by water mass and temperature. Shelf and slope occurrences of *O. mucofloris* are linked to NE Atlantic- and coastal waters with temperatures ranging from 7 to 10°C. Going deeper into the Nordic Seas and the Arctic the temperature decreases rapidly and is negative below 600–1000 m depth. The site of our deployment is characterized by Norwegian Sea deep water with a temperature of −0.5 to −0.9°C, which is likely to be too cold for *O. mucofloris*. It should also be noted that only cow bones were deployed in this experiment, and as *Osedax* species appear to have different preferences when it comes to the settlement substrate (Rouse et al., 2018), cow bones might not attract all *Osedax* species. Additional experiments with a wide range of bone substrates, both in terms of size and animal origin, would be desirable to capture the entire diversity of *Osedax* in the region.

The phylogeny shows that *O. fenrisi* sp. nov. belongs to a different clade than *O. mucofloris*, which refutes the hypothesis that these two species might be part of a regional

North Atlantic/Arctic radiation. Most of the species in clade V are from the Pacific, which could indicate a Pacific origin of the clade. It has previously been suggested that some of the hydrothermal vent fauna of the LCVF may have originated from the Pacific (Pedersen et al., 2010). However, recent advances on the taxonomy and distributions of the annelids from LCVF has called this hypothesis into question (Kongsrud et al., 2017; Eilertsen et al., 2018). In other groups there are apparent links both to the Polar basin and the Pacific on one hand, and to the Mid-Atlantic Ridge on the other (Antje, 2015; Tandberg et al., 2017). It should be noted that there is an over-representation of Pacific *Osedax* species in the phylogeny compared to other oceans due to unbalanced sampling efforts, and the prevalence of Pacific species in clade V may thus be an artifact. A more complete sampling of the global diversity of *Osedax* is necessary to infer biogeographic patterns and evolutionary pathways.

DATA AVAILABILITY STATEMENT

The datasets generated for this study can be found in GenBank and Figshare.

AUTHOR CONTRIBUTIONS

ME participated in the deployment and retrieval of the colonization experiment, sampling of *Osedax*, performed the DNA analyses, and drafted the manuscript. TD did the morphological work and wrote the species descriptions. HR came up with the study design and coordinated the study. All authors contributed to the general text and read and approved the final manuscript.

ACKNOWLEDGMENTS

We thank the crew, scientists and students onboard the R/V G.O. Sars during the cruises in 2017 and 2018, and the operators of the ROV Ægir6000 for their assistance at sea. We are especially grateful to Tone Ulvatn and Anne Helene Tandberg for their help with deployment and retrieval of the colonization experiments. We thank David J. Rees for help with the molecular work, which was performed at the Biodiversity Laboratories, University of Bergen. We also thank Jon A. Kongsrud and Katrine Kongshavn, University Museum of Bergen for assisting with SEM images. Finally, we would like to thank the two reviewers for their feedback, which helped improve this manuscript. This work is a contribution from the KG Jebsen Centre for Deep Sea Research (funded through Stiftelsen Kristian Gerhard Jebsen).

SUPPLEMENTARY MATERIAL

The Supplementary Material for this article can be found online at: https://www.frontiersin.org/articles/10.3389/fmars.2020.00443/full#supplementary-material

REFERENCES

Altschul, S. F., Gish, W., Miller, W., Myers, E. W., and Lipman, D. J. (1990). Basic local alignment search tool. *J. Mol. Biol.* 215, 403–410. doi: 10.1006/jmbi.1990.9999

Amon, D. J., Wiklund, H., Dahlgren, T. G., Copley, J. T., Smith, C. R., Jamieson, A. J., et al. (2014). Molecular taxonomy of *Osedax* (Annelida: Siboglinidae) in the Southern Ocean. *Zool. Scr.* 43, 405–417. doi: 10.1111/zsc.12057

Antje, B. (2015). The Expedition PS86 of the Research Vessel POLARSTERN to the Arctic Ocean in 2014. (Germany: Berichte zur Polar- und Meeresforschung = Reports on Polar and Marine Research), 685:133. doi: 10.2312/BzPM_0685_2015

Bienhold, C., Ristova, P. P., Wenzhofer, F., Dittmar, T., and Boetius, A. (2013). How deep-sea wood falls sustain chemosynthetic life. *PLoS One* 8:e53590. doi: 10.1371/journal.pone.0053590

Cohen, B. L., Gawthrop, A., and Cavalier-Smith, T. (1998). Molecular phylogeny of brachiopods and phoronids based on nuclear-encoded small subunit ribosomal RNA gene sequences. *Philos. Trans. R. Soc. B* 353, 2039–2061. doi: 10.1098/rstb.1998.0351

Dahlgren, T. G., Wiklund, H., Kallstrom, B., Lundalv, T., Smith, C. R., and Glover, A. G. (2006). A shallow-water whale-fall experiment in the north Atlantic. *Cah. Biol. Mar.* 47, 385–389.

Edgar, R. C. (2004). MUSCLE: multiple sequence alignment with high accuracy and high throughput. *Nucleic Acids Res.* 32, 1792–1797. doi: 10.1093/nar/gkh340

Eilertsen, M. H., Georgieva, M. N., Kongsrud, J. A., Linse, K., Wiklund, H., Glover, A. G., et al. (2018). Genetic connectivity from the Arctic to the Antarctic: *Sclerolinum contortum* and *Nicomache lokii* (Annelida) are both widespread in reducing environments. *Sci. Rep.* 8:4810. doi: 10.1038/s41598-018-23076-0

Fujikura, K., Fujiwara, Y., and Kawato, M. (2006). A new species of *Osedax* (Annelida: Siboglinidae) associated with whale carcasses off Kyushu. *Jpn. Zool. Sci.* 23, 733–740. doi: 10.2108/zsj.23.733

Fujiwara, Y., Jimi, N., Sumida, P. Y. G., Kawato, M., and Kitazato, H. (2019). New species of bone-eating worm *Osedax* from the abyssal South Atlantic Ocean (Annelida: Siboglinidae). *Zookeys* 814, 53–69. doi: 10.3897/zookeys.814.28869

Glover, A. G., Källström, B., Smith, C. R., and Dahlgren, T. G. (2005). World-wide whale worms? A new species of *Osedax* from the shallow north Atlantic. *Proc. Royal Soc. B* 272, 2587–2592. doi: 10.1098/rspb.2005.3275

Glover, A. G., Kemp, K. M., Smith, C. R., and Dahlgren, T. G. (2008). On the role of bone-eating worms in the degradation of marine vertebrate remains. *Proc. Royal Soc. B* 275, 1959–1961. doi: 10.1098/rspb.2008.0177

Glover, A. G., Wiklund, H., Taboada, S., Avila, C., Cristobo, J., Smith, C. R., et al. (2013). Bone-eating worms from the Antarctic: the contrasting fate of whale and wood remains on the Southern Ocean seafloor. *Proc. Royal Soc. B* 280:1768. doi: 10.1098/rspb.2013.1390

Goffredi, S. K., Johnson, S. B., and Vrijenhoek, R. C. (2007). Genetic diversity and potential function of microbial symbionts associated with newly discovered species of *Osedax* polychaete worms. *Appl. Environ. Microbiol.* 73, 2314–2323. doi: 10.1128/aem.01986-06

Goffredi, S. K., Orphan, V. J., Rouse, G. W., Jahnke, L., Embaye, T., Turk, K., et al. (2005). Evolutionary innovation: a bone-eating marine symbiosis. *Environ. Microbiol.* 7, 1369–1378. doi: 10.1111/j.1462-2920.2005.00824.x

Guindon, S., Dufayard, J. F., Lefort, V., Anisimova, M., Hordijk, W., and Gascuel, O. (2010). New algorithms and methods to estimate maximum-likelihood phylogenies: assessing the performance of PhyML 3.0. *Syst. Biol.* 59, 307–321. doi: 10.1093/sysbio/syq010

Halanych, K. M., Bacheller, J. D., Aguinaldo, A. M., Liva, S. M., Hillis, D. M., and Lake, J. A. (1995). Evidence from 18S ribosomal DNA that the lophophorates are protostome animals. *Science* 267, 1641–1643. doi: 10.1126/science.7886451

Hilário, A., Capa, M., Dahlgren, T. G., Halanych, K. M., Little, C. T. S., Thornhill, D. J., et al. (2011). New perspectives on the ecology and evolution of siboglinid tubeworms. *PLoS One* 6:e16309. doi: 10.1371/journal.pone.0016309

Hilario, A., Cunha, M. R., Génio, L., Marçal, A. R., Ravara, A., Rodrigues, C. F., et al. (2015). First clues on the ecology of whale falls in the deep Atlantic Ocean: results from an experiment using cow carcasses. *Mar. Ecol.* 36, 82–90. doi: 10.1111/maec.12246

Hillis, D. M., and Dixon, M. T. (1991). Ribosomal DNA: molecular evolution and phylogenetic inference Q. *Rev. Biol.* 66, 411–453. doi: 10.1086/417338

Jones, W. J., Johnson, S. B., Rouse, G. W., and Vrijenhoek, R. C. (2008). Marine worms (genus *Osedax*) colonize cow bones. *Proc. Royal Soc. B* 275, 387–391. doi: 10.1098/rspb.2007.1437

Katoh, K., and Standley, D. M. (2013). MAFFT multiple sequence alignment software version 7: improvements in performance and usability. *Mol. Biol. Evol.* 30, 772–780. doi: 10.1093/molbev/mst010

Kongsrud, J. A., Eilertsen, M. H., Alvestad, T., Kongshavn, K., and Rapp, H. T. (2017). New species of *Ampharetidae* (Annelida: Polychaeta) from the Arctic loki castle vent field. *Deep Sea Res. Pt II* 137, 232–245. doi: 10.1016/j.dsr2.2016.08.015

Kongsrud, J. A., and Rapp, H. T. (2012). *Nicomache* (*Loxochona*) *lokii* sp. nov. (Annelida, Polychaeta, Maldanidae) from the Loki's Castle vent field – an important structure builder in an Arctic vent system. *Pol. Biol.* 35, 161–170. doi: 10.1007/s00300-011-1048-4

Lanfear, R., Frandsen, P. B., Wright, A. M., Senfeld, T., and Calcott, B. (2016). PartitionFinder 2: new methods for selecting partitioned models of evolution for molecular and morphological phylogenetic analyses. *Mol. Biol. Evol.* 34, 772–773. doi: 10.1093/molbev/msw260

Lundsten, L., Schlining, K. L., Frasier, K., Johnson, S. B., Kuhnz, L. A., Harvey, J. B. J., et al. (2010). Time-series analysis of six whale-fall communities in Monterey Canyon, California, USA. *Deep Sea Res. Pt I* 57, 1573–1584. doi: 10.1016/j.dsr.2010.09.003

Miller, M. A., Pfeiffer, W., and Schwartz, T. (2010). "Creating the CIPRES science gateway for inference of large phylogenetic trees," in *Proceedings of the Gateway Computing Environments Workshop (GCE)* (New Orleans, LA: IEEE), 1–8.

Passamaneck, Y. J., Schander, C., and Halanych, K. M. (2004). Investigation of molluscan phylogeny using large-subunit and small-subunit nuclear rRNA sequences. *Mol. Phylogenet. Evol.* 32, 25–38. doi: 10.1016/j.ympev.2003.12.016

Pedersen, R. B., Rapp, H. T., Thorseth, I. H., Lilley, M. D., Barriga, F., Baumberger, T., et al. (2010). Discovery of a black smoker vent field and vent fauna at the Arctic Mid-Ocean Ridge. *Nat. Commun.* 1:126. doi: 10.1038/ncomms1124

Rambaut, A. (2012). *FigTree. Version 1.4.0*. Available online at: http://tree.bio.ed.ac.uk/software/figtree (accessed October 1, 2019).

Ronquist, F., and Huelsenbeck, J. P. (2003). MrBayes 3: bayesian phylogenetic inference under mixed models. *Bioinformatics* 19, 1572–1574. doi: 10.1093/bioinformatics/btg180

Rouse, G. W., Goffredi, S. K., Johnson, S. B., and Vrijenhoek, R. C. (2011). Not whale-fall specialists, *Osedax* worms also consume fishbones. *Biol. Lett.* 7, 736–739. doi: 10.1098/rsbl.2011.0202

Rouse, G. W., Goffredi, S. K., Johnson, S. B., and Vrijenhoek, R. C. (2018). An inordinate fondness for *Osedax* (Siboglinidae: Annelida): fourteen new species of bone worms from California. *Zootaxa* 4377, 451–489. doi: 10.11646/zootaxa.4377.4.1

Rouse, G. W., Goffredi, S. K., and Vrijenhoek, R. C. (2004). *Osedax*: bone-eating marine worms with dwarf males. *Science* 305, 668–671. doi: 10.1126/science.1098650

Schander, C., Rapp, H. T., and Dahlgren, T. G. (2010). *Osedax mucofloris* (Polychaeta, Siboglinidae), a bone-eating marine worm new to Norway. *Fauna Norv.* 30, 5–8. doi: 10.5324/fn.v30i0.632

Schulze, A., and Halanych, K. M. (2003). Siboglinid evolution shaped by habitat preference and sulfide tolerance. *Hydrobiologia* 496, 199–205. doi: 10.1023/A:1026192715095

Shimabukuro, M., and Sumida, P. Y. G. (2019). Diversity of bone-eating *Osedax* worms on the deep Atlantic whale falls—bathymetric variation and inter-basin distributions. *Mar. Biodivers.* 49, 2587–2599. doi: 10.1007/s12526-019-00988-2

Smith, C. R., and Baco, A. R. (2003). Ecology of whale falls at the deep-sea floor. *Oceanogr. Mar. Biol.* 41, 311–354.

Stamatakis, A. (2014). RAxML version 8: a tool for phylogenetic analysis and post-analysis of large phylogenies. *Bioinformatics* 30, 1312–1313. doi: 10.1093/bioinformatics/btu033

Struck, T., Hessling, R., and Purschke, G. (2002). The phylogenetic position of the Aeolosomatidae and Parergodrilidae, two enigmatic oligochaete-like taxa of the "Polychaeta", based on molecular data from 18SrDNA sequences. *J. Zool. Syst. Evolut. Res.* 40, 155–163. doi: 10.1046/j.1439-0469.2002.00200.x

Struck, T. H., Purschke, G., and Halanych, K. M. (2005). A scaleless scale worm: molecular evidence for the phylogenetic placement of *Pisione remota* (Pisionidae: Annelida). *Mar. Biol. Res.* 1, 243–253. doi: 10.1080/17451000500261951

Taboada, S., Riesgo, A., Bas, M., Arnedo, M. A., Cristobo, J., Rouse, G. W., et al. (2015). Bone-eating worms spread: insights into shallow-water *Osedax* (Annelida, Siboglinidae) from Antarctic, Subantarctic, and Mediterranean waters. *PLoS One* 10:e0140341. doi: 10.1371/journal.pone.0140341

Tandberg, A. H. S., Olsen, B. R., and Rapp, H. T. (2017). Amphipods from the arctic hydrothermal vent field «Loki's Castle», Norwegian Sea. *Biodiver. J.* 8, 553–554.

Vrijenhoek, R. C., Johnson, S. B., and Rouse, G. W. (2009). A remarkable diversity of bone-eating worms (*Osedax*; Siboglinidae; Annelida). *BMC Biol.* 7:74. doi: 10.1186/1741-7007-7-74

Xia, X., and Lemey, P. (2009). "Assessing substitution saturation with DAMBE," in *The Phylogenetic Handbook*, eds P. Lemey, M. Salemi, and A. M. Vandamme (Cambridge: Cambridge University Press), 615–630. doi: 10.1017/cbo9780511819049.022

Zhou, Y., Wang, Y., Li, Y., Shen, C., Liu, Z., and Wang, C. (2020). First report of *Osedax* in the Indian Ocean indicative of trans-oceanic dispersal through the Southern Ocean. *Mar. Biodiver.* 50:4. doi: 10.1007/s12526-019-01034-x

Conflict of Interest: The authors declare that the research was conducted in the absence of any commercial or financial relationships that could be construed as a potential conflict of interest.

Copyright © 2020 Eilertsen, Dahlgren and Rapp. This is an open-access article distributed under the terms of the Creative Commons Attribution License (CC BY). The use, distribution or reproduction in other forums is permitted, provided the original author(s) and the copyright owner(s) are credited and that the original publication in this journal is cited, in accordance with accepted academic practice. No use, distribution or reproduction is permitted which does not comply with these terms.

frontiers in Marine Science

ORIGINAL RESEARCH
published: 30 June 2020
doi: 10.3389/fmars.2020.00480

Diversity, Abundance, Spatial Variation, and Human Impacts in Marine Meiobenthic Nematode and Copepod Communities at Casey Station, East Antarctica

Jonathan S. Stark[1†], Mahadi Mohammad[2‡], Andrew McMinn[2] and Jeroen Ingels[3*]*

[1] Antarctic Conservation and Management Program, Australian Antarctic Division, Kingston, TAS, Australia, [2] Institute for Marine and Antarctic Studies, University of Tasmania, Hobart, TAS, Australia, [3] Coastal and Marine Laboratory, Florida State University, Saint Teresa, FL, United States

The composition, spatial structure, diversity and abundance of Antarctic nematode and copepod meiobenthic communities was examined in shallow (5–25 m) marine coastal sediments at Casey Station, East Antarctica. The sampling design incorporated spatial scales ranging from 10 meters to kilometers and included testing for human impacts by comparing polluted (metal and hydrocarbon contaminated sediments adjacent to old waste disposal sites) and control areas. A total of 38 nematode genera and 20 copepod families were recorded with nematodes being dominant, comprising up to 95% of the total abundance. Variation was greatest at the largest scale (km's) but each location had distinct assemblages. At smaller scales there were different patterns of variation for nematodes and copepods. There were significant differences between communities at control and impacted locations. Community patterns had strong correlations with concentrations of metals introduced by human activity in sediments as well as sediment grain size and total organic content. Given the strong association with environmental patterns, particularly those associated with human impacts, we provide further evidence that meiofauna are very useful indicators of anthropogenic environmental changes in Antarctica.

Keywords: meiofauna, benthic community, marine sediments, metals, Antarctic, human impacts, nematodes, copepods

OPEN ACCESS

Edited by:
Rui Rosa,
University of Lisbon, Portugal

Reviewed by:
Thomas Soltwedel,
Alfred Wegener Institute, Helmholtz Centre for Polar and Marine Research (AWI), Germany
Marcos Rubal,
University of Porto, Portugal

****Correspondence:***
Jonathan S. Stark
jonny.stark@aad.gov.au
Jeroen Ingels
jingels@fsu.edu

†ORCID:
Jonathan S. Stark
orcid.org/0000-0002-4268-8072

‡Present address:
Mahadi Mohammad,
School of Biological Sciences, Universiti Sains Malaysia, George Town, Malaysia

Specialty section:
This article was submitted to Global Change and the Future Ocean, a section of the journal Frontiers in Marine Science

Received: *29 November 2019*
Accepted: *28 May 2020*
Published: *30 June 2020*

Citation:
Stark JS, Mohammad M, McMinn A and Ingels J (2020) Diversity, Abundance, Spatial Variation, and Human Impacts in Marine Meiobenthic Nematode and Copepod Communities at Casey Station, East Antarctica. Front. Mar. Sci. 7:480. doi: 10.3389/fmars.2020.00480

INTRODUCTION

Knowledge of Antarctic meiobenthic communities (here limited to metazoans, excluding foraminifera) is limited to only a few areas and shallow water (< 100 m) ecological studies are limited to the Antarctic Peninsula region, including Signy Island (Vanhove et al., 1998, 2000), King George Island (Skowronski and Corbisier, 2002; Petti et al., 2006; Pasotti et al., 2012, 2014),

and Adelaide Island (Fonseca et al., 2017); and the Ross Sea (Danovaro et al., 1999; Fabiano and Danovaro, 1999). There have also been some studies of deeper water Antarctic meiobenthos: in the Weddell Sea, Ross Sea, Bransfield Strait and Drake Passage (Vanhove et al., 1995, 1999; Lee et al., 2001a; Veit-Köhler et al., 2018). Almost nothing is known of meiobenthic communities from the majority of the Antarctic coast or shelf.

The structure, composition and diversity of Antarctic meiobenthic communities are poorly understood, especially in East Antarctica. Meiobenthic studies in Antarctica, particularly the Antarctic Peninsula, have focused on their distribution (Danovaro et al., 1999; Vanhove et al., 2000; Petti et al., 2006; Pasotti et al., 2014), relationship to environmental influences and food availability (Vanhove et al., 1998; Skowronski and Corbisier, 2002; Pasotti et al., 2012), recolonization following disturbance (Peck et al., 1999; Lee et al., 2001b; Stark et al., 2017), and more recently in the context of ice-shelf disintegration and collapse (Rose et al., 2015). In most polar regions there is a pronounced dominance of nematodes, which comprise 80 to 95% of the community; the next most abundant component is usually copepods (< 1 to 27%), based on available literature. This dominance is thought to be due to the ability of nematodes to adapt, with high diversification and niche segregation between many genera and species, and generally being resilient to varied environmental conditions (Lee and Van de Velde, 1999). Worldwide, nematode genera respond to a number of environmental factors such as organic content of the sediments (i.e., food availability), grain size, physical disturbance (Ingels et al., 2009, 2011a,b; Ingels and Vanreusel, 2013) and this is also the case in the Antarctic (Vanhove et al., 1998, 2000; Lee et al., 2001a,b). Meiofauna in polar regions display large spatial variability, but the parameters controlling their distribution and community structure are unclear (Fabiano and Danovaro, 1999). One of the problems with examining meiofaunal communities is that the vast majority of species remain undescribed (Boucher and Lambshead, 1995) and this is particularly true for Antarctica (e.g., nematodes, Ingels et al., 2014). Thus most studies focus on coarser level taxonomy such as genus or family.

Coastal benthic habitats are among the most productive of marine environments (Suchanek, 1994; Borum and Sand-Jensen, 1996). They typically have high nutrient concentrations, which are influenced by both terrestrial nutrient sources and coastal phytoplankton production. In Antarctica, however, terrestrial nutrient supply is extremely limited or almost entirely absent as there are no rivers and little terrestrial primary production. In Antarctic coastal areas nutrients are relatively high throughout the year and are only briefly lowered during summer (McMinn and Hodgson, 1993; McMinn et al., 1995). Almost nothing is known of meiofaunal communities from the vast majority of the Antarctic coast, as most studies to date are from the South Shetland or South Orkney Islands.

Casey station, in the Windmill Islands in East Antarctica, is situated in a permanently ice free area of low-lying rocky peninsulas and islands. This area comprises a range of benthic habitats (Stark, 2000), from partially ice-covered, exposed coast dominated by macroalgae, to mostly ice-covered and sheltered embayments dominated by invertebrate communities including sponges, ascidians, tubeworms, echinoderms and other invertebrates (Thompson et al., 2007). Fragmented in nature, and sensitive to change owing to the adapted benthic communities, shallow water coastal habitats in Antarctica are considered to be rare and important for maintaining ecosystem function in coastal Antarctica (Clark et al., 2015). Information on the spatial distributions of benthic communities and understanding of their response to change and subsequent recovery is important given that human activities are concentrated in these types of habitat in the Antarctic (Clark et al., 2015).

The aims of this study at Casey Station were to: (1) determine the composition, diversity and spatial variability of nematode and copepod meiobenthic communities in shallow marine sediments. Spatial variation was examined at three scales: Locations (kms); Sites within locations (∼100 m); and Plots within sites (∼10 m); (2) to examine the relationship between nematode and copepod communities and local environmental influences; and (3) to investigate human impacts on nematode and copepod communities by comparing three control locations and three locations adjacent to waste disposal sites and exposed to pollution.

MATERIALS AND METHODS

Sampling Design

Sampling was undertaken using a hierarchical, nested design with three spatial scales, Locations (separated by kms); within each location there were two sites (∼ 100 m apart) and at each site there were two plots (∼10m apart). Within each plot (1m diameter), two replicate cores were taken for meiofauna and two for environmental analysis, making a total of 8 meiofauna and 8 environmental cores per location, except at O'Brien Bay-5 where one meiofauna core was lost during sampling. Six locations were sampled around Casey Station. There were three control locations, two of which were within O'Brien Bay to the south of Casey [O'Brien Bay-1 (OB-1) and O'Brien Bay-5 (OB-5)]; and one within Newcomb Bay, in McGrady Cove (**Figure 1**). There were three locations adjacent to waste disposal sites: two locations were situated along a gradient of pollution within Brown Bay (Inner and Middle) (Stark et al., 2004; Stark, 2008); and a third location was at Wilkes, adjacent to the abandoned waste disposal site at the derelict Wilkes station (Stark et al., 2003a), all within Newcomb Bay (**Figure 1**). These waste disposal sites were used historically to dispose of all waste and rubbish generated on station and included used oil, building materials, electronics and batteries, food, clothing and chemicals (Snape et al., 2001; Stark et al., 2006). Both waste disposal sites are contaminated with metals and hydrocarbons above background levels (Stark et al., 2008, 2014b; Fryirs et al., 2015).

Location Description

Casey Station is situated at 66°17′ S, 110°32′E on Bailey Peninsula in the Windmill Islands, East Antarctica (**Figure 1**). The shallow (< 50 m) benthic marine environment in the near shore region at Casey is very heterogeneous, comprising a mosaic of sediments of varying grain sizes, gravels, cobbles, boulders and bedrock

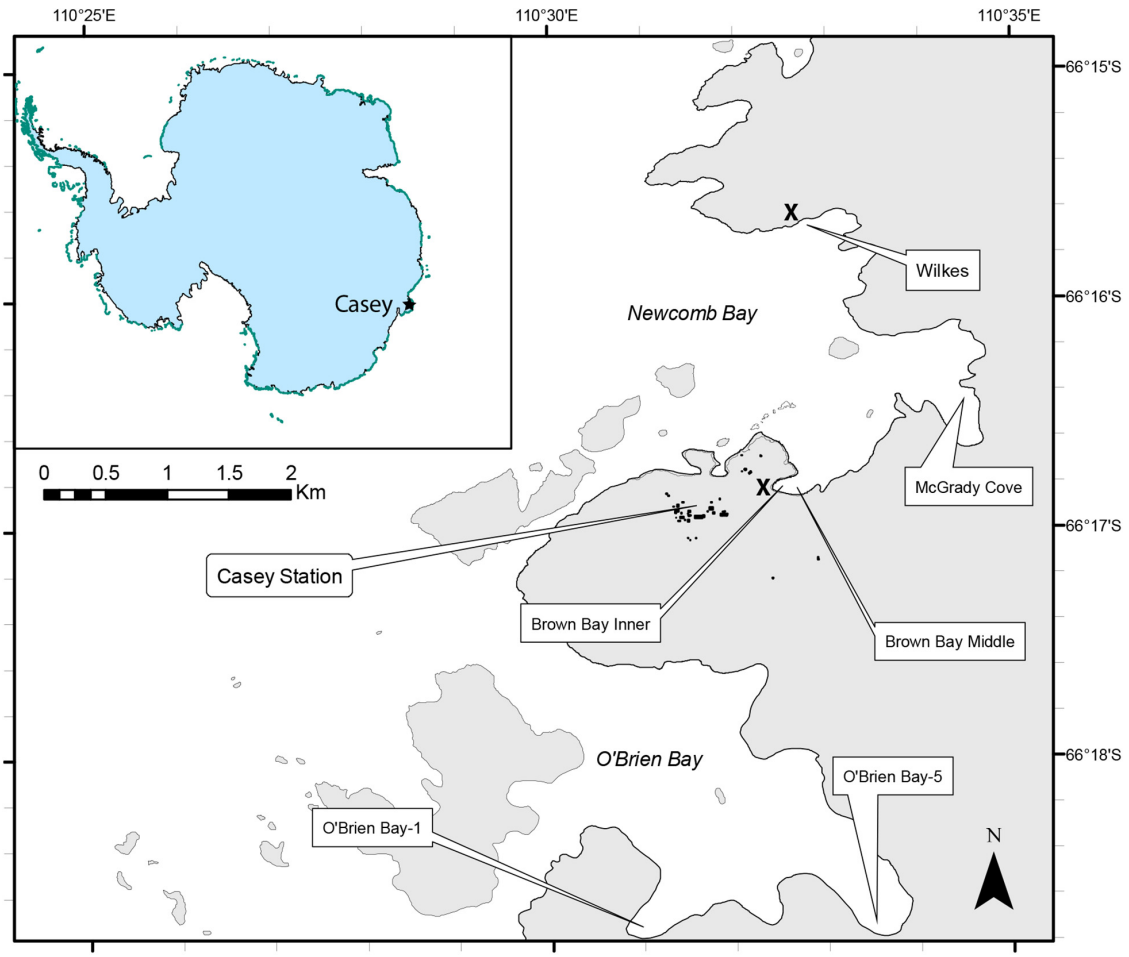

FIGURE 1 | Map of sampling locations around Casey Station, East Antarctica. The approximate locations of the former waste disposal sites at Casey and Wilkes stations are shown by the X symbol.

(Stark et al., 2003b). All locations have relatively similar sea ice regimes, although there can be considerable local variation in timing of ice break out and duration of periods of open water. Wilkes usually has an earlier sea ice loss than the other locations by between 2 and 6 weeks. Bathymetry varies significantly in the area, but within the two large bays in the study the bathymetry is similar, with deep basins at around 90 m depth, and the small bays around the edges, where samples were taken, usually have a maximum depths of approximately 25 to 30 m. Very little is known of oceanographic patterns in the region but all the bays in this study are considered to be connected and experience similar tidal and oceanographic regimes. Sediment properties are presented in the results, but general conditions at each location are described below.

Brown Bay

Brown Bay is a small embayment at the southern end of the larger Newcomb Bay with rocky sides grading to a muddy bottom to a maximum depth of approximately 15 m. Brown Bay is typically ice-free for 1–2 months in a year, between January and March. It is adjacent to the former Casey waste disposal site, abandoned in 1986, which was on the foreshore of the bay, at the base of Thala Valley. Samples were taken from 2 locations within Brown Bay: Brown Bay Inner at a depth of 7 m was 30 m from the waste dump directly in front of the point where summer melt water from the valley enters the bay (Stark et al., 2006). Brown Bay Middle was 150 m from the waste dump and ranged from 12 to 15 m in depth. Brown Bay is polluted with metals and hydrocarbons which came from the former waste disposal site situated on the foreshore of the bay (Stark et al., 2003b, 2005).

Wilkes

Wilkes was the first research station built in the Windmill Islands area, by the United States in 1957 on Clark Peninsula on the shore of Newcomb Bay; it was abandoned in 1969. The Wilkes waste disposal site is on the foreshore of a small embayment on the northern side of Newcomb Bay. The marine benthic environment adjacent to the site consists of sandy sediments and areas of exposed rock covered with macroalgae in summer (Stark et al., 2003b). Samples were collected approximately 50 m from shore,

approximately 200 m from the front of the waste dump, in 10–15 m depth. Sediment metal levels are generally similar to control locations except for cadmium, although hydrocarbons have not been measured at this location (Stark et al., 2003b).

O'Brien Bay

O'Brien Bay is a large bay several kilometers south of Casey station and is visually unaffected by human activities or contamination. The benthic environment consists of slopes and terraces of rock, boulders, cobbles and gravel, with patches of sediment dispersed among them (Stark et al., 2003a). O'Brien Bay-1 and O'Brien Bay-5 are small embayments within O'Brien Bay, with rocky sides sloping to mixed habitat of rock and sediment patches. Samples were taken at depths of 12–18 m.

McGrady Cove

McGrady Cove is a small embayment within the larger Newcomb Bay and is not directly affected by human activities or contamination. Samples were taken on the northern side of the bay which is bordered by ice cliffs which extend to the seabed at depths of 5–7 m. The benthic habitat consists of patches of rocky reef and boulders interspersed with large patches of muddy sediments. Samples were collected in 12–18 m water depth.

Sample Collection, Meiofauna Preparation, and Identification

Sediment samples were collected by divers using modified 60 ml syringes with their intake end cut off to form a small core tube (28mm internal diameter). Cores were pushed into the sediment to a depth of 10 cm, extracted, and the bottom end was capped. In a few cases samples were only taken down to 5–7 cm, where sediments were less than 10 cm deep due to underlying rock. No sediments less than 5 cm deep were sampled. Samples were collected between 25 November and 14 December 2005.

Cores were transported to Casey Station laboratories where they were emptied into sample jars and 4% formalin was added to each sample. Prior to processing, each sample was washed through a 500 μm sieve to remove the macrofauna and the coarser sediment fraction. A 32 μm sieve was used to retain the meiofauna size fraction. Meiofauna were extracted through a modified gravity gradient centrifugation technique (Heip et al., 1985; Pfannkuche et al., 1988) using a% solution of Ludox HS40 and Ludox AS in distilled water (Witthoft-Muhlmann et al., 2005). Ludox is a silica sol (a colloidal solution of Si02) which causes no plasmolysis. Samples were rinsed thoroughly over a sieve of 32 μm with tap water to prevent flocculation of Ludox. The samples were then transferred from the sieve to a large centrifuge tube. Ludox was diluted with water to specific gravity 1.18 g/ml (60% Ludox and 40% water; density = 1.18) and added to each tube until the level of the mixture was balanced for centrifuging. The sample was then centrifuged at 2800 rpm for 10 min. The supernatant was decanted and collected, and the remaining sediment pellet was resuspended. This process was repeated three times.

All supernatants were filtered on a 32 μm sieve, which was rinsed with tap water to avoid a reaction between the Ludox and formalin. After the extraction, 4% formalin and 1% of Rose Bengal (to facilitate counting) was added to preserve meiofauna before identification.

Nematodes and copepods retained on the 32 μm sieve were counted and sorted using a dissecting microscope at 25× magnification (Zeiss Stemi 2000; Zeiss Inc., Germany). Two hundred nematodes per sample were picked out at random and mounted on slides in glycerine after a slow evaporation procedure (modified after Riemann, 1988) and identified to genus level using Platt and Warwick (1983, 1988) and Warwick et al. (1998) and NeMys online identification (Steyaert et al., 2005). All copepods were picked out and mounted on slides in glycerine without evaporation for identification to family level using THAO: the Taxonomische Harpacticoida Archiv Oldenburg 2005 and Bodin (1997). The identification of nematodes and copepods was conducted on a compound microscope (1000 x magnification).

Environmental Variables

Sediment samples were taken for analysis of grain size, metals and total organic matter (TOM) using a 5 cm diameter core pushed 10 cm into the sediment. Cores were frozen at −20°C until analysis. Each core was subsampled from the top 5 cm of the frozen core, which was then homogenized by stirring and then subsampled further for separate analysis of grain size, metals and TOM. Full details of analytical methods can be found in Stark et al. (2014a) and are briefly summarized below.

Total organic matter was calculated by mass-loss on ignition at 550° for 4 h to determine ash free dry weight following Heiri et al. (2001), on a 2 g homogenized wet sub-sample, from 2 replicate cores in each plot for a total of 4 cores per location.

Grain size analysis: The outer 5 mm edge of the top 5 cm of the core was removed with a scalpel blade and dried at 45°C, then sieved through a 2mm sieve. The < 2 mm fraction and the > 2 mm fraction were weighed separately. A 5 g sample of the < 2mm fraction was analyzed using a Mastersizer 2000 Particle Size Analyzer with Hydro 2000MU accessory at the Department of Physical Geography, Macquarie University, Sydney.

Analysis of metals in sediments were done on a 3 g sub-sample of homogenized wet sediment. A 1:10 w/v 1 M HCl digest was used as recommended by Scouller et al. (2006), which gives an estimate of bioavailable elements and those more likely to have an anthropogenic source. Samples were analyzed by ICP-MS at the Central Science Laboratories (CSL), University of Tasmania for a suite of ions which included: Sr, Mo, Ag, Cd, Sn, Sb, Pb, Mg, Cr, Mn, Fe, Co, Ni, Cu, Zn, As, Al, Ba.

Statistical Methods

Abundances of nematodes were standardized to the total number per sample and the proportion of each genera was multiplied by the total number of nematodes in each sample to estimate their abundance per core. Multivariate analyses were performed on merged nematode and copepod abundances after square-root transformation as well as on separate nematode and copepod community data. Data was square root transformed to reduce the effect of dominant taxa and the Bray-Curtis resemblance measure

was used. Multivariate analyses of community composition were undertaken using non-metric multidimensional scaling (nMDS), PERMANOVA, Analysis of Similarities (ANOSIM), group-average CLUSTER (including SIMPROF 5%), PERMDISP and similarity percentages (SIMPER) procedures using the PRIMER v7.0.13 statistical software package (Clarke and Gorley, 2006; Anderson et al., 2008). Spatial differences between communities were analyzed in a hierarchical 3-factor design with Location (fixed factor), Site (nested in location) and plot (nested in site). To compare control and potentially impacted locations, a series of planned contrasts were done using PERMANOVA, to further partition the variation within the Location level (Anderson et al., 2008). Brown Bay (Inner and Middle) was compared to the control locations (McGrady, O'Brien Bay-1 and -2); and Wilkes was compared to the control locations, in planned contrasts. This allows a higher level comparison of control and impacted locations without potentially confounding different impacts at Brown Bay and Wilkes by combining under the same factor of impact. The null hypotheses of no relationship among samples or variables was tested using *P*-values from permutation techniques [if less than 100 permutations were available Monte Carlo routine was used (Anderson and Robinson, 2001)]. The Pseudo-F ratio and *p*-value (from permutation) were calculated using type III sums of squares and permuting residuals under a reduced model. PERMDISP and one-way ANOSIM was performed in *post hoc* tests to determine which groups were different and if differences were due to multivariate location or dispersion. PERMANOVA was used to examine the relative variance component contribution of each factor to overall variance, as an estimate of magnitude of effects (Graham and Edwards, 2001).

The relationship between meiofaunal communities and environmental variables was examined using distance-based linear modeling (DSTLM) and visualized using distance-based redundancy analysis (dbRDA) to obtain an ordination of the fitted values from the selected model (Anderson et al., 2008), as well as by overlying vectors of environmental variables on community multivariate ordinations. A stepwise and a forward selection process were used in DISTLM with the AICc model selection criteria, to model the community data (Bray Curtis resemblance matrix) against the normalized environmental data which were checked for collinearity (and removed when necessary).

To further distinguish patterns in nematode genera and copepod families a coherence analysis following Somerfield and Clarke (2013) was conducted using PRIMER v7. This analysis distinguishes subsets of taxa (based on SIMPROF on species variables) in the dataset that have coherent abundance patterns across a set of samples or gradient of samples, and can be separated based on significance levels in statistical tests. In essence, the routine finds groups of taxa that have similar responses across a set of samples.

Differences in environmental conditions were explored using Principal Component analysis (PCA). Relationships among variables were visualized using Draftsman plots and skewed variables were transformed (log(x + 1) or square root) to achieve even distributions. Environmental variables with correlations > 0.95 were removed leaving a single variable to represent these groups to prevent over-parameterization. Environmental variables were normalized prior to PCA or DSTLM analysis.

For comparison of nematode and copepod abundances with other studies, data were obtained either directly from published studies or from figures in published studies using the program WebPlotDigitizer V4.1[1].

RESULTS

Nematode and Copepod Abundance and Taxon Richness

Sediment meiofaunal communities at Casey were dominated by nematodes (95% of abundance), followed by copepods (5%). Other taxa were not included in this study. A total of 38 nematode genera (belonging to 16 families) and 20 harpacticoid copepod families (**Table 1**) were identified in the 47 samples from the six locations. Nematode abundance was highest at the two control locations in O'Brien Bay (**Figure 2**). Nematode diversity was greatest at Wilkes (37 genera) but the highest mean number of genera per core was found at OB-5. Copepod abundance was relatively consistent among locations ranging from a mean of 44 to 55 copepods per core (**Figure 2**). Mean abundance of copepods was not significantly different between locations. The number of copepod families was also relatively consistent among locations, ranging from 15 to 18 (**Figure 2**). Wilkes was the most taxa-rich location for both nematodes and copepods. OB-1 had the lowest number of taxa with 32 genera of nematodes and 15 families of harpacticoid copepods.

Nematode abundances ranged from 1.45 to 2.01 $\times$ 10^6 individuals m^{-2}. The control locations in O'Brien Bay had a significantly greater total abundance of nematodes than the impacted and control locations in Newcomb Bay (PERMANOVA p(perm.) = 0.003). Copepod abundances ranged from 0.072 to 0.089 $\times$ 10^6 individuals m^{-2}, and there was no significant differences among locations (**Figure 2**). The most abundant nematode genera (as % of total abundance averaged across all locations) were *Monhystera* (13.7%), *Daptonema* (9.5%), *Neochromadora* (7.6%), *Odonthopora* (4.3%), *Halalaimus* (4.2%), and *Chromadorina* (4.1%) and the most abundant copepod families were Tisbidae (1%) and Ectinosomatidae (0.5%) (**Table 1**).

Nematode and Copepod Community Spatial Structure

Multivariate analysis of community composition revealed significant differences at the location scale for both nematode and copepod communities. Patterns for the combined nematode/copepod community data were very similar to those of the nematode community, due to the dominance of nematodes in the assemblages, and thus the nematode and copepod community data were analyzed separately. The location scale contributed most to the overall variation in

[1]https://automeris.io/WebPlotDigitizer

TABLE 1 | Average abundances of nematodes and copepods in cores at six locations at Casey Station (n = 8, except at O'Brien Bay-5 n = 7).

	Brown Bay Inner	Brown Bay Middle	Wilkes	McGrady	O'Brien Bay-1	O'Brien Bay-5	Rank
Nematode genera – average % abundance of total nematodes in cores (based on 200 nematodes identified per sample).							
Acanthonchus	0.63	0.38	0.38	1.81	2.06	0.71	29
Aegialoalaimus	0.19	0.31	1.25	0	1.19	1.07	36
Aponema	0	0.69	0.38	0	0.75	0.43	38
Ascolaimus	3.00	3.00	0.25	0.56	6.06	4.64	11
Bolbolaimus	2.75	2.06	1.63	1.44	3.44	3.86	13
Chromadora	3.81	2.75	1.38	3.25	5.94	5.36	7
Chromadorella	2.81	3.94	1.38	3.06	3.31	3.79	10
Chromadorina	4.38	7.38	3.94	4.81	2.13	2.86	6
Chromadorita	0	0	1.75	4.31	0.88	0.71	25
Daptonema	8.56	2.69	12.38	15.38	11.25	9.43	2
Desmodora	2.56	0	0.69	1.00	1.19	2.07	26
Desmodorella	1.13	0	2.00	0	0.19	0.64	37
Dichromadora	1.81	0.50	2.19	1.94	3.25	3.21	15
Draconema	2.88	0	1.88	0	0.56	0.57	32
Gammanema	0	3.31	0.38	2.19	2.13	2.07	21
Halalaimus	0.88	0.88	5.81	11.94	3.44	3.50	5
Ixonema	0	8.13	0.75	0	0.56	0.71	20
Leptolaimus	1.75	1.44	5.75	0.75	0.94	1.14	17
Linhomoeus	7.31	0.63	1.50	0.19	1.94	2.36	14
Megadesmolaimus	0	1.56	1.25	0.13	9.75	8.43	8
Metalinhomoeus	0.94	2.25	3.00	0.13	7.69	6.79	9
Microlaimus	0.50	1.00	2.63	0.13	2.81	3.29	18
Molgolaimus	0.38	0	1.31	0.69	3.00	3.57	23
Monhystera	11.75	17.38	15.13	15.19	13.00	13.50	1
Neochromadora	7.19	11.25	10	9.25	5.06	4.36	3
Odonthopora	7.88	4.31	8.75	1.81	2.19	1.64	4
Paracanthonchus	0.25	2.81	4.94	1.31	1.56	1.71	16
Paralinhomoeus	5.25	6.19	0.25	1.31	1.50	2.00	12
Paramesonchium	2.38	2.25	1.50	0.31	0.75	0.86	24
Paramonohystera	0	3.19	0.06	0	0.81	1.43	33
Pierrickia	1.19	1.94	0.19	0	0.19	0.71	35
Promonhystera	3.44	4.75	0	2.06	0	0	19
Sabatiera	2.06	1.13	1.69	0.31	0.25	0.50	31
Southerniella	2.25	0.50	0.38	2.88	0	0	28
Sphaerolaimus	2.06	0.44	0.31	5.06	0	1.14	22
Spirobolbolaimus	2.44	0	0.63	1.56	0	0.14	34
Theristus	2.56	0.19	1.50	1.06	0	0.64	30
Wieseria	2.50	0.38	0.63	3.81	0	0	27
Copepod families – average abundance in cores							
Aegisthidae	1.63	1.25	2.63	3.88	0.38	1.14	11
Ameiridae	1.13	1.88	1.50	0.13	2.13	0	16
Ancorabolidae	0	1.88	0.50	1.63	2.63	4.00	12
Argestidae	4.63	3.13	2.25	3.13	4.50	1.86	4
Canthocamptidae	1.13	4.00	1.00	3.13	0	0	13
Canuellidae	1.63	2.38	0.88	4.50	2.38	3.43	7
Cletodidae	0	0	1.63	0.63	0	0	20
Dactylopusiidae	0	0	5.25	0.63	2.25	6.43	8
Ectinosomatidae	2.13	5.50	6.13	6.63	6.25	3.57	2
Huntemanniidae	2.75	2.63	3.50	2.50	2.38	5.00	6
Idyanthidae	0.63	3.13	1.63	2.50	0.25	0.71	14
Miraciidae	2.50	2.75	1.75	4.50	0	0.71	10

(Continued)

TABLE 1 | Continued

	Brown Bay Inner	Brown Bay Middle	Wilkes	McGrady	O'Brien Bay-1	O'Brien Bay-5	Rank
Neobradyidae	1.38	1.00	1.13	1.00	0	0.71	18
Parameiropsidae	2.63	1.00	0.50	0	0	0.86	19
Paramesochridae	5.50	7.38	3.25	0	9.25	4.71	3
Pseudotachidiidae	4.38	3.50	0	1.25	2.00	2.00	9
Rhizothricidae	0.75	3.13	1.13	0.75	1.13	0.29	15
Rometidae	0	0	0	0.50	1.00	4.00	17
Tisbidae	9.13	7.25	14.38	12.00	8.88	7.57	1
Zosimidae	2.50	1.50	2.13	5.50	5.25	2.29	5

Rank based on average abundance over all locations.

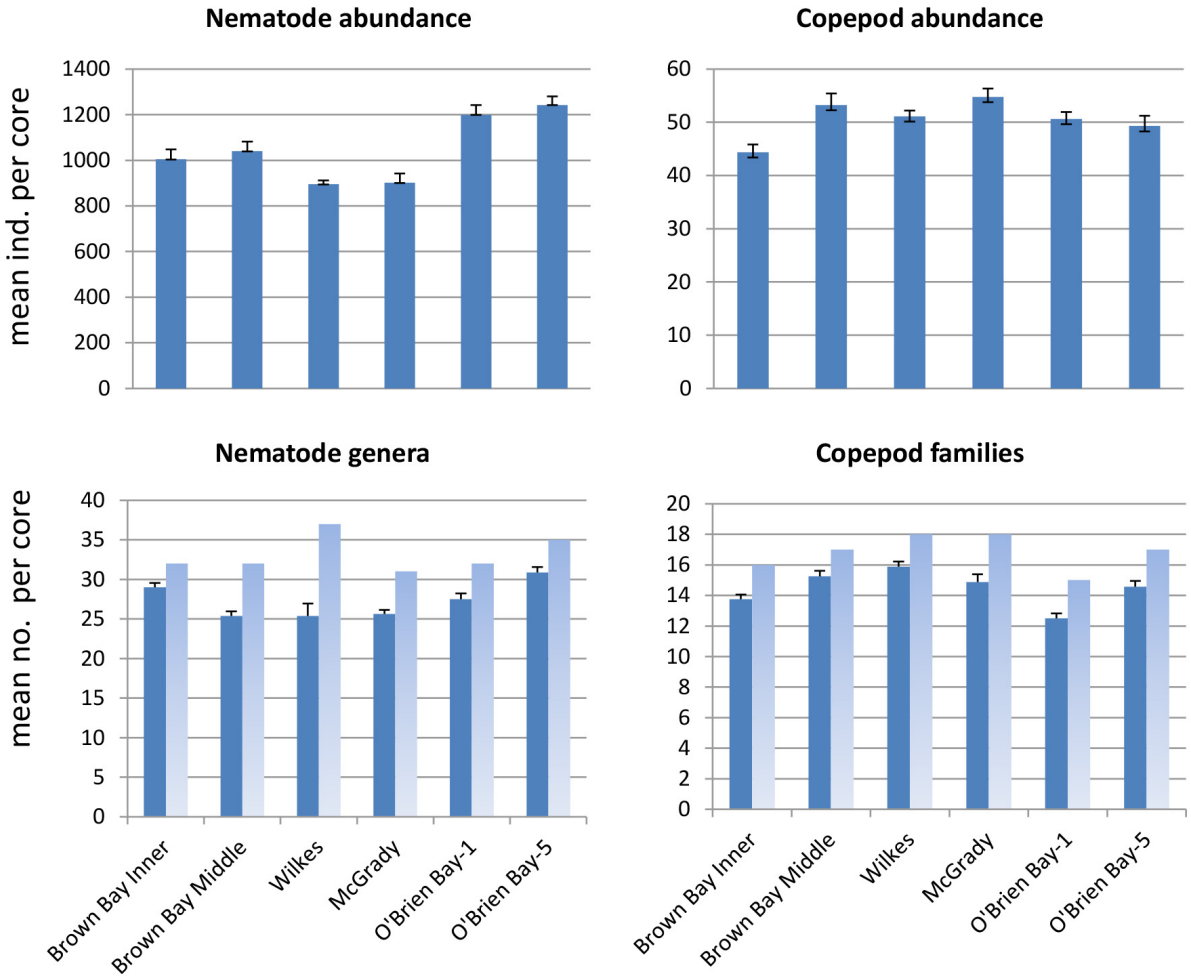

FIGURE 2 | Mean abundance and number of taxa per core at each location (± SE). Dark bars represent mean per core (n = 8, except O'Brien Bay-5: n = 7); light bars represent total number of taxa found at each location.

communities (largest estimated component of variation, ECV) with remarkably distinct meiofaunal communities at each location, as evidenced by the distinct location groupings in the nMDS ordinations (**Figure 3**). All locations had significantly different copepod and nematode communities (**Tables 2**, **3**), and form non-overlapping groups in the nMDS ordinations (**Figure 3**). There was also significant variation among sites (100 m scale, copepods only) within locations and among plots within sites (10 m, for nematodes). Analysis of the ECV values revealed that variation among locations accounted for about 70% of the total variation (for copepods and nematodes), with both sites and plots contributing less than the residual variation (< 18%, **Figure 3** and **Table 2**). Variation in copepod communities increased with increasing spatial scale, with no

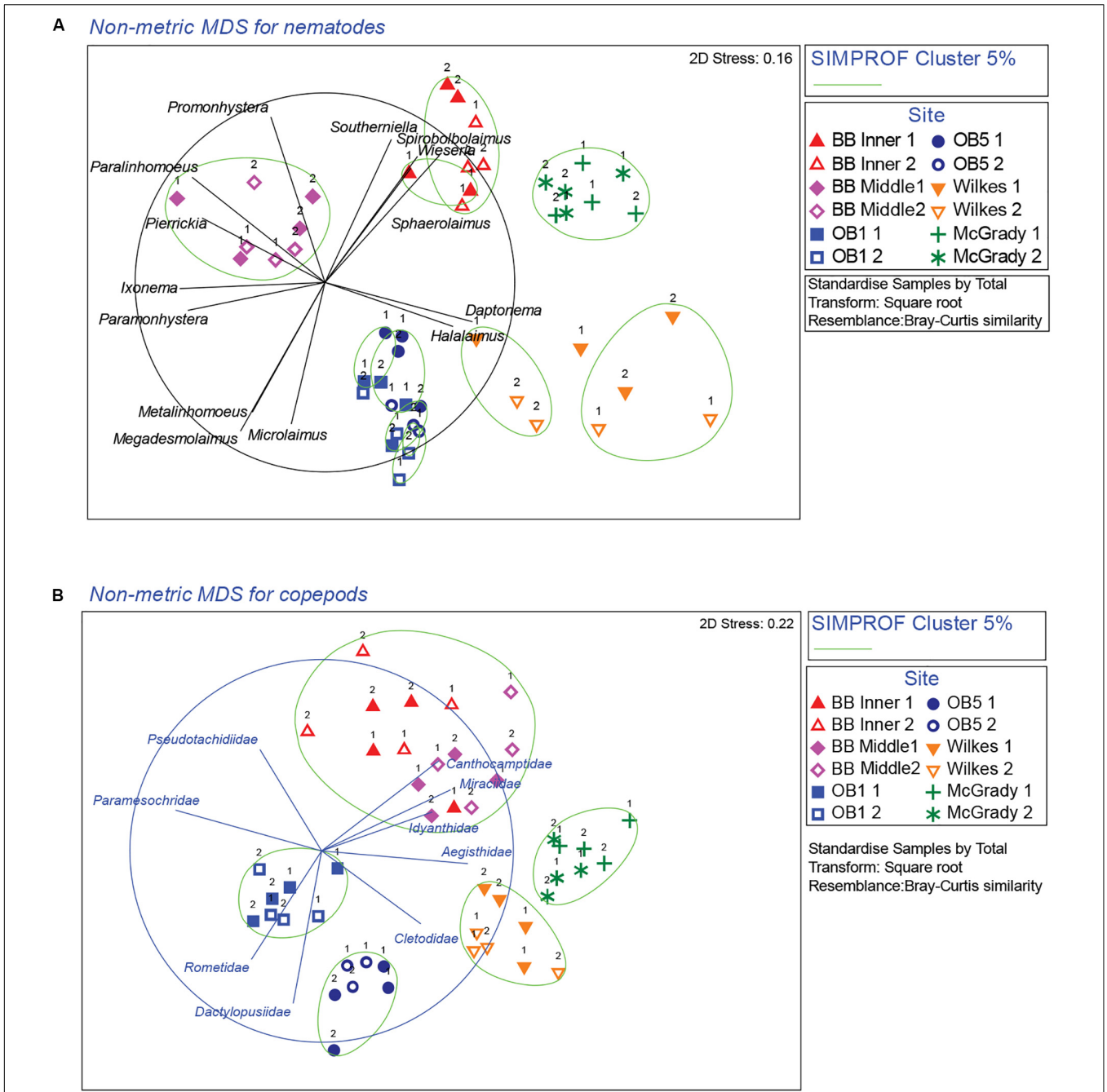

FIGURE 3 | nMDS ordinations of nematode and copepod communities around Casey Station. Numbers next to symbols represent the different plots within each site. The taxa most responsible for contributing to differences among locations were determined using vector plots overlaid on the nMDS and similarity percentage analysis (SIMPER). **(A)** Nematodes, **(B)** copepods. Vectors are taxon correlations with nMDS axes (nematode correlation cut-off: 0.7, copepod correlation cut-off: 0.6; with circle representing correlation value of 1). Ellipses on the plot represent significant cluster groups based on SIMPROF analysis.

significant variation at the 10m scale. In contrast, nematode communities varied significantly at the 10m site scale, and not at the 100m plot scale (**Table 2**). Further analysis of community structure was done by PERMDISP which tests for differences in multivariate dispersion, which can affect differences between groups [their multivariate location *sensu* Anderson (2006)]. There were significant differences in multivariate dispersion for nematodes, with Wilkes more variable than all other locations; and for copepods, with Brown Bay Inner and Middle more variable than all other locations (**Table 4**). However given that there is no overlap among locations in MDS plots, this difference in variation does not affect the main test of differences between

TABLE 2 | Results of PERMANOVA analyses for nematode and copepod communities at Casey Station, with estimated components of variation (ECV) derived from PERMANOVAs.

Source	PERMANOVA results					Est. components of variation	
	df	MS	Pseudo-F	P(perm)	P(MC)	Estimate	%
Nematodes							
Location	5	4334.20	15.97	0.0002	0.0001	525.97	71
Brown Bay vs controls*	(1)	5722.8	3.38	0.01	0.025		
Wilkes vs controls*	(1)	3410.8	2.35	0.06	0.10		
Site(Location)	6	271.61	1.01	0.48	0.48	0.41	0.06
Plot[Site(Location)]	12	270.69	1.76	0.0006	0.0029	60.05	8
Residual	23	153.93				153.93	21
Total	46						
Copepods							
Location	5	3442.80	12.40	0.0001	0.0001	409.78	69
Brown Bay vs controls*	(1)	4722.3	3.38	0.008	0.02		
Wilkes vs controls*	(1)	3307.4	2.20	0.10	0.12		
Site(Location)	6	277.76	1.88	0.026	0.038	33.53	6
Plot[Site(Location)]	12	148.12	1.02	0.47	0.46	1.49	0.25
Residual	23	145.23				145.23	25
Total	46						

**Indicates planned comparisons (or contrasts), which further partition the sums of squares in the factor Location. These provide a test of impacted versus control locations, but enables separate tests for Wilkes and the Brown Bay locations.*

TABLE 3 | Results from ANOSIM analysis showing R values from pairwise tests for differences in meiofauna among locations.

	Brown Bay Inner	Brown Bay Middle	O'Brien Bay-1	O'Brien Bay-5	Wilkes
(A) Nematodes					
Brown Bay					
Middle	1				
OB1	1	1			
OB5	1	1	0.26		
Wilkes	0.88	0.97	0.80	0.71	
McGrady	1	1	1	1	0.90
(B) Copepods					
Brown Bay					
Middle	0.59				
OB1	0.98	0.97			
OB5	0.98	0.99	0.99		
Wilkes	0.89	0.96	1	1	
McGrady	0.96	0.93	1	1	1

All comparisons significantly different.

locations. These PERMDISP results could be interpreted as a separate effect, with nematode communities at Wilkes and copepod communities at both Brown Bay locations being significantly more variable than other locations.

Human Impacts

The planned comparisons in the PERMANOVA analyses demonstrated that the Brown Bay locations were significantly different to the controls but that Wilkes was not different, for both nematode and copepod communities (**Table 2**).

The taxa most responsible for contributing to differences among locations were determined using vector plots and bubble plots overlaid on the nMDS and similarity percentage analysis (SIMPER).

Nematodes

Cluster analysis (group average) confirmed the patterns seen in the nMDS ordination, with cluster groups strongly aligned to each location (**Figure 3A**). Each location had distinct assemblages of nematodes. The species that drove differences among locations most strongly (correlation > 0.7) are shown in the vector plot (**Figure 3A**), with some of the strongest patterns reflected in bubble plots (**Figures 4A,B**), indicating strong genera selectivity between locations. In particular the genera *Promonhystera, Paralinhomoeus* and *Pierrickia* were consistently more abundant at Brown Bay than the controls, while *Daptonema, Halalaimus* and *Microlaimus* were more abundant at controls (**Figure 3** and **Table 1**).

Coherence analysis of nematode genera indicated five subsets of nematode genera that showed similar abundance patterns across the locations, along a pollution gradient (**Figure 5**): (1) there was a large group of genera with no distinguishable abundance patterns across polluted and non-polluted locations (**Figure 5A**); (2) a group of nematode genera that were more abundant at the two O'Brien Bay and the Wilkes locations, and that had either very low abundances or were absent at the Brown Bay locations (**Figure 5B**); (3) a group of nematode genera that were more abundant at the McGrady location, and had medium to low abundances at the other locations (**Figure 5C**); (4) nematode genera that were generally more

TABLE 4 | PERMDISP analysis of multivariate dispersion in nematode and copepod communities at each location at Casey.

Groups	Nematodes		Copepods	
	t	P(perm)	t	P(perm)
(Brown Bay Inner, Brown Bay Middle)	0.79	0.48	1.30	0.21
(BB Inn., OB1)	0.65	0.54	3.33	**0.005**
(BB Inn., OB5)	1.54	0.15	4.55	**0.001**
(Brown Bay Inner, Wilkes)	7.67	**0.0003**	4.40	**0.001**
(Brown Bay Inner, McGrady)	1.03	0.35	4.42	**0.002**
(BB Mid., OB1)	1.33	0.22	1.91	**0.05**
(BB Mid., OB5)	2.27	**0.04**	3.22	**0.004**
(Brown Bay Middle, Wilkes)	6.42	**0.0002**	3.01	**0.005**
(Brown Bay Middle, McGrady)	1.70	0.12	3.04	**0.005**
(OB1, OB5)	0.60	0.57	1.70	0.10
(OB1, Wilkes)	7.69	**0.0002**	1.35	0.20
(OB1, McGrady)	0.34	0.73	1.38	0.14
(OB5, Wilkes)	10.22	**0.0001**	0.30	0.76
(OB5, McGrady)	0.19	0.84	0.26	0.79
(Wilkes, McGrady)	8.14	**0.0002**	0.03	0.97

Means and standard errors	Size	Nematodes		Copepods	
Group		Average	SE	Average	SE
Brown Bay Inner	8	11.76	0.71	15.63	1.15
Brown Bay Middle	8	12.62	0.82	13.58	1.07
OB1	8	11.05	0.84	11.09	0.73
OB5	7	10.46	0.38	9.48	0.58
Wilkes	8	20.01	0.81	9.75	0.68
McGrady	8	10.65	0.82	9.72	0.68

Significant differences indicated in bold type. Means show average distance from group centroid.

abundant at the polluted Brown Bay Inner location, with medium or high abundance at Wilkes, and medium to low abundances at Brown Bay Middle locations (**Figure 5D**); and (5) a group of nematode genera that were more abundant at both Brown Bay Inner and Middle, and medium to low abundance at the other locations (**Figure 5E**).

Copepods

Copepod communities were very distinct at each location, with a number of taxa contributing strongly to these differences (**Figure 3B**). Brown Bay Inner and Middle locations grouped together, demonstrating similarity among copepod communities within Brown Bay, although they also showed the most variation overall (**Table 4**). Cluster analysis (group average) confirmed the patterns seen in the nMDS ordination, with groups strongly aligned to each location (**Figure 3B**). Although most taxa were found at each location, there were unique presence and abundance combinations at each location, clearly distinguishing them from each other (**Figure 3B**, and genera bubble plots in **Figures 4C,D**). Pseudotachidiidae were consistently more abundant at Brown Bay locations, while Dactylopusiidae and Rometidae were more abundant at controls (**Figure 3** and **Table 1**). In contrast to nematodes, coherence analysis of copepod families did not indicate any general patterns of abundance across locations so these are not shown.

Environmental Influences on Nematode and Copepod Communities

Sediments ranged from very fine sands to medium sands, with generally unimodal distributions, and were poorly sorted. There were significant differences in grain size distribution among locations, with most variation associated with the location scale (approx. 50% of total variance), but no difference between sites within locations, due to differences between plots within sites or residual variation between replicate cores (**Table 5**). Sediment grain size distributions were most different at O'Brien Bay-1, which had higher proportions of coarser sediments than the other locations (**Figure 6**) and the largest mean particle diameter MPD (**Table 6**). In contrast McGrady Cove had the highest proportion of fine sediments, the smallest MPD and high levels of organic matter (**Figure 6** and **Table 6**). The very coarse silt fraction, 31–62.5 μm, was strongly positively correlated with organic content of sediment ($r = 0.96$).

Multivariate analysis of sediment environmental variables including grain size, TOC and metal concentrations showed strong differences between locations (**Figure 7**). A PCA of all environmental data shows most locations as distinct groups, with OB-1 being most separate from all other locations (**Figure 7A**). Results of ANOSIM analysis (**Table 7**) demonstrated that all locations were significantly different. When separating grain size and metal variables these patterns changed slightly, with less differences among locations in grain size and greater differences in metals. For grain size, essentially two groups can be distinguished: OB-1 was a highly variable group on its own with the rest of the locations forming a loose grouping together (**Figure 7B**), yet, within the latter, the distinction of separate locations was still evident (**Figure 7B**). There were also strong differences between the two sites at Wilkes. For metal concentrations, both sampling locations in Brown Bay were clearly separate from the other locations in the PCA ordination (**Figure 7C**) with particularly high concentrations of iron, tin, copper, lead, antimony, silver and zinc. All locations had maximal differences in ANOSIM tests, baring Brown Bay Middle and McGrady (**Table 7**). OB-1 also formed a separate metal group but was much more similar in its metal content to OB-5. There was a gradient of metal concentration aligned with the PC2 axis, increasing toward the top of the ordination (**Figure 7C**).

Relationships between the meiofauna communities and the environmental variables were assessed using the DISTLM modeling procedure. DISTLM results are shown in **Table 8**, and patterns are visualized in the PCO (copepod and nematode communities), and dbRDA plots (copepod and nematode communities modeled against environmental variables) in **Figure 8**. To avoid multi-collinearity (where two or more

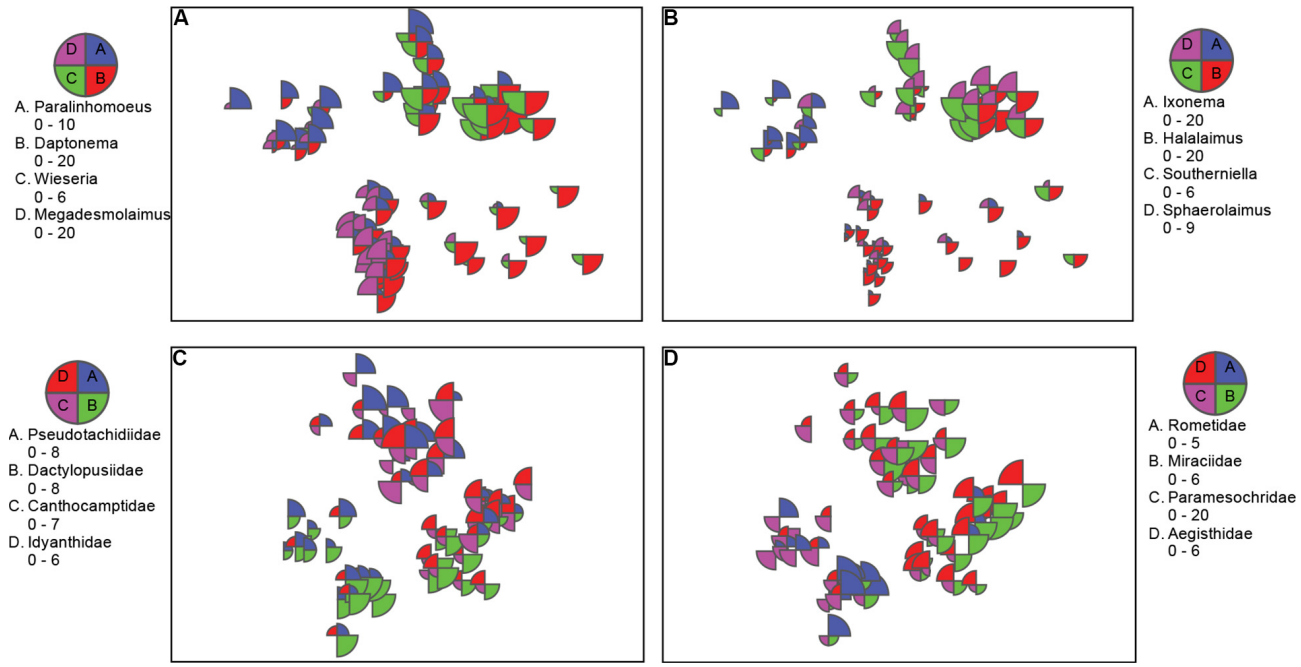

FIGURE 4 | nMDS bubble plots with scaled abundance showing taxa with substantial contributions to location differences. **(A,B)** Nematode genera from nMDS in **Figure 3A**; and **C,D**) copepod families from nMDS **Figure 3B**. Data was standardized, square rooted, and Bray-Curtis resemblance measure was used.

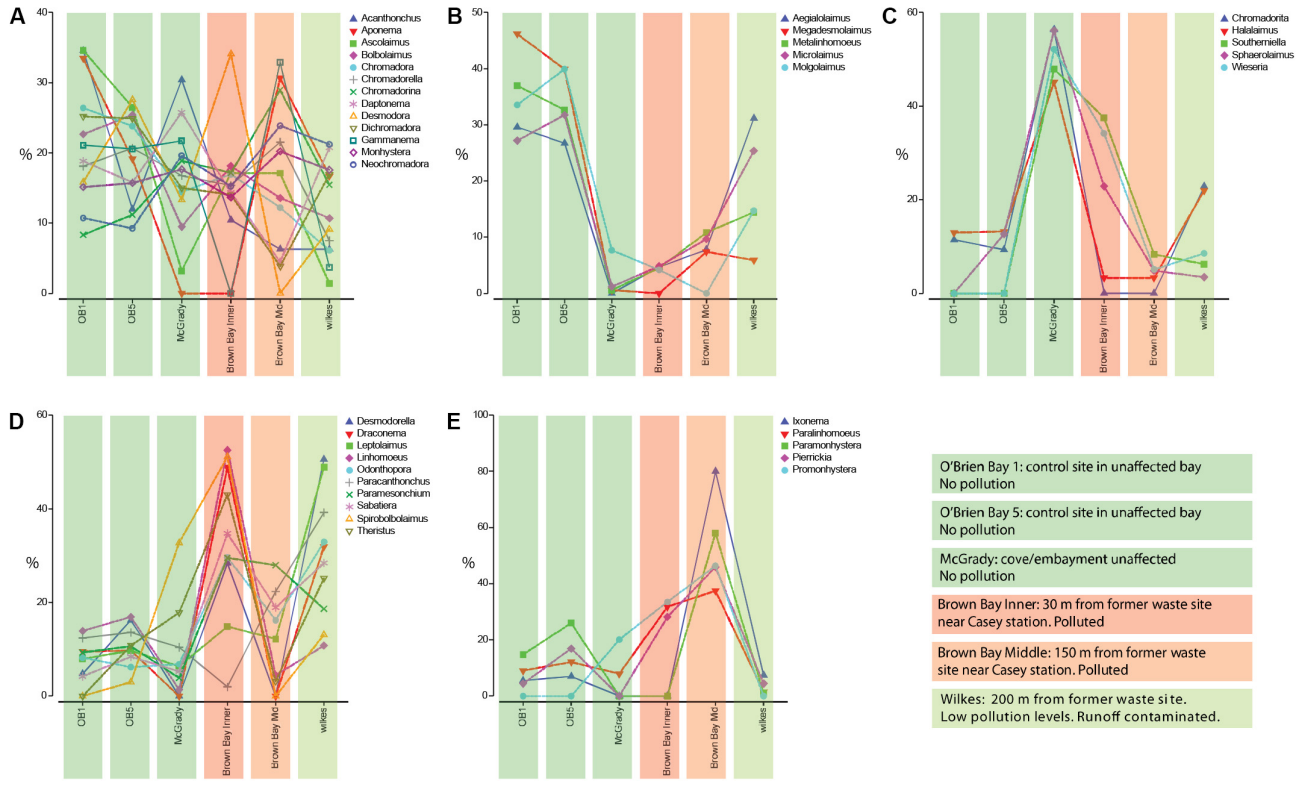

FIGURE 5 | (A–E) Different patterns of abundance from coherance analysis of the 38 nematode genera, standardized by genus across locations, which produced five statistically different subsets of nematode genera. Colored bars are associated with each station and indicate pollution levels as explained in the color legend.

TABLE 5 | Results of PERMANOVA analyses for grain size of sediments at Casey Station, with estimated components of variation (ECV) derived from PERMANOVAs.

Source	PERMANOVA results			P(perm)	Estimates of components of variation		
	df	MS	Pseudo-F		Estimate	Sq. root	%
Location	5	2.35	10.96	0.0011	0.28	0.53	48.6
Site(Location)	6	0.21	0.50	0.9094		−0.24	0
Plot[Site(Location)]	12	0.43	2.98	0.0004	0.15	0.38	26.0
Residual	23	0.14			0.14	0.38	25.5
Total	46						

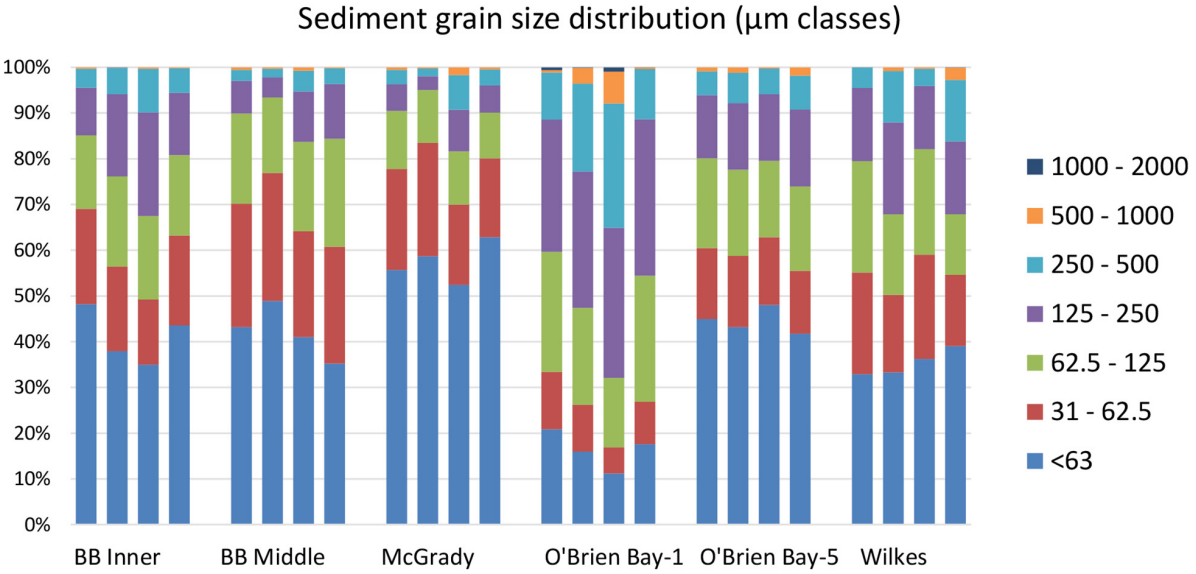

FIGURE 6 | Average sediment grain size category% in each of four plots (n = 2) at each location.

variables are highly co-linear with correlation $|r| \geq 0.95$ for example), whereby variables contain the same information and are redundant for the purposes of the dbRDA analysis (Anderson et al., 2008), one or more redundant variables were dropped from the analysis. Correlations between all variables were examined and where $|r| \geq 0.95$ one variable was removed to be represented by the other variable to avoid multi-collinearity and over-parameterization. These were: tin was used to represent lead and antimony; zinc was used to represent vanadium; copper was used to represent iron; nickel to represent chromium; strontium to represent magnesium, 31–62.5 µm to represent TOC; 250–500 µm to represent mean particle diameter; and 2–7.8 µm to represent 0.01–2 µm. The best DISTLM models correspond strongly with the unconstrained PCO ordination of nematode and copepod communities (**Figure 8**).

DISTLM/dbRDA Nematodes

The single variables with the strongest correlations identified in marginal tests for nematodes were: arsenic, zinc, silver, copper, barium, tin and sediment 15.6–31 µm (**Table 8**). For nematodes the best multivariate explanatory models included a group of 5 variables (from a total of 26 variables), which accounted for approximately 68% of the variation in the nematode community. These included metals likely to have an anthropogenic source: arsenic which was higher at Brown and McGrady; tin (also represents lead and antimony) which was higher at Brown Bay than all other locations; barium which was lower at the two O'Brien Bay locations; manganese; and sediment in the 31–62.5 µm very coarse silt range (also represents TOC), which was lower at the two O'Brien Bay locations. Selected models were visualized using dbRDA ordinations (**Figure 8**), bearing a strong resemblance to the unconstrained PCO ordination of nematode communities (**Figures 8A,B**), explaining almost 70% of the fitted model variation and nearly 50% of the total variation in nematode communities. The impacted locations of Brown Bay Inner and Middle have higher metal concentrations (note the Sn (represents Pb, Sb) and As vectors overlaid on **Figure 8B**), and finer sediments, separating these locations from the others in these ordinations. McGrady also has fine sediments but higher concentrations of barium. The two O'Brien Bay locations had lower metal concentrations as well as higher manganese (**Figure 8B**).

DISTLM/dbRDA Copepods

For copepods there was a slightly different set of variables with barium, zinc, cadmium, coarse silt 15.6–31 µm, arsenic, tin and

TABLE 6 | Sediment properties at locations used in this study including: MPD = mean particle diameter; SE = standard error; TOM = total organic matter.

	Brown Bay Inner	Brown Bay Middle	McGrady	Wilkes	O'Brien Bay-1	O'Brien Bay-5
MPD um	156.34	133.68	119.66	173.48	276.80	152.37
MPD SE	10.59	7.52	8.55	9.52	32.40	3.92
TOM	5.78	9.12	7.05	7.04	1.56	3.61
TOM SE	0.82	0.51	1.03	1.13	0.11	0.18
Sn	3.52	0.40	0.04	0.12	0.00	0.00
Cd	0.04	0.26	0.15	0.22	0.01	0.03
Pb	7.17	2.23	0.25	0.57	0.04	0.20
Cu	4.48	0.46	0.45	0.37	0.15	0.42
Zn	3.07	3.41	1.83	1.88	0.39	0.21
Fe	567.62	168.17	77.79	32.13	8.46	32.37
Ba	0.89	1.39	2.22	1.55	0.31	0.18
As	2.73	0.80	6.76	1.30	0.00	0.88
Mg	1039.41	638.49	1084.31	1919.28	231.90	614.76
Sr	8.10	3.59	7.23	10.54	1.45	5.00
Mo	0.12	0.15	0.29	0.69	0.02	0.10
Ag	0.03	0.03	0.02	0.01	0.00	0.00
Sb	0.015	0.005	0.005	0.004	0.004	0.001
Cr	0.58	2.83	2.62	2.00	0.12	1.70
Mn	0.32	0.35	0.42	0.47	0.28	0.50
Co	0.018	0.035	0.037	0.029	0.009	0.013
Ni	0.36	1.62	1.56	1.33	0.12	1.15
Al	60.92	38.29	29.23	20.81	24.88	39.19

All metal concentrations in mg/kg.

copper among the highest correlations with copepod patterns (**Table 8A**). For copepods the best explanatory model included barium, tin (representing lead and antimony), manganese, arsenic, strontium and very coarse silt (31–63 μm), with the best dbRDA model explaining 64% of fitted and 50% of total variation (**Figures 8C,D**). There are two clear groups of copepod communities, those in O'Brien Bay, correlated with higher concentrations of manganese; and those in Newcomb Bay, correlated with higher concentrations of metals (tin (lead, antimony), arsenic) strongly differentiating the Brown Bay locations, and finer sediments (**Figures 8C,D**). Wilkes and McGrady were also differentiated from the O'Brien locations along the dbRDA 1 axis, which had a strong positive correlation with barium. Both O'Brien Bay locations were negatively correlated with fine sediments but positively correlated with manganese (**Figure 8D**).

DISCUSSION

This study provides the first description of the spatial distribution, diversity and relationship to environmental influences for benthic nematode and copepod meiofaunal communities in east Antarctica. The dominance of nematodes (which comprised over 90% of the meiobenthic community) is similar to other areas of Antarctica, whether in shallow or in deep waters (**Table 9**).

Abundance

Abundances of copepods and nematodes in shallow waters around Casey are at the lower end of, but within, the range of abundances found to date in shallow-water Antarctic sediments (**Table 9**). Comparisons among studies, however, are heavily affected by sampling, preservation, extraction and sorting methods (Rudnick et al., 1985) and should be interpreted with caution. In our study, the minor deviation of core depth for a few samples below the 5 cm horizon (most samples were 10 cm, but some were only 5–7 cm) is not a major concern, as meiofauna abundance rapidly declines below the first 2 to 3 cm sediment depth. This is especially the case in coastal Antarctic sediments (as a result of high food availability at the surface) as reported by Vanhove et al. (1998) who showed a rapid decline of meiofauna abundance from 5170 ind./10cm^2 in the 0–1cm layer, to 182 ind./10cm^2 in the 4–5cm layer (representing only 1.38% of abundance in the top 5 cm) and at another site found that only 1.11% of total 0–5 cm meiofauna abundance was found in the 4–5cm depth layer. Pasotti et al. (2012) reported similar meiofauna declines with depth of sediment profile, with only a fraction of the total abundance in the 4–5cm layer.

Most other shallow water studies are from the Antarctic Peninsula region (including South Shetlands and South Orkneys) where densities of meiofauna have generally been found to be much higher, but which have somewhat different marine environments, with generally higher primary productivity, less sea ice (and thus more light in the water column) and warmer summer seawater temperatures (Stark et al., 2019). Such conditions may be favorable for more abundant meiobenthic communities, with abundances up to 11.5×10^6 ind. m^{-2} found on King George Island (**Table 9**). Meiofaunal abundance, however, can vary greatly over relatively small scales, for example on King George Island abundances of nematodes in shallow water vary from a mean of 0.43×10^6m^{-2} (Marion Cove) to

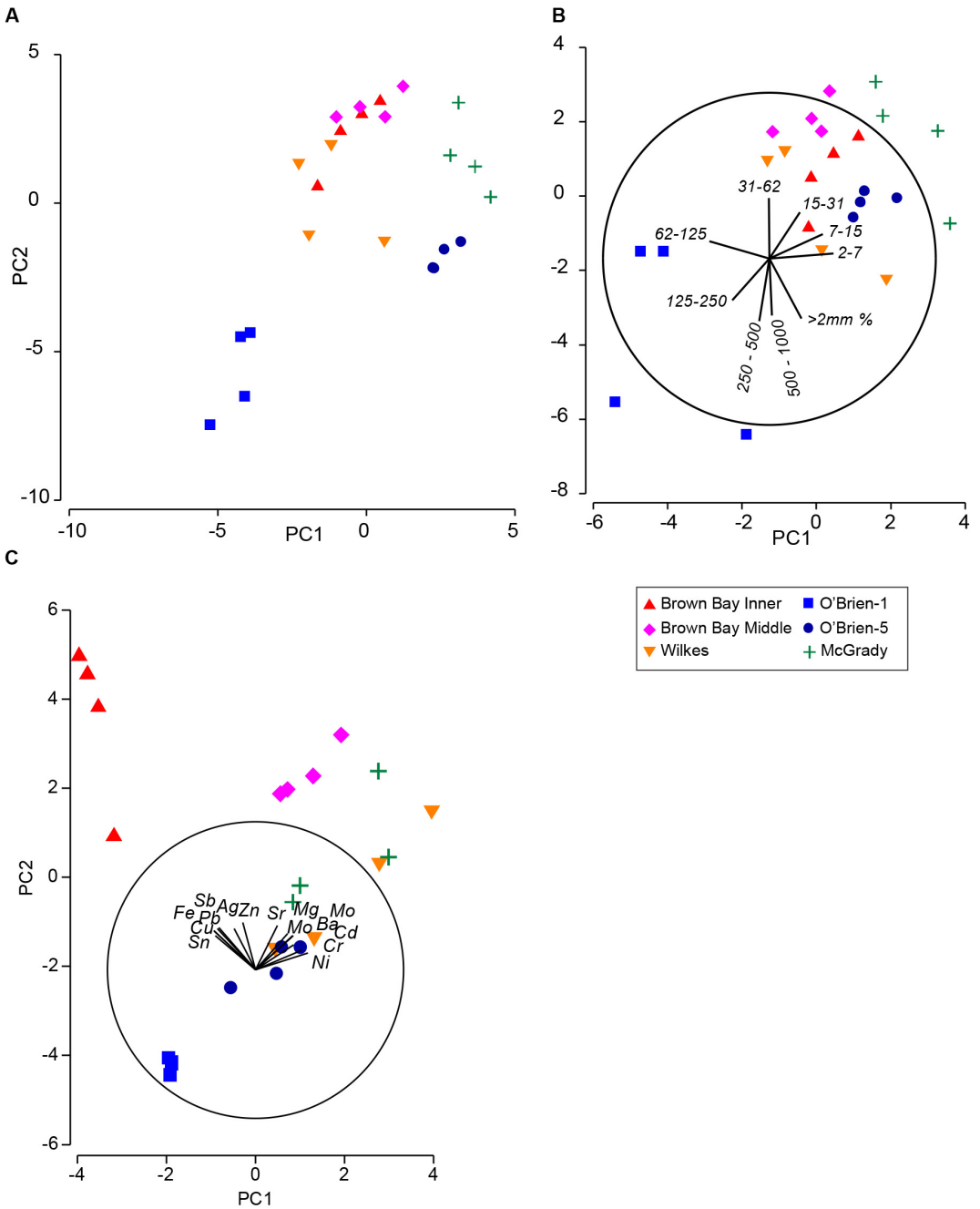

FIGURE 7 | (A) PCA ordination of combined environmental variables; **(B)** PCA ordination of sediment grain size variables; **(C)** PCA ordination of metal concentrations in sediment. Vector plots indicate the direction and size of the correlation between PC axes and variables.

5.6×10^6 m^{-2} in Potter Cove (**Table 9**), approximately 9km apart over water. In comparison, abundances at Casey were relatively even over the areas sampled ($1.5–2.0 \times 10^6$ m^{-2}) and are more similar to abundances found in sediments on the Antarctic shelf (**Table 9**). As Casey is further south it may more closely resemble the shelf than the Antarctic Peninsula in environmental conditions with longer duration of sea ice leading to lower productivity and lower food availability for meiobenthos.

Diversity

While there have been several Antarctic shallow water studies of meiobenthic abundance, there have been very few which have examined diversity. We recorded 38 nematode genera and 20 copepod families at Casey but identification was not done to species level, and there is very little data on species diversity in other shallow water Antarctic meiofauna studies. In the only two shallow water Antarctic studies to examine

TABLE 7 | ANOSIM results testing for differences among locations for environmental variables.

Group comparison	All (metals and GS)		Grain size		Metals	
	R	P%	R	P%	R	P%
Brown Bay Inner, Brown Bay Middle	0.906	2.9	0.594	2.9	1	2.9
Brown Bay Inner, McGrady	0.979	2.9	0.604	2.9	1	2.9
Brown Bay Inner, OB1	0.927	2.9	0.583	2.9	1	2.9
Brown Bay Inner, OB5	1	2.9	0.625	2.9	1	2.9
Brown Bay Inner, Wilkes	0.979	2.9	0.104	25.7	1	2.9
Brown Bay Middle, McGrady	0.76	2.9	0.646	2.9	0.948	2.9
Brown Bay Middle, OB1	0.99	2.9	0.635	2.9	1	2.9
Brown Bay Middle, OB5	1	2.9	1	2.9	1	2.9
Brown Bay Middle, Wilkes	0.813	2.9	0.344	2.9	1	2.9
McGrady, OB1	1	2.9	0.948	2.9	1	2.9
McGrady, OB5	0.948	2.9	0.813	2.9	1	2.9
McGrady, Wilkes	1	2.9	0.781	2.9	1	2.9
OB1, OB5	0.833	2.9	0.594	2.9	1	2.9
OB1, Wilkes	0.854	2.9	0.479	2.9	1	2.9
OB5, Wilkes	0.948	2.9	0.469	2.9	1	2.9

nematode diversity, at Signy Island, Vanhove et al. (1998) found 19 nematode genera but Lee et al. (2001b) found 49 genera representing 65 species. Our study found similar diversity to the deep continental shelf in the eastern Weddell Sea, where a total of 38 nematode genera were found by Lee et al. (2001a). In contrast, nematode diversity is generally much higher in Antarctic shelf waters, for example: Vanhove et al. (1999) found 158 genera in the deeper waters of Kapp Norvegia and the Halley Bay shelf and slope (211–2080 m); Raes et al. (2010) found 80 genera in deep shelf waters of the Larsen ice-shelf area; and Hauquier et al. (2011) found 66 nematode genera in only 4 replicate cores in a supposedly impoverished Larsen Ice Shelf area which had only recently become ice free. New approaches, however, have revealed that shallow-water diversity may be much higher than described to date. Using a metabarcoding approach, the shallow water meiofaunal diversity at Adelaide Island on the Antarctic peninsula was found to be potentially as diverse as in temperate regions, with over 90 nematode operational taxonomic units (OTUs) (Fonseca et al., 2017). Such approaches have not yet been tried elsewhere specifically for meiofauna in Antarctica. There are insufficient studies to determine whether the diversity of nematodes observed in our study at Casey is generally representative of Antarctic shallow water ecosystems.

Very few studies have examined meiobenthic copepod diversity in the Antarctic region. We observed 20 copepod families in this study. The only other shallow water locality in Antarctica where copepods have been identified to family is on King George Island, where 14 copepod families have been recorded, representing 34 species (Hong et al., 2011). This suggests that the 20 families observed in our study may represent more than 20 species, which would presumably change community patterns. In a study of deeper water continental shelf and slope sediments of the subantarctic Magellan region of South America, George (2005) reported 25 families of copepods, of which 6 families comprised at least 52 genera and 122 species, 80% of which were undescribed. In the Magellan region, however, species are potentially restricted to small geographic areas and families and genera display a much wider distribution than the species they enclose, and represent a broad spectrum of ecological habitats and roles (George, 2005). Shallow water environments such as in this study are likely to be less diverse due to the narrower niche of ecological habitats compared to a broad area of shelf and slope such as the Magellan region.

Spatial Variation

Significant spatial variation in meiofaunal communities at Casey Station was observed at all scales measured, from 10's to 1000's of meters. The greatest variation was found at the largest scale, between locations, which accounted for approximately 70% of the variation in nematode and copepod communities. Perhaps the most striking feature of this variation was that all locations had distinctly different communities, with very little overlap of samples in multivariate ordinations. This suggests that unique conditions and adaptation to those conditions at the different locations have shaped the nematode and copepod communities over potentially a long time.

At smaller scales, nematodes and copepods had very different distribution patterns. At scales of 100 m (between sites) there was very little variation in nematode communities but significant variation (6% of overall) for copepods; while in contrast at the 10 m scale (between plots within sites) there was significant variation in nematode communities (8% of overall) and no significant variation for copepods. There was a similar amount of variation between individual replicate cores for both nematodes and copepods and this comprised the second largest source of variation (approximately 21 to 25%), indicating large variation at scales < 1 m. Potential explanations of why nematode communities may exhibit greater variability at 10 m scale and for the copepods at 100-m scale may be related to the life style and mobility range of nematodes and copepods. Nematodes are confined to the sediment as they occupy interstitial space. The different response of copepods could be related to their life style,

TABLE 8 | Results of distance-based linear modeling (DISTLM) of environmental variables against nematode and copepod communities.

(A) Marginal tests results (single variable tests)

Nematodes			Copepods		
Variable	***P***	**Prop. variance**	**Variable**	***P***	**Prop. variance**
Log(As + 1)	0.0001	0.24	Log(Ba + 1)	0.0001	0.26
Log(Zn + 1)	0.0001	0.24	Log(Zn + 1)	0.0001	0.24
Log(Ag + 1)	0.0001	0.23	Log(Cd + 1)	0.0001	0.23
Log(Cu + 1)	0.0001	0.23	15.6–31	0.0001	0.22
Log(Pb + 1)	0.0001	0.23	Log(As + 1)	0.0001	0.22
Log(Ba + 1)	0.0001	0.22	Log(Pb + 1)	0.0001	0.22
15.6–31	0.0001	0.21	Log(Sn + 1)	0.0001	0.21
Log(Sn + 1)	0.0001	0.21	Log(Cu + 1)	0.0001	0.21
Log(Fe + 1)	0.0001	0.2	TOC	0.0002	0.21
Log(Sb + 1)	0.0003	0.2	Log(Sr + 1)	0.0002	0.2
31–62.5	0.0003	0.19	Log(Mo + 1)	0.0001	0.2
TOC	0.0008	0.17	31–62.5	0.0001	0.2
Log(Sr + 1)	0.0006	0.17	125–250	0.0002	0.2
Log(Mo + 1)	0.0006	0.16	Log(Sb + 1)	0.0001	0.19
Log(Cd + 1)	0.0015	0.15	Log(Ag + 1)	0.0003	0.18
125–250	0.0018	0.15	Log(Fe + 1)	0.0009	0.17
IGS	0.0021	0.14	IGS	0.0005	0.16
7.8–15.6	0.0034	0.14	7.8–15.6	0.0008	0.16
62.5–125	0.0048	0.13	graphic mean	0.0009	0.16
graphic mean	0.0085	0.13	250–500	0.0019	0.14
250–500	0.0072	0.12	Log(Mn + 1)	0.004	0.14
Log(Al + 1)	0.0209	0.11	Log(Ni + 1)	0.0064	0.13
Log(Mn + 1)	0.0341	0.1	2–7.8	0.0061	0.13
500–1000	0.0227	0.1	62.5–125	0.0091	0.12
2–7.8	0.0995	0.08	Log(Al + 1)	0.0196	0.11
1000–2000	0.0611	0.08	IGK	0.0221	0.1
Log(Ni + 1)	0.1159	0.07	Log(Co + 1)	0.0257	0.1
IGSD	0.1768	0.06	500–1000	0.033	0.09
IGK	0.2332	0.06	1000–2000	0.0478	0.09
Log(Co + 1)	0.3503	0.05	IGSD	0.0941	0.08
< 2mm%	0.8297	0.03	<2mm%	0.2526	0.05
> 2mm%	0.8246	0.03	>2mm%	0.2382	0.05

(B) DSTLM best model solutions

	Nematodes			Copepods		
	AICc	R^2	**Variables**	**AICc**	R^2	**Variables**
Forward selection	141.3	0.68	As, Sn, Ba, 31–62.5, Mn	129.8	0.79	Ba, Sn, Mn, As, 31–62.5, Sr
Stepwise selection	141.3	0.68	As, Sn, Ba, 31–62.5, Mn	129.8	0.79	Ba, Sn, Mn, As, 31–62.5, Sr

IGS = Inclusive graphic skewness; IGK = Inclusive graphic kurtosis; IGSD = inclusive graphic standard deviation.

and while copepods are also interstitial, they can also have a epibenthic-pelagic life style and may emerge and move across sediment surfaces more easily than nematodes (Rubal et al., 2011), giving them a larger range, and hence their potential responses to heterogeneity on the seafloor may be expressed at greater spatial scales compared to nematodes. The epibenthic life style of copepods may also allow them to actively avoid polluted sediments (Rubal et al., 2011). The two most abundant copepod families in our study, Tisbidae and Ectinosomatidae (**Table 1**), are known to actively move between the sediment to the water column, and such behavior has been described as a way to cope with pollution (Calow, 1991).

Previous studies investigating the role of drivers of meiofaunal variation at different spatial scales have shown that the smaller scales are important determinants of community composition and structure as they relate to the biogeochemical (e.g., sediment heterogeneity and micro-patchiness) and trophic environment of the meiofauna organisms in their interstitial space (Fonseca et al., 2010; Ingels and Vanreusel, 2013; Rosli et al., 2018). Small-scale environmental heterogeneity and associated trophic and biogeochemical conditions, as well as disturbance events and seasonal variability may drive the spatially contrasting settings in this area. It has been proposed that heterogeneity of habitats is an important determinant

TABLE 9 | Mean abundance ($\times 10^6$) and range of nematodes and copepods in Antarctic marine sediments.

			Nematodes			Copepods			Reference
	Depth m	Method	Mean	Range	% of total	Mean	Range	% of total	
Shallow (< 150 m)									
Casey	5–20	Manual corer	1.7	1.5–2.0	95	0.082	0.07–0.09	5	This study
Signy Island–Factory Cove	7–9	Manual corer	7.5	3.7–11.4	86–90	1.3	1.1–1.5	11–16	Vanhove et al., 1998
Signy Island–Factory Cove	8–9	Manual corer	1.8	1.2–1.4	84–94	0.045	0.038–0.052	2.0–2.6	Lee et al., 2001b
King George Island–Martel Inlet	15	manual corer	2.4	1.2–4.4	64	0.37	0.16–0.7	9.5	Skowronski and Corbisier, 2002
King George Island–Marion Cove	30–40	remote corer	0.43	0.11–0.81	93	0.014	0.004–0.028	3.2	Hong et al., 2011
King George Island–Potter Cove	15	manual corer	5.6	1.2–11.5	92–98	0.1	0.004–0.2	0.3–1.8	Pasotti et al., 2014
Terra Nova Bay	40–127	Van Veen grab	2.45	0.15–5.1	46–91	0.14	0.012–0.33	1.8–5.7	Danovaro et al., 1999
Deep (> 200 m)									
Weddell Sea–Halley Bay to Kapp Norvegia	500–2000	multiboxcorer/multicorer	1.6	0.73–3.0	95	0.05	0.02–0.12	3	Herman and Dahms, 1992
Weddell Sea–Kapp Norvegia	211–2080	multiboxcorer	0.09	0.08–0.096	83–97	0.08	0.03–0.23		Vanhove et al., 1995
Weddell Sea–Kapp Norvegia	255–298	multiboxcorer	1.23	1.1–1.3	92	0.03	0.02–0.04	2.3	Lee et al., 2001a
Ross Sea–Joides Basin	556–587	box corer	1.16	0.6–1.7	97	0.015	0.007–0.02	1.3	Fabiano and Danovaro, 1999
Ross Sea–Mawson Bank	432–446	box corer	0.11	0.06–0.16	56	0.05	0.03–0.07	27	Fabiano and Danovaro, 1999
Bransfield Strait	222–518	Multicorer	5.85	4.25–7.96	73–93	0.97	1.14–3.64	3.0–25.4	Veit-Köhler et al., 2018
Drake Passage	423–756	Multicorer	3.84	1.44–6.19	57–96	0.26	0.14–0.53	2.6–10.7	Veit-Köhler et al., 2018
Weddell Sea	350–498	Multicorer	3.18	2.32–3.95	83–91	0.28	0.15–4.25	5.1–11.8	Veit-Köhler et al., 2018
Larsen A/B	275–427	Multicorer	0.96	0.39–1.60	69–95	0.027	0.041–0.084	2.4–11.8	Rose et al., 2015
Elephant Island	400–412	Multicorer	1.31	1.31	90.4	0.027	0.027	1.9	Rose et al., 2015
Western Weddell Sea	1085–4063	Multicorer	0.49	0.36–0.63	89–94	0.019	0.019	2.3–4.7	Rose et al., 2015

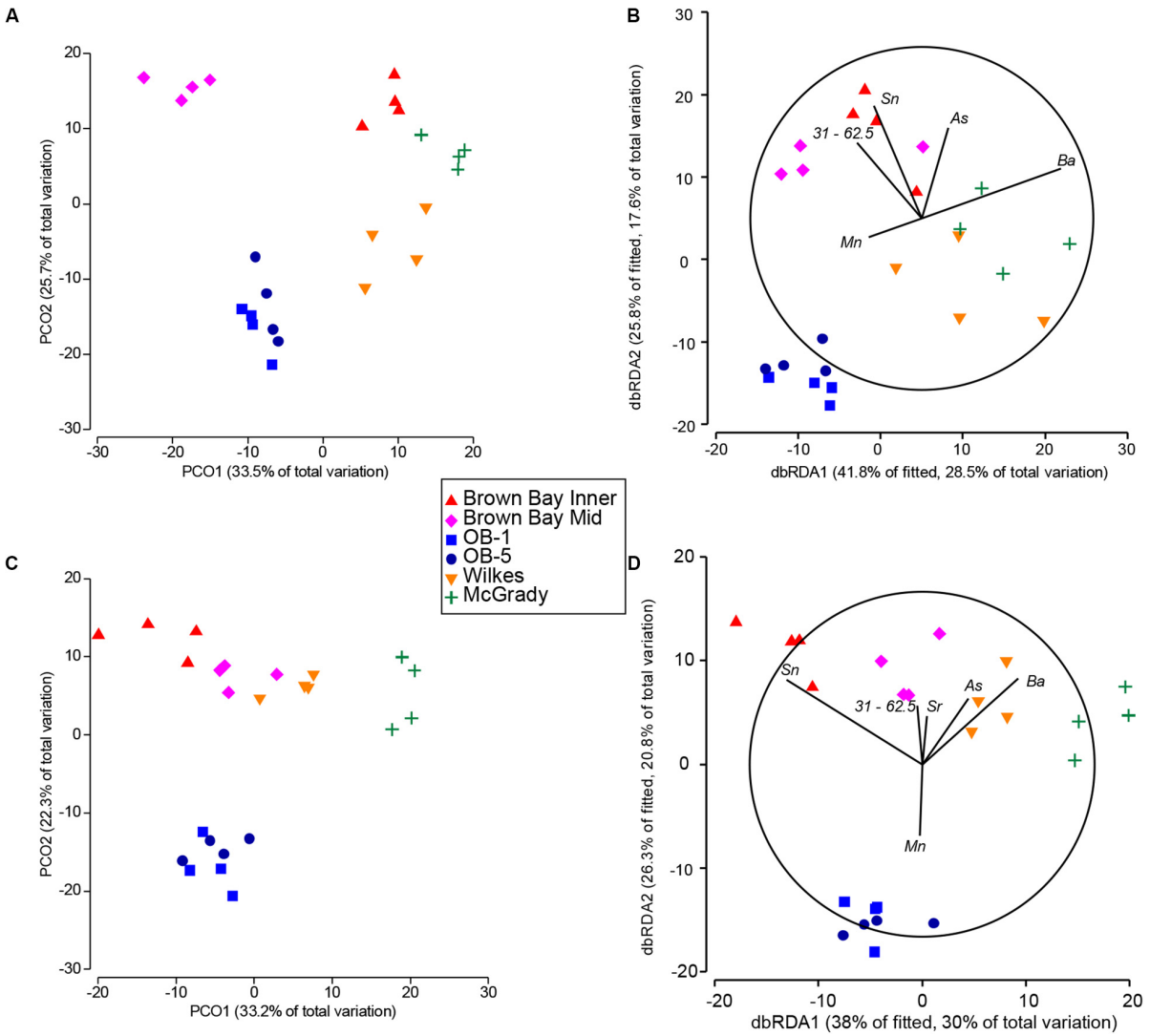

FIGURE 8 | Comparison of fitted DSTLM environmental models with respective PCO ordinations of nematode and copepod communities. **(A)** PCO ordination of nematode communities; **(B)** dbRDA ordination of fitted best environmental model explaining nematode community patterns; **(C)** PCO ordination of copepod communities; **(D)** dbRDA ordination of fitted best environmental model explaining copepod community patterns. Sb (antimony) represents iron, lead and copper.

of meiofaunal biodiversity in shallow waters (Mokievsky and Azovsky, 2002; Vanreusel et al., 2010).

Similar patterns of spatial variation were observed for macrofaunal communities at the same locations (Stark et al., 2003a) suggesting that the same environmental drivers are influencing both meiofaunal and macrofaunal communities at similar scales (Stark et al., 2003b). However, meiofaunal communities displayed greater differentiation between locations than macrofauna, indicating a high degree of suitability of meiofauna for environmental monitoring purposes.

Environmental Influences on Meiofaunal Communities

Of all the environmental drivers examined in this study it was metals that were able to explain the most variation in meiofaunal community patterns, particularly those metals associated with anthropogenic sources. These had some of the strongest correlations with community patterns at the location scale. This was principally due to the large differences in metal concentrations between Brown Bay and other locations, however, this does not necessarily infer causality, as there could be other unmeasured differences in environmental conditions between Brown Bay and other locations. Cause and effect can only be established by experimental studies, either in field experiments (e.g., Thompson et al., 2007) or laboratory experiments (e.g., Stark, 1998). The effects of metals and hydrocarbons have been experimentally demonstrated on macrofaunal communities in Brown Bay (Stark et al., 2003c). Contamination in Brown Bay also includes hydrocarbons (Stark et al., 2005) and may also include persistent organic pollutants, which are known to occur around some Antarctic stations and waste

disposal sites (Lenihan and Oliver, 1995; Wild et al., 2015; Stark et al., 2016).

Sediment grain-size properties and organic matter content also had strong correlations with community patterns and were included in the best explanatory models. Sediment grain size can be particularly variable in shallow marine sediments, and was found to be highly variable in this study, not only between locations but also at the plot (10 m) and replicate level, with each accounting for approximately 25% of variation in grain size. Meiofaunal diversity can be regulated by the grain size of the sediments (Steyaert et al., 1999) and the differences in grain size between locations in this study were strongly correlated with differences in meiofaunal communities. Sediment properties (grain size and food content) have been found to be important determinants of meiofaunal community patterns generally (Coull, 1999), and this has also found to apply in studies from Antarctica, such as King George Island (Skowronski and Corbisier, 2002) and Signy Island (Vanhove et al., 1998).

In our study the influence of sediment metals on meiofauna appears to be stronger than that of grain size. The differences found between nematode and copepod communities at Brown Bay and other locations were strongly correlated with higher concentrations of metals including lead, copper, iron and antimony, which were known to occur in the adjacent waste disposal site (Stark et al., 2008). Despite having very different sediment grain size properties the meiofaunal communities at the two locations in O'Brien Bay were very similar, particularly nematode communities. Meiofauna are well known to respond to metal contamination, from both laboratory and field surveys and experimental studies (Coull and Chandler, 1992; Somerfield et al., 1994; Schratzberger et al., 2000). As concentrations of all metals increases there is increased mortality of meiofauna and reduced reproductive output (*in vitro*) and some fauna such as copepods have been shown to be more affected by paired metal mixtures than by single metals (Coull and Chandler, 1992). Mixed pollutants, such as metals and hydrocarbons, have been shown to inhibit life-history progressions in the laboratory, and to cause synergistic reductions in the diversity and abundance of meiofauna in the field (Coull and Chandler, 1992).

Physical disturbance is another potential influence on meiobenthic communities, such as that caused by calving of ice cliffs and large snow banks that form in the lee of the ice cliffs, which can break off during summer when the sea ice breaks out. Physical disturbance caused by this would be intermittent and patchy, and not necessarily throughout the whole bay, but it may nevertheless influence the benthic communities (Schratzberger et al., 2009). The McGrady area is characterized by ice cliffs which are bigger than at Wilkes or Brown Bay, extending to the seabed at 5–7m water depth, so this may be potentially more of an influence there. The nematode communities at McGrady were more similar to Brown Bay than to the Wilkes and O'Brien locations, possibly due to physical disturbance induced by the specific glacial conditions in the bay.

There was also a difference in nematode and copepod communities between the two large bays: Newcomb Bay (which contained Brown Bay, McGrady and Wilkes) and O'Brien Bay (which contained O'Brien Bay-1 and -5). Larger scale factors such as the hydrographic characteristics of Newcomb and O'Brien Bay may also have had an effect on meiofaunal communities. Despite significant differences in sediment grain size and organic matter content between the two O'Brien Bay locations, they had very similar meiofaunal communities and together they displayed distinct differences from the locations in Newcomb Bay. Hydrographic characteristics influence food availability in benthic habitats, by influencing benthic-pelagic coupling, and can have a strong effect on meiofaunal communities (Veit-Köhler et al., 2018) and is driven by oceanographic conditions such as water temperature, salinity, sea-ice cover and pelagic primary production. Not only is food supply (quantity) very influential in structuring meiofaunal communities, but food quality can also be important (Fabiano and Danovaro, 1999), such as the concentrations of protein, carbohydrate and lipids. The distribution of deep-sea Antarctic meiofauna can be strongly related to the amount of utilizable organic matter in the sediment (Fabiano and Danovaro, 1999), which is controlled by sedimentation and organic degradation rates. Some of the differences between the two large bays and among locations observed in this study are likely to be influenced by local variation in hydrographic characteristics (currents, sea ice regime), which would also influence benthic pelagic coupling and thus sedimentation, food availability and organic degradation rates. Modeling has indicated that differences in meiofaunal communities between the two bays were also correlated with higher concentrations of organic matter (and very coarse silt) and barium in Newcomb Bay. Barium is considered to be a useful proxy for primary productivity in paleo studies (Prakash Babu et al., 2002; Liguori et al., 2016) and together with generally higher levels of organic matter in sediments may indicate generally higher levels of primary production in Newcomb Bay.

Human Impacts

Another large scale difference between the two bays could be from generally higher contamination throughout Newcomb Bay (Wilkes, McGrady, Brown Bay Inner and Middle). There is evidence for this for many metals at the locations examined in Newcomb Bay (**Table 6**) but there may be other contaminants present throughout the bay that have not been measured, such as hydrocarbons. Newcomb Bay has a long history of continuous human occupation, which to date has comprised three separate Antarctic research stations dating back to 1957. Prior to modern environmental management there were many practices and activities which could have led to widespread pollution, such as igniting full drums of fuel on the shoreline to farewell ships and disposing of old vehicles on the sea ice (personal communication by previous expeditioners to J. Stark). Such anecdotal evidence is not captured by official records but may have had long term consequences. A few metals are generally higher in Newcomb than O'Brien Bay including iron, arsenic and zinc, which may also explain why nematode communities at McGrady were more similar to Brown Bay than O'Brien Bay.

Meiofauna are considered to be sentinels of environmental changes making them useful bioindicators of human impacts

(Somerfield et al., 1994; Kennedy and Jacoby, 1999; Semprucci and Balsamo, 2012; Alves et al., 2013; Semprucci et al., 2015; Schratzberger and Ingels, 2017). In this study there were distinctive differences in nematode and copepod communities between control and polluted locations. Activities associated with the waste disposal site in Brown Bay have resulted in increased metals, organic content (Stark, 2000; Stark et al., 2003b) and hydrocarbons (Stark et al., 2005) in sediments, which have likely contributed to the differences in meiofaunal communities between Brown Bay and control locations. Other studies have found that meiofaunal assemblages, and nematodes in particular, are indicative of differences in metal contamination and of metal gradients in sediments (Somerfield et al., 1994; Coull, 1999; Schratzberger et al., 2000).

Differences in nematode communities between the Inner and Middle locations within Brown Bay, though only several hundred meters apart, were as great as between other locations separated by many kilometers. Copepod communities at the two Brown Bay locations, however, were the most similar among all locations. Some metals have higher concentrations at Brown Bay Inner (Cu, Fe, Pb, Sn) and others are higher at Brown Bay Middle (Ag, As, Cr, Ni, Sb, Zn) (Stark et al., 2003b). It is not understood why this is the case although it may relate to the contamination history of the dump site, as large items of rubbish have been observed on the sea bed (metal components, fuel drums, treated timber) and may have contributed to localized patterns or hot spots of contamination. Previous waste management practices included using explosives to create a hole in the sea ice and bulldozing rubbish into it, although such practices have long since been discontinued (Stark et al., 2006). As discussed above, the lifestyle of copepods, with the potential for epibenthic dispersal and movement, may serve to dampen small-scale localized pollution effects, which are better reflected in nematode communities. Hydrocarbon levels are generally greater at the Inner than the Middle location (Stark et al., 2005). It is thus difficult to determine which part of Brown Bay is the more polluted but copepods appear to be responding in the same manner in both locations, while nematodes are responding differently. Warwick (1986) suggested that copepods are generally more sensitive to the effects of pollution than nematodes, however our study indicates that Antarctic nematodes may be more sensitive on small scales than copepods.

In comparison to other regions of Antarctica Brown Bay could be considered to be low to moderately polluted (Stark et al., 2014b). Contamination levels are lower than observed at the severely polluted Winter Quarters Bay at McMurdo Station, but impacts resulting from this pollution are very clear and in some respects are as large as seen at McMurdo (Stark et al., 2014b), not only in meiofauna but also in benthic diatom (Cunningham et al., 2005), macrofaunal (Stark et al., 2003a, 2004) and epifaunal communities (Stark, 2008).

Meiofaunal communities at Wilkes, however, do not appear to be impacted by the former waste disposal site at Wilkes Station. Nematode communities at Wilkes were not significantly different from controls and were most similar to the control locations in O'Brien Bay. Whereas the copepod communities at Wilkes, while also not significantly different to the controls, were more similar to the control location McGrady Cove in Newcomb Bay. Despite evidence for contamination of meltwater from sites at Wilkes flowing into the marine environment at concentrations well in excess of the Australian and New Zealand (ANZECC) guidelines (Fryirs et al., 2015), metal levels in marine sediments are generally not significantly different from the control locations, although other contaminants, such as hydrocarbons, have not been measured. The Wilkes waste dumpsite is much older than the Casey site, dating back to 1957 and was abandoned in 1969. Contaminants may not have accumulated in adjacent marine sediments to the same extent or marine communities may have recovered from pollution impacts or may not have been as strongly impacted as Brown Bay. Stark et al. (2003c) found that the macrofaunal communities at Wilkes were similar in some ways to those of the control locations (O'Brien Bay) but in other ways resembled Brown Bay, suggesting that perhaps it was impacted at some point since human occupation.

While clear patterns related to disturbance were observed at the community level, patterns for individual taxa in relation to disturbance were less clear. A few taxa were consistently more abundant at impacted locations at Brown Bay including the nematode genera *Promonhystera, Paralinhomoeus* and *Pierrickia* and the copepod family Pseudotachidiidae. A few taxa were more abundant at control locations including the nematode genera *Daptonema, Halalaimus* and *Microlaimus* and the copepod families Dactylopusiidae and Rometidae. Coherence curves for nematodes (**Figure 5**) provided some insights into the use of certain genera as indicators, particularly when compared to findings in previous studies. Each location exhibited a group of nematode taxa genera which were characteristic of that location (**Figure 5**) and in some instances may be indicative of a pollution response., e.g., Bianchelli et al. (2018). Several genera that have been shown to respond to different types of disturbances in other studies are highlighted below.

There is a subset of nematode genera with high abundance at the polluted and organic matter loaded Brown Bay Inner location (**Figure 5D**). *Leptolaimus* has been previously recognized as tolerant to high organic matter levels as well as physical disturbance (Schratzberger et al., 2009; Losi et al., 2013). *Odontophora* has been recognized as opportunistic in conditions with high Ni content (Balsamo et al., 2012 and references within). *Sabatieria* and *Theristus* (**Figure 5D**) are two genera that have often been mentioned as tolerant and opportunistic in various disturbed conditions such as physical disturbance, general pollution, hypoxia or anoxia, and in the context of metal contamination (Somerfield et al., 1994; Millward and Grant, 1995; Austen and Somerfield, 1997; Gyedu-Ababio et al., 1999; Balsamo et al., 2012). It is not surprising then that these genera are abundant at the Brown Bay Inner location as they are able to colonize disturbed or impacted sediments rapidly and persist in adverse conditions. Also striking are the abundant genera associated with the polluted Brown Bay Middle location (**Figure 5E**). *Paramonhystera* and *Promonhystera* are members of the monhysterid family, traditionally recognized as containing opportunistic and tolerant genera (Balsamo et al., 2012; Semprucci et al., 2015). *Pierrickia* has also been recognized as a genus that is tolerant to high organic matter levels and

contaminated sediments (Danovaro et al., 2009; Losi et al., 2013). These genera provide some context in which to interpret the usefulness of nematode in indicating sediment disturbance and contamination. However, in this study, a number of other genera that have been postulated as either sensitive or tolerant to pollution, contamination, and disturbed conditions in other studies did not adhere to the expected abundance or presence-absence in that context. *Paracanthonchus* was assigned to the same subset of nematode genera in the coherence analysis, but did not generally conform to the same pattern as other taxa in the group as it had minimum abundance in Brown Bay Inner samples. Danovaro et al. (1995) and Balsamo et al. (2012) indicate that this genus is sensitive to hydrocarbon impacts and was one of the first genera to disappear following an oil spill, and hydrocarbon concentrations are generally higher at Brown Bay Inner (Stark et al., 2005). This highlights that care should be taken when interpreting individual nematode genera patterns, since communities are driven not just by individual responses, but also by a wide range of abiotic and biotic interactions. Complex succession patterns in response to disturbance and interactions with other benthic components as part of food webs or through competitive interactions may also confound clear patterns. Another example is the genus *Halalaimus,* which has been recognized as being sensitive to organic loads (Essink and Keidel, 1998; Mirto et al., 2002; Vezzulli et al., 2008). This is inconsistent with the observations in our study, with sediments at Brown Bay (where it was least abundant) and McGrady (where it was most abundant) both containing high levels of organic matter. This suggests that in this study it was more responsive to contaminants than organic loading of sediments. In addition, responses to pollution, disturbance or other environmental change may differ among species within the same genus.

Meiofauna as Environmental Indicators in Antarctica

While it is well documented that meiofauna are generally excellent indicators for natural or anthropogenic environmental change (Zeppilli et al., 2015), caution should be used in interpreting abundance data when little is known of their temporal or spatial distribution and heterogeneity at specific locations. For example, significant seasonal variations in meiofaunal abundance were found in shallow water at Signy Island (Vanhove et al., 2000) and at King George Island (Pasotti et al., 2014). In the present study, the specific environmental conditions related to the geographic and glacial conditions and sediment heterogeneity at the different locations likely have some influence on the nematode and copepod communities, but these varied together with the metal signatures and their impacts on the faunal communities. Temporal variability can also be related to spatial heterogeneity, particularly in the Antarctic, where glacial characteristics and influences vary seasonally with ice melt and sea ice break up.

Other benthic community components have been well studied in coastal areas of east Antarctica at Casey Station including the macrobenthos (Stark et al., 2003a,b) and microphytobenthos (Cunningham et al., 2003, 2005; Polmear et al., 2015) but the meiofauna are an important component of benthic ecosystems for which little was previously known in this region. Given the clear differences in both nematode and copepod communities at the location scale and their strong correlation with environmental patterns, particularly anthropogenic disturbance, this study adds further evidence that these taxa may be excellent indicators of environmental change in Antarctic coastal waters. While there is a clear signature of human impacts at the polluted Brown Bay locations which can be detected using nematode and copepod communities, there are also important differences among locations driven by a range of natural environmental variables. These need to be taken into account when drawing comparisons and disentangling the nature and effect of the anthropogenic and natural drivers of these communities. Further understanding of responses of Antarctic meiofauna to environmental change would be gained by examining species level responses, as well as including other less abundant elements of the meiofaunal community such as kinorhynchs, gastrotrichs, tardigrades, polychaetes and crustaceans such as amphipods.

SAMPLING AND FIELD STUDIES

All necessary permits for sampling and observational field studies were obtained by the authors from the competent authorities. The study is compliant with CBD and Nagoya protocols.

DATA AVAILABILITY STATEMENT

The datasets generated for this study are available at https://data.aad.gov.au/metadata/records/AAS_2201_Casey_Monitoring_Meiofauna.

AUTHOR CONTRIBUTIONS

JS designed the study and contributed to the field work, collection of samples, and laboratory analysis of environmental samples. MM conducted the laboratory analysis and identification of meiofaunal communities. JS, JI, MM, and AM contributed to the statistical analysis and interpretation. JS and JI prepared the figures. All authors contributed to the writing and editing of the manuscript.

FUNDING

This study was funded by the Universiti Sains Malaysia, Australian Antarctic Division (AAS projects 2201 and 4180) and Institute for Marine and Antarctic Studies at the University of Tasmania.

ACKNOWLEDGMENTS

We are grateful to the following people for their assistance and support in this study: Sazlina Salleh, Martin Riddle, Glenn

Johnstone, Scott Stark, Anne Palmer, Kate Stark, and the Casey dive team in 2005/06 season. Some of the content of this study was part of a postgraduate Ph.D. thesis of MM (Mohammad, 2011) and is the only medium it has appeared in, and is in line with the University of Tasmania policy, and can be accessed online at http://encore.lib.utas.edu.au/iii/encore/record/C__Rb1570829.

REFERENCES

Alves, A. S., Adão, H., Ferrero, T., Marques, J., Costa, M. J., and Patrício, J. (2013). Benthic meiofauna as indicator of ecological changes in estuarine ecosystems: the use of nematodes in ecological quality assessment. *Ecol. Indic.* 24, 462–475. doi: 10.1016/j.ecolind.2012.07.013

Anderson, M. J. (2006). Distance-based tests for homogeneity of multivariate dispersions. *Biometrics* 62, 245–253. doi: 10.1111/j.1541-0420.2005.00440.x

Anderson, M. J., Gorley, R. N., and Clarke, K. R. (2008). *PERMANOVA+ for PRIMER: Guide to Software and Statistical Methods*. Plymouth, UK: PRIMER-E.

Anderson, M. J., and Robinson, J. (2001). Permutation tests for linear models. *Aust. New Zeal. J. Stat.* 43, 75–88.

Austen, M. C., and Somerfield, P. J. (1997). A community level sediment bioassay applied to an estuarine heavy metal gradient. *Mar. Environ. Res.* 43, 315–328. doi: 10.1016/s0141-1136(96)00094-3

Balsamo, M., Semprucci, F., Frontalini, F., and Coccioni, R. (2012). "Meiofauna as a tool for marine ecosystem biomonitoring," in *Marine Ecosystems*, ed. C. Antonio (Rijeka: In Tech).

Bianchelli, S., Buschi, E., Danovaro, R., and Pusceddu, A. (2018). Nematode biodiversity and benthic trophic state are simple tools for the assessment of the environmental quality in coastal marine ecosystems. *Ecol. Indicat.* 95, 270–287. doi: 10.1016/j.ecolind.2018.07.032

Bodin, P. (1997). Catalogue of the new marine harpacticoid copepods. *Doc. Trav. Inst. Roy. Sci. Nat. Belg.* 89:304.

Borum, J., and Sand-Jensen, K. (1996). Is total primary production in shallow coastal marine waters stimulated by nitrogen loading?. *Oikos* 76, 406–410.

Boucher, G., and Lambshead, P. J. D. (1995). Ecological biodiversity of marine nematodes in samples from temperate, tropical, and deep-sea regions. *Conserv. Biol.* 9, 1594–1604. doi: 10.1046/j.1523-1739.1995.09061594.x

Calow, P. (1991). Physiological costs of combating chemical toxicants: ecological implications. *Comp. Biochem. Physiol. C* 100, 3–6. doi: 10.1016/0742-8413(91)90110-f

Clark, G. F., Raymond, B., Riddle, M. J., Stark, J. S., and Johnston, E. L. (2015). Vulnerability of shallow Antarctic invertebrate-dominated ecosystems. *Aust. Ecol.* 40, 482–491. doi: 10.1111/aec.12237

Clarke, K. R., and Gorley, R. N. (2006). *PRIMER v6. User Manual/Tutorial Plymouth Routine in Mulitvariate Ecological Research*. Plymouth: Plymouth Marine Laboratory

Coull, B. C. (1999). Role of meiofauna in estuarine soft-bottom habitats. *Aust. J. Ecol.* 24, 327–343. doi: 10.1046/j.1442-9993.1999.00979.x

Coull, B. C., and Chandler, G. T. (1992). Pollution and meiofauna: field, laboratory, and mesocosm studies. *Oceanogr. Mar. Biol.* 30, 191–271.

Cunningham, L., Snape, I., Stark, J. S., and Riddle, M. J. (2005). Benthic diatom community response to environmental variables and metal concentrations in a contaminated bay adjacent to Casey Station. Antarctica. *Mar. Pollut. Bull.* 50, 264–275. doi: 10.1016/j.marpolbul.2004.10.012

Cunningham, L., Stark, J. S., Snape, I., McMinn, A., and Riddle, M. J. (2003). Effects of metal and petroleum hydrocarbon contamination on benthic diatom communities near Casey Station, Antarctica: an experimental approach. *J. Phycol.* 39, 490–503. doi: 10.1046/j.1529-8817.2003.01251.x

Danovaro, R., Fabiano, M., and Vincx, M. (1995). Meiofauna response to the Agip Abruzzo oil spill in subtidal sediments of the Ligurian Sea. *Mar. Pollut. Bull.* 30, 133–145. doi: 10.1016/0025-326x(94)00114-o

Danovaro, R., Gambi, C., Höss, S., Mirto, S., Traunspurger, W., and Zullini, A. (2009). *Case Studies Using Nematode Assemblage Analysis in Aquatic Habitats. Nematodes as Enviornmental Indicators*. Wallingford: CABI publishing, 146–171.

Danovaro, R., Pusceddu, A., Mirto, S., and Fabiano, M. (1999). Meiofaunal assemblages associated with scallop beds (Adamussium colbecki) in the coastal sediments of Terra Nova Bay (Ross Sea, Antarctica). *Antarctic Sci.* 11, 415–418. doi: 10.1017/s0954102099000528

Essink, K., and Keidel, H. (1998). Changes in estuarine nematode communities following a decrease of organic pollution. *Aquatic Ecol.* 32, 195–202.

Fabiano, M., and Danovaro, R. (1999). Meiofauna distribution and mesoscale variability in two sites of the Ross Sea (Antarctica) with contrasting food supply. *Polar Biol.* 22, 115–123. doi: 10.1007/s003000050398

Fonseca, G., Soltwedel, T., Vanreusel, A., and Lindegarth, M. (2010). Variation in nematode assemblages over multiple spatial scales and environmental conditions in Arctic deep seas. *Progr. Oceanogr.* 84, 174–184. doi: 10.1016/j.pocean.2009.11.001

Fonseca, V., Sinniger, F., Gaspar, J., Quince, C., Creer, S., Power, D. M., et al. (2017). Revealing higher than expected meiofaunal diversity in Antarctic sediments: a metabarcoding approach. *Sci. Rep.* 7:6094.

Fryirs, K. A., Hafsteinsdóttir, E. G., Stark, S. C., and Gore, D. B. (2015). Metal and petroleum hydrocarbon contamination at Wilkes Station, East Antarctica. *Antarctic Sci.* 27, 118–133. doi: 10.1017/s0954102014000443

George, K. H. (2005). Sublittoral and bathyal Harpacticoida (Crustacea, Copepoda) of the Magellan region. Composition, distribution and species diversity of selected major taxa. *Sci. Mar.* 69, 147–158. doi: 10.3989/scimar.2005.69s2147

Graham, M. H., and Edwards, M. S. (2001). Statistical significance vs. fit: estimating relative importance of individual factors in ecological analysis of variance. Oikos 93, 505–513

Gyedu-Ababio, T., Furstenberg, J., Baird, D., and Vanreusel, A. (1999). Nematodes as indicators of pollution: a case study from the Swartkops River system, South Africa. *Hydrobiologia* 397, 155–169.

Hauquier, F., Ingels, J., Gutt, J., Raes, M., and Vanreusel, A. (2011). Characterisation of the nematode community of a low-activity cold seep in the recently ice-shelf free Larsen B area, Eastern Antarctic Peninsula. *PLoS One* 6:e22240. doi: 10.1371/journal.pone.0022240

Heip, C., Vincx, M., and Vranken, G. (1985). The ecology of marine nematodes. *Oceanogr. Mar. Biol.* 23, 399–489.

Heiri, O., Lotter, A. F., and Lemcke, G. (2001). Loss on ignition as a method for estimating organic and carbonate content in sediments: reproducibility and comparability of results. *J. Paleolimnol.* 25, 101–110.

Herman, R., and Dahms, H. (1992). Meiofauna communities along a depth transect off Halley Bay (Weddell Sea-Antarctica). *Polar Biol.* 12, 313–320. doi: 10.1007/978-3-642-77595-6_36

Hong, J.-H., Kim, K.-C., Lee, S.-H., Back, J.-W., Lee, D.-J., and Lee, W.-C. (2011). The community structure of meiofauna in Marian cove, King George island, Antarctica. *Ocean Polar Res.* 33, 265–280. doi: 10.4217/opr.2011.33.3.265

Ingels, J., Billett, D. S. M., Kiriakoulakis, K., Wolff, G. A., and Vanreusel, A. (2011a). Structural and functional diversity of Nematoda in relation with environmental variables in the Setúbal and Cascais canyons, Western Iberian Margin. *Deep Sea Res. Part II* 58, 2354–2368. doi: 10.1016/j.dsr2.2011.04.002

Ingels, J., Tchesunov, A. V., and Vanreusel, A. (2011b). Meiofauna in the Gollum Channels and the Whittard Canyon, Celtic Margin–how local environmental conditions shape nematode structure and function. *PLoS One* 6:e20094. doi: 10.1371/journal.pone.0020094

Ingels, J., Kiriakoulakis, K., Wolff, G. A., and Vanreusel, A. (2009). Nematode diversity and its relation to the quantity and quality of sedimentary organic matter in the deep Nazare Canyon, Western Iberian Margin. *Deep-Sea Res. Part I Oceanogr. Res. Pap.* 56, 1521–1539. doi: 10.1016/j.dsr.2009.04.010

Ingels, J., and Vanreusel, A. (2013). The importance of different spatial scales in determining structural and functional characteristics of deep-sea infauna communities. *Biogeosciences* 10, 4547–4563. doi: 10.5194/bg-10-4547-2013

Ingels, J., Hauquier, F., Raes, M., Vanreusel, A. (2014). "Antarctic free-living marine nematodes," in *Biogeographic atlas of the Southern Ocean*, eds C. De Broyer, P. Koubbi, H. Griffiths, B. Raymond, C. D. Udekem d'Acoz and A. Van de Putte (Cambridge: Scientific Committee on Antarctic Research).

Kennedy, A. D., and Jacoby, C. A. (1999). Biological indicators of marine environmental health: meiofauna – a neglected benthic component? *Environ. Monit. Assess.* 54, 47–68.

Lee, H. J., Gerdes, D., Vanhove, S., and Vincx, M. (2001a). Meiofauna response to iceberg disturbance on the Antarctic continental shelf at Kapp Norvegia (Weddell Sea). *Polar Biol.* 24, 926–933. doi: 10.1007/s003000100301

Lee, H. J., Vanhove, S., Peck, L. S., and Vincx, M. (2001b). Recolonisation of meiofauna after catastrophic iceberg scouring in shallow Antarctic sediments. *Polar Biol.* 24, 918–925. doi: 10.1007/s003000100300

Lee, H. J., and Van de Velde, J. (1999). "Biodiversity of Antarctic nematodes," in *Reports on Polar Research, the Expedition ANTARKTIS ZX/3 (EASIZ II)*, eds W. E. Aaa and J. Gaa (Bremerhaven: Boehl & Oppermann).

Lenihan, H. S., and Oliver, J. S. (1995). Anthropogenic and natural disturbances to marine benthic communities in Antarctica. *Ecol. Appl.* 5, 311–326.

Liguori, B. T., Almeida, M., and Rezeende, C. (2016). Barium and its Importance as an Indicator of (Paleo) Productivity. *Anais Acad. Bras. Ciências* 88, 2093–2103. doi: 10.1590/0001-3765201620140592

Losi, V., Ferrero, T., Moreno, M., Gaozza, L., Rovere, A., Firpo, M., et al. (2013). The use of nematodes in assessing ecological conditions in shallow waters surrounding a Mediterranean harbour facility. *Estuar. Coast. Shelf Sci.* 130, 209–221. doi: 10.1016/j.ecss.2013.02.017

McMinn, A., Gibson, J., and Hodgson, D. (1995). Nutrient limitation in Ellis Fjord, eastern Antarctica. *Polar Biol.* 15, 269–276.

McMinn, A., and Hodgson, D. (1993). Summer phytoplankton succession in Ellis Fjord, eastern Antarctica. *J. Plankton Res.* 15, 925–938. doi: 10.1093/plankt/15.8.925

Millward, R. N., and Grant, A. (1995). Assessing the impact of copper on nematode communities from a chronically metal-enriched estuary using pollution-induced community tolerance. *Mar. Pollut. Bull.* 30, 701–706. doi: 10.1016/0025-326x(95)00053-p

Mirto, S., La Rosa, T., Gambi, C., Danovaro, R., and Mazzola, A. (2002). Nematode community response to fish-farm impact in western Mediterranean. *Environ. Pollut.* 116, 203–214. doi: 10.1016/s0269-7491(01)00140-3

Mohammad, M. (2011). *Meiofaunal communities and human impacts at Casey Station, Antarctica*. PhD Thesis PhD, University of Tasmania, Hobart.

Mokievsky, V., and Azovsky, A. (2002). Re-evaluation of species diversity patterns of free-living marine nematodes. *Mar. Ecol. Prog. Ser.* 238, 101–108. doi: 10.3354/meps238101

Pasotti, F., Convey, P., and Vanreusel, A. (2014). Potter Cove, west Antarctic Peninsula, shallow water meiofauna: a seasonal snapshot. *Antarctic Sci.* 26, 554–562. doi: 10.1017/s0954102014000169

Pasotti, F., De Troch, M., Raes, M., and Vanreusel, A. (2012). Feeding ecology of shallow water meiofauna: insights from a stable isotope tracer experiment in Potter Cove, King George Island, Antarctica. *Polar Biol.* 35, 1629–1640. doi: 10.1007/s00300-012-1203-6

Peck, L. S., Brockington, S., Vanhove, S., and Beghyn, M. (1999). Community recovery following catastrophic iceberg impacts in a soft-sediment shallow-water site at Signy Island, Antarctica. *Mar. Ecol. Prog. Ser.* 186, 1–8. doi: 10.3354/meps186001

Petti, M. A. V., Nonato, E. F., Skowronski, R. S., and Corbisier, T. N. (2006). Bathymetric distribution of the meiofaunal polychaetes in the nearshore zone of Martel Inlet, King George Island, Antarctica. *Antarctic Sci.* 18, 163–170. doi: 10.1017/s0954102006000186

Pfannkuche, O., Thiel, H., and Samples, M. (1988). *9. Sample processing Introduction to the Study of Meiofauna*. Washington DC: Smithsonian Institution Press.

Platt, H. M., and Warwick, R. M. (1983). *Freeliving marine nematodes. Part 1: British enoplids. Pictorial key to World Genera and Notes for the Identification of British Species*. Cambridge, UK: Cambridge University Press.

Platt, H., and Warwick, R. (1988). "Freeliving marine nematodes. Part II: British chromadorids. Pictorial key to World Genera and Notes for the Identification of British Species," *Synopses of the British fauna (new series)*, eds D. M. Kermack and RSK Barnes (Shrewsbury, UK: Field Studies Council (FSC)), 38:502.

Polmear, R., Stark, J. S., Roberts, D., and McMinn, A. (2015). The effects of oil pollution on Antarctic benthic diatom communities over 5 years. *Mar. Pollut. Bull.* 90, 33–40. doi: 10.1016/j.marpolbul.2014.11.035

Prakash Babu, C., Brumsack, H. J., Schnetger, B., and Böttcher, M. E. (2002). Barium as a productivity proxy in continental margin sediments: a study from the eastern Arabian Sea. *Mar. Geol.* 184, 189–206. doi: 10.1016/s0025-3227(01)00286-9

Raes, M., Rose, A., and Vanreusel, A. (2010). Response of nematode communities after large-scale ice-shelf collapse events in the Antarctic Larsen area. *Glob. Change Biol.* 16, 1618–1631. doi: 10.1111/j.1365-2486.2009.02137.x

Riemann, F. (1988). "Nematoda," in *Introduction to the Study of Meiofauna*, eds R. Higgins and H. Thiel (Washington, DC: Smithsonian Press), 293–301.

Rose, A., Ingels, J., Raes, M., Vanreusel, A., and Arbizu, P. M. (2015). Long-term iceshelf-covered meiobenthic communities of the Antarctic continental shelf resemble those of the deep sea. *Mar. Biodiv.* 45, 743–762. doi: 10.1007/s12526-014-0284-6

Rosli, N., Leduc, D., Rowden, A. A., and Probert, P. K. (2018). Review of recent trends in ecological studies of deep-sea meiofauna, with focus on patterns and processes at small to regional spatial scales. *Mar. Biodiv.* 48, 13–34. doi: 10.1007/s12526-017-0801-5

Rubal, M., Guilhermino, L. M., and Medina, M. H. (2011). Two strategies to live in low chronic pollution estuaries: the potential role of lifestyle. *Ecotoxicol. Environ. Saf.* 74, 1226–1231. doi: 10.1016/j.ecoenv.2011.02.017

Rudnick, D., Elmgren, R., and Frithsen, J. (1985). Meiofaunal prominence and benthic seasonality in a coastal marine ecosystem. *Oecologia* 67, 157–168. doi: 10.1007/bf00384279

Schratzberger, M., Gee, J., Rees, H., Boyd, S., and Wall, C. (2000). The structure and taxonomic composition of sublittoral meiofauna assemblages as an indicator of the status of marine environments. *J. Mar. Biol. Assoc.* 80, 969–980. doi: 10.1017/s0025315400003039

Schratzberger, M., and Ingels, J. (2017). Meiofauna matters: the roles of meiofauna in benthic ecosystems. *J. Exp. Mar. Biol. Ecol.* 502, 12–25. doi: 10.1016/j.jembe.2017.01.007

Schratzberger, M., Lampadariou, N., Somerfield, P., Vandepitte, L., and Berghe, E. V. (2009). The impact of seabed disturbance on nematode communities: linking field and laboratory observations. *Mar. Biol.* 156, 709–724. doi: 10.1007/s00227-008-1122-9

Scouller, R. C., Snape, I., Stark, J. S., and Gore, D. B. (2006). Evaluation of geochemical methods for the discrimination of metal contamination in Antarctic marine sediments: a case study from Casey Station, East Antarctica. *Chemosphere* 65, 294–309. doi: 10.1016/j.chemosphere.2006.02.062

Semprucci, F., and Balsamo, M. (2012). Free-living marine nematodes as bioindicators: past, present and future perspectives. *Environ. Res. J.* 6, 17–35.

Semprucci, F., Frontalini, F., Sbrocca, C., Du Châtelet, E. A., Bout-Roumazeilles, V., Coccioni, R., et al. (2015). Meiobenthos and free-living nematodes as tools for biomonitoring environments affected by riverine impact. *Environ. Monit. Assess.* 187, 251.

Skowronski, R. S. P., and Corbisier, T. N. (2002). Meiofauna distribution in Martel Inlet, King George Island (Antarctica): sediment features versus food availability. *Polar Biol.* 25, 126–134. doi: 10.1007/s003000100320

Snape, I., Riddle, M. J., Stark, J. S., Cole, C. M., King, C. K., Duquesne, S., et al. (2001). Management and remediation of contaminated sites at Casey Station. Antarctica. *Polar Rec.* 37, 199–214. doi: 10.1017/s0032247400027236

Somerfield, P. J., and Clarke, K. R. (2013). Inverse analysis in non-parametric multivariate analyses: distinguishing groups of associated species which covary coherently across samples. *J. Exp. Mar. Biol. Ecol.* 449, 261–273. doi: 10.1016/j.jembe.2013.10.002

Somerfield, P. J., Gee, J. M., and Warwick, R. M. (1994). Soft sediment meiofaunal community structure in relation to a long-term heavy metal gradient in the Fal estuary system. *Mar. Ecol. Prog. Ser.* 105, 79–88. doi: 10.3354/meps105079

Stark, J. S. (1998). Effects of copper on macrobenthic assemblages in soft-sediments: a laboratory experimental study. *Ecotoxicology* 7, 161–173.

Stark, J. S. (2000). The distribution and abundance of soft-sediment macrobenthos around Casey Station. East Antarctica. *Polar Biol.* 23, 840–850. doi: 10.1007/s003000000162

Stark, J. S. (2008). Patterns of higher taxon colonisation and development in sessile marine benthic assemblages at Casey Station, Antarctica, and their use in environmental monitoring. *Mar. Ecol. Prog. Ser.* 365, 77–89. doi: 10.3354/meps07559

Stark, J. S., Bridgen, P., Dunshea, G., Galton-Fenzi, B., Hunter, J., Johnstone, G., et al. (2016). Dispersal and dilution of wastewater from an ocean outfall at Davis Station, Antarctica, and resulting environmental contamination. *Chemosphere* 152, 142–157. doi: 10.1016/j.chemosphere.2016.02.053

Stark, J. S., Johnstone, G., Stark, S. C., and Palmer, A. (2014a). *Analytical Methods Used to Measure Chemical and Physical Properties of Davis Station Wastewater and Marine Sediments*. Hobart: Australian Antarctic Data Centre, doi: 10.4225/15/5472BCFBA5E10

Stark, J. S., Kim, S. L., and Oliver, J. S. (2014b). Anthropogenic disturbance and biodiversity of marine benthic communities in antarctica: a regional comparison. *PLoS One* 9:e98802. doi: 10.1371/journal.pone.0098802

Stark, J. S., Mohammad, M., McMinn, A., and Ingels, J. (2017). The effects of hydrocarbons on meiofauna in marine sediments in Antarctica. *J. Exp. Mar. Biol. Ecol.* 496, 56–73. doi: 10.1016/j.jembe.2017.07.009

Stark, J. S., Raymond, T., Deppeler, S. L., and Morrison, A. K. (2019). "Antarctic seas," in *World Seas: an Environmental Evaluation (Second Edition), Book 3*, ed. C. Sheppard (Cambridge, MA: Academic Press).

Stark, J. S., Riddle, M. J., and Simpson, R. D. (2003a). Human impacts in soft-sediment assemblages at Casey Station, East Antarctica: spatial variation, taxonomic resolution and data transformation. *Aust. Ecol.* 28, 287–304. doi: 10.1046/j.1442-9993.2003.01289.x

Stark, J. S., Riddle, M. J., Snape, I., and Scouller, R. C. (2003b). Human impacts in Antarctic marine soft-sediment assemblages: correlations between multivariate biological patterns and environmental variables. *Estuar. Coast. Shelf Sci.* 56, 717–734. doi: 10.1016/s0272-7714(02)00291-3

Stark, J. S., Snape, I., and Riddle, M. J. (2003c). The effects of hydrocarbon and heavy metal contamination of marine sediments on recruitment of Antarctic soft-sediment assemblages: a field experimental investigation. *J. Exp. Mar. Biol. Ecol.* 283, 21–50.

Stark, J. S., Riddle, M. J., and Smith, S. D. A. (2004). Influence of an Antarctic waste dump on recruitment to near-shore marine soft-sediment assemblages. *Mar. Ecol. Prog. Ser.* 276, 53–70. doi: 10.3354/meps276053

Stark, J. S., Snape, I., and Riddle, M. J. (2006). Abandoned waste disposal sites in Antarctica: monitoring remediation outcomes and limitations at Casey Station. *Ecol. Manag. Restor.* 7, 21–31. doi: 10.1111/j.1442-8903.2006.00243.x

Stark, J. S., Snape, I., Riddle, M. J., and Stark, S. C. (2005). Constraints on spatial variability in soft-sediment communities affected by contamination from an Antarctic waste disposal site. *Mar. Pollut. Bull.* 50, 276–290. doi: 10.1016/j.marpolbul.2004.10.015

Stark, S. C., Snape, I., Graham, N. J., Brennan, J. C., and Gore, D. B. (2008). Assessment of metal contamination using X-ray fluorescence spectrometry and the toxicity characteristic leaching procedure (TCLP) during remediation of a waste disposal site in Antarctica. *J. Environ. Monit.* 10, 60–70. doi: 10.1039/b712631j

Steyaert, M., Deprez, T., Raes, M., Bezerra, T., Demesel, I., Derycke, S., et al. (2005). *Electronic key to the Free-Living Marine Nematodes. World Wide Web Electronic Publication*. Available online at: http://www.marinespecies.org/aphia.php?p=idkeys_redirect&page=licence&taxon=280&keyid=13 (accessed September, 2005).

Steyaert, M., Garner, N., van Gansbeke, D., and Vincx, M. (1999). Nematode communities from the North Sea: environmental controls on species diversity and vertical distribution within the sediment. *J. Mar. Biol. Assoc.* 79, 253–264. doi: 10.1017/s0025315498000289

Suchanek, T. H. (1994). Temperate coastal marine communities: biodiversity and threats. *Am. Zool.* 34, 100–114. doi: 10.1093/icb/34.1.100

Thompson, B. A. W., Goldsworthy, P. M., Riddle, M. J., Snape, I., and Stark, J. S. (2007). Contamination effects by a conventional and a biodegradable lubricant oil on infaunal recruitment to Antarctic sediments: a field experiment. *J. Exp. Mar. Biol. Ecol.* 340, 213–226. doi: 10.1016/j.jembe.2006.09.010

Vanhove, S., Arntz, W., and Vincx, M. (1999). Comparative study of the nematode communities on the southeastern Weddell Sea shelf and slope (Antarctica). *Mar. Ecol. Prog. Ser.* 181, 237–256. doi: 10.3354/meps181237

Vanhove, S., Beghyn, M., Van Gansbeke, D., Bullough, L., and Vincx, M. (2000). A seasonally varying biotope at Signy Island, Antarctic: implications for meiofaunal structure. *Mar. Ecol. Prog. Ser.* 202, 13–25. doi: 10.3354/meps202013

Vanhove, S., Lee, H., Beghyn, M., Van Gansbeke, D., Brockington, S., and Vincx, M. (1998). The metazoan meiofauna in its biogeochemical environment: the case of an Antarctic coastal sediment. *J. Mar. Biol. Assoc. U. K.* 78, 411–434. doi: 10.1017/s0025315400041539

Vanhove, S., Wittoeck, J., Desmet, G., Van den Berghe, B., Herman, R., Bak, R., et al. (1995). Deep-sea meiofauna communities in Antarctica: structural analysis and relation with the environment. *Mar. Ecol. Prog. Ser.* 127, 65–76. doi: 10.3354/meps127065

Vanreusel, A., Fonseca, G., Danovaro, R., Da Silva, M. C., Esteves, A. M., Ferrero, T., et al. (2010). The contribution of deep-sea macrohabitat heterogeneity to global nematode diversity. *Mar. Ecol.* 31, 6–20. doi: 10.1111/j.1439-0485.2009.00352.x

Veit-Köhler, G., Durst, S., Schuckenbrock, J., Hauquier, F., Suja, L. D., Dorschel, B., et al. (2018). Oceanographic and topographic conditions structure benthic meiofauna communities in the Weddell Sea, Bransfield Strait and Drake Passage (Antarctic). *Progr. Oceanogr.* 162, 240–256. doi: 10.1016/j.pocean.2018.03.005

Vezzulli, L., Moreno, M., Marin, V., Pezzati, E., Bartoli, M., and Fabiano, M. (2008). Organic waste impact of capture-based Atlantic bluefin tuna aquaculture at an exposed site in the Mediterranean Sea. *Estuar. Coast. Shelf Sci.* 78, 369–384. doi: 10.1016/j.ecss.2008.01.002

Warwick, R. M. (1986). A new method for detecting pollution effects on marine macrobenthic communities. *Mar. Biol.* 92, 557–562. doi: 10.1007/BF00392515

Warwick, R. M., Platt, H. M., and Somerfield, P. J. (1998). "Freeliving marine nematodes: part III. Monhysterida," *Synopses of the British Fauna (New Series)* (Shrewsbury: Field Studies Council), 53:296.

Wild, S., McLagan, D., Schlabach, M., Bossi, R., Hawker, D., Cropp, R., et al. (2015). An antarctic research station as a source of brominated and perfluorinated persistent organic pollutants to the local environment. *Environ. Sci. Tech.* 49, 103–112. doi: 10.1021/es5048232

Witthoft-Muhlmann, A., Traunspurger, W., and Rothhaupt, K. O. (2005). Meiobenthic response to river-borne benthic particulate matter-a microcosm experiment. *Freshw. Biol.* 50, 1548–1559. doi: 10.1111/j.1365-2427.2005.01425.x

Zeppilli, D., Sarrazin, J., Leduc, D., Arbizu, P. M., Fontaneto, D., Fontanier, C., et al. (2015). Is the meiofauna a good indicator for climate change and anthropogenic impacts? *Mar. Biodiv.* 45, 505–535. doi: 10.1007/s12526-015-0359-z

Conflict of Interest: The authors declare that the research was conducted in the absence of any commercial or financial relationships that could be construed as a potential conflict of interest.

Copyright © 2020 Stark, Mohammad, McMinn and Ingels. This is an open-access article distributed under the terms of the Creative Commons Attribution License (CC BY). The use, distribution or reproduction in other forums is permitted, provided the original author(s) and the copyright owner(s) are credited and that the original publication in this journal is cited, in accordance with accepted academic practice. No use, distribution or reproduction is permitted which does not comply with these terms.

frontiers in Marine Science

ORIGINAL RESEARCH
published: 07 July 2020
doi: 10.3389/fmars.2020.00490

Benthic Communities on the Mohn's Treasure Mound: Implications for Management of Seabed Mining in the Arctic Mid-Ocean Ridge

Eva Ramirez-Llodra[1], Ana Hilario[2], Emil Paulsen[1,3,4], Carolina Ventura Costa[2], Torkild Bakken[3], Geir Johnsen[4,5] and Hans Tore Rapp[6,7]*

[1] Marine Biology, Norwegian Institute for Water Research, Oslo, Norway, [2] Centre for Environmental and Marine Studies, Department of Biology, University of Aveiro, Aveiro, Portugal, [3] NTNU University Museum, Norwegian University of Science and Technology, Trondheim, Norway, [4] Centre of Autonomous Marine Operations and Systems, Trondheim Biological Station, Department of Biology, Norwegian University of Science and Technology, Trondheim, Norway, [5] Department of Arctic Biology, The University Centre in Svalbard, Longyearbyen, Norway, [6] Department of Biological Sciences and K.G. Jebsen Centre for Deep-Sea Research, University of Bergen, Bergen, Norway, [7] Norwegian Research Centre AS, NORCE Environment, Bergen, Norway

OPEN ACCESS

Edited by:
Sarah Mincks Hardy, University of Alaska Fairbanks, United States

Reviewed by:
Lauren Sutton, University of Alaska Fairbanks, United States
Malcolm Ross Clark, National Institute of Water and Atmospheric Research (NIWA), New Zealand

****Correspondence:***
Eva Ramirez-Llodra
eva.ramirez@niva.no

Specialty section:
This article was submitted to Global Change and the Future Ocean, a section of the journal Frontiers in Marine Science

Received: *06 December 2019*
Accepted: *02 June 2020*
Published: *07 July 2020*

Citation:
Ramirez-Llodra E, Hilario A, Paulsen E, Costa CV, Bakken T, Johnsen G and Rapp HT (2020) Benthic Communities on the Mohn's Treasure Mound: Implications for Management of Seabed Mining in the Arctic Mid-Ocean Ridge. Front. Mar. Sci. 7:490. doi: 10.3389/fmars.2020.00490

The Mohn's Treasure, described as an inactive sulfide mound, was discovered at 2,600-m depth on the Arctic Mid-Ocean Ridge (AMOR) in 2002. In 2015, we conducted the first biological survey of Mohn's Treasure using remotely operated vehicle (ROV) photo transects and sampling. This site is covered by a thick layer of fine sediments, where hard substratum is only visible as rocky outcrops on ridges. The observed benthic community was typical of Arctic bathyal systems. A total of 46 species (identified as morphospecies) were recorded, with densities varying from 12.2 to 31.6 ind.m^{-2}. The two most abundant phyla were Porifera and Echinodermata. The sediment is dominated by fields of the stalked crinoid *Bathycrinus carpenterii*, whereas areas of hard substratum were characterized by high abundances of several sponge species and associated fauna. Interest in commercial exploration and exploitation of minerals from massive sulfide deposits is rising globally, and the AMOR is being targeted for mineral exploration within Norwegian waters. Gathering baseline ecological data from these poorly known sites is thus urgent and essential if robust resource management measures are to be developed and implemented. The results of this ecological survey are discussed in relation to the designation of deep-sea vulnerable marine ecosystems (VMEs) and their implication in management and conservation of areas targeted by the emerging deep-sea mining industry.

Keywords: deep-sea benthos, Arctic Mid-Ocean Ridge, inactive hydrothermal vent, seabed mining, vulnerable marine ecosystem

INTRODUCTION

Since hydrothermal vents were discovered in 1977, scientific research has been the primary source of anthropogenic disturbance in these ecosystems. However, there is increasing interest in commercial exploration of seabed minerals in general and a special focus on potential exploitation of seafloor massive sulfide (SMS) deposits that also host vent communities and habitats

(Van Dover et al., 2014). SMS are large deposits of polymetallic-bearing sulfides on and below the seabed, formed through precipitation of metals contained in the hydrothermal fluids emanating from active vents. SMS deposits can be found associated to active vents, as well as at inactive ones, where fluid flow has stopped, and the chemosynthetic-based faunal communities have disappeared (Van Dover, 2019). At active hydrothermal vents, large biomass of highly adapted organisms is sustained by the primary production of chemoautotrophic microorganisms, both free-living and in symbiosis with the fauna (Van Dover, 2010). Mining SMS deposits represents a whole new level of impact on these unique and rare vent ecosystems (Van Dover et al., 2018), and a better understanding of the community composition, ecosystem function, and population connectivity is essential for the development of sound environmental management, conservation measures, and decision making.

The ultraslow-spreading Arctic Mid-Ocean Ridge (AMOR) comprises the Kolbeinsey Ridge, Mohn's Ridge, and Knipovich Ridge (**Figure 1**), with the sections from Jan Mayen to off Svalbard within the Norwegian exclusive economic zone (EEZ) and Extended Continental Shelf. Several active areas have been discovered and studied in the AMOR since 2005, ranging from upper bathyal (140–700 m) vents at the Jan Mayen Vent Field and Seven Sisters Vent Field, to deep bathyal sites (2,400–2,200 m) at the Loki's Castle and AEgir vent sites (Pedersen et al., 2010a; Schander et al., 2010; Olsen et al., 2016). In 2018, a new active site was observed at more than 3,000-m depth on the Mohn's Ridge between Loki's Castle and AEgir, during an exploration survey for potential mineral deposits in the AMOR commissioned by the Norwegian Petroleum Directorate. In addition to the active sites, two inactive sites have been reported so far along the AMOR: Copper Hill (900-m depth) on the central Mohn's Ridge, for which very limited geological information is available (Pedersen et al., 2010b) and Mohn's Treasure (2,600 m). Mohn's Treasure is located at the edge of an inner rift wall, 30 km southwest of Loki's Castle, and was described as a massive inactive sulfide deposit based on hydrothermal deposits collected in a rock dredge in 2002 (Pedersen et al., 2010b). Lim et al. (2019) provided magnetic data of the fossil sedimented-hosted hydrothermal deposit, delineating a deposit of approximately 200 × 150 m buried under 15 m of sediments, as well as two new deposits. The ecology of AMOR vents has been studied for the shallow active vent fields and Loki's Castle. While the shallower vents at Seven Sisters and Jan Mayen vent fields do not support typical vent communities, the Loki's Castle vent field is characterized by chemosynthetic-based fauna, including gastropods, siboglinid polychaetes, and an endemic species of amphipod (Pedersen et al., 2010a; Tandberg et al., 2011, 2018; Kongsrud and Rapp, 2012; Kongsrud et al., 2017). The AEgir vent field, discovered in 2015 and poorly studied to date, seems to host a similar fauna to Loki's Castle communities, with, however, a lower diversity of vent specialists (Olsen et al., 2016). No biological information was available for the inactive Copper Hill and Mohn's Treasure sites.

Interest in potential seabed mineral resources has increased rapidly in the last decades, and 30 exploration licenses are currently (November 2019) active within international waters, seven of which are for SMS deposits (ISA, 2019). The International Seabed Authority (ISA) Mining Code that will regulate mineral exploitation in The Area (i.e., the seafloor in the area beyond national jurisdiction) is being developed based on the United Nations Convention on the Law of the Sea (UNCLOS). The Mining Code contains environmental regulations that should ensure that the marine environment is protected from any harmful effects, which may arise during mining activities, including, among others, a precautionary approach and the use of best environmental practices such as environmental impact assessments (EIAs), baseline data collection that follows an ecosystem-based approach and monitoring programs (Jaeckel, 2015; UNCLOS articles 137, 145, 153). Norway's interest in its potential seabed resources has also increased rapidly, and a new "Act on Mineral Activities on the Continental Shelf" entered into force on 1 July 2019, regulating all exploration for and exploitation of subsea minerals on the Norwegian Continental Shelf (Seabed Mineral Law, 2019). The act includes provisions to avoid damage to the marine environment and seabed cultural heritage, as well as avoiding pollution and litter. These provisions include, among others, the requirement for an EIA prior to opening a geographic area for mineral activity. The EIA should contribute to highlight interests from different stakeholders in the area, identify to what degree the mining activity would impact the environment, and estimate potential industrial, economic, and societal impact. However, knowledge on the biological composition, ecological functions, and population connectivity of microbial and faunal communities at many vent sites in international waters and most of the AMOR active and inactive sites within Norwegian jurisdiction is still utterly scarce (Eilertsen et al., 2018), strongly limiting the robustness of any environmental regulations and/or management measures. This is particularly true for inactive sites, as most research so far has focused on the abundant and exotic communities of active vents. Van Dover (2019) reviews current knowledge of inactive sites worldwide and highlights the limited geological and ecological understanding currently available of these habitats and a lack of consensus of what characterizes inactive hydrothermal sites. No biological information was available for Mohn's Treasure prior to this study. The aim of this study was to provide the first biological data of the region by assessing the faunal composition, community structure, and biodiversity of the megabenthic community to provide initial baseline information that can inform management measures related to seabed mining in the AMOR region.

MATERIALS AND METHODS

Study Area

The Mohn's Treasure site is situated at 73°44′N–07°27′E, at the edge of an inner rift wall 30 km southwest of the active Loki's Castle vent field, at 2,600- to 2,800-m depth (**Figure 1**). All data were gathered on board the multipurpose subsea vessel CSV Polar King during a research cruise in the framework of the MarMine project in the summer of 2016. The study area was divided into four sampling sites, based on differences in

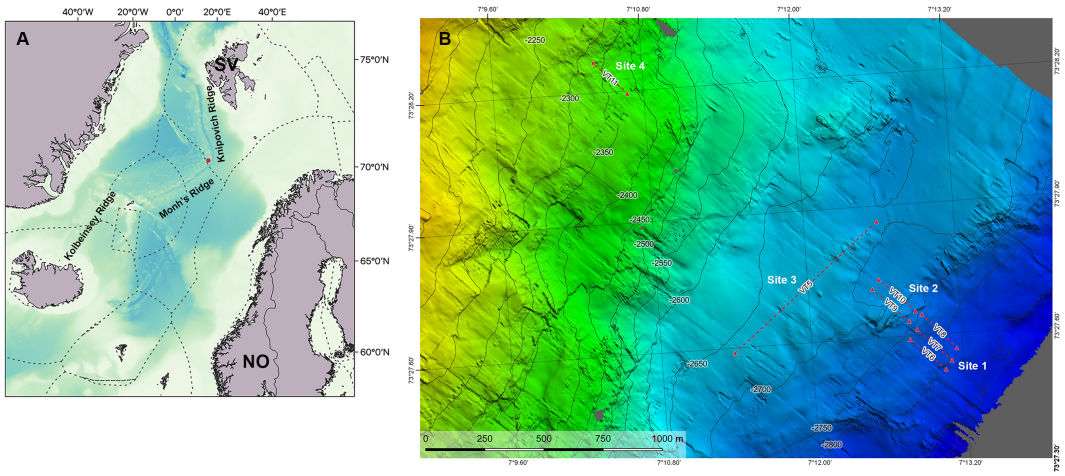

FIGURE 1 | Map of the study area. **(A)** Regional map showing the Arctic Mid-Ocean Ridge with the location of Mohn's Treasure (red dot) and the three main ridges: KOR, Kolbeinsey Ridge; MR, Mohn's Ridge; KR, Knipovich Ridge on the Mohn's Treasure. **(B)** Bathymetry of the study area showing the video transects (VT). Mohn's Treasure map made by Christian Malmquist, NTNU AUR Lab.

depth and seafloor steepness identified from the low-resolution multibeam data that were available prior to the cruise (**Figure 1**). Site 1 comprises the deepest parts of the Mohn's Treasure region, with a gentle slope at ca. 2,810-m depth. Site 2 is located between 2,745- and 2,750-m depth and is located at the start of what resembles a plateau because of its very low steepness. Site 3 is in the middle of the plateau at 2,720 m, and Site 4 is located at 2,385-m depth and has the greatest steepness gradient.

Sampling

All data were gathered during systematic remotely operated vehicles (ROVs)-based video/photo transects using low light navigation cameras Kongsberg OE13-124 and a CCD color camera Kongsberg 14-366 for still photos (Ludvigsen et al., 2016) mounted on a Triton work-class ROV (XLR 02). The ROV was equipped with two green lasers (532 nm), projecting two parallel lines on the seafloor with a distance of 10 cm, which were used to calibrate the field of view and size of object of interest. The video transects (VTs) were conducted flying the ROV at 1 m above the seafloor at a constant speed of 0.4 knots (0.2 m s^{-1}), using the approach detailed by Ludvigsen et al. (2016). Because of the low resolution of the video cameras on the ROV, color photographs were taken at ca. 15-s interval (one photo every 3 m of seafloor). A total of eight transects were conducted (**Table 1**), with one transect of 800-m length (VT5, Site 3) perpendicular to the other shorter transects (200-m length): three replicates (VT6–VT8) at Site 1, two replicates (VT9–VT10) at Site 2, and two replicates (VT11–VT12) at Site 4. However, we had a technical issue in the still camera during VT12, so this transect is not included in the analyses. Between 68 and 108 images were taken during transects VT6–VT11, but overlapping images were excluded from the data set (**Table 1**). On transect VT5, 560 images were taken, but only 70 randomly selected photographs (average of number of photographs analyzed from the other transects) were included in the analyses. The field of view (area covered by each image in m^2) was calculated based on the ROV height above seafloor, seafloor angle, camera angle, image width/height, and camera vertical/horizontal field of view.

Analyses

The transects were analyzed both qualitatively and quantitatively. All specimens observed were identified to the lowest taxonomic level possible from the ROV images, based on expert knowledge (HR, TB, and EP) and additional literature (Clark, 1970; Clark and Downey, 1992; Madsen and Hansen, 1994; Cárdenas et al., 2013; Hestetun et al., 2017; Plotkin et al., 2018).

All individuals in each image along each transect were identified to the lowest taxonomic level possible and counted. The total abundance within a transect was divided by the transect area (**Table 1**) to obtain the density (ind.m^{-2}) for each morphospecies per transect. The density data were grouped by phylum for graphic representation (**Table 2**). The community structure was assessed with multidimensional scaling (MDS) using PRIMER v.6 based on Bray–Curtis similarity and square-root transformation of the morphospecies density matrix. Basic biodiversity indices [Margalef's species richness, Shannon–Weaver diversity, ES(50), and Pielou's evenness] were computed for each transect based on morphospecies data. The lack of replicates in Sites 3 and 4 did not allow conducting statistical analyses so the data could only be compared qualitatively among sites.

RESULTS

Environmental and Biological Observations

The ROV video surveys analyzed four sites at different depth ranges on Mohn's Treasure (**Table 1**). The survey showed a highly sedimented habitat as would be typical for lower bathyal and abyssal regions, with sparse rocky outcrops (**Figure 2**). Site

TABLE 1 | Overview of the video transects on the Mohn's Treasure analyzed in this study.

Site	Transect	ROV dive	Date	Start LAT/LON	End LAT/LON	Length (m)	Depth start–end (m)	No. of images (no. analyzed)	Area analyzed (m^2)
1	VT6	ROV8	24.08.2016	73,458,647/7,217,581	73,459,874/7,213,105	200	2,806–2,764	108 (76)	104.44
1	VT7	ROV8	25.08.2016	73,458,972/7,218,446	73,460,230/7,214,076	200	2,805–2,757	94 (69)	125.38
1	VT8	ROV10	26.08.2016	73,459,427/7,219,194	73,460,790/7,214,884	200	2,811–2,756	99 (99)	148.5
2	VT9	ROV5	23.08.2016	73,460,560/7,213,141	73,461,860/7,208,557	200	2,739–2,705	99 (63)	95.76
2	VT10	ROV5	23.08.2016	73,460,927/7,214,049	73,462,197/7,209,472	200	2,743–2,708	68 (52)	75.12
3	VT5	ROV8	24.08.2016	73,459,819/7,189,748	73,464,403/7,209,727	800 (200)	2,657–2,698	560 (70)	103.50
4	VT11	ROV9	25.08.2016	73,469,900/7,177,835	73,471,163/7,173,581	200	2,378–2,328	102 (62)	84.77

VT, video transect; Start LAT/LON and End LAT/LON, start and end positions of each transect in WGS84 coordinate system.

1 in the deeper surveyed area (average depth 2,783 m) was covered by soft sediments. At the end of the transects in Site 1 (VT6, VT7, and VT8), we came across a small rocky ridge, with hard substrate making up approximately 8% of the area. Site 2 started at this ridge and progressed to shallower depths (average depth 2,724 m) on a steeper sedimented slope. Hard substrate covered approximately 22% of the surveyed area. Site 3 (average depth 2,678 m) was surveyed by a long (800 m) perpendicular transect to the other transects, along a low steepness area covered with fine sediment. This area was intercepted by rocky outcrops (10%) colonized by sponges and associated fauna. Site 4 was the shallowest area surveyed, on a steeper slope (average depth 2,353 m). This region had a mixture of coarse and fine sediment with more rocky outcrops. Site 4 had approximately 35% of its surface represented by hard substrate.

In general, areas of soft sediment were mainly inhabited by stalked crinoids and mobile fauna such as holothurians, asteroids, and crustaceans, whereas the rocky outcrops were colonized by abundant sponges of different species/morphotypes, non-stalked crinoids, and crustaceans. Site 1 was mostly covered by high densities (21.4 ind.m^{-2}) of the stalked crinoid *Bathycrinus carpenterii* on the soft sediment (**Figure 2A**). This species was observed forming in dense crinoid fields in the deepest part of Monh's Treasure, both along the VTs and during other ROV dives that were not dedicated to linear VTs. Site 2 included also large abundances of stalked crinoids on the sediment, while sponges and associated fauna dominated the rocky outcrops (**Figure 2B**). Site 3 was covered mostly by fine sediment with deposit feeders such as holothurians and asteroids, and rocky outcrops with sponges (**Figure 2C**). Site 4 had a higher proportion of hard substrate and the communities shifted to more sessile, filter feeder communities, mostly of a variety of sponges, crinoids, and associated fauna (**Figure 2D**).

Community Structure

A total of 491 ROV photos were analyzed, comprising a seafloor area of 741 m^2 (**Table 1**) with mean area per photo of 1.51 ± 0.41 m^2 ($\pm$SD). The mean density per site varied from 12.2 to 31.6 ind. m^{-2} in Sites 3 and 2, respectively (**Figure 3**). A total of 46 species or morphotypes were identified, belonging to seven phyla. Porifera was the most diverse phylum with 25 different species/morphotypes, followed by Echinodermata with seven different species/morphotypes. Porifera and Echinodermata were also the most abundant groups in all sites representing, respectively, 42 and 47% of the total density. Sponges were most abundant in Site 2 (16.8 ind.m^{-2}), Site 3 (9.1 ind.m^{-2}), and Site 4 (22.4 ind.m^{-2}), whereas echinoderms were most abundant in Site 1 (22.6 ind.m^{-2}). Within these two phyla, the sponges *Lissodendoryx complicata* and *Hymedesmia* sp. were the most abundant in all transects, representing 17% of all observed individuals, and the stalked crinoid *B. carpenterii* was the most abundant echinoderm, representing 43% of all observations. The latter was particularly abundant in Site 1, reaching an average density of 21.4 ind.m^{-2}.

The species accumulation curves indicated that the 200-m VTs were a good representation of the megafauna community found in the surveyed area of Mohn's Treasure. Most of the curves started leveling off after 75 m (25 photos) of survey (**Figure 4**). In VT5, the species accumulation curve had a steeper increase in number of species, potentially caused by the number of rocky ridges that were crossed by this longer transect. The multidimensional analysis showed that the communities from the three transects in Site 1 and the two transects in Site 3 grouped well together and were different from the communities in Sites 3 and 4 at 60% similarity (**Figure 5**).

Biodiversity

Although no statistical analyses could be conducted because of the lack of replicates in Sites 3 and 4, the four computed indices followed a similar pattern, with Margalef's species richness, Pielou's evenness, Shannon diversity, and ES(30) lower at Site 1 (**Figure 6**). This site was characterized by fields of stalked crinoids, which explain the low species richness, the low evenness caused by the dominance of one species, and low Shannon diversity.

DISCUSSION

Although Mohn's Treasure has been described as a massive sulfide deposit, the only evidence of mineralization found during the entire MarMine survey over the area (13 ROV dives) was a few meters of oxidized basalt outcrops comprising minor pyrites and features possibly formed by diffuse discharges (Ludvigsen et al., 2016). Subsequent analyses of magnetic data collected during the cruise suggest the presence of deposits buried under 15 m of sediments (Lim et al., 2019). The general

TABLE 2 | Density (ind.m^{-2}) of the different morphospecies observed in Mohn's Treasure.

			Site 1			Site 2		Site 3	Site 4
PHYLUM	**Class**	**Morphospecies**	**VT6**	**VT7**	**VT8**	**VT9**	**VT10**	**VT5**	**VT11**
PORIFERA			**2.470**	**3.677**	**9.623**	**19.162**	**14.630**	**8.251**	**22.402**
	Hexactinellida		0.048	0.008	0.121	0.230	0.160	0.193	0.153
		Caulophacus arcticus	0.000	0.008	0.074	0.042	0.027	0.174	0.071
		Asconema sp.	0.029	0.000	0.047	0.115	0.120	0.010	0.012
		Hexactinellida sp. 1	0.019	0.000	0.000	0.052	0.000	0.000	0.024
		Hexactinellida sp. 2	0.000	0.000	0.000	0.021	0.013	0.010	0.047
	Calcarea		0.642	0.080	0.027	0.668	0.825	0.010	0.153
		Brattegardia sp.	0.642	0.080	0.027	0.668	0.825	0.010	0.153
	Desmospongia		1.781	3.589	9.475	18.264	13.645	8.048	22.095
		Lyssodendoryx complicate!	0.163	0.702	3.926	6.328	4.034	2.947	1.239
		Asbestopluma sp.l	0.000	0.000	0.000	0.021	0.000	0.010	0.047
		Cladorhiza sp.l	0.000	0.000	0.000	0.000	0.000	0.000	0.118
		Hymedesmia sp.l	0.402	1.236	1.367	4.271	4.087	0.947	2.442
		Axinellidae sp.l	0.278	0.183	0.532	0.710	0.493	0.309	0.944
		Thenea sp.l	0.000	0.000	0.007	0.042	0.000	0.000	0.000
		Demospongiae sp. 1	0.211	0.112	0.128	1.316	0.466	0.106	0.672
		Demospongiae sp. 2	0.000	0.000	0.000	0.010	0.000	0.000	0.059
		Demospongiae sp. 3	0.622	1.101	0.027	3.582	2.796	0.106	1.781
		Demospongiae sp. 4	0.000	0.000	0.000	0.000	0.000	0.010	0.295
		Demospongiae sp. 5	0.048	0.056	0.000	0.919	0.466	0.000	0.236
		Demospongiae sp. 6	0.000	0.000	0.000	0.031	0.000	0.000	0.389
		Demospongiae sp. 7	0.010	0.136	0.007	0.512	0.759	0.000	0.389
		Encrusting sp. 1	0.000	0.016	0.000	0.000	0.120	0.174	1.545
		Encrusting sp. 3	0.000	0.016	0.000	0.063	0.160	0.000	0.047
		Encrusting sp. 4	0.000	0.000	0.007	0.000	0.240	0.000	1.003
		Encrusting sp. 5	0.048	0.032	0.215	0.198	0.027	0.222	0.177
		Encrusting sp. 6	0.000	0.000	0.000	0.094	0.000	0.000	0.035
		Encrusting sp. 7	0.000	0.000	0.000	0.167	0.000	0.029	10.676
		Encrusting sp. 11	0.000	0.000	3.259	0.000	0.000	3.188	0.000
CNIDARIA			**1.312**	**1.587**	**0.761**	**4.751**	**3.927**	**0.435**	**3.173**
	Anthozoa		1.312	1.587	0.761	4.751	3.927	0.425	3.173
		Gersemia fruticosa	0.000	0.000	0.000	0.219	0.000	0.048	2.961
		Amphianthus sp.l	0.670	1.069	0.418	0.950	2.223	0.155	0.000
		Bathyphellia margaritacea	0.642	0.518	0.343	3.582	1.704	0.222	0.212
	Hydrozoa		0.000	0.000	0.000	0.000	0.000	0.010	0.000
		Benthic meduse spl	0.000	0.000	0.000	0.000	0.000	0.010	0.000
MOLLUSCA			**0.134**	**0.112**	**0.155**	**0.115**	**0.106**	**0.010**	**0.000**
	Gastropoda		0.134	0.112	0.020	0.115	0.106	0.000	0.000
		Buccinidae sp. 1	0.134	0.112	0.020	0.115	0.106	0.000	0.000
	Bivalvia		0.000	0.000	0.135	0.000	0.000	0.010	0.000
		Bivalvia sp.	0.000	0.000	0.135	0.000	0.000	0.010	0.000
ANNELIDA									**0.000**
	Polychaeta		0.096	0.024	0.007	0.146	0.173	0.010	0.000
		Polychaeta sp. 1 (white)	0.048	0.024	0.007	0.104	0.106	0.000	0.000
		Polychaeta sp. 2 (red)	0.048	0.000	0.000	0.042	0.067	0.010	0.000
ARTHROPODA			**0.785**	**0.742**	**0.471**	**0.439**	**0.293**	**0.329**	**0.366**
	Pycnogonida		0.488	0.367	0.236	0.178	0.133	0.029	0.024
		Ascorhynchus abyssi	0.488	0.367	0.236	0.178	0.133	0.029	0.024
	Malacostraca		0.297	0.375	0.236	0.261	0.160	0.300	0.342
		Isopoda sp.l	0.144	0.199	0.013	0.000	0.000	0.000	0.000
		Amphipoda sp.l	0.077	0.064	0.088	0.000	0.000	0.068	0.000
		Bythocarididae sp.l	0.077	0.112	0.135	0.261	0.160	0.232	0.342

(Continued)

TABLE 2 | Continued

			Site 1			Site 2		Site 3	Site 4
PHYLUM	**Class**	**Morphospecies**	**VT6**	**VT7**	**VT8**	**VT9**	**VT10**	**VT5**	**VT11**
ECHINODERMATA			**19.628**	**28.202**	**19.966**	**4.898**	**14.031**	**3.179**	**4.648**
	Crinoidea		19.313	27.692	19.758	4.323	13.791	2.570	4.565
		Bathycrinus carpenterii	18.432	27.516	18.370	3.133	13.325	1.816	3.350
		Poliometra prolixa	0.881	0.175	1.387	1.190	0.466	0.754	1.215
	Holothuroidea		0.278	0.367	0.114	0.188	0.040	0.367	0.000
		Kolga hyalina	0.010	0.000	0.000	0.000	0.000	0.309	0.000
		Elpidia sp.	0.268	0.367	0.114	0.188	0.040	0.058	0.000
	Asteroidea		0.038	0.144	0.094	0.324	0.200	0.242	0.083
		Hymenaster pellucidus	0.019	0.088	0.081	0.251	0.160	0.213	0.083
		Poraniomorpha sp.I	0.019	0.056	0.013	0.073	0.040	0.029	0.000
	Echinoidea		0.000	0.000	0.000	0.063	0.000	0.000	0.000
		Pourtalesia Jeffreys/	0.000	0.000	0.000	0.063	0.000	0.000	0.000
CHORDATA			**0.153**	**0.215**	**0.047**	**0.125**	**0.532**	**0.000**	**0.672**
	Ascidiacea		0.153	0.199	0.007	0.125	0.493	0.000	0.661
		Didemnidae sp.	0.153	0.199	0.007	0.125	0.493	0.000	0.661
	Actinopterygii		0.000	0.016	0.040	0.000	0.040	0.000	0.012
		Lycodes frigidus	0.000	0.016	0.040	0.000	0.040	0.000	0.012
TOTAL faunal density (ind. m^{-2})			24.579	34.559	31.030	29.637	33.693	12.213	31.261

Bold numbers indicate total density for each phylum.

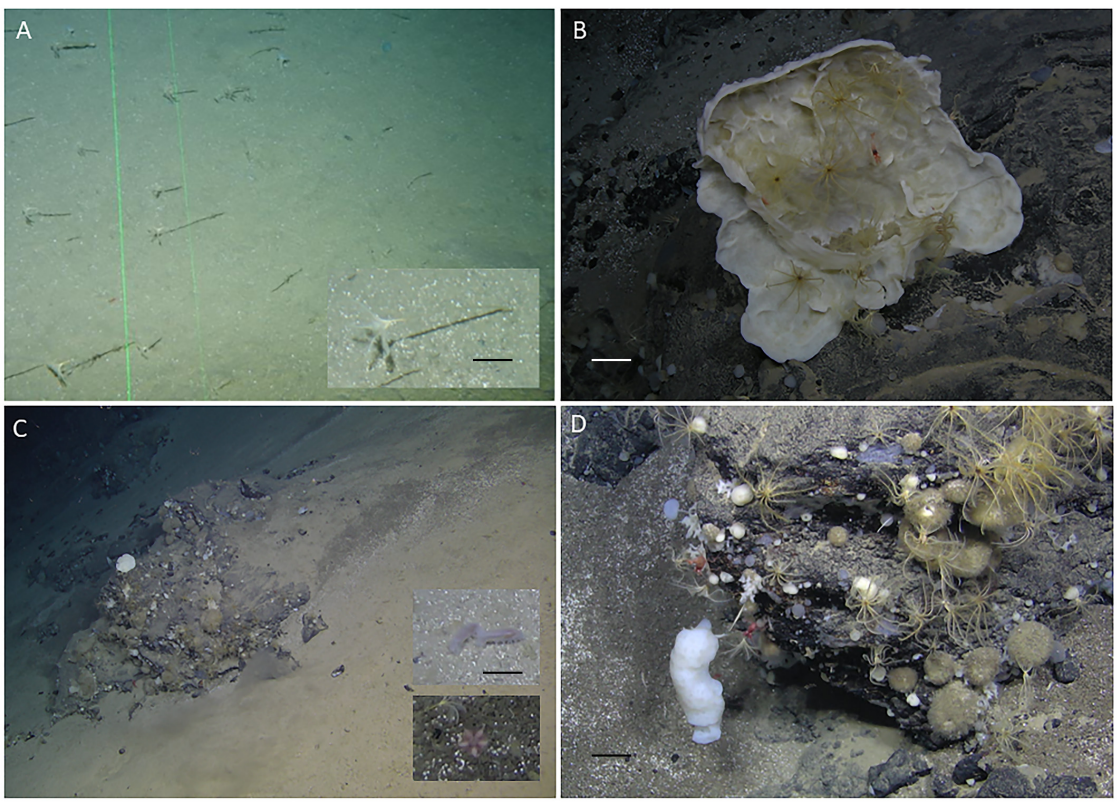

FIGURE 2 | Mohn's Treasure fauna. **(A)** Sedimentary plain at Site 1 with dense aggregations of the stalked crinoid *Bathycrinus carpenterii*. Insert: close-up of one individual (scale bar = 2 cm). **(B)** Rocky outcrop with sponges and associated fauna on Site 2 (scale bar = 10 cm). **(C)** Site 3 was dominated by fine sediments with holothurians and asteroids as well as rocky outcrops with sponges. The insert shows the holothurian *Kolga* species and the asteroid *Hymenaster pellucidus* (scale bar = 5 cm). **(D)** Site 4 was dominated by hard substrates with high abundance of filter feeders, in particular sponges (scale bar = 10 cm).

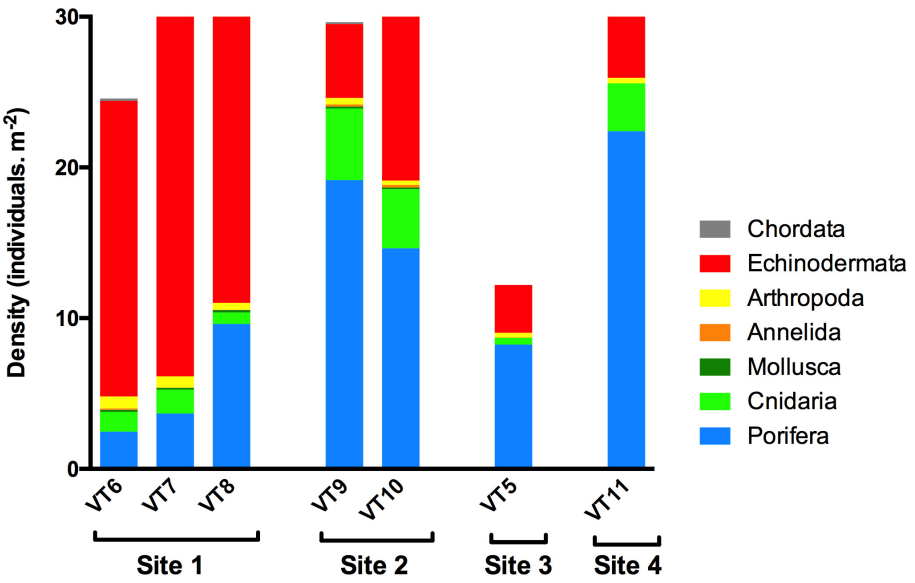

FIGURE 3 | Density (individuals.m^{-2}) of the different phyla observed during the photo transects on Mohn's Treasure.

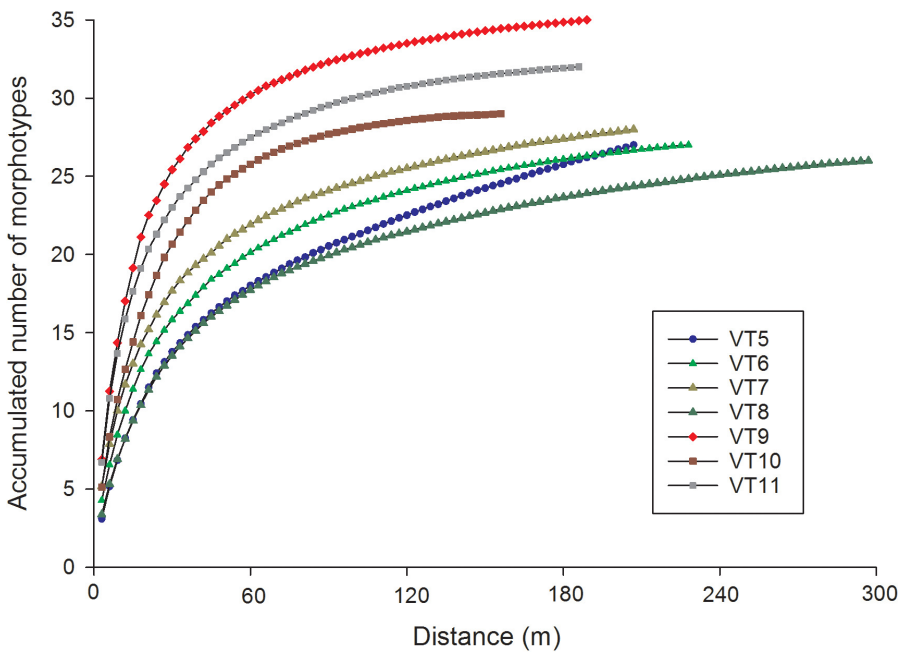

FIGURE 4 | Species accumulation curves for the six ROV transects in Site 1 (VT6, 7, and 8), Site 2 (VT9 and 10), Site 3 (VT5), and Site 4 (VT11).

seascape was that of a sedimented rift valley, with the seafloor composed mainly of soft sediment with basalt outcrops. Although biological data of the region around Monh's Treasure are relatively scarce, the fauna observed in our survey resembles that of communities described from other lower bathyal Arctic regions such as the Shultz Bank, a seamount to the east of Mohn's Treasure (Meyer et al., 2019), or a deep-water reef in the Fram Straight, west of Svalbard (Meyer et al., 2014).

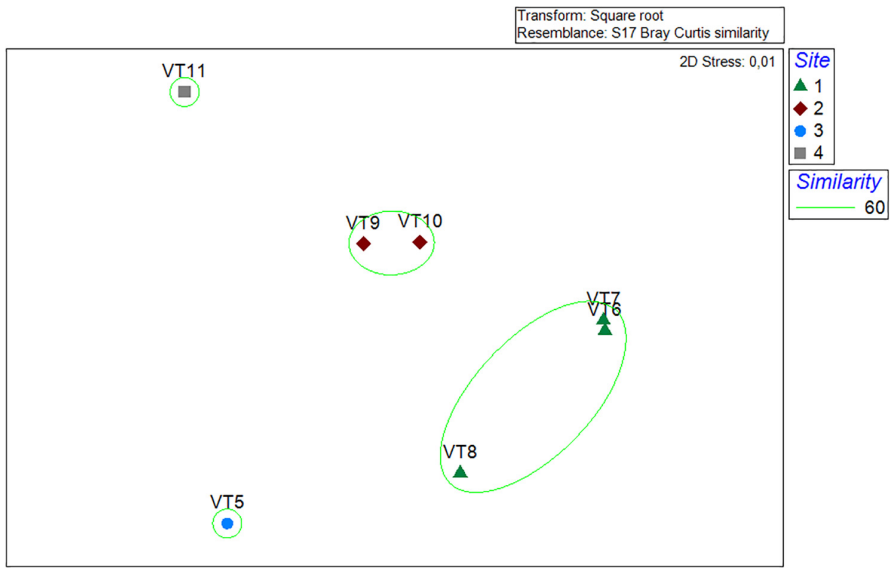

FIGURE 5 | Multidimensional scaling plot. Green circle represents 60% similarity. Site 1: VT6, 7, and 8. Site 2: VT8 and 9. Site 3: VT5. Site 4: VT11.

In all these regions, echinoderms dominate the sedimentary habitats, whereas suspension feeders, mostly sponges, and their associated fauna such as crinoids and arthropods dominate the hard substratum (Meyer et al., 2014, 2019; Roberts et al., 2018). In Mohn's Treasure, the most abundant taxa were sponges, representing 42% of the fauna and dominated by desmosponges, similar to what has been described for the Shultz Bank communities (Meyer et al., 2019), and echinoderms in the lower region of Mohn's Treasure where high-density fields of the stalked crinoid *B. carpenterii* were observed. The fauna is very different from that of the active Loki's castle vent field, which is characterized by chemosynthetic-based fauna, including the amphipod *Exitomelita sigynae*, the siboglinid worm *Sclerolinum contortum*, and the rissoid gastropod *Pseudosetia griegi* (Tandberg et al., 2011, 2018; Kongsrud and Rapp, 2012; Olsen et al., 2016; Kongsrud et al., 2017). The Mohn's Treasure fauna differs also from the communities described from the Seven Sisters and Jan Mayen vent fields. The fauna in these active, upper-bathyal hydrothermal vents (120–700 m) is characterized by non-vent endemic fauna dominated by anemones and calcareous sponges (Schander et al., 2010; Sweetman et al., 2013). The difference to the Mohn's Treasure fauna is probably related to depth and enhanced food supply at the active vents through microbial production (Sweetman et al., 2013). Within Mohn's Treasure, the differences observed among the sites in the MDS can reflect local variability, where the VT crossed one or more rocky ridges at which different sponge species dominate (Beazley et al., 2018; Meyer et al., 2019). The sponge grounds support a rich community of other invertebrates, providing habitat and food (Maldonado et al., 2016). In contrast, the sedimentary areas are characterized by scarce megafauna that can be analyzed from ROV imaging, with only some echinoderms or fish observed sporadically. In addition, the deeper site surveyed at Mohn's Treasure was characterized by fields of the stalked crinoid *B. carpenterii*, not observed at the other sites. These differences result in lower biodiversity indices at the deepest site where *B. carpenterii* dominates.

In relation to the increasing interest for seabed minerals, seven licenses for exploration of SMS deposits in areas beyond national jurisdiction have been granted by the ISA (2019), whereas exploration is also rapidly developing in national waters of some countries such as Japan and Norway. Following the publication of the Norwegian Minerals Act in July 2019 (Seabed Mineral Law, 2019), interest in the seafloor mineral resources of Norway has been increasing dramatically, leading to two exploration cruises in the AMOR, in 2018 and 2019. Although previously described as a massive sulfide deposit (Pedersen et al., 2010b), no resource exploration has been conducted at Mohn's Treasure to date. In addition, our ROV observations and magnetic data collected during the MarMine cruise (Lim et al., 2019) indicate that this is a highly sedimented system, which would not be, in principle, interesting to mineral exploration in the current technological and economical context. However, Mohn's Treasure is situated only 30 km to the south of Loki's Castle active hydrothermal vent field and other active vents with potential sulfide deposits, which have been identified along the Mohn's Ridge since 2015 (Olsen et al., 2016). The exploitation of mineral resources from the seabed is expected to lead to widespread environmental impacts. These include both direct impacts on the targeted habitat and associated fauna caused by the mining machinery and indirect impacts on adjacent ecosystems caused by the creation and dispersal of sediment plumes with high concentrations of particles, potentially including the dispersal of toxic chemicals (Boschen et al., 2013; Van Dover et al., 2018). If commercial exploration for, and subsequent exploitation of, mineral resources was to be conducted in the AMOR region, robust environmental baseline studies and EIAs will need to be conducted. Our survey provided the first biological study of the Mohn's Treasure

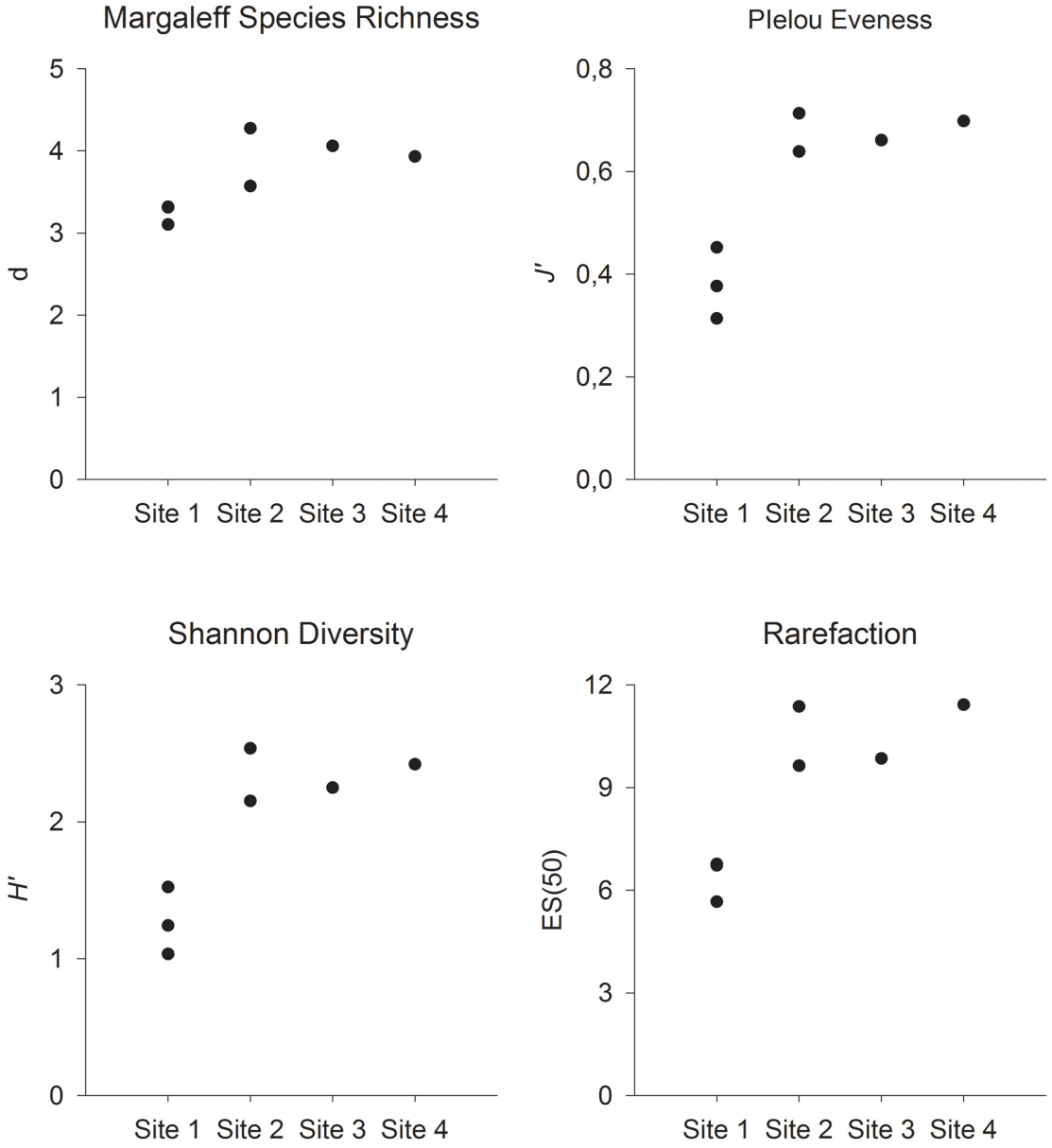

FIGURE 6 | Margalef's species richness (d), Pielou's evenness (*J'*), Shannon biodiversity (*H'*), and estimated number of species (ES50) at the four sites on Mohn's Treasure. Site 1: VT6, 7, and 8. Site 2: VT8 and 9. Site 3: VT5. Site 4: VT11.

region that can be used to design and support future baselines studies in the region.

In the framework of a full-scale baseline study of the region, an important component would be the assessment of the benthic communities, including the potential presence of vulnerable marine ecosystems (VMEs) (Burgos et al., 2020). VMEs are characterized by the uniqueness or rarity of the ecosystem, its fragility, the functional significance of its habitat, and the presence of key species with life-history traits that make recovery difficult and structural complexity (FAO, 2009). The VME guidelines identify a series of taxa as indicators, including, among others, cold-water corals, sponges, ophiuroids and stalked crinoids, bryozoans, ascidians, brachiopods, and xenophyophore foraminifera (FAO, 2019). Dense aggregations of stalked crinoids are considered VMEs when present in dense aggregations, as they can provide habitat for small invertebrates and are vulnerable to physical impact (Murillo et al., 2011). In our survey of Mohn's Treasure, we observed dense aggregations of the stalked crinoid *B. carpenterii* with 21.4 individuals per m^2, whereas other observations in the NE Atlantic/Arctic of *B. carpenterii* report much lower densities: 0.76 $ind.m^{-2}$ on the Hausgarten Observatory in the Fram Strait (Taylor et al., 2016) and

1.3 ind.m^{-2} on a deep-water reef in the Fram Strait (Meyer et al., 2014). Although our survey of the lower Mohn's Treasure area was limited to three transects, we suggest that the observations of dense fields of stalked crinoids, together with the presence of sponges aggregations on rocky outcrops throughout our transects, would need to be taken under consideration prior to any commercial activity for the exploitation of seabed minerals in the central Mohn's Ridge. In the last years, interest on the mineral resources along the AMOR within Norwegian jurisdiction has increased rapidly, as evidenced by the two seabed mineral mapping surveys of the Norwegian Petroleum Directorate on behalf of the Ministry of Petroleum and Energy in 2018 and 2019. Although mining exploitation on Mohn's Treasure seems unlikely currently, as any potential resources would be covered by a thick (ca. 15 m) sediment layer (Lim et al., 2019), new sites may be found in proximity. The potential exploitation of mineral resources in the region may result in harmful effects on the crinoid and sponge communities that we observed and on the ecosystem services they provide, such as nutrient regeneration and habitat provision. For example, close associations between ground-forming sponges and specialized microbes have proven to be key players in the biogeochemical cycling of nutrients along the ridge (Rooks et al., 2020). Stressors such as enhanced sedimentation or release of bioavailable metals caused by commercially exploited seabed minerals may have serious effects on ecosystem function, potentially changing these sponge communities from being nutrient sources to nutrient sinks (Rooks et al., 2020).

In addition, it is already well established that hydrothermally active and non-active areas of the AMOR host unique and poorly studied macrofauna, as well as a wide diversity of novel and uncultured microbial biodiversity (e.g., Dahle et al., 2015, 2018; Steen et al., 2016; Stokke et al., 2020). Metagenomic studies from the AMOR have identified novel archaeal lineages, which have challenged our views on the origin and evolution of eukaryotes and the topology of the tree of life (Spang et al., 2015). In addition, recent *in situ* enrichment and culture of rare sedimentary microbes at AMOR vents have revealed great potential for biodiscovery of novel enzymes for use in biorefining and bioconversion of industrially relevant substrates such as those produced in fish farming and wood-pulping industries (Stokke et al., 2020). Given the high degree of novel findings during work in the area over the most recent years, it is likely that they represent only the tip of the iceberg when it comes to the amount of potentially valuable genetic resources present in the AMOR region. Potential biodiversity loss from seabed mining (Niner et al., 2018), particularly in poorly investigated regions such as the AMOR, may result in the loss of biological knowledge, ecosystem services, and valuable marine genetic resources before we know them (Arrieta et al., 2010; Rabone et al., 2019).

Biological surveys such as the one conducted in this study are essential as a first step toward robust, ecosystem approach, baseline studies that would improve understanding of the ecosystems composition and functioning and their response to stressors (Levin and Le Bris, 2015). Although our study had limitations in terms of replication of transects and analyses of other community components (microbes and meio- and macro-infauna), we provide a first overview of the megabenthos communities of the Mohn's Treasure and in particular observations of dense stalked crinoid populations and abundant sponge aggregations, which can inform future studies and instigate a dialog with the relevant stakeholders, including industry, authorities, and non-governmental organizations. Conducting thorough environmental baselines and EIAs of these poorly known regions, including both the target area and adjacent areas that may be indirectly impacted by exploitation activities, are necessary to avoid harmful effects to the ecosystem and the services it provides (Van Dover, 2010; Boschen et al., 2013; Van Dover et al., 2018). In addition to currently used technologies and methods for environmental baselines and EIAs, the development of new technologies such as the use of autonomous underwater vehicles (AUVs) and hyperspectral cameras mounted on AUVs and ROVs (Dumke et al., 2018) will greatly contribute to time- and cost-effective large-scale surveys of unknown regions, such as the AMOR, and their faunal communities. These data will provide essential information that is necessary to develop management measures for seabed mining.

DATA AVAILABILITY STATEMENT

This article contains previously unpublished data. The name of the repository and accession number(s) are not available. The data can be available upon request to the lead author.

AUTHOR CONTRIBUTIONS

EP and CC conducted the image analyses and preliminary data analyses. All authors contributed to the in-depth data analyses and to the writing of the manuscript.

DEDICATION

This manuscript is dedicated to the memory of Hans Tore Rapp, who passed away on 7 March 2020.

FUNDING

The research was conducted in the framework of the project MarMine, funded by the Research Council of Norway (Project No. 247626/O30) and associated industrial partners. AH was funded by CESAM (UIDP/50017/2020 + UIDB/50017/2020) that is financed by FCT/MCTES through national funds. HR was funded by the European Research Council (ERC) under the European Union's Horizon 2020 research and innovation program (Grant Agreement No. 679849; the SponGES project). GJ was supported by the Research Council of Norway through the Centres of Excellence funding scheme (Grant No. 223254–NTNU AMOS).

ACKNOWLEDGMENTS

The authors would like to acknowledge the support of the Officers, crew, and scientific party on board CVS Polar King during the MarMine cruise for assistance at sea. The authors would like to thank Stein Nornes Melvaer and Øystein Sture (NTNU) for their assistance in the calculation of the image field of view area. We thank Christian Malmquist (NTNU AUR Lab) for making the Mohn's Treasure map in **Figure 1**. The authors would like to thank the two reviewers for their valuable comments that have contributed to considerably improving the manuscript.

REFERENCES

Arrieta, J. M., Arnaud-Haond, S., and Duarte, C. M. (2010). What lies underneath: conserving the oceans' genetic resources. *PNAS* 107, 18318–18324. doi: 10.1073/pnas.0911897107

Beazley, L. I., Wang, Z., Kenchington, E. L., Yashayaev, I., Rapp, H. T., Xavier, J. R., et al. (2018). Predicted distribution and climatic tolerance of the glass sponge Vazella pourtalesi on the Scotian Shelf and its persistence in the face of climatic variability. *PLoS One* 13:e0205505. doi: 10.1371/journal.pone.0205505

Boschen, R. E., Rowden, A. A., Clark, M. R., and Gardner, J. P. A. (2013). Mining of deep-sea seafloor massive sulfides: a review of the deposits, their benthic communities, impacts from mining, regulatory frameworks and management strategies. *Ocean Coast. Manag.* 84, 54–67. doi: 10.1016/j.ocecoaman.2013.07.005

Burgos, J. M., Buhl-Mortensen, L., Buhl-Mortensen, P., Ólafsdóttir, S. H., Steingrund, P., Ragnarsson, S. Á, et al. (2020). Predicting the distribution of indicator taxa of vulnerable marine ecosystems in the Arctic and Sub-Arctic waters of the Nordic Seas. *Front. Mar. Sci.* 7:131. doi: 10.3389/fmars.2020.00131

Cárdenas, P., Rapp, H. T., Klitgaard, A. B., Best, M., Thollesson, M., and Tendal, O. S. (2013). Taxonomy, biogeography and DNA barcodes for *Geodia species* (Porifera, Demospongiae, Astrophorida) in the Atlantic Boreo-Arctic region. *Zool. J. Linnean Soc.* 169, 251–311. doi: 10.1111/zoj.12056

Clark, A. M. (1970). Crinoidea. *Mar. Inverteb. Scand.* 3, 1–55.

Clark, A. M., and Downey, M. E. (1992). *Starfishes of the Atlantic. Natural History Museum Publications*. London: Chapman and Hall.

Dahle, H., Le Moine Bauer, S., Baumberger, T., Stokke, R., Pedersen, R. B., Thorseth, I. H., et al. (2018). Energy landscapes in hydrothermal chimneys shape distributions of primary producers. *Front. Microbiol.* 9:1570. doi: 10.3389/fmicb.2018.01570

Dahle, H., Økland, I. E., Thorseth, I. H., Pedersen, R. B., and Steen, I. H. (2015). Energy landscapes shape microbial communities in hydrothermal systems on the Arctic Mid-Ocean Ridge. *ISME J.* 9, 1593–1606. doi: 10.1038/ismej.2014.247

Dumke, I., Purser, A., Marcon, Y., Nornes, S. M., Johnsen, G., Ludvigsen, M., et al. (2018). Underwater hyperspectral imaging as an in situ taxonomic tool for deep-sea megafauna. *Sci. Rep.* 8:12860. doi: 10.1038/s41598-018-31261-4

Eilertsen, M. H., Georgieva, M. N., Kongsrud, J. A., Wiklund, H., Glover, A. G., and Rapp, H. T. (2018). Genetic connectivity from the Arctic to the Antarctic: *Sclerolinum contortum* and *Nicomache lokii* (Annelida) are both widespread in reducing environments. *Sci. Rep.* 8:4810. doi: 10.1038/s41598-018-23076-0

FAO (2009). *International Guidelines For The Management Of Deep-Sea Fisheries In The High Seas*. Rome: Food and Agricultural Organisation of the United Nations.

FAO (2019). *VME Indicators, Thresholds And Encounter Responses Adopted By R(F)Mos In Force During 2019*. Avaliavle at http://www.fao.org/in-action/vulnerable-marine-ecosystems/vme-indicators/en/ (accessed December 3, 2019).

Hestetun, J. T., Tompkins-MacDonald, G., and Rapp, H. T. (2017). A review of carnivorous sponges from the boreal North Atlantic and Arctic Oceans. *Zool. J. Linnean Soc.* 181, 1–69. doi: 10.1093/zoolinnean/zlw022

ISA (2019). *International Seabed Authority Website*. Available online at: https://www.isa.org.jm/deep-seabed-minerals-contractors?qt-contractors_tabs_alt=1#qt-contractors_tabs_alt (accessed November 15, 2019).

Jaeckel, A. (2015). An environmental management strategy for the international seabed authority? the legal basis. *Intern. J. Mar. Coast. Law* 30, 1–27.

Kongsrud, J. A., and Rapp, H. T. (2012). *Nicomache (Loxochona) lokii* sp. nov. (Annelida, Polychaeta, Maldanidae) from the Loki's Castle vent field – an important structure builder in an Arctic vent system. *Pol. Biol.* 35, 161–170. doi: 10.1007/s00300-011-1048-4

Kongsrud, J. A., Eilertsen, M. H., Alvestad, T., and Rapp, H. T. (2017). Two new species of *Ampharetidae* (Polychaeta) from the loki castle vent field. *Deep Sea Res. Part II* 137, 232–245. doi: 10.1016/j.dsr2.2016.08.015

Levin, L. A., and Le Bris, N. (2015). The deep ocean under climate change. *Science* 350, 766–768. doi: 10.1126/science.aad0126

Lim, A., Bronner, M., Johansen, S. E., and Dumais, M. A. (2019). Hydrothermal activity at the ultraslow-spreading Mohns ridge: new insights from near-seafloor magnetics. *Geochem. Geophys. Geosyst.* 20, 5691–5709. doi: 10.1029/2019GC008439

Ludvigsen, M., Aasly, K., Ellefmo, S. L., Hilário, A., Ramirez-Llodra, E., Søreide, F. X., et al. (2016). *MarMine Cruise Report-Arctic Mid-Ocean Ridge*. Trondheim, NO: NTNU.

Madsen, F. J., and Hansen, B. (1994). *Echinodermata Holothuroidea*. Oslo: Scandinavian University Press.

Maldonado, M., Aguilar, R., Bannister, R. J., Bell, J. J., Conway, K. W., Dayton, P. K., et al. (eds) (2016). "Sponge grounds as key marine habitats: a synthetic review of types, structure, functional roles, and conservation concerns," in *Marine Animal Forests: the Ecology of Benthic Biodiversity Hotspots*, (Berlin: Springer), 1–39. doi: 10.1007/978-3-319-17001-5_24-1

Meyer, H. K., Roberts, E. M., Rapp, H. T., and Davies, A. J. (2019). Spatial patterns of arctic sponge ground fauna and demersal fish are detectable in autonomous underwater vehicle (AUV) imagery. *Deep Sea Res.* 153:103137. doi: 10.1016/j.dsr.2019.103137

Meyer, K. S., Soltwedel, T., and Bergmann, M. (2014). High Biodiversity on a deep-water reef in the Eastern fram strait. *PLoS One* 9:e105424. doi: 10.1371/journal.pone.0105424

Murillo, F. J., Kenchington, E., Sacau, M., Piper, D. J. W., Wareham, V., and Muñoz, A. (2011). *New VME Indicator Species (Excluding Corals And Sponges) and Some Potential VME Elements of the NAFO Regulatory Area. SC WG on the Ecosystem Approach To Approach Fisheries Management*. Dartmouth: Northwest Atlantic Fisheries Organization.

Niner, H. J., Ardron, J. A., Escobar, E. G., Gianni, M., Jaeckel, A., Jones, D. O. B., et al. (2018). Deep-sea mining with no net loss of biodiversity—an impossible aim. *Front. Mar. Sci.* 5:53. doi: 10.3389/fmars.2018.00053

Olsen, B. R., Økland, I. E., Thorseth, I. H., Pedersen, R. B., and Rapp, H. T. (2016). *Environmental Challenges Related To Offshore Mining And Gas Hydrate Extraction*. Norway: Norwegian Environment Agency.

Pedersen, R. B., Rapp, H. T., Thorseth, I. H., Lilley, M., Barriga, F., Baumberger, T., et al. (2010a). Discovery of a black smoker field and a novel vent fauna at the ultraslow spreading Arctic Mid-Ocean Ridges. *Nat. Commun.* 1, 1–6.

Pedersen, R. B., Thorseth, I. H., Nygård, T. E., Lilley, M. D., and Kelley, D. S. (2010b). "Hydrothermal activity at the arctid mid-ocean ridges," in *Diversity of Hydrothermal Systems on Slow Spreading Ocean Ridges. Geophysical Monographs Series*, Vol. 118, eds P. A. Rona, C. W. Devey, J. Dyment, and B. J. Murton (Washington, DC: American Geophysical Union), 67–89.

Plotkin, A., Gerasimova, E., and Rapp, H. T. (2018). Polymastiidae (Porifera: Demospongiae) of the Nordic and Siberian Seas. *J. Mar. Biol. Assoc.* 98, 1273–1335. doi: 10.1017/S0025315417000285

Rabone, M., Harden-Davies, H., Collins, J. E., Zajderman, S., Appeltans, W., Droege, G., et al. (2019). Access to marine genetic resources (MGR): raising awareness of best-practice through a new agreement for biodiversity beyond national jurisdiction (BBNJ). *Front. Mar. Sci.* 6:520. doi: 10.3389/fmars.2019.00520

Roberts, E. M., Mienis, F., Rapp, H. T., Hanz, U., Meyer, H. K., and Davies, A. J. (2018). Oceanographic setting and short-timescale environmental variability at an Arctic seamount sponge ground. *Deep Sea Res. I* 138, 98–113. doi: 10.1016/j.dsr.2018.06.007

Rooks, C., Fang, J. K.-H., Mørkved, P. T., Zhao, R., Rapp, H. T., Xavier, J. R., et al. (2020). Deep-sea sponge grounds as nutrient sinks: denitrification is common in boreo-Arctic sponges. *Biogeosciences* 17, 1231–1245. doi: 10.5194/bg-17-1231-2020

Schander, C., Rapp, H. T., Kongsrud, J. A., Bakken, T., Berge, J., Cochrane, S., et al. (2010). The fauna of the hydrothermal vents on the Mohn Ridge (North Atlantic). *Mar. Biol. Res.* 6, 155–171. doi: 10.1080/17451000903147450

Seabed Mineral Law (2019). *Lov om Mineralvirksomhet På Kontinentalsokkelen (Law On Mineral Activities On The Continental Shelf), LOV-2019-03-22-7 (in Norwegian), Norwegian Ministry of Oil and Energy*. Available online at: https://lovdata.no/dokument/NL/lov/2019-03-22-7 (accessed April 2020).

Spang, A., Saw, J., Jørgensen, S., Zaremba-Niedzwiedzka, K., Martijn, K., Lind, A. E., et al. (2015). Complex archaea that bridge the gap between prokaryotes and eukaryotes. *Nature* 521, 173–179. doi: 10.1038/nature14447

Steen, I. H., Dahle, H., Stokke, R., Roalkvam, I., Daae, F. L., Rapp, H. T., et al. (2016). Novel barite chimneys at the Loki's Castle vent field shed light on key factors shaping microbial communities and functions in hydrothermal systems. *Front. Microbiol.* 6:1510. doi: 10.3389/fmicb.2015.01510

Stokke, R., Reeves, E., Dahle, H., Fedoy, A.-E., Viflot, T., Onstad, S. L., et al. (2020). Tailoring hydrothermal vent biodiversity toward improved biodiscovery using a novel in situ enrichment strategy. *Front. Microbiol.* 11:249. doi: 10.3389/fmicb.2020.00249

Sweetman, A. K., Levin, L. A., Rapp, H. T., and Schander, C. (2013). Faunal trophic structure at hydrothermal vents on the southern Mohn's Ridge, Arctic Ocean. *Mar. Ecol. Prog. Ser.* 473, 115–131. doi: 10.3354/meps10050

Tandberg, A. H. S., Vader, W., Olsen, B. R., and Rapp, H. T. (2018). *Monoculodes bousfieldi* n. sp. from the arctic hydrothermal vent Loki's Castle. *Mar. Biodiv.* 48, 927–937. doi: 10.1007/s12526-018-0869-6

Tandberg, A. H., Rapp, H. T., Schander, C., Vader, W., Sweetman, A. K., and Berge, J. (2011). *Exitomelita sigynae* gen. et sp. nov.: a new amphipod from the Arctic Loki castle vent field with potential gill ectosymbionts. *Pol. Biol.* 35, 705–716. doi: 10.1007/s00300-011-1115-x

Taylor, J., Krumpen, T., Soltwedel, T., Gutt, J., and Bergmann, M. (2016). Regional- and local-scale variations in benthic megafaunal composition at the Arctic deep-sea observatory Hausgarten. *J. Deep Sea Res. I* 108, 58–72. doi: 10.1016/j.dsr.2015.12.009

Van Dover, C. L. (2010). Mining seafloor massive sulphides and biodiversity: what is at risk? *ICES J. Mar. Sci.* 68, 341–348. doi: 10.1093/icesjms/fsq086

Van Dover, C. L. (2019). Inactive sulfide ecosystems in the deep sea: a review. *Front. Mar. Sci.* 6:461. doi: 10.3389/fmars.2019.00461

Van Dover, C. L., Arnaud-Haond, S., Gianni, M., Helmreich, S., Huber, J. A., Jaeckel, A., et al. (2018). Scientific rationale and international obligations for protection of active hydrothermal vent ecosystems from deep-sea mining. *Mar. Policy* 90, 20–28. doi: 10.1016/j.marpol.2018.01.020

Van Dover, C. L., Aronson, J., Pendleton, L., Smith, S., Arnaud-Haond, S., Moreno-Mateos, D., et al. (2014). Ecological restoration in the deep sea: desiderata. *Mar. Policy* 44, 98–106. doi: 10.1016/j.marpol.2013.07.006

Conflict of Interest: The authors declare that the research was conducted in the absence of any commercial or financial relationships that could be construed as a potential conflict of interest.

Copyright © 2020 Ramirez-Llodra, Hilario, Paulsen, Costa, Bakken, Johnsen and Rapp. This is an open-access article distributed under the terms of the Creative Commons Attribution License (CC BY). The use, distribution or reproduction in other forums is permitted, provided the original author(s) and the copyright owner(s) are credited and that the original publication in this journal is cited, in accordance with accepted academic practice. No use, distribution or reproduction is permitted which does not comply with these terms.

frontiers in Marine Science

ORIGINAL RESEARCH
published: 21 July 2020
doi: 10.3389/fmars.2020.00591

Species and Functional Diversity of Deep-Sea Nematodes in a High Energy Submarine Canyon

Jian-Xiang Liao[1], *Chih-Lin Wei*[1]* *and Moriaki Yasuhara*[2,3]

[1] Institute of Oceanography, National Taiwan University, Taipei, Taiwan, [2] School of Biological Sciences, The University of Hong Kong, Hong Kong, China, [3] Swire Institute of Marine Science, The University of Hong Kong, Hong Kong, China

Gaoping Submarine Canyon (GPSC) off southwestern Taiwan is a high energy canyon connected to a small mountain river with extremely high sediment load (~10 kt km^{-2} y^{-1}). Due to heavy seasonal precipitation (>3,000 mm y^{-1}) and high tectonic activity in the region, the GPSC is known for active sediment transport processes and associated submarine geohazards (e.g., submarine cable breaks). More importantly, strong internal tides have been recorded in the GPSC to drive head-ward, bottom-intensified currents, which result in sediment erosion and resuspension in response to the tidal cycles. To understand the effects of extreme physical conditions on marine nematodes, we sampled the surface sediments along the thalweg of upper GPSC and adjacent slope (200–1,100 m) using a multicorer in the summer and fall of 2015. We found that the nematode species, functional, trophic diversity and maturity dropped significantly in the GPSC as compared with slope communities, but the nematode abundances were not affected by the adverse conditions in the canyon. The non-selective deposit-feeding, fast colonizing nematodes (e.g., *Sabatieria*, *Daptonema*, *Axonolaimus*, and *Metadesmolaimus*) dominated the canyon seafloor. In contrast, other species of non-selective deposit feeders (*Setosabatieria* and *Elzalia*), epigrowth feeders (*Craspodema*), omnivores/predators (*Paramesacanthion*), and other species constituted the diverse nematode assemblages on the slope. We found that the strong bottom currents in the GPSC may depress the local nematode diversity by removing the organic-rich, fine-grained sediments; therefore, only the resilient or fast recovering nematode species could survive and prevail. The high species turnover with depth and between the canyon and slope habitats demonstrates that strong environmental filtering processes were the primary mechanism shaping the nematode community assembly off SW Taiwan. Between the canyon and slope, a considerable contribution of nestedness pattern also indicates some degree of local extinction and dispersal limitation in the dynamic GPSC.

Keywords: meiobenthos, nematode, submarine canyon, continental slope, community structure, functional groups, diversity

OPEN ACCESS

Edited by:
Rui Rosa,
University of Lisbon, Portugal

Reviewed by:
Chiara Romano,
Center for Advanced Studies of Blanes (CSIC), Spain
Henko De Stigter,
Royal Netherlands Institute for Sea Research (NIOZ), Netherlands
Natalya D. Gallo,
Scripps Institution of Oceanography, University of California, San Diego, United States
Sofia P. Ramalho,
University of Aveiro, Portugal

***Correspondence:**
Chih-Lin Wei
clwei@ntu.edu.tw;
chihlinwei@gmail.com

Specialty section:
This article was submitted to Global Change and the Future Ocean, a section of the journal Frontiers in Marine Science

Received: *14 December 2019*
Accepted: *29 June 2020*
Published: *21 July 2020*

Citation:
Liao J-X, Wei C-L and Yasuhara M (2020) Species and Functional Diversity of Deep-Sea Nematodes in a High Energy Submarine Canyon. Front. Mar. Sci. 7:591. doi: 10.3389/fmars.2020.00591

INTRODUCTION

Gaoping Submarine Canyon (GPSC) is the largest underwater canyon off SW Taiwan (Yu et al., 2009). The head of GPSC connects to a small mountain river, the Gaoping River, which originates from the Mt. Jade at more than 3,000 m above sea level. The thalweg of the canyon meanders approximately 260 km to the south and eventually connects to the Manila Trench, which reaches

depths of over 5,000 m. The high bedrock erodibility, heavy precipitations, steep topography and high tectonic activities in the Gaoping River catchment make the GPSC prone to receive extremely high fluvial sediment loads (~10 kt km^{-2} y^{-1}) and frequent turbidity currents (Liu et al., 2013, 2016; Gavey et al., 2017). The rugged, steep, and tectonically active margin off SW Taiwan also subjects the GPSC to high risk of slope failure, producing debris flows which cascade down the canyon axis, occasionally resulting in breakage of telecommunication cables (Hsu et al., 2008; Su et al., 2012; Gavey et al., 2017). Besides these episodic events, the GPSC is close to the source of the world's largest internal solitary waves in the Luzon Strait (Jan et al., 2008; Alford et al., 2015). The energy of internal tides propagates along the axis of the GPSC following tidal cycles to drive bottom and headward intensified currents with observed current velocity exceeding 1 m/s at the canyon head (Wang et al., 2008; Chiou et al., 2011). These unique physical settings make the GPSC an example of source-to-sink sediment transports from the high mountains to the deep sea and also an ideal location to study submarine geohazards (Liu et al., 2013, 2016). However, despite a wealth of literature and interests in the GPSC's unique geology, information is lacking on how benthic communities, especially the very small but numerically dominant meiofauna, respond to such extreme environmental conditions. This study thus attempts to conduct the first meiofauna diversity investigation in the GPSC and to contribute to the growing interests in understanding the ecological processes in the benthic communities in highly dynamic conditions.

Many studies have documented enriched benthic communities in submarine canyons and suggested that the organic accumulation in these prominent topographic depressions might be the primary driver of enhanced benthic production (Baguley et al., 2006; Ingels et al., 2009; De Leo et al., 2010; Kiriakoulakis et al., 2011; Leduc et al., 2014; Amaro et al., 2016; Román et al., 2016; Gambi et al., 2019). Due to the higher food availability within canyons, the abundance and biomass of meiofauna are generally higher than on the adjacent slope (Danovaro et al., 2009; Ingels et al., 2009, 2011; De Leo et al., 2010; Leduc et al., 2014; Gambi et al., 2019), although the opposite has also been found in active canyons with substantial sediment disturbances (Garcia et al., 2007; Van Gaever et al., 2009). The elevated density and biomass of benthos in the submarine canyon are thus considered as the typical "canyon effect" (Vetter and Dayton, 1998; Fernandez-Arcaya et al., 2017; Román et al., 2019). Also, opportunistic species may become dominant in the canyons so the local diversity could be comparable to or lower than in slope communities (Van Gaever et al., 2009; Ingels et al., 2011; Leduc et al., 2014; Gambi et al., 2019; Wei and Rowe, 2019; Wei et al., 2020). In the upper GPSC off SW Taiwan, however, Liao et al. (2017) found that strong, continuous, and recurrent bottom currents driven by the internal tides may cause sediment erosion which may negatively impact the densities and alter the taxonomic composition of meiofaunal taxa. The faunal patterns observed in the GPSC probably resemble those observed under high physical disturbance by strong near-bed flows and sediment erosion, as in the upper Nazaré Canyon and Congo Channel (Garcia et al., 2007; Van Gaever et al., 2009). The strong bottom shear not only may erode sediment and remove the local benthic communities but also likely re-suspend or prevent the organic-rich particles from settling on the seafloor and thus reduce the sedimentary organic carbon contents and the food supply to the meiofauna (Liao et al., 2017). While meiofauna abundance and the number of taxa were found to be depressed in the canyon (Liao et al., 2017), it is still unknown how species diversity, species composition, and functional traits may be affected. These biodiversity attributes are known to predict the ecosystem functioning of the benthic community, reflecting the ability of meiobenthos in moderating carbon and nutrient cycling and converting the available energy into biomass and transferring this energy up the food chain (Covich et al., 2004; Ieno et al., 2006; Radwell and Brown, 2008; Karlson et al., 2010).

Moreover, Liao et al. (2017) hypothesized that the extreme conditions in the GPSC might result in the environmental filtering of the less-fitted species or even local extinction if the disturbance is too strong. In such a case, meiofauna should exhibit varying degrees of spatial turnover (i.e., replaced by better-fitted species) or nestedness pattern (i.e., species-poor as subsets of species-rich assemblages) (Baselga, 2010, 2012). From the relative proportion of the turnover and nestedness inferences can be made regarding the process of community assembling under strong environmental perturbations. Therefore, the high-resolution, species-level data are required for quantitatively assessing these ecological mechanisms.

In this study, we used free-living marine nematodes as a model organism to examine the species and functional diversity of meiofauna in the GPSC and adjacent slope habitat. Nematodes are the most abundant metazoan in sediments, accounting for more than 90% of the meiofaunal abundance in deep-sea environments (Giere, 2009; Danovaro, 2012). They are also one of the most diverse organisms in the ocean. A conservative estimation suggests that there may be 6,900 described species to up to 50,000 species if the undescribed species are also included (Appeltans et al., 2012). Not only are nematodes abundant and diverse, they are also ubiquitous, not highly mobile, and sensitive to environmental changes and pollution; therefore, nematodes have been widely used as an indicator for environmental monitoring (Coull and Chandler, 1992; Bongers and Ferris, 1999; Schratzberger et al., 2000; Giere, 2009; Moreno et al., 2011). Due to their small sizes, short generation times, and high metabolic rates, nematodes process a considerable amount of energy in the benthic ecosystem (Giere, 2009). The grazing, excretion, bioturbation, and mechanical breakdown of detrital particles by nematodes can stimulate bacterial activities (Giere, 2009). These interactions may affect the organic carbon remineralization, oxygen dynamics, and nutrient cycling in the sediment (Aller and Aller, 1992; Rysgaard et al., 2000; Moens et al., 2005; Nascimento et al., 2012; Bonaglia et al., 2014; Schratzberger and Ingels, 2018). More importantly, the feeding guilds and morphological traits affecting the locomotion and life-history strategies of nematodes are well-developed (Wieser, 1953; Jensen, 1987; Bongers et al., 1991; Thistle et al., 1995; Soetaert et al., 2002; Schratzberger et al., 2007). These studies allow us

to quickly assemble the species functional traits from the known species list and compute nematode functional diversity.

Our objective was to examine how species and functional diversity and community composition of deep-sea nematodes may respond to a high energy environment in the GPSC. We compared the GPSC and the adjacent slope by surveying parallel transects at equivalent depths across the continental margin off SW Taiwan. We hypothesized that: (1) the extreme physical conditions in the GPSC may depress the nematode species, functional and trophic diversity, and maturity, as well as alter their life strategies (e.g., feeding guilds, morphology, and lifestyles) and species composition; (2) nestedness patterns of species loss may be the dominant mechanism shaping the GPSC community if the adverse environment caused local extinction; otherwise, spatial turnover of species replacement may play a more dominant role indicating the effect of environmental filtering. Ultimately, with the species-level information on nematodes, we hope to contribute to the understanding of the responses of meiofauna to the strong internal tides and thus fast bottom currents and consequent physical disturbances in a high-energy submarine canyon.

MATERIALS AND METHODS

Environmental Setting

GPSC is a major conduit on the active margin offshore SW Taiwan. The collision between the Luzon Volcanic Arc and the South China Sea margin created the Taiwan central mountain belt, foreland shelf and slope, and Manila Trench, which significantly affects the geomorphology of GPSC (Liu et al., 2016). The head of GPSC is deeply incised into the continental shelf (i.e., vertical relief >400 meters, **Figure 1**) with a clear bathymetric connection to a small mountain river, the Gaoping River (Chiang et al., 2020). The canyon head is believed to have formed by subaerial erosion; the head later submerged during the Holocene transgression following the last glacial maximum (∼18,000 years BP) and then was re-excavated by sediment movement processes (Yu et al., 1991). The meandering, V-shaped, and entrenched thalweg with deep-cutting outer bends are characteristic features of the GPSC (**Figure 1**). These erosive features are believed to be maintained by turbidity currents triggered by (1) flood events (Liu et al., 2013, 2016), (2) turbulence mixing related to internal and surface waves (Wang et al., 2008; Lee et al., 2009; Chiou et al., 2011), (3) submarine groundwater discharges (Su et al., 2012), and (4) sediment collapses from over- steepening canyon walls following earthquakes (Hsu et al., 2008; Su et al., 2012; Gavey et al., 2017). The GPSC is filled with the effluent of Gaoping River, Kuroshio Current Water, and South China Sea Water, in which the mixing of these water masses is controlled by internal tides (Liu et al., 2002, 2006). The internal tides in the GPSC follow semidiurnal cycles (M_2), in which the intensity increases toward the canyon head, or in other words, decreases with depth and with distance from the canyon head (Wang et al., 2008). The energy flux of internal tide in the GPSC is estimated to be 3–7 times greater than that in the Monterey Canyon (Lee et al., 2009); therefore, the isothermal displacement by the internal tides can be easily over 200 meters in the GPSC (Liu et al., 2016). Another consequence of the strong internal waves is the year-round existence of a benthic nepheloid layer as thick as 100 m with the suspended sediment concentration reaching 30 mg/l (Liu et al., 2010). The turbulence mixing associated with internal tides and high suspended-sediment concentrations near the seabed are believed to result in significant sediment transport (Liu et al., 2016).

Field Sampling

Two cruises (cruises 1114 and 1126) were conducted off SW Taiwan by R/V Ocean Researcher 1 in August and November 2015 (i.e., summer and fall, respectively). A total of eight stations were repeatedly sampled from 200 to 1,100 m in the upper Gaoping Submarine Canyon (GPSC) and the adjacent slope (**Figure 1** and **Table 1**). The sampling was designed to collect biological and environmental information on four equally spaced depth strata (200–400 m, 400–600 m, 600–800 m, and 800–1,100 m) along the canyon thalweg and on the adjacent slope. At each station, a CTD-Rosette cast was made and surface sediment was sampled by means of a multicorer (OSIL megacorer). One multicore tube (i.d., =105 mm) per station was selected for meiofaunal analysis and three subsamples were taken with a cut-off syringe (i.d., 28 mm; area 616 mm^2) from the top 5 cm of the sediment. The subsamples were immediately fixed on board in formalin solution with Rose Bengal. During Cruise 1126, only one subsample for meiofauna analysis was retrieved from the deepest canyon station (GC4). Altogether, 46 meiofauna subsamples were retrieved during the two cruises.

The fixed sediment samples were washed with tap water through a 1,000-μm sieve and a 40-μm sieve. The meiofauna samples retained on a 40-μm sieve were extracted by Ludox HS40 (gravity = 1.18 g/cm^3; centrifuged for 10 min at 8,000 rpm and repeated three times) (Danovaro, 2010), after which meiofauna were picked and counted under a stereomicroscope (Olympus SZ61). From each subsample, 100 nematode individuals (or all the individuals if fewer than 100 were present) were randomly picked out and transferred to a solution of 5% glycerol and 5% ethanol in water. The mixture was allowed to evaporate gradually on a warm hotplate, leaving the nematodes in pure glycerol. The nematodes were mounted onto permanent slides. Putative morphospecies were identified using pictorial keys (Platt and Warwick, 1983, 1988; Warwick et al., 1998; Schmidt-Rhaesa, 2014). Based on the morphology of the buccal cavities, the nematodes were classified to four feeding traits, namely selective deposit feeders (1A), non-selective deposit feeders (1B), epigrowth feeders (2A), and omnivores/predators (2B) (Wieser, 1953). Of the gutless chemotrophic nematode genus Astomonema, allocated to a fifth feeding trait by Ingels et al. (2011), only one specimen was identified, which was not included in the analysis. Furthermore, nematodes were classified to four classes of tail shape, namely short/round, elongated/filiform, conical, and clavate, because these traits might relate to the movement and vertical distribution of nematodes, which depends on the sediment type (Riemann, 1974; Thistle et al., 1995). Also, following Bongers et al. (1991), nematodes were assigned to four life-history strategy classes, using c-p values ranging from 1 for

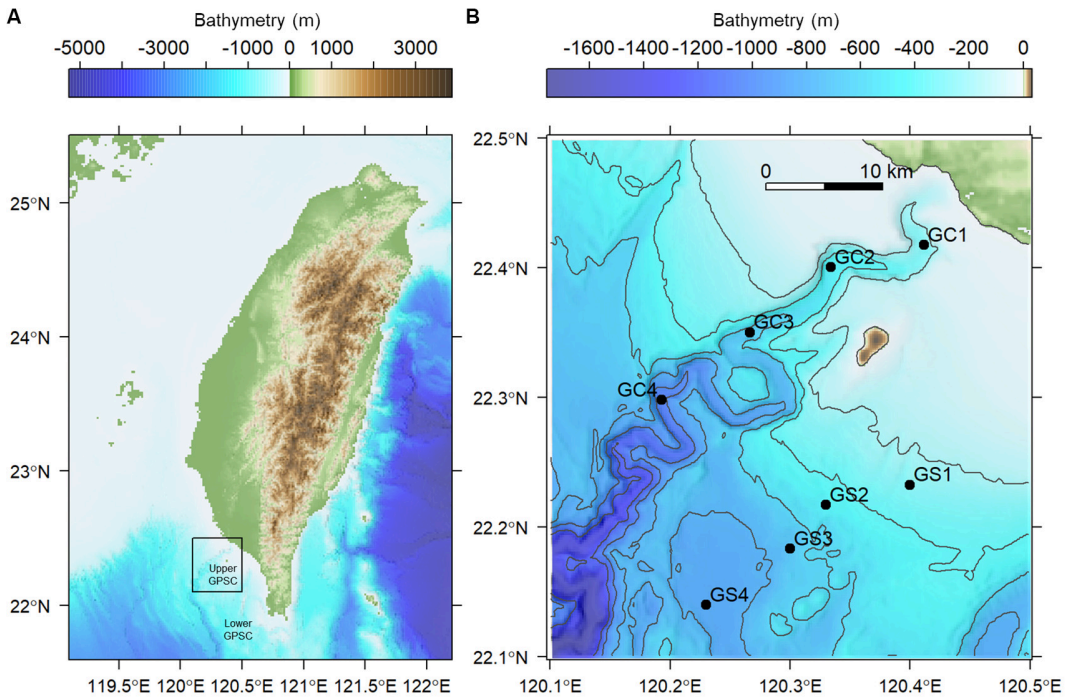

FIGURE 1 | Map of sampling stations visited in August and November 2015. **(A)** The sampling area off the continental margin of SW Taiwan. **(B)** Sampling transects along the upper Gaoping Submarine Canyon (GC) and Gaoping Slope (GS).

TABLE 1 | Dates, coordinates, and water depths of sample sites during August and November 2015.

Cruise	Date	Habitat	Station	Longitude	Latitude	Depth
1114	2015-08-04	Canyon	GC1	120.4111	22.4173	318
1114	2015-08-04	Canyon	GC2	120.3348	22.4007	478
1114	2015-08-04	Canyon	GC3	120.2665	22.3500	655
1114	2015-08-05	Canyon	GC4	120.1928	22.2980	1051
1114	2015-08-05	Slope	GS1	120.3998	22.2322	279
1114	2015-08-05	Slope	GS2	120.3297	22.2172	462
1114	2015-08-05	Slope	GS3	120.2998	22.1833	690
1114	2015-08-05	Slope	GS4	120.2304	22.1401	848
1126	2015-11-21	Canyon	GC1	120.4117	22.4176	318
1126	2015-11-21	Canyon	GC2	120.3330	22.4000	487
1126	2015-11-20	Canyon	GC3	120.2667	22.3500	655
1126	2015-11-20	Canyon	GC4	120.1933	22.2981	1073
1126	2015-11-19	Slope	GS1	120.4000	22.2330	277
1126	2015-11-19	Slope	GS2	120.3300	22.2168	463
1126	2015-11-19	Slope	GS3	120.3000	22.1830	690
1126	2015-11-20	Slope	GS4	120.2301	22.1402	848

colonizers (r-selected species with short generation time, high colonization ability, and adaptation of unstable environments) to 4 for persisters (K-selected species with strong competition ability in crowded niches).

Temperature, salinity, dissolved oxygen concentration, fluorescence, and light transmission of the bottom water were measured by a conductivity-temperature-depth (CTD) recorder (Sea-Bird SBE 911) and other attached sensors. Surface sediment grain sizes (non-carbonate fraction) were measured by a laser diffraction particle size analyzer (Beckman Coulter LS13 320). Total organic carbon (TOC) and total nitrogen (TN) were analyzed with a Flash EA 1112 elemental analyzer. The detailed descriptions of hydrological and sediment sampling can be found in Liao et al. (2017). Hourly bottom current velocity at each site was derived from a 3-D, hydrodynamic internal tide model from Chiou et al. (2011). Based on the internal tide model, we

calculated the hourly mean velocity of bottom currents and the duration for which bottom current velocity exceeded 20 cm/s for 1 month preceding the sampling campaign to evaluate the possible disturbances of near-bottom currents on nematodes. The environmental data were derived from Liao et al. (2017, **Supplementary Figure S1**), in which the canyon head and upper canyon had the highest modeled bottom current velocity and the most prolonged duration of sediment erosion. The lowest bottom water light transmission and surface sediment TOC coincided with the strongest hydrodynamic energy near the canyon head. While the temperature and dissolved oxygen concentration both declined with depth, surface sediment TOC increased with depths in both the canyon and slope transects (Liao et al., 2017). Nevertheless, the dissolved oxygen concentration never dropped below the threshold of hypoxia (2 mg/L), presumably, due to turbulence mixing by internal tides. To avoid autocorrelations, redundant environmental variables (correlations > 0.9) were removed. For example, the bottom water temperature, density, and dissolved oxygen measured in this study were highly correlated (**Supplementary Figure S1**). Therefore, the dissolved oxygen was not retained because the bottom water was not hypoxic in all stations. The density was not retained because it's not an important factor known to affect nematode assemblages. Only the ecologically relevant variables, including bottom water temperature, salinity, light transmission, percent sand, silt and clay, sediment TOC and C/N ratio, mean bottom current velocity, and duration of bottom current velocity exceeding 20 cm/s were retained for the analysis. These variables were logarithm (base of 10) transformed, centered (subtracted from the mean), and normalized (divided by the standard deviation) prior to use in statistical analyses involving environmental variables.

Data Analysis

Species diversity was determined using Hill numbers (Hill, 1973), or the effective numbers of equally abundant species in a hypothetical assemblage (Chao and Jost, 2010). The Hill number, ${}^{q}D$, is expressed as a function of the *q-th* power sum of the relative species abundance. Thus, the order q controls the sensitivity of Hill numbers to the relative species abundance. For example, when $q = 0$, ${}^{0}D$ weights all species equally and reduces to the number of species. For $q = 1$, ${}^{1}D$ weights species in proportion to their abundance and can be interpreted as the effective number of abundant species. For $q = 2$, ${}^{2}D$ then measures the effective number of highly abundant species. The Hill numbers of order $q = 0, 1, 2$ are mathematically equivalent to the species richness, the exponential of Shannon entropy, and the inverse of Simpson concentration index (Chao et al., 2014). We, therefore, adopted these three most commonly used diversity indices and referred to them as the species richness, Shannon diversity, and Simpson diversity following Chao et al. (2014). To make a fair comparison across samples, the Hill numbers of order $q = 0, 1, 2$ were rarefied or extrapolated to equal sample coverage of 80.8% (the lowest sample coverage among samples, **Supplementary Figure S2**). The standard error and 95% confidence intervals of the Hill numbers were estimated by 1000 bootstrap resampling. The rarefaction, extrapolation, and resampling of Hill numbers follow the description by Chao et al. (2013).

Functional diversity was calculated from species abundance and functional dissimilarities (Gower distances) between species based on nematode functional traits (buccal morphology, tail shape, and life history). We adopt a Hill-number based approach to estimate the effective number of equally abundant and equally distinct functional groups in an assemblage (Chao et al., 2019). In this new approach, Chao et al. (2019) introduce a positive parameter τ to the ordinary Hill numbers to indicate a threshold of functional distinctiveness between any two species (based on Gower distance in functional trait space). Any two species with functional dissimilarity $\geq\tau$ are considered functionally distinct. When τ approaches 0, every species is functionally distinct; therefore, the functional diversity reduces to the ordinary Hill numbers. Following the recommendation by Chao et al. (2019), we set the τ = Rao's quadratic entropy (Q) of the pooled assemblages, or the abundance-weighted mean functional dissimilarity (based on Gower distance) between any two taxa (Botta-Dukát, 2005). Similarly, we computed the functional diversity of order $q = 0, 1, 2$ to estimate the functional richness, effective number of abundant functional group, and effective number of highly abundant functional group, respectively. Unfortunately, the functional diversities were not standardized by sample coverage. The rarefied and extrapolated functional diversity is still under development and not available at the time of writing this paper (Chao, personal communication).

Trophic diversity (TD) was determined from four trophic groups based on the buccal morphologies (1A, 1B, 2A, 2B) (Wieser, 1953) and calculated as the sum of square of the relative abundance of each trophic group (Heip et al., 1985; Gambi et al., 2003; Gambi and Danovaro, 2016). Maturity index (MI) was computed as the mean individual genus c-p value (from colonizers to persisters) weighted by their relative abundance (Bongers et al., 1991).

We scaled the relative abundance of each nematode species (from 100 randomly selected individuals) by the total nematode abundance in each sample. The species abundance in each sample was square-root transformed, and converted to Bray-Curtis dissimilarity between samples. The same matrix was subjected to the agglomerative hierarchical clustering based on the group average (=UPGMA) method and Non-metric Multi-dimensional Scaling (nMDS). The species which contributed most to the average Bray-Curtis dissimilarity in each cluster were identified by the Similarity Percentage (SIMPER) routine. These characteristic species were projected on to the nMDS plot by the abundance-weighted averages of the ordination scores. Distance-based Redundancy Analysis (dbRDA) was used to select the subset of environmental variables which best explained (with the smallest AIC) the nematode species composition. The selected variables were projected as vectors on to the same nMDS ordination with the length of vectors indicating their correlations with the nMDS ordination scores and direction of vectors indicating the direction of increasing environmental values.

We used multiple-site Sørensen dissimilarity to examine nematode β-diversity among the four sites within the GPSC and adjacent slope transects, as well as between the canyon

and slope site pair across four depth strata (i.e., 200–400 m, 400–600 m, 600–800 m, 800–1,100 m). The dissimilarities within-habitat (canyon or slope) or between-habitat (canyon vs. slope) were respectively partitioned to their turnover and nestedness components (Baselga, 2010, 2012). Average dissimilarity, turnover, and nestedness over the two cruises in 2015 were calculated. We used the turnover dissimilarity to examine the contributions of environmental filtering in structuring the nematode species composition within and between the habitats. The nestedness dissimilarity explored the contribution of source-sink dynamics or local extinction.

Nematode community attributes, such as total abundance, number of species, species diversity, functional diversity, trophic diversity, and maturity index of each subsample were averaged per core (i.e., average of three subsamples) before further statistical tests. We used Generalized Least Squares (GLS) modeling to examine the effects of habitat (canyon vs. slope), depth strata, and sampling time (Cruise 1114 vs. 1126) on the mean values of the community attributes mentioned above. Also, we performed a three-way cross permutation analysis of variance (PERMANOVA) to examine the effects of habitat, depth, and sampling time on the average nematode species composition per core. The number of permutation was set to 999. All statistical tests used α-value = 0.05 and pairwise tests used α-value = 0.05/numbers of tests (i.e., Bonferroni correction).

Statistical analyses used software R version 3.6.1 (R Core Team, 2019). Hill numbers were computed by the "iNEXT" package. Functional diversity was computed by R code available at https://github.com/AnneChao/FunD/blob/master/FunD_Rcode.txt. Multivariate analyses used the "vegan" package and β-diversity partition used the "betapart" package. Generalized Least Squares (GLS) modeling used the "nlme" package. All relevant analyses can be reproduced and the data are deposited in an R data package "nema" available at https://github.com/chihlinwei/nema.

RESULTS

A total of 163 nematode species belonging to 32 families and 105 genera were identified from 3,577 individuals. Among them, 53 and 156 species were found in the GPSC and adjacent slope, respectively. In other words, 46 species co-occurred in both habitats and only seven species were exclusively found in the GPSC. Among the nematode species identified in this study, there was a total of 32 different combinations of functional types (excluding the gutless *Astomonema* sp.) based on their buccal morphologies, tail shapes, and life-history strategies. Only 15 combinations were found in the GPSC, whereas all functional types existed on the slope. The non-selective deposit feeders (1B) with clavate tail and r-selection strategy (c-p value = 2) flourished in the GPSC (GLS, $P < 0.01$, **Supplementary Table S1**). In contrast, the different buccal morphologies, tail shapes, and life-history strategies were more evenly represented in the slope assemblages (**Figure 2**). The relative contributions of epigrowth feeders (2A), conical and elongated/filiform tails, and persisters (c-p value = 4) were higher on the slope (GLS, $P < 0.01$, **Supplementary Table S1**). The relative contributions of deposit feeders (1A, 1B) increased, but the omnivores/predators (2B) decreased with depth (GLS, $P < 0.05$, **Supplementary Table S1** and **Figure 2A**). In the GPSC, the r-selection strategists contributed more toward the head of the canyon, reflected in a decreasing contribution of persisters (GLS, $P < 0.01$, **Supplementary Table S1**). Albeit weakly, on the slope, the relative contributions of persisters declined with depth (GLS, $P = 0.026$, **Supplementary Table S1** and **Figure 2C**).

Nematode abundances were not significantly different between the canyon and slope and among different depth strata (**Figure 3** and **Table 2**). The observed number of species (**Figure 3B**), Shannon diversity, functional diversity ($q = 1$), trophic diversity and maturity index were significantly depressed in the GPSC compared to the adjacent slope (**Figure 4** and **Table 2**). Similar patterns (i.e., depressed diversity in the GPSC) were also found for the species richness, Simpson diversity, and functional diversity of order $q = 0$ and 2 (**Supplementary Figures S2**, **S3** and **Supplementary Table S2**). Individual linear regressions for the canyon and slope samples show that the species diversity (including species richness, Shannon diversity, and Simpson diversity) both increased with depth; however, the increase was more rapid on the slope than in the canyon (**Supplementary Figures S4A–C**). On the slope, the number of species increased and trophic diversity declined with depth, but no bathymetric pattern was evident in the canyon (**Supplementary Figures S4D,E**). These subtle discrepancies in bathymetric patterns between the canyon and slope may contribute to the significant interaction between habitat and depth in the GLS model for the number of species, Shannon diversity, trophic diversity and maturity index (**Table 2**). Similar interactions were also evident for species richness and Simpson diversity, probably for the same reason (**Supplementary Table S2**). Nevertheless, the effect size of habitat (in the variables mentioned above) is much stronger than the effect of habitat and depth interactions (see GLS coefficients in **Table 2** and **Supplementary Table S2**), which warrants the observation of depressed nematode diversity (all aspects from species, functional to trophic diversity) and maturity in the GPSC. Among the two sampling times, none of the GLS tests suggest significant cruise effect ($P > 0.05$, **Table 2** and **Supplementary Table S2**); however, the inconclusive time effect might have been confounded by the significant interaction between habitat and cruise for total abundance and Shannon diversity ($P < 0.05$, **Table 2**), as well as for the species richness and Simpson diversity ($P < 0.05$, **Supplementary Table S2**). Nevertheless, further pairwise GLS tests (with depth, cruise and their interaction as factors) in each of the canyon and slope habitats confirmed no cruise effect ($P > 0.05/2$, Bonferroni Correction).

Habitats were clearly separated in the nMDS ordination of nematode assemblages without any overlap (**Figure 5**). This was also reflected by the significant difference found between nematode species composition of canyon and slope habitats (habitat, $P = 0.001$) in the PERMANOVA (**Table 3**). In the meantime, no statistical depth effect ($P = 0.135$) but marginal cruise effect ($P = 0.052$) and marginal interaction

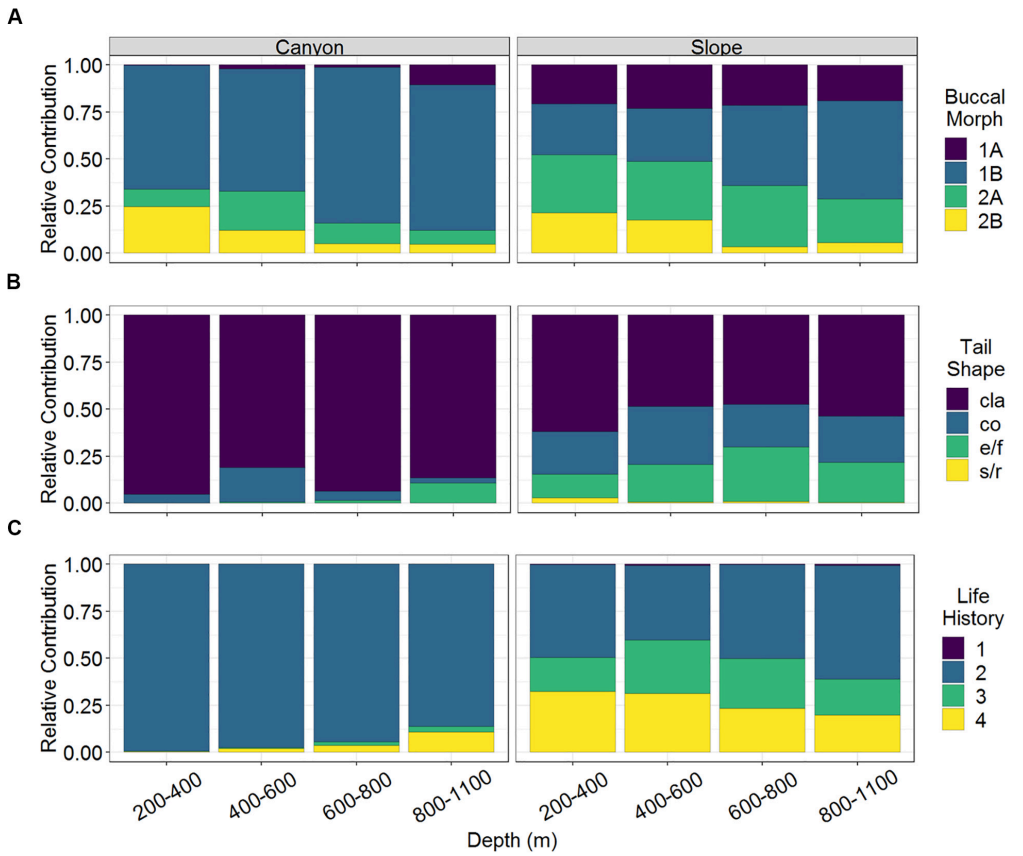

FIGURE 2 | The relative abundance of **(A)** buccal morphology, **(B)** tail shape, and **(C)** life history strategy of nematodes of the GPSC and adjacent slope. Buccal cavities classified according to Wieser (1953): selective deposit feeders (1A), non-selective deposit feeders (1B), epigrowth feeders (2A), and omnivores/predators (2B). Tail shapes included clavate (cla), conical (co), elongated/filiform (e/f), and short/round (s/r). Life history denoted as c-p values 1–4 from colonizer to persister.

between habitat and depth were detected (P = 0.061, **Table 3**). Although not statistically significant, the temporal change in nematode composition is visible in the nMDS ordination (**Figure 5**), especially for the canyon (i.e., better separation between cruises). Based on the similarity percentage (SIMPER) analysis, *Metadesmolaimus* sp. 1, *Daptonema* sp. 4, *Axonolaimus* sp. 1, *Sabatieria* sp. 2, and *Sabatieria* sp. 3 have the highest contribution to the average dissimilarity in the GPSC (**Figure 5A** and **Supplementary Table S3**). *Sabatieria* sp. 1, *Elzalia gerlachi*, *Dorylaimopsis variabilis*, *Cervonema tenuicaudatum,* and *Sphaerolaimus* sp. 1 were the top five most contributing species on the slope (**Supplementary Table S3**). In terms of species abundance, *Daptonema* sp. 2, *Axonolaimus* sp. 1, *Metadesmolaimus* sp. 1, *Daptonema* sp. 4, and *Sabatieria* sp. 2 dominated in the GPSC, whereas *Craspodema* sp. 1, *Elzalia gerlachi*, *Paramesacanthion tricuspis*, *Setosabatieria hilarula,* and *Sabatieria* sp. 1 flourished on the slope. For the most contributing species identified by SIMPER (**Supplementary Tables S3**, **S4**), the top five species in the GPSC were non-selective deposit feeders (1B) with clavate tail and r-selection strategy, whereas the highly contributed species on the slope including *Dorylaimopsis variabilis* and *Sphaerolaimus* sp. 1 were epigrowth feeders (2A) and omnivores/predators (2B), respectively. The same pattern was also found for the most abundant species. The top five most abundant canyon species were non-selective deposit feeders (1B) with clavate tail and r-selection strategy. In contrast, *Craspodema* sp. 1 and *Paramesacanthion tricuspis* from the slope habitats belonged to epigrowth feeder (2A) and omnivore/predator (2B), respectively.

Based on distance-based redundancy analysis (dbRDA), the best subset of environmental factors explaining nematode species composition (adjusted R^2 = 58.8%, $p < 0.05$) were variables related to:

1. Internal-tide energy, i.e., mean bottom current velocity (*Spd*), duration of bottom current velocity exceeding 20 cm/s (*Over20*), and light transmission (*Trans*),
2. Food supply, i.e., total organic carbon contents (*TOC*) and carbon to nitrogen ratio (*CN*),
3. Water masses, i.e., salinity (*Salin*) and temperature (*Temp*).

These variables are mapped onto the same nMDS plot using their correlations with the ordination axes (**Figure 5B**), showing that the canyon assemblages were characterized by increasing *Over20* and *Spd* and the slope assemblages by increasing *TOC* and *Trans*.

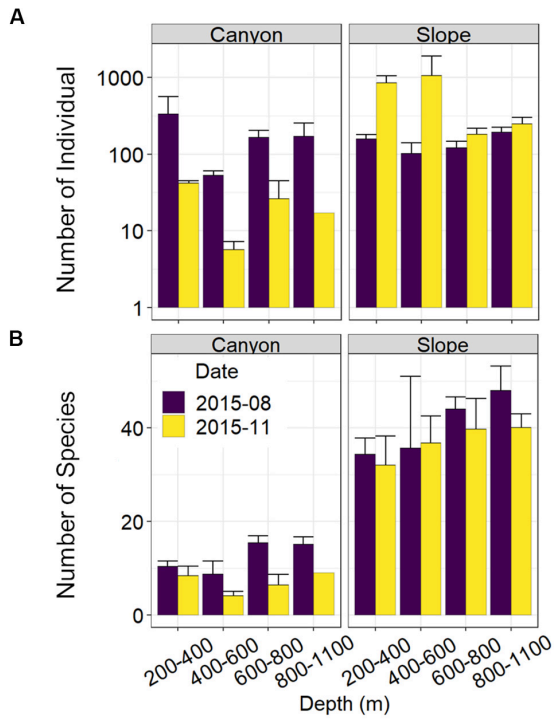

FIGURE 3 | Nematode abundance and number of species along the upper GPSC and adjacent slope. The bar chart and error bars show the mean and standard deviation of the nematode **(A)** abundance and **(B)** observed number of species per station during the August and November 2015 sampling.

Multiple-site Sørensen dissimilarities were 78 and 81% along the GPSC and slope transects, in which the spatial turnover component contributed to 88 and 96% and the nestedness component contributed only 12 and 4% of the total β-diversity, respectively (**Figure 6A**). Between the canyon and slope habitats, the Sørensen dissimilarities were between 72 and 79% across the four depth strata (**Figure 6B**). The spatial turnover processes still dominated and accounted for 69–75% of the total β-diversity, but the nestedness patterns also played considerable roles and contributed 25–31% of the between-habitat dissimilarity across the four depth strata.

Shannon diversity, functional diversity (q = 1), trophic diversity, and maturity index were negatively correlated with the mean bottom current velocity and positively correlated with total organic carbon (TOC) contents (**Figure 7**). Environmental gradients mainly drove these significant correlations, which arose from strong bottom currents and low TOC in the GPSC as well as relatively weak currents and high TOC on the adjacent slope (**Figure 7**).

DISCUSSION

Study Limitations

Despite that 163 nematode species were uncovered from the GPSC and adjacent slope for the first time, the current study is by-no-means a comprehensive inventory of the nematode species diversity in the region. Given the small area of seafloor sampled (i.e., only 283 cm^2 of surface sediment from 46 subsamples), the gamma diversity estimate of nematodes is no doubt an underestimation. Thus, the interpretation of our results should only focus on comparisons between the canyon and non-canyon communities rather than the absolute alpha, beta, and gamma diversities. Moreover, like many deep-sea benthic studies, we took only one multicore per station and allocated resources to cover a larger survey area. In any deep-sea survey, there is always a trade-off between whether to sample more replicates to give higher statistical power or more stations to cover a larger sampling area. To resolve such dichotomy in the sampling design, Montagna et al. (2017) partitioned the variability of abundance and diversity of macrofauna among sampling locations, multicorer deployments, and core tubes of a multicorer. Gallucci et al. (2009) also partitioned the variability of total and species abundance and assemblage composition of nematodes among core tubes (i.e., from a multicorer) and within a core tube (i.e., subcores). Both studies found that the smaller-scale heterogeneity (i.e., core tubes for macrofauna or subcores for meiofauna) explained more variability in the nested sampling designs. Therefore, given limited resources in deep-sea researches, it may be more cost-effective to allocate efforts to increase the spatial cover rather than repeat deployments at a single location (Montagna et al., 2017). In this study, we have taken a more conservative approach by using the true replication (i.e., averages of subsamples per core) from two short repeated cruises to ensure robust statistical hypothesis testing. Nevertheless, the interpretation of our results still requires caution. While a conservative approach may be effective in reducing Type I error (i.e., false-positive), the risk of Type II error (i.e., false negative) may increase.

Response of Diversity to Disturbance

Submarine canyons represent remarkably heterogeneous habitats on the otherwise seemingly monotonous, mud-covered seafloor of the continental margins. Due to the funneling effect, the seafloor of the canyon thalweg often receives and accumulates a large amount of terrestrial and oceanic organic matter. The highly diverse microhabitats and the ample food supplies in the canyon likely allow species to coexist and thus sustain high biodiversity and ecosystem functioning (McClain and Barry, 2010; Leduc et al., 2014; Fernandez-Arcaya et al., 2017). Therefore, the majority of the studies have found that the diversity and abundance of meiofauna were significantly higher in the canyons than the adjacent slopes (Baguley et al., 2006; Ingels et al., 2009; Román et al., 2016; Gambi et al., 2019). However, contrasting results or lack of difference between the canyon and slope communities have also been found, especially in large-scale comparative studies (Soltwedel et al., 2005; Garcia et al., 2007; Bianchelli et al., 2010; Leduc et al., 2014; Bianchelli and Danovaro, 2019). For example, lower abundance and diversity of meiofauna have been found in the Congo Canyon than on the adjacent slope, presumably, related to the strong bottom currents and unstable seafloor conditions within the canyon (Van Gaever et al., 2009).

TABLE 2 | Generalized Least Square (GLS) modeling on mean Shannon diversity, functional diversity (q = 1), trophic diversity, and maturity index of nematodes per station.

	Coefficient	Std. error	DF	*t*-value	*p*-value		Coefficient	Std. error	DF	*t*-value	*p*-value
Abundance						**Functional diversity (q = 1)**					
Intercept	2.04	0.38	9	5.33	**0.001**	Intercept	1.60	0.83	9	1.92	0.086
Habitat	0.24	0.47	9	0.52	0.619	Habitat	4.58	1.03	9	4.45	**0.002**
Depth	0.00	0.00	9	0.38	0.713	Depth	0.00	0.00	9	0.58	0.578
Cruise	−0.53	0.49	9	−1.10	0.300	Cruise	−0.37	1.05	9	−0.35	0.733
Habitat:Depth	0.00	0.00	9	−0.67	0.519	Habitat:Depth	0.00	0.00	9	−0.68	0.514
Habitat:Cruise	1.39	0.34	9	4.11	**0.003**	Habitat:Cruise	−0.30	0.73	9	−0.41	0.689
Depth:Cruise	0.00	0.00	9	−0.90	0.390	Depth:Cruise	0.00	0.00	9	0.37	0.722
Number of species						**Trophic diversity**					
Intercept	6.56	2.40	9	2.73	**0.023**	Intercept	1.83	0.49	9	3.77	**0.004**
Habitat	20.47	2.98	9	6.87	**0.000**	Habitat	2.73	0.60	9	4.54	**0.001**
Depth	0.01	0.00	9	2.67	**0.026**	Depth	0.00	0.00	9	−0.04	0.968
Cruise	−0.66	3.05	9	−0.22	0.832	Cruise	−0.53	0.62	9	−0.87	0.408
Habitat:Depth	0.01	0.00	9	3.31	**0.009**	Habitat:Depth	0.00	0.00	9	−2.60	**0.029**
Habitat:Cruise	1.59	2.12	9	0.75	0.472	Habitat:Cruise	0.04	0.43	9	0.09	0.932
Depth:Cruise	−0.01	0.00	9	−1.80	0.105	Depth:Cruise	0.00	0.00	9	0.96	0.361
Shannon diversity						**Maturity index**					
Intercept	0.70	1.99	9	0.35	0.732	Intercept	1.89	0.13	9	14.58	**0.000**
Habitat	15.68	2.47	9	6.35	**0.000**	Habitat	1.05	0.16	9	6.55	**0.000**
Depth	0.01	0.00	9	2.67	**0.026**	Depth	0.00	0.00	9	1.91	0.088
Cruise	3.44	2.53	9	1.36	0.206	Cruise	0.14	0.16	9	0.85	0.420
Habitat:Depth	0.02	0.00	9	5.72	**0.000**	Habitat:Depth	0.00	0.00	9	−2.84	**0.019**
Habitat:Cruise	−7.29	1.76	9	−4.15	**0.003**	Habitat:Cruise	−0.05	0.11	9	−0.46	0.655
Depth:Cruise	0.00	0.00	9	−1.05	0.319	Depth:Cruise	0.00	0.00	9	−1.08	0.308

Bold font means significant effect (P < 0.05).

The inhabitants of the Gaoping Submarine Canyon (GPSC) are no stranger to extreme environmental conditions including high sediment loads originating from the small mountain river, extreme monsoonal and typhoon rainfalls triggering subsequent turbidity currents, strong internal-tide energy causing swift bottom currents, and high tectonic activity leading to frequent debris flows (Jan et al., 2008; Chiou et al., 2011; Liu et al., 2013, 2016). These physical disturbances within the GPSC substantially suppressed the vulnerable macrofauna taxa (Liao et al., 2017) and depressed the species and functional diversity of nematode assemblages (this study). Nevertheless, the nematode abundance was not affected by the adverse condition in the GPSC, suggesting rapid recovery of the more resilient nematode species. In fact, the dominant species in the GPSC, including members of *Daptonema*, *Sabatieria*, and *Metadesmolaimus* (belonging to Families Comesomatidae and Xylidae), were eurytopic, opportunistic species with short generation time (c-p value = 2). These r-selection strategists may quickly occupy the empty niches left by eliminated predecessors to maintain the population size after disturbance. In comparison, extremely high biomass but low diversity of nematode assemblages was found in the active Kaikoura Canyon off eastern New Zealand, where the *Daptonema* and *Sabatieria pulchra* were the dominant taxa due to their ability to adapt to hypoxia and eutrophic conditions (Leduc et al., 2014). This scenario is also common in the benthic communities under turbidite impact or hypoxia after eutrophication (Tsujimoto et al., 2008, 2020; Vanreusel et al., 2010; Zeppilli et al., 2018).

Characteristic Species and Functional Traits

Nematode assemblages of submarine canyons often share a considerable number of genera with adjacent slope habitats, although the canyon communities may comprise more dominant taxa with a lower species evenness (Vanreusel et al., 2010). In this study, we found that the GPSC and the adjacent slope harbored distinct nematode assemblages. On the slope, the species, functional, and trophic diversity and maturity index of nematodes were significantly higher than those in the GPSC. Except for the 46 common species that occurred in both the canyon and slope, seven species were restricted to the GPSC, and 110 species were only found on the slope. The canyon nematode assemblages were dominated by the non-selective deposit feeding (1B) species with r-selection strategy and clavate tail (e.g., *Daptonema*, *Axonolaimus*, *Metadesmolaimus*, and *Sabatieria*). These same species also contributed highly to the average dissimilarity within the canyon. The *Daptonema* and *Sabatieria* species are commonly found in the disturbed, organic-rich, and polluted sediment

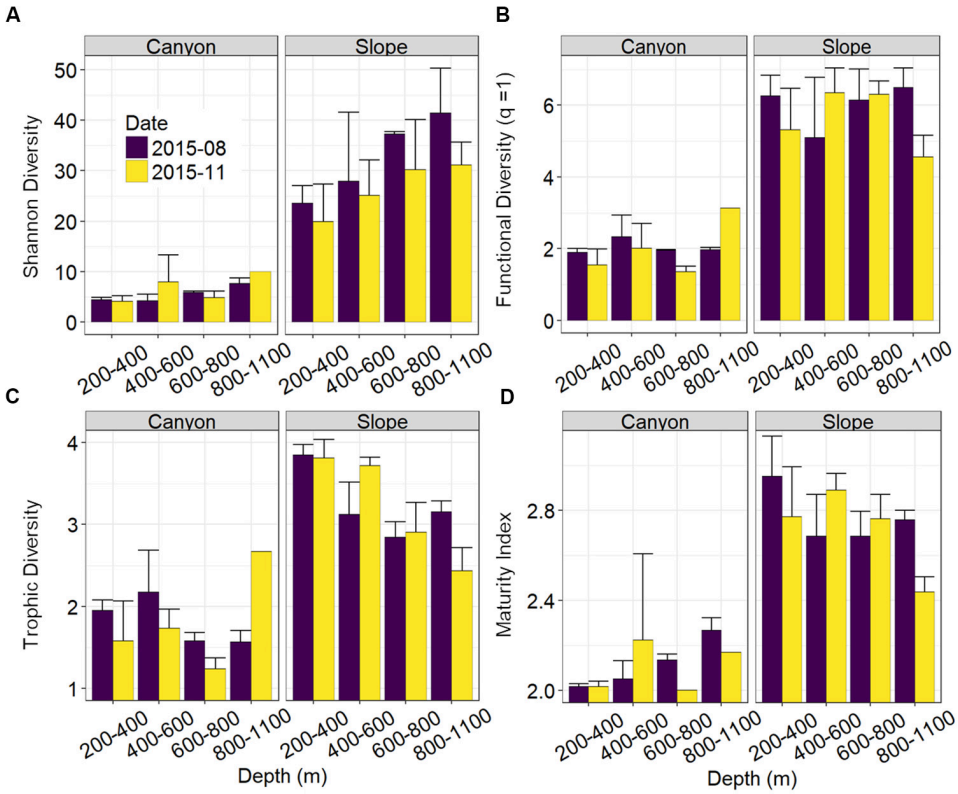

FIGURE 4 | Nematode species and functional diversity along the upper GPSC and adjacent slope. The bar chart and error bars show the mean and standard deviation of the nematode **(A)** species diversity as Hill number of order $q = 1$ or effective numbers of abundant species, **(B)** functional diversity of order $q = 1$ or effective numbers of abundant functional group, **(C)** trophic diversity, and **(D)** maturity index per station during the August and November 2015 sampling.

(Vanreusel, 1990; Schratzberger and Jennings, 2002; Moreno et al., 2008). The *Sabatieria* species is also known to adapt to anoxic conditions and thus prevalent in reduced sediment (Jensen, 1984; Soetaert and Heip, 1995; Steyaert et al., 2007). The dominance of r-selection strategists and depressed maturity index in the GPSC indicated that not just a few dominant species have low c-p value (=2), but that the canyon assemblage almost entirely consisted of colonizers. The canyon nematodes may benefit from the colonization strategy so they can quickly recover from the extremely unstable conditions associated with the recurrent disturbances by internal tides or periodic disturbances by turbidity currents (Wang et al., 2008; Chiou et al., 2011; Liu et al., 2013; Hsu et al., 2014). Moreover, the clavate-shape tails have been considered as typical morphology of interstitial inhabitants of high-energy, sandy habitats, in which the long tail might be used as a tool to anchor the body (Riemann, 1974; Thistle et al., 1995). The slope assemblages, on the other hand, were dominated (also highly contributed) by species with more diverse feeding guilds including non-selective deposit feeders (1B, e.g., *Sabatieria*, *Setosabatieria*, *Cervonema* and *Elzalia*), epigrowth feeders (2A, e.g., *Dorylaimopsis* and *Craspodema*), and omnivores/predators (2B, e.g., *Sphaerolaimus* and *Paramesacanthion*). Some selective deposit-feeding species (1A, e.g., *Quadricoma*, *Pselionema*, and *Halalaimus*) and omnivores/predators (2B, e.g., *Abelbolla*) with K-selection strategy (c-p value = 4) also had high contribution to the average assemblage dissimilarity on the slope (**Supplementary Table S4**), indicating that the slope offers a stable habitat where persister species can thrive. In contrast to the canyon assemblages, the slope nematodes had more diverse feeding guilds, tail shapes, and life strategies, which resulted in more functional groups with higher trophic diversity. The increasing relative abundance of nematodes with conical and elongated/filiform tails on the slope also signals the change of sediment types (Riemann, 1974; Thistle et al., 1995). These tail shapes are well-represented in fine sand and muddy sediments with little interstitial space, where nematodes may burrow or push sediment particles to create their own space (Singh and Ingole, 2016; Armenteros et al., 2019).

Environmental Controls on Diversity and Composition

The canyon assemblages differed from those of the adjacent slope in that they experienced stronger internal tide energy, including higher modeled bottom current velocity (i.e., *Spd*) and longer duration of currents stronger enough to induce sediment erosion (i.e., *Over20*). The organic matter might be rapidly buried after episodic turbidity currents such as occurred during the 2011 Tohoku Earthquake (Tsujimoto et al., 2020). The strong internal tides may cause intermittent resuspension of

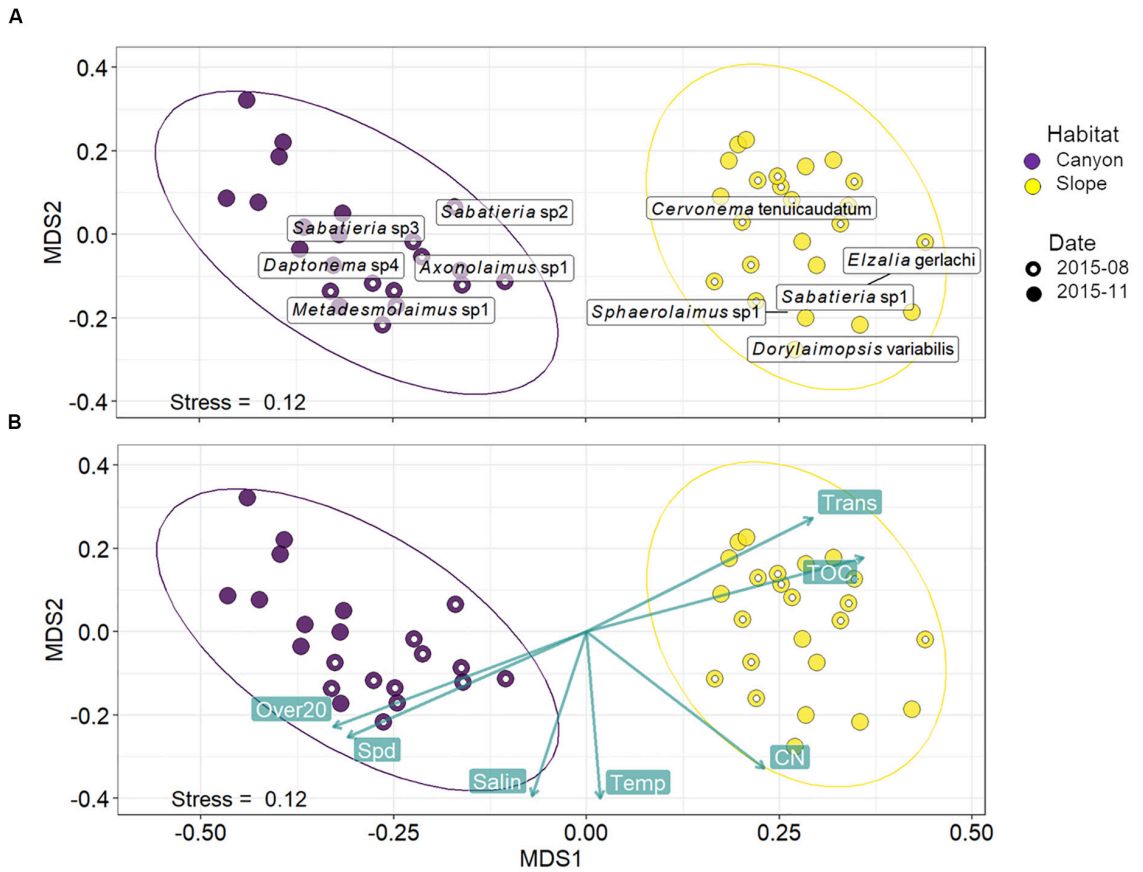

FIGURE 5 | Non-metric multi-dimensional scaling (nMDS) based on squared-root transformed species abundance. The rectangular labels in panel **(A)** indicate the abundance-weighted averages scores for the top five most contributing species in the GPSC and adjacent slope, respectively. The species contributions were decomposed from the average Bray-Curtis dissimilarity within the GPSC and adjacent slope using SIMPER (**Supplementary Tables S3**, **S4**). In other words, the label shows where the high abundance of the five most contributing species may occur on the nMDS ordination. Panel **(B)** shows the correlations between the best-subset of environmental variables and nMDS ordination axes. The environmental subset was selected by distance-based redundancy analysis (dbRDA) with the smallest AIC. The green labels show mean bottom current velocity (Spd) and duration of bottom current velocity exceeding 20 cm/s (Over20), salinity (Salin), temperature (Temp), C/N ratio (CN), total organic carbon (TOC), and light transmission (Trans).

sediment and transport of the resuspended material in the bottom nepheloid layer (Liu et al., 2010). The internal tides may also lead to long-lasting sediment winnowing and prevent the organic-rich particles from settling on the seafloor and thus decrease the total organic carbon (TOC) contents in the sediments (Liao et al., 2017). As a result, the slope assemblages were separated from the canyon by the higher TOC contents in the surface sediment and the clearer bottom water (with higher light transmission). In submarine canyons, frequent physical disturbances and abundant organic inputs may favor opportunistic nematode species and lead to high dominance and low evenness assemblages (Garcia et al., 2007; Ingels et al., 2009; Leduc et al., 2014; Gambi and Danovaro, 2016). In the GPSC, unlike most other canyons, the total organic carbon (TOC) was also in short supplies due to the sorting and winnowing of particles by strong bottom currents (Liao et al., 2017). The contrast between the physically dynamic canyon and more tranquil slope habitat not only drove the species composition of nematode assemblages but also caused the species and functional diversity to decrease with the increasing bottom-current velocity and decreasing TOC contents from the slope into the canyon. Within the individual canyon and slope transects, we found that the observed number of species and the species diversity (i.e., Hill numbers of order q = 0–2) both increased with depth. The rates of increase, however, were different between the canyon and slope, suggesting that the underlying drivers may be different. The head of GPSC is known to experience frequent submarine geohazards (Hsu et al., 2008; Su et al., 2012; Gavey et al., 2017). The bottom currents at the canyon head regularly exceed 1 m/s, but then the internal-tide energy and near-bottom currents weaken away from the head region along the thalweg (Wang et al., 2008; Chiou et al., 2011; Liao et al., 2017). Due to the relaxation of physical disturbance, it may be expected that the nematode diversity increased slightly with depth (or away from the canyon head). Other physical disturbances such as bottom trawling could also remove the organic-rich sediment and cause a reduction of meiofauna diversity and ecosystem function (Puig et al., 2012; Pusceddu et al., 2014; Román et al., 2019). In our study region,

TABLE 3 | Three-way cross permutation analysis of variance (PERMANOVA) on nematode species composition.

	DF	SS	MS	F	R2	Pr(>F)
Habitat	1	1.92	1.92	16.02	0.46	**0.001**
Depth	1	0.21	0.21	1.71	0.05	0.135
Cruise	1	0.29	0.29	2.43	0.07	0.052
Habitat:Depth	1	0.27	0.27	2.28	0.07	0.061
Habitat:Cruise	1	0.26	0.26	2.13	0.06	0.103
Depth:Cruise	1	0.16	0.16	1.35	0.04	0.206
Residuals	9	1.08	0.12		0.26	
Total	15	4.19			1.00	

Bold font means significant effect (P < 0.05).

the bottom trawl fishery typically targets water depths between 100 and 400 m, while the GPSC is avoided to prevent gear damage. Therefore, we cannot rule out the possibility that the upper slope sites (i.e., GS1, GS2, **Figure 1** and **Table 1**) may have experienced some fishing impacts and thus had low nematode diversity. In the meantime, the increasing nematode diversity with depth on the slope could also be explained by a unimodal diversity-depth relationship (Etter and Grassle, 1992; Boucher and Lambshead, 1995), in which the slope sites (278–848 m) happened to be on the ascending limb of the general unimodal diversity gradient.

Mechanisms Shaping the Nematode Assemblages

Along the GPSC and adjacent slope, the spatial turnover (or species replacement) was the main contributor of β-diversity, suggesting that the environmental filtering, not the nestedness, was the primary mechanism driving the bathymetric variation of species composition. Although the depth range of this study was less than 1,000 m, there were large environmental variations with depth, including increasing pressure, decreasing temperature and dissolved oxygen, as well as the increasing total organic carbon (TOC), total nitrogen (TN) and porosity in the sediment (Liao et al., 2017). Within the GPSC, the internal tide energy also weakened considerably with depth, resulting in declining bottom current velocity, duration of sediment erosion, and increasing water clarity or light transmission toward the deeper regions of the canyon (Liao et al., 2017). These environmental variations may replace (or filter) the poorly fitted species with the better-fitted one to cause a gradual, continued species turnover along the length of the continental margin (McClain and Rex, 2015). Moreover, the physical disturbances by bottom currents, turbidity and debris flows may contribute to the heterogeneity of the canyon seafloor (Liu et al., 2016; Chiang et al., 2020) and thus drive the bathymetric variation in species composition (Zeppilli et al., 2016, 2018). In the GPSC, we found that the selective deposit feeding (1A) and K-selection species tend to increase toward the deeper depth strata, providing some indirect evidence of decreasing physical disturbance toward the deeper canyon. Since the environmental conditions in the submarine canyons are obviously more dynamic than the gentle sloping seafloor, many studies found conspicuous bathymetric difference in the canyon nematodes as opposed to the more homogeneous slope assemblages (Ingels et al., 2009; Leduc et al., 2014; Gambi and Danovaro, 2016; Rosli et al., 2016; Román et al., 2019). Nevertheless, we found that the bathymetric β-diversity was comparable between the GPSC and the adjacent slope.

Strikingly, even at a similar depth, the β-diversity between the pairs of GPSC and slope sites were just as high as the

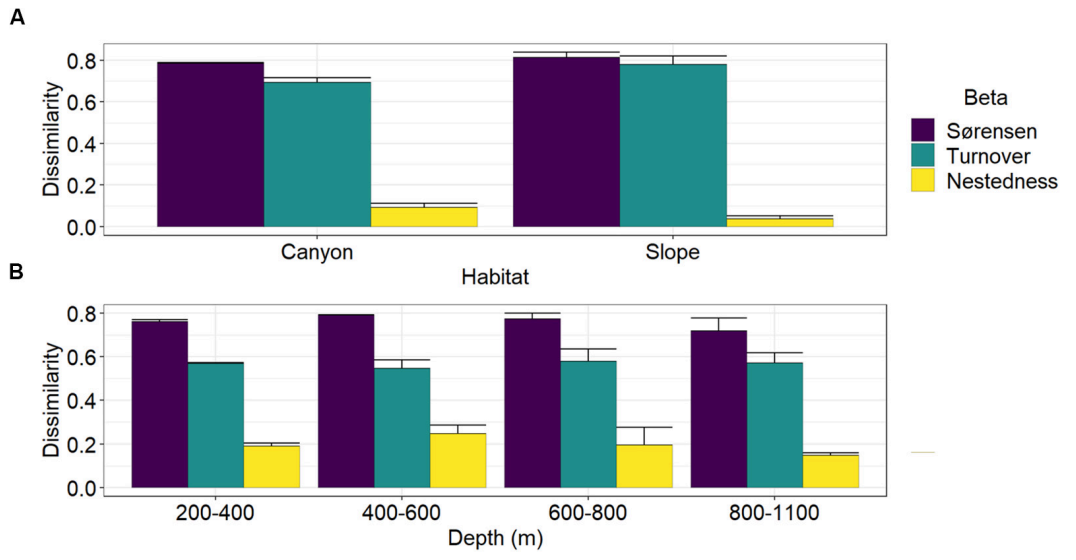

FIGURE 6 | Partition of multiple-site nematode (Sørensen) dissimilarity into spatial turnover and nestedness components. Panel **(A)** shows the Sørensen dissimilarity and its turnover and nestedness components among the four sites within the GPSC and adjacent slope transects. Panel **(B)** shows the Sørensen dissimilarity and its turnover and nestedness components between the canyon and slope site pair across different depth strata. The bar chart and error bars show the mean and standard deviation of the multiple-site dissimilarity and its components across different sampling times.

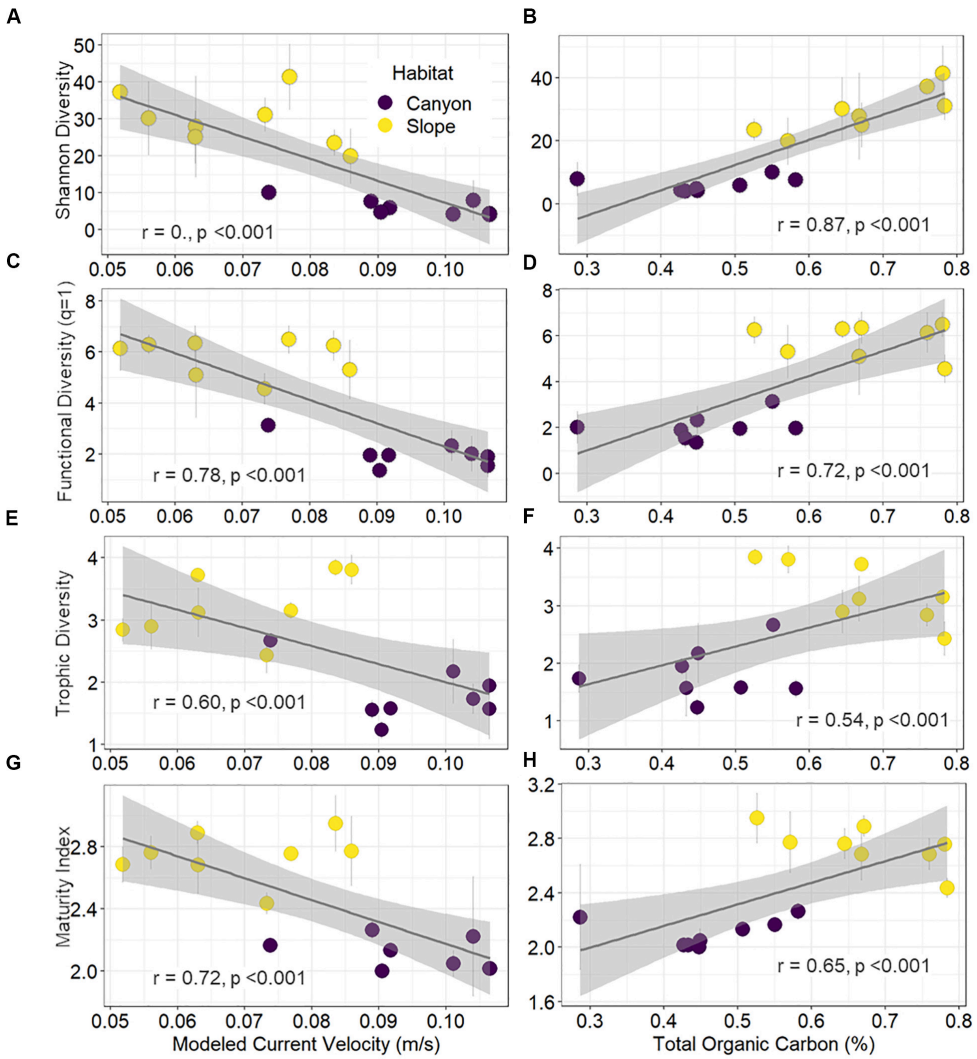

FIGURE 7 | Correlations of diversity and maturity indices to proxies of internal tide energy and food supplies. The mean effective number of abundant species **(A,B)**, effective number of abundant functional group **(C,D)**, trophic diversity **(E,F)**, and maturity index **(G,H)** per station are plotted against the mean bottom current velocity and total organic carbon in the surface sediments. Error bar indicates standard deviation.

bathymetric β-diversity along the canyon or slope transects. For the canyon-slope β-diversity comparison, the spatial turnover still dominated, but the nestedness also played a considerable role (25–31% of the β-diversity) across the four depth strata. For the spatial turnover, it is apparent that the majority of the slope nematode species did not occur in the canyon. The abrupt change in species composition or rapid species replacement is evident in the nMDS ordination, in which the canyon and slope assemblages were clearly separated without overlap. It may be possible that the environmental stress in the GPSC prevented the colonization of K-selection species or larger individuals, which effectively filtered out ∼71% of the slope species. The seven endemic species from the canyon might be well-adapted to the extreme environmental conditions but unable to compete with the abundant persisters on the slope. Possibly, these species also occur on the slope, but in too low numbers to be detected by our sampling. In terms of the 46 species that occurred in both the canyon and slope, these nematodes might be the tolerant species that adapt to the strong physical disturbance and lower TOC in the GPSC and probably immigrated from the adjacent slope by ocean currents (Palmer, 1988). Despite that the nematodes are generally considered as inferior swimmers (Jensen, 1981), they can be suspended by weak currents and move a notable distance (Boeckner et al., 2009). Active colonization by nematode assemblages with different species composition may also influence the recolonized communities and increase the patchiness in a new habitat (Ullberg and Ólafsson, 2003; Fonsêca-Genevois et al., 2006; Lins et al., 2013). This may have given rise to the nestedness pattern in the canyon, where some of the species appear to be subsets of slope communities (e.g., ∼87% of the canyon species also occurred on the slope). It is also possible that some shared species might be morphologically similar (so

identified as the same species) from the same genus but displayed distinct ecological functions and adapted to both the canyon and slope conditions (De Meester et al., 2016). The majority of species could be sensitive species from the slope, which may have been subjected to local extinction and disappearance from the canyon or experienced some degree of dispersal limitation (e.g., washed away by strong currents) as they immigrated into the GPSC to contribute to the nestedness patterns between the canyon and slope (Baselga, 2010, 2012).

Contrast Between Meiofauna and Macrofauna

Although all aspects of the nematode diversity (i.e., species, functional, and trophic diversity) measured in this study appeared depressed in the GPSC, the nematode abundance was not affected by the adverse conditions in the GPSC. In contrast, the macrofauna abundance was significantly depressed in the GPSC, especially toward the canyon head, where the internal-tide energy is the strongest (Liao et al., 2017). Within the macrofauna taxa, the peracarid crustaceans (i.e., amphipods, cumaceans, isopods, and tanaids) appeared most sensitive to environmental perturbations and thus declined or disappeared altogether in the GPSC, whereas the tolerant harpacticoids, nematodes, and polychaetes (macrofaunal or meiofaunal size) were common in both the canyon and the slope (Liao et al., 2017). Nematodes are known to be more resilient to physical disturbances such as sediment resuspension and deposition than the larger macrofauna taxa (Lambshead et al., 2001; Schratzberger and Jennings, 2002; Whomersley et al., 2009). After disturbances, nematodes typically show higher turnover and lower mortality rates than macrofauna in the early successional stages (Schratzberger and Jennings, 2002). The meiofaunal abundance may quickly recover within a few months but the diversity tends to remain low and species composition does not recover to its original state for prolonged time (Kitahashi et al., 2014, 2016; Tsujimoto et al., 2020). Considering that the GPSC may be subject to disturbance by internal tide flushing on a daily basis, only the resilient nematode taxa (e.g., *Daptonema*, *Sabatieria*, and *Axonolaimus*) may quickly recover from the disturbance events and flourish in the canyon. The fast growth rates and short generation times (i.e., weeks to months) of these tolerant nematode taxa may help them to recover rapidly from the recurrent disturbance events (Giere, 2009). Nevertheless, some uncertainty remains. During the fall sampling, the nematode abundance appeared lower in the GPSC than on the adjacent slope, but the habitat effect was not detected when both the summer and fall sampling were taken into consideration. The episodic flooding in the Gaoping River and the subsequent turbidity currents in the GPSC were unpredictable but mostly followed the monsoonal rainfalls and typhoons which mostly occurred between May and October (Liu et al., 2016); therefore, the abundance variations between habitats may have been smeared by the potential seasonal effect or unpredictable sediment flows. A long-term, repeated sampling will be needed to resolve the potential effect of seasonality or episodic events on the nematode assemblages.

CONCLUSION

The Gaoping Submarine Canyon (GPSC), which is subject to frequent turbidity currents and debris flows and strong near-bottom currents driven by internal tides, is an ideal testbed to study the effect of large-scale disturbance on deep-sea benthic communities. In the summer and fall of 2015, we conducted the first detailed deep-sea nematode diversity investigation in the GPSC and adjacent slope. When considering the average effect across both the sampling campaigns, we found no statistical difference in nematode abundance across the depth transects and between the GPSC and adjacent slope. This suggests that the canyon environment had little effect on the nematode population densities. Most strikingly, we found that the nematode species, functional and trophic diversity and maturity were significantly depressed in the GPSC, corresponding to stronger near-bottom currents and lower total organic carbon (TOC) contents in the surface sediments. We also found that the nematode species diversity increased with depth in the upper GPSC and adjacent slope, consistent with the classical paradigm of unimodal diversity-depth relationship in the deep sea. Between the GPSC and adjacent slope, the distinct species composition was mainly contributed by species replacement due to environmental filtering. The canyon assemblages were mainly driven by stronger internal tide energy, and the slope assemblages were associated with higher total organic matter in the surface sediments from which a higher food supply may be inferred. As a result, the canyon nematode assemblages were dominated by non-selective deposit-feeding species with r-selection strategy and clavate tail (e.g., most species of Comesomatidae and Xylidae), whereas on the slope, the longer life-span species with diverse feeding strategies and tail shapes may co-exist. While environmental filtering was the dominant mechanism, the considerable contribution of nestedness to between-habitat nematode dissimilarity suggests that species immigration and local extinction may also play an important role in shaping the canyon assemblages (e.g., opportunistic species from adjacent slope became dominant in the canyon).

In the age of global climate change, the deep seafloor is expected to experience warming, deoxygenation, acidification, and decline in food supplies (Mora et al., 2013; Sweetman et al., 2017; Breitburg et al., 2018). On the continental slope, the changes in climatic drivers may lead to species range shift (Smith et al., 2012), reduction of suitable habitat (Morato et al., 2020), reduction of abundance and biomass (Jones et al., 2014), decline in biodiversity (Sperling et al., 2016; Brito-Morales et al., 2020), and eventually shift of relative contribution of carbon-processing from the large to small benthic size classes (Jones et al., 2014; Sweetman et al., 2017). River-connected canyons such as GPSC may not only be affected by the marine expressions of climate change, but also by terrestrial climate change impacts due to their close association with fluvial processes. For example, the changes in storm and precipitation patterns may lead to changes in the frequency and intensity of flood events (Knutson et al., 2010; Westra et al., 2014; Bacmeister et al., 2018), which may cascade down to trigger turbidity currents and the associated submarine geohazards. Understanding the impact on species

and functional diversity from large-scale natural disturbance in submarine canyons like GPSC will enhance our ability to predict the potential impacts of climate change and other anthropogenic effects on deep-sea ecosystems.

DATA AVAILABILITY STATEMENT

The datasets generated for this study can be found in the https://github.com/chihlinwei/nema.

AUTHOR CONTRIBUTIONS

J-XL and C-LW designed and conceived the study, to which all authors contributed the ideas and discussion. J-XL and C-LW executed the field sampling. J-XL conducted the laboratory work and drafted the manuscript with substantial inputs from C-LW and MY. J-XL, C-LW, and MY contributed to the data analysis. All authors contributed to the article and approved the submitted version.

FUNDING

This project was part of an integrated project, Fate of Terrestrial/Non-terrestrial Sediments in High Yield Particle-Export River-sea Systems (FATES-HYPERS) and South China Sea Marine Research – Toward the south (SCSMART): Environment Change and Marine Biodiversity, sponsored by the Ministry of Science and Technology (MOST 108-2611-M-002-001 and 108-2119-M-001-019). J-XL was supported by the NTU and MOST Postdoctoral Fellowship (MOST 108-2811-M-002-622).

ACKNOWLEDGMENTS

We would like to thank the Institute of Oceanography (IO), the National Taiwan University (NTU), and the Ministry of Science and Technology for supporting the field work, analysis, and manuscript preparation. We also thank Anne Chao for providing R code to compute functional diversity and for valuable suggestions to improve the manuscript. We also thank Sen Jan and Ming-Da Chiou for providing the internal tide model. We also thank captain, crew members, and technicians of the R/V Ocean Researcher I, as well as the graduate students who participated in OCEAN 7090 Field Work in Marine Biology. The majority of samples and data were collected by students through the field course.

SUPPLEMENTARY MATERIAL

The Supplementary Material for this article can be found online at: https://www.frontiersin.org/articles/10.3389/fmars.2020.00591/full#supplementary-material

REFERENCES

Alford, M. H., Peacock, T., MacKinnon, J. A., Nash, J. D., Buijsman, M. C., Centuroni, L. R., et al. (2015). The formation and fate of internal waves in the South China Sea. *Nature* 521, 65–69. doi: 10.1038/nature14399

Aller, R. C., and Aller, J. Y. (1992). Meiofauna and solute transport in marine muds. *Limnol. Oceanogr.* 37, 1018–1033. doi: 10.4319/lo.1992.37.5.1018

Amaro, T., Huvenne, V., Allcock, A., Aslam, T., Davies, J., Danovaro, R., et al. (2016). The Whittard Canyon: a case study of submarine canyon processes. *Prog. Oceanogr.* 146, 38–57. doi: 10.1016/j.pocean.2016.06.003

Appeltans, W., Ahyong, S. T., Anderson, G., Angel, M. V., Artois, T., Bailly, N., et al. (2012). The magnitude of global marine species diversity. *Curr. Biol.* 22, 2189–2202. doi: 10.1016/j.cub.2012.09.036

Armenteros, M., Pérez-García, J. A., Marzo-Pérez, D., and Rodríguez-García, P. (2019). The influential role of the habitat on the diversity patterns of free-living aquatic nematode assemblages in the Cuban Archipelago. *Diversity* 11:166. doi: 10.3390/d11090166

Bacmeister, J. T., Reed, K. A., Hannay, C., Lawrence, P., Bates, S., Truesdale, J. E., et al. (2018). Projected changes in tropical cyclone activity under future warming scenarios using a high-resolution climate model. *Clim. Change* 146, 547–560. doi: 10.1007/s10584-016-1750-x

Baguley, J. G., Montagna, P. A., Hyde, L. J., Kalke, R. D., and Rowe, G. T. (2006). Metazoan meiofauna abundance in relation to environmental variables in the northern Gulf of Mexico deep sea. *Deep Sea Res. I Oceanogr. Res. Pap.* 53, 1344–1362. doi: 10.1016/j.dsr.2006.05.012

Baselga, A. (2010). Partitioning the turnover and nestedness components of beta diversity. *Glob. Ecol. Biogeogr.* 19, 134–143. doi: 10.1111/j.1466-8238.2009.00490.x

Baselga, A. (2012). The relationship between species replacement, dissimilarity derived from nestedness, and nestedness. *Glob. Ecol. Biogeogr.* 21, 1223–1232. doi: 10.1111/j.1466-8238.2011.00756.x

Bianchelli, S., and Danovaro, R. (2019). Meiofaunal biodiversity in submarine canyons of the Mediterranean Sea: a meta-analysis. *Prog. Oceanogr.* 170, 69–80. doi: 10.1016/j.pocean.2018.10.018

Bianchelli, S., Gambi, C., Zeppilli, D., and Danovaro, R. (2010). Metazoan meiofauna in deep-sea canyons and adjacent open slopes: a large-scale comparison with focus on the rare taxa. *Deep Sea Res. Part I Oceanogr. Res. Pap.* 57, 420–433. doi: 10.1016/j.dsr.2009.12.001

Boeckner, M. J., Sharma, J., and Proctor, H. C. (2009). Revisiting the meiofauna paradox: dispersal and colonization of nematodes and other meiofaunal organisms in low- and high-energy environments. *Hydrobiologia* 624, 91–106. doi: 10.1007/s10750-008-9669-5

Bonaglia, S., Nascimento, F. J. A., Bartoli, M., Klawonn, I., and Brüchert, V. (2014). Meiofauna increases bacterial denitrification in marine sediments. *Nat. Commun.* 5:5133. doi: 10.1038/ncomms6133

Bongers, T., Alkemade, R., and Yeates, G. W. (1991). Interpretation of disturbance-induced maturity decrease in marine nematode assemblages by means of the Maturity Index. *Mar. Ecol. Prog. Ser.* 76, 135–142. doi: 10.3354/meps076135

Bongers, T., and Ferris, H. (1999). Nematode community structure as a bioindicator in environmental monitoring. *Trends Ecol. Evol.* 14, 224–228. doi: 10.1016/S0169-5347(98)01583-3

Botta-Dukát, Z. (2005). Rao's quadratic entropy as a measure of functional diversity based on multiple traits. *J. Veg. Sci.* 16, 533–540. doi: 10.1111/j.1654-1103.2005.tb02393.x

Boucher, G., and Lambshead, P. J. D. (1995). Ecological biodiversity of marine nematodes in samples from temperate, tropical, and deep-sea regions. *Conserv. Biol.* 9, 1594–1604. doi: 10.1046/j.1523-1739.1995.09061594.x

Breitburg, D., Levin, L. A., Oschlies, A., Grégoire, M., Chavez, F. P., Conley, D. J., et al. (2018). Declining oxygen in the global ocean and coastal waters. *Science* 359:eaam7240. doi: 10.1126/science.aam7240

Brito-Morales, I., Schoeman, D. S., Molinos, J. G., Burrows, M. T., Klein, C. J., Arafeh-Dalmau, N., et al. (2020). Climate velocity reveals increasing exposure

of deep-ocean biodiversity to future warming. *Nat. Clim. Change* 10, 576–581. doi: 10.1038/s41558-020-0773-5

Chao, A., Chiu, C.-H., and Jost, L. (2014). Unifying species diversity, phylogenetic diversity, functional diversity, and related similarity and differentiation measures through hill numbers. *Annu. Rev. Ecol. Evol. Syst.* 45, 297–324. doi: 10.1146/annurev-ecolsys-120213-091540

Chao, A., Chiu, C.-H., Villéger, S., Sun, I.-F., Thorn, S., Lin, Y., et al. (2019). An attribute-diversity approach to functional diversity, functional beta diversity, and related (dis)similarity measures. *Ecol. Monogr.* 89:e01343. doi: 10.1002/ecm.1343

Chao, A., Gotelli, N. J., Hsieh, T. C., Sander, E. L., Ma, K. H., Colwell, R. K., et al. (2013). Rarefaction and extrapolation with Hill numbers: a framework for sampling and estimation in species diversity studies. *Ecol. Monogr.* 84, 45–67. doi: 10.1890/13-0133.1

Chao, A., and Jost, L. (2010). *Diversity Analysis*, 1 Edn. London: Chapman & Hall/CRC.

Chiang, C.-S., Hsiung, K.-H., Yu, H.-S., and Chen, S.-C. (2020). Three types of modern submarine canyons on the tectonically active continental margin offshore southwestern Taiwan. *Mar. Geophys. Res.* 41:4. doi: 10.1007/s11001-020-09403-z

Chiou, M.-D., Jan, S., Wang, J., Lien, R.-C., and Chien, H. (2011). Sources of baroclinic tidal energy in the Gaoping Submarine Canyon off southwestern Taiwan. *J. Geophys. Res. Oceans* 116:C12016. doi: 10.1029/2011JC007366

Coull, B. C., and Chandler, G. T. (1992). Pollution and meiofauna: field, laboratory, and mesocosm studies. *Oceanogr. Mar. Biol. Ann. Rev.* 30, 191–271.

Covich, A. P., Austen, M. C., Bärlocher, F., Chauvet, E., Cardinale, B. J., Biles, C. L., et al. (2004). The role of biodiversity in the functioning of freshwater and marine benthic ecosystems. *Bioscience* 54, 767–775.

Danovaro, R. (2010). *Methods for the Study of Deep-Sea Sediments, their Functioning and Biodiversity*. Boca Ration, FL: CRC Press, 428.

Danovaro, R. (2012). "Extending the approaches of biodiversity and ecosystem functioning to the deep ocean," in *Marine Biodiversity and Ecosystem Functioning*, eds M. Solan, R. J. Aspden, and D. M. Paterson (Oxford: Oxford University Press), 115–126. doi: 10.1093/acprof:oso/9780199642250.003.0009

Danovaro, R., Bianchelli, S., Gambi, C., Mea, M., and Zeppilli, D. (2009). α-, β-, γ-, δ- and ε-diversity of deep-sea nematodes in canyons and open slopes of Northeast Atlantic and Mediterranean margins. *Mar. Ecol. Prog. Ser.* 396, 197–209. doi: 10.3354/meps08269

De Leo, F. C., Smith, C. R., Rowden, A. A., Bowden, D. A., and Clark, M. R. (2010). Submarine canyons: hotspots of benthic biomass and productivity in the deep sea. *Proc. R. Soc. Lond. B Biol. Sci.* 277, 2783–2792. doi: 10.1098/rspb.2010.0462

De Meester, N., Gingold, R., Rigaux, A., Derycke, S., and Moens, T. (2016). Cryptic diversity and ecosystem functioning: a complex tale of differential effects on decomposition. *Oecologia* 182, 559–571. doi: 10.1007/s00442-016-3677-3

Etter, R. J., and Grassle, J. F. (1992). Patterns of species diversity in the deep sea as a function of sediment particle size diversity. *Nature* 360, 576–578. doi: 10.1038/360576a0

Fernandez-Arcaya, U., Ramirez-Llodra, E., Aguzzi, J., Allcock, A. L., Davies, J. S., Dissanayake, A., et al. (2017). Ecological role of submarine canyons and need for Canyon conservation: a review. *Front. Mar. Sci.* 4:5. doi: 10.3389/fmars.2017.00005

Fonsêca-Genevois, V., Somerfield, P. J., Neves, M. H. B., Coutinho, R., and Moens, T. (2006). Colonization and early succession on artificial hard substrata by meiofauna. *Mar. Biol.* 148, 1039–1050. doi: 10.1007/s00227-005-0145-8

Gallucci, F., Moens, T., and Fonseca, G. (2009). Small-scale spatial patterns of meiobenthos in the Arctic deep sea. *Mar. Biodivers.* 39, 9–25. doi: 10.1007/s12526-009-0003-x

Gambi, C., Carugati, L., Martire, M. L., and Danovaro, R. (2019). Biodiversity and distribution of meiofauna in the Gioia, Petrace and Dohrn Canyons (Tyrrhenian Sea). *Prog. Oceanogr.* 171, 162–174. doi: 10.1016/j.pocean.2018.12.016

Gambi, C., and Danovaro, R. (2016). Biodiversity and life strategies of deep-sea meiofauna and nematode assemblages in the Whittard Canyon (Celtic margin, NE Atlantic Ocean). *Deep Sea Res. I Oceanogr. Res. Pap.* 108, 13–22. doi: 10.1016/j.dsr.2015.12.001

Gambi, C., Vanreusel, A., and Danovaro, R. (2003). Biodiversity of nematode assemblages from deep-sea sediments of the Atacama Slope and Trench (Southern Pacific Ocean). *Deep Sea Res. I Oceanogr. Res. Pap.* 50, 103–117. doi: 10.1016/S0967-0637(02)00143-7

Garcia, R., Koho, K. A., De Stigter, H. C., Epping, E., Koning, E., and Thomsen, L. (2007). Distribution of meiobenthos in the Nazaré canyon and adjacent slope (western Iberian Margin) in relation to sedimentary composition. *Mar. Ecol. Prog. Ser.* 340, 207–220. doi: 10.3354/meps340207

Gavey, R., Carter, L., Liu, J., Talling, P., Hsu, R. T., Pope, E., et al. (2017). Frequent sediment density flows during 2006 to 2015, triggered by competing seismic and weather events: observations from subsea cable breaks off southern Taiwan. *Mar. Geol.* 384, 147–158. doi: 10.1016/j.margeo.2016.06.001

Giere, O. (2009). *Meiobenthology. The Microscopic Motile Fauna of Aquatic Sediments*, 2nd Edn. Berlin: Springer.

Heip, C., Vinx, M., and Vranken, G. (1985). The ecology of marine nematode. *Oceanogr. Mar. Biol. Annu. Rev.* 23, 399–489.

Hill, M. O. (1973). Diversity and evenness: a unifying notation and its consequences. *Ecology* 54, 427–432. doi: 10.2307/1934352

Hsu, F.-H., Su, C.-C., Wang, C.-H., Lin, S., Liu, J., and Huh, C.-A. (2014). Accumulation of terrestrial organic carbon on an active continental margin offshore southwestern Taiwan: source-to-sink pathways of river-borne organic particles. *J. Asian Earth Sci.* 91, 163–173. doi: 10.1016/j.jseaes.2014.05.006

Hsu, S.-K., Kuo, J., Lo, C.-L., Tsai, C.-H., Doo, W.-B., Ku, C.-Y., et al. (2008). Turbidity Currents, Submarine Landslides and the 2006 Pingtung Earthquake off SW Taiwan. *Terr. Atmos. Ocean Sci.* 19, 767–772. doi: 10.3319/TAO.2008.19.6.767(PT)

Ieno, E. N., Solan, M., Batty, P., and Pierce, G. J. (2006). How biodiversity affects ecosystem functioning: roles of infaunal species richness, identity and density in the marine benthos. *Mar. Ecol. Prog. Ser.* 311, 263–271. doi: 10.3354/meps311263

Ingels, J., Kiriakoulakis, K., Wolff, G. A., and Vanreusel, A. (2009). Nematode diversity and its relation to quantity and quality of sedimentary organic matter in the Nazaré Canyon, Western Iberian margin. *Deep Sea Res. I Oceanogr. Res. Pap.* 56, 1521–1539. doi: 10.1016/j.dsr.2009.04.010

Ingels, J., Tchesunov, A. V., and Vanreusel, A. (2011). Meiofauna in the Gollum Channels and the Whittard Canyon, Celtic margin—how local environmental conditions shape nematode structure and function. *PLoS One* 6:e20094. doi: 10.1371/journal.pone.0020094

Jan, S., Lien, R.-C., and Ting, C.-H. (2008). Numerical study of baroclinic tides in Luzon Strait. *J. Oceanogr.* 64, 789–802. doi: 10.1007/s10872-008-0066-5

Jensen, P. (1981). Phyto-chemical sensitivity and swimming behavior of the free-living marine nematode Chromadorita tenuis. *Mar. Ecol. Prog. Ser.* 4, 203–206. doi: 10.3354/meps004203

Jensen, P. (1984). Ecology of benthic and epiphytic nematodes in brackish waters. *Hydrobiologia* 108, 201–217. doi: 10.1007/BF00006329

Jensen, P. (1987). Feeding ecology of free-living aquatic nematodes. *Mar. Ecol. Prog. Ser.* 35, 187–196. doi: 10.3354/meps035187

Jones, D. O. B., Yool, A., Wei, C.-L., Henson, S. A., Ruhl, H. A., Watson, R. A., et al. (2014). Global reductions in seafloor biomass in response to climate change. *Glob. Change Biol.* 20, 1861–1872. doi: 10.1111/gcb.12480

Karlson, A. M. L., Nascimento, F. J. A., Näslund, J., and Elmgren, R. (2010). Higher diversity of deposit-feeding macrofauna enhances phytodetritus processing. *Ecology* 91, 1414–1423. doi: 10.1890/09-0660.1

Kiriakoulakis, K., Blackbird, S., Ingels, J., Vanreusel, A., and Wolff, G. A. (2011). Organic geochemistry of submarine canyons: the Portuguese Margin. *Deep Sea Res. II Top. Stud. Oceanogr.* 58, 23–24. doi: 10.1016/j.dsr2.2011.04.010

Kitahashi, T., Jenkins, R. G., Nomaki, H., Shimanaga, M., Fujikura, K., and Kojima, S. (2014). Effect of the 2011 Tohoku Earthquake on deep-sea meiofaunal assemblages inhabiting the landward slope of the Japan Trench. *Mar. Geol.* 358, 128–137. doi: 10.1016/j.margeo.2014.05.004

Kitahashi, T., Watanabe, H., Ikehara, K., Jenkins, R. G., Kojima, S., and Shimanaga, M. (2016). Deep-sea meiofauna off the Pacific coast of Tohoku and other trench slopes around Japan: a comparative study before and after the 2011 off the Pacific coast of Tohoku Earthquake. *J. Oceanogr.* 72, 129–139. doi: 10.1007/s10872-015-0323-3

Knutson, T. R., McBride, J. L., Chan, J., Emanuel, K., Holland, G., Landsea, C., et al. (2010). Tropical cyclones and climate change. *Nat. Geosci.* 3, 157–163. doi: 10.1038/ngeo779

Lambshead, P. J. D., Tietjen, J., Glover, A., Ferrero, T., Thistle, D., and Gooday, A. J. (2001). Impact of large-scale natural physical disturbance on the diversity

of deep-sea North Atlantic nematodes. *Mar. Ecol. Prog. Ser.* 214, 121–126. doi: 10.3354/meps214121

Leduc, D., Rowden, A. A., Nodder, S. D., Berkenbusch, K., Probert, P. K., and Hadfield, M. G. (2014). Unusually high food availability in Kaikoura Canyon linked to distinct deep-sea nematode community. *Deep Sea Res. II Top. Stud. Oceanogr.* 104, 310–318. doi: 10.1016/j.dsr2.2013.06.003

Lee, I.-H., Wang, Y.-H., Liu, J. T., Chuang, W.-S., and Xu, J. (2009). Internal tidal currents in the Gaoping (Kaoping) Submarine Canyon. *J. Mar. Syst.* 76, 397–404. doi: 10.1016/j.jmarsys.2007.12.011

Liao, J.-X., Chen, G.-M., Chiou, M.-D., Jan, S., and Wei, C.-L. (2017). Internal tides affect benthic community structure in an energetic submarine canyon off SW Taiwan. *Deep Sea Res. I Oceanogr. Res. Pap.* 125, 147–160. doi: 10.1016/j.dsr.2017.05.014

Lins, L., Vanreusel, A., van Campenhout, J., and Ingels, J. (2013). Selective settlement of deep-sea canyon nematodes after resuspension – an experimental approach. *J. Exp. Biol. Ecol.* 410, 110–116. doi: 10.1016/j.jembe.2013.01.021

Liu, J. T., Hsu, R. T., Hung, J.-J., Chang, Y.-P., Wang, Y.-H., Rendle-Buhring, R., et al. (2016). From the highest to the deepest: the Gaoping-River-Gaoping Submarine Canyon dispersal system. *Earth Sci. Rev.* 153, 274–300. doi: 10.1016/j.earscirev.2015.10.012

Liu, J. T., Kao, S.-J., Huh, C.-A., and Hung, C.-C. (2013). Gravity flows associated with flood events and carbon burial: Taiwan as instructional source area. *Annu. Rev. Mar. Sci.* 5, 47–68. doi: 10.1146/annurev-marine-121211-172307

Liu, J. T., Lin, H.-L., and Hung, J.-J. (2006). A submarine canyon conduit under typhoon conditions off Southern Taiwan. *Deep Sea Res. I Oceanogr. Res. Pap.* 53, 223–240. doi: 10.1016/j.dsr.2005.09.012

Liu, J. T., Liu, K., and Huang, J. C. (2002). The effect of a submarine canyon on the river sediment dispersal and inner shelf sediment movements in southern Taiwan. *Mar. Geol.* 181, 357–386. doi: 10.1016/S0025-3227(01)00219-5

Liu, J. T., Wang, Y. H., Lee, I.-H., and Hsu, R. T. (2010). Quantifying tidal signatures of the benthic nepheloid layer in Gaoping Submarine Canyon in Southern Taiwan. *Mar. Geol.* 271, 119–130. doi: 10.1016/j.margeo.2010.01.016

McClain, C. R., and Barry, J. P. (2010). Habitat heterogeneity, disturbance, and productivity work in concert to regulate biodiversity in deep submarine canyons. *Ecology* 91, 964–976. doi: 10.1890/09-0087.1

McClain, C. R., and Rex, M. A. (2015). Toward a conceptual understanding of β-Diversity in the deep-sea Benthos. *Annu. Rev. Ecol. Evol. Syst.* 46, 623–642. doi: 10.1146/annurev-ecolsys-120213-091640

Moens, T., dos Santos, G. A. P., Thompson, F., Swings, J., Fonsêca-Genevois, V., and De Mesel, I. (2005). Do nematode mucus secretions affect bacterial growth? *Aquat. Microb. Ecol.* 40, 77–83. doi: 10.3354/ame040077

Montagna, P. A., Baguley, J. G., Hsiang, C.-Y., and Reuscher, M. G. (2017). Comparison of sampling methods for deep-sea infauna. *Limnol. Oceanogr. Methods* 15, 166–183. doi: 10.1002/lom3.10150

Mora, C., Wei, C.-L., Rollo, A., Amaro, T., Baco, A. R., Billett, D., et al. (2013). Biotic and Human Vulnerability to Projected Changes in Ocean Biogeochemistry over the 21st Century. *PLoS Biol.* 11:e1001682. doi: 10.1371/journal.pbio.1001682

Morato, T., González-Irusta, J.-M., Dominguez-Carrió, C., Wei, C.-L., Davies, A., Sweetman, A. K., et al. (2020). Climate-induced changes in the suitable habitat of cold-water corals and commercially important deep-sea fishes in the North Atlantic. *Glob. Change Biol.* 26, 2181–2202. doi: 10.1111/gcb.14996

Moreno, M., Semprucci, F., Vezzulli, L., Balsamo, M., Fabiano, M., and Albertelli, G. (2011). The use of nematodes in assessing ecological quality status in the Mediterranean coastal ecosystems. *Ecol. Indic.* 11, 328–336. doi: 10.1016/j.ecolind.2010.05.011

Moreno, M., Vezzulli, L., Marin, V., Laconi, P., Albertelli, G., and Fabiano, M. (2008). The use of meiofauna diversity as an indicator of pollution in harbours. *ICES J. Mar. Sci.* 65, 1428–1435. doi: 10.1016/j.ecolind.2010.05.011

Nascimento, F. J. A., Näslund, J., and Elmgren, R. (2012). Meiofauna enhances organic matter mineralization in soft sediment ecosystems. *Limnol. Oceanogr.* 57, 338–346. doi: 10.4319/lo.2012.57.1.0338

Palmer, M. A. (1988). Dispersal of marine meiofauna: a review and conceptual model explaining passive transport and active emergence with implications for recruitment. *Mar. Ecol. Prog. Ser.* 48, 81–91. doi: 10.3354/meps048081

Platt, H. M., and Warwick, R. M. (1983). *Free-living Marine Nematodes. Part I. British Enoplids*. Cambridge: Cambridge University Press.

Platt, H. M., and Warwick, R. M. (1988). *Free-living Marine Nematodes. Part II. British Chromadorids*. Cambridge: Cambridge University Press.

Puig, P., Canals, M., Company, J. B., Martín, J., Amblas, D., Lastras, G., et al. (2012). Ploughing the deep sea floor. *Nature* 489, 286–289. doi: 10.1038/nature11410

Pusceddu, A., Bianchelli, S., Martín, J., Puig, P., Palanques, A., Masqué, P., et al. (2014). Chronic and intensive bottom trawling impairs deep-sea biodiversity and ecosystem functioning. *Proc. Natl. Acad. Sci. U.S.A.* 111, 8861–8866. doi: 10.1073/pnas.1405454111

R Core Team (2019). *R: A Language and Environment for Statistical Computing*. Vienna: R Foundation for Statistical Computing. Available online at: http://www.R-project.org/

Radwell, A. J., and Brown, A. V. (2008). Benthic meiofauna assemblage structure of headwater streams: density and distribution of taxa relative to substrate size. *Aquat. Ecol.* 42, 405–414. doi: 10.1007/s10452-007-9108-0

Riemann, F. (1974). On hemisessile nematodes with flagilliform tails living in marine soft bottoms and on microtubes found in deep sea sediments. *Mikrofauna Meeresbod.* 40, 1–15.

Román, S., Lins, L., Ingels, J., Romano, C., Martin, D., and Vanreusel, A. (2019). Role of spatial scales and environmental drivers in shaping nematode communities in the Blanes Canyon and its adjacent slope. *Deep Sea Res. I Oceanogr. Res. Pap.* 146, 62–78. doi: 10.1016/j.dsr.2019.03.002

Román, S., Vanreusel, A., Romano, C., Ingels, J., Puig, P., Company, J. B., et al. (2016). High spatiotemporal variability in meiofaunal assemblages in Blanes Canyon (NW Mediterranean) subject to anthropogenic and natural disturbances. *Deep Sea Res. I Oceanogr. Res. Pap.* 117, 70–83. doi: 10.1016/j.dsr.2016.10.004

Rosli, N., Leduc, D., Rowden, A. A., Clark, M. R., Probert, P. K., Berkenbusch, K., et al. (2016). Differences in meiofauna communities with sediment depth are greater than habitat effects on the New Zealand continental margin: implications for vulnerability to anthropogenic disturbance. *PeerJ* 4:e2154. doi: 10.7717/peerj.2154

Rysgaard, S., Christensen, P. B., Sørensen, M. V., Funch, P., and Berg, P. (2000). Marine meiofauna, carbon and nitrogen mineralization in sandy and soft sediments of Disko Bay, West Greenland. *Aquat. Microb. Ecol.* 21, 59–71. doi: 10.3354/ame021059

Schmidt-Rhaesa, A. (2014). *Handbook of Zoology. Gastrotricha, Cycloneuralia and Gnathifera, Volume 2, Nematoda*. Berlin: De Gruyter.

Schratzberger, M., and Ingels, J. (2018). Meiofauna matters: the roles of meiofauna in benthic ecosystems. *J. Exp. Mar. Biol. Ecol.* 502, 12–25. doi: 10.1016/j.jembe.2017.01.007

Schratzberger, M., and Jennings, S. (2002). Impacts of chronic trawling disturbance on meiofaunal communities. *Mar. Biol.* 141, 991–1000. doi: 10.1007/s00227-002-0895-5

Schratzberger, M., Rees, H. L., and Boyd, S. E. (2000). Effects of simulated deposition of dredged material on structure of nematode assemblages – the role of contamination. *Mar. Biol.* 137, 613–622. doi: 10.1007/s002270000386

Schratzberger, M., Warr, K., and Rogers, S. I. (2007). Functional diversity of nematode communities in the southwestern North Sea. *Mar. Environ. Res.* 63, 368–389. doi: 10.1016/j.marenvres.2006.10.006

Singh, R., and Ingole, B. S. (2016). Structure and function of nematode communities across the Indian western continental margin and its oxygen minimum zone. *Biogeosciences* 13, 191–209. doi: 10.5194/bg-13-191-2016

Smith, C. R., Grange, L. J., Honig, D. L., Naudts, L., Huber, B., Guidi, L., et al. (2012). A large population of king crabs in Palmer Deep on the west Antarctic Peninsula shelf and potential invasive impacts. *Proc. R. Soc. B* 279, 1017–1026. doi: 10.1098/rspb.2011.1496

Soetaert, K., and Heip, C. (1995). Nematode assemblages of deep-sea and shelf break sites in the North Atlantic and Mediterranean sea. *Mar. Ecol. Prog. Ser.* 125, 171–183. doi: 10.3354/meps125171

Soetaert, K., Muthumbi, A., and Heip, C. (2002). Size and shape of ocean margin nematodes: morphological diversity and depth-related patterns. *Mar. Ecol. Prog. Ser.* 242, 179–193. doi: 10.3354/meps242179

Soltwedel, T., Hasemann, C., Queric, N. V., and von Juterzenka, K. (2005). Gradients in activity and biomass of the small benthic biota along a channel system in the deep Western Greenland Sea. *Deep Sea Res. I Oceanogr. Res. Pap.* 52, 815–835. doi: 10.1016/j.dsr.2004.11.011

Sperling, E. A., Frieder, C. A., and Levin, L. A. (2016). Biodiversity response to natural gradients of multiple stressors on continental margins. *Proc. R. Soc. B* 283:20160637. doi: 10.1098/rspb.2016.0637

Steyaert, M., Moodley, L., Nadong, T., Moens, T., Soetaert, K., and Vincx, M. (2007). Responses of intertidal nematodes to short-term anoxic events. *J. Exp. Mar. Biol. Ecol.* 345, 175–184. doi: 10.1016/j.jembe.2007.03.001

Su, C.-C., Tseng, J.-Y., Hsu, H.-H., Chiang, C.-S., Yu, H.-S., Lin, S., et al. (2012). Records of submarine natural hazards off SW Taiwan. *Geol. Soc. Lond. Spec. Publ.* 361, 41–60. doi: 10.1144/SP361.5

Sweetman, A. K., Thurber, A. R., Smith, C. R., Levin, L. A., Mora, C., Wei, C.-L., et al. (2017). Major impacts of climate change on deep-sea benthic ecosystems. *Elem. Sci. Anth.* 5, 1–23. doi: 10.1525/elementa.203

Thistle, D., Lambshead, P. J. D., and Sherman, K. M. (1995). Nematode tail-shape groups respond to environmental differences in the deep sea. *Vie Milieu* 45, 107–115.

Tsujimoto, A., Nomura, R., Arai, K., Nomaki, H., Inoue, M., and Fujikura, K. (2020). Changes in deep-sea benthic foraminiferal fauna caused by turbidites deposited after the 2011 Tohoku-oki earthquake. *Mar. Geol.* 419:106045. doi: 10.1016/j.margeo.2019.106045

Tsujimoto, A., Yasuhara, M., Nomura, R., Yamazaki, H., Sampei, Y., Hirose, K., et al. (2008). Development of modern benthic ecosystems in eutrophic coastal oceans: the foraminiferal record over the last 200 years, Osaka Bay, Japan. *Mar. Micropaleontol.* 69, 225–239. doi: 10.1016/j.marmicro.2008.08.001

Ullberg, J., and Ólafsson, E. (2003). Free-living marine nematodes actively choose habitat when descending from the water column. *Mar. Ecol. Prog. Ser.* 260, 141–149. doi: 10.3354/meps260141

Van Gaever, D., Galéron, J., Sibuet, M., and Vanreusel, A. (2009). Deep-sea habitat heterogeneity influence on meiofaunal communities in the Gulf of Guinea. *Deep Sea Res. II Top. Stud. Oceanogr.* 56, 2259–2269. doi: 10.1016/j.dsr2.2009.04.008

Vanreusel, A. (1990). Ecology of the free-living marine nematodes from the Voordelta (Southern Bight of the North Sea): I. Species composition and structure of the nematode communities. *Cah. Biol. Mar.* 31, 439–462.

Vanreusel, A., Fonseca, G., Danovaro, R., da Silva, M. C., Esteves, A. M., Ferrero, T., et al. (2010). The contribution of deep-sea macrohabitat heterogeneity to global nematode diversity. *Mar. Ecol. Evol. Perspect.* 31, 6–20. doi: 10.1111/j.1439-0485.2009.00352.x

Vetter, E. W., and Dayton, P. K. (1998). Macrofaunal communities within and adjacent to a detritus-rich submarine canyon system. *Deep Sea Res. II Top. Stud. Oceanogr.* 45, 25–54. doi: 10.1016/S0967-0645(97)00048-9

Wang, Y. H., Lee, I. H., and Liu, J. T. (2008). Observation of internal tidal currents in the Kaoping Canyon off southwestern Taiwan. *Estuar. Coast. Shelf Sci.* 80, 153–160. doi: 10.1016/j.ecss.2008.07.016

Warwick, R. M., Platt, H. M., and Somerfield, P. J. (1998). *Free-living Marine Nematodes. Part III: Monhysterids*. Shrewsbury: Field Studies Council.

Wei, C.-L., Chen, M., Wicksten, M. K., and Rowe, G. T. (2020). Macrofauna bivalve diversity from the deep northern Gulf of Mexico. *Ecol. Res.* 35, 343–361. doi: 10.1111/1440-1703.12077

Wei, C.-L., and Rowe, G. T. (2019). Productivity controls macrofauna diversity in the deep northern Gulf of Mexico. *Deep Sea Res. I Oceanogr. Res. Pap.* 143, 17–27. doi: 10.1016/j.dsr.2018.12.005

Westra, S., Fowler, H. J., Evans, J. P., Alexander, L. V., Berg, P., Johnson, F., et al. (2014). Future changes to the intensity and frequency of short-duration extreme rainfall. *Rev. Geophys.* 52, 522–555. doi: 10.1002/2014RG000464

Whomersley, P., Huxham, M., Schratzberger, M., and Bolam, S. (2009). Differential response of meio- and macrofauna to in situ burial. *J. Mar. Biol. Assoc. U.K.* 89, 1091–1098. doi: 10.1017/s0025315409000344

Wieser, W. (1953). Die beziehung zwischen mundhöhlengestalt, ernährungsweise und vorkommen bei freilebenden marinen nematoden. 2. *Arkiv. Zool.* 4, 439–484.

Yu, H.-S., Chiang, C.-S., and Shen, S.-M. (2009). Tectonically active sediment dispersal system in SW Taiwan margin with emphasis on the Gaoping (Kaoping) Submarine Canyon. *J. Mar. Syst.* 76, 369–382. doi: 10.1016/j.jmarsys.2007.07.010

Yu, H.-S., Huang, C.-S., and Ku, J.-W. (1991). Morphology and possible origin of the Kaoping submarine canyon head of southwest Taiwan. *Acta Oceanogr. Taiwan.* 27, 40–50.

Zeppilli, D., Leduc, D., Fontanier, C., Fontaneto, D., Fuchs, S., Gooday, A. J., et al. (2018). Characteristics of meiofauna in extreme marine ecosystems: a review. *Mar. Biodivers.* 48, 35–71. doi: 10.1007/s12526-017-0815-z

Zeppilli, D., Pusceddu, A., Trincardi, F., and Danovaro, R. (2016). Seafloor heterogeneity influences the biodiversity–ecosystem functioning relationships in the deep sea. *Sci. Rep.* 6:26352. doi: 10.1038/srep26352

Conflict of Interest: The authors declare that the research was conducted in the absence of any commercial or financial relationships that could be construed as a potential conflict of interest.

The reviewer NG declared a past co-authorship with one of the authors C-LW to the handling editor.

Copyright © 2020 Liao, Wei and Yasuhara. This is an open-access article distributed under the terms of the Creative Commons Attribution License (CC BY). The use, distribution or reproduction in other forums is permitted, provided the original author(s) and the copyright owner(s) are credited and that the original publication in this journal is cited, in accordance with accepted academic practice. No use, distribution or reproduction is permitted which does not comply with these terms.

frontiers in Marine Science

ORIGINAL RESEARCH
published: 28 July 2020
doi: 10.3389/fmars.2020.00578

Community Composition and Habitat Characterization of a Rock Sponge Aggregation (Porifera, Corallistidae) in the Cantabrian Sea

Pilar Ríos[1,2†], Elena Prado[1*†], Francisca C. Carvalho[3], Francisco Sánchez[1], Augusto Rodríguez-Basalo[1], Joana R. Xavier[3,4], Teodoro P. Ibarrola[5] and Javier Cristobo[2,5]*

[1] Centro Oceanográfico de Santander, Instituto Español de Oceanografía, Santander, Spain, [2] Departamento de Ciencias de la Vida, Universidad de Alcalá, Madrid, Spain, [3] Department of Biological Sciences and K.G. Jebsen Centre for Deep Sea Research, University of Bergen, Bergen, Norway, [4] CIIMAR – Interdisciplinary Centre of Marine and Environmental Research, University of Porto, Porto, Portugal, [5] Centro Oceanográfico de Gijón, Instituto Español de Oceanografía, Gijón, Spain

OPEN ACCESS

Edited by:
Jeroen Ingels, Florida State University, United States

Reviewed by:
Georgios Kazanidis, The University of Edinburgh, United Kingdom
Dorte Janussen, Senckenberg Museum, Germany

***Correspondence:**
Pilar Ríos
pilar.rios.lopez@gmail.com
Elena Prado
elena.prado@ieo.es

[†] *These authors have contributed equally to this work*

Specialty section:
This article was submitted to Global Change and the Future Ocean, a section of the journal Frontiers in Marine Science

Received: *16 December 2019*
Accepted: *22 June 2020*
Published: *28 July 2020*

Citation:
Ríos P, Prado E, Carvalho FC, Sánchez F, Rodríguez-Basalo A, Xavier JR, Ibarrola TP and Cristobo J (2020) Community Composition and Habitat Characterization of a Rock Sponge Aggregation (Porifera, Corallistidae) in the Cantabrian Sea. Front. Mar. Sci. 7:578. doi: 10.3389/fmars.2020.00578

Deep-sea sponge-dominated communities are complex habitats considered hotspots of biodiversity and ecosystem functioning. They are classified as Vulnerable Marine Ecosystem and are listed as threatened or declining as a result of anthropogenic activities. Yet, studies into the distribution, community structure and composition of these habitats are scarce, hampering the development of appropriate management measures to ensure their conservation. In this study we describe a diverse benthic community, dominated by a lithistid sponge, found in two geomorphological features of important conservation status —Le Danois Bank and El Corbiro Canyon— of the Cantabrian Sea. Based on the analyses of visual transects using a photogrammetric towed vehicle and samples collected by rock dredge, we characterize the habitat and the associated community in detail. This deep-sea sponge aggregation was found on bedrock. It is dominated by one lithistid sponge, *Neoschrammeniella* aff. *bowerbankii* (0.2 ind./m^2) and further composed of various sponge species as well as of other benthic invertebrates such as cnidarians, bryozoans and crustaceans. Using a non-invasive methodology (SfM – Structure from Motion) and empirical relationships of individuals size and biomass/volume obtained in laboratory for *N*. aff. *bowerbankii*, we were able to estimate a total biomass of 41 kg and volume of 39 l of this species in the surveyed area. This approach allows a fine tune methodology for estimating biomass and volume by image-based-observed area avoiding destructive techniques for this species.

Keywords: sponge grounds, lithistids, demosponges, vulnerable marine ecosystems, ecology, taxonomy, structure from motion, underwater photogrammetry

INTRODUCTION

Sponges constitute an important component of the benthic marine communities, particularly in deeper environments where they play fundamental ecological roles (Pomponi et al., 2019). In areas where they aggregate in high density and biomass they form structurally complex ecosystems (sponge aggregations or grounds) providing habitat, nursery and rearing areas for other organisms

often augmenting biodiversity levels locally (Murillo et al., 2012; Beazley et al., 2013; Kazanidis et al., 2016; Hawkes et al., 2019). Due to their filter-feeding capacity, they also contribute significantly to the biogeochemical cycles of carbon, nitrogen and silica (Yahel et al., 2007; De Goeij et al., 2008, 2013; Kutti et al., 2013; Cathalot et al., 2015; Maldonado et al., 2019).

The deep-sea ecosystems of the Cantabrian Sea and particularly of the Le Danois Bank (LDB) and Avilés Canyon System (ACS) have been studied in the scope of several projects (ECOMARG, INDEMARES, SponGES, INTEMARES, among others) of the Spanish Institute of Oceanography (IEO) since 2003. Initially, the projects were focused on the characterization of sediments, bathymetry and water masses dynamics, but further developed into an integrated study of the benthic communities and the trophic ecology of these ecosystems (Cartes et al., 2007; Sánchez et al., 2008, 2017; Preciado et al., 2009).

Many of the studies, focusing on Vulnerable Marine Ecosystems (FAO, 2009) of this area have been carried out over the last years, some of which aimed to characterize the sponge-dominated habitat. Protecting and restoring sponge aggregations are considered crucial from an environmental perspective. They are recognized as singular vulnerable habitats that deserve special research attention and legal protection. Deep-water sponge aggregations are now emerging as a key component of deep-sea ecosystems, creating complex habitats hosting many other species (Hogg et al., 2010; Maldonado et al., 2017). Under particular ecological conditions sponges are able to form concentrations or beds of high abundances building habitats for other species and increasing the biodiversity with respect to surrounding areas, especially the associated fauna of other invertebrate and fish (Bett and Rice, 1992; Klitgaard, 1995; Kunzmann, 1996; Bo et al., 2012; Beazley et al., 2013; Fillinger et al., 2013). These evidences indicate that efforts to close areas dominated by deep-sea sponge aggregations to bottom-tending gears will serve to meet the conservation objectives of the UNGA Resolution 61/105, that drew attention to the importance of the benthic megafauna, in vulnerable marine ecosystems. Despite the ecological importance for the deep-sea, sponge aggregations are poorly mapped and understood (Hogg et al., 2010). This lack of knowledge is most evident in deep-sea species due to the complexity of their study.

In the El Cachucho MPA, that include Le Danois Bank and its intraslope basin, the presence of sponges habitats dominated by the hexactinellids *Asconema setubalense* and *Pheronema carpenteri* and more recently demosponges habitats for *Phakellia ventilabrum*, *P. robusta,* and *Geodia barretti* have been described (Sánchez et al., 2008, 2009, 2017; García-Alegre et al., 2014).

In the Avilés Canyon System the presence of habitats characterized by different sponge species was also described (Sánchez et al., 2015). These studies were focused mainly on the identification of diversity hotspots and presence of vulnerable species associated with the habitat "1170 Reefs" defined by the EU Habitat Directive (E.C, 2013), toward the creation of a coherent network of Marine Protected Areas in Spain (Rodríguez-Basalo et al., 2019). As a result of these studies, Le Danois Bank and its intraslope basin were designated as a Special Area of Conservation (SAC) category and the Avilés Canyon System as a Site of Community Importance (SCI) and integrated into the Natura 2000 network.

In the Cantabrian Sea, only one other deep-sea sponge aggregation dominated by *Artemisina transiens* Topsent, 1890, has been reported and characterized, although in a considerably shallower area (Ríos et al., 2018).

However, due to the need to improve the management that applies in these two areas, it is necessary to identify, map and describe other benthic communities which are in these vulnerable habitats to ensure their protection.

Understanding the community composition and the population structure of key habitat-forming species is critical to understand and quantify their ecological roles, and to assess their resilience to disturbance with the aim to develop appropriate management measures to ensure their conservation.

But nowadays, there are still few studies focused on high resolution mapping techniques to determine the distribution patterns and spatial structure of sponge aggregations in the deep-sea (Klitgaard and Tendal, 2004; Chu and Leys, 2010; Kazanidis et al., 2019; Ramiro-Sánchez et al., 2019). Remotely Operated Vehicles (ROVs) and Remotely Operated Towed Vehicles (ROTVs), which integrate video and still cameras, are increasingly used by the scientific community as a means to explore and characterize deep-sea ecosystems in a non-invasive way. In recent years, applied studies have been carried out for mapping deep-sea sponge aggregations in detail based on visual or quantitative analysis of images acquired from different platforms, i.e., ROVs and AUVs (Beazley et al., 2013; Kutti et al., 2013; McIntyre et al., 2016; Powell et al., 2018; Hawkes et al., 2019; Meyer et al., 2019). The application of quantitative image analysis to deep-sea sponge aggregations habitat characterization, in general terms, has not been used to estimate biomass and population size structure.

In order to increase our knowledge about deep-sea sponges, it is essential to know specimens volume and surface area. These data also contribute to describe the population structure and biomass of species of interest. The access to these data is very difficult in the deep-sea. Most of the available methods are invasive or require removing the organisms from their natural habitat, in order to measure these parameters. Recently, approaches using underwater photogrammetry to create digital models of deep-sea communities are providing non-invasive methods to explore morphometry of individual organisms. Techniques based on Structure-from-motion (SfM) allow the reconstruction of digital, true-scale, 3D model (James and Robson, 2012; Westoby et al., 2012). This photogrammetric approach offers the possibility of creating advanced cartographic products of the ocean floor, such as 3D models and very high spatial resolution orthomosaic, in a fast and low-cost way (Kwasnitschka et al., 2013; McCarthy and Benjamin, 2014). Structure-from-Motion (SfM) techniques have been used to determine surface area and volume of corals and marine sponges from *in situ* images and compare them to measurements obtained in the lab (Lavy et al., 2015).

In compliance with the EU Habitats Directive, follow-up surveys are being performed to further characterize and monitor the identified habitats including the deep-sea sponge

aggregations. Such efforts are linked to the objectives of the EU-funded SponGES project which aims to develop an integrated ecosystem-based approach to preserve and sustainably use vulnerable sponge ecosystems of the North Atlantic. Through the SponGES project some of these areas (Le Danois Bank and Avilés Canyon System in the Cantabrian sea) were revisited since there was evidence that a sponge aggregation dominated by a lithistid sponge species was present. The importance of this group of sponges has been recently highlighted by Maldonado et al. (2015) which reported large aggregations of *Leiodermatium pfeifferae* (Carter, 1876) with extensive signs of habitat damage in the Mediterranean Sea.

Thus, the main aim of this study was to (a) characterize and describe the habitat of a benthic community dominated by a lithistid sponge, and (b) establish morphometric relationships of this species to estimate population structure parameters from underwater imagery, in the Avilés Canyon System and Le Danois Bank. This study is the first descriptive and quantitative analysis of lithistid aggregations in the Cantabrian Sea and contributes to our understanding of the population structure of this species as well as the composition of the overall benthic community in the area.

MATERIALS AND METHODS

Study Area

The Cantabrian Sea central area is characterized by a complex topography, including, deep-sea canyons and seamounts, and a very narrow continental shelf. Within it, two small areas have been selected for our study for having high numbers of *Neoschrammeniella* aff. *bowerbankii* (**Figure 1A**).

The western study area corresponds to the so-called El Corbiro Canyon (ECC) (**Figure 1B**), which forms part of the Aviles Canyon System (ACS). The ACS is a complex region of canyons and valleys comprising three main canyons of different morpho-structural characteristics: Avilés, El Corbiro, and La Gaviera canyons. The ACS has been integrate into the Natura 2000 as a Site of Community Importance (SCI) (Boletín Oficial del Estado, 2014). The continental shelf is generally narrow; the width varies from 12 km (where the head of the Avilés Canyon is incised) to 40 km. The ACS extends from the continental shelf to the abyssal plain, at 4800 m depth, and is controlled by the tectonic regime of the area. The El Corbiro Canyon is characterized by a V-shaped profile and a pronounced axial incision at its head that starts at 176 m depth on the continental shelf. Its head is made up of several gullies, particularly on the eastern wall, that converge to form the main channel (Gomez-Ballesteros et al., 2014). In our study, we have identified a rocky outcrop located on the west side of the canyon head, suitable for the settlement of lithistids. The strong currents over the canyon and his strong slope are responsible for the scarce sedimentary cover in the area.

The second study area is Le Danois Bank (LDB), a large seamount (marginal shelf) located on the Cantabrian Sea central area at 5°W longitude and 44°N latitude (**Figure 1A**). The Bank presents an elongated form about 72 km long in an E-W direction and about 15 km wide from north to south; it has an almost flat summit with a minimum depth of 424 m, and is separated 25 km from the continental shelf by a deeper intraslope basin (Van Rooij et al., 2010). This structure is a "horst" type, presenting a dissymmetry between its northern and southern flanks. The northern side of Le Danois Bank has a steep continental slope with a relief of 3600 m; its base is located at a 4400 m depth on the Biscay abyssal plain. The sedimentary cover is scarce in the bank summit and particularly in its western flank (**Figure 1C**), where the rocky outcrops and boulders are quite abundant. Gorgonian forests and deep-sea sponge aggregations are two of the most important habitats of ecological values in the Le Danois Bank and its intraslope basin. These types of habitats are included in the EU Habitat Directive that urges national governments to ensure the conservation and protect these vulnerable ecosystems. In this way, "El Cachucho" became the first Marine Protected Area (MPA) in Spain, and was included in the Natura 2000 network in 2011 (Boletín Oficial del Estado, 2011).

Data Collection

Oceanographic Cruises

Data were collected at 27 stations (**Supplementary Table 1**) during five expeditions within the framework of the different projects, namely INDEMARES AVILES_0511, ESMAREC_0514, SponGES_0617, ECOMARG_0717 and ECOMARG_2019 (see details in funding). The surveys were carried out onboard the R/V *Vizconde de Eza* (SGM) in May 2011, the R/V *Ángeles Alvariño* (IEO) in May 2014, in June and July 2017 and the R/V *Ramón Margalef* (IEO) in July 2019.

Sampling

Sampling on hard substrate was conducted using a rock dredge RD (80 × 30 cm; 10 mm mesh size net) towed on the seafloor during 5−15 min at a speed of 1.5 knots (**Figure 2A**).

The sampling stations to collect sponges (2 on each study area) were selected after studying the data provided by the multibeam echosounder or after previous visualization of images from photogrammetric towed vehicle, following gradient of deep and geological structures: DR7_AVILES0511 and DR4_SponGES0617 in ECC; DR9_SponGES0617 and DR15_SponGES0617 in LDB.

Collected material was sorted onboard, and when large catches were obtained, a representative sub-sample was kept (**Figures 2D,E**).

The collected biological material was photographed, anesthetized and preserved in 96% ethanol for further study in the laboratory. Identifications were performed to the lowest taxonomic level possible from the analyses of taxon-specific morphological features using specialized literature such us Bowerbank (1866), Sollas (1888), Hooper and van Soest (2002), and Cárdenas et al. (2018) (Porifera); Alder (1856), Stephens and Hickson (1909), Gravier (1920), Zibrowius (1978, 1980), Zibrowius and Cairns (1992), Molodtsova (2006), Cairns and Bayer (2009), Altuna (2013), Altuna and Ríos (2014), Addamo et al. (2016), and Cairns and Taylor (2019) (Cnidaria); Thomson (1872), Kœhler (1896), Mortensen (1935), Cherbonnier (1969), Clark (1980), Paterson (1985), Clark and Downey (1992),

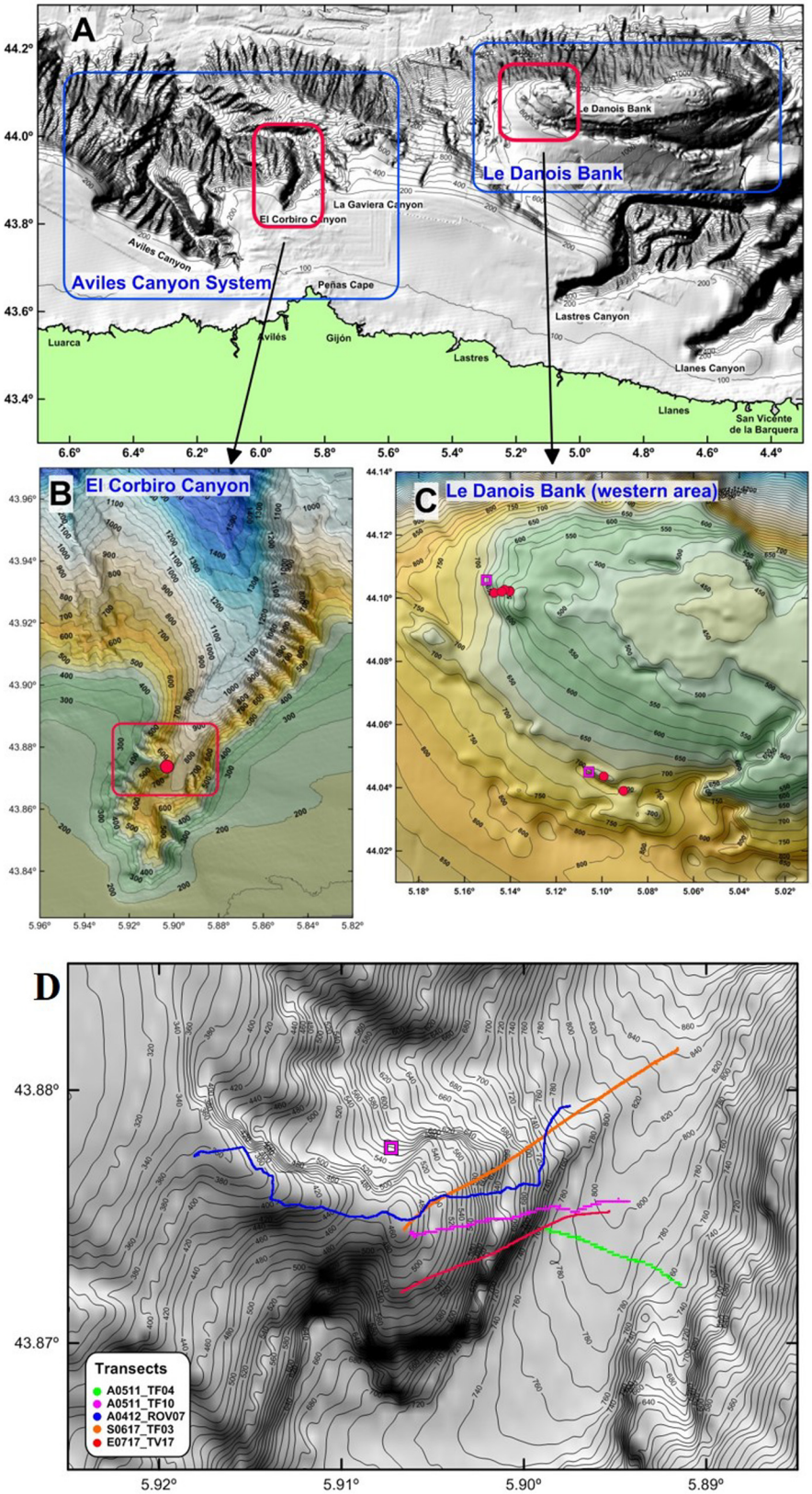

FIGURE 1 | (A) The Cantabrian Sea central area. **(B)** El Corbiro Canyon and sampling zone. **(C)** Le Danois Bank western area and sampling stations (squares for rock dredge and dots for ROTV). **(D)** Video transects in El Corbiro Canyon. In red the transect analyzed with SfM (TV17, ECOMARG_2017).

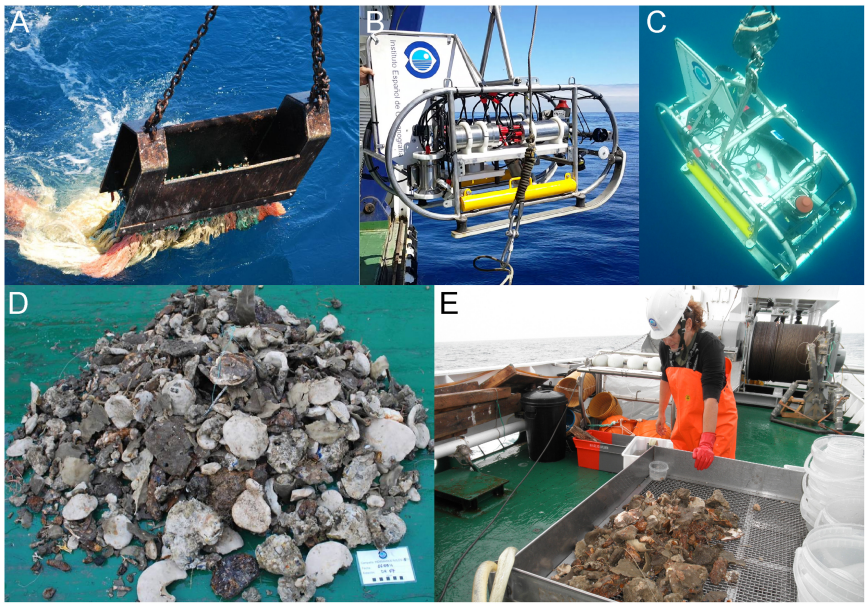

FIGURE 2 | Sampling methods. **(A)** Rock dredge. **(B,C)** Photogrammetric towed vehicle. **(D)** Sample of *Neoschrammeniella* aff. *bowerbankii* agreggations on deck. **(E)** Seaving tower.

Southward and Campbell (2006), Míguez (2009), Manjón-Cabeza et al. (2014), and Fernández-Rodríguez et al. (2019) (Echinodermata); and Jullien and Calvet (1903), Calvet (1907, 1931), Rioja (1931), Zariquiey (1968), D'Hondt (1974), Brunton and Curry (1979), Rouse and Pleijel (2001), Louisy (2002), Wisshak et al. (2009), Velasco et al. (2013), Lloris (2015), Negri and Corselli (2016), and Álvarez-Campos et al. (2018) (others).

A total of 668 organism were sampled (339 in ECC and 329 in LDB) and compared with 6321 underwater images analyzed. In ECC we collected 111 specimens of *N.* aff. *bowerbankii* and in LDB we collected 10 specimens.

Spicules on Porifera and other skeletal structures, with taxonomic value, were prepared and cleaned with bleach, distilled water and ethanol. Skeletal arrangement and spicules of *Neoschrammeniella* aff. *bowerbankii* were examined with a ZEISS SEM at Bergen University (**Suplement A**). Taxonomic assignments followed the classification proposed by Morrow and Cárdenas (2015) and the World Porifera Database[1] for Porifera, and the World Register of Marine Species (WORMS[2]) for other invertebrates.

ROTV Underwater Images

The images analyzed in this study were obtained at LDB and ECC during the ESMAREC_0514, SponGES_0617, ECOMARG_0717, and ECOMARG_2019 surveys, using the Remotely Operated Towed Vehicle (ROTV) *Politolana* (**Figures 2B,C**). The vehicle can be operated up to a maximum of 2000 m in depth and transects were carried out navigating to 0.8 – 1.0 knot of speed at 2 – 4 m over the sea floor. This ROTV acquires simultaneously still pictures and HD video, and synchronizes it with environmental variables (pressure, temperature, and salinity). The *Politolana* uses telemetry to send and receive data in real-time from the equipment that composes the monitoring system: altimeter, CTD, positioning system and cameras (Sánchez and Rodríguez, 2013).

The acoustic positioning system Kongsberg HIPAP 502 was used to obtain the absolute position of the underwater vehicle. It is based on Super (Ultra) Short Base Line (SSBL) principle that establishes a three-dimensional position of the transponder. An SSBL system measured the horizontal and vertical angles together with the range to the ROTV. Then, OFOP (Ocean Floor Observation Protocol) software (Huetten and Greinert, 2008) processed the coordinate observation files and merges them with additional sensor data. Finally a complete data set for each ROTV trajectory deployment is obtained allowing georeferencing image data.

The photographs were revised for habitat characterization and description of associated communities. The ROTV *Politolana* is provided with a Nikon D90 camera with a Subtronic strobe. Four parallel laser beams spaced 25 cm apart and integrated in the still camera provided scale for photographs. Each 10 s the equipment takes a picture, obtaining representative data of the habitat and benthic communities to be characterized (Sánchez and Rodríguez, 2013; Sánchez et al., 2017).

The video-transect was used to generate an orthomosaic and to measure population of *N.* aff. *bowerbankii* sizes. It was recorded in July 2017 at ECC during the ECOMARG_2017 survey (TV17), in a range of depths going from 500 to 800 m (**Figure 1D**). A full-HD video-camera (Sony HD-700-CX) with two LED lights (12600 lumens/6000° Kelvin) attached to the image system. Two parallel laser beams spaced 20 cm apart

[1]http://www.marinespecies.org/porifera/

[2]http://www.marinespecies.org

provided scale for videos and constant distances to validate results. The video transect analyzed in this study was about 450 m long and ran close to steep slope in ECC. The optical sensors shows a portion of around 3 m of the seafloor, this area is referred to as the swath. This footprint varies depending of height over the seafloor and its bathymetry. The area covered and analyzed using this photogrammetric approach was 1450 m^2.

Sponge Density Estimation and Faunal Identification

The pictures analyzed are scaled in the PescaWin software (Sánchez, 2015). This allows estimating the surface covered by each photograph and sponge density. In each photograph all macro and megafauna were labeled, and identified to the lowest taxonomic level possible. When the external characteristics made it impossible to identify to the species level, observed specimens were assigned to morphotypes. All records were stored in a database of the IEO that allows multiple data queries on existing species throughout the Central Cantabrian Sea, their geographical location, the type of substrate, water depth, etc.

Lithistid Morphometry

Morphometric parameters such as biomass (drained weight), surface area, perimeter and thickness were measured for 41 specimens of *Neoschrammeniella* aff. *bowerbankii* collected at ECC (N = 35) and LDB (N = 6) covering a range of individual's sizes (**Figure 3**). Obtained measurements were used to establish size (perimeter) – volume – biomass (drained weight) relationships. The volume was calculated for 25 samples from ECC by measuring the liquid displacement (Jokiel et al., 1978; Hughes, 2005). Weight, surface, area, perimeter and thickness were measured in all samples.

FIGURE 3 | Samples collected with Rock Dredge. **(A)** In El Corbiro (INDEMARES AVILES_0511 cruise). **(B)** In Le Danois Bank (SponGES_0617 cruise). Scale bar 1 cm.

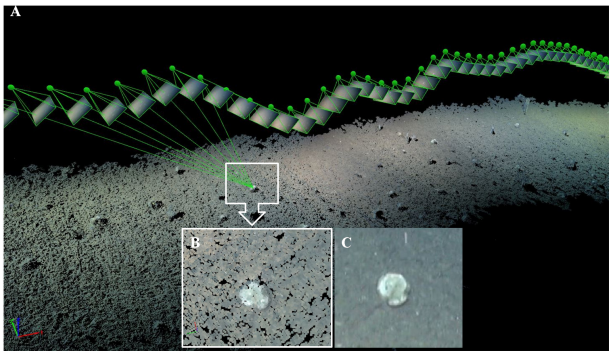

FIGURE 4 | Sampling methods. Video Transect: 3D reconstruction of video transect using Pix4D Mapper Pro. **(A)** Decomposing video-sectioning thousands of geo-positioned overlapping images processed. Green points show the camera's position. **(B)** Zoom 3D point cloud. **(C)** Zoom original video-frame.

Image Morphometry

The measurement of the morphometry of *N.* aff. *bowerbankii* specimens was made using an orthomosaic of images covering 450 m of video-transect. This orthomosaic is obtained using a photogrammetric reconstruction approach. This methodology was done decomposing video-sections in thousands of geo-positioned overlapping images processed using photogrammetric Pix4D Mapper Pro software (Pix4D SA, Switzerland). Pix4D uses the Structure-from-Motion (SfM) approach. SfM is the process of estimating the 3-D structure of a scene from a set of 2-D images. It requires point correspondences between images and finds corresponding points by matching features. Pix4D software also uses a dense image matching, an automated process based on dense image matching technology (Tola et al., 2010). Integration of the point measurements, camera calibration, and the position data given by the cameras, the software provides 3D dense point clouds (**Figure 4**), Digital Surface Models (DSM) and orthomosaics. Since all the information is geo-referenced in a cartographic system (UTM-WGS84), all the geographic layers obtained can be included in a GIS environment thus allowing the subsequent morphometric analysis.

Constant distances between laser pointers projected on the frames were used to evaluate the reconstruction of the geometric model. In this way, the geometric uncertainty of the model and errors associated to measurements over the orthomosaic were estimated.

Thousand five hundred video-frames were used as image input in the photogrammetric adjustment of the 3D block, only 11 images were discarded. The size of 203 specimens of *N.* aff. *bowerbankii* were measured; the area covered by each specimen was selected as a suitable parameter of size and the area covered by the video section was also measured. The direct measurement of this parameter is possible using a complete orthomosaic with a

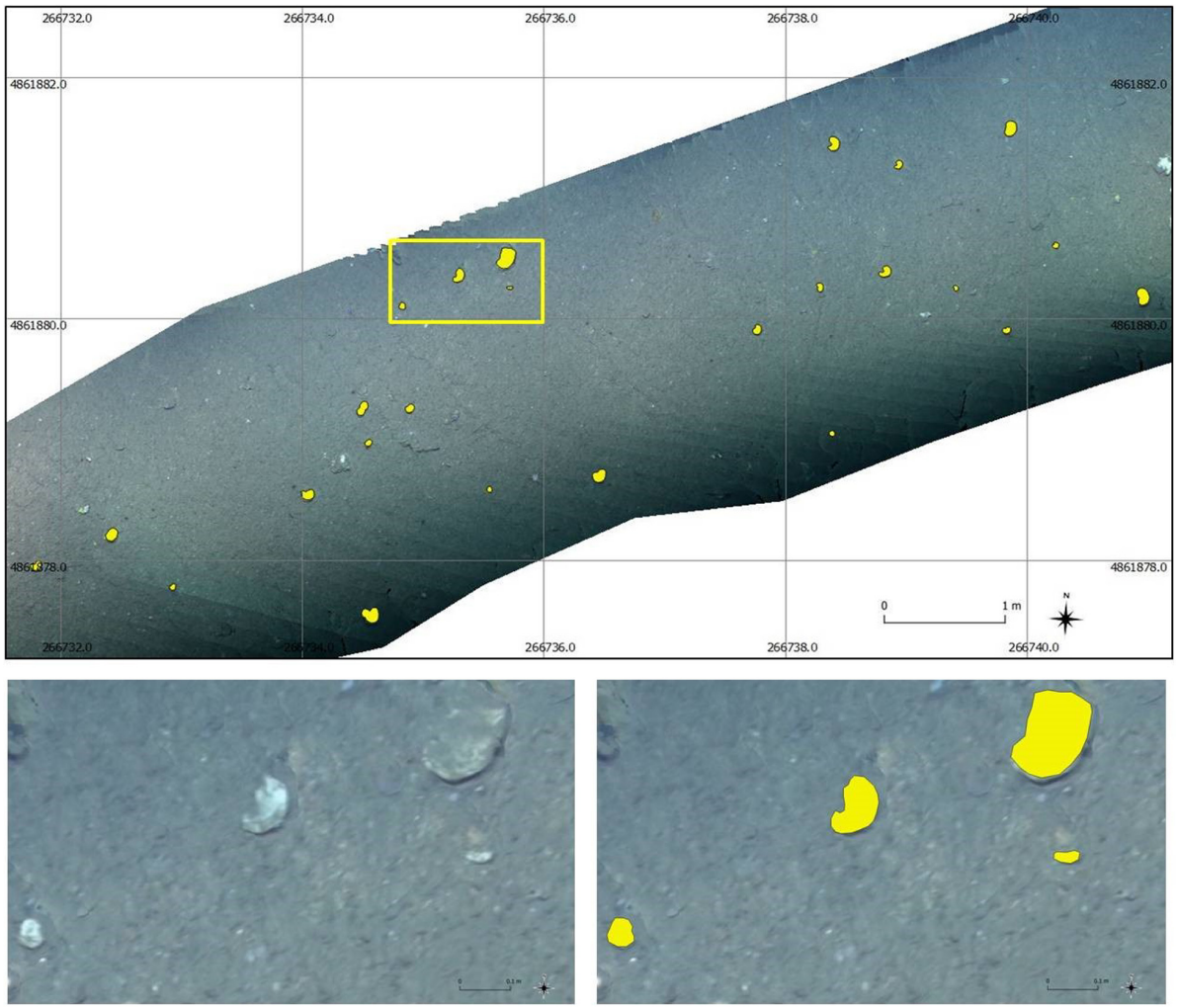

FIGURE 5 | Measurement of size using photogrametric technics.

very high spatial resolution (0.16 cm/pixel) of the area. Using the QGis software, the area enclosed within each lithistid's perimeter was calculated (**Figure 5**).

These image-based perimeter data were compared with *in situ* data measured in the laboratory for evaluation of the equivalence of the samples. To verify this similarity, the Mann Whitney test was used. This test can be used to investigate whether two independent samples from different populations have the same distribution. Then, empirical relationships between *in situ* morphometric (perimeters) and biological parameters (drained weight biomass and volume) were established for this species. This empirical relationship can be applied to infer biomass from image morphometric data.

RESULTS

Here, we report the discovery of a benthic community dominated by a lithistid sponge in two areas of the Cantabrian Sea, providing a characterization of this community and its habitat. We also established the empirical relationship for *Neoschrammeniella* aff. *bowerbankii* surface area with drained weight biomass and volume, improving our knowledge in the relationship between 2D and 3D metrics for this species, in addition to inferring biomass data per unit of surface present in a specific area or aggregation both in weight and in volume occupied by the specimens.

We annotated 509 specimens seen in the videos at 23 stations, between 486 and 672 m depth and we collected 121 samples at 4 stations of RD, between 551 and 695 m depth (**Supplementary Table 1**).

Benthic Community Composition

In these study cases, 3691 animals belonging to eight Phyla were observed (**Figure 6**). In the El Corbiro Canyon area, 20 sponge morphotypes were identified from the video and photographs of the photogrammetric towed vehicle. These included the habitat-forming lithistid sponge *Neoschrammeniella* aff. *bowerbankii*,

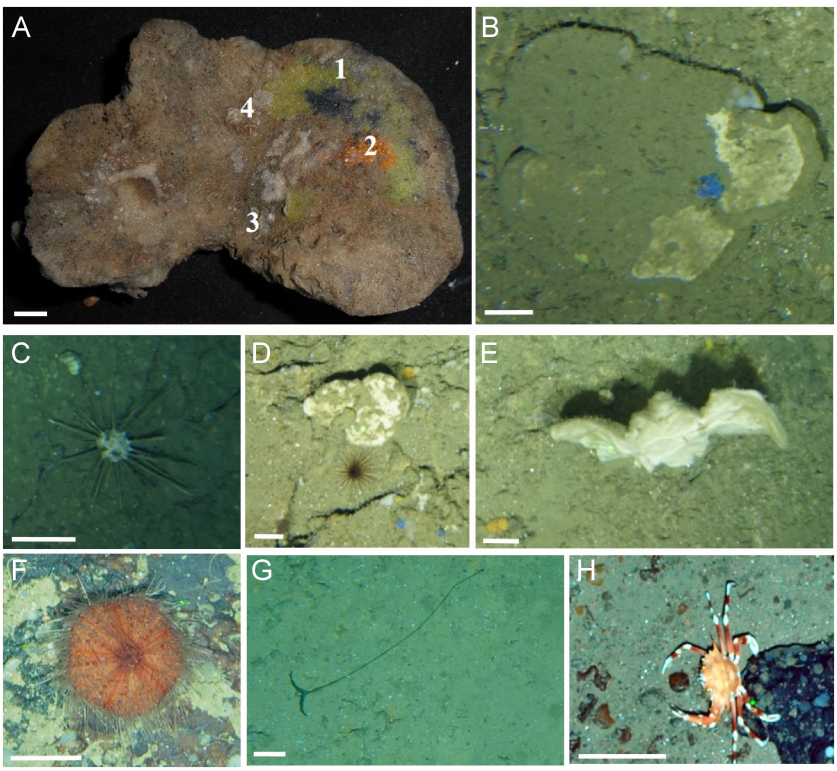

FIGURE 6 | Associated fauna in El Corbiro **(A,B)** and Co-occurrent fauna, species that structure the *Neoschrammeniella* aff. *bowerbankii* community **(C–H)**. **(A)** Dead specimen on which different species live, (1) *Hexadella* sp. (2) *Hymedesmia* sp. (3) *Desmacella* sp. (4) *Disporella* sp. **(B)** *Hymedesmia* (*Hymedesmia*) *paupertas*. **(C)** *Cidaris cidaris*. **(D)** *Cerianthus* sp. **(E)** *Phakellia hirondellei*. **(F)** *Araeosoma fenestratum*. **(G)** *Bonellia viridis*. **(H)** *Bathynectes maravigna*. Scale bar **(A)**: 1 cm. **(C–H)**: 10 cm. **(B–G)**: 5 cm. El Corbiro **(A–E)**. Le Danois Bank **(F–H)**.

Axinellida (*Phakellia robusta* and *P. hirondellei* and other fun shape sponges), Tetractinellida, (*Pachastrella monilifera*, *P. ovisternata*, *P.* cf. *nodulosa*), Verongiida (*Hexadella* sp.), Halichondriidae (*Topsentia* sp.), Desmacellida (*Desmacella* spp.), Haplosclerida and Poecilosclerida (*Hymedesmia* (*Hymedesmia*) *paupertas,* and other *Hymedesmia* spp.) and other small or encrusting sponges (see **Table 1**). We also recorded other invertebrates, including the solitary Scleractinian *Desmophyllum* spp., the black coral *Parantipathes hirondelli*, the echinoids *Cidaris cidaris* and *Araeosoma fenestratum*, the echiuran *Bonellia viridis*, the asteroid *Henricia* sp. and the cnidarians *Cerianthus* spp. However, there were a number of species not easily distinguished and impossible to identify only by video.

In Le Danois Bank, several species of Demospongiae and Hexactinellida were present alongside *N.* aff. *bowerbankii* contributing to the 3D structure of the community. Analysis of the samples collected and annotation of the video transects confirmed that there are a number of erect, massive or encrusting species that play an important role because of their size, volume or abundance: erect and fan–shaped species as *Phakellia hirondellei* and *Phakellia robusta*; massive Tetractinellida, with three large Geodiid species: *Geodia* cf. *barretti*, *G. pachydermata*, *Geodia* sp. and the presence of three species of the genus *Pachastrella* were frequently recorded. In this area, we also collected other Tetractinellida such as *Characella pachastrelloides*, *Calthropella* (*Calthropella*) *geodioides* and *Calthropella* (*Calthropella*) *durissima* these last ones smaller than the previous ones. *Hymedesmia* (*Hymedesmia*) *paupertas* is one of the most common species recognizable using ROTV by its characteristic encrusting shape and bright blue color. The Hexactinellid *Aphrocallistes beatrix* was also detected not forming a biogenic framework, but as solitary individuals. Some specimens of *Pheronema carpenteri* were observed but in soft bottons near the *N.* aff. *bowerbankii* community.

In ECC, we collected more cnidarians (colonies or individuals) (44 samples) than in LDB (9 samples), where the most abundant are two different species of *Cerianthus* Anthozoa, the scleractinian *Desmophyllum* spp. and *Balanophyllia* (*Balanophyllia*) *thalassae*, the Alcyonacea *Callogorgia verticillata*, *Paramuricea* cf. *placomus* and *Anthomastus* sp., these two only present in LDB.

Including samples collected with RD and analyzed images with ROTV. The species richness is very similar in both areas (**Figure 7**), but slightly higher in LDB for almost all the taxonomic groups, with the phylum Porifera being dominant (35.44% ECC – 38.64% LDB), and consisting nearly entirely of species belonging to the class Demospongiae. As for Cnidarians (17.72% ECC – 20.45% LDB), they are also found in both areas, but images show that they are more frequent in the surrounding areas than in the habitat occupied by the sponges. Mollusca (6.33% ECC – 2.27%

TABLE 1 | Species in associated fauna (AF) and co-occurrence (CO) in populations of *Neoschrammeniella* aff. *bowerbanki* in El Corbiro Canyon (SCA) and Le Danois Bank (LDB).

Phyllum	Species	AF	El Corbiro Canyon (ECC)		Le Danois Bank (LDB)	
			CO – DR	CO – TF	CO – DR	CO – TF
Porifera						
Demospongiae	*Antho* sp.				X	
	Axinellida indet.			X		X
	Axinella sp.			X		
	Calthropella (Calthropella) geodioides (Carter, 1876)				X	
	Calthropella (Calthropella) durissima Topsent, 1892				X	
	Caminella pustula (Cárdenas et al., 2018)				X	
	Characella pachastrelloides (Carter, 1876)				X	
	Clathria sp.				X	
	Coelosphaera (Histodermion) sp.		X			
	Coelosphaera sp.		X			
	Desmacella sp.	X	X	X		X
	Demospongiae indet.			X		X
	Geodia anceps (Vosmaer, 1894)				X	
	Geodia cf. *barretti*				X	X
	Geodia nodastrella Carter, 1876				X	
	Geodia pachydermata (Sollas, 1886)		X	X	X	X
	Geodia sp.			X	X	X
	Haliclona (Flagellia) sp.				X	
	Haliclona (Gellius) sp.		X		X	
	Haliclona sp.			X		X
	Halicnemia sp.		X			X
	Hamacantha sp.		X			
	Haplosclerida indet.			X		X
	Hexadella sp.	X	X	X		X
	Hymedesmia (Hymedesmia) paupertas (Bowerbank, 1866)	X	X	X	X	X
	Hymedesmia sp.	X	X	X		X
	Janulum spinispiculum (Carter, 1876)		X		X	
	Latrunculia sp.		X		X	X
	Microcionidae indet.	X	X			
	Pachastrella cf. *nodulosa*		X	X		X
	Pachastrella monilifera Schmidt, 1868		X	X		X
	Pachastrella ovisternata Lendenfeld, 1894		X	X	X	X
	Pachastrella sp.			X		
	Pachastrellidae indet.			X		X
	Phakellia hirondellei Topsent, 1890			X	X	X
	Phakellia robusta Bowerbank, 1866		X	X	X	X
	Plocamione hystrix (Ridley and Duncan, 1881)				X	
	Plocamionida sp.		X			
	Polymastia sp.		X			
	Sceptrella sp.				X	
	Siphonodictyon sp.		X		X	
	Spirorhabdia vidua (Schmidt, 1875)				X	
	Spongosorites sp.					X
	Sulcastrella sp.		X			
	Tentorium semisuberites (Schmidt, 1870)		X		X	
	Tetractinellida indet.		X			
	Thenea schmidti (Sollas, 1886)		X			X
	Thrombus sp.				X	

(Continued)

TABLE 1 | Continued

Phyllum	Species	AF	El Corbiro Canyon (ECC)		Le Danois Bank (LDB)	
			CO – DR	CO – TF	CO – DR	CO – TF
	Thymosia sp.				X	
	Topsentia sp.		X	X	X	
	Triptolemma sp. nov.				X	
	Vulcanella gracilis (Sollas, 1888)				X	
Hexactinellida	Hexactinellida indet.			X		
	Aphrocallistes beatrix Gray, 1858				X	
	Pheronema carpenteri (Thomson, 1869)				X	
Cnidaria						
Anthozoa	Cnidaria indet.			X		
	Balanophyllia (*Balanophyllia*) *thalassae* Zibrowius, 1980		X	X	X	X
	Caryophyllia sp.					X
	Deltocyathus moseleyi Cairns, 1979					X
	Dendrophyllia cornigera (Lamarck, 1816)		X			
	Desmophyllum dianthus (Esper, 1794)		X	X		X
	Desmophyllum pertusum (Linnaeus, 1758)		X	X		X
	Desmophyllum sp.					X
	Scleractinia indet.					X
	Acanthogorgia armata Verrill, 1878				X	
	Acanthogorgia sp.					X
	Anthomastus sp.					X
	Callogorgia verticillata (Pallas, 1766)		X	X	X	X
	Gersemia sp.					X
	Narella versluysi (Stephens and Hickson, 1909)		X			X
	Paramuricea cf. *placomus*				X	X
	Paramuricea sp.					X
	Placogorgia sp.		X	X	X	X
	Stolonifera indet.		X			
	Swiftia dubia (Thomson, 1929)				X	
	Viminella flagellum (Johnson, 1863)		X			X
	Actiniaria indet.					X
	Antipatharia indet.			X		X
	Allopathes sp.					X
	Leiopathes sp.					X
	Parantipathes hirondelle Molodtsova, 2006			X		
	Schizopathes sp.					X
	Cerianthus sp.			X		X
	Epizoanthus sp.		X		X	
Hydrozoa	Hydrozoa indet.					X
	Campanularia hincksii Alder, 1856		X			
	Diphasia alata (Hincks, 1855)		X			
	Lafoea dumosa (Fleming, 1820)		X			
	Stenohelia maderensis (Johnson, 1862)				X	X
Brachiopoda	*Macandrevia* sp.		X			
	Platidia sp.		X			
	Terebratulina retusa (Linnaeus, 1758)		X			
Bryozoa	Buguloidea indet.		X	X	X	
	Disporella sp.	X	X			
	Reteporella sp.		X		X	X
	Bryozoa indet.	X	X			
Sipuncula	Sipuncula indet.		X		X	

(Continued)

TABLE 1 | Continued

Phyllum	Species	AF	El Corbiro Canyon (ECC)		Le Danois Bank (LDB)	
			CO – DR	CO – TF	CO – DR	CO – TF
Mollusca						
Solenogastres	Solenogastres indet.				X	
Polyplacophora	*Hanleya hanleyi* (Bean, 1844)		X			
Gastropoda	*Calliostoma leptophyma* Dautzenberg and Fischer, 1896		X	X		
	Emarginula sp.				X	
Bivalvia	*Spondylus gussonii* Costa, 1830 ["1829"]		X			
	Karnekampia sulcata (Müller, 1776)		X			
	Neopycnodonte zibrowii Wisshak et al., 2009		X			
Cephallopoda	*Eledone* sp.			X		
Annelida	Amphinomidae indet.				X	
	Bonellia viridis Rolando, 1822			X		X
	Eunicidae indet.	X	X		X	
	Haplosyllis sp.	X				
	Hesionidae indet.		X		X	
	Hyalinoecia tubicola (Müller, 1776)					X
	Maldanidae indet.	X	X		X	
	Phyllodocidae indet		X		X	
	Polynoidae indet.	X	X		X	
	Syllis sp.	X	X		X	
	Terebellidae indet.				X	
	Trypanosyllis sanchezi (Álvarez-Campos et al., 2018)				X	
	Trypanosyllis sp.	X			X	
	Vermiliopsis sp.	X	X			
Arthropoda Crustacea	*Dichelopandalus bonnieri* Caullery, 1896					X
	Munida perarmata Milne-Edwards and Bouvier, 1894		X	X		X
	Bathynectes maravigna (Prestandrea, 1839)		X	X	X	X
	Polybius henslowii Leach, 1815–1875			X		X
	Pagurus sp.					X
	Uroptychus sp.					X
Echinodermata						
Echinoidea	*Araeosoma fenestratum* (Thomson, 1872)		X	X		X
	Cidaris cidaris (Linnaeus, 1758)		X	X		X
	Phormosoma placenta Thomson, 1872					X
Asteroidea	*Brisinga endecacnemos* Asbjørnsen, 1856					X
	Ceramaster sp.					X
	Culcitopsis borealis (Süssbach and Breckner, 1911)		X			
	Henricia caudani (Kœhler, 1895)		X	X	X	X
	Novodinia pandina					X
	Peltaster placenta (Müller and Troschel, 1842)					X
	Porania sp.					X
	Pterasteridae indet.		X			
	Asteroidea indet.			X		X
Ophiuroidea	*Ophiotreta valenciennesi* (Lyman, 1879)		X			
Crinoidea	*Koehlermetra porrecta* (Carpenter, 1888)		X		X	
	Leptometra celtica (M'Andrew and Barrett, 1857)		X			X
	Crinoidea indet.			X		X
Holothuroidea	*Benthogone rosea* Kœhler, 1895					X
	Parastichopus tremulus (Gunnerus, 1767)					X
	Psolidium cf. *complanatum*				X	
	Psolus sp.	X			X	X

(Continued)

TABLE 1 | Continued

Phyllum	Species	AF	El Corbiro Canyon (ECC)		Le Danois Bank (LDB)	
			CO – DR	CO – TF	CO – DR	CO – TF
Chordata Actinopterygii	*Conger conger* (Linnaeus, 1758)					X
	Hymenocephalus italicus Giglioli, 1884					X
	Lepidion lepidion (Risso, 1810)					X
	Molva molva (Linnaeus, 1758)					X
	Trachyscorpia echinata (Kœhler, 1896)					X
Holocephali	*Chimaera monstrosa* Linnaeus, 1758			X		

DR, rock dredged. TF, Photogrammetric towed vehicle.

LDB), Crustacea (3.8% ECC – 5.69% LDB); Annelida (12.66% ECC – 12.5% LDB) and Echinodermata (12.66% ECC – 14.77% LDB) are other groups well represented in the area, with high density of the taxon Echinoidea.

The presence of Brachiopoda (5 ECC) and Sipuncula (5 ECC – 9 LDB) was only detected with the specimens collected by the RD.

Habitat Characterization

In the two Cantabrian Sea areas we studied, habitats have a similar structure and taxonomic composition with only slight differences. In ECC the aggregation of *Neoschrammeniella* aff. *bowerbankii* occurs on the west wall (**Figures 1B,D**) attached by their bases on a rocky bottom with a steep slope between 520 and 760 m in depth (**Figure 8A**).

The massive skeletons have a very hard consistency neither disaggregate nor easily dissolved after sponge death; they persist attached to the bottom and they are an available substrate for other organisms. Sponge densities estimated by image analysis were 0.43 indiv./m^2 in the TF17_ECOMARG_0717 transect (ECC) and 0.05 indiv./m^2 in the TF9_ESMAREC_0514 transect (LDB). Individuals were not clustered nor densely aggregated as in other deep-sea sponge aggregations. They presented an average distance of 79.6 cm between individuals (with minimum distances of 8.30 and maximum distances of 212.40 cm).

In LDB, the aggregation occurs mainly on the rocky ridges of the western and SW flanks of the seamount (**Figure 1C**), at 477–760 m in depth (**Figure 8B**). The substrate type is quite different in both areas. In ECC, we find that the area is continuous and well defined and is formed by bedrock covered with a thin layer of mud, with a slope range o 45−60°. At LDB, facies are formed by rock ridges, large boulders and mixed sediments producing a more patchy habitat both along the seamount and inside our study area. The water temperature at the seafloor during the survey periods was 10.30−10.86°C in ECC and 10.50−11.14°C in LDB. The salinity ranged between 35.56−35.72 ppm in ECC and 35.59−35.66 ppm in LDB.

Neoschrammeniella aff. *bowerbankii* Morphometry

The form of the collected samples in the Cantabrian Sea is a small cup in the case of the younger specimens and the shape of a round tray with undulated margin in that of the adults. Dimensions (height, width) varied between 3.1 × 4.1 in the smallest and 19.5 × 19.6 in the largest collected specimens, with wall thickness ranging from 1.2 to 2.8 cm. The perimeter varies from 10.10 to 64.7 cm.

Morphometric parameters (perimeter, thickness, weight, and volume) obtained in the laboratory for 41 specimens allowed us to establish logarithmic morphometric relationships, with high adjustment for perimeter – drained weight (R^2 = 0.93) and perimeter – volume (R^2 = 0.91) for *Neoschrammeniella* aff. *bowerbankii* (**Figures 9B,C**).

The size of 203 *Neoschrammeniella* aff. *bowerbankii* specimens were obtained through manual digitalized perimeter and area enclosed measurements. Both specimens measured in the laboratory and those measured on the image orthomosaic belonged to the same study area, the El Corbiro Canyon, in ACS, at two different stations, separated at 678m.

The lithistid perimeter data of the two samples sets (measured in the lab and from the images) have been compared to verify their similarity, using Mann Whitney test (**Figure 9A**). The result shows that *U*-value is 3352; the *Z*-Score is 0.53167 and the *p*-value is 0.59612. Subsequently, we cannot reject the null hypothesis at 5% significance, indicating not significant differences between the obtained measurements.

The density of this species as assessed by the video is 0.2 indiv./m^2. Using the surface data enclosed in the perimeters of the lithistids measured by digitizing on the orthomosaic image, a histogram with the population size distribution of *N.* aff. *bowerbankii* was obtained showing that specimens range from 7 to 497 cm^2 (**Figure 9D**). Applying the relationships established with the *in situ* samples and empirical lab measures, we can infer the drained weight biomass and volume of each of the copies of *N.* aff. *bowerbankii* measured in the images and the total weight (41.13 kg) and volume (39.34 l) of the aggregation of lithistids present in the area, without the need for extractive sampling.

DISCUSSION

The biology and ecology of present-day lithistid fauna remain poorly known (Carvalho et al., 2015; Maldonado et al., 2015). With this study we focus on the knowledge of lithistid aggregation in the Cantabrian Sea at two Natura 2000 sites.

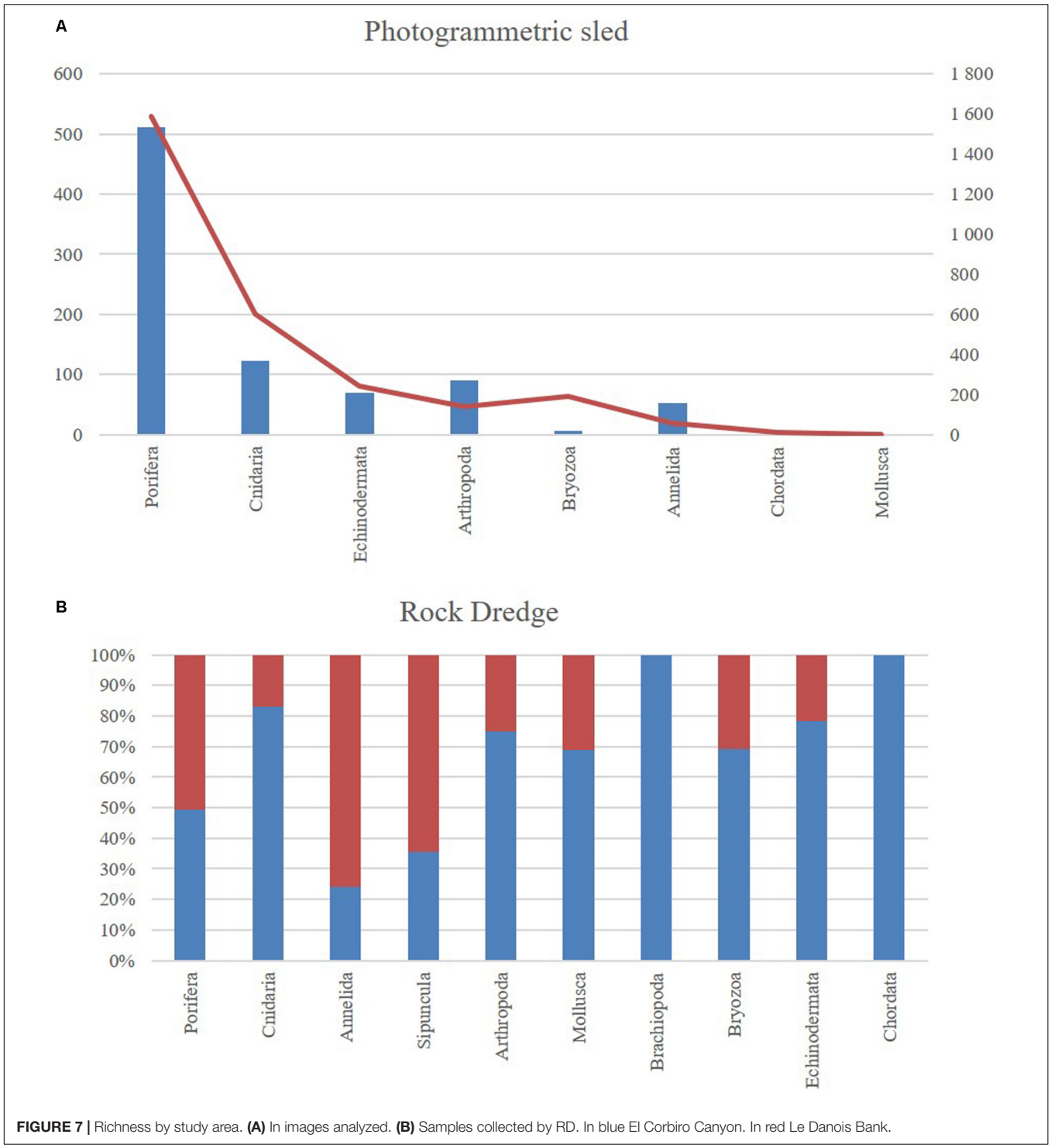

FIGURE 7 | Richness by study area. **(A)** In images analyzed. **(B)** Samples collected by RD. In blue El Corbiro Canyon. In red Le Danois Bank.

Deep-sea sponge aggregations have been considered a type of habitat under the OSPAR Convention for the Protection of the Marine Environment of the North-East Atlantic (Christiansen, 2010). The document mentions grounds of Astrophorids and Hexactinellida, and in particular the genera *Geodia* and *Pheronema*, which are the predominant habitat-forming species in the NE Atlantic. Hogg et al. (2010), in the frame of United Nations Environment Programme World Conservation Monitoring Centre (UNEP-WCMC), report outlines of what is known about deep-water sponge grounds habitats and Maldonado et al. (2015), reported a distinct reef-like type from the Mediterranean, the monospecific formation built by the lithistid demosponge *Leiodermatium pfeifferae*. Other regions where lithistids dominate the fauna are the tropical

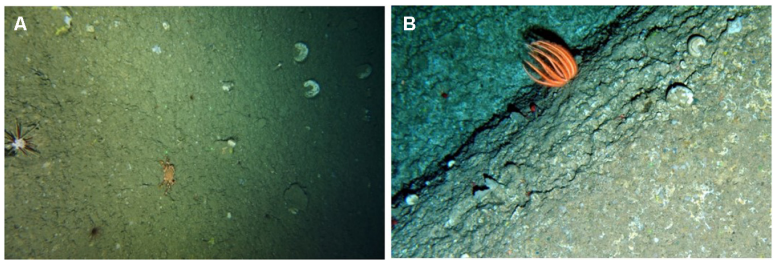

FIGURE 8 | Population of *N*. aff. *bowerbankii*. **(A)** In El Corbiro Canyon (TF17, ECOMARG_0717). **(B)** In Le Danois Bank (TF9, ESMAREC_0514).

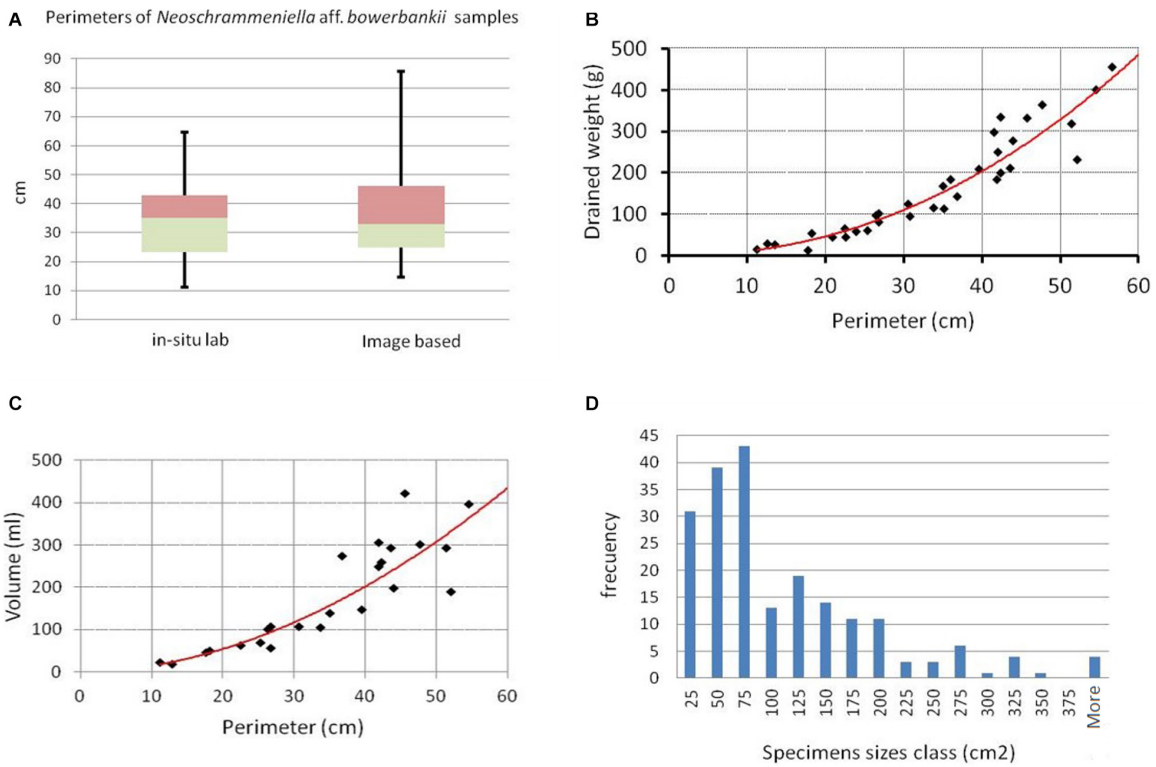

FIGURE 9 | (A) Perimeters of samples measured (lab *vs*. Image). **(B)** Relation Perimeter-Weight. **(C)** Relation Perimeter-Volume. **(D)** Population size distribution.

and subtropical Atlantic (Pomponi et al., 2001; Maldonado et al., 2017) and the south of New Caledonia (Lévi, 1991) and New Zealand (Kelly, 2007; Kelly et al., 2007).

The study area is subject to some management measures in the context of the Natura 2000 Framework, the "El Cachucho" MPA, that include Le Danois Bank, and the Site of Community Importance (SCI) Avilés Canyon System. For both Natura 2000 areas the main environmental value that has conditioned its protection policies is the presence of the habitat "1170 Reefs" of the European Habitat Directive (E.C, 2013). The sponge aggregations located on hard bottoms are included in this classification of vulnerable habitats on which it is mandatory for the European countries to establish conservation measures. In this sense, the knowledge of the habitats structured by lithistids sponges is essential to provide managers with indicators for monitoring the degree of the habitat's recovery in order to know the success of management measures and to ensure their adequate protection. Within the implementation of Marine Strategy Framework Directive (MSFD, E.C, 2008) it would be good to monitor those indicators that could help assess the environmental status of this vulnerable habitat. The methodologies described in this work will facilitate future monitoring of the MPAs using different indicators within the descriptor "Biological Diversity," such as the species distribution, the size and condition of their populations and some indicators in relation of deep-sea sponge aggregations (as distributional range, pattern and area covered) and condition of the typical species and communities (Borja et al., 2011, 2014). Among the indicators of "Sea-floor Integrity" descriptor of MSFD (Rice et al., 2012), the most suitable are estimates of the type, abundance, biomass

and the real extent of the biogenic substrate as well as all those indicators related to benthic community condition such as the presence of species on the seabed particularly sensitive and/or tolerant to human activities. Considering just those indicators in successive surveys and applying ground-truth sampling and photogrammetric techniques in representative biotopes of deep-sea sponge aggregations (using fixed sampling stations), the monitoring could be affordable and provide reliable results (Sánchez et al., 2017).

On the basis of the environmental characteristics required for the settlement of these sponges it is possible to obtain high resolution maps of their spatial distribution and identify potential impacts of anthropogenic uses. These approaches have already been used successfully in the study area by providing detailed maps needed for effective protection of gorgonians forest, deep-sea sponge aggregations and cold-water corals (Sánchez et al., 2014, 2017; Rodríguez-Basalo et al., 2019). The present study of the lithistids sponges should be taken into consideration for the design of the new management plan of the ACS.

The approach presented here to obtain the size of sponges demonstrate the consistency and reliability of SfM methodology. This is especially relevant in deep-sea environments where the access to the sizes of species is limited. The obtained results, giving a quadratic mean error of 0.10 cm in distance (using laser bean constant distance) and a retroprojection error of 0.154 pixels in image block adjustments, show very low values of geometric uncertainty, which validate the application of this approach for the measurement of parameters related to the size of sessile organism living on the sea bottom. Mean retroprojection errors values of less than 2 pixels were assumed as indicators of the effectiveness of SfM programs for creating highly accurate 3D reconstructions of underwater habitats (Burns and Delparte, 2017).

The relationship between surface area (2D) and volume (3D) metrics estimated using SfM, are particularly relevant when estimating the ecosystem services and functions performed by corals (House et al., 2018).

Surface area can be used as an indicator of structural habitat availability, which is an important ecosystem service of coral reefs and sponges (Santavy et al., 2013). The SfM technique shows a great potential for characterization and monitoring habitats and benthic communities. Thanks to the non-destructive nature it can be used in vulnerable habitats and protected areas, across multiple depths, scales, and reef types (Bythell et al., 2001; Cocito et al., 2003; Courtney et al., 2007; Burns et al., 2015a,b; Prado et al., 2019; Price et al., 2019). The high resolution cartographic outputs can increase the speed, scale and accuracy of species morphometric assessment. In addition, the methodologies based on SfM are quantitative and replicable, so these techniques, therefore allows detailed, spatially explicit observation of community change through time rather than purely typical qualitative descriptions (Ferrari et al., 2016).

"For sponges (Porifera), the amount of food available is directly proportional to the amount they can pump. All the mechanisms which could lead to induced current, depend on the flow regime around the sponge, the morphology of the sponge (mound-shaped or cylindrical) and the direction the apertures open into the flow" (Leys et al., 2011). It is, therefore key to fine-tune methodologies to evaluate the shape and size of the specimens of the different species. The relationship of these parameters to filtration rates is a complex matter in the deep-sea that has so far barely been addressed, with the exception of some experiments conducted with monitoring hoods placed on-site (Yahel et al., 2007; Maldonado et al., 2012, 2017; De Goeij et al., 2017). The progress in relating size (surface area) to volume and even biomass measurements (weight or volume) is essential to be able to understand basic processes of the biology of the species.

The accuracy of the adjustments obtained in the ratio of the size measures (perimeters) to weight and volume (R2 greater than 0.9 in both cases) make us consider a robust and logical relationship between the size of the specimens and the biomass and volume they provide in the habitat. These aspects are key not only for sponge aggregations but also for coral reefs, in this case with morphotype specific conversion parameters, the surface area and volume scale consistently with planar area (House et al., 2018) based on the SfM method. But this approach is still rarely mentioned in literature.

Photogrammetry provides accurate estimates of the surface and perimeters and the establishment of the relationship between *in situ* measurements and image-based measurements describing a relationship between lab conenchymal surface *versus* mesh surface calculation for *Paramuricea clavata* (Palma et al., 2018) but no known similar approximation has been made for lithistid sponges aggregations.

Common methods for measuring surface, area and volume of marine organisms include water displacement (Jokiel et al., 1978) and paraffin dipping (Stimson and Kinzie, 1991; Veal et al., 2010) and require in all cases the extraction of the specimens from seafloors. The use of extractive methodologies is usually banned for highly vulnerable species or in areas of special conservation. It is thus very important to develop and validate non-invasive methodologies to obtain morphometric parameters of the different species and subsequently, establish the empirical relationships between biological characteristics and the morphometry of the specimens. The morphometric measurements of a species can be determined using non-invasive methods and by applying obtained empirical relations, important information can be inferred from the biology of highly unknown benthic species.

DATA AVAILABILITY STATEMENT

The datasets generated for this study can be found at: https://doi.pangaea.de/10.1594/PANGAEA.910127.

AUTHOR CONTRIBUTIONS

All the authors conceived and designed the study. EP, PR, and FS analyzed the data. EP, FS, PR, and AR-B contributed to the

photogrammetry and structure from motion techniques. FS and JC led the ship surveys. PR, EP, and AR-B processed the video and image material. FS, JC, and JX acquired the funding. FC, AR-B, PR, and TI identified the fauna. All the authors helped to collect process and map field data, prepared the figures and tables, reviewed drafts of the manuscript, and helped to writing the manuscript.

FUNDING

This research has been performed in the scope of the SponGES project, which received funding from the European Union's Horizon 2020 Research and Innovation Programme under grant agreement no. 679849. This study was partially funded by the European Commission LIFE + "Nature and Biodiversity" call, and included in the INDEMARES (07/NAT/E/000732) and INTEMARES (LIFE15 IPE ES 012) projects. The Biodiversity Foundation, of the Ministry of Environment, was the institution responsible for coordination these projects.

ACKNOWLEDGMENTS

This study was made possible thanks to the invaluable work of all the participants in the five surveys involved and the crews of the R/Vs. *Vizconde de Eza* (SGPM), *Ramón Margalef* (IEO), and *Angeles Alvariño* (IEO). We appreciate the helpful assistance of Álvaro Altuna, Eugenia Manjón, Sergio Taboada, and Serge Gofas which helped identify associated fauna. We would like to thank Elena Isla for the careful revision of English, as well as to two reviewers for their valuable comments on the manuscript. We are especially grateful to Ines Fernández, Alejandra Calvo, and Cristina Boza for their help and technical support in the laboratory.

SUPPLEMENTARY MATERIAL

The Supplementary Material for this article can be found online at: https://www.frontiersin.org/articles/10.3389/fmars.2020.00578/full#supplementary-material

REFERENCES

Addamo, A. M., Vertino, A., Stolarski, J., García-Jiménez, R., Taviani, M., and Machordom, A. (2016). Merging scleractinian genera: the overwhelming genetic similarity between solitary *Desmophyllum* and colonial *Lophelia*. *BMC Evolut. Biol.* 16:108. doi: 10.1186/s12862-016-0654-8

Alder, J. (1856). A notice of some new genera and species of British hydroid zoophytes. *Ann. Magaz. Nat. History* 18, 12–14. doi: 10.1080/00222935608697652

Altuna, A. (2013). Scleractinia (Cnidaria: Anthozoa) from ECOMARG 2003, 2008 and 2009 expeditions to bathyal waters off north and northwest Spain (northeast Atlantic). *Zootaxa* 3641, 101–128. doi: 10.11646/zootaxa.3641.2.1

Altuna, A., and Ríos, P. (2014). Scleractinia (Cnidaria: Anthozoa) from INDEMARES 2010–2012 expeditions to the Avilés Canyon System (Bay of Biscay, Spain, northeast Atlantic). *Helgol Mar. Res.* 68, 399–430. doi: 10.1007/s10152-014-0398-z

Álvarez-Campos, P., Taboada, S., San Martín, G., Leiva, C., and Riesgo, A. (2018). Phylogenetic relationships and evolution of reproductive modes within flattened syllids (Annelida: Syllidae) with the description of a new genus and six new species. *Inverteb. Syst.* 32, 224–251. doi: 10.1071/IS17011

Asbjørnsen, P. C. (1856). Description d'un nouveau genre des Astéries in Sars, Koren, Danielssen eds. *Fauna Litt. Norw.* 2, 95–101.

Bean, T. C. (1844). *British Marine Conchology; Being a Descriptive Catalogue, Arranged According to the Lamarckian System, of The Salt Water Shells of Great Britain*. London: Edward Lumley.

Beazley, L. I., Kenchington, E. L., Murillo, F. J., and Sacau, M. (2013). Deep-sea sponge grounds enhance diversity and abundance of epibenthic megafauna in the Northwest Atlantic. *ICES J. Mar. Sci.* 70, 1471–1490. doi: 10.1093/icesjms/fst124

Bett, B. J., and Rice, A. L. (1992). The influence of hexactinellid sponge (*Pheronema carpenteri*) spicules on the patchy distribution of macrobenthos in the Porcupine Seabight (bathyal NE Atlantic). *Ophelia* 36, 217–226. doi: 10.1080/00785326.1992.10430372

Bo, M., Bertolino, M., Bavestrello, G., Canese, S., Giusti, M., Angiolillo, M., et al. (2012). Role of deep sponge grounds in the Mediterranean Sea: a case study in southern Italy. *Hydrobiologia* 687, 163–177. doi: 10.1007/s10750-011-0964-1

Boletín Oficial del Estado (2011). *(295) 130084–130138. 8 de Diciembre de 2011 (BOE-A-2011-19246)*. Madrid: Boletín Oficial del Estado.

Boletín Oficial del Estado (2014). *(293) 100065–100076. 4 de Diciembre de 2014 (BOE-A-2014-12628)*. Madrid: Boletín Oficial del Estado.

Borja, A., Galparsoro, I., Irigoien, X., Iriondo, A., Menchaca, I., Muxika, I., et al. (2011). Implementation of the European Marine Strategy Framework Directive: a methodological approach for the assessment of environmental status, from the Basque Country (Bay of Biscay). *Mar. Pollut. Bull.* 62, 889–904. doi: 10.1016/j.marpolbul.2011.03.031

Borja, A., Prins, T. C., Nomiki, S., Andersen, J. H., Torsten, B., Joao-Carlos, M., et al. (2014). Tales from a thousand and one ways to integrate marine ecosystem components when assessing the environmental status. *Front. Mar. Sci.* 1:72. doi: 10.3389/fmars.2014.00072

Bowerbank, J. S. (1866). *A Monograph of the British Spongiadae*, Vol. 2. London: Ray Society, 1–388.

Brunton, C. H. C., and Curry, G. B. (1979). *British Brachiopods. Keys and Notes for the Identification of the Species. Synopses of the British Fauna (New Series), N.S. 17*. London: Academic Press.

Burns, J. H. R., and Delparte, D. (2017). "Comparison of commercial structure-from-motion photogrammety software used for underwater three-dimensional modeling of coral reef environments," in *The International Archives of the Photogrammetry, Remote Sensing and Spatial Information Sciences. Vol. XLII-2/W3*, Nafplio, 127–131. doi: 10.5194/isprs-archives-XLII-2-W3-127-2017

Burns, J. H. R., Delparte, D., Gates, R. D., and Takabayashi, M. (2015a). Integrating structure-from-motion photogrammetry with geospatial software as a novel technique for quantifying 3D ecological characteristics of coral reefs. *PeerJ* 3:e1077. doi: 10.7717/peerj.1077

Burns, J. H. R., Delparte, D., Gates, R. D., and Takabayashi, M. (2015b). "Utilizing underwater three-dimensional modeling to enhance ecological and biological studies of coral reefs," in *The International Archives of the Photogrammetry, Remote Sensing and Spatial Information Sciences, XL-5/W5*, Italy. doi: 10.5194/isprsarchives-XL-5-W5-61-2015

Bythell, J., Pan, P., and Lee, J. (2001). Three-dimensional morphometric measurements of reef corals using underwater photogrammetry techniques. *Coral Reefs* 20, 193–199. doi: 10.1007/s003380100157

Cairns, S. D. (1979). The deep-water Scleractinia of the Caribbean and adjacent waters. *Stud. Fauna Curacao.* 57:341.

Cairns, S. D., and Bayer, F. M. (2009). *A generic revision and phylogenetic analysis of the Primnoidae (Cnidaria:Octocorallia). Smithsonian Contributions to Zoology, 629*. Washington DC: Smithsonian Institution Press, 79. doi: 10.5479/si.00810282.629

Cairns, S. D., and Taylor, M. L. (2019). An illustrated key to the species of the genus *Narella* (Cnidaria, Octocorallia, Primnoidae). *ZooKeys* 822, 1–15. doi: 10.3897/zookeys.822.29922

Calvet, L. (1907). Bryozoaires. Expeditions scientifiques du "Travailleur" et du "Talisman" pendant les annees 1880–1883. *Paris* 8, 355–495.

Calvet, L. (1931). Bryozoaires provenant des campagnes scientifiques du prince albert ier de monaco. *Rés. Camp. Sci. Prince Monaco* 83, 1–152.

Cárdenas, P., Vacelet, J., Chevaldonné, P., Pérez, T., and Xavier, J. R. (2018). "From marine caves to the deep sea, a new look at *Caminella* (Demospongiae, Geodiidae) in the Atlanto-Mediterranean region," in *Deep Sea and Cave Sponges*, Vol. 4466, eds M. Klautau, T. Pérez, P. Cárdenas, and N. de Voogd (Auckland: Magnolia Press), 174–196. doi: 10.11646/zootaxa.4466.1.14

Carter, H. J. (1876). Descriptions and Figures of Deep-Sea Sponges and their Spicules, from the Atlantic Ocean, dredged up on board H.M.S.'Porcupine', chiefly in 1869 (concluded). *Ann. Mag. Natl. History* 18, 226–240. doi: 10.1080/00222937608682035

Cartes, J. E., Huguet, C., Parra, S., and Sanchez, F. (2007). Trophic relationships in deep-water decapods of Le Danois bank (Cantabrian Sea, NE Atlantic): trends related with depth and seasonal changes in food quality and availability. *Deep Sea Res. Part I* 54, 1091–1110. doi: 10.1016/j.dsr.2007.04.012

Carvalho, F. C., Pomponi, S. A., and Xavier, J. R. (2015). Lithistid sponges of the upper bathyal of Madeira, Selvagens and Canary Islands, with description of a new species of *Isabella*. *J. Mar. Biol. Assoc. U. K.* 95, 1287–1296. doi: 10.1017/S0025315414001179

Carpenter, P. H. (1888). Report on the Crinoidea collected during the voyage of H.M.S. Challenger, during the years 1873-76. Part II. The Comatulae. Reports of the Scientific Results of the Voyage of H.M.S. Challenger. *Zoology* 26(Pt 60), 1–70.

Cathalot, C., van Oevelen, D., Cox, T. J. S., Kutti, T., Lavaleye, M., Duineveld, G., et al. (2015). Cold-water coral reefs and adjacent sponge grounds: hot spots of benthic respiration and organic carbon cycling in the deep sea. *Front. Mar. Sci.* 2:37. doi: 10.3389/fmars.2015.00037

Caullery, M. (1896). Résultats scientifiques de la Campagne du "Caudan" dans le Golfe de Gascogne. Aout-Septembre 1985. Crustacés schizopodes et décapodes. *Ann. Univ. Lyon* 2, 365–419.

Cherbonnier, G. (1969). Echinodermes récoltés par la Thalassa au large des côtes ouest de Bretagne et du golfe de Gascogne (3-12 aout 1967). *Bull. Mus. Natl. His. Nat. Paris. Ser.* 2, 343–361.

Christiansen, S. (2010). Background document for deep-sea sponge aggregations. *Ospar Convent. Biodivers. Ser.* 46:508.

Chu, J. W. F., and Leys, S. P. (2010). High resolution mapping of community structure in three glass sponge reefs (Porifera, Hexactinellida). *Mar. Ecol. Progr. Ser.* 417, 97–113. doi: 10.3354/meps08794

Clark, A. M. (1980). Crinoidea collected by the Meteor and Discovery in the NE Atlantic. *Bull. Br. Mus. Nat. History (Zoology)* 38, 187–210.

Clark, A. M., and Downey, M. E. (1992). *Starfishes of the Atlantic. Chapman & Hall Identification Guides, 3*, Vol. xxvi. London: Chapman & Hall, 794.

Cocito, S., Sgorbini, S., Peirano, A., and Valle, M. (2003). 3-D reconstruction of biological objects using underwater video technique and image processing. *J. Exp. Mar. Biol. Ecol.* 297, 57–70. doi: 10.1016/S0022-0981(03)00369-1

Costa, O. G. (1830 ["1829"]). Catalogo sistematico e ragionato de' testacei delle Due Sicilie. *Tipogr. Della Min. Napoli* 30, 1–3.

Courtney, L. A., Fisher, W. S., Raimondo, S., Oliver, L. M., and Davis, W. P. (2007). Estimating 3-dimensional colony surface area of field corals. *J. Exp. Mar. Biol. Ecol.* 351, 234–242. doi: 10.1016/j.jembe.2007.06.021

De Goeij, J. M., Lesser, M. P., and Pawlik, J. R. (2017). "Nutrient fluxes and ecological functions of coral reef sponges in a changing ocean," in *Climate Change, Ocean Acidification and Sponges*, eds J. L. Carballo and J. J. Bell (Berlin: Springer), 373–410. doi: 10.1007/978-3-319-59008-08

De Goeij, J. M., Moodley, L., and Houtekamer, M. (2008). Tracing 13C-enriched dissolved and particulate organic carbon in the bacteria-containing coral reef sponge *Halisarca caerulea*: evidence for DOM feeding. *Limnol. Oceanogr.* 53, 1376–1386. doi: 10.4319/lo.2008.53.4.1376

De Goeij, J. M., van Oevelen, D., and Vermeij, M. J. A. (2013). Surviving in a marine desert: the sponge loop retains resources within coral reefs. *Science* 342, 108–110. doi: 10.1126/science.1241981

D'Hondt, J. L. (1974). Bryozoaires récoltés par la « Thalassa » dans le Golfe de Gascogne. (Campagnes de 1968 à 1972). *Cah. Biol. Mar.* 15, 27–50.

Dautzenberg, P., and Fischer, H. (1896). Dragages effectués par l'Hirondelle et par la Princesse Alice 1888-1895. 1. Mollusques gastéropodes. *Mém. Soc. Zool. France* 9, 395–498.

E.C. (2008). *Directive 2008/56/EC of the European Parliament and of the Council of 17 June 2008, Establishing a Framework for Community Action in the field of Marine Environmental Policy (Marine Strategy Framework Directive). Official Journal of the European Union L164*. Maastricht: European Union, 19–40.

E.C. (2013). *Interpretation Manual of European Union Habitats. EUR28. European Commision DG Environment*. Maastricht: European Union, 144.

FAO (2009). *International Guidelines for the Management of Deep-Sea Fisheries in the High Seas*. Rome: FAO, 73.

Esper, E. J. C. (1794). Fortsetzungen der Pflanzenthiere. *Nürnberg* 1:64.

Fernández-Rodríguez, I., Arias, A., Anadón, N., and Acuña, J. L. (2019). Holothurian (Echinodermata) diversity and distribution in the central cantabrian sea and the avilés canyon system (Bay of Biscay). *Zootaxa* 4567, 293–325. doi: 10.11646/zootaxa.4567.2.5

Ferrari, R., McKinnon, D., He, H., Smith, R. N., Corke, P., González-Rivero, M., et al. (2016). Quantifying multiscale habitat structural complexity: a cost-effective framework for underwater 3D modelling. *RemoteSensing* 8:113. doi: 10.3390/rs8020113

Fillinger, L., Janussen, D., Lundälv, T., and Richter, C. (2013). Rapid glass sponge expansion after climate-induced Antarctic ice shelf collapse. *Curr. Biol.* 23, 1–5. doi: 10.1016/j.cub.2013.05.051

Fleming, J. (1820). Observations on the natural history of Sertularia gelatinosa of Pallas. *Edinbur. Philos. J.* 2, 82–89.

García-Alegre, A., Sánchez, F., Gómez-Ballesteros, M., Hinz, H., Serrano, A., and Parra, S. (2014). Modelling and maping the local distribution of representative species on the Le Danois Bank, El Cachucho Marine Protected Area (Cantabrian Sea). *Dep Sea Res. II* 106, 151–164. doi: 10.1016/j.dsr2.2013.12.012

Giglioli, E. H. (1884). "Esplorazione talassografica del Mediterraneo eseguita sotto gli auspici del governo italiano," in *Pelagos. Saggi Sulla Vita e Sui Prodotti Del Mare. Reale Instituto de' Sordo-Muti*, eds F. Gigliogli, E. Haa, and A. Issel (Genova: Esplorazione talassografica del Mediterraneo eseguita sotto gli auspici del governo italiano), 199–291.

Gomez-Ballesteros, M., Druet, M., Muñoz, A., Arrese, B., Rivera, J., Sánchez, F., et al. (2014). Geomorphology of the avilés canyon system, cantabrian sea (Bay of Biscay). *Deep Sea Res.* 106, 99–117. doi: 10.1016/j.dsr2.2013.09.031

Gravier, C. (1920). Madréporaires provenant des campagnes des yachts Princesse Alice et Hirondelle II (1893-1913). *Rés. Cam. Sci. Prince Monaco* 55, 1–123. doi: 10.5962/bhl.title.50363

Gray, J. E. (1858). On *Aphrocallistes*, a new genus of *Spongiadae* from malacca. *Proc. Zool. Soc. Lond.* 26, 114–115.

Gunnerus, J. E. (1767). Beskrifning på trenne Norrska Sjö-Kråk, Sjö-Pungar kallade. Kungl. *Svens. Vetenskaps. Handl.* 28, 114–124.

Hawkes, N., Korabik, M., Beazley, L., Rapp, H. T., Xavier, J. R., and Kenchington, E. L. (2019). Glass sponge grounds on the Scotian Shelf and their associated biodiversity. *Mar. Ecol. Prog. Ser.* 614, 91–109. doi: 10.3354/meps12903

Hincks, T. (1855). Notes on British zoophytes, with description of new species. *Ann. Mag. nat. Hist.* 215, 127–130.

Hogg, M. M., Tendal, O. S., Conway, K. W., Pomponi, S. A., van Soest, R. W. M., Gutt, J., et al. (2010). *Deep-Sea Sponge Grounds: Reservoirs of Biodiversity. UNEP-WCMC Biodiversity Series No. 32*. Cambridge: UNEP-WCMC.

Hooper, J. N. A., and van Soest, R. W. M. (2002). *A guide to the classification of sponges*, Vol. 2. New York, NY: Kluwer Academic/ Plenum Publishers, 1706.

House, J. E., Brambilla, V., Bidaut, L. M., Christie, A. P., Pizarro, O., Madin, J. S., et al. (2018). Moving to 3D: relationships between coral planar area, surface area and volume. *PeerJ* 6:e4280. doi: 10.7717/peerj.4280

Huetten, E., and Greinert, J. (2008). Software controlled guidance, recording and post-processing of seafloor observations by ROV and other towed devices: The software package OFOP. *Geophys. Res. Abstr.* 10:3088.

Hughes, S. W. (2005). Archimedes revisited: a faster, better, cheaper method of accurately measuring the volume of small objects. *Phys. Educ.* 40, 468–474. doi: 10.1088/0031-9120/40/5/008

James, M. R., and Robson, S. (2012). Straightforward reconstruction of 3D surfaces and topography with a camera: accuracy and geosciences application. *J. Geophys. Res.* 117:F03017. doi: 10.1029/2011JF002289

Johnson, J. Y. (1862). Descriptions of some new corals from Madeira. *Proc. Zool. Soc. Lond.* 1862, 194–197.

Johnson, J. Y. (1863). Description of a new siliceous sponge from the coast of Madeira. *Proc. Zool. Soc. Lond.* 1863, 257–259.

Jokiel, R. L., Maragos, J. E., and Franzisket, L. (1978). "Coral growth: buoyant weight technique," in *Coral Reef Research Methods*, eds D. R. Stoddart and R. E. Johannes (Paris: United Nations Educational, Scientific and Cultural Organization), 529–542.

Jullien, J., and Calvet, L. (1903). Bryozoaires provenant des campagnes de l'Hirondelle (1886-1888). *Result. Campag. Sci. Accom. Yacht Albert Prince Souver. Monaco.* 23, 1–188.

Kazanidis, G., Henry, L. A., Roberts, J. M., and Witte, U. F. M. (2016). Biodiversity of *Spongosorites coralliophaga* (Stephens, 1915) on coral rubble at two contrasting cold-water coral reef settings. *Coral Reefs* 35, 193–208. doi: 10.1007/s00338-015-1355-2

Kazanidis, G., Vad, J., Henry, L. A., Neat, F., Berx, B., Georgoulas, K., et al. (2019). *Seabed Images and Corresponding Environmental Data From Deep-Sea Sponge Aggregations in the Faroe-Shetland Channel Nature Conservation Marine Protected Area*. Amsterdam: PANGAEA, doi: 10.1594/PANGAEA.897604

Kelly, M. (2007). *The Marine Fauna of New Zealand. Porifera: Lithistid Demospongiae (Rock Sponges). The Marine Fauna of New Zealand*. Wellington: National Institute of Water and Atmospheric Research (NIWA).

Kelly, M., Ellwood, M., Tubbs, L., and Buckeridge, J. (2007). "The lithistid Demospongiae in New Zealand waters: species composition and distribution," in *Porifera Research: Biodiversity, Innovation and Sustainability*, eds M. R. Custódio, G. Lôbo-Hajdu, E. Hajdu, and G. Muricy (Rio de Janeiro: Museu Nacional du Rio de Janeiro, vol série livros), 393–404.

Klitgaard, A. B. (1995). The fauna associated with outer shelf and upper slope sponges (Porifera, Demospongiae) at the Faroe Islands, northeastern Atlantic. *Sarsia* 80, 1–22. doi: 10.1080/00364827.1995.10413574

Klitgaard, A. B., and Tendal, O. S. (2004). Distribution and species composition of mass occurrences of large-sized sponges in the northeast Atlantic. *Prog. Oceanogr.* 61, 57–98. doi: 10.1016/j.pocean.2004.06.002

Kœhler, R. (1895). Dragages profonds executes a bord du Caudan dans le Golfe de Gascogne. Rapport préliminaire sur le Échinodermes. *Revue biologique du Nord de la France* 7, 439–496.

Kœhler, R. (1896). "Échinodermes," in *Résultats scientifiques de la campagne du "Caudan" dans le Golfe de Gascogne — août-septembre 1895*, Vol. 26, ed. R. Koehler (Lyon: Université de Lyon), I–IV. doi: 10.5962/bhl.title.65730

Kunzmann, K. (1996). Associated fauna of selected sponges (Hexactinellida and Demospongiae) from the Weddell Sea. Antarctica. *Rep. Polar Res.* 210, 1–93.

Kutti, T., Bannister, R. J., and Fossa, J. H. (2013). Community structure and ecological function of deep-water sponge grounds in the Traenadypet MPA-Northern Norwegian continental shelf. *Cont. Shelf Res.* 69, 21–30. doi: 10.1016/j.csr.2013.09.011

Kwasnitschka, T., Hansteen, T. H., Devey, C. W., and Kutterolf, S. (2013). Doing fieldwork on the seafloor: photogrammetric techniques to yield 3D visual models from ROV video. *Comput. Geosci.* 52, 218–226. doi: 10.1016/j.cageo.2012.10.008

Lamarck, J. B. M. (1816). *Histoire Naturelle des Animaux sans Vertèbres. Tome Second*. Paris: Verdière, 568.

Lavy, A., Eyal, G., Neal, B., Keren, R., Loya, Y., Ilan, M., et al. (2015). A quick, easy and non-intrusive method for underwater volume and surface area evaluation of benthic organisms by 3D computer modelling. *Methods Ecol. Evol.* 6, 521–531. doi: 10.1111/2041-210X.12331

Leach (1815-1875). *Malacostraca Podophthalmata Britanniae; or Descriptions of Such British Species of the Linnean Genus Cancer as Have Their Eyes Elevated on Footstalks*. London: John Sowerby, 124.

Lendenfeld, R. (1894). Eine neue pachastrella. sitzungsberichte der kaiserlichen akademie der wissenschaften. *Mathem. Naturwissens. Classe* 103, 439–442.

Lévi, C. (1991). "Lithistid sponges from the Norfolk Rise: recent and Mesozoic genera," in *Fossil and Recent Sponges*, eds J. Reitner and H. Keupp (Berlin: Springer-Verlag Publishers), 72–82. doi: 10.1007/978-3-642-75656-6_7

Leys, S. P., Yahel, G., Reidenbach, M. A., Tunnicliffe, V., Shavit, U., and Reiswig, H. M. (2011). The sponge pump: the role of current induced flow in the design of the sponge body plan. *PLoS One* 6:e27787. doi: 10.1371/journal.pone.0027787

Linnaeus, C. (1758). *Systema Naturae per Regna tria Naturae, Secundum Classes, Ordines, Genera, Species, cum Characteribus, Differentiis, Synonymis, Locis. Editio Decima, Reformata [10th Revised Edition]*, Vol. 1. Holmiae: Laurentius Salvius, 824.

Lloris, D. (2015). Ictiofauna marina. Manual de identificación de los peces marinos de la península ibérica y Baleares. *Edit. Omega* 15:674.

Louisy, P. (2002). Guide d'identification des Poissons Marins. Europe et Méditerranée. *Edit. Ulmer* 2:429.

Lyman, T. (1879). *Ophiuridae and Astrophytidae of the "Challenger" Expedition. Part II*, Vol. 6. Cambridge, Ma: Harvard College, 17–83.

M'Andrew, R., and Barrett, L. (1857). List of the echinodermata dredged between drontheim and the north cape. *Ann. Mag. Nat. History* 20, 43–44.

Maldonado, M., Aguilar, R., Bannister, R. J., Bell, J. J., Conway, K. W., Dayton, P. K., et al. (2017). "Sponge grounds as key marine habitats: a synthetic review of types, structure, functional roles, and conservation concerns," in *Marine Animal Forests: The Ecology of Benthic Biodiversity Hotspots*, eds S. Rossi, L. Bramanti, A. Gori, and C. Orejas (Berlín: Springer International Publishing), 145–183. doi: 10.1007/978-3-319-17001-5_24-1

Maldonado, M., Aguilar, R., Blanco, J., García, S., Serrano, A., and Punzón, A. (2015). Aggregated clumps of lithistid sponges: a singular, reef-like bathyal habitat with relevant paleontological connections. *PloS One* 10:e0125378. doi: 10.1371/journal.pone.0125378

Maldonado, M., López-Acosta, M., Sitjà, C., et al. (2019). Sponge skeletons as an important sink of silicon in the global oceans.Nat. *Geosci.* 12, 815–822. doi: 10.1038/s41561-019-0430-7

Maldonado, M., Ribes, M., and van Duyl, F. C. (2012). Nutrient fluxes through sponges: biology, budgets, and ecological implications. *Adva. Mar. Biol.* 62, 114–182. doi: 10.1016/B978-0-12-394283-8.00003-5

Manjón-Cabeza, M. E., Palma-Sevilla, N., Gómez-Delgado, A. I, Andrino-Abelaira, J., and Ríos, P. (2014). "Echinoderms assemblages of Aviles canyons (preliminary results) (Biscay Bay) (INDEMARES+LIFE Project)," in *XVIII Simposio Ibérico de Estudios de Biología Marina. Libro de resúmenes*, eds P. Ríos, L. A. Suárez, and J. Cristobo (Gijón : Centro Oceanográfico de Gijón).

McCarthy, J., and Benjamin, J. (2014). Multi-image photogrammetry for underwater archaeological site recording: an accessible, diverbased approach. *J. Mar. Archaeol.* 9, 95–114. doi: 10.1007/s11457-014-9127-7

McIntyre, F. D., Drewery, J., Eerkes-Medrano, D., and Neat, F. C. (2016). Distribution and diversity of deep-sea sponge grounds on the rosemary bank seamount, NE Atlantic. *Mar. Biol.* 163:143. doi: 10.1007/s00227-016-2913-z

Meyer, H. K., Roberts, E. M., Rapp, H. T., and Davies, A. J. (2019). Spatial patterns of arctic sponge ground fauna and demersal fish are detectable in autonomous underwater vehicle (AUV) imagery. *Deep Sea Res. Part I* 19:103137 doi: 10.1016/j.dsr.2019.103137

Milne-Edwards, A., and Bouvier, E. L. (1894). Considerations génerales sur la famille des Galatheides. *Ann. Sci. Nat. Zool.* 16, 191–327.

Míguez, L. J. (2009). *Equinodermos (Crinoideos, Equinoideos y Holothuroideos) Litorales, Batiales y Abisales de Galicia*. 864. Ph.D. Thesis, Universidad de Santiago de Compostela, Santiago de Compostela.

Molodtsova, T. N. (2006). "Black corals (Antipatharia: Anthozoa: Cnidaria) of North-East Atlantic," in *Biogeography of the North Atlantic seamounts*, eds A. N. Mironov, A. V. Gebruk, and A. J. Southward (Moscow: KMK Press), 141–151.

Morrow, C., and Cárdenas, P. (2015). Proposal for a revised classification of the Demospongiae (Porifera). *Front. Zool.* 12:7. doi: 10.1186/s12983-015-0099-8

Mortensen, T. (1935). *A Monograph of the Echinoidea. II. Bothriocidaroida, Melonechinoida, Lepidocentroida, and Stirodonta*, ed. C. A. Reitzel (London: Oxford University Press), 647.

Müller, O. F. (1776). *Zoologiæ Danicæ Prodromus, seu Animalium Daniæ et Norvegiæ Indigenarum Characteres, Nomina, et Synonyma Imprimis Popularium*. Copenhagen: Hallageri, 274.

Müller, J., and Troschel, F. H. (1842). *System der Asteriden. 1. Asteriae. 2. Ophiuridae*. Vieweg: Braunschweig, 12.

Murillo, F. J., Durán Muñoz, P., Cristobo, J., Ríos, P., González, C., Kenchington, E., et al. (2012). Deep-sea sponge grounds of the Flemish Cap, Flemish Pass and the Grand Banks of Newfoundland (Northwest Atlantic Ocean): Distribution and species composition. *Mar. Biol. Res.* 8, 842–854. doi: 10.1080/17451000.2012.682583

Negri, M. P., and Corselli, C. (2016). Bathyal Mollusca from the cold-water coral biotope of Santa Maria di Leuca (Apulian margin, southern Italy). *Zootaxa* 4186, 1–97. doi: 10.11646/zootaxa.4186.1.1

Pallas, P. S. (1766). *Elenchus Zoophytorum Sistens Generum Adumbrationes Generaliores et Specierum Cognitarum Succintas Descriptiones, Cum Selectis Auctorum Synonymis*. Hagae: Fransiscum Varrentrapp, 451.

Palma, M., Rivas, M., Pantaleo, U., Pavoni, G., Pica, D., and Cerrano, C. (2018). SfM-based method to assess gorgonian forests (*Paramuricea clavata* (Cnidaria, Octocorallia)). *Remote Sensing* 10:1154. doi: 10.3390/rs10071154

Paterson, G. L. J. (1985). The deep-sea Ophiuroidea of the north Atlantic Ocean. *Bull. Br. Mus. (Natl. Hist.) Zool.* 49, 1–162.

Pomponi, S. A., Diaz, M. C., Vs, R. W. M., Bell, L. J., Busutil, L., Gochfeld, D. J., et al. (2019). "Sponges," in *Mesophotic Coral Ecosystems. Coral Reefs of the World*, Vol. 12, eds Y. Loya, K. Puglise, and T. Bridge (Cham: Springer).

Pomponi, S. A., Kelly, M., Reed, J. K., and Wright, A. (2001). Diversity and bathymetric distribution of lithistid sponges in the tropical western Atlantic region. *Bull. Biol. Soc. Washing.* 10, 344–353.

Pouliquen, L. (1972). Les spongiaires des grottes sous-marines de la région de Marseille: Ecologie et systématique. *Téthys* 3, 717–758.

Powell, A., Clarke, M. E., Fruh, E., Chaytor, J. D., Reiswig, H. M., and Whitmire, C. E. (2018). Characterizing the sponge grounds of grays canyon, Washington, USA. *Deep Sea Res. Part II Top. Stud. Oceanogr.* 150, 146–155. doi: 10.1016/j dsr2.2018.01.004

Prado, E., Sánchez, F., Rodríguez-Basalo, A., Altuna, A., and Cobo, A. (2019). Analysis of the population structure of a gorgonian forest (*Placogorgia* sp.) using a photogrammetric 3D modeling approach at Le Danois Bank, Cantabrian Sea. *Deep Sea Res. Part I* 153:3124. doi: 10.1016/j.dsr.2019.103124

Preciado, I., Cartes, J. E., Serrano, A., Velasco, F., Olaso, I., Sánchez, F., et al. (2009). Resource utilisation by deepsea sharks at the Le Danois Bank, Cantabrian Sea, north-east Atlantic Ocean. *J. Fish Biol.* 75, 1331–1351. doi: 10.1111/j.1095-8649.2009.02367.x

Prestandrea, N. (1839). Descrizione di due nuovi crustacei dei mari di messina. *Atti Accad. Gioe. Sci. Nat. Cat.* 2, 131–136.

Price, D., Robert, K., Callaway, A., Lo lacono, C., Hall, R. A., and Huvenn, V. A. I. (2019). Using 3D photogrammetry from ROV video to quantify coldwater coral reef structural complexity and investigate its influence on biodiversity and community assemblage. *Coral Reefs* 38, 1007–1021. doi: 10.1007/s00338-019-01827-3

Ramiro-Sánchez, B., González-Irusta, J. M., Henry, L. A., Cleland, J., Yeo, I., Xavier, J. R., et al. (2019). Characterization and mapping of a deep-sea sponge ground on the tropic seamount (northeast tropical atlantic): implications for spatial management in the high seas. *Front. Mar. Sci.* 6:278. doi: 10.3389/fmars.2019.00278

Rice, J., Arvanitidis, C., Borja, A., Frid, C., Hiddink, J., Krause, J., et al. (2012). Indicators for sea-floor integrity under the european marine strategy framework directive. *Ecol. Indic.* 12, 174–184. doi: 10.1016/j.ecolind.2011.03.021

Ridley, S. O., and Duncan, P. M. (1881). On the genus *Plocamia*, schmidt, and on some other sponges of the order echinonemata. with descriptions of two additional new species of dirrhopalum. *J. Linn. Soc. Zool.* 15, 476–497.

Rioja, E. (1931). Estudio de los poliquetos de la Península Iberica. Memorias de la Academia de Ciencias Exactas, Físicas y Naturales de Madrid. *Serie Cienc. Natur.* 2, 1–471.

Ríos, P., Aguilar, R., Torriente, A., Muñoz, A., and Cristobo, J. (2018). Sponge grounds of *Artemisina* (Porifera, Demospongiae) in the Iberian Peninsula, ecological characterization by ROV techniques. *Zootaxa* 4466, 095–123. doi: 10.11646/zootaxa.4466.1.10

Risso, A. (1810). Ichthyologie de Nice, ou histoire naturelle des poissons du Département des Alpes Maritimes. *F. Schoell Paris* 10, 1–11.

Rodríguez-Basalo, A., Sánchez, F., Punzón, A., and Gómez-Ballesteros, M. (2019). Updating the Master Management Plan for El Cachucho MPA (Cantabrian Sea) using a spatial planning approach. *Cont. Shelf Res.* 19:10. doi: 10.1016/j.csr.2019.06.010

Rolando, L. (1822). (1821 volume). Description d'un animal nouveau qui appartient à la classe des Echinodermes. *Mem. Della Reale Accad. Delle Sci. Torino.* 26, 539–556.

Rouse, G., and Pleijel, F. (2001). *Polychaetes*. Oxford: Oxford University Press, 354.

Sánchez, F. (2015). *Manual PescaWin 2015. Programa de Monitorización de Muestreos en Campañas de Investigación*. Madrid: Instituto Español de Oceanografía, doi: 10.13140/RG.2.1.3786.5684

Sánchez, F., González-Pola, C., Druet, M., García-Alegre, A., Acosta, J., Cristobo, J., et al. (2014). Habitat characterization of deep-water coral reefs in La Gaviera canyon (Avilés Canyon System, Cantabrian Sea). *Deep Sea Res. Part II.* 106, 118–140. doi: 10.1016/j.dsr2.2013.12.014

Sánchez, F., Rodríguez, A., García-Alegre, A., and Gómez-Ballesteros, M. (2015). Mapping the 1170 reefs habitat of EU Directive of bathial grounds of Le Danois Bank (El Cachucho MPA, Cantabrian Sea). VIII Simposio sobre el Margen Ibérico Atlántico. *Abstract Book* 15, 683–686.

Sánchez, F., and Rodríguez, J. M. (2013). POLITOLANA, a new low cost towed vehicle designed for the characterization of the deep-sea floor. *Instrument. Viewpoint* 15:69.

Sánchez, F., Rodríguez-Basalo, A., García-Alegre, A., and Gómez-Ballesteros, M. (2017). Hard-bottom bathyal habitats and keystone epibenthic species on Le Danois Bank (Cantabrian Sea). *J. Sea Res.* 130, 134–153. doi: /10.1016/j.seares.2017.09.005

Sánchez, F., Serrano, A., Parra, S., Ballesteros, M., and Cartes, J. E. (2008). Habitat characteristics as determinant of the structure and spatial distribution of epibenthic and demersal communities of Le Danois Bank (Cantabrian Sea, N. Spain). *J. Mar. Syst.* 72, 64–86. doi: 10.1016/j.jmarsys.2007.04.008

Sánchez, F. M., Serrano, A. G., and Ballesteros, M. G. (2009). Photogrammetric quantitative study of habitat and benthic communities of deep Cantabrian Sea hard grounds. *Contin. Shelf Res.* 29, 1174–1188. doi: 10.1016/j.csr.2009.01.004

Santavy, D. H., Courtney, L. A., Fisher, W. S., Quarles, R. L., and Jordan, S. J. (2013). Estimating surface area of sponges and gorgonians as indicators of habitat availability on Caribbean coral reefs. *Hydrobiologia* 707, 1–16. doi: 10.1007/s10750-012-1359-7

Schmidt, O. (1868). *Die Spongien der Küste von Algier. Mit Nachträgen zu den Spongien des Adriatischen Meeres (Drittes Supplement)*, Vol. i–iv. Leipzig: Wilhelm Engelmann, 1–44.

Schmidt, O. (1870). *Grundzüge Einer Spongien-Fauna des Atlantischen Gebietes*, Vol. iii-iv. Leipzig: Wilhelm Engelmann, 1–88.

Schmidt, O. (1875). Spongien. die expedition zur physikalisch-chemischen und biologischen untersuchung der nordsee im sommer 1872. *Jahresb. Commis. Wissensch. Untersuch. Deuts. Meere Kiel* 2–3, 115–120.

Sollas, W. J. (1886). Preliminary account of the Tetractinellid sponges Dredged by H.M.S. 'Challenger' 1872-76. Part I. The choristida. *Sci. Proc. R. Dublin Soc. (New Ser.)* 5, 177–199.

Sollas, W. J. (1888). Report on the Tetractinellida collected by H.M.S. Challenger, during the years 1873–1876. *Zoology* 25(Pt 63), 1–458.

Southward, E. C., and Campbell, A. C. (2006). *Echinoderms. Linnean Society Synopses of the British Fauna (New Series)*, Vol. 56. Telford: FSC Publications, 272.

Stephens, J., and Hickson, S. J. (1909). Alcyonarian and madreporarian corals of the Irish coasts, with description of a new species of *Stachyodes*. department of agriculture and technical instruction for fisheries, ireland, fisheries branch, Scientific. *Investigations.* 1907, 1–18. doi: 10.5962/bhl.title.33355

Stimson, J., and Kinzie, R. A. I. I. I. (1991). The temporal pattern and rate of release of zooxanthellae from the reef coral *Pocillopora damicornis*(Linnaeus) under nitrogen-enrichment and control conditions. *J. Exp. Mar. Biol. Ecol.* 153, 63–74. doi: 10.1016/S0022-0981(05)80006-1

Süssbach, S., and Breckner, A. (1911). Die Seeigel, Seesterne und Schlangensterne der Nord- und Ostsee. Wissenschaftliche Meeresuntersuchungen, Kommission zur wissenschaftlichen Untersuchung der deutschen Meere in Kiel. *Neue Folge* 12, 167–300.

Topsent, E. (1892). Contribution à l'étude des Spongiaires de l'Atlantique Nord (Golfe de Gascogne, Terre-Neuve, Açores). Résultats des campagnes scientifiques accomplies par le Prince Albert I. *Monaco* 2, 1–165.

Thomson, C. W. (1869). On holtenia, a Genus and of *Vitreus sponges*. *Proc. R. Soc. Lond.* 18, 32–35.

Thomson, C. W. (1872). "On the echinidea of the 'porcupine' deep-sea dredging-expeditions," in *Proceedings of the Royal Society of London*, Vol. 20, London, 491–497. doi: 10.1098/rspl.1871.0095

Thomson, J. A. (1929). Alcyonaires des environs de Monaco et de localités diverses. *Bulletin de l'Institut Océanographique* 10:534

Tola, E., Lepetit, V., and Fua, P. (2010). DAISY: an efficient dense descriptor applied to wide-baseline stereo. *IEEE Transact. Patt. Anal. Mach. Intell.* 32, 815–830. doi: 10.1109/TPAMI.2009.77

Topsent, E. (1890). Notice préliminaire sur les spongiaires recueillis durant les campagnes de l'Hirondelle. *Bull. Soc. Zool. France* 15, 65–71. doi: 10.5962/bhl.part.18721

Van Rooij, D., Iglesias, J., Hernández-Molina, F. J., Ercilla, G., Gomez-Ballesteros, M., Casas, D., et al. (2010). The le danois contourite depositional system:

interactions between the mediterranean outflow water and the upper cantabrian slope (north iberian margin). *Mar. Geol.* 274, 1–20. doi: 10.1016/j.margeo.2010.03.001

Veal, C. J., Carmi, M., Fine, M., and Hoegh-Guldberg, O. (2010). Increasing the accuracy of surface area estimation using single wax dipping of coral fragments. *Coral Reefs* 29, 893–897. doi: 10.1007/s00338-010-0647-9

Velasco, E. M., Amez, M. A., and Punzón, A. (2013). *Especies de Interés Pesquero en Galicia, Asturias y Cantabria*. Madrid: Ministerio de Economía y Competitividad, 218.

Verrill, A. E. (1878). Notice of recent additions to the marine fauna of the eastern coast aof North America, No. 2. Brief contributions to zoology from the Museum of Yale College, No. 39. *Am. J. Sci. Arts Third Ser.* 16, 371–378.

Vosmaer, G. C. J. (1894). Preliminary notes on some tetractinellids of the Bay of Naples. *Tijdschr. Nederland. Dierkund. Vereeniging.* 4, 269–286.

Westoby, M. J., Brasington, J., Glasser, N. F., Hambrey, M. J., and Reynolds, J. M. (2012). Structure-from-Motion' photogrammetry: a low-cost, effective tool for geoscience applications. *Geomorphology* 179, 300–314. doi: 10.1016/j.geomorph.2012.08.021

Wisshak, M., López Correa, M., Gofas, S., Salas, C., Taviani, M., Jakobsen, J., et al. (2009). Shell architecture, element composition, and stable isotope signature of the giant deep-sea oyster *Neopycnodonte zibrowii* sp. n. from the NE Atlantic. *Deep Sea Res. I* 56, 374–404. doi: 10.1016/j.dsr.2008.10.002

Yahel, G., Whitney, F., Reiswig, H. M., Eerkes-Medrano, D. I., and Leys, S. P. (2007). In situ feeding and metabolism of glass sponges (Hexactinellida, Porifera) studied in a deep temperate fjord with a remotely operated submersible. *Limnol. Oceanogr.* 52, 428–440. doi: 10.4319/lo.2007.52.1.0428

Zariquiey, ÁR. (1968). Crustáceos decápodos ibéricos. *Invest. Pesq.* 32, 1–520.

Zibrowius, H. (1978). Les Scléractiniaires des grottes sous-marines en Méditerranée et dans l'Atlantique nor-oriental (Portugal, Madère, Canaries, Azores). *Pubbl. Staz. Zool. Napoli* 40, 516–544.

Zibrowius, H. (1980). Les Scléractiniaires de la Méditerranée et de l'Atlantique nord-oriental. *Mém. Inst. Océanogr. Monaco* 11, 1–284.

Zibrowius, H., and Cairns, S. D. (1992). Revision of the northeast Atlantic and Mediterranean Stylasteridae (Cnidaria: Hydrozoa). Memoires du Museum National d'Histoire Naturelle. *Serie A Zool.* 153:135.

Conflict of Interest: The authors declare that the research was conducted in the absence of any commercial or financial relationships that could be construed as a potential conflict of interest.

Copyright © 2020 Ríos, Prado, Carvalho, Sánchez, Rodríguez-Basalo, Xavier, Ibarrola and Cristobo. This is an open-access article distributed under the terms of the Creative Commons Attribution License (CC BY). The use, distribution or reproduction in other forums is permitted, provided the original author(s) and the copyright owner(s) are credited and that the original publication in this journal is cited, in accordance with accepted academic practice. No use, distribution or reproduction is permitted which does not comply with these terms.

frontiers in Marine Science

ORIGINAL RESEARCH
published: 19 August 2020
doi: 10.3389/fmars.2020.00665

Dragons of the Deep Sea: Kinorhyncha Communities in a Pockmark Field at Mozambique Channel, With the Description of Three New Species

Diego Cepeda[1], Fernando Pardos[1], Daniela Zeppilli[2] and Nuria Sánchez[2]*

[1] *Departamento de Biodiversidad, Ecología y Evolución, Facultad de Ciencias Biológicas, Universidad Complutense de Madrid, Madrid, Spain,* [2] *Laboratoire Environnement Profond, Institut Français de Recherche pour l'Exploitation de la Mer (IFREMER), Plouzané, France*

Cold seep areas are extremely reduced habitats with spatiotemporal variation of hydrocarbon-rich fluid seepage, low oxygen levels, and great habitat heterogeneity. Cold seeps can create circular to ellipsoid shallow depressions on the seafloor called pockmarks. We investigated two selected pockmarks, characterized by different gas emission, and two sites outside these geological structures at the Mozambique Channel to understand whether and how their environmental conditions affect the kinorhynch fauna in terms of density, richness, and community composition. A total of 11 species have been found living in the studied area, of which three are new species: *Fissuroderes cthulhu* sp. nov., *Fujuriphyes dagon* sp. nov., and *Fujuriphyes hydra* sp. nov. Densities outside the pockmarks are low and regularly decrease from the upper sediment layers, whereas inside the pockmarks, density reaches its highest value at layer 1–2 cm, strongly decreasing along the vertical profile from this depth. Areas under pockmark influence and locations outside pockmarks are similar in terms of species richness, but kinorhynchs showed a significant remarkable higher density at the pockmark sites. Additionally, species composition changes between habitats (inside and outside pockmarks) and between the two sampled pockmarks, with most of the species restricted to one of the studied habitats, except for *Condyloderes* sp. and *Echinoderes unispinosus* present both outside and inside the pockmarks. *Echinoderes hviidarum, E. unispinosus*, and *Fi. cthulhu* sp. nov., present at sites with gas emission, do not only survive under the specific pockmark conditions (characterized by hydrogen sulfide toxicity, methane high concentration, and low availability of dissolved oxygen) but even profit from a habitat with a likely lower competition for space and resources, flourishing and enhancing the density, most likely through the replacement with specialized species. Contrarily, species that only appear outside the pockmarks do not seem to cope with the presence of hydrogen sulfide and methane. Therefore, environmental factors linked to gas emissions have a major role driving the kinorhynch community composition.

Keywords: cold seeps, deep sea, ecology, kinorhynchs, meiofauna, diversity, taxonomy

OPEN ACCESS

Edited by:
Rui Rosa,
University of Lisbon, Portugal

Reviewed by:
Martin Vinther Sørensen,
University of Copenhagen, Denmark
Matteo Dal Zotto,
University of Modena and Reggio Emilia, Italy

****Correspondence:***
Diego Cepeda
diegocepeda@ucm.es

Specialty section:
This article was submitted to Global Change and the Future Ocean, a section of the journal Frontiers in Marine Science

Received: *30 November 2019*
Accepted: *21 July 2020*
Published: *19 August 2020*

Citation:
Cepeda D, Pardos F, Zeppilli D and Sánchez N (2020) Dragons of the Deep Sea: Kinorhyncha Communities in a Pockmark Field at Mozambique Channel, With the Description of Three New Species. Front. Mar. Sci. 7:665. doi: 10.3389/fmars.2020.00665

INTRODUCTION

Worldwide oceans cover about 361.9 million km^2 of the earth's surface, of which ∼70% are deep sea plains (Eakins and Sharman, 2010). Nowadays, ocean floor studies have experienced a strong revitalization, showing that the deep sea possesses prosperous, complex biological communities and a huge variety of geochemical environments that host unique species (Levin and Sibuet, 2012; Kennedy et al., 2019). Cold seeps are extreme, reduced habitats on the seafloor where hydrogen sulfide, methane, and other hydrocarbon-rich fluid seepage occurs (Kumar, 2017), causing a fall in oxygen levels and peaks of primary production due to chemoautotrophic organisms (Sibuet and Olu, 1998; Levin, 2005; Zeppilli et al., 2018). Cold seeps generate several geological structures such as pockmarks, circular to ellipsoid shallow depressions on the seafloor where the fluid emission varies spatiotemporally, cones (as mud volcanoes), carbonated structures, and brine pools, oval to rounded-shaped bodies of water that have a salinity higher than the surrounding ocean (Hovland and Judd, 1988; Dando et al., 1991).

Organisms inhabiting cold seeps take advantage of the habitat heterogeneity formed by the variable fluid release intensity and the hydrocarbon-rich fluid concentration of the sediment to occupy extreme, reduced niches that other organisms are unable to inhabit (Levin, 2005; Guillon et al., 2017). These adapted species can reach high levels of abundance and biomass (Rouse and Fauchald, 1997; Levin, 2005; Seitzinger et al., 2010; Vanreusel et al., 2010; Guillon et al., 2017; Sun et al., 2017) as a consequence of few species having evolved the morpho-physiological adaptations required to live in such a challenging habitat (Hourdez and Lallier, 2006; Zeppilli et al., 2018).

Studies of Kinorhyncha from the deep sea have frequently reported unidentified species, mostly from the Indian, Pacific, and Atlantic Oceans (Neuhaus, 2013; Zeppilli et al., 2018). More recently, studies to the species level have received a strong boost, and up to 45 species have recently been described or reported from this environment (Neuhaus and Blasche, 2006; Sørensen, 2008a; Neuhaus and Sørensen, 2013; Sánchez et al., 2014a,b, 2019a; Adrianov and Maiorova, 2015, 2016, 2018a,b; Grzelak and Sørensen, 2018, 2019; Sørensen and Grzelak, 2018; Sørensen et al., 2018, 2019; Yamasaki et al., 2018a,b,c, 2019; Cepeda et al., 2019a). Of these, some species seem to possess wider ranges of distribution than their congeners from the coastal zone. For instance, *Condyloderes kurilensis* Adrianov and Maiorova (2016), and *Fissuroderes higginsi* Neuhaus and Blasche (2006), were originally described from the Kuril-Kamchatka Trench (northwestern Pacific) and New Zealand (southwestern Pacific), respectively, and later found in the deep-sea waters off Oregon and California (northeastern Pacific) and the Clarion-Clipperton Zone (Neuhaus and Blasche, 2006; Adrianov and Maiorova, 2016; Sørensen et al., 2018; Sánchez et al., 2019a). More striking are the cases of *Campyloderes vanhoeffeni* Zelinka, 1913, distributed worldwide in both coastal waters and deep sea (Neuhaus and Sørensen, 2013) and *Echinoderes unispinosus* present in the deep sea of the Atlantic and the Pacific Oceans (Sørensen et al., 2018; Yamasaki et al., 2019; Álvarez-Castillo et al., 2020). This apparent cosmopolitanism might suggest that the deep sea environmental homogeneity promotes much wider distributional ranges than those observed from shallow water species (Sørensen et al., 2018). However, the possibility of having complexes of cryptic species must also be taken into account, since speciation in deep sea environments is not always accompanied by conspicuous morphological changes (Janssen et al., 2015).

Despite these hypotheses, little is known about the main environmental factors that shape the kinorhynch communities in general and particularly in deep sea, extreme environments. Some recent studies performed in the Arctic Ocean and the Gulf of Mexico determined that sediment grain size and trace metals are the variables that most seem to affect the Kinorhyncha species composition (Landers et al., 2018; Grzelak and Sørensen, 2019). Additionally, Álvarez-Castillo et al. (2015) concluded that kinorhynchs are somehow affected by pore water pH in reduced environments such as CO_2 vents. Also, kinorhynch densities have been proven to vary with the sulfide and organic matter concentrations of the seafloor (Sutherland et al., 2007; Mirto et al., 2012; Dal Zotto et al., 2016; Landers et al., 2020). In this context, the main aim of the present paper is to characterize the kinorhynch community associated with pockmarks in the Mozambique Channel deep sea to (1) identify and describe the new species inhabiting the area, (2) report potential kinorhynch species as indicators of cold seep areas, and (3) determine possible differences in richness, density, and species composition inside and outside pockmarks and along the vertical profile.

MATERIALS AND METHODS

Study Area, Sampling, and Processing

A pockmark cluster area was selected for the present study in the deep sea Mozambique Channel, off Mozambique and Madagascar (western Indian Ocean). Samples were collected during the *PAMELA-MOZ01* and *PAMELA-MOZ04* campaigns aboard the R/V *L'Atalante* and *Pourquoi pas?* (Genavir-Ifremer), respectively (Olu, 2014; Jouet and Deville, 2015). Multibeam echosounders and seabed inspection with a deep-towed camera Scampi were used to detect the location of pockmarks obtaining bathymetric data and identifying cold seep macrofauna indicators. Two active pockmarks and two sites outside any pockmark were selected.

MOZ04_MTB2: S 15 21.685; E 45 57.378; 754 m.
MOZ01_MTB3: S 15°21.695; E 45°57.388; 757 m.
MOZ04_MTB1: S 15°21.812; E 45°57.628; 735 m.
MOZ01_MTB6: S 15°31.148; E 45°42.931; 789 m depth.

Samples were obtained with a Barnett-type multi-corer (MTB) with three cores by deployment. Each core of 6.2 cm inner diameter (total surface area of 30.2 cm^2) was horizontally sliced into five layers: layer 1 (0–1 cm depth), layer 2 (1–2 cm depth), layer 3 (2–3 cm depth), layer 4 (3–4 cm depth), and layer 5 (4–5 cm depth). Each subsample was fixed in 4% formalin. Subsequently, the sediment of each slice was sieved on 1-mm and 32-μm sieves at the Ghent laboratory (Belgium) and the IFREMER laboratory (France), and the metazoan meiofauna was separated from the sediment by Ludox centrifugation (Heip et al., 1985) and subsequently fixed in 4% formalin.

Species Identification and Description

Kinorhynchs were separated from the remaining meiofauna using an Irwin loop and washed with distilled water to remove formalin remnants. Kinorhynchs were mounted and identified to species level, except for the juveniles that could be identified only to class level.

For light microscopy (LM), specimens were dehydrated through a graded series of 25, 50, 75, and 100% glycerine to be mounted on glass slides with Fluoromount G®. The mounted specimens were studied, identified, and photographed with a Leica DM2500® LED compound microscope equipped with differential interference contrast (DIC).

For scanning electron microscopy (SEM), specimens were sonically cleaned and transferred to 70% ethanol and progressively dehydrated through a graded series of 80, 90, 95, and 100% ethanol. Hexamethyldisilazane (HMDS) was used for chemical drying through a HMDS-ethanol series. Specimens were coated with gold and mounted on aluminum stubs to be examined with a JSM 6335-F JEOL SEM at the "ICTS Centro Nacional de Microscopía Electrónica" (Universidad Complutense de Madrid, Spain). For species descriptions, line art and image plates composition were done using Adobe Photoshop and Illustrator CC-2014 software. Type and additional material were deposited at the Natural History Museum of Denmark (NHMD).

Environment Characterization

To test the influence of the environment over the kinorhynch communities and detect potential species as indicators of seepages, we selected hydrogen sulfide (H_2S) and methane (CH_4) as a proxy of cold seep activity.

H_2S concentration was quantified by colorimetry (Fonselius, 1983) after precipitation of the sulfide with zinc chloride on board. The concentration was detected in a high level only at the pockmark site MOZ04-MTB1. CH_4 was determined by gas chromatography headspace technique (GC/HSS) (Sarradin and Caprais, 1996), following different sampling techniques between the two cruises. In MOZ-01, 5 ml of pore waters was collected in 10-ml vials by Rhizon samplers (Rhizosphere Research Products R.V., Wageningen), which are thin rods covered by hydrophilic porous polymer designed to extract water from sediment using a vacuum (Seeberg-Elverfeldt et al., 2005); then, 20 μl of a saturated mercuric hydrochloride solution was added to preserve samples. In MOZ-04, 3 ml of sediment was collected in 20-ml vials, where 5 ml of a solution of sodium hydroxide at 1 M was added to avoid any bacterial activity. CH_4 was found at the two study pockmarks. The methodology followed during the cruise MOZ01, using Rhizon samplers, induced a degassing step of dissolved methane in the pore waters, while methane is more preserved by collecting directly the sediment, as done during the cruise MOZ04.

Data Processing and Statistical Analyses

The effect of the environmental conditions on kinorhynch community structure and assemblage was assessed using three community descriptors as response variables: (1) richness, (2) density, and (3) species composition. Richness was measured as number of species, and density as number of individuals per 10 cm^2, including both adults and juveniles.

Kruskal–Wallis analyses (KW) were conducted through R v.6.3.1 software to test differences in kinorhynch richness and density. We assessed changes in community structure through different approaches: along the vertical profile of each habitat (inside and outside pockmarks, considering five layers: 0–1, 1–2, 2–3, 3–4, and 4–5 cm), between habitats (inside vs. outside pockmarks), and between sites sampled at the same habitat.

Differences in adult community composition between habitats and between sites of the same habitat were tested by permutational multivariate analysis of variance (PERMANOVA) calculated with the function "adonis" in the R package *vegan* v. 2.2-1 (Oksanen et al., 2018). Distance matrices were calculated using both Jaccard (incidence) and Ružièka [abundance transformed to $\log_{10}$(abundance + 1)] dissimilarity indices through the function "beta" of the R package *vegan* v. 2.2-1 (Oksanen et al., 2015). In order to further investigate the environmental factors that drive the community composition, H_2S was used as categorical covariate variable (two levels: absence, all layers with concentration of 0 μM; high, layers with concentrations > 200 Mm). CH_4 was detected at both pockmark sites (MOZ01-MTB06 and MOZ04-MTB1), but the concentration was measured following different methods and therefore data cannot be truly comparable. We conducted a principal component analysis (PCA) in abundance using the function "rda" of the R package *vegan* v. 2.2-1 (Oksanen et al., 2015) to visualize community composition variations among sites. Abundance data were transformed in order to use the Hellinger distance among samples using the function "decostand" of the R package *vegan* 2.4-4 (Oksanen et al., 2018), since double absence is not considered as an indicator of similarity and it gives a lower weight to dominant species (Legendre and Gallagher, 2001). A *post hoc* explaining of the PCA axes by adding environmental variables was performed by the function "envfit" of the R package *vegan* 2.4-4 (Oksanen et al., 2018).

RESULTS

Taxonomic Account

Class Allomalorhagida Sørensen et al., 2015.

Family Pycnophyidae Zelinka, 1896.

Genus *Fujuriphyes* Sánchez et al., 2016.

Fujuriphyes dagon sp. nov.

urn:lsid:zoobank.org:act:28C303EF-46AE-4304-887C-9202B7386AB9 (**Figures 1–4**).

Material examined

Holotype, adult female, collected in October 2014 at Mahavavy area, Mozambique Channel, western Indian Ocean (−15° 32.532′, 45° 42.894′) at 775 m depth; mounted in Fluoromount G®, deposited at NHMD under accession number: 669762. Paratypes, three adult males, with same collecting data as

holotype; mounted in Fluoromount G®, deposited at NHMD under accession numbers: 669763–669765. Two additional specimens mounted for SEM, same collecting data as type material, deposited at the Meiofauna Collection of the UCM.

Diagnosis

Fujuriphyes without middorsal processes or elevations. Unpaired paradorsal setae on segments 2, 4, 6, and 8. Laterodorsal setae on segments 2–10. Lateroventral setae on even segments. One pair of ventrolateral setae on segments 2–4 and 6–9, and two pairs on segment 5. Males with ventromedial tubes on segment 2. Lateral terminal spines present.

Etymology

The species is named after the fictional deity Dagon (also known as Father Dagon), created by the American writer of horror fiction H.P. Lovecraft (1890–1937) and firstly introduced in the short story "Dagon," published in 1919. In the pantheon of Lovecraftian cosmic entities, Dagon presides over the Deep Ones, an amphibious humanoid race indigenous to Earth's oceans.

Description

See **Supplementary Table 1.1** for measurements and dimensions and **Supplementary Table 1.2** for summary of seta, spine, tube, glandular cell outlet, and sensory spot locations.

Ring 00 of mouth cone with nine equally sized outer oral styles (**Figure 2**) composed of a single, flexible unit, wider at the base, which bears a fringed sheath, progressively tapering toward a distal, pointed tip. Outer oral styles located anterior to each introvert sector, except in the middorsal section 6 where a style is missing (**Figure 2**).

Introvert with six transverse rings of scalids and 10 longitudinal sectors defined by the arrangement of the primary spinoscalids (**Figures 2**, **3H**). Ring 01 with 10 primary spinoscalids, larger than remaining ones, each one composed of a basal, rectangular, wide sheath and a distal, elongated, flexible, distally pointed end piece (**Figures 2**, **3H**). Ring 02 with 10 regular-sized scalids, arranged as one medially in each sector (**Figure 2**). Scalids of this and the following rings are morphologically similar to the primary spinoscalids but smaller (**Figure 3H**). Ring 03 with 20 regular-sized scalids, arranged as 2 in each sector (**Figures 2**, **3H**). Ring 04 with 5 regular-sized scalids, arranged as 1 medially in each odd-numbered sector (**Figures 2**, **3H**). Ring 05 with 15 regular-sized scalids, arranged as 1 medially in each even-numbered sector and 2 in each odd-numbered sector (**Figure 2**). Ring 06 also with 15 regular-sized scalids, arranged as 2 in each even-numbered sector and 1 medially in each odd-numbered sector (**Figure 2**). The location of scalids in rings 01–06 follows a strict pattern around the introvert: each even-numbered sector carries six regular-sized scalids as two chevrons, whereas each odd-numbered sector bears seven regular-sized scalids as a double diamond (**Figures 2**, **3H**).

Neck with four dorsal and two ventral sclerotized placids (**Figures 1A–C**). Dorsal placids rectangular, wide, mesial ones broader (ca. 30–32 μm wide at the base) than lateral ones (ca. 20–23 μm wide at the base), with a notch in the middle region (**Figure 1B**). Ventral placids (ca. 29–31 μm wide at the base) more quadrangular than dorsal ones, with the posterolateral margins curved toward the sternal plates of the first trunk segment (**Figures 1A,C**). A ring of 14 trichoscalids posterior to the scalid rings, arranged as 2 in the odd-numbered sectors (except sector 1 with a single trichoscalid) and 1 in the even-numbered sectors of the introvert (**Figures 2**, **3H**).

Trunk rectangular, stout, triangular in cross-section, composed of 11 segments (**Figures 1A,B**, **3A**, **4A**). Segment 1 with one tergal, two episternal, and one midsternal plate (**Figures 1A–C**, **3A–C**); remaining segments with one tergal and two sternal plates (**Figures 1A–D**, **3A**). Maximum sternal width at segment 6, almost constant throughout the trunk, progressively tapering at the last trunk segments (**Figures 1A,B**, **3A**, **4A**). Sternal cuticular plates relatively narrow in the ratio of maximum sternal width to trunk length (MSW-6:TL interval ratio = 21.9–24.9), giving the animal a slender appearance (**Figures 1A,B**, **3A**, **4A**). Segments 1–10 with oval glandular cell outlets in subdorsal and ventromedial positions (**Figures 1A–C**, **3B–G,I,J**). Segments 2–10 with paired cuticular ridges in laterodorsal and ventrolateral positions, the latter with adjacent, minute glandular cell outlets (**Figures 1A–D**, **3A–G,I,J**). Cuticular hairs acicular, densely covering the cuticular surface of segments 2–10 from paralateral to ventromedial positions (**Figures 4D–G, H–K**). Muscular scars very conspicuous in laterodorsal and ventromedial positions (**Figures 1A–D**, **3B–G,I,J**). Areas with superficially wrinkled cuticle present in ventrolateral position on segments 2–10 and paralateral position on segment 1 (**Figures 1A,C**). Pachycycli and ball-and-socket joints well-developed and thick on segments 2–10 (**Figures 1A–D**, **3A**). Apodemes present on segments 8–10 (**Figures 1A**, **3A**). Posterior margin of segments straight, showing primary pectinate fringes with weakly serrated free flaps; secondary pectinate fringes also straight and finely serrated (**Figures 1A–D**).

Segment 1 without middorsal cuticular process or elevation. Anterolateral margins of the tergal plate as horn-like, distally rounded extensions (**Figures 1A–C**, **3A**, **4A,B**). Anterior margin of tergal plate smooth, followed by a crenulated area (**Figures 1B**, **3B**, **4A,B**). Anterior margin of sternal plates with a wavy median ridge of cuticle (**Figures 1A,C**, **3C**). Midsternal plate trapezoidal, laterally extended at its base, with a lateral constriction near its anterior margin and a straight posterior margin (**Figures 1A,C**, **3C**). Sensory spots in subdorsal (two pairs), laterodorsal (one pair), ventrolateral (two pairs), and ventromedial (one pair) positions (**Figures 1A–C**, **3B,C**, **4B,C**).

Segment 2 without middorsal process or elevation. Unpaired seta in paradorsal position; paired setae in laterodorsal, lateroventral, and ventrolateral positions (**Figures 1A–C**, **3D,E**, **4H,I**). Sensory spots in subdorsal (one pair), laterodorsal (one pair), and ventromedial (two pairs) positions (**Figures 1A–C**, **3D,E**, **4H,I**). Males with sexually dimorphic tubes in ventromedial position (**Figures 1C**, **4I**).

Segment 3 without middorsal process or elevation. Paired setae in laterodorsal and ventrolateral positions (**Figures 1A,B**, **3D,E**). Sensory spots in subdorsal (one pair), laterodorsal (one pair), and ventromedial (two pairs) positions (**Figures 1A,B**, **3D,E**).

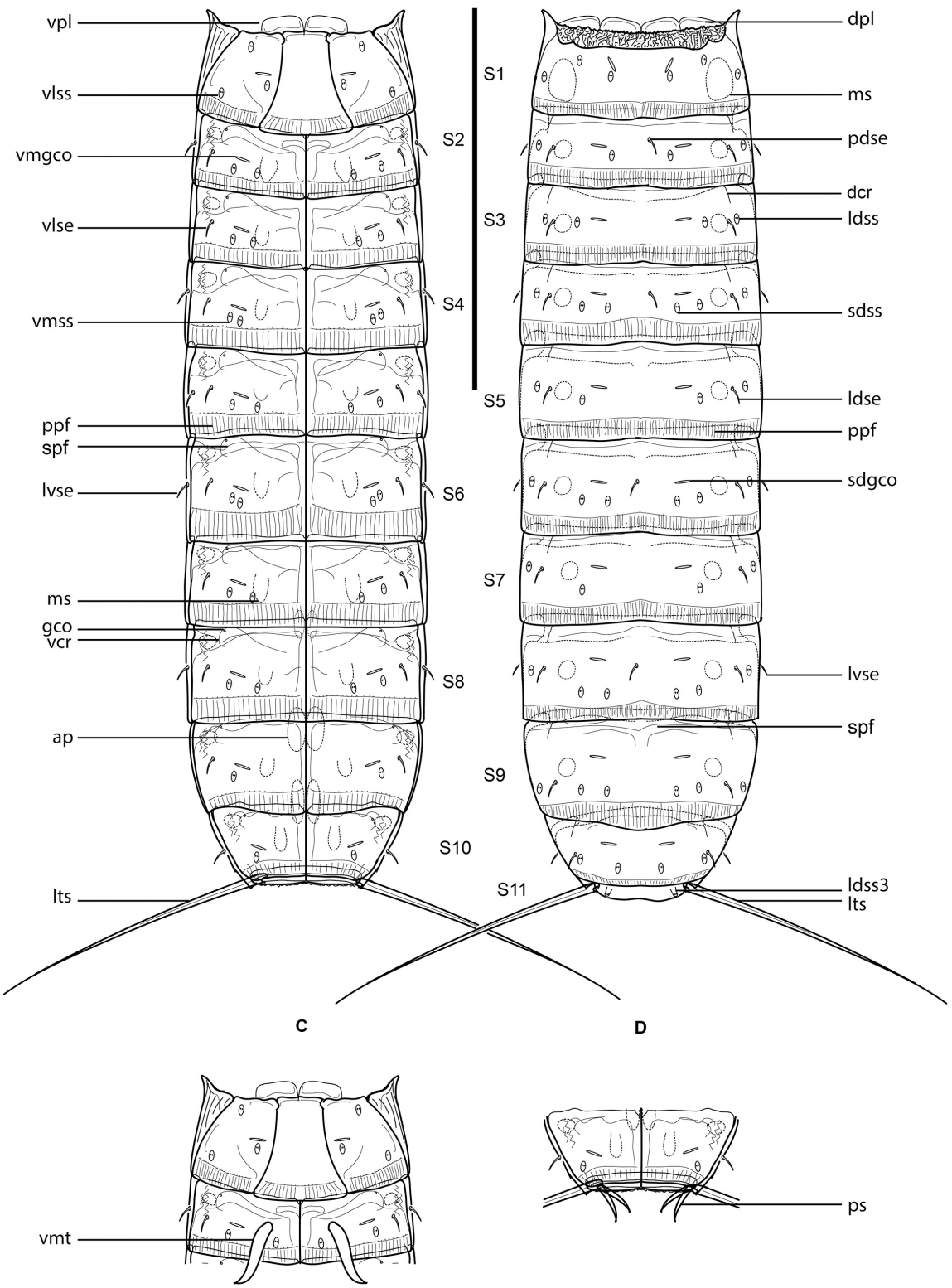

FIGURE 1 | Continued

FIGURE 1 | Line art illustrations of *Fujuriphyes dagon* sp. nov. **(A)** Female, ventral view; **(B)** female, dorsal view; **(C)** male, segments 1–2, ventral view; **(D)** male, segments 10–11, ventral view. Scale bar: 250 μm. Abbreviations: ap, apodeme; dcr, dorsal cuticular ridge; dpl, dorsal placid; gco, glandular cell outlet; ldse, laterodorsal seta; ldss, laterodorsal sensory spot; ldss3, laterodorsal type 3 sensory spot; lts, lateral terminal spine; lvse, lateroventral seta; ms, muscular scar; pdse, paradorsal seta; ppf, primary pectinate fringe; ps, penile spine; sdgco, subdorsal glandular cell outlet; sdss, subdorsal sensory spot; spf, secondary pectinate fringe; vcr, ventral cuticular ridge; vlse, ventrolateral seta; vlss, ventrolateral sensory spot; vmgco, ventromedial glandular cell outlet; vmss, ventromedial sensory spot; vmt, ventromedial tube; vpl, ventral placid.

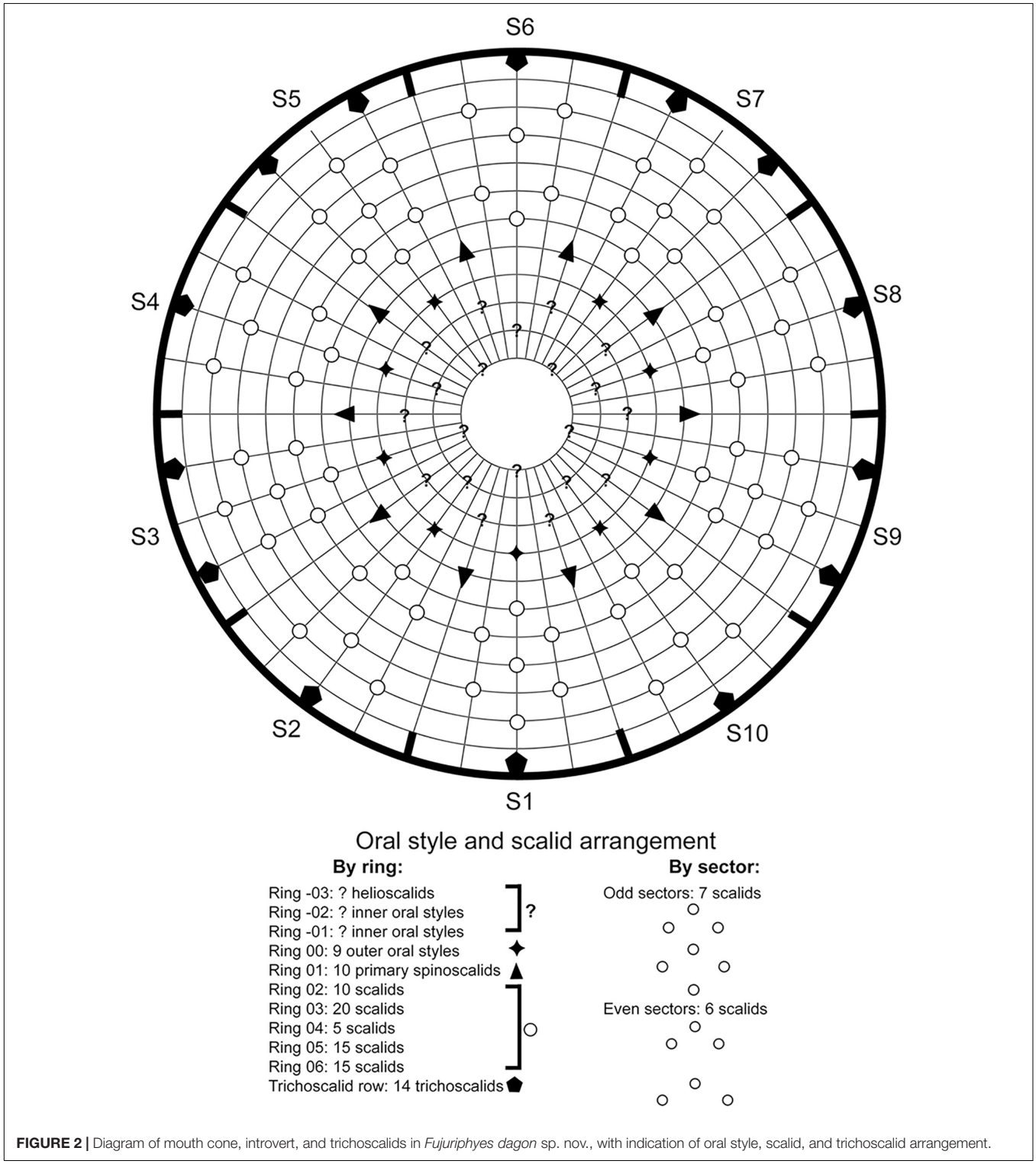

FIGURE 2 | Diagram of mouth cone, introvert, and trichoscalids in *Fujuriphyes dagon* sp. nov., with indication of oral style, scalid, and trichoscalid arrangement.

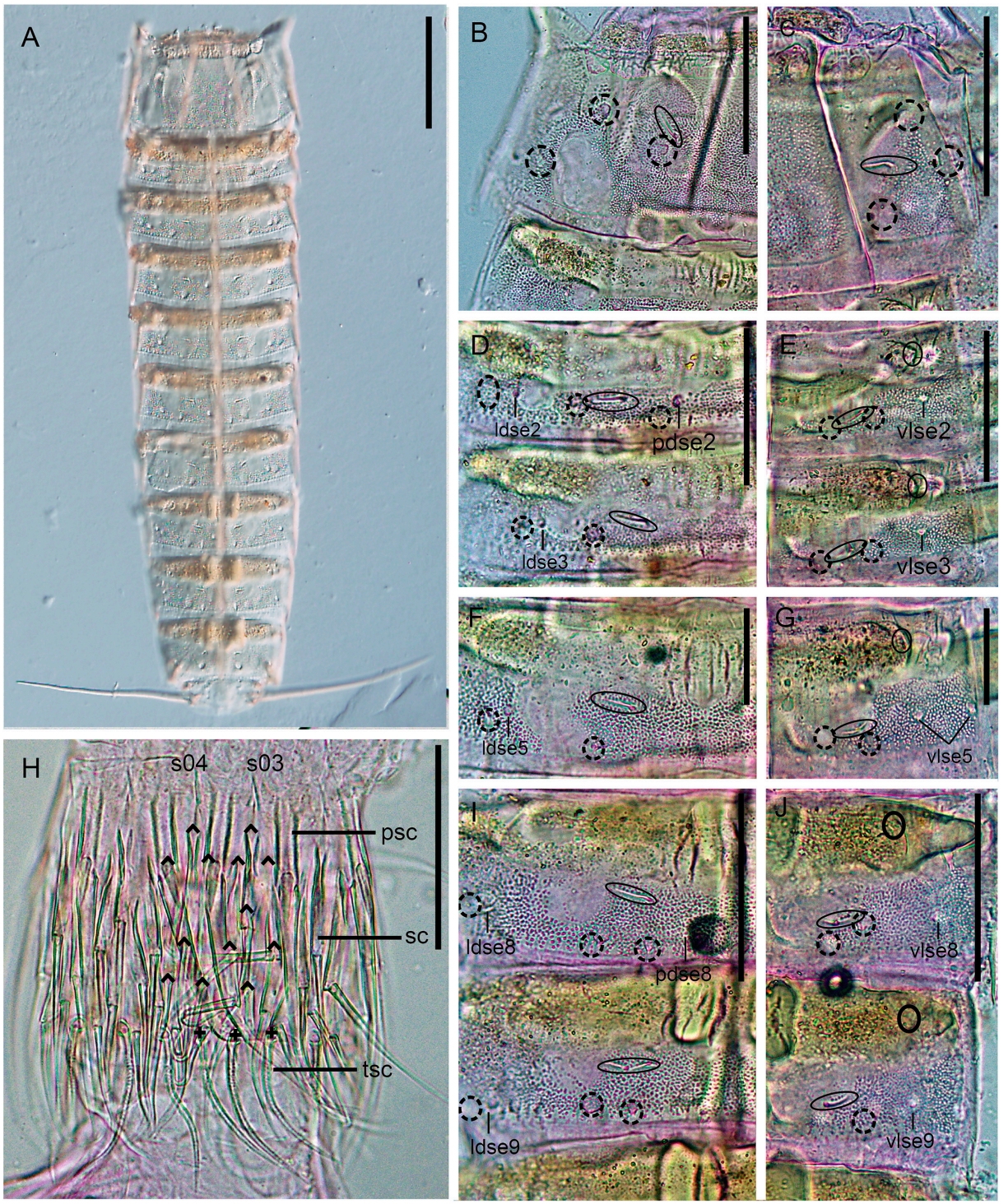

FIGURE 3 | Light micrographs showing trunk overview and details in the head and main trunk cuticular characters of female holotype NHMD 669762 **(B–J)** and male paratype NHMD 669763 **(A)** of *Fujuriphyes dagon* sp. nov. **(A)** Dorsal overview of trunk; **(B)** middorsal to paralateral view on right half of tergal plate of segment 1; **(C)** ventrolateral to ventromedial view on left half of sternal plates of segment 1; **(D)** middorsal to laterodorsal view on right half of tergal plate of segments 2–3; **(E)** left sternal plates of segments 2–3; **(F)** middorsal to laterodorsal view on right half of tergal plate of segment 5; **(G)** left sternal plate of segment 5; **(H)** introvert, with detail of primary spinoscalid, regular-sized scalid, and trichoscalid arrangement of sectors 03–04; **(I)** middorsal to laterodorsal view on right half of tergal plate of segments 8–9; **(J)** left sternal plates of segments 8–9. Scale bars **(A):** 250 μm; **(B–E, H–J)**: 62 μm; **(F)** and **(G):** 31 μm. Abbreviations: ldse, laterodorsal seta; pdse, paradorsal seta; psc, primary spinoscalid; s, sector of introvert; sc, regular-sized scalid; tsc, trichoscalid; vlse, ventrolateral seta; numbers after abbreviations indicate corresponding segment or sector of introvert; carets indicate the arrangement of scalids, and crosses that of trichoscalids; sensory spots are marked as dashed circles, and glandular cell outlets as continuous circles.

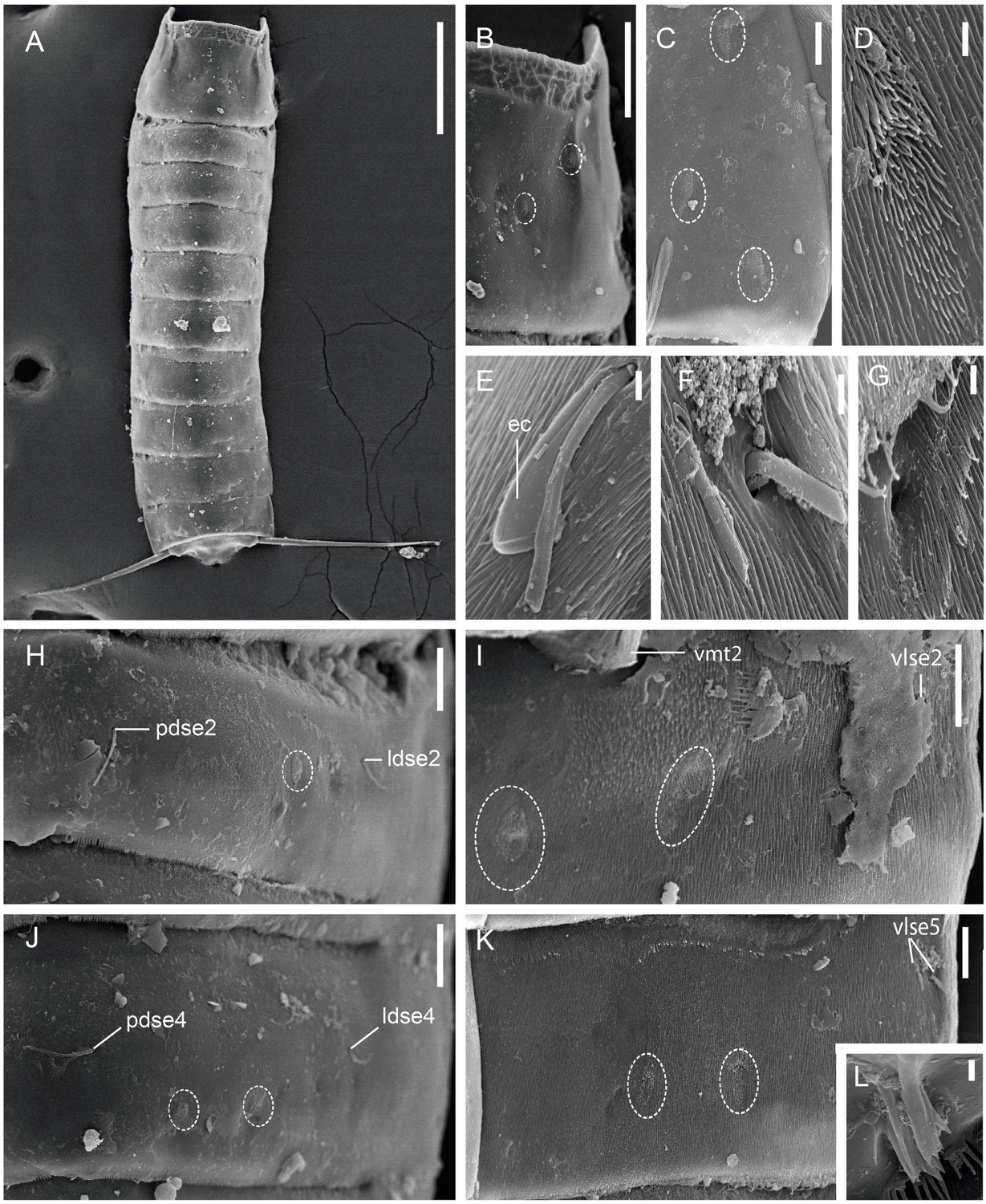

FIGURE 4 | Scanning electron micrographs showing trunk overview and details in the main trunk cuticular appendages of a male of *Fujuriphyes dagon* sp. nov. **(A)** Dorsal overview of trunk; **(B)** middorsal to subdorsal view on left half of tergal plate of segment 1; **(C)** left episternal plate of segment 1; **(D)** ventromedial sensory spot of segment 5; **(E)** lateroventral seta of segment 10; **(F)** ventrolateral setae of segment 5; **(G)** ventral cuticular ridge and associated glandular cell outlet of segment 6; **(H)** middorsal to laterodorsal view on left half of tergal plate of segment 2; **(I)** left sternal plate of segment 2; **(J)** middorsal to laterodorsal view on left half of tergal plate of segment 4; **(K)** left sternal plate of segment 5; **(L)** laterodorsal type 3 sensory spot of segment 11. Scale bars: **(A):** 300 μm; **(B):** 30 μm; **(C,E,H–L)**: 10 μm; **(D,F,G):** 1 μm. Abbreviations: ec, epibiontic Ciliophora; ldse, laterodorsal seta; pdse, paradorsal seta; vlse, ventrolateral seta; vmt, ventromedial tube; numbers after abbreviations indicate corresponding segment; sensory spots are marked as dashed circles.

Segment 4 without middorsal process or elevation. Unpaired seta in paradorsal position; paired setae in laterodorsal, lateroventral, and ventrolateral positions (**Figures 1A,B**, **4J**). Sensory spots in subdorsal (two pairs), laterodorsal (one pair), and ventromedial (two pairs) positions, with the more mesial ventromedial pair laterally shifted compared to those of previous segments (**Figures 1A,B**, **4J**).

Segment 5 without middorsal process or elevation. Two pairs of setae in ventrolateral position; one pair in laterodorsal position (**Figures 1A,B**, **3F,G**, **4F,K**). Sensory spots in subdorsal (one pair), laterodorsal (one pair), and ventromedial (two pairs) positions, the latter aligned with those of segment 3 (**Figures 1A,B**, **3F,G**, **4D,K**).

Segment 6 similar to segment 4 in the arrangement of setae and sensory spots (**Figures 1A,B**, **4G**).

Segment 7 similar to segment 3 in the arrangement of setae and sensory spots (**Figures 1A,B**).

Segment 8 without middorsal process or elevation. Unpaired seta in paradorsal position; paired setae in laterodorsal, lateroventral, and ventrolateral positions (**Figures 1A,B**, **3I,J**). Sensory spots in subdorsal (two pairs), laterodorsal (one pair), and ventromedial (two pairs) positions, the latter aligned with those of the previous segment (**Figures 1A,B**, **3I,J**).

Segment 9 without middorsal process or elevation. Paired setae in laterodorsal and ventrolateral positions (**Figures 1A,B**, **3I,J**). Sensory spots in subdorsal (two pairs), laterodorsal (one pair), and ventromedial (one pair) positions (**Figures 1A,B, 3I,J**). Nephridiopores not observed.

Segment 10 without middorsal process or elevation. Paired setae in laterodorsal and lateroventral positions (**Figures 1A,B,D**, **4E**). One pair of sensory spots in subdorsal, laterodorsal, and ventromedial positions (**Figures 1A,B,D**).

Segment 11 with one pair of type 3 sensory spots in laterodorsal position (**Figures 1B**, **4L**). Males with two pairs of sexually dimorphic penile spines and genital pores (**Figure 1D**). Lateral terminal spines long (LTS:TL interval ratio = 30.1–31.9), robust, widely spread, apparently rigid (**Figures 1A,B**, **3A**, **4A**).

Associated kinorhynch fauna

Fujuriphyes dagon sp. nov. co-occurred with *Condyloderes* sp., *E. unispinosus* and *Fissuroderes cthulhu* sp. nov. in the analyzed samples.

Fujuriphyes hydra sp. nov.

urn:lsid:zoobank.org:act:28E6A464-9534-46AC-A113-16492D6E52BE (**Figures 5**, **6**).

Material examined

Holotype, adult female, collected in November 2015 at Betsiboka area, Mozambique Channel, western Indian Ocean (−15° 21.685′, 45° 57.392′) at 754 m depth; mounted in Fluoromount G®, deposited at NHMD under accession number: 669766. Paratypes, two adult males and one adult female, with same collecting data as holotype; mounted in Fluoromount G®, deposited at NHMD under accession numbers: 669767–669769.

Diagnosis

Fujuriphyes with middorsal elevations on segments 1–10, with the elevation of segment 10 appearing smaller and thinner than the others. Unpaired paradorsal setae on segments 2, 4, and 6, and paired on segment 8. Paralateral setae on segment 1. Laterodorsal setae on segments 2–9. One pair of lateroventral setae on segments 2, 4, 6, and 8, and two pairs on segment 10. One pair of ventrolateral setae on segments 3–4 and 6–8, and two pairs on segment 5. Ventromedial setae on segments 2 (only females) and 9. Males with ventromedial tubes on segment 2. Lateral terminal spines present.

Etymology

The species is named after the fictional deity Hydra (also known as Mother Hydra), created by the American writer of cosmic horror fiction H.P. Lovecraft (1890–1937) and firstly introduced in the short story "The Shadow over Innsmouth," published in 1936. In the pantheon of Lovecraftian cosmic entities, Mother Hydra is the consort of Father Dagon.

Description

See **Supplementary Table 1.3** for measurements and dimensions, and **Supplementary Table 1.4** for summary of cuticular elevation, seta, spine, tube, glandular cell outlet, and sensory spot locations.

The analyzed specimens were not suitable for head examinations; hence, data on morphology, number, and arrangement of scalids and oral styles are not available.

Neck with four dorsal and two ventral, slightly sclerotized placids (**Figures 5A–C**). Dorsal placids rectangular, wide, longitudinally compressed; mesial ones broader (ca. 25–26 μm wide at the base), with the margins closest to the lateral ones more elevated; lateral ones narrower (ca. 20–21 μm wide at the base), with the margins closest to the mesial ones more elevated (**Figure 5B**). Ventral placids also rectangular but much more elongated (ca. 37–40 μm wide at the base), getting narrower toward the lateral sides (**Figures 5A,C**).

Trunk rectangular, stout, strongly sclerotized, triangular in cross-section, composed of 11 segments (**Figures 5A,B**, **6A**). Segment 1 with one tergal, two episternal, and one midsternal plate; remaining segments with one tergal and two sternal plates (**Figures 5A–D**, **6A–J**). Maximum sternal width at segment 6, almost constant throughout the trunk, slightly tapering at the last trunk segments (**Figures 5A,B**, **6A**). Sternal cuticular plates wide in ratio of maximum sternal width to trunk length (MSW-6:TL average ratio = 32.81%), giving the animal a plump appearance (**Figures 5A,B**, **6A**). Middorsal elevations on segments 1–10, with intracuticular, butterfly-like atria of paradorsal sensory spots; middorsal elevation of segment 10 smaller and thinner than previous ones (**Figures 5B**, **6B,D,F,I**). Segments 1–10 with rounded glandular cell outlets in subdorsal and ventromedial positions (**Figures 5A–D**, **6B–J**). Segments 2–10 with paired cuticular ridges in laterodorsal and ventrolateral positions, the latter with adjacent, minute glandular cell outlets (**Figures 5A–D**, **6B–J**). Cuticular hairs not observed. Muscular scars very conspicuous in laterodorsal and ventromedial positions (**Figures 5A–D**, **6B–J**). Pachycycli and

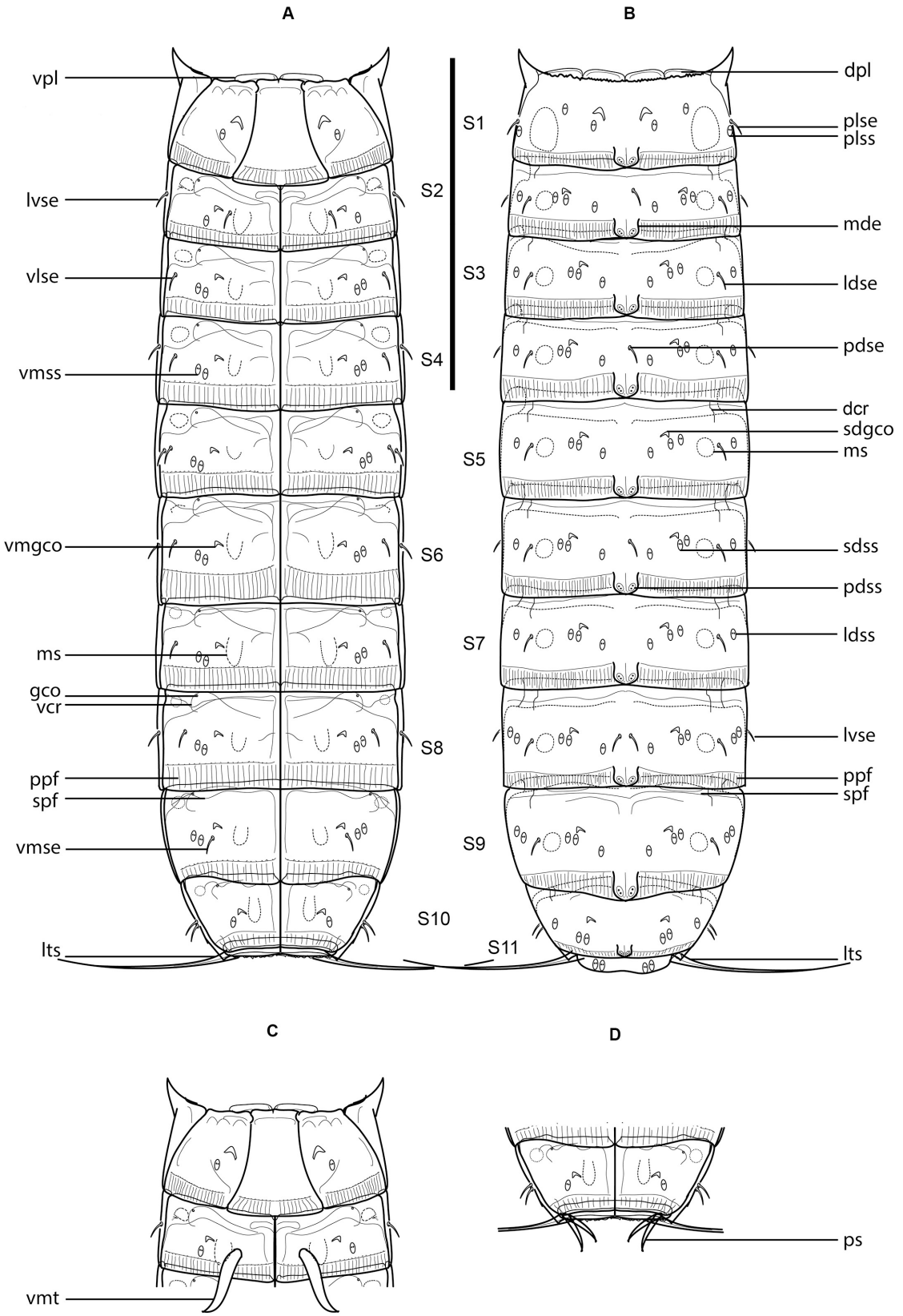

FIGURE 5 | Continued

FIGURE 5 | Line art illustrations of *Fujuriphyes hydra* sp. nov. **(A)** Female, ventral view; **(B)** female, dorsal view; **(C)** male, segments 1–2, ventral view; **(D)** male, segments 10–11, ventral view. Scale bar: 250 μm. Abbreviations: dcr, dorsal cuticular ridge; dpl, dorsal placid; gco, glandular cell outlet; ldse, laterodorsal seta; ldss, laterodorsal sensory spot; lts, lateral terminal spine; lvse, lateroventral seta; mde, middorsal elevation; ms, muscular scar; pdse, paradorsal seta; pdss, paradorsal sensory spot; plse, paralateral seta; plss, paralateral sensory spot; ppf, primary pectinate fringe; ps, penile spine; sdgco, subdorsal glandular cell outlet; sdss, subdorsal sensory spot; spf, secondary pectinate fringe; vcr, ventral cuticular ridge; vlse, ventrolateral seta; vmgco, ventromedial glandular cell outlet; vmse, ventromedial seta; vmss, ventromedial sensory spot; vpl, ventral placid; vmt, ventromedial tube.

ball-and-socket joints well-developed, thick, on segments 2–10 (**Figures 5A–D**, **6A**). Apodemes absent. Posterior margin of segments straight, showing primary pectinate fringes with weakly serrated free flaps (**Figures 5A–D**); secondary pectinate fringes not detectable under LM.

Segment 1 with middorsal elevation and associated butterfly-like intracuticular atria of the paradorsal sensory spots (**Figures 5B**, **6B**). Anterolateral margins of tergal plate as horn-like, distally pointed extensions (**Figures 5A–C**, **6A–C**). Anterior margin of tergal plate finely denticulate (**Figures 5B**, **6B**). Anterior margin of sternal plates with a wavy median ridge of cuticle (**Figures 5A,C**, **6A,C**). Midsternal plate trapezoidal, laterally extended at its base, with a lateral constriction near its anterior margin and a straight posterior margin (**Figures 5A,C**, **6A,C**). Paired setae in paralateral position (**Figures 5B**, **6B**). Sensory spots in paradorsal (one pair), subdorsal (two pairs), paralateral (one pair), and ventromedial (one pair) positions; all of them located at the anterior half of the cuticular plates except the paradorsal and paralateral ones (**Figures 5A–C**, **6B,C**).

Segment 2 with middorsal elevation as on the preceding segment (**Figures 5B**, **6D**). Unpaired seta in paradorsal position, and paired setae in laterodorsal and lateroventral positions; females with paired, sexually dimorphic setae in ventromedial position (**Figures 5A–C**, **6D,E**). Sensory spots in paradorsal (one pair), subdorsal (three pairs), laterodorsal (one pair), and ventromedial (one pair) positions (**Figure 5A–C**, **6D,E**). Males with sexually dimorphic tubes in ventromedial position (**Figure 5C**).

Segment 3 with middorsal elevation as on preceding segments (**Figures 5B**, **6D**). Paired setae in laterodorsal and ventrolateral positions (**Figures 5A,B**, **6D,E**). Sensory spots in paradorsal (one pair), subdorsal (three pairs), laterodorsal (one pair), and ventromedial (two pairs) positions (**Figures 5A,B**, **6D,E**). Subdorsal sensory spots more mesial than those of segment 2; ventromedial sensory spots closely located to each other (**Figures 5A,B**, **6D,E**).

Segment 4 with middorsal elevation as on preceding segments (**Figure 5B**). Unpaired seta in paradorsal position, and paired setae in laterodorsal, lateroventral, and ventrolateral positions, the former aligned with those of segment 3 (**Figures 5A,B**). Sensory spots in paradorsal (one pair), subdorsal (three pairs), laterodorsal (one pair), and ventromedial (two pairs) positions (**Figures 5A,B**).

Segment 5 similar to segment 3 in the arrangement of cuticular elevation, setae, and sensory spots, but with two pairs of ventrolateral setae, situated very close to each other (**Figures 5A,B**, **6F,G**).

Segment 6 similar to segment 4 in the arrangement of cuticular elevation, setae, and sensory spots (**Figures 5A,B**, **6F,G**).

Segment 7 similar to segment 3 in the arrangement of cuticular elevation, setae, and sensory spots (**Figures 5A,B**).

Segment 8 with middorsal elevation as on preceding segments (**Figures 5B**, **6I**). Paired setae in paradorsal, laterodorsal, lateroventral, and ventrolateral positions, the latter more mesial than those of previous segments but still in ventrolateral position (**Figures 5A,B**, **6I,J**). Sensory spots in paradorsal (one pair), subdorsal (three pairs), laterodorsal (two pairs), and ventromedial (two pairs) positions (**Figures 5A,B**, **6I,J**).

Segment 9 with middorsal elevation as on preceding segments (**Figures 5B**, **6I**). Paired setae in laterodorsal and ventromedial positions (**Figure 5A,B**, **6I,J**). Sensory spots in paradorsal (one pair), subdorsal (three pairs), laterodorsal (two pairs), and ventromedial (two pairs) positions (**Figure 5A,B**, **6I,J**). Nephridiopores not observed.

Segment 10 with middorsal elevation smaller and thinner than previous ones (**Figures 5B**, **6H**). Two pairs of setae in lateroventral position (**Figure 5B**). Sensory spots in paradorsal (one pair), subdorsal (two pairs), laterodorsal (one pair), and ventromedial (one pair) positions (**Figures 5A,B**, **6H**).

Segment 11 with two pairs of sensory spots in laterodorsal position (**Figure 5B**). Males with two pairs of sexually dimorphic penile spines and genital pores (**Figure 5D**). Lateral terminal spines long (LTS:TL average ratio = 30.97%), slender, narrow, apparently flexible (**Figures 5A,B**, **6A**).

Associated kinorhynch fauna

Fujuriphyes hydra sp. nov. co-occurred with the species *E. unispinosus* and *Ryuguderes* sp. in the analyzed samples.

Class Cyclorhagida (Zelinka, 1896) Sørensen et al., 2015.
Family Echinoderidae Zelinka, 1894.
Genus *Fissuroderes* Neuhaus and Blasche, 2006.

Fissuroderes cthulhu sp. nov.

urn:lsid:zoobank.org:act:8C27FAF4-0CD2-4767-9FE3-F46DEDDE9147 (**Figures 7–9**).

Material examined

Holotype, adult female, collected in October 2014 at Mahavavy area, Mozambique Channel, western Indian Ocean (−15° 32.532′, 45° 42.894′) at 775 m depth; mounted in Fluoromount G®, deposited at NHMD under accession number: 669727. Paratypes, five adult males and four adult females, with same collecting data as holotype; mounted in Fluoromount G®, deposited at NHMD under accession numbers: 669728–669736. Nineteen additional specimens mounted for LM, same collecting data as type material, deposited at NHMD under accession numbers: 669737–669755; one additional specimen mounted for

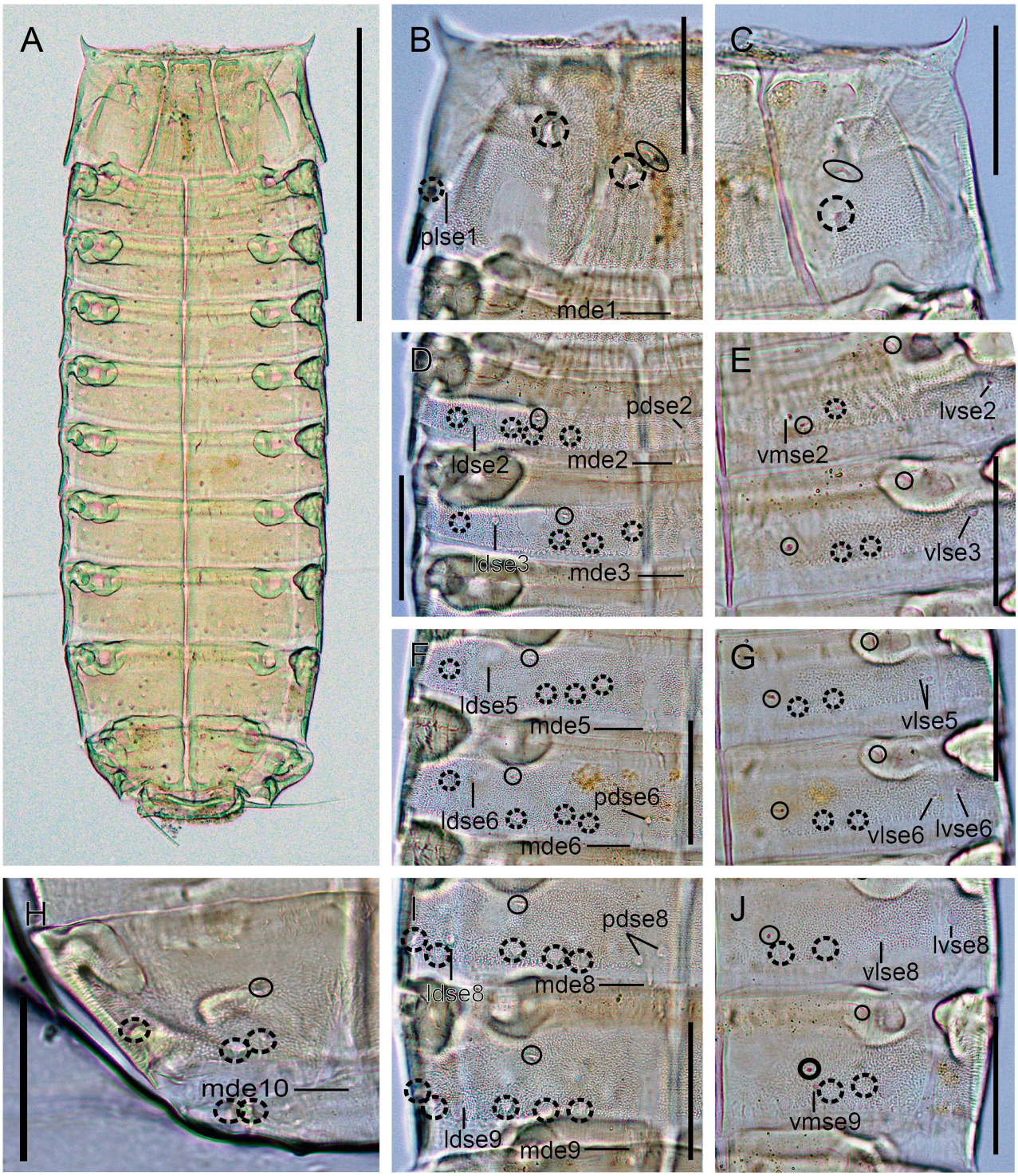

FIGURE 6 | Light micrographs showing trunk overview and details in the main trunk cuticular appendages of female holotype NHMD 669766 of *Fujuriphyes hydra* sp. nov. **(A)** Ventral overview of trunk; **(B)** middorsal to paralateral view on right half of tergal plate of segment 1; **(C)** ventrolateral to ventromedial view on left half of sternal plates of segment 1; **(D)** middorsal to laterodorsal view on right half of tergal plates of segments 2–3; **(E)** left sternal plates of segments 2–3; **(F)** middorsal to laterodorsal view on right half of tergal plates of segments 5–6; **(G)** left sternal plates of segments 5–6; **(H)** middorsal to laterodorsal view on right half of tergal plate of segment 10; **(I)** middorsal to laterodorsal view on right half of tergal plate of segments 8–9; **(J)** left sternal plates of segments 8–9. Scale bars: **(A):** 250 μm; **(B–J)**: 62 μm. Abbreviations: ldse, laterodorsal seta; mde, middorsal elevation; pdse, paradorsal seta; plse, paralateral seta; vlse, ventrolateral seta; vmse, ventromedial seta; numbers after abbreviations indicate corresponding segment; sensory spots are marked as dashed circles (except paradorsal ones), and glandular cell outlets as closed circles.

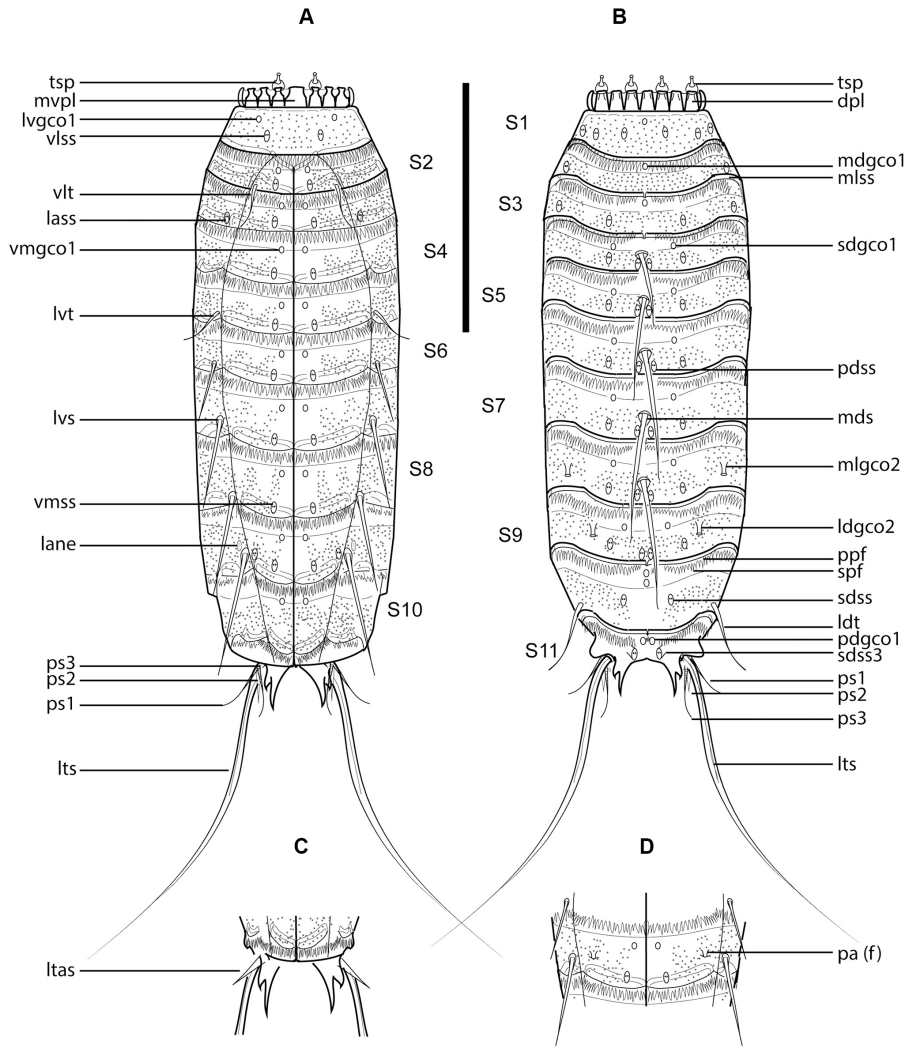

FIGURE 7 | Line art illustrations of *Fissuroderes cthulhu* sp. nov. **(A)** Male, ventral view; **(B)** male, dorsal view; **(C)** female, segments 10–11, ventral view; **(D)** female, segment 7, ventral view. Scale bar: 250 μm. Abbreviations: dpl, dorsal placid; f, female condition of sexually dimorphic character; lane, lateral accessory nephridiopore; lass, lateral accessory sensory spot; ldgco2, laterodorsal type 2 glandular cell outlet; ldss, laterodorsal sensory spot; ldt, laterodorsal tube; ltas, lateral terminal accessory spine; lts, lateral terminal spine; lvgco1, lateroventral type 1 glandular cell outlet; lvs, lateroventral spine; lvt, lateroventral tube; mdgco1, middorsal type 1 glandular cell outlet; mds, middorsal spine; mlgco2, midlateral type 2 glandular cell outlet; mlss, midlateral sensory spot; mvpl, midventral placid; pa, papilla; pdgco1, paradorsal type 1 glandular cell outlet; pdss, paradorsal sensory spot; ppf, primary pectinate fringe; ps, penile spine (followed by number of corresponding pair); sdgco1, subdorsal type 1 glandular cell outlet; sdss, subdorsal sensory spot; sdss3, subdorsal type 3 sensory spot; spf, secondary pectinate fringe; tsp, trichoscalid plate; vlss, ventrolateral sensory spot; vlt, ventrolateral tube; vmgco1, ventromedial type 1 glandular cell outlet; vmss, ventromedial sensory spot.

SEM, same collecting data as type material, deposited at the Meiofauna Collection of the UCM.

Diagnosis

Fissuroderes with spines in middorsal position on segments 4–8 and in lateroventral position on segments 6–9, increasing progressively in length toward the posterior segments; broad, elongated, and distally pointed tubes in ventrolateral position on segment 2, in lateroventral position on segment 5, and in laterodorsal position on segment 10. Tergal extensions of segment 11 elongated, distally bifurcated, with pointed tips. Type 2 glandular cell outlets in midlateral position on segment 8 and in laterodorsal position of segment 9. Females with sexually dimorphic papillae in ventrolateral position on segment 7.

Etymology

The species is named after the fictional cosmic entity Cthulhu, created by the American writer of horror fiction H.P. Lovecraft (1890-1937) and firstly introduced in the short story "The Call of Cthulhu," published in 1928. Considered a Great Old One within the pantheon of Lovecraftian cosmic entities, Cthulhu is a gigantic being of great power described as looking like an octopus or a dragon that lies in a death-like torpor in the sunken city of R'lyeh.

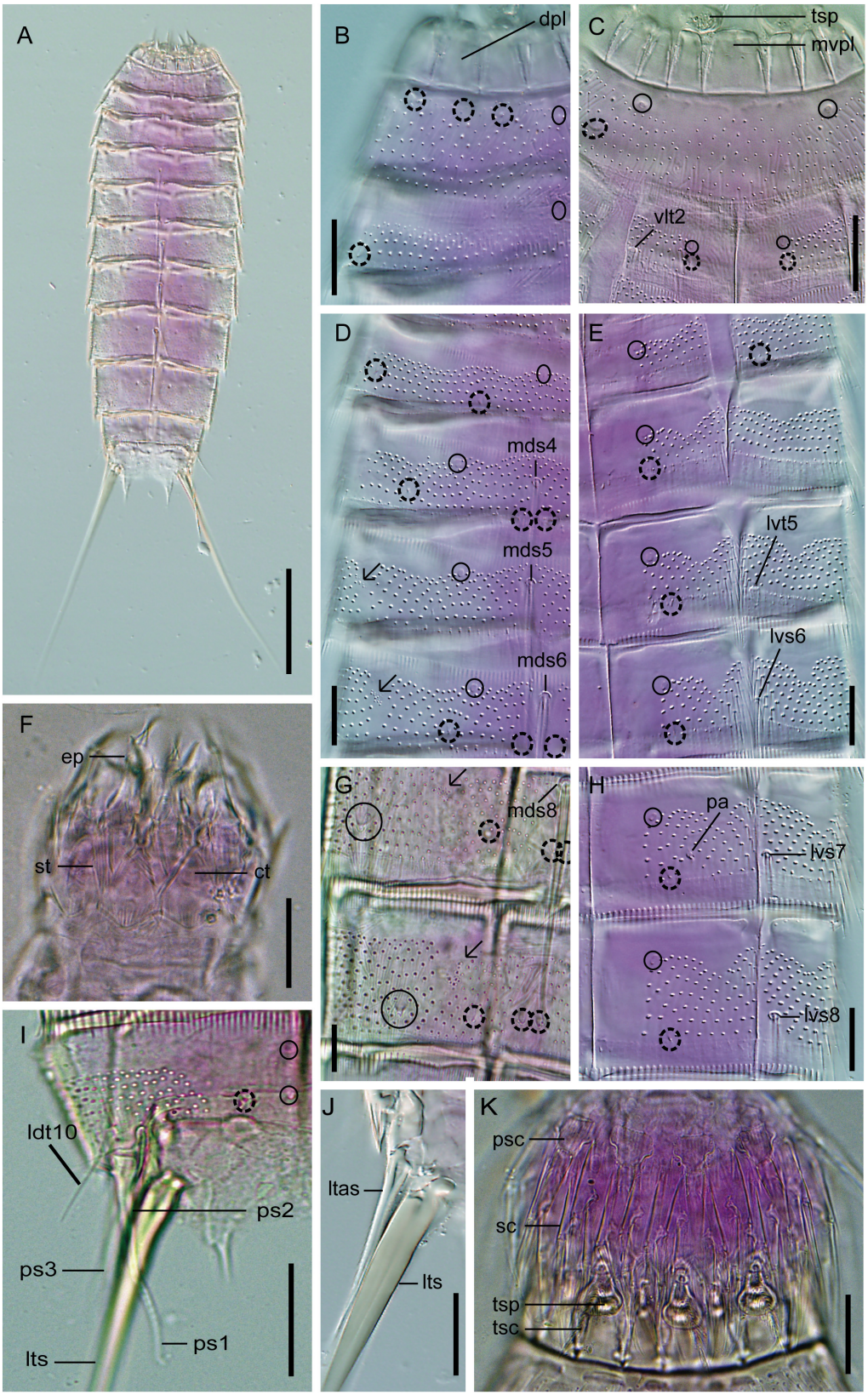

FIGURE 8 | Continued

FIGURE 8 | Light micrographs showing trunk overview and details in the head, neck, and main trunk cuticular characters of female holotype NHMD 669727 **(A–E,H,J)** and male paratype NHMD 669728 **(F,G,I,K)** of *Fissuroderes cthulhu* sp. nov. **(A)** Dorsal overview of trunk; **(B)** neck and middorsal to midlateral view on right half of tergal plates of segments 1–2; **(C)** neck and sublateral to ventromedial view tergal and sternal plates of segments 1–2; **(D)** middorsal to midlateral view on right half of tergal plates of segments 3–6; **(E)** sublateral to ventromedial view on left half of tergal and sternal plates of segments 3–6; **(F)** mouth cone; **(G)** middorsal to midlateral view on right half of tergal plates of segments 8–9; **(H)** sublateral to ventromedial view on left half of tergal and sternal plates of segments 7–8; **(I)** middorsal to midlateral view on right half of tergal plate of segment 10; **(J)** lateral terminal accessory spine; **(K)** introvert. Scale bars: **(A):** 100 μm; **(B–K)**: 20 μm. Abbreviations: ct, cuticular thickening; dpl, dorsal placid; ep, end-piece of outer oral style; ldt, laterodorsal tube; ltas, lateral terminal accessory spine; lts, lateral terminal spine; lvs, lateroventral spine; lvt, lateroventral tube; mds, middorsal spine; mvpl, midventral placid; pa, female papilla; ps, penile spine (followed by number of corresponding pair); psc, primary spinoscalid; sc, regular-sized scalid; st, spinous tuft of outer oral style; tsc, trichoscalid; tsp, trichoscalid plate; vlt, ventrolateral tube; numbers after abbreviations indicate corresponding segment; sensory spots are marked as dashed circles, and glandular cell outlets as closed circles; arrows indicate the muscular scars with several perforations as microsculpture.

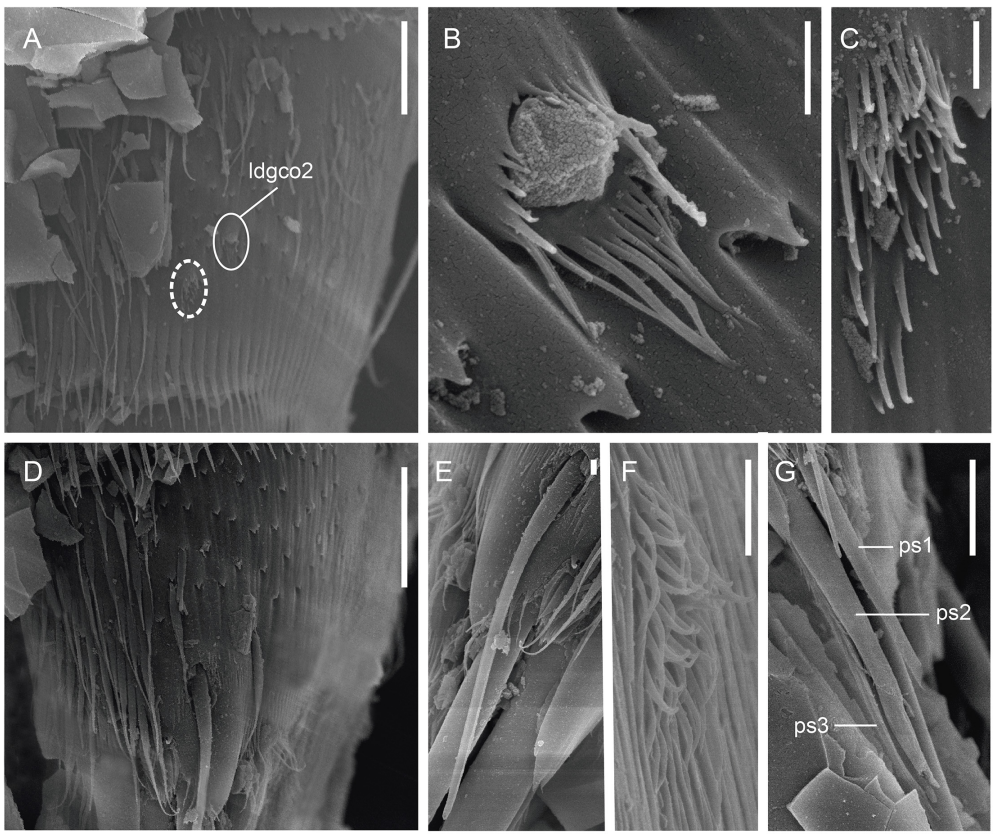

FIGURE 9 | Scanning electron micrographs showing some cuticular characters of segments 9–11 of a male of *Fissuroderes cthulhu* sp. nov. **(A)** Lateral view of segment 9; **(B)** detail of the laterodorsal type 2 glandular cell outlet of segment 9; **(C)** detail of the midlateral sensory spot of segment 9; **(D)** lateral view of segment 10; **(E)** detail of the laterodorsal tube of segment 10; **(F)** detail of the subdorsal sensory spot of segment 10; **(G)** detail of the penile spines of segment 11. Scale bars: **(A,D):** 10 μm; **(B,C,E–G)**: 1 μm. Abbreviations: ldgco2, laterodorsal type 2 glandular cell outlet; ps, penile spine (followed by number of corresponding pair); sensory spots are marked as dashed circles.

Description

See **Supplementary Table 1.5** for measurements and dimensions and **Supplementary Table 1.6** for summary of spine, tube, nephridiopore, glandular cell outlet, and sensory spot locations.

Head with retractable mouth cone and introvert (**Figures 8F,K**). Although some of the specimens have the introvert partially everted, oral styles and scalids tended to be collapsed when mounted for LM; furthermore, specimens for SEM were not suitable for head examination, so only some details on the exact number, arrangement, and morphology of oral styles and scalids can be provided.

Ring 00 of mouth cone with nine outer oral styles alternating in size between slightly larger and smaller ones (**Figure 8F**). Outer oral styles composed of two jointed subunits: a rectangular basal piece with a proximal sheath bearing a long, spinous tuft; and a triangular, curved end piece distally sharped (**Figure 8F**). Triangular, cuticular thickenings flanking the outer oral styles' bases (**Figure 8F**). Outer oral styles located anterior to each introvert sector, except in the middorsal section 6 where a style is missing.

Introvert with six transverse rings of scalids and 10 longitudinal sectors defined by the arrangement of the primary

spinoscalids. Ring 01 with 10 primary spinoscalids, larger than the remaining ones, laterally compressed, composed of a trapezoidal, wide basal sheath and a distal, elongated, flexible, distally blunt end piece (**Figure 8K**). The basal sheath bears two long, thread-like projections laterally and a median fringe of several long and flexible tips (**Figure 8K**). Rings 02–06 with regular-sized, laterally compressed scalids, much smaller than the primary spinoscalids, each one composed of a rectangular basal sheath carrying a median fringe and a distal, pointed end piece (**Figure 8K**). Exact arrangement of these scalids cannot be provided.

Neck with 16 trapezoidal placids, wider at bases, with a distinct joint between the neck and segment 1 (**Figures 7A,B**, **8B,C,K**). Midventral placid widest (ca. 17–19 μm wide at base), remaining ones narrower (ca. 12–13 μm wide at base) (**Figures 7A,B**, **8B,C,K**). Placids closely situated at base, distally separated by cuticular folds (**Figures 7A,B**, **8B,C,K**). A ring of six long, hairy trichoscalids associated with the placids of the neck is present, attached to large, bottle-like trichoscalid plates (**Figures 7A,B**, **8C,K**).

Trunk with 11 segments, triangular in cross-section (**Figures 7A,B**, **8A**). Segment 1 as closed cuticular ring, remaining ones with one tergal and two sternal cuticular plates (**Figures 7A–D**, **8A**). Tergal plates middorsally bulging. Maximum width at segment 6, progressively tapering toward the last trunk segments (**Figures 7A,B**, **8A**). Sternal plates relatively narrow compared to the total trunk length (MSW-6:TL average ratio = 22.3%), giving the animal a rectangular general appearance (**Figures 7A,B**, **8A**). Cuticular hairs present on segments 1–10, acicular, elongated, distally pointed, with rounded to oval-shaped perforation sites (**Figures 7A–D**, **8B–E,G,H**, **9A,D**). Cuticular hairs distributed in 5–7 wavy, transverse rows at the middle part of the plates on segments 2–9; in 6–7 straight, transverse rows almost covering the whole cuticular surface on segment 1; and segment 10 with 5–7 wavy, transverse rows at the middle part of the plates, from subdorsal to ventromedial regions (**Figures 7A–D**, **8B–E,G–I**). Muscular scars with several perforations as microsculpture throughout the trunk (**Figure 8D,G**). Posterior margin of segments 1–10 straight, showing a long, conspicuous primary pectinate fringe with a strong serration with bifid tips (**Figures 7A,B,D**, **8B–E,G,H**, **9A,D**). Secondary pectinate fringes on segments 2–11, with a very weak serration and usually hidden by the primary pectinate fringe of the previous segment (**Figures 7A,B,D**).

Segment 1 without spines and tubes. Unpaired type 1 glandular cell outlet in middorsal position, and paired type 1 glandular cell outlets in lateroventral position (**Figures 7A,B**, **8B,C**). Type 1 glandular cell outlets on this and remaining segments situated at the anterior half of the segment, sometimes hidden under the pectinate fringe of the previous segment. Paired sensory spots in subdorsal, laterodorsal, midlateral, and ventrolateral positions (**Figures 7A,B**, **8B,C**). Sensory spots on this and remaining segments composed of several long micropapillae and sometimes with a single, central cilium (**Figures 9C,F**).

Segment 2 with a pair of wide, flexible tubes in ventrolateral position (**Figures 7A**, **8C**). Tubes on this and remaining segments are composed of a short, rectangular, wide basal-piece and a flexible, elongated, distally pointed end piece that resembles an acicular spine in LM (**Figure 9E**). Unpaired type 1 glandular cell outlet in middorsal position, and paired type 1 glandular cell outlets in ventromedial position (**Figures 7A,B**, **8B,C**). Paired sensory spots in midlateral and ventromedial positions (**Figures 7A,B**, **8B,C**).

Segment 3 without spines and tubes. Unpaired type 1 glandular cell outlet in middorsal position, and paired type 1 glandular cell outlets in ventromedial position (**Figures 7A,B**, **8D,E**). Paired sensory spots in subdorsal, midlateral, lateral accessory, and ventromedial positions (**Figures 7A,B**, **8D,E**).

Segment 4 with a middorsal spine not exceeding the posterior edge of the following segment (**Figures 7B**, **8D**). Spines on this and remaining segments are acicular and flexible, increasing in length toward the end of the trunk throughout both the middorsal and lateroventral series (**Figures 7A,B**, **8D,E,G,H**). Paired type 1 glandular cell outlets in subdorsal and ventromedial positions (**Figures 7A,B**, **8D,E**). Paired sensory spots in paradorsal, laterodorsal, and ventromedial positions (**Figures 7A,B**, **8D,E**).

Segment 5 with a middorsal spine reaching the posterior edge of the following segment, and paired lateroventral tubes (**Figures 7A,B**, **8D,E**). Paired type 1 glandular cell outlets in subdorsal and ventromedial positions (**Figures 7A,B**, **8D,E**). Paired sensory spots in paradorsal, subdorsal, and ventromedial positions (**Figures 7A,B**, **8D,E**).

Segment 6 with a middorsal spine exceeding the posterior edge of the following segment, and paired lateroventral spines (**Figures 7A,B**, **8D,E**). Paired type 1 glandular cell outlets in subdorsal and ventromedial positions (**Figures 7A,B**, **8D,E**). Paired sensory spots in paradorsal, subdorsal, and ventromedial positions (**Figures 7A,B**, **8D,E**).

Segment 7 similar to segment 6 in the arrangement of spines, type 1 glandular cell outlets, sensory spots, and cuticular hairs, as well as in the morphology of the posterior margin of segment, primary and secondary pectinate fringes, except females that have sexually dimorphic papillae in ventrolateral position (**Figures 7A,B,D**, **8H**).

Segment 8 with a middorsal spine exceeding the posterior edge of the following segment, and paired lateroventral spines (**Figures 7A,B**, **8G,H**). Paired type 1 glandular cell outlets in subdorsal and ventromedial positions, and paired type 2 glandular cell outlets in midlateral position (**Figures 7A,B**, **8G,H**). Type 2 glandular cell outlets consist of a big, elevated pore surrounded by a single ring of long micropapillae (**Figure 9B**). Paired sensory spots in paradorsal, subdorsal, and ventromedial positions (**Figures 7A,B**, **8G,H**).

Segment 9 with paired lateroventral spines (**Figure 7A**). Paired type 1 glandular cell outlets in subdorsal and ventromedial positions, and paired type 2 glandular cell outlets in laterodorsal position (**Figures 7A,B**, **8G**, **9B**). Paired sensory spots in paradorsal, subdorsal, and ventromedial positions (**Figures 7A,B**, **8G**, **9C**). Nephridiopores as small sieve plates in lateral accessory position (**Figure 7A**).

Segment 10 with paired laterodorsal tubes (**Figures 7B**, **8I**, **9E**). Two unpaired type 1 glandular cell outlets in middorsal

position, and paired type 1 glandular cell outlets in ventromedial position (**Figures 7A,B**, **8I**). Paired sensory spots in subdorsal position (**Figures 7B**, **8I**, **9F**).

Segment 11 with type 1 glandular cell outlets in paradorsal position and type 3 sensory spots in subdorsal position (**Figure 7B**). Slender, flexible lateral terminal spines (**Figures 7A,B**, **8A,I,J**). Females with paired short, robust lateral accessory spines (LTAS:LTS average ratio = 28.4%) (**Figures 7C**, **8J**). Males with three pairs of penile spines: first and third pairs long, flexible and crenulated, second pair shorter, robust and superficially smooth (**Figures 7A,B**, **8I**, **9G**). Tergal extensions of segment 11 elongated, distally bifurcated, with pointed tips (**Figures 7A–C**, **8I**). Sternal plates distally rounded (**Figures 7A,C**).

Associated kinorhynch fauna

Fissuroderes cthulhu sp. nov. co-occurred with *Condyloderes* sp., *E. unispinosus* and *F. dagon* sp. nov. in the analyzed samples.

Community Structure Along the Vertical Profile and Intra-Habitats Comparison

Densities outside the pockmarks are low and significantly decrease from the upper to the bottom sediment layers (p = 0.0242), varying more gradually than those inside the pockmarks. Densities significantly vary along the vertical profile inside the pockmarks (p = 0.0117), reaching a peak in layer 1–2 cm (means of ca. 34 specimens per 10 cm^2 at MTB06 and 4 specimens per 10 cm^2 at MTB1), and strongly decreasing from this depth (**Table 1** and **Figures 10**, **11**). Likewise, species richness outside the pockmarks is low and changes significantly with sediment depth (p = 0.0389), having its highest value in the uppermost layer, 0–1 cm (means of ca. 1 species at both MTB2 and MTB03), and no specimens in the deepest layers, 3–4 and 4–5 cm (**Table 1** and **Figure 10**). Species richness is more stable along the vertical profile inside the pockmarks, and no significant differences are observed. The highest values are found in the second sediment layer (means of ca. 3 species at MTB06 and ca. 1 species in MTB1), and kinorhynchs are still present in the bottom layers (highest means at MTB06 of ca. 2 and 1 species at 3–4 and 4–5 cm depth, respectively) (**Table 1** and **Figure 10**).

Considering the whole cores, analyses between sites of the same habitat found no differences comparing sites outside the pockmarks (density, p = 0.5066; richness, p = 0.5002), or between the pockmark sites (density, p = 0.1266; richness, p = 0.0722), except for the species assemblage between the two pockmark sites (see below).

Inter-Habitats Comparison

Both habitats are similar in terms of species richness (p = 0.6831), with means of ca. 1–2 species outside the pockmarks (per site: ca. 2 species at MTB03 and 1 species at MTB2), and means of ca. 2 species inside the pockmarks (per site: ca. 3 species at MTB06 and 1 species at MTB1) (**Table 2** and **Figure 12**). However, kinorhynchs show a significant higher density inside the pockmarks (p = 0.0039), with means of ca. 35–36 specimens per 10 cm^2 inside the pockmarks (per site: 56 specimens at

TABLE 1 | Species richness and specimen abundance of Kinorhyncha present at the study sites.

		OUTSIDE POCKMARK MTB03					OUTSIDE POCKMARK MTB2					INSIDE POCKMARK MTB06					INSIDE POCKMARK MTB1				
	Sediment layer	A	B	C	X	Total	A	B	C	X	Total	A	B	C	X	Total	A	B	C	X	Total
Species Richness	0–1	1	0	2	1 ± 1	3	0	3	1	1.3 ± 1.5	3	-	2	2	2 ± 0	4	0	1	1	0.7 ± 0.6	2
	1–2	4	0	1	1.7 ± 2.1	5	0	0	0	0	0	1	3	4	2.7 ± 1.5	8	2	1	1	1.3 ± 0.6	4
	2–3	1	0	0	0.3 ± 0.6	1	0	0	0	0	0	2	1	2	1.7 ± 0.6	5	0	1	1	0.7 ± 0.6	2
	3–4	0	0	0	0	0	0	0	0	0	0	2	2	2	2 ± 0	6	0	0	1	0.3 ± 0.6	1
	4–5	0	0	0	0	0	0	0	0	0	0	2	1	1	1.3 ± 0.6	4	0	0	1	0.3 ± 0.6	1
Abundance	0–1	2	0	4	2 ± 2	6	0	3	1	1.3 ± 1.5	4	-	44	24	34 ± 14.1	68	0	46	15	20.3 ± 23.5	61
	1–2	11	0	3	4.7 ± 5.7	14	1	1	0	0.7 ± 0.6	2	84	16	210	103.3 ± 98.4	310	7	24	9	13.3 ± 9.3	40
	2–3	2	0	2	1.3 ± 1.2	4	0	0	0	0	0	19	8	68	31.7 ± 31.9	95	6	9	5	6.7 ± 2.1	20
	3–4	0	0	0	0	0	0	0	0	0	0	10	4	10	8 ± 3.5	24	12	1	1	4.7 ± 6.4	14
	4–5	0	0	0	0	0	0	0	0	0	0	2	1	4	2.3 ± 1.5	7	2	0	1	1 ± 1	3
Density (ind/10 cm^2)	0–1	0.7	0	1.3	0.7 ± 0.7		0	1	0.3	0.43 ± 0.51		-	14.6	8	11.3 ± 4.7		0	15.2	5	6.7 ± 7.7	
	1–2	3.6	0	1	1.5 ± 1.8		0.3	0.3	0	0.2 ± 0.17		27.8	5.3	69.6	34.2 ± 32.6		2.3	8	3	4.4 ± 3.1	
	2–3	0.7	0	0.7	0.5 ± 0.4		0	0	0	0		6.3	2.7	22.5	10.5 ± 10.5		2	3	1.7	2.2 ± 0.68	
	3–4	0	0	0	0		0	0	0	0		3.3	1.3	3.3	2.6 ± 1.1		4	0.3	0.3	1.5 ± 2.1	
	4–5	0	0	0	0		0	0	0	0		0.7	0.3	1.3	0.77 ± 0.5		0.7	0	0.3	0.33 ± 0.35	

Data are specified by cores and layers along the vertical profile. Total numbers show the data merging the information of the three cores. X refers to average values ± standard deviation.

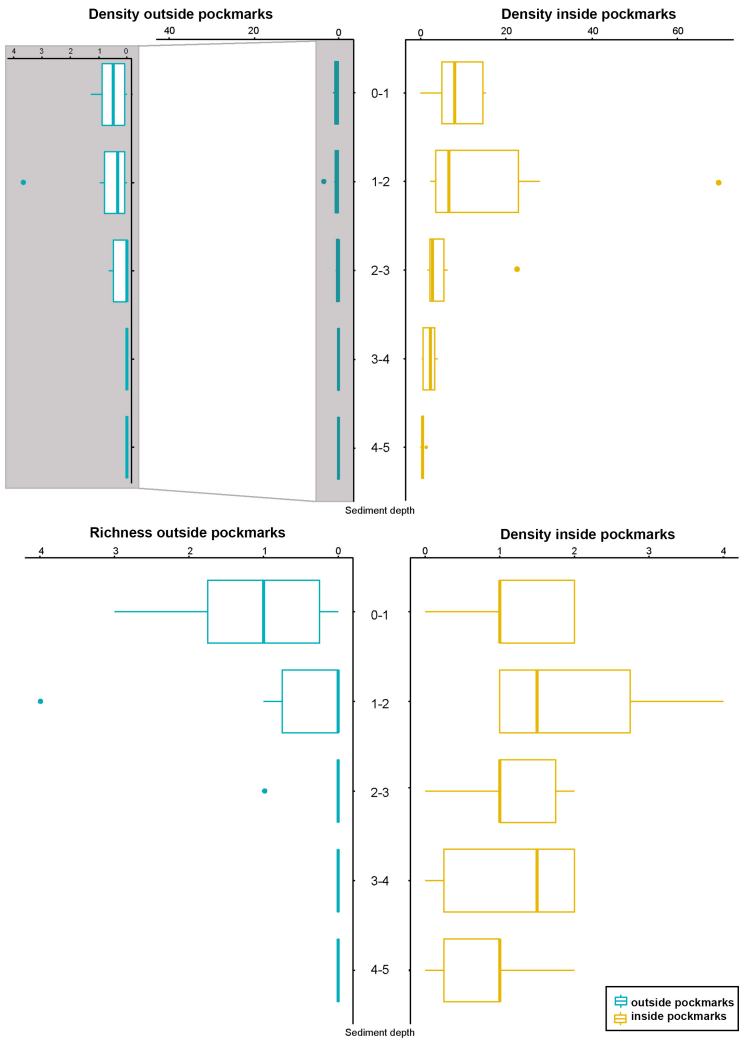

FIGURE 10 | Kinorhynch density and richness along the vertical profile of the two study habitats, inside pockmark (yellow) and outside pockmark (blue). Image enlargement of density outside the pockmark is provided to allow discerning variation of kinorhynch densities along the vertical profile. Boxplots represent the median value (horizontal line within the box), the distributions of 50% of the data (the box), and the highest and lowest values within 95% of the distribution (the whisker).

MTB06 and 15 specimens at MTB1) vs. means of ca. 1–2 specimens per 10 cm^2 outside the pockmarks (per site: ca. 3 specimens per 10 cm^2 at MTB03 and 0 specimens at MTB2) (**Table 2** and **Figures 11**, **12**). Juveniles were always present and relatively abundant both inside and outside the pockmarks, with means of ca. 3–4 specimens per 10 cm^2 outside (per site: ca. 5 specimens, 20.8% of the total kinorhynch abundance at MTB03 and 2 specimens, 33.3% at MTB2) and means of ca. 30–31 specimens per 10 cm^2 inside the pockmarks (per site: ca. 169 specimens, 33.5% of the total kinorhynch abundance at MTB06 and 92 specimens, 65.2% at MTB1) (**Table 2** and **Figure 12**).

It appears that most of the species are restricted to one of the studied habitats, except *Condyloderes* sp. and *E. unispinosus* Yamasaki et al., 2018b that are present both outside and inside the pockmarks. *E. unispinosus* is the dominant species inside the pockmarks (63.1% of the total adult kinorhynch community), followed far behind by *Fi. cthulhu* sp. nov. (15% of the adult community), *Echinoderes hviidarum* Sørensen et al., 2018 (11.8% of the adult community) and *F. dagon* sp. nov. (6.6% of the adult community) (**Table 2** and **Figure 12**). All the referred species were recovered only at the pockmark site MTB06, except for *E. hviidarum* that only appeared at MTB1 (**Table 2** and **Figure 12**). The remaining species were recovered only at one of the sites in low number: *Echinoderes apex* Yamasaki et al. (2018c), *Echinoderes* cf. *dubiosus*, *Echinoderes* sp., *Ryuguderes* sp., and *F. hydra* sp. nov. outside the pockmarks; and *Sphenoderes* cf. *indicus* as a singleton inside the pockmark MTB1 (**Table 2** and **Figure 12**).

Differences in community composition between the two study habitats, inside and outside the pockmarks, were observed (occurrence: $p = 0.005$, $F.Model = 3.8761$, $R^2 = 0.222$; abundance: $p = 0.003$, $F.Model = 3.8926$, $R^2 = 0.235$). Moreover, H_2S

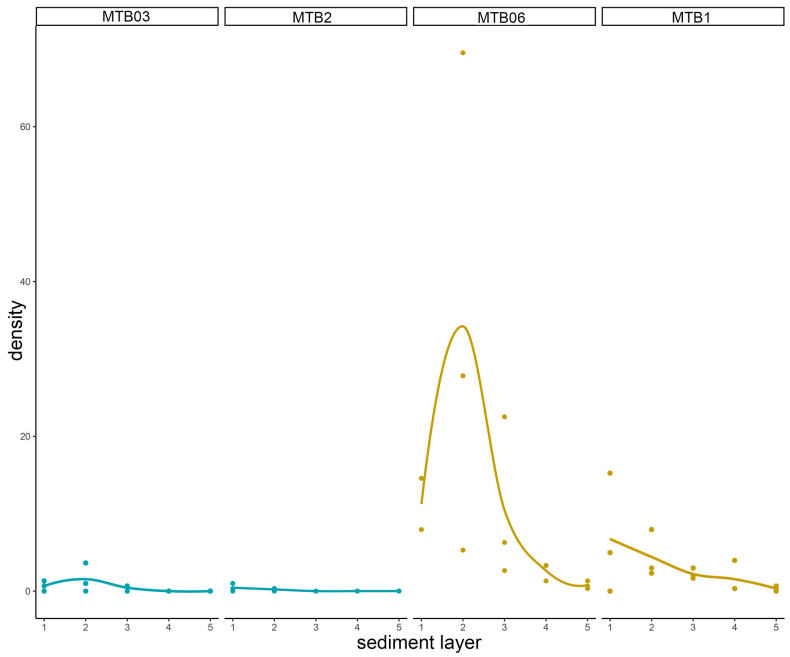

FIGURE 11 | Kinorhynch total density (including both adults and juveniles) along the vertical profile of the four study sites: MTB03 and MTB2 as outside pockmark sites (blue), and MTB06 and MTB1 (purple) as inside pockmark sites (yellow). Layers per core were determined as follows: layer 1 (0–1 cm), layer 2 (1–2 cm), layer 3 (2–3 cm), layer 4 (3–4 cm), and layer 5 (4–5 cm).

was found as a covariate explanatory variable (occurrence: $p = 0.001$, *F.Model* = 6.6067, $R^2 = 0.3779$; abundance: $p = 0.001$, *F.Model* = 5.6791, $R^2 = 0.343$). Differences in community composition were found between the two study pockmarks as well (occurrence: $p = 0.001$, *F.Model* = 44.255, $R^2 = 0.678$; abundance: $p = 0.001$, *F.Model* = 18.3670, $R^2 = 0.467$). None of the analyses showed significant differences to discriminate between sites outside the pockmarks. PCA for illustrating kinorhynch trends in community composition discriminated among sites: PC2 distinguished between sites located inside and outside the pockmarks, whereas PC1 discriminated between the two pockmarks (**Figure 13**). PC1 explained 39.8% of the variance and was mainly affected by the high abundance of *E. hviidarum* at the pockmark site MTB1 (site with the highest concentrations of H_2S and detection of CH_4), whereas *E. unispinosus* followed by *Fi. cthulhu* sp. nov. distinguished the pockmark site MTB06 (site with emission of CH_4 only, H_2S not detected), and PC2 explained 25.7% of the variance, with *Condyloderes* sp., *Echinoderes* cf. *dubious*, and *Ryuguderes* sp. characterizing the sites located outside the pockmarks and *E. unispinosus* and *E. hviidarum* characterizing the sites inside the pockmarks (**Figure 13**). We are aware that a larger total variance explained by the two PCAs would have been desirable and therefore other factors not included in the present study could be responsible for the remaining percentage of variance, but still the studied pockmark conditions explained some differences in the kinorhynch community composition between both pockmarks and between pockmarks and sites outside pockmarks.

DISCUSSION

Remarks on Diagnostic and Taxonomic Features of *F. dagon* sp. nov. and *F. hydra* sp. nov.

The two new species of *Fujuriphyes* agree with the main diagnostic characters of the genus, including the presence of ventrolateral setae on segment 5 and on additional segments from segment 3 to 9 where ventromedial setae are absent, as well as long lateral terminal spines (LTS:TL average ratio > 30%) (Sánchez et al., 2016). Until now, the genus was composed of seven species: three from the Caribbean Sea, *Fujuriphyes dalii* Cepeda et al., 2019b, *F. deirophorus* (Higgins, 1983), and *F. distentus* (Higgins, 1983); one from the Gulf of Mexico, *F. viserioni* Sánchez et al., 2019a,b; one from the East China Sea, *F. longispinosus* Sánchez and Yamasaki, 2016; and two from the Mediterranean Sea, *F. ponticus* (Reinhard, 1881) and *F. rugosus* (Zelinka, 1928).

The presence of lateral terminal spines in both *F. dagon* sp. nov. and *F. hydra* sp. nov. easily allows their differentiation from *F. deirophorus* and *F. distentus* that lack these structures (Higgins, 1983).

The absence of middorsal cuticular specializations (processes or elevations) throughout the trunk in *F. dagon* sp. nov. is only shared with *F. dalii* (Cepeda et al., 2019b). However, both species may be easily distinguished by the arrangement of setae. *F. dalii* has a pair of paralateral setae on segment 1 (Cepeda et al., 2019b), which are absent in *F. dagon* sp. nov. The lateroventral

TABLE 2 | Kinorhyncha species identified at study sites.

	OUTSIDE POCKMARK MTB03					OUTSIDE POCKMARK MTB2					INSIDE POCKMARK MTB06					INSIDE POCKMARK MTB1				
Species	**A**	**B**	**C**	**X**	**Total**	**A**	**B**	**C**	**X**	**Total**	**A**	**B**	**C**	**X**	**Total**	**A**	**B**	**C**	**X**	**Total**
Condyloderes sp.	0	0	0	0	0	0	1	1	0.67 ± 0.58	2	0	0	1	0.33 ± 0.58	1	0	0	0	0	0
Echinoderes apex	1	0	0	0.33 ± 0.58	1	0	0	0	0	0	0	0	0	0	0	0	0	0	0	0
Echinoderes cf. *dubiosus*	0	0	3	1 ± 1.7	3	0	1	0	0.33 ± 0.58	1	0	0	0	0	0	0	0	0	0	0
Echinoderes hviidarum	0	0	0	0	0	0	0	0	0	0	0	0	0	0	0	5	24	16	15 ± 9.5	45
Echinoderes unispinosus	2	0	1	1 ± 1	3	0	0	0	0	0	77	24	151	84 ± 63.8	252	0	0	0	0	0
Echinoderes sp.	0	0	2	0.67 ± 1.2	2	0	0	0	0	0	0	0	0	0	0	0	0	0	0	0
Fissuroderes cthulhu sp. nov.	0	0	0	0	0	0	0	0	0	0	12	3	42	19 ± 20.4	57	0	0	0	0	0
Ryuguderes sp.	4	0	0	1.3 ± 2.3	4	0	1	0	0.33 ± 0.58	1	0	0	0	0	0	0	0	0	0	0
Sphenoderes cf. *indicus*	0	0	0	0	0	0	0	0	0	0	0	0	0	0	0	1	0	0	0.33 ± 0.58	1
Fujuriphyes dagon sp. nov.	0	0	0	0	0	0	0	0	0	0	0	6	19	8.3 ± 9.7	25	0	0	0	0	0
Fujuriphyes hydra sp. nov.	6	0	0	2 ± 3.5	6	0	0	0	0	0	0	0	0	0	0	0	0	0	0	0
Adult abundance	13	0	6	6.3 ± 6.5	19	0	3	1	1.3 ± 1.5	4	89	33	213	111.7 ± 92.11	335	6	24	16	15.3 ± 9	46
Total abundance	15	0	9	8.0 ± 7.6	24	1	4	1	2 ± 1.7	6	115	73	316	168 ± 129.9	504	27	80	31	46 ± 29.5	138
Total density (ind/10 cm^2)	5	0	3	2.6 ± 2.5		0.5	0.2	0.5	0.37 ± 0.15		38.1	24.2	105	55.6 ± 43		8.9	26.5	10.3	15.2 ± 9.8	
Total species richness	4	0	3	2.3 ± 2.1	6	0	3	1	1.3 ± 1.5	3	2	3	4	3 ± 1	4	2	1	1	1.3 ± 0.6	2

Abundance of each species is specified by cores and merging the data of the three cores in the total. Data are specified by cores and merging the data of the three cores. Total abundance includes adults and juvenile stages. X refers to average values ± standard deviation.

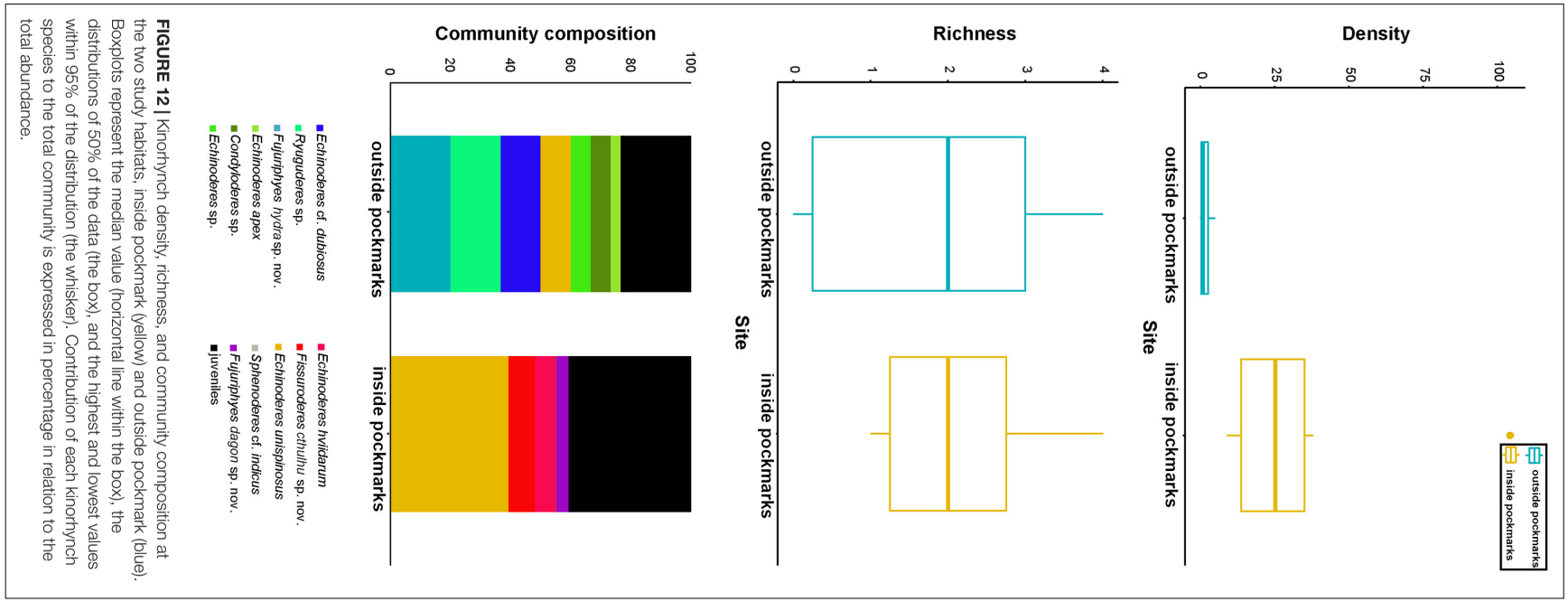

FIGURE 12 | Kinorhynch density, richness, and community composition at the two study habitats. inside pockmark (yellow) and outside pockmark (blue). Boxplots represent the median value (horizontal line within the box), the distributions of 50% of the data (the box), and the highest and lowest values within 95% of the distribution (the whisker). Contribution of each kinorhynch species to the total community is expressed in percentage in relation to the total abundance.

setae of *F. dalii* are only present on segments 2, 4, and 10 (Cepeda et al., 2019b), while those of *F. dagon* sp. nov. are present on all the even-numbered segments. *F. dagon* sp. nov. has ventrolateral setae on segment 2, which are absent in *F. dalii* sp. nov. (Cepeda et al., 2019b). Additionally, *F. dalii* possesses ventromedial setae on segments 8–9 (Cepeda et al., 2019b), whereas *F. dagon* sp. nov. lacks setae in ventromedial position throughout the trunk.

The presence of middorsal elevations throughout segments 1–10 in *F. hydra* is unique within the genus, as the remaining species possess a different arrangement of middorsal elevations. *F. ponticus* and *F. rugosus* bear these structures on segments 1–9; *F. viserioni*, on segment 3; and *F. longispinosus*, on segments 1–6 (Reinhard, 1881; Zelinka, 1928; Sánchez and Yamasaki, 2016; Sánchez et al., 2016, 2019b). Regarding the setae arrangement, *F. hydra* sp. nov. is most similar to *F. dalii* and *F. longispinosus*, as the three species possess two pairs of ventrolateral setae on segment 5 and a relatively low number of ventromedial setae. Thus, *F. dalii* has ventromedial setae on segments 8–9, and *F. longispinosus* bears these structures on segments 2 and 9 in both sexes (Sánchez et al., 2016; Cepeda et al., 2019b). *F. hydra* sp. nov. also has ventromedial setae on segments 2 and 9, but those of segment 2 are only present in females. Moreover, the two pairs of ventrolateral setae of segment 5 of *F. hydra* sp. nov. are situated very close together, a feature that has not been observed in the remaining congeners.

Remarks on Diagnostic and Taxonomic Features of *Fi. cthulhu* sp. nov.

Currently, the genus *Fissuroderes* is morphologically defined by the combination of one tergal and two sternal plates on segment 2 plus paired, sexually dimorphic ventral papillae in females (Herranz and Pardos, 2013), despite the fact that females of one of the species, *Fi. papai* Neuhaus and Blasche, 2006, lack these structures. The newly described species, *Fi. cthulhu* sp. nov., matches the aforementioned condition of sexually dimorphic papillae, as only females bear these structures in ventrolateral position on segment 7. *Polacanthoderes* is the only genus of the family Echinoderidae that shares the arrangement of cuticular plates of segment 2 with *Fissuroderes* (Claparède, 1863; Adrianov and Malakhov, 1999; Neuhaus and Blasche, 2006; Sørensen, 2008a; Herranz et al., 2012), but it is furthermore characterized by possessing unusual morphological features never found in the remaining kinorhynch genera, including acicular spines in subdorsal, laterodorsal, midlateral, ventrolateral, and ventromedial positions (Sørensen, 2008a). This led us to include the new species in the genus *Fissuroderes*. Nevertheless, a total-evidence systematic revision of the family Echinoderidae is needed in order to describe new reliable characters of the different genera (Sørensen, 2008b; Sørensen et al., 2015).

Regarding the spine and tube arrangements, *Fi. cthulhu* sp. nov. is most similar to *Fi. novaezealandia* Neuhaus and Blasche (2006) and *Fi. thermoi* Neuhaus and Blasche (2006), as the three species share the presence of middorsal spines on segments 4–8, lateroventral spines on segments 6–9, ventrolateral tubes on segment 2, and lateroventral tubes on segment 5 (Neuhaus and Blasche, 2006). However, *Fi. novaezealandia* lacks laterodorsal tubes on segment 10, which are present and easily recognizable in *Fi. thermoi* and *Fi. cthulhu* sp. nov. (Neuhaus and Blasche, 2006). The main morphological differences between *Fi. thermoi* and *Fi. cthulhu* sp. nov. are the arrangement of the type 2 glandular cell outlets and female papillae, and the shape of the tergal extensions. *Fissuroderes thermoi* possesses type 2 glandular cell outlets in midlateral position on segments 5, 6, 8, and 9 (females furthermore with papillae in ventromedial position of segment 7), and its tergal extensions are short and distally rounded (Neuhaus and Blasche, 2006), while *Fi. cthulhu* sp. nov. has type 2 glandular cell outlets in midlateral position on segment 8 and in laterodorsal position on segment 9 (females furthermore with papillae in ventrolateral position of segment 7), and its tergal extensions are long, bifurcated, and distally pointed.

New Kinorhynch Records

The species *E. apex*, *E.* cf. *dubiosus*, *E. hviidarum*, *E. unispinosus*, *Ryuguderes* sp., and *Sphenoderes* cf. *indicus* were also reported in the analyzed pockmark field for the first time. In addition, *Condyloderes* sp. and *Echinoderes* sp. were also recorded, but the material was badly preserved and did not allow us to identify them to the species level.

A single specimen of *E. apex* was found at MOZ01-MTB03 (outside pockmarks). The species is characterized by having spines in middorsal position on segments 4, 6, and 8 and in lateroventral position throughout segments 6–9, together with tubes in ventrolateral position on segment 2, lateroventral position on segment 5, and laterodorsal position on segment 10, and type 2 glandular cell outlets in subdorsal position on segment 2, sublateral position on segment 6, and lateral accessory position on segment 8 (Yamasaki et al., 2018c). Moreover, *E. apex* has a relatively short trunk, ranging from 165 to 215 μm, and long lateral terminal spines, ranging from 60.0 to 80.2% of the total trunk length (Yamasaki et al., 2018c). The specimen found in the present study agrees with these diagnostic characters (see **Supplementary Figure 2.1**), except the length of the lateral terminal spines that are slightly shorter than those of the type material, ranging from 54.5 to 56.0% of the total trunk length, but we do not consider this difference important enough to assign the specimen to a different species. *E. apex* has been reported in the Great Meteor Seamount (eastern Atlantic Ocean) at depths of 287–856 m (Yamasaki et al., 2018c). This finding supposes an extension of the distributional range of the species to the Mozambique Channel (Indian Ocean).

Three specimens of *Echinoderes* cf. *dubiosus* were recorded at MOZ01-MTB03 and one was recorded at MOZ04-MTB2 (outside pockmarks). *Echinoderes dubiosus* is characterized by having spines in middorsal position throughout segments 4–8 and in lateroventral position on segments 6–9 (with those of segment 9 extending beyond segment 11), as well as tubes in lateroventral position on segment 5, sublateral position on

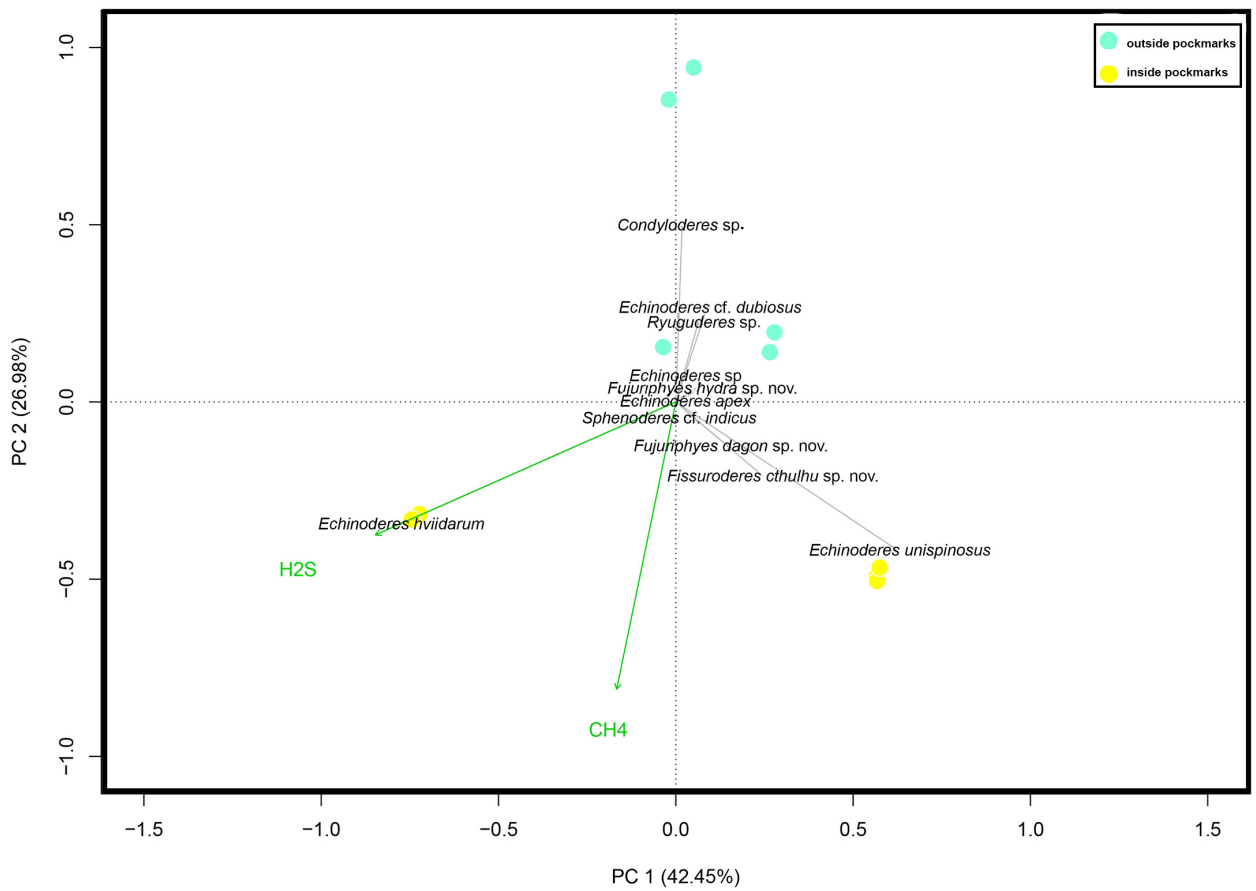

FIGURE 13 | Principal component analysis scaling two bi-plots based on Hellinger-transformed data on kinorhynch species composition considering the four study sites: two sites inside pockmarks (yellow) and two sites outside pockmarks (blue). Passive (*post hoc*) explanations of axis were conducted using environmental variables (CH_4, methane; and H_2S, hydrogen sulfide concentrations).

segment 8, and laterodorsal position on segment 10, and type 2 glandular cell outlets in midlateral position on segment 2 (Sørensen et al., 2018). The species also has middorsal cuticular structures on segment 9 forming a pore with a posterior papillary flap flanked by paired sensory spots (Sørensen et al., 2018). This last character was not observed in the specimens from the Mozambique Channel (see **Supplementary Figure 2.2**), which led us to tentatively identify them as *E.* cf. *dubiosus*. The species was previously known from the northern California (eastern Pacific Ocean) at 2702–3853 m depth (Sørensen et al., 2018), and this finding increases its bathymetrical and distributional range.

Echinoderes hviidarum was consistently found at MOZ04-MTB1 (within pockmark). The species has spines in middorsal position on segments 6 and 8 and lateroventral position throughout segments 6–9, as well as tubes in lateroventral position on segment 5, lateral accessory position on segment 8, and laterodorsal position on segments 9–10, and a middorsal protuberance on segment 11 (Sørensen et al., 2018). The specimens reported in the Mozambique Channel agree well with the aforementioned diagnostic characters of the species (see **Supplementary Figure 2.3**). *E. hviidarum* was exclusively reported off northern California (eastern Pacific Ocean) at 2702–3853 m depth (Sørensen et al., 2018), but with these findings, the bathymetrical and distributional range of the species is increased.

Echinoderes unispinosus was consistently reported at MOZ01-MTB03 (outside pockmarks) and MOZ01-MTB06 (within pockmark) and can be distinguished from its congeners by possessing spines in middorsal position on segment 4 and lateroventral position on segments 6–7, together with type 2 glandular cell outlets in midlateral position on segment 1; in subdorsal, laterodorsal, sublateral, and ventrolateral positions on segment 2; in lateral accessory position on segment 5; and in sublateral position on segment 8 (Yamasaki et al., 2018b). The species is furthermore characterized by having a narrow primary pectinate fringe with short tips throughout segments 1–10 and tergal extensions long, smoothly pointed (Yamasaki et al., 2018b). The specimens from the Mozambique Channel agree with these diagnostic characters of the species

(see **Supplementary Figure 2.4**), and the only morphological difference observed was the presence of subdorsal sensory spots on segment 4, which were not detected in the type material. *E. unispinosus* is known to possess a wide distributional range, being present in the northeast Atlantic Ocean, the northeast Pacific Ocean, and the Gulf of Mexico (Sørensen et al., 2018; Yamasaki et al., 2018b; Álvarez-Castillo et al., 2020). Now, its distributional range is furthermore increased to the Indian Ocean.

Three specimens from MOZ01-MTB03 and one from MOZ04-MTB02 (outside pockmarks) were tentatively assigned to *Ryuguderes* sp. This recently established genus of Campyloderidae can be distinguished from *Campyloderes* by having outer oral styles partially fused throughout the basal regions and free distal parts bearing lateral cuticular structures, as well as by the absence of lateroventral spines throughout the first trunk segments (Yamasaki, 2016). Currently, only a single species is known from the Ryukyu Islands (western Pacific Ocean), namely, *Ryuguderes iejimaensis* Yamasaki, 2016. The specimens from the Mozambique Channel seem to possess the diagnostic outer oral styles of *Ryuguderes*, but the lack of SEM material did not allow us to surely confirm this character. In addition, these specimens have important morphological discrepancies with *R. iejimaensis*, including the presence of a middorsal spine on segment 1, lateroventral spines on segment 3, a single pair of lateroventral spines on segment 5, females with middorsal spines on segment 10, and a different arrangement of sensory spots and glandular cell outlets (see **Supplementary Figure 2.5**).

A single specimen of *Sphenoderes* cf. *indicus* was found at MOZ04-MTB01 (within pockmark). *Sphenoderes indicus*, widely reported through the Bay of Bengal (Indian Ocean) at 6–40 m depth, is characterized by having acicular spines in middorsal position throughout segments 1–11 and lateroventral position on segments 3–9, as well as cuspidate spines in lateroventral position on segments 5 and 8–9, with those of segments 5 and 8 located more ventral than the acicular spines (Higgins, 1969). These characters were also found in the specimens from the Mozambique Channel (see **Supplementary Material 9**), but the arrangement of the sensory spots could not be completely determined because of the bad preservation of the specimens, which led us to tentatively identify them as *S.* cf. *indicus*. These findings increase the bathymetrical and distributional range of the species throughout the Indian Ocean.

Kinorhynch Community Structure and Composition

Our results show that kinorhynch density and community composition seem to be influenced by the environmental conditions of each study habitat, whereas similar values of richness were found in the inter-habitat comparison (**Figure 12**).

Kinorhynchs are more abundant inside the pockmarks, where environmental conditions are extreme due to reduced chemical compounds and the shortage of dissolved oxygen (Kumar, 2017; Pastor et al., 2020). Indeed, inside the pockmarks, hydrogen sulfide concentration increases with depth along the vertical profile while the dissolved oxygen plummets (Coull, 1988; Ritt et al., 2011; Ristova et al., 2015; Pastor et al., 2020). Specifically, most of the animals were found in the upper sediment layers (0–1 cm and 1–2 cm) (**Figure 10**). These layers are well-oxygenated (Coull, 1988; Pastor et al., 2020), and in one of the study pockmarks, there is a still relatively low concentration of hydrogen sulfide, a toxic reduced compound (Somero et al., 1989; Bagarinao, 1992; Giere, 2009). These findings agree with the hypothesis of Sánchez et al. (under review) and seem to evidence that the pockmark conditions enhance the abundance of Kinorhyncha, likely through the replacement with opportunistic, specialized species. These species would be able to cope with the pockmark conditions where other meiofaunal organisms cannot live (including other non-adapted species of Kinorhyncha), profiting about this and thriving rapidly (Ritt et al., 2010; Vanreusel et al., 2010; Sánchez et al., under review). This is also supported by the presence of a relatively high juvenile abundance inside the pockmarks, which shows that these species not only manage to survive under such extreme conditions but also are able to intensely flourish there. Indeed, certain groups of meiofauna, such as nematodes and harpacticoid copepods, can reach high peaks of abundance in extreme environments where competition with other taxa is lower, which makes their prosperity possible (Coull, 1985; Colangelo et al., 2001; Van Gaever et al., 2009; Zeppilli and Danovaro, 2009; Zeppilli et al., 2012, 2018). Alternatively, the elevated kinorhynch density, including the high number of juveniles, may be explained, in the context of pockmarks, as they are considered potential colonizers at sulfide seepages of deep sea vents (Mullineaux et al., 2012).

Additionally, pockmarks are rich in reduced compounds, resulting in higher chemosynthetic microbial densities that live in these habitats as hydrocarbon degraders, acting in the anaerobic oxidation of methane and sulfate reduction processes (Giovannelli et al., 2016). The bacterial mats form a major source of food for meiofauna, including kinorhynchs who likely feed on them (Neuhaus, 2013). Thus, pockmarks may also enhance high kinorhynch densities because of the abundant bacteria, also in those layers where the hydrogen sulfide concentration (formed as a waste product of the anaerobic respiration of reducing microorganisms) is still tolerable. However, as soon as the hydrogen sulfide concentration increases in the subsequent layers, it seems to turn toxic and both kinorhynch density and richness decrease (**Figure 10**).

Cold seeps also increase the spatial heterogeneity of the habitat through geochemical gradients, driving the distribution of the biological communities (Levin, 2005; Guillon et al., 2017). This fact furthermore supports the differences in the community composition between pockmarks and areas outside pockmarks' influence, so the greater availability of geochemically heterogeneous microhabitats inside the pockmark may enable the maintenance of a community made up of highly adapted kinorhynch species to the particular conditions of each pockmark.

Thus, even though a similar kinorhynch richness was found in areas under pockmark influence and outside pockmarks,

community composition drastically differs from one habitat to another (**Figures 12**, **13**), suggesting that only certain species are well-adapted and able to tolerate the extreme conditions of this kind of cold seeps, characterized by methane and hydrogen sulfide emissions, as was already confirmed for other meiofaunal groups (Vanreusel et al., 2010; Zeppilli et al., 2012, 2018). The pockmark conditions seem to prevent the survival of non-adapted species, with their consequent fading, as occur for *E. apex*, *E.* cf. *dubiosus*, *Echinoderes* sp., *F. hydra* sp. nov., and *Ryuguderes* sp., only found outside the pockmark sites.

Condyloderes sp., *E. hviidarum*, *E. unispinosus*, *Fi. cthulhu* sp. nov., *F. dagon* sp. nov., and *Sphenoderes* cf. *indicus* characterize the kinorhynch community in the areas under the pockmark's influence. Of these, only *Condyloderes* sp. and *E. unispinosus* seem to be generalistic species capable of living in both habitats, but their abundances are higher inside pockmarks by far. These two species, together with *E. hviidarum* and *Fi. cthulhu* sp. nov., do not simply survive under such harsh conditions but take advantage of a habitat with a likely lower competition for space and resources, flourishing there (Sánchez et al., under review). Additionally, the dissimilarity in kinorhynch community composition between the two study pockmarks is remarkable as well. *E. hviidarum* seems to be the most tolerant species to hydrogen sulfide as it largely dominated the community at the more active pockmark with higher concentrations of hydrogen sulfide. Indeed, *E. hviidarum* was also present in deep layers where the highest concentrations of hydrogen sulfide were detected. On the other hand, *E. unispinosus*, *Fi. cthulhu* sp. nov., and *F. dagon* sp. nov. only appeared in the pockmark with methane but without hydrogen sulfide emission (**Figure 13**). Therefore, methane and hydrogen sulfide, among other ecological factors, turn out to significantly drive kinorhynch community structure and composition, but we cannot conclude that all the aforementioned species are truthful bioindicators of cold seeps activity, as some of them were originally described from habitats free of seepages influence (Higgins, 1983; Sørensen et al., 2018; Yamasaki et al., 2018b). It remains to be clarified if the species described in the present article, *Fi. cthulhu* sp. nov. and *F. dagon* sp. nov., are only present in cold seepages or not.

CONCLUSION

Despite the fact that data interpretation of the present study must be taken with caution due to the reduced number of sampling sites and the possible effect of spatiotemporal variation among samples, we could make the following conclusions:

- Deep-sea environments host a highly biodiverse community of still undescribed species of Kinorhyncha.
- Kinorhynch richness is similar inside and outside the pockmarks, but the species composition completely changes because of exclusive species at both habitats.
- Contrarily to kinorhynch species richness, abundance is affected by the pockmarks' conditions, being higher within pockmarks than outside them. The extreme conditions of these habitats boost the kinorhynch abundance likely through the replacement with opportunistic specialized species, such as *E. hviidarum*, *E. unispinosus*, and *Fi. cthulhu* sp. nov., able to thrive rapidly under such features where competition is lower by far as hydrogen sulfide is toxic for most metazoans.

DATA AVAILABILITY STATEMENT

All datasets generated for this study are included in the article/**Supplementary Material**.

AUTHOR CONTRIBUTIONS

NS and DZ conceived the general idea of the study. DC, NS, and FP conducted the experimental process, and NS statistically analyzed the results. DC wrote the background and taxonomic part of the manuscript, and NS wrote the methods and the ecological part of the study. All the authors reviewed the manuscript.

FUNDING

This study was done within the framework of the Passive Margin Exploration Laboratories (PAMELA) project, funded by TOTAL and IFREMER. IFREMER furthermore funded the contract of NS to study the meiofauna collected during the PAMELA-MOZ04 campaign. DC was supported by a predoctoral fellowship of the Complutense University of Madrid (CT27/16-CT28-16) and a short-term predoctoral fellowship also of the Complutense University of Madrid (EB14/19).

ACKNOWLEDGMENTS

We would like to thank all the participants and the staff of the R/V *L'Atalante* and *Pour quoi pas?* Vessel, Scampi team and all scientists and students who participated in the PAMELA MOZ1 and MOZ4 cruises, specially to Dr. Karine Olu, chief of the mission, and Lara Macheriotou for processing the cores on board. Moreover, we are grateful to the Ghent meiofauna laboratory for the meiofauna processing and Dr. Lucie Pastor and Christophe Brandily (IFREMER) for the geochemical analyses and advises in the treatment of geo-chemical data. We would also like to thank Dr. Martin V. Sorensen and Dr. Matteo Dal Zotto for their suggestions and comments that kindly improved the present article.

SUPPLEMENTARY MATERIAL

The Supplementary Material for this article can be found online at: https://www.frontiersin.org/articles/10.3389/fmars.2020.00665/full#supplementary-material

REFERENCES

Adrianov, A. V., and Maiorova, A. S. (2015). *Pycnophyes abyssorum* sp. n. (Kinorhyncha: Homalorhagida), the deepest kinorhynch species described so far. *Deep Sea Res. II Top. Stud. Oceanogr.* 111, 49–59. doi: 10.1016/j.dsr2.2014.08.009

Adrianov, A. V., and Maiorova, A. S. (2016). *Condyloderes kurilensis* sp. nov. (Kinorhyncha: Cyclorhagida)—a new deep water species from the abyssal plain near the Kuril-Kamchatka Trench. *Russ. J. Mar. Biol.* 42, 11–19. doi: 10.1134/S1063074016010028

Adrianov, A. V., and Maiorova, A. S. (2018a). *Meristoderes okhotensis* sp. nov. – The first deepwater representative of kinorhynchs in the Sea of Okhotsk (Kinorhyncha: Cyclorhagida). *Deep Sea Res. II Top. Stud. Oceanogr.* 154, 99–105. doi: 10.1016/j.dsr2.2017.10.011

Adrianov, A. V., and Maiorova, A. S. (2018b). *Parasemnoderes intermedius* gen. n., sp. n.—the First Abyssal Representative of the Family Semnoderidae (Kinorhyncha: Cyclorhagida). *Russ. J. Mar. Biol.* 44, 355–362. doi: 10.1134/S1063074018050024

Adrianov, A. V., and Malakhov, V. V. (1999). *Cephalorhyncha of the World Ocean*. Moscow: KMK Scientific Press.

Álvarez-Castillo, L., Cepeda, D., Pardos, F., Rivas, G., and Rocha-Olivares, Á (2020). *Echinoderes unispinosus* (Kinorhyncha: Cyclorhagida), a new record from deep-sea sediments in the Gulf of Mexico. *Zootaxa* 4821, 196–200.

Álvarez-Castillo, L., Hermoso-Salazar, M., Estradas-Romero, A., Prol-Ledesma, R. M., and Pardos, F. (2015). First records of *Kinorhyncha* from the Gulf of California: horizontal and vertical distribution of four genera in shallow basins with CO2 venting activity. *Cah. Biol. Mar.* 56, 271–281.

Bagarinao, T. (1992). Sulfide as an environmental factor and toxicant: tolerance and adaptations in aquatic organisms. *Aquat. Toxicol.* 24, 21–62. doi: 10.1016/0166-445X(92)90015-F

Cepeda, D., Álvarez-Castillo, L., Hermoso-Salazar, M., Sánchez, N., Gómez, S., and Pardos, F. (2019a). Four new species of Kinorhyncha from the Gulf of California, eastern Pacific Ocean. *Zool. Anz.* 282, 140–160. doi: 10.1016/j.jcz.2019.05.011

Cepeda, D., Sánchez, N., and Pardos, F. (2019b). First extensive account of the phylum Kinorhyncha from Haiti and the Dominican Republic (Caribbean Sea), with the description of four new species. *Mar. Biodivers.* 49, 2281–2309. doi: 10.1007/s12526-019-00963-x

Claparède, A. R. E. (1863). *Zur Kenntnis der Gattung Echinoderes Duj. Beobachtungen über Anatomie und Entwicklungsgeschichte wirbelloser Thiere an der Küste von Normandie angestellt*. Leipzig: Engelmann.

Colangelo, M. A., Bertasi, F., Dall'Olio, P., and Ceccherelli, V. H. (2001). "Meiofaunal biodiversity on hydrothermal seepage off Panarea (Aeolian Islands, Tyrrhenian Sea)," in *Mediterranean Ecosystems: Structures and Processes*, eds F. M. Faranda, L. Guglielmo, and G. Spezie (Berlin: Springer-Verlag), 353–359. doi: 10.1007/978-88-470-2105-1_46

Coull, B. C. (1985). Long-term variability of estuarine meiobenthos: an 11 year study. *Mar. Ecol. Prog. Ser.* 24, 205–218. doi: 10.3354/meps024205

Coull, B. C. (1988). "Ecology of the marine meiofauna," in *Introduction to the Study of Meiofauna*, eds R. P. Higgins and H. Thiel (Washington D.C: Smithsonian Institution Press), 18–38.

Dal Zotto, M., Santulli, A., Simonini, R., and Todaro, M. A. (2016). Organic enrichment effects on a marine meiofauna community, with focus on Kinorhyncha. *Zool. Anz.* 265, 127–140. doi: 10.1016/j.jcz.2016.03.013

Dando, P. R., Austen, M. C., Burke, R. A., Kendall, M. A., Kennicutt, M. C., Judd, A. G., et al. (1991). Ecology of a North Sea pockmark with an active methane seep. *Mar. Ecol. Prog. Ser.* 70, 49–63. doi: 10.3354/meps070049

Eakins, B. W., and Sharman, G. F. (2010). *Volumes of the World's Oceans from ETOPO1*. Boulder, CO: NOAA National Geophysical Data Center.

Fonselius, S. H. (1983). "Determination of hydrogen sulphide," in *Methods of Seawater Analysis*, eds K. Grasshoff, K. Kremling, and M. Ehrhardt (Weinheim: Verlag Chemie), 73–80.

Giere, O. (2009). *Meiobenthology. The Microscopic Motile Fauna of Aquatic Sediments*. Berlin: Springer.

Giovannelli, D., D'Errico, G., Fiorentino, F., Fattorini, D., Regoli, F., Angeletti, L., et al. (2016). Diversity and distribution of prokaryotes within a shallow-water pockmark field. *Front. Microbiol.* 7:941. doi: 10.3389/fmicb.2016.00941

Grzelak, K., and Sørensen, M. V. (2018). New species of Echinoderes (Kinorhyncha: Cyclorhagida) from Spitsbergen, with additional information about known Arctic species. *Mar. Biol. Res.* 14, 113–147. doi: 10.1080/17451000.2017.1367096

Grzelak, K., and Sørensen, M. V. (2019). Diversity and community structure of kinorhynchs around Svalbard: first insights into spatial patterns and environmental drivers. *Zool. Anz.* 282, 31–43. doi: 10.1016/j.jcz.2019.05.009

Guillon, E., Menot, L., Decker, C., Krylova, E., and Olu, K. (2017). The vesicomyd bivalve habitat at cold-seeps supports heterogeneous and dynamic macrofaunal assemblages. *Deep Sea Res. I Oceanogr. Res. Pap.* 120, 1–13. doi: 10.1016/j.dsr.2016.12.008

Heip, C. H. R., Vincx, M., and Vranken, G. (1985). The ecology of marine nematodes. *Oceanogr. Mar. Biol.* 23, 399–489.

Herranz, M., and Pardos, F. (2013). *Fissuroderes sorenseni* sp. nov. and *Meristoderes boylei* sp. nov.: first Atlantic recording of two rare kinorhynch genera, with new identification keys. *Zool. Anz.* 2013, 93–111. doi: 10.1016/j.jcz.2013.09.005

Herranz, M., Thormar, J., Benito, J., Sánchez, N., and Pardos, F. (2012). *Meristoderes* gen. nov., a new kinorhynch genus, with the description of two new species and their implications for echinoderid phylogeny (Kinorhyncha: Cyclorhagida, Echinoderidae). *Zool. Anz.* 251, 161–179. doi: 10.1016/j.jcz.2011.08.004

Higgins, R. P. (1969). Indian Ocean Kinorhyncha: 1. *Condyloderes* and Sphenoderes, new cyclorhagid genera. *Smith. Contr. Zool.* 14, 1–13. doi: 10.5479/si.00810282.14

Higgins, R. P. (1983). The Atlantic barrier reef ecosystem at Carrie Bow Cay, Belize, II. *Kinorhyncha. Smith. Contr. Mar. Sci.* 1, 1–131. doi: 10.5479/si.01960768.18.1

Hourdez, S., and Lallier, F. H. (2006). Adaptations to hypoxia in hydrothermal-vent and cold-seep invertebrates. *Rev. Environ. Sci. Biotechnol.* 6, 143–159. doi: 10.1007/s11157-006-9110-3

Hovland, M., and Judd, A. G. (1988). *Seabed Pockmarks and Seepages: Impact on Geology, Biology and Marine Environment*. London: Grahamand Trotman.

Janssen, A., Kaiser, S., Meißner, K., Brenke, N., Menot, L., and Arbizu, P. (2015). A reverse taxonomic approach to assess macrofaunal distribution patterns in abyssal Pacific polymetallic nodule fields. *PLoS One* 10:e0117790. doi: 10.1371/journal.pone.0117790

Jouet, G., and Deville, E. (2015). *PAMELA-MOZ04 cruise, R/V Pourquoi pas? Flotte océanographique française opérée par l'Ifremer*. Netherlands: EAGE.

Kennedy, B. R. C., Cantwell, K., Malik, M., Kelley, C., Potter, J., Elliott, K., et al. (2019). The unknown and the unexplored: insights into the Pacific deep-sea following NOAA CAPSTONE expeditions. *Front. Mar. Sci.* 6:480. doi: 10.3389/fmars.2019.00480

Kumar, A. (2017). "Foreword," in *Investigating Seafloors and Oceans, from Mud Volcanoes to Giant Squid*, ed. A. Joseph (Amsterdam: Elsevier), 9–26.

Landers, S. C., Basshman, R. D., Miller, J. A., Ingels, J., Sánchez, N., and Sørensen, M. V. (2020). Kinorhynch communities from Alabama coastal waters. *Mar. Biol. Res.* doi: 10.1080/17451000.2020.1789660

Landers, S. C., Sørensen, M. V., Beaton, K. R., Jones, C. M., Miller, J. M., and Stewart, P. M. (2018). Kinorhynch assemblages in the Gulf of Mexico continental shelf collected during a two-year survey. *J. Exp. Mar. Biol. Ecol.* 02, 81–90. doi: 10.1016/j.jembe.2017.05.013

Legendre, P., and Gallagher, E. D. (2001). Ecologically meaningful transformations for ordination of species data. *Oecology* 129, 271–280. doi: 10.1007/s004420100716

Levin, L. A. (2005). Ecology of cold seep sediments: interactions of fauna with flow, chemistry and microbes. *Oceanogr. Mar. Biol.* 43, 1–46. doi: 10.1201/9781420037449-3

Levin, L. A., and Sibuet, M. (2012). Understanding continental margin biodiversity: a new imperative. *Annu. Rev. Mar Sci.* 4, 79–112. doi: 10.1146/annurev-marine-120709-142714

Mirto, S., Gristina, M., Sinopoli, M., Maricchiolo, G., Genovese, L., Vizzini, S., et al. (2012). Meiofauna as an indicator for assessing the impact of fish farming at an exposed marine site. *Ecol. Indic.* 18, 468–476. doi: 10.1016/j.ecolind.2011.12.015

Mullineaux, L. S., Le Bris, N., Mills, S. W., Henri, P., Bayer, S. R., Secrist, R. G., et al. (2012). Detecting the influence of initial pioneers on succession at deep-sea vents. *PLoS One* 7:e50015. doi: 10.1371/journal.pone.0050015

Neuhaus, B. (2013). "Kinorhyncha (=Echinodera)," in *Handbook of Zoology. Gastrotricha, Cycloneuralia and Gnathifera, Volume 1: Nematomorpha,*

Priapulida, Kinorhyncha, Loricifera, ed. A. Schmidt-Rhaesa (Hamburg: De Gruyter), 181–350.

Neuhaus, B., and Blasche, T. (2006). Fissuroderes, a new genus of Kinorhyncha (Cyclorhagida) from the deep sea and continental shelf of New Zealand and from the continental shelf of Costa Rica. *Zool. Anz.* 245, 19–52. doi: 10.1016/j.jcz.2006.03.003

Neuhaus, B., and Sørensen, M. V. (2013). Populations of *Campyloderes* sp. (Kinorhyncha, Cyclorhagida): one global species with significant morphological variation? *Zool. Anz.* 252, 48–75. doi: 10.1016/j.jcz.2012.03.002

Oksanen, F. J., Blanchet, F. G., Friendly, M., Kindt, R., Legendre, P., McGlinn, D., et al. (2018). *vegan: Community Ecology Package. R Package Version 2.4-4*. Available online at: https://github.com/vegandevs/vegan (accessed October 02, 2019).

Oksanen, F. J., Blanchet, F. G., Kindt, R., Legendre, P., Minchin, P. R., O'Hara, R. B., et al. (2015). *vegan: Community Ecology Package. R Package Vegan, Version 2.2-1*. Available online at: https://github.com/vegandevs/vegan (accessed October 02, 2019).

Olu, K. (2014). *PAMELA-MOZ01 cruise, R/V L'Atalante. Flotte océanographique française opérée par l'Ifremer*. Netherlands: EAGE.

Pastor, L., Brandily, C., Schmidt, S., Miramontes, E., Péron, M., Apperé, D., et al. (2020). Modern sedimentation and geochemical imprints in sediments from the NW Madagascar margin. *Mar. Geol.* 426:106184. doi: 10.1016/j.margeo.2020.106184

Reinhard, W. (1881). Über Echinoderes und Desmoscolex der Umgebung von Odessa. *Zool. Anz.* 4, 588–592.

Ristova, P. P., Wenzhöfer, F., Ramette, A., Felden, J., and Boetius, A. (2015). Spatial scales of bacterial community diversity at cold seeps (eastern Mediterranean Sea). *ISME J.* 9, 1306–1318. doi: 10.1038/ismej.2014.217

Ritt, B., Pierre, C., Gauthier, O., Wenzhöfer, F., Boetius, A., and Sarrazin, J. (2011). Diversity and distribution of cold-seep fauna associated with different geological and environmental settings at mud volcanoes and pockmarks of the Nile deep-sea fan. *Mar. Biol.* 158, 1187–1210. doi: 10.1007/s00227-011-1679-6

Ritt, B., Sarrazin, J., Caprais, J. C., Noël, P., Gauthier, O., Pierre, C., et al. (2010). First insights into the structure and environmental setting of cold-seep communities in the Marmara Sea. *Deep Sea Res. I Oceanogr. Res. Pap.* 57, 1120–1136. doi: 10.1016/j.dsr.2010.05.011

Rouse, G. W., and Fauchald, K. (1997). Cladistics and polychaetes. *Zool. Scr.* 26, 139–204. doi: 10.1111/j.1463-6409.1997.tb00412.x

Sánchez, N., Pardos, F., and Martínez-Arbizu, P. (2019a). Deep-sea Kinorhyncha diversity of the polymetallic nodule fields at the clarion-clipperton fracture zone (CCZ). *Zool. Anz.* 282, 88–105. doi: 10.1016/j.jcz.2019.05.007

Sánchez, N., Pardos, F., and Sørensen, M. V. (2014a). A new kinorhynch genus, Mixtophyes (Kinorhyncha: Homalorhagida), from the Guinea Basin deep-sea, with new data on the family Neocentrophyidae. *Helgol. Mar. Res.* 68, 221–239. doi: 10.1007/s10152-014-0383-6

Sánchez, N., Pardos, F., and Sørensen, M. V. (2014b). Deep-sea Kinorhyncha: two new species from the Guinea Basin, with evaluation of an unusual male feature. *Org. Divers. Evol.* 14, 349–361. doi: 10.1007/s13127-014-0182-6

Sánchez, N., Sørensen, M. V., and Landers, S. C. (2019b). Pycnophyidae (Kinorhyncha: Allomalorhagida) from the Gulf of Mexico: *Fujuriphyes viserioni* sp. nov. and a re-description of *Leiocanthus langi* (Higgins, 1964), with notes on its intraspecific variation. *Mar. Biodivers.* 49, 1857–1875. doi: 10.1007/s12526-019-00947-x

Sánchez, N., and Yamasaki, H. (2016). Two new Pycnophyidae species (Kinorhyncha: Allomalorhagida) from Japan lacking ventral tubes in males. *Zool. Anz.* 265, 80–89. doi: 10.1016/j.jcz.2016.04.001

Sánchez, N., Yamasaki, H., Pardos, F., Sørensen, M. V., and Martínez, A. (2016). Morphology disentangles the systematics of a ubiquitous but elusive meiofaunal group (Kinorhyncha: Pycnophyidae). *Cladistics* 32, 479–505. doi: 10.1111/cla.12143

Sarradin, P. M., and Caprais, J. C. (1996). Analysis of dissolved gases by headspace sampling gas chromatography with column and detector switching. Preliminary results. *Anal. Commun.* 33, 371–373. doi: 10.1039/ac9963300371

Seeberg-Elverfeldt, J., Schlüter, M., Feseker, T., and Koelling, M. (2005). Rhizon sampling of pore waters near the sediment/water interface of aquatic systems. *Limnol. Oceanogr. Meth.* 3, 361–371. doi: 10.4319/lom.2005.3.361

Seitzinger, S. P., Mayorga, E., Bouwman, A. F., Kroeze, C., Beusen, A. H. W., Billen, G., et al. (2010). Global river nutrient export: a scenario analysis of past and future trends. *Glob. Biogeochem. Cycles* 24:GB0A08. doi: 10.1029/2009GB003587

Sibuet, M., and Olu, K. (1998). Biogeography, biodiversity and fluid dependence of deep-sea cold-seep communities at active and passive margins. *Deep Sea Res. II Top. Stud. Oceanogr.* 45, 517–567. doi: 10.1016/S0967-0645(97)00074-X

Somero, G. N., Childress, J. J., and Anderson, A. E. (1989). Transport, metabolism and detoxification of hydrogen sulphide in animals from sulphide-rich marine environments. *Aquat. Sci.* 1, 591–614.

Sørensen, M. V. (2008a). A new kinorhynch genus from the Antarctic deep sea and a new species of Cephalorhyncha from Hawaii (Kinorhyncha: Cyclorhagida: Echionoderidae). *Org. Divers. Evol.* 8, e1–e232. doi: 10.1016/j.ode.2007.11.003

Sørensen, M. V. (2008b). Phylogenetic analysis of the Echinoderidae (Kinorhyncha: Cyclorhagida). *Org. Divers. Evol.* 8, 233–246. doi: 10.1016/j.ode.2007.11.002

Sørensen, M. V., Dal Zotto, M., Rho, H. S., Herranz, M., Sánchez, N., Pardos, F., et al. (2015). Phylogeny of Kinorhyncha based on morphology and two molecular loci. *PLoS One* 10:e0133440. doi: 10.1371/journal.pone.0133440

Sørensen, M. V., and Grzelak, K. (2018). New mud dragons from Svalbard: three new species of Cristaphyes and the first Arctic species of *Pycnophyes* (Kinorhyncha: Allomalorhagida: Pycnophyidae). *PeerJ* 6:e5653. doi: 10.7717/peerj.5653

Sørensen, M. V., Rohal, M., and Thistle, D. (2018). Deep-sea Echinoderidae (Kinorhyncha: Cyclorhagida) from the Northwest Pacific. *Eur. J. Taxon.* 456, 1–75. doi: 10.5852/ejt.2018.456

Sørensen, M. V., Thistle, D., and Landers, S. C. (2019). North American *Condyloderes* (Kinorhyncha: Cyclorhagida: Kentrorhagata): female dimorphism suggests moulting among adult *Condyloderes*. *Zool. Anz.* 282, 232–251. doi: 10.1016/j.jcz.2019.05.015

Sun, J., Zhang, Y., Xu, T., Zhang, Y., Mu, H., Zhang, Y., et al. (2017). Adaptation to deep-sea chemosynthetic environments as revealed by mussel genomes. *Nat. Ecol. Evol.* 1:0121. doi: 10.1038/s41559-017-0121

Sutherland, T. F., Levings, C. D., Petersen, S. A., Poon, P., and Piercey, B. (2007). The use of meiofauna as an indicator of benthic organic enrichment associated with salmonid aquaculture. *Mar. Poll. Bull.* 54, 1249–1261. doi: 10.1016/j.marpolbul.2007.03.024

Van Gaever, S., Olu, K., Derycke, S., and Vanreusel, A. (2009). Metazoan meiofaunal communities at cold-seeps along the Norwegian margin: influence of habitat heterogeneity and evidence for connection with shallow-water habitats. *Deep Sea Res. I Oceanogr. Res. Pap.* 56, 772–785. doi: 10.1016/j.dsr.2008.12.015

Vanreusel, A., De Groote, A., Gollner, S., and Bright, M. (2010). Ecology and biogeography of free-living nematodes associated with chemosynthetic environments in the deep-sea: a review. *PLoS One* 5:e12449. doi: 10.1371/journal.pone.0012449

Yamasaki, H. (2016). Ryuguderes iejimaensis, a new genus and species of Campyloderidae (Xenosomata: Cyclorhagida: Kinorhyncha) from a submarine cave in the Ryukyu Islands, Japan. *Zool. Anz.* 265, 69–79. doi: 10.1016/j.jcz.2016.02.003

Yamasaki, H., Grzelak, K., Sørensen, M. V., Neuhaus, B., and George, K. H. (2018a). Echinoderes pterus sp. n. showing a geographically and bathymetrically wide distribution pattern on seamounts and on the deep-sea floor in the Arctic Ocean, Atlantic Ocean, and the Mediterranean Sea (Kinorhyncha, Cyclorhagida). *ZooKeys* 771, 15–40. doi: 10.3897/zookeys.771.25534

Yamasaki, H., Neuhaus, B., and George, K. H. (2018b). New species of Echinoderes (Kinorhyncha: Cyclorhagida) from Mediterranean seamounts and from the deep-sea floor in the North-eastern Atlantic Ocean, including notes of two undescribed species. *Zootaxa* 4387, 541–556. doi: 10.11646/zootaxa.4387.3.8

Yamasaki, H., Neuhaus, B., and George, K. H. (2018c). Three new species of Echinoderidae (Kinorhyncha: Cyclorhagida) from two seamounts and the adjacent deep-sea floor in the Northeast Atlantic Ocean. *Cah. Biol. Mar.* 59, 79–106. doi: 10.21411/CBM.A.124081A9

Yamasaki, H., Neuhaus, B., and George, K. H. (2019). Echinoderid mud dragons (Cyclorhagida: Kinorhyncha) from Senghor Seamount (NE Atlantic Ocean) including general discussion of faunistic characters and distribution patterns of seamount kinorhynchs. *Zool. Anz.* 282, 64–87. doi: 10.1016/j.jcz.2019.05.018

Zelinka, K. (1894). Über die Organisation von *Echinoderes*. *Verh. Dtsch. Zool. Ges.* 4, 46–49.

Zelinka, K. (1896). Demonstration der Tafeln der Echinoderes-Monographie. *Verh. Dtsch. Zool. Ges.* 6, 197–199.

Zelinka, K. (1913) Die Echinoderen der Deutschen Südpolar-Expedition 1901–1903. *Deutsche Südpolar Expedition XIV Zoologie* 6, 419–437.

Zelinka, K. (1928). *Monographie der Echinodera*. Leipzig: Engelmann.

Zeppilli, D., Canals, M., Danovaro, R., and Gambi, C. (2012). Meiofauna abundance of westerm Mediterranean Sea seep sediments. *PANGAEA*. doi: 10.1594/PANGAEA.803358

Zeppilli, D., and Danovaro, R. (2009). Meiofaunal diversity and assemblage structure in a shallow-water hydrothermal vent in the Pacific Ocean. *Aquat. Biol.* 5, 75–84. doi: 10.3354/ab00140

Zeppilli, D., Leduc, D., Fontanier, C., Fontaneto, D., Fuchs, S., Gooday, A. J., et al. (2018). Characteristics of meiofauna in extreme marine ecosystems: a review. *Mar. Biodivers.* 48, 35–71. doi: 10.1007/s12526-017-0815-z

Conflict of Interest: The authors declare that the research was conducted in the absence of any commercial or financial relationships that could be construed as a potential conflict of interest.

Copyright © 2020 Cepeda, Pardos, Zeppilli and Sánchez. This is an open-access article distributed under the terms of the Creative Commons Attribution License (CC BY). The use, distribution or reproduction in other forums is permitted, provided the original author(s) and the copyright owner(s) are credited and that the original publication in this journal is cited, in accordance with accepted academic practice. No use, distribution or reproduction is permitted which does not comply with these terms.

Advantages of publishing in Frontiers

OPEN ACCESS
Articles are free to read for greatest visibility and readership

FAST PUBLICATION
Around 90 days from submission to decision

HIGH QUALITY PEER-REVIEW
Rigorous, collaborative, and constructive peer-review

TRANSPARENT PEER-REVIEW
Editors and reviewers acknowledged by name on published articles

Frontiers
Avenue du Tribunal-Fédéral 34
1005 Lausanne | Switzerland

Visit us: www.frontiersin.org
Contact us: frontiersin.org/about/contact

REPRODUCIBILITY OF RESEARCH
Support open data and methods to enhance research reproducibility

DIGITAL PUBLISHING
Articles designed for optimal readership across devices

FOLLOW US
@frontiersin

IMPACT METRICS
Advanced article metrics track visibility across digital media

EXTENSIVE PROMOTION
Marketing and promotion of impactful research

LOOP RESEARCH NETWORK
Our network increases your article's readership